THE UNIVERSITY OF QUEENSLAND

AUSTRALIA

β-hairpin antimicrobial peptides:

structure, function and mode of action

Ingrid Alexia Edwards

MSc Chemistry and chemical engineering

A thesis submitted for the degree of Doctor of Philosophy at

The University of Queensland in 2018

Institute for Molecular Bioscience

Abstract

A ‘state of emergency’ was declared by the World Health Organization three years ago to combat the increasing rate of resistance arising in bacteria to all currently available antibiotics on the market. Antimicrobial resistance is now a worldwide concern, and renewed efforts are needed in the search for new replacement drugs for obsolete antibiotics. Antimicrobial peptides (AMPs) have been discovered and studied over decades; importantly very limited bacterial resistance has been reported to date. The work here aims to better characterize and understand the structure-function relationships of select β-hairpin AMPs, leading to the design of novel, optimized and potentially therapeutically valuable peptides.

Chapter 1 reviews the field of β-hairpin AMPs and provides a background for the specific AMPs studied in this thesis. Chapter 2 consists of an original data set that strengthens the current knowledge of β-hairpin AMPs by comparing their activity profile under similar conditions. This work analysed the contribution of amphipathicity and hydrophobicity to antimicrobial activity and cytotoxicity of β-hairpin peptides, concluding that a very fine balance between charge, hydrophobicity, amphipathicity, secondary and tertiary structure and mode of action is needed for a peptide to be therapeutically valuable. From this study, two distinct but linked areas of further investigation were identified (i) a structure activity and function relationship study and (ii) a determination of the mode of action of select β-hairpin AMPs.

Chapter 2 identified that tachyplesin-1, a 17 amino acids β-hairpin AMP originating from the hemocyte debris of a horseshoe crab, *Tachypleus tridentatus*, was an ideal β-hairpin AMP candidate to study structure-activity and -toxicity relationships, as it possessed an 8-fold higher therapeutic index than other β-hairpin AMPs studied. Thus, chapter 3 contains an evaluation of the role of each amino acid of tachyplesin-1 through an alanine scan. New analog peptides were designed as a systematic approach to develop more therapeutically valuable peptides as replacements for antibiotics that have become ineffective. Measurements of activity and toxicity, combined with preliminary ADME data, led to the identification of two tachyplesin-1 analogs with great potential for future drug development.

Chapters 4 and 5 consist of studies of the mode of action of arenicin-3, a 21 amino acid β-hairpin AMP originating from the coelomocytes of marine polychaeta lugworm, *Arenicola marina*, and its synthetic analog AA139. AA139 is a lead drug candidate of Adenium Biotech Ltd. currently in preclinical development for MDR urinary tract infection and MDR Gram-negative pneumonial diseases. Their 3D NMR solution structures revealed right handed twisted β-hairpin structures of 21

amino acids rigidified by two disulfide bridges (Cys3-Cys20 and Cys7-Cys16). The mode of action of arenicin peptides and their selectivity toward bacteria cells, and more specifically their interaction toward different lipid membrane systems, were examined. Chapter 4 focused on label free mode of action investigations, leading to a proposed model of arenicin mode of action involving three steps: (1) binding to the outer membrane through electrostatic interactions, (2) insertion into the hydrophobic core of the outer membrane creating partial permeabilization due to the ability of the peptide to modify its secondary structure allowing it to enter into the lipid bilayer without pore formation, (3) accessing and partially permeabilizing the cytoplasmic membrane. To provide further evidence of the arenicin peptides mode of action, chapter 5 contains a comprehensive structural investigation employing NMR experiments with ^{15}N labelled AA139 in the presence of lipid bilayer model membranes, nanodiscs or vesicles, using solution and solid-state NMR, respectively. This work suggested that the *C*- and *N*-terminal of AA139 are the first point of interaction with lipid bilayer membranes. Following that first interaction, AA139 possibly undergoes a loss of its well-defined 3D solution structure, becoming dynamic and without a distinct fold whilst embedded in the membrane and causing the permeabilization of both outer and inner membranes. This study allowed us to gain a deeper understanding of AA139 mode of action, and of the differences between the successful lead drug candidate, AA139 and its therapeutically less valuable progenitor, arenicin-3. This study provides an example of potential approaches to employ when designing other improvements to antimicrobial peptides. More importantly, this study allowed us to confirm the great potential of nanodiscs, not only to study membrane proteins, but also to evaluate the mode of action of membrane-active peptides.

Declaration by author

This thesis is composed of my original work, and contains no material previously published or written by another person except where due reference has been made in the text. I have clearly stated the contribution by others to jointly-authored works that I have included in my thesis.

I have clearly stated the contribution of others to my thesis as a whole, including statistical assistance, survey design, data analysis, significant technical procedures, professional editorial advice, financial support and any other original research work used or reported in my thesis. The content of my thesis is the result of work I have carried out since the commencement of my higher degree by research candidature and does not include a substantial part of work that has been submitted to qualify for the award of any other degree or diploma in any university or other tertiary institution. I have clearly stated which parts of my thesis, if any, have been submitted to qualify for another award.

I acknowledge that an electronic copy of my thesis must be lodged with the University Library and, subject to the policy and procedures of The University of Queensland, the thesis be made available for research and study in accordance with the Copyright Act 1968 unless a period of embargo has been approved by the Dean of the Graduate School.

I acknowledge that copyright of all material contained in my thesis resides with the copyright holder(s) of that material. Where appropriate I have obtained copyright permission from the copyright holder to reproduce material in this thesis and have sought permission from co-authors for any jointly authored works included in the thesis.

Publications included in this thesis

Edwards, IA, Elliott, AG, Kavanagh, AM, Zuegg, J, Blaskovich, MAT, Cooper, MA, (2016), Contribution of amphipathicity and hydrophobicity to the antimicrobial activity and cytotoxicity of β-hairpin peptides, *ACS Inf. dis*. DOI: 10.1021/acsinfecdis.6b00045

Edwards, IA, Elliott, AG, Kavanagh, AM, Blaskovich, MAT, Cooper, MA, (2017), Structure-activity and -toxicity relationships of the antimicrobial peptide tachyplesin-1, *ACS Inf. dis.* DOI:10.1021/acsinfecdis.7b00123

Submitted manuscripts included in this thesis

No manuscripts submitted for publication.

Other publications during candidature

Conference abstracts

Edwards, IA, Mobli, M, Zuegg, J, Cooper, MA. Arenicin-3 peptides: β-hairpin AMPs structures and mode of action. *11th Australian peptides conferences*, Kingscliff, Australia, October 2015

Edwards, IA, Elliott, AG, Blaskovich, MAT and Cooper, MA. Contribution of physicochemical parameters to the antimicrobial activity / toxicity index of β-hairpin peptides. *34th European peptide conference*, Leipzig, Germany, September 2016.

Edwards, IA, Elliott, AG, Blaskovich, MAT and Cooper, MA. Contribution of physicochemical parameters to the antimicrobial activity / toxicity index of β-hairpin peptides. *Queensland Annual Chemistry Symposium*, Brisbane, Australia, November 2016.

Edwards, IA, Elliott, AG, Blaskovich, MAT and Cooper, MA. Contribution of physicochemical parameters to the antimicrobial activity / toxicity index of β-hairpin peptides. *Solution for drug resistant infections*, Brisbane, Australia, April 2017.

Edwards, IA, Elliott, AG, Blaskovich, MAT, Mobli, M, Solution NMR characterisation of β-hairpin antimicrobial peptides in lipid bilayer nanodiscs, *12th Australian peptides conferences*, Noosa, Australia, October 2017

Edwards, IA, Elliott, AG, Blaskovich, MAT, Mobli, M, Solution NMR characterisation of β-hairpin antimicrobial peptides in lipid bilayer nanodiscs, *ANZMAG (Australian New Zealand Magnetic Resonance) conference*, Kingscliff, Australia, December 2017

Contributions by others to the thesis

Zhenling Cui designed the plasmid vector mentioned in chapter 5, page 5-110.

Alan Zhang performed the expression and purification of cNW9 mentioned in chapter 5, page 5-113.

Statement of parts of the thesis submitted to qualify for the award of another degree

No works submitted towards another degree have been included in this thesis.

Research Involving Human or Animal Subjects

The work in this thesis was performed under the ethics approval number 2014000031 granted by NHMRC/ARC agent for the duration period: 17 March 2015 to 31 December 2019, to perform hemolytic assay of red blood cells for compounds with antimicrobial activity.

Acknowledgements

Many people have contributed to make my journey through my PhD as smooth as possible and I would like to thank them for their time, patience and their trust in me.

I would like to sincerely thank my supervisors Prof. Matthew Cooper, A/Prof. Mehdi Mobli, Dr Alysha Elliott and Dr Mark Blaskovich who have provided support and encouragement throughout my thesis. Matt, thank you for the opportunity to work in your lab, your expert advices and your continual optimism. Mehdi, you have been a great support throughout my thesis, you always made time to help and offer advice. Thank you for your patience in teaching me the world of NMR. Alysha, your attention to detail and high expectations made me a better researcher and I thank you for your availability, feedback and guiding me through my PhD journey. Mark, thank you for your guidance and advice. I would like to also thank the other members of my thesis committee, Prof. David Craik and Dr Johan Rosengren, for providing me with highly valuable advice to further direct my project along the three years.

A special thanks to Greg Pierens for his help with NMR and Matthias Floetenmeyer for his help with EM. A particular thanks to Sonia Henriques for her teaching, encouragement and expert advice in membrane biology. The Cooper and Mobli group members past and present not only for their discussions and technical advice but for their friendship. I would like to specially acknowledge the support of postgraduate team for help and kindness throughout the whole administrative process. Amanda and Cody thank you for caring for each student within IMB, you are making our journey very special.

Finally a huge thank you to my husband, David and son, Owen. You are the two most amazing people in the world. Thank you for your love, trust and specially thank you for making me laugh at home when in the lab there was not much room for laugher. Thank you also to my parents for your support and your travel visits making 17000 km feel like nothing.

Financial support

I would like to acknowledge the financial support of a University of Queensland International PhD scholarship. I have also had the privilege of travelling to conferences thanks to travel grants from the IMB, the Australian Peptide Society and the European Peptides Society.

Keywords

Antimicrobial peptides, arenicin, tachyplesin, bilayer lipid model membranes, nanodiscs, mode of action, biological membrane.

Australian and New Zealand Standard Research Classifications (ANZSRC)

ANZSRC code: 030406, Proteins and Peptides, 40%

ANZSRC code: 029901, Biological Physics, 30%

ANZSRC code: 111504, Pharmaceutical Sciences, 30%

Fields of Research (FoR) Classification

FoR code: 0601, Biochemistry and Cell Biology, 30%

FoR code: 0306, Physical Chemistry (incl. Structural), 40%

FoR code: 1115, Pharmacology and Pharmaceutical Sciences, 30%

Table of content

List of figures

List of tables

Abbreviations

Abbreviations	Definition
A3D	aggrescan 3D
ADME	adsorption distribution metabolism elimination
AMPs	antimicrobial peptides
ApoA1	apolipoprotein A1
ATR-FTIR	attenuated total reflectance – fourier transform infrared
BCA	bicinchoninic acid
BMRB	biological magnetic resonance bank
CCPNMR	collaborative computational project for NMR
CD	circular dichroism
CF	carboxyfluorescein
CHAPS	3-[(3-cholamidopropyl)dimethylammonio]-1-propanesulfonate
cNW9	cicularized MSP1D1ΔH5
CP	cross polarization
CSI	chemical shift indices
cUTI	complicated urinary tract infection
dH5	MSP1D1ΔH5
DHPC	1,2-diheptanoyl-*sn*-glycero-3-phosphocholine
DLPC	1,2-Dilauroyl-sn-glycero-3-phosphocholine
DLS	dynamic light scattering
DMPC	1,2-dimyristoyl-sn-glycero-3-phosphocholine
DOSY	diffusion ordered spectroscopy
DPC	dodecylphosphocholine
DSS	2,2-dimethylsilapentane-5-sulfonic acid
E.coli	escherichia coli
EDTA	ethylenediaminetetraacetic acid
ELSD	evaporative light scattering detector
EM	electron microscopy
ESBL	extended spectrum beta lactamase
ESI	electrospray ionization
FA	formic acid
FACS	fluorescence activated cell sorting
FPLC	fast protein liquid chromatogrraphy
G+ve	gram positive
G-ve	gram negative
HDL	high density lipoprotein
HPLC	high performance liquid chromatography
HSQC	heteronuclear single quantum correlation
IPTG	isopropyl beta-D-1-thiogalactopyranoside
LB	luria broth
LC-MS	liquid chromatography-mass spectrometry
LPS	lipid lipopolysaccharide
LUVs	large unilamellar vesicles
MAS	magic angle spinning

MBP	maltose binding protein
MDR	multi drug resistant
MIC	minumim inhibitory concentration
MM	minimal media
MRSA	methicillin resistant staphylococcus aureus
MS	mass spectrometry
MSP	membrane scaffold protein
MW	molecular weight
ND	nanodisc
NDM-1	new delhi metallo-beta-lactamase-1
NEB	new england biolabs
NMR	nuclear magnetic resonance
NOE	nuclear overhauser effect
NOESY	nuclear overhauser effect spectroscopy
OD_{600}	optical density at 600 nm
OPM	orientation of protein in membrane
P/L	peptide to lipid molar ratio
PBS	phosphate buffer saline
PCR	polymerase chain reaction
PDB	protein data bank
POPC	palmitoyloleoylphosphatidylcholine
POPE	palmytoyloleoylphosphatidylethanolamine
POPG	palmytoyloleoylphosphatidylglycerol
POPS	palmitoyleoylphosphatidylserine
RBC	red blood cells
SDS-PAGE	sodium dodecyl sulfate - polyacrylamide gel electrophoresis
SEC	size exclusion chromatography
SPR	surface plasmom resonance
ssNMR	solid state NMR
SUMO	small ubiquitin like modifier
SUVs	small unilamellar vesicles
TFA	trifluoroacetic acid
TFE	trifluoroethanol
TIC	total ion chromatography
tm	mixing time
TOCSY	total correlation spectroscopy
TOF	time of flight
TP1	tachyplesin-1
TROSY	transverse relaxation optimized spectroscopy
VRE	vancomycin resistant enterococci
WHO	world health organisation
ΔH5	MSP1D1ΔH5

Chapter 1 - Introduction

1.1 Antibiotic development

Antibiotics, or antibacterial drugs, are chemicals used for the treatment of bacterial infections. Bacteria are all around us, being one of the first life forms to appear on earth and still constituting the biggest biomass present on the planet. We encounter bacteria on and inside us, from our fingerprints to the nooks and crannies of our intestines, with the human body consisting of about 10 bacterial cells for every human cell. Bacteria are part of our lives and to stay healthy we need to maintain a healthy ecosystem of bacterial flora that can fight against harmful, pathogenic or opportunistic species that can cause infection. Even though the body's immune system is powerful enough to regulate its own bacterial flora, external help is sometimes required from antibiotics, to fight against the more persistent pathogenic bacteria. However, antibiotics can cause unintended side effects by causing dysbiosis via collateral damage to the beneficial microbiome.

Antibiotics first appeared during the 1930's with Alexander Fleming in 1928[1-3] discovering Penicillin, the first member of the β-lactam family. It was the first drug to show activity against bacterial infections caused by staphylococci and streptococci. Infections that were a common cause of death before, became curable. The mass production of penicillin expanded in the 1940's followed by numerous other antibiotic families (Figure 1-1).

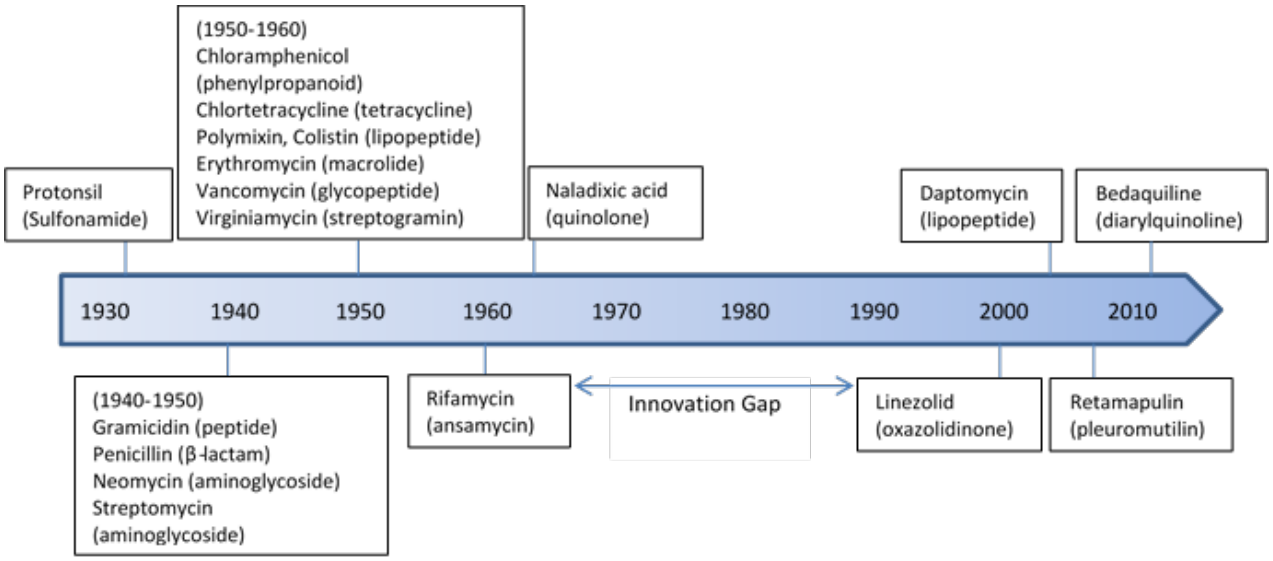

Figure 1-1 - Chronological discovery of antibiotics. Antibiotic class in brackets.

The so-called “Golden-Age of Discovery” was the period between 1945 and 1960, which showed a rapid expansion in the number of new antibiotics discovered and developed, almost all derived from natural products (Figure 1-1). The discovery of antibiotics, able to prevent and cure deadly infections, facilitated the development of revolutionary medical interventions possible such as organ transplants, chemotherapy and invasive surgery. This period was followed closely by the “Golden Age of Medicinal Chemistry”, from 1970 to 2000, where antibiotics were synthesized or semi-synthesized from naturally existing ones, improving their pharmacokinetic profiles and antibacterial potency (for example, from erythromycin to clarithromycin and later to roxithromycin and finally to solithromycin).[4-8]

Unfortunately, the end of the 20th century marked the end of antibiotic discovery as no new families of drugs have been developed into clinically used antibiotics for the last 20 years. Almost all antibacterial classes, such as β-lactams, tetracyclines, chloramphenicol, aminoglycosides, macrolides, glycopeptides, streptogramines and quinolones, each with different mechanisms of action, were initially introduced into clinical practice during this Golden-Age of antibiotics. After this prolific period, very few antibiotic class have entered into the clinic. Despite the numerous efforts to find and develop new antibiotics and improve existing ones, bacteria continue to evolve, responding to exposure to antibiotics.

Antibiotics are classified according to their chemical structure, their mode of action and their spectrum of activity. Two main classes of antibiotics can be distinguished (i) bacteriostatic agents, restricting the growth and reproduction of the bacteria, such as chloramphenicol, oxazolidinones, sulfonamides, tetracyclines and macrolides and (ii) bactericidal agents, causing bacterial cell death, like β-lactams, aminoglycosides, glycopeptides, quinolones, ansamycines, streptogramins and lipopeptides. Their modes of action to act against bacteria are diverse and can be classified into five main categories (Figure 1-2): cell wall synthesis, protein synthesis, bacterial cell membrane, nucleic acid synthesis and antimetabolite activity.

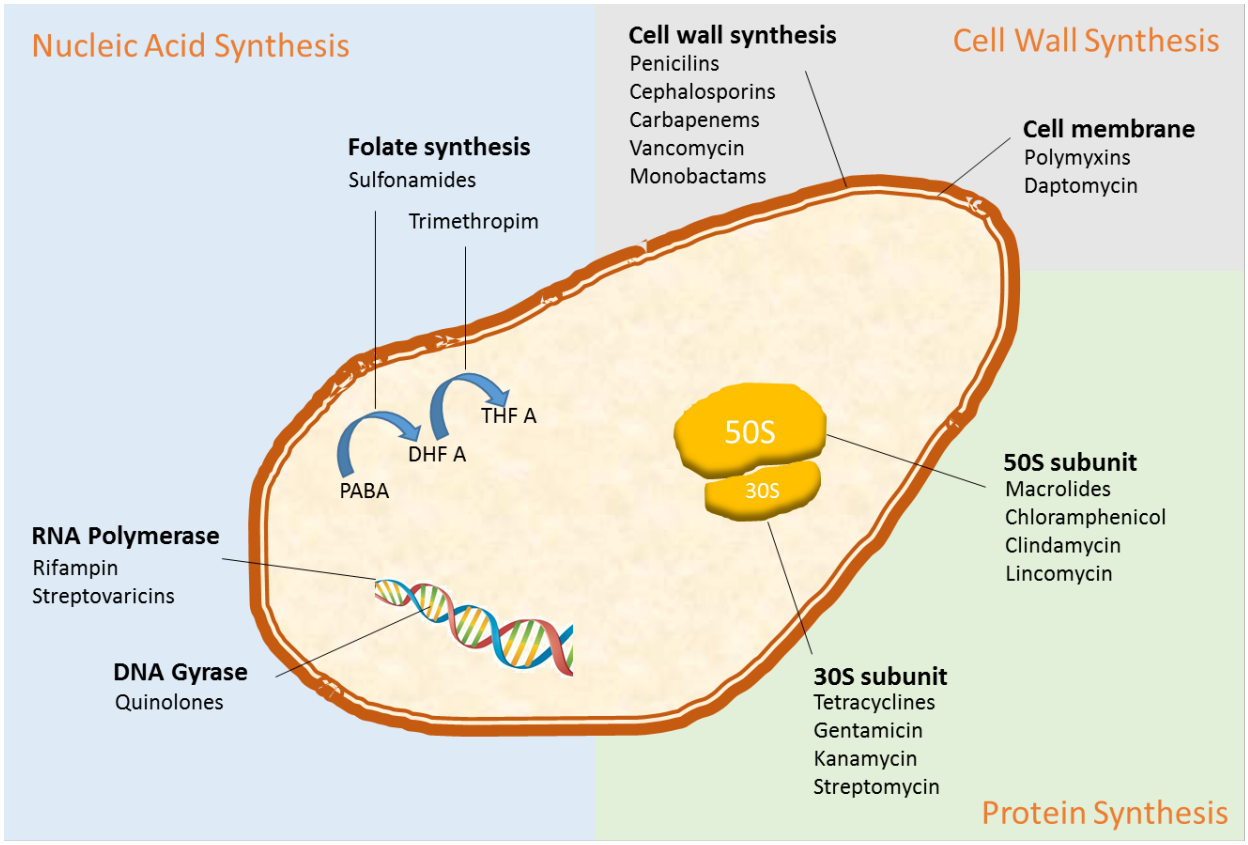

Figure 1-2 - Classes of antibiotics/antibacterial agents and their modes of action on bacteria.[9]

1.2 Bacterial resistance

The lack of new discoveries and decrease of pharmaceutical companies being involved in antimicrobial research and development, coupled with the increasing development of antimicrobial resistance, has triggered a serious threat to human health. The appearance of antibiotic resistant bacteria, where the bacteria are no longer controlled or killed by the antibiotic, is often observed only a few years after the antibiotic was first introduced into clinical use. Antibiotic resistant bacteria either spontaneously mutate to be able to counteract the efficacy of the antibiotics or transfer antibiotic resistance genes from one bacterium to another. Antibiotic resistant bacteria are able to survive and even multiply in the presence of antibiotics. Bacteria can be resistant to one or more antibiotics, with multi-drug resistant (MDR) bacteria known as 'superbugs'. Figure 1-3 illustrates the correlation between the introduction of antibiotic use in the clinic versus the evolution of resistance that has arisen to those clinical antibiotics.[10-18] On average, antibiotic resistance develops only 8 years following introduction of the drug's use in the clinic. In earlier years, 1950s to 1960s, the time for resistance development was much longer than during the 21st century due to the high number of antibiotics available.

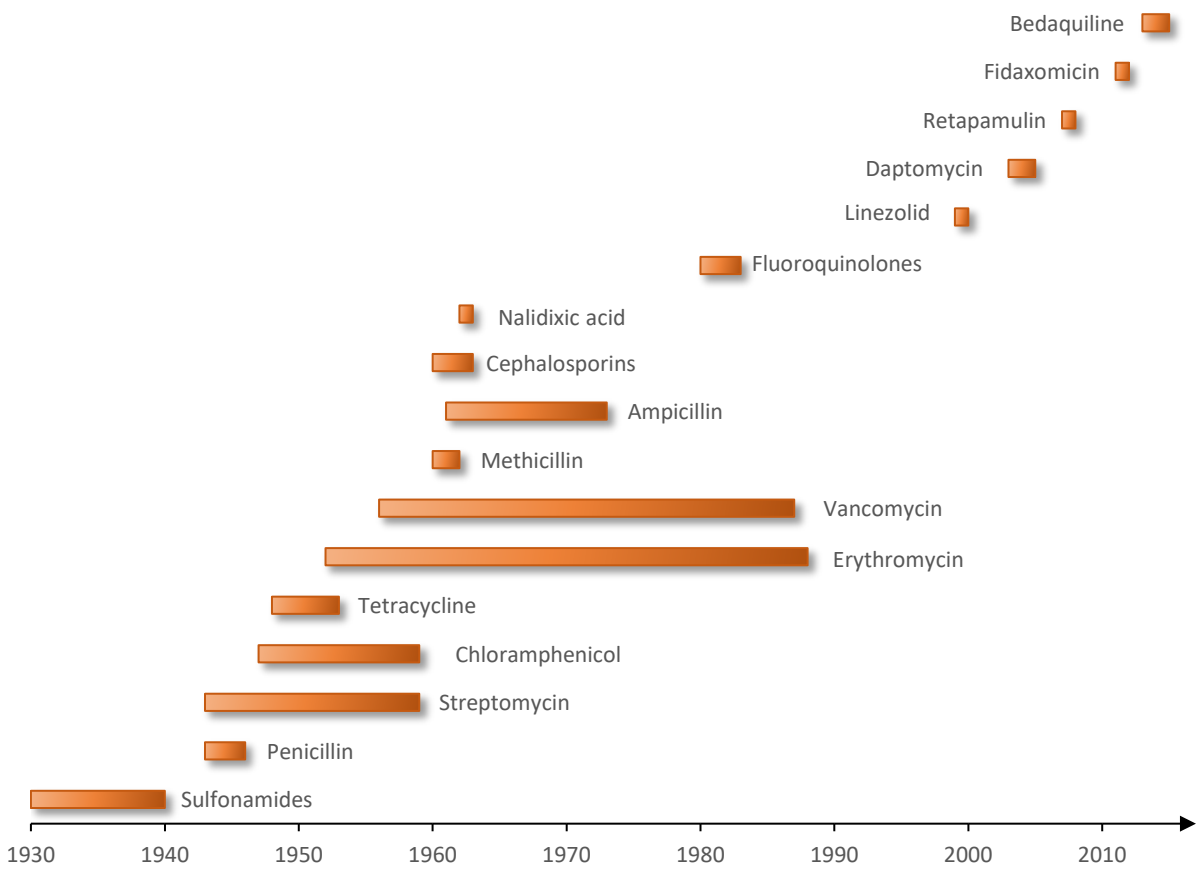

Figure 1-3 - Discovery to consequent development of antibiotic resistance timeline. The bars mark the time from the introduction of an antibiotic to the clinic until the first clinical case of resistance to that antibiotic was reported.

Antimicrobial resistance occurs naturally over time, however, the rapid expansion of antimicrobial resistance is facilitated by the misuse and over prescription of antibiotics. Bacteria acquire several mechanisms to become resistant to antibiotics. It can be through the inactivation of the drug by enzymes, the alteration of the drug target, or by prevention of the drug reaching its target via modification of cell wall or the activation of a drug efflux pump (Figure 1-4). This is the case for Vancomycin Resistant Enterococci (VRE) for example, where the first case of resistance was reported in 1987.[19] VRE became resistant to vancomycin via biochemical changes to its target, Lipid II. By changing an Lipid II alanine to a lactate or a serine, a hydrogen bond normally formed with vancomycin is eliminated, decreasing the *in vitro* binding affinity by 1000-fold.[20] Methicillin Resistant *Staphylococcus aureus* (MRSA) is resistant to most β-lactam antibiotics with the first case reported in 1968. The mechanism of this resistance is mediated through the production of an enzyme known as beta-lactamase which is capable of deactivating penicillin via lactam hydrolysis, thus rendering it ineffective.[21]

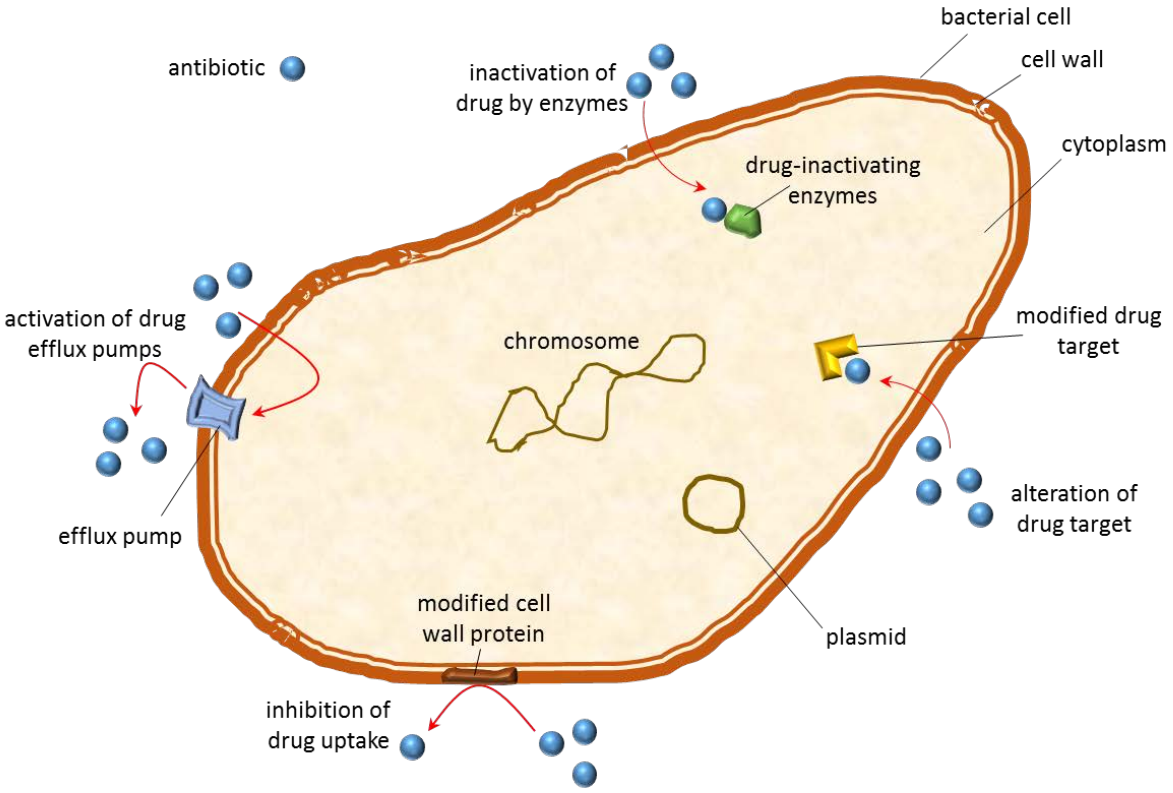

Figure 1-4 - Mechanisms of antibiotic resistance.

Current antibiotics generally target pathways susceptible to generate drug resistance via protein mutation, like folic acid synthesis, protein synthesis, RNA and DNA synthesis. Bacterial membrane is still a domain showing the least resistance mechanisms, making it a valuable target for new antibiotics. The only membrane-targeting antibiotic currently available to treat MDR Gram-negative (G-ve) bacterial infections is the lipopeptide colistin (polymyxin E). Unfortunately, colistin is poorly membrane-selective, highly nephrotoxic and imparts severe adverse effects in humans. Therefore, there is a definite need for safer drugs that can target G-ve bacterial membranes with high selectivity over mammalian membranes.

1.3 New antibiotics, approaches to development

In 2014, the World Health Organization (WHO) declared a ‘state of emergency’ to combat the increasing rate of resistance arising in bacteria to all current antibiotics on the market.[22] More recently, in November 2015, WHO launched a multiyear campaign themed “Antibiotics: Handle with care” tackling antimicrobial resistance. Considering the urgency needed to find new antibacterial compounds, it begs the question; which techniques could be applied for their discovery? Historically, two main approaches of research have been fruitful (i) finding a new molecule from a natural source

and (ii) synthetic modification of existing antibacterial drugs.[23] Mining the world for new antibacterial molecules is a big challenge. Molecules could be found in microorganisms, prokaryotes and eukaryotes. This work requires high sampling volumes and sensitive scanning techniques in order to identify bioactive molecules unknown to date. Most of the currently used antibiotics come from bacteria in the soil which produce them naturally in order to compete in their environment. However, to date, still 99% of the known microbial species are yet uncultured.[24] Therefore, the potential for new antibacterial compounds from natural sources is promising, if they can be grown. The other way to find new antibacterial agents, is to synthetically modify existing ones. The most common and successful synthetic modifications are the ones which have been performed on existing successful drug classes. However, modifications could also be made to potent antibacterial molecules that have not been pushed for clinical trials due to their high degree of toxicity against mammalian cells, converting them into therapeutically valuable derivatives. Several pathways could be followed (i) study the mode of action of a successful antibacterial agent in order to replicate the mechanism on a different molecule (ii) characterize each amino acid of a potent antimicrobial peptide (AMP), by alanine scan for instance, to identify modifiable regions of the peptide in order to create a new peptide maintaining potency while reducing mammalian toxicity, (iii) modulate the structure by combinatorial chemistry. In this thesis, the latter two pathways are investigated with the aim of discovering a replacement for obsolete antibiotics and will be further discussed in chapters 2 to 5.

Additional alternative pathways of finding new antibacterial agents could also be investigated. The reexamination of discarded antibiotics is an option. This was the case for daptomycin first discovered by Eli Lilly in 1980s, discarded due to toxicity concerns but brought back to market by the Cubist group in 2003 using a different dosage composition.[25] The combination of several antibiotics together or hybrid antibiotics with non-antibiotics is another successful pathway, as shown by the very successful antibiotic Augmentin, a combination of ampicillin with the β-lactamase inhibitor clavulanic acid.

1.4 Antimicrobial peptides (AMPs)

The initial work requirement for synthetic modifications of an existing compound resides on the choice of the template molecule candidate for drug design. In general, microbes are considered to have developed little or no resistance to AMPs, in contrast to antibiotics, which have developed marked resistance. AMPs could thereby be a valuable starting point for synthetic modifications. AMPs are oligopeptides, ranging from five to a hundred amino acids, ubiquitous in nature. AMPs are produced by the innate immune defense system of multicellular organisms, microorganisms, plants

and animals to help them fight against external invading pathogens. Being mobilized shortly after microbial invasion, AMPs are expressed to act broadly and quickly. AMPs have the common characteristics of being amphipathic, cationic and membranolytic, properties which make them suitable for development as a drug candidate if selectivity for bacterial cells over mammalian cells can be established. AMPs were first discovered in 1939 by Dubos,[26] who identified an AMP from the soil and named it gramicidin, which later became a topical therapeutic agent for wounds and ulcers.[27] Since then, thousands of antimicrobial molecules have been reported, with more than 2300 AMPs reported from eukaryotes (http://aps.unmc.edu/AP/about.php). AMPs are classified according to their source, their secondary structure and their mode of action.[28-30] From all the AMPs reported only about 40% of them have had their structure characterized. Approximately 90% of them have been determined to adopt α-helical secondary structure, Figure 1-5. This α-helical AMP category has been extensively examined.[31-33] However, less known are the AMPs which adopt a β-sheet structure; these include peptides with a β-sheet structure consisting of three strands (most vertebrate defensins), two strands with a β-hairpin structure, or a mixed structure that includes both β-sheets and α-helices.[34] The α-helical AMPs are abundant in the extracellular fluids of insects and frogs and mostly exist as extended or unstructured conformers in solution. Many of these peptides only become helical when interacting with the cell membrane. However, β-sheet peptides adopt more ordered structures. Despite such differences, all AMPs share common features, including amphipathic composition, with distinct hydrophilic and hydrophobic surfaces.

Figure 1-5 - Clustering of antimicrobial peptides according to backbone torsion angles and antimicrobial activity.[35] Helixes are represented in cyan and β-sheet in magenta.

1.5 β-hairpin AMPs

The subcategory, β-hairpin AMPs, have the common characteristic of two anti-parallel β-sheets linked by a small turn of 3 to 7 amino acids, forming a hairpin shape. Twelve families of β-hairpin AMPs have been discovered and reported so far, from mammals and invertebrates. For most β-hairpin classes, representative members have been analyzed for their 3D solution structures by nuclear magnetic resonance (NMR) spectroscopy. Their structures vary from one disulfide bond to four and from linear to cyclic (head-to-tail) backbones, Table 1-1. Although the 3D NMR structures have never been assessed for either tigerinin-1 or bactenecin, computer modelling propose that their peptide chains also adopt β-hairpin secondary structure.[36]

The β-hairpin AMPs share close sequence homology, with conserved disulfide bridges to stabilize the β–sheets, a β–turn motif, cationic Arg or Lys residues adjacent to the turn and distal C- and N-termini flanked by hydrophobic, membrane-insertive Val, Leu, Ile, Tyr or Trp residues. Together these motifs describe an amphipathic structure with one hydrophobic face and a basic face, which creates a hydrophobic moment in the structure. Amphipathicity is one of the key characteristics of AMPs and Fernandes-Vidal et al.[37] showed that amphipathicity is more important than hydrophobicity for binding to microbial membranes. This makes AMPs an attractive candidate class to develop as new antibiotics.

Table 1-1 - β-hairpin AMPs origin, sequence and cartoon representation using Pymol 1.7.2.3. Disulfide bridges are shown as thin lines in the sequences and are yellow stick in the 3D structures. The bold line denotes the peptide bond that forms a θ-defensin cycle. (*) – C-terminal amidation, Z – N-terminal pyroglutamic acid.

Name	Source	Amino acid sequence	Cartoon representation	PDB/Ref.
tigerinin-1	*Rana tigerina* (frog skin secretion)	FCTMIPIPRCY*	-	[36]
bactenecin	*Bos taurus* (bovine neutrophils)	RLCRIVVIRVCR	-	[38]
tachyplesin-1	*Tachypleus tridentatus* (horseshoe crab hemocytes)	KWCFRVCYRGICYRRCR*		1WO0/[39]
polyphemusin-1	*Limulus polyphemus* (horseshoe crab hemocytes)	RRWCFRVCYRGFCYRKCR	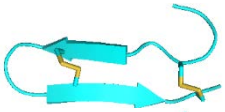	1RKK/[40]
protegrin-1	*Sus scrofa* (porcine leukocytes)	RGGRLCYCRRRFCVCVGR*	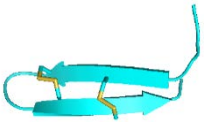	1PG1/[41]
gomesin	*Acanthoscurria gomesiana* (spider hemocytes)	ZCRRLCYKQRCVTYCRGR*		1KFP/[42]
retrocyclin-2	*Macaca mulattav* (rhesus monkey leukocytes)	GFCRCLCRRGVCRCICTR	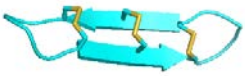	2LRI/[43]
arenicin-1	*Arenicola marina* (lugworm coelomocytes)	RWCVYAYVRVRGVLVRYRRCW		2JSB/[44]
thanatin	*Podisus maculiventris* (spined soldier bug hemolymph)	GSKKPVPIIYCNRRTGKCQRM	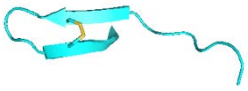	8TFV/[45]
alvinellacin	*Alvinella pompejana* (Pompeii worm)	RGCYTRCWKVGRNGRVCMRVCT	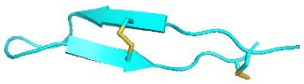	2LLR/[46]
androctonin	*Androctonus australis* (scorpion hemolymph)	RSVCRQIKICRRRGGCYYKCTNRPY		1CZ6/[47]
lactoferricin B	*Bos taurus taurus* (bovine milk)	FKCRRWQWRMKKLGAPSITCVRRAF		1LFC/[48]
hepcidin 25	*Homo sapiens* (human hepatocytes)	DTHFPICIFCCGCCHRSKCGMCCKT	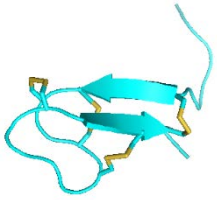	2KEF/[49]

1.6 Cell membrane

The cell membrane has been extensively studied over the past 100 years. This protecting barrier was first proposed by Gorter et al.[50] in 1925 as a lipid bilayer membrane with the polar group orientated toward the inside of the cell. Their proposed theory of the cell membrane consisting of a lipid bilayer contained several experimental issues that were later corrected. Several modifications of the Gorter et al. lipid bilayer theory were discussed up until 1972, where Singer et al.[51], proposed the "fluid mosaic model", a model still in use to date. The model describes the cell membrane as a liquid matrix comprising lipids and proteins that restricts the lateral diffusion of membrane components. The liquid matrix was then found to be inhomogeneous and prone to forming lipid rafts, caused by stabilizing lipid-lipid and lipid-protein interactions.[52]

The composition of the cell membranes is very complex and cell type dependent. Mostly constituted of lipids of various kinds, membrane proteins and a small amount of carbohydrates, the lipid matrix of biological membranes is formed asymmetrically in order to ensure the unique functionality of the cell type (Figure 1-6). This bilayer is composed of two leaflets of amphipathic lipid molecules, whose polar head groups are in contact with the intra- or extracellular aqueous phases, whereas their non-polar tails face each other, constituting the hydrophobic interior of the membrane.

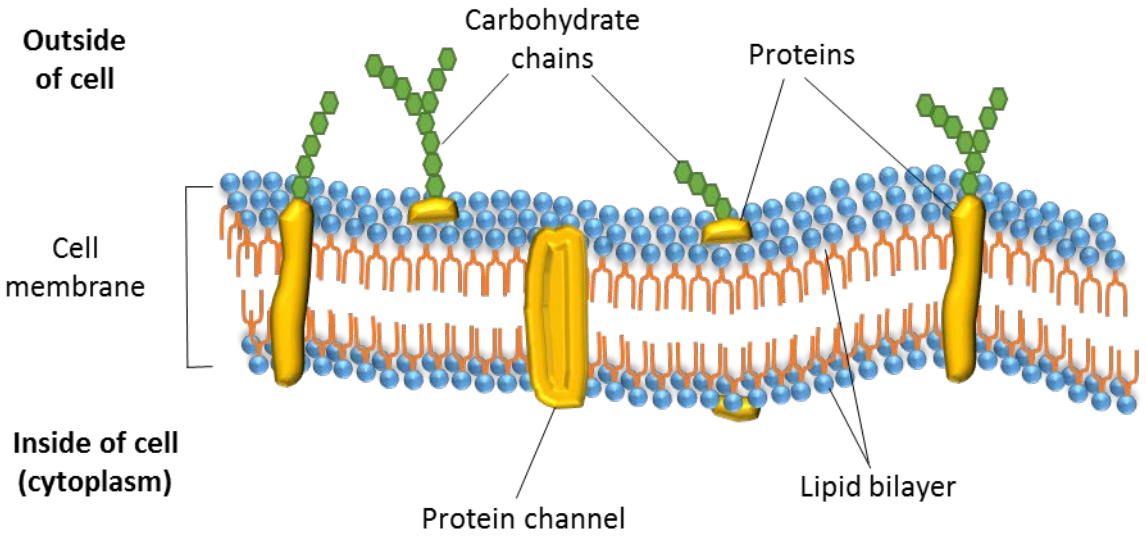

Figure 1-6 - Fluid mosaic model.

Whilst the cell membrane of human cells can be represented using the fluid mosaic model presented above, bacteria cell walls differ considerably.

Bacteria were first classified into two main categories by the Danish bacteriologist Hans Christian Gram who developed the Gram stain test that identified bacteria as belonging to one of two main categories, Gram positive (G+ve) and G-ve bacteria. The Gram test differentiates the bacteria according to the chemical and physical properties of their cell wall, detecting in particular the properties of the peptidoglycan. In this test, the G+ve bacteria appear a purple color, as the stain is retained in the larger and denser peptidoglycan structure, while G-ve bacteria appear pink, as their thin and light peptidoglycan is not able to retain the stain. Even though G-ve bacteria possess a second, outer membrane which acts as an additional barrier, the Gram staining process disrupts the membrane with alcohol, making the Gram staining a marker for the structure of the peptidoglycan rather than the presence or absence of a second membrane (Figure 1-7).

The bacterial cytoplasmic cell content is surrounded by a plasma membrane followed by the inner peptidoglycan cell wall, and for G-ve bacteria an outer lipid bilayer. In G-ve bacteria, the peptidoglycan layer contains about 10% of the cell wall dry weight while in G+ve bacteria the peptidoglycan layer is thicker (about 40 layers) and constitutes about 20% of the cell wall dry weight.

The structure of peptidoglycan contains a carbohydrate backbone of alternating units of *N*-acetylglucosamine (GlcNAc) and *N*-acetylmuramic acid, with the *N*-acetylmuramic acid residues cross-linked to peptides. This is the peptidoglycan layer that confers the rigidity and strength to the bacterial cell.

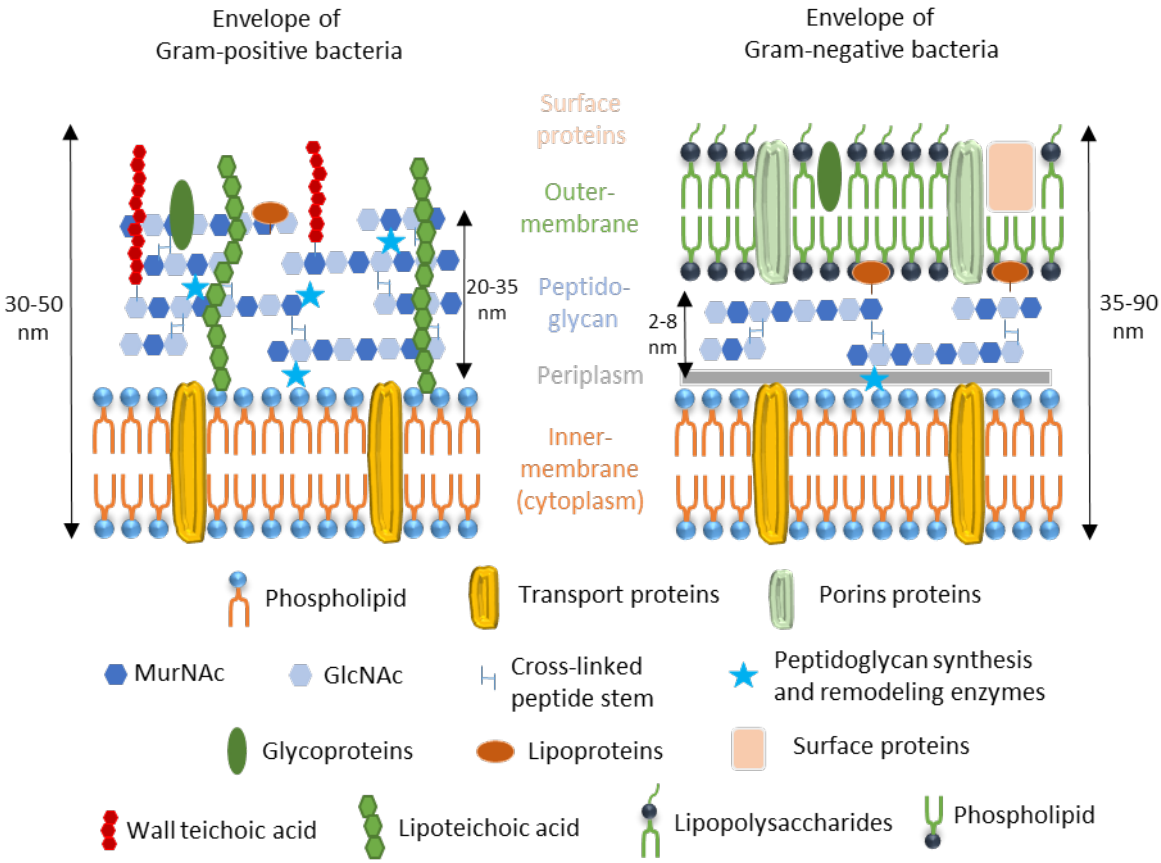

Figure 1-7 - Schematic views of Gram-negative (top) and Gram-positive (bottom) bacteria cell walls, showing the complex assembly of high molecular weight compounds.

However, the bacteria cell membrane constitutes many other components. For both types of bacteria, the cytoplasmic membrane (or inner bacterial membrane for G-ve bacteria) is constituted of a symmetric double layer of phospholipid molecules, the hydrophilic (polar) heads of which face the peptidoglycan and the cytoplasm while their hydrophobic (apolar) tails are hidden in the middle of the cell membrane. Embedded in the lipid bilayer are proteins and glycoproteins (proteins with carbohydrates attached) serving different functions. For G-ve bacteria only, the distinctive outer membrane is even more complex featuring an asymmetric membrane, an inner phospholipid and an outer glycolipid leaflet. The glycolipid leaflet is a lipopolysaccharide (LPS) layer composed of O-specific polysaccharide, core polysaccharide and lipid A attached to the surface. Traversing this membrane are outer membrane proteins such as porins that allow the diffusion of essential molecules across the otherwise impermeable barrier.

1.7 Lipid model membranes

In this thesis, the cell membranes of human cell and bacteria cells are modelled in order to study the interaction and mode of action of peptides against the different types of cell membrane. Lipids constituting the lipid bilayer are mostly dominated by different types of phospholipids followed by a very small proportion of glycolipids and sterols.[53] Phospholipids are amphipathic, containing a hydrophilic head comprised of a phosphate group functionalized with two hydrophobic fatty acid tail chains varying in length and saturation level. Phospholipids are often classified by their head group composition; predominantly phosphatidylcholine (PC), phosphatidylglycerol (PG) or phosphatidylethanolamine (PE). Bacteria cell membranes are overall very negatively charged and therefore contain a significant proportion of negatively charged PG, negatively charged phospholipids, whereas mammalian cells are more positively charged, thus composed of zwitterionic phospholipids such as PC or PE.

Phospholipids, being amphipathic, aggregate in solution, naturally forming vesicles in solution. Vesicles are a very important tool used in many different areas of research. They serve as models for cell membranes, as delivery vehicles for drugs into living cells and through other hydrophobic barriers, and as useful components of other specialized applications, such as a support for semiconductor particles for the photoconversion of solar energy.[54] In this thesis, lipid vesicles help us to model cell membranes to investigate the mode of action of AMPs. However, in order to understand the mechanisms of action, the models need to replicate as closely as possible the real cell membrane environment. Different lipid formations can be taken as a membrane mimicking environment. Micelles are the oldest mimic commonly used, however they do not reflect the true complexity of the bacteria and/or mammalian cell membranes due to their monolayer feature. Phospholipids tend to form liposomes, or lipid vesicles, made of bilayers, able to more accurately mimic the complexity and charge of different type of cell membrane. Vesicles vary in size and the number of bilayers present, from multilamellar vesicles (MLV) bigger than 500 nm to lipid bilayers as small as 8 nm, such as nanodiscs (ND). The latter are relatively recent innovations that incorporate a membrane scaffold protein (MSP) that considerably reduces the size of the lipid bilayer, allowing for a new way of membrane analysis and characterization via NMR.[55] Figure 1-8, represents the basic structure of lipid vesicles and nanodisc models, used in this thesis (Chapters 3, 4 and 5).

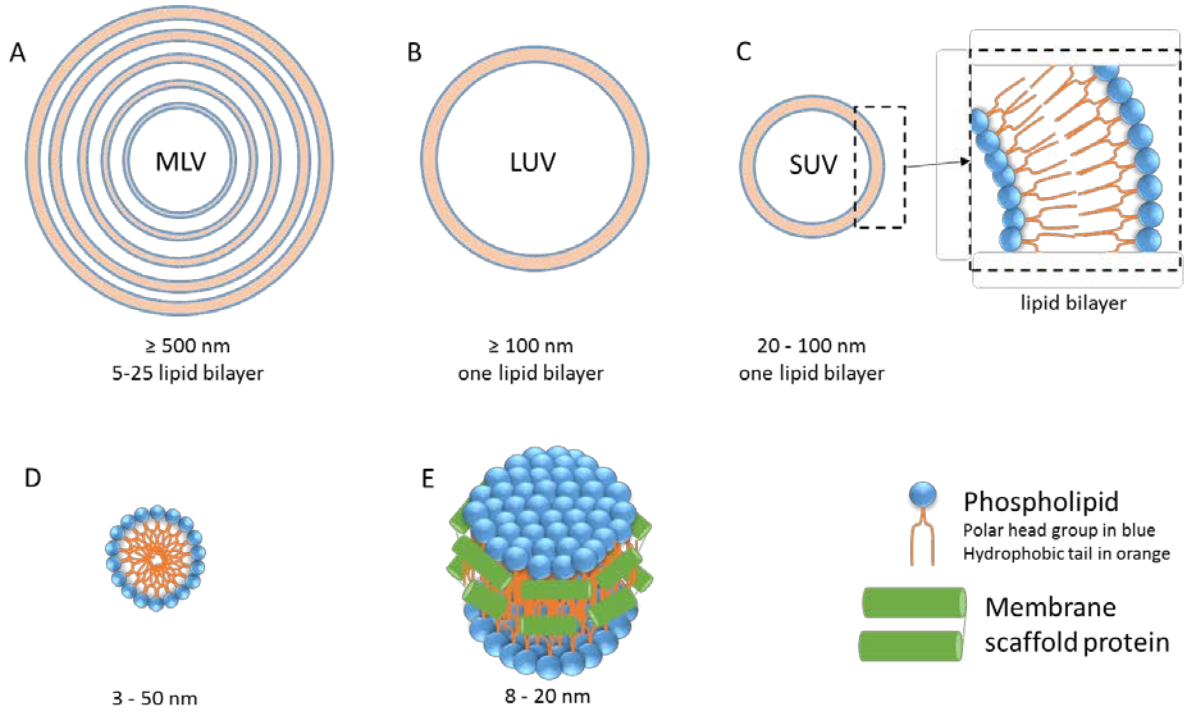

Figure 1-8 - Lipid formation. (A) Multilamellar vesicle (MLV), (B) Large unilamellar vesicle (LUV), (C) Small unilamellar vesicle (SUV), (D) Micelle and (E) Nanodisc (ND).

Whilst lipid vesicle formation occurs naturally once the lipid concentration meets a certain threshold, the formation of nanodiscs require additional membrane constraint. The MSP surrounding the lipid bilayer of nanodiscs comes from the truncation of the human apolipoprotein A1 (ApoA1). ApoA1 is the major protein constituent of reverse cholesterol transport in the human body. ApoA1 is a 30 kDa protein consisting of 267 amino acids produced and excreted from the liver, and its structure consists of 10 helixes forming a half circle, Figure 1-9.

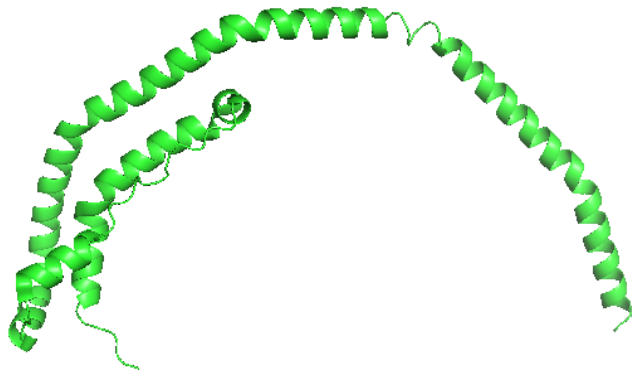

Figure 1-9 - Crystal structure of apolipoprotein A-1. PDB entry 3R2P.

Sligar et al., when investigating the structure of reconstituted HDL from ApoA1 and synthetic phospholipids, discovered that ApoA1 could be used as a self-assembling phospholipid bilayer

support.[56] In order to optimize the particle for nanodisc use, they produced a truncated version of ApoA1 that lacked the globular *N*-terminal domain. This modified protein, MSP, is also able to self-assemble into discoidal monodisperse particles in the presence of synthetic phospholipids.[57] The diameter of the nanodiscs will thus vary according to the length of MSP, forming discs of 8 to 12 nm. In this thesis, the MSP proteins used for the formation of nanodiscs are the MSP1D1ΔH5 and cNW9. MSP1D1 refers to the ApoA1 signal and globular motif that has been replaced by a histidine-TEV-tag and the helix 1 truncated to helix 0.5. ΔH5 refers to the deletion of helix 5, Table 1-2. TEV is a protease recognition site used for removal of the affinity tag during purification. cNW9 is the same construct as MSP1D1ΔH5 but able to covalently circularize via linkage by sortase.[58]

Table 1-2 - MSP protein motifs and sequence construct.

Protein	Motifs
ApoA1	SIGNAL-GLOBULAR-H1-H2-H3-H4-H5-H6-H7-H8-H9-H10
MSP1D1	HisTEV-H0.5 -H2-H3-H4-H5-H6-H7-H8-H9-H10
MSP1D1ΔH5	HisTEV-H0.5 -H2-H3-H4-H6-H7-H8-H9-H10
cNW9	HisTEV-H0.5 -H2-H3-H4-H6-H7-H8-H9-H10-LinkerHis

Protein	Sequence
ApoA1	MKAAVLTLAVLFLTGSQARHFWQQDEPPQSPWDRVKDLATVYVDVLKDSGRDYVS QFEGSALGKQLNLKLLDNWDSVTSTFSKLREQLGPVTQEFWDNLEKETEGLRQEMS KDLEEVKAKVQPYLDDFQKKWQEEMELYRQKVEPLRAELQEGARQKLHELQEKLSP LGEEMRDRARAHVDALRTHLAPYSDELRQRLAARLEALKENGGARLAEYHAKATE HLSTLSEKAKPALEDLRQGLLPVLESFKVSFLSALEEYTKKLNTQ
MSP1D1	MGHHHHHHHHDYDIPTTENLYFQGSTFSKLREQLGPVTQEFWDNLEKETEGLRQEMS KDLEEVKAKVQPYLDDFQKKWQEEMELYRQKVEPLRAELQEGARQKLHELQEKLSP LGEEMRDRARAHVDALRTHLAPYSDELRQRLAARLEALKENGGARLAEYHAKATE HLSTLSEKAKPALEDLRQGLLPVLESFKVSFLSALEEYTKKLNTQ
MSP1D1ΔH5	MGHHHHHHHHDYDIPTTENLYFQGSTFSKLREQLGPVTQEFWDNLEKETEGLRQEMS KDLEEVKAKVQPYLDDFQKKWQEEMELYRQKVEPLGEEMRDRARAHVDALRTHLA PYSDELRQRLAARLEALKENGGARLAEYHAKATEHLSTLSEKAKPALEDLRQGLLPV LESFKVSFLSALEEYTKKLNTQ
cNW9	MGSSHHHHHHENLYFQGSTFSKLREQLGPVTQEFWDNLEKETEGLRQEMSKDLEEV KAKVQPYLDDFQKKWQEEMELYRQKVEPLGEEMRDRARAHVDALRTHLAPYSDEL RQRLAARLEALKENGGARLAEYHAKATEHLSTLSEKAKPALEDLRQGLLPVLESFKV SFLSALEEYTKKLNTQLPGTGAAALEHHHHHH

Nanodiscs are able to self-assemble in only a few steps via addition of an adequate ratio of phospholipids to the MSP, stored in detergent, followed by the addition of non-polar polystyrene beads, biobeads, which trigger the formation of nanodiscs by removing the detergent, Figure 1-10. Subsequently, homogeneous nanodiscs are purified from the reconstitution mixture by gel filtration.[59]

Each nanodisc is constituted of two MSPs wrapped around the phospholipid bilayer. The composition of phospholipids can be varied in order to mimic different types of cell membranes.

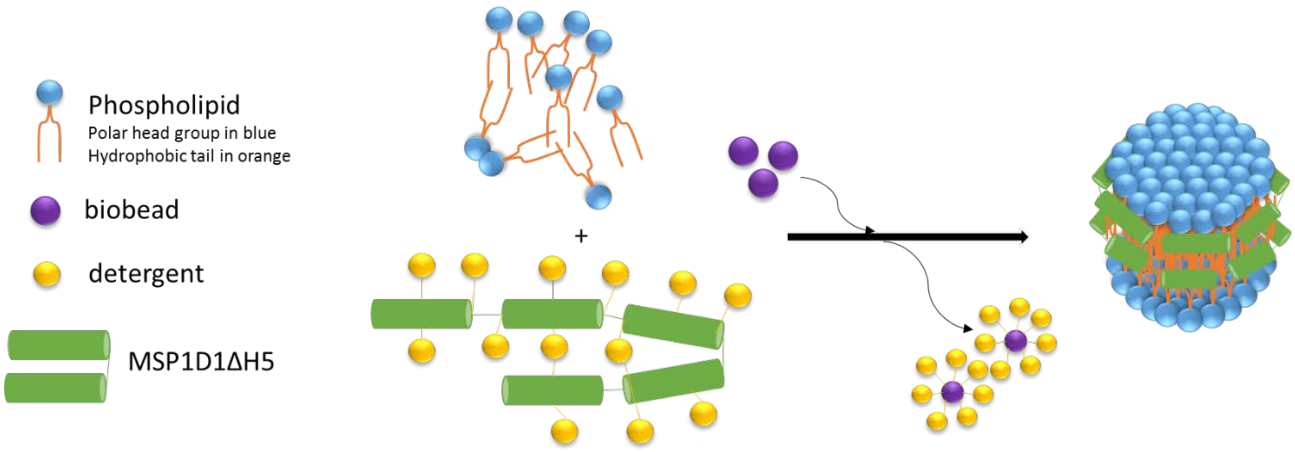

Figure 1-10 - Nanodiscs formation process.

1.8 Mode of action

The capacity of AMPs to kill microorganisms relies on their ability to disrupt and/or permeate the organisms' cell membrane. The AMPs, generally being cationic, are well designed to bind and interact with the negatively charged lipophilic outer membrane of the bacteria cell. The mode of action of AMPs, especially α-helical AMPs, have been well studied, demonstrating very diverse and complex mechanisms. For cell destruction, the cell membrane can be disrupted or not. Most of the AMPs studied disrupt the cell membrane either via pore formation, with either barrel stave (Alamethicin[60]) or toroidal (Magainin-2[60]) pore structures, or by non-pore mechanisms, such as a carpet-like mechanism (Cecropin[61]), Figure 1-11. In all cases, the peptides initially accumulate at the membrane surface. Then, above a certain concentration threshold, toroidal or barrel stave pores are formed by peptides aligned perpendicular to the membrane plane together with phospholipid molecules. Alternatively, the peptides cover the membrane surface like a carpet and ultimately disrupt the bilayer. Some AMPs polarize the membrane to form anionic lipid clusters.[62] A minority of AMPs, however, do not cause membrane disruption, but instead act on intracellular targets such as nucleic acids and functional proteins to activate cell death, after crossing the bacterial cell wall and the cytoplasmic membrane.[63,64]

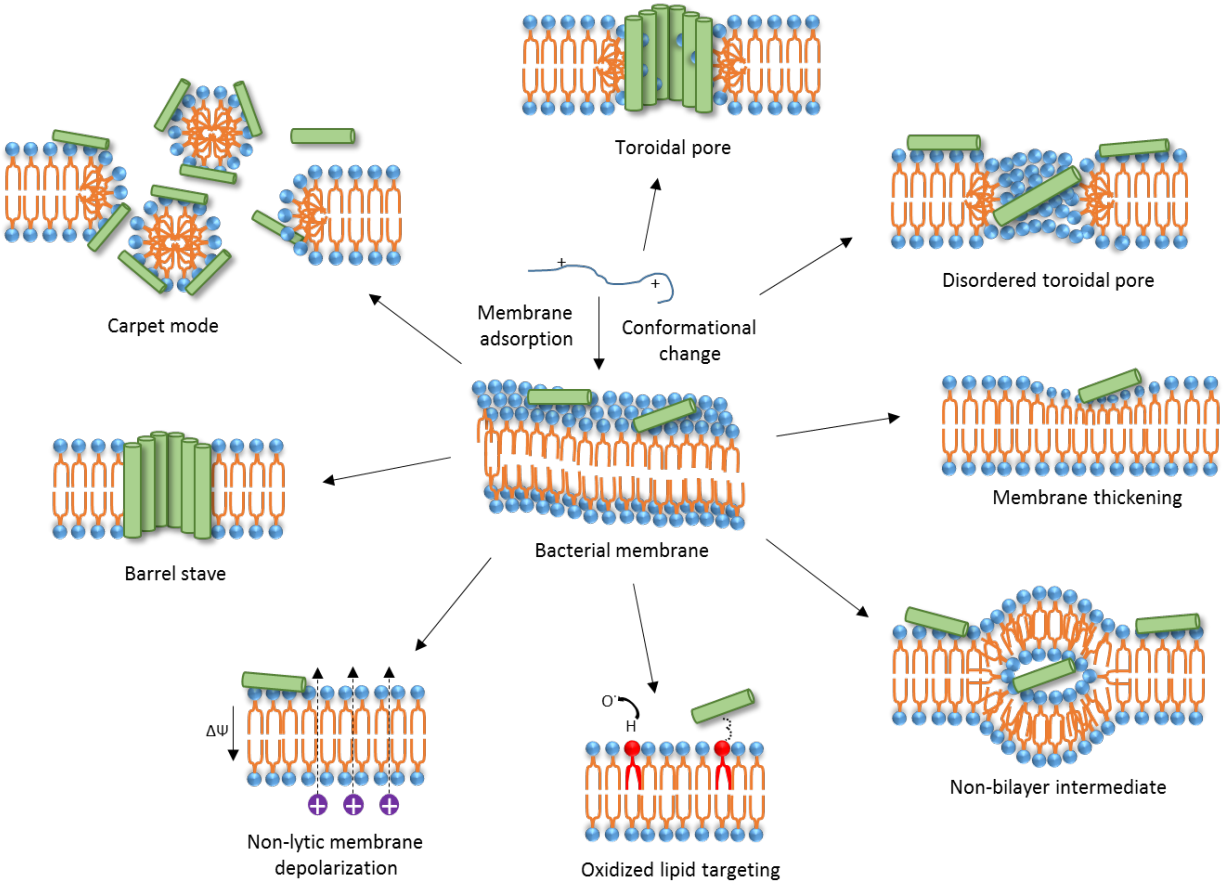

Figure 1-11 - Mechanisms of action for cell destruction.

A summary of the modes of action of the β-hairpin AMPs are presented in Table 1-3. Like any other AMPs, the β-hairpin AMPs act via diverse and complex mechanisms of action, where one or more mechanisms are combined to yield the unique activity of the peptide. Pore formation has been suggested for arenicin-1, bactenecin, androctonin, gomesin and protegrin-1.[65-71] The initial binding of the AMP to the bacteria is driven by electrostatic interactions with the negatively charged cell surface. The peptide then adopts a parallel orientation to the lipid bilayer. From this point, the AMPs adopt one of two mechanisms (i) they stay parallel to the lipid bilayer forming clusters similar to a carpet-like model and, as the concentration increases, the membrane weakens and the peptide eventually intercalates into the cell causing the membrane to disrupt, or (ii) they are positioned parallel to the surface of the membrane, but then insert perpendicularly into it and cause deformation, creating a toroidal pore mechanism. Additionally, a lipid flip-flop mechanism has been observed for tachyplesin-1 and polyphemusin-1.[72-74] The peptide first binds to the outer leaflet of the lipid bilayer then translocates to the other side of the membrane using surrounding lipids to internalize into the intracellular compartment of the cell. A translocation mechanism has been suggested with spontaneous internalization or nonspecifically, for lactoferricin B and thanatin, respectively.[75-78] To

date, tigerinin-1 is the only AMP reported to create membrane depolarization to finally open and disrupt the membrane.[36] Hepcidin 25 is an interesting AMP, as the activity as well as the mode of action is dependent on the environmental pH, and therefore this AMP will act differently in the body according to the location (e.g. the gut intestinal track has a different pH to other tissues).[64] Each AMP finds its own unique way to kill its target by combining one or more of the models discussed above, and potentially with mechanisms that have yet to be identified.

To assess these mechanisms of action, a variety of techniques are utilized, such as fluorescence assays and NMR, relying on membrane models mimicking the bacterial cell. Although, the membrane models are established to mimic bacteria as closely as possible, the models are far from perfect and must be applied carefully, in the context of a good understanding of the differences between the models and true cell membrane architecture and dynamics. Every model has its benefits, matching one or more characteristics to the real membrane, but at the same time they displays imperfections which could lead to an incorrect interpretation of the true mode of action. Therefore, much research is still ongoing to establish new ways of modelling cell membranes that could replicate the cell membrane far better than the models currently in use.

Table 1-3 - Mode of action of the β-hairpin AMPs.

Peptide	Mode of action		Ref.
tigerinin-1	disruption	membrane depolarization model	36
bactenecin	disruption	carpet/toroidal pore model	65
tachyplesin-1	translocation and disruption	lipid flip-flop with vesicle leakage of outer membrane followed by toroidal pore formation of cytoplasmic membrane and intracelular target	72,73
polyphemusin-1	translocation	lipid flip-flop model	73,74
protegrin-1	disruption	disordered toroidal pore model	66, 67
gomesin	disruption	carpet-like model	68,69
rectrocyclin-2	disruption	mechanism not elucidated yet	79
arenicin-1	disruption	carpet/toroidal pore model	70,71
thanatin	translocation	nonspecific mechanism	75
alvinellacin	not studied yet		
androctonin	disruption	carpet-like model	80
lactoferricin B	translocation	spontaneous internalization, pore formation model	77,76,78
hepcidin 25	translocation	pore formation with pH dependant model	64

1.9 Bacterial resistance to AMPs

Although very limited, bacterial resistance to AMPs has been reported, and is mainly focused on cell membrane modifications. For instance, the bacterial membrane can remodel to inhibit the first electrostatic binding between negatively charge membrane and positively charged AMPs. This could be seen as modification of the teichoic acid in G+ve bacteria or modification of the lipid A in G-ve bacteria to neutralize the cell membrane surface charge.[81,82] Bacterial protease and peptidases can

degrade and inactivate AMPs, for example in the cases of cathelicidin LL-37 or C18G.[83,84] Additionally, bacteria can also sequester AMPs and inhibit their antimicrobial activity.[85]

1.10 Significance and aims

Antibiotic resistant bacteria are a major public health concern today, highlighted by the World Health Organization in its 2014 report: "Antibiotic resistance is no longer a prediction for the future as it is happening right now, across the world, and is putting at risk the ability to treat common infections in the community and hospitals. Without urgent, coordinated action, the world is heading towards a post-antibiotic era, in which common infections and minor injuries, which have been treatable for decades, can once again kill."[22] Treatment failure reports for gonorrhea usually treated by third generation cephalosprins, urinary tract infections caused by *Escherichia coli* normally solved by fluoroquinolones, and intestinal bacteria medically treated by carbapenem antibiotics are now widespread across the world. Multi-drug resistant (MDR) G-ve infections normally cured by last resort antibiotics, colistin (polymyxin E), has seen rapid resistance developing around the world, aided by plasmid-mediated transmission of *mcr-1*. Therefore, there is a definite need for safer membranolytic drugs with higher selectivity for G-ve bacteria cells over mammalian cells.

AMPs are one of the only classes of compounds thus far against which bacteria have developed little resistance. Even though having been discovered and studied for over 80-years, commercialization of AMPs is mainly limited by their inherently low stability in human serum and potential storage degradation, their immunogenicity and the need to establish selectivity over mammalian cell toxicity. My thesis focuses on the subclass of β-hairpin AMPs which have not yet been extensively explored. Whilst limited in number, β-hairpin AMPs are very attractive molecules due to their very potent and broad spectrum of antibacterial and antifungal activities as well as their very limited bacterial resistance reported to date. Thus, β-hairpin AMPs provide an attractive starting point for the design of new antimicrobial drugs to replace obsolete ones.

Given that β-hairpin AMPs are not naturally safe for clinical development due to their toxicity against mammalian cells, the overall aim of this thesis is to understand the relationship and correlation between antimicrobial activity and toxicity, membrane activity and microbial activity, of β-hairpin AMPs. These findings will be used to create a safe and effective alternative to colistin for the treatment of infections caused by MDR G-ve bacteria.

1.11 Thesis outline

The thesis comprises four research chapters. The first two chapters cover the characterization of β-hairpin AMPs and more specifically tachyplesin-1. The last two investigate the mode of action of arenicin-3 and its synthetic analog, AA139.

Chapter 2 focuses on a comparative study between the physicochemical properties (amphipathicity and hydrophobicity) and the antimicrobial activity and toxicity of six β-hairpin AMPs (arenicin-3, tachyplesin-1, polyphemusin-1, gomesin, protegrin-1 and thanatin). The outcome of this study shows that β-hairpin AMPs display a complex and fine balance between charge, hydrophobicity, amphipathicity, secondary and tertiary structure, and mode of action. This study also identified tachyplesin-1 as a leading candidate for further optimisation, with 7-fold higher therapeutic index than any of the other β-hairpin AMPs investigated here. This work was published in April 2016 in ACS Infectious Diseases.

Chapter 3 investigates the β-hairpin AMP tachyplesin-1 (TP1). TP1 exhibits potent antimicrobial activity against a broad range of G+ve and G-ve bacteria, as well as fungi. However, it also displays high toxicity towards mammalian cells, making it unsuitable to be developed as a therapeutic in its own right. This study evaluates structure-function and structure-toxicity relationships using an alanine scan to assess the impact of each amino acid of TP1, to assist in the design of novel therapeutically valuable peptides. This template-based approach focused not only on an alanine scan of TP1, but also modified the overall hydrophobicity / amphipathicity by amino acid replacement at select positions. My findings revealed three newly designed peptides TP1[F4A], TP1[I11A] and TP1[C3A,C16A] with 26- to 64-fold improved antimicrobial activity / toxicity index, rendering them very attractive as potential drug candidates. Structural studies of TP1[F4A] and TP1[I11A] identified a conserved β-hairpin secondary structure motif correlating with their very high stability in mouse and human plasma. This study was published in September 2017 in ACS Infectious Diseases.

Chapter 4 evaluates the mode of action of AA139, a synthetic analog of arenicin-3 discovered by Adenium Pty Ltd, and under advanced preclinical development by this company. The aim of this chapter is to understand the structural and functional changes between the two analogs, arenicin-3 and AA139 that leads to different activity. In this study, I have characterized arenicin-3 and its synthetic analog, AA139, with elucidation of their 3D structures in aqueous solution confirming disulfide-bridged β-hairpin peptide structures. The mode of action of both arenicin peptides was investigated using lipid model membranes and *Escherichia coli* bacterial cells. This work suggested that arenicin peptides bind, insert and partially permeabilize both negatively charged lipid vesicles and the cell membranes of G-ve bacteria. Interestingly, the mode of action of arenicin peptides seems

to not only depend on electrostatic interaction and membrane permeabilization, but also rely on additional mode(s) of action.

Chapter 5 investigates the mode of action of AA139 from a structurally focused point of view. In this study, three approaches were explored: (i) a computational modelling study to provide an experimental speculation of the orientation of the peptide at the interface with the cell membrane, (ii) a solution NMR study using lipid bilayer nanodiscs, and (iii) a solid-state NMR study using lipid bilayer vesicles. This study allowed the refinement of the mode of action studied in chapter 4. The solution NMR results identified the *N*- and *C*- terminal ends of the peptide as the first point of contact with the cell membrane. The preliminary work performed using solid-state NMR suggests that the peptide loses its well-defined 3D structure upon insertion in the hydrophobic core of the membrane.

1.12 References

1. Ligon, B. L. (2004) Penicillin: its discovery and early development, *Semin. Pediatr. Infect. Dis. 15*, 52-57. DOI:10.1053/j.spid.2004.02.001
2. Wainwright, M. (1993) The mystery of the plate: Fleming's discovery and contribution to the early development of penicillin, *J. Med. Biogr. 1*, 59-65. DOI:10.1177/096777209300100113
3. Swann, J. P. (1985) The discovery and early development of penicillin, *Med. Herit. 1*, 375-386.
4. Clardy, J., Fischbach, M. A., and Walsh, C. T. (2006) New antibiotics from bacterial natural products, *Nat. Biotechnol. 24*, 1541-1550. DOI:10.1038/nbt1266
5. Miller, J. R., and Waldrop, G. L. (2010) Discovery of novel antibacterials, *Expert Opin. Drug Discovery 5*, 145-154. DOI:10.1517/17460440903493449
6. Silver, L. L. (2011) Challenges of antibacterial discovery, *Clin. Microbiol. Rev. 24*, 71-109. DOI:10.1128/CMR.00030-10
7. von Nussbaum, F., Brands, M., Hinzen, B., Weigand, S., and Habich, D. (2006) Antibacterial natural products in medicinal chemistry--exodus or revival?, *Angew. Chem., Int. Ed. Engl. 45*, 5072-5129. DOI:10.1002/anie.200600350
8. Wright, G. D. (2007) The antibiotic resistome: the nexus of chemical and genetic diversity, *Nat. Rev. Microbiol. 5*, 175-186. DOI:10.1038/nrmicro1614
9. Bbosa G. S., M. N., Odda J., Kyegombe D. B., Ntale M. (2014) Antibiotics/antibacterial drug use, their marketing and promotion during the post-antibiotic golden age and their role in emergence of bacterial resistance, *Health 6*, 410-425. DOI:10.4236/health.2014.65059
10. Cohen, J. (2013) Infectious disease. Approval of novel TB drug celebrated--with restraint, *Science 339*, 130. DOI:10.1126/science.339.6116.130
11. Goldstein, E. J., Citron, D. M., Sears, P., Babakhani, F., Sambol, S. P., and Gerding, D. N. (2011) Comparative susceptibilities to fidaxomicin (OPT-80) of isolates collected at baseline, recurrence, and failure from patients in two phase III trials of fidaxomicin against Clostridium difficile infection, *Antimicrob. Agents Chemother. 55*, 5194-5199. DOI:10.1128/AAC.00625-11
12. Gentry, D. R., McCloskey, L., Gwynn, M. N., Rittenhouse, S. F., Scangarella, N., Shawar, R., and Holmes, D. J. (2008) Genetic characterization of Vga ABC proteins conferring reduced susceptibility to pleuromutilins in Staphylococcus aureus, *Antimicrob. Agents Chemother. 52*, 4507-4509. DOI:10.1128/AAC.00915-08

13. Lewis, J. S., 2nd, Owens, A., Cadena, J., Sabol, K., Patterson, J. E., and Jorgensen, J. H. (2005) Emergence of daptomycin resistance in Enterococcus faecium during daptomycin therapy, *Antimicrob. Agents Chemother. 49*, 1664-1665. DOI:10.1128/AAC.49.4.1664-1665.2005
14. Tsiodras, S., Gold, H. S., Sakoulas, G., Eliopoulos, G. M., Wennersten, C., Venkataraman, L., Moellering, R. C., and Ferraro, M. J. (2001) Linezolid resistance in a clinical isolate of Staphylococcus aureus, *Lancet 358*, 207-208. DOI:10.1016/S0140-6736(01)05410-1
15. Palumbi, S. R. (2001) Humans as the world's greatest evolutionary force, *Science 293*, 1786-1790. DOI:10.1126/science.293.5536.1786
16. Kresken, M., and Wiedemann, B. (1988) Development of resistance to nalidixic acid and the fluoroquinolones after the introduction of norfloxacin and ofloxacin, *Antimicrob. Agents Chemother. 32*, 1285-1288. DOI:10.1128/AAC.32.8.1285
17. Ronald, A. R., Turck, M., and Petersdorf, R. G. (1966) A critical evaluation of nalidixic acid in urinary-tract infections, *N. Engl. J. Med. 275*, 1081-1089. DOI:10.1056/NEJM196611172752001
18. Walsh, C. T., and Wencewicz, T. A. (2014) Prospects for new antibiotics: a molecule-centered perspective, *J. Antibiot. 67*, 7-22. DOI:10.1038/ja.2013.49
19. Hiramatsu, K. (1998) Vancomycin resistance in staphylococci, *Drug Resist. Updates 1*, 135-150.
20. Périchon, B., and Courvalin, P. (2012) Glycopeptide Resistance, In *Antibiotic Discovery and Development* (Dougherty, T. J., and Pucci, M. J., Eds.), pp 515-542, Springer US.
21. Lowy, F. D. (2003) Antimicrobial resistance: the example of Staphylococcus aureus, *J. Clin. Invest. 111*, 1265-1273. DOI:10.1172/JCI18535
22. WHO. Antimicrobial Resistance: Global report on Surveillance, 2014, WHO, Geneva, Switzerland,2014 <http://www.who.int/drugresistance/documents/surveillancereport/en/>.
23. Blaskovich, M. A., Butler, M. S., and Cooper, M. A. (2017) Polishing the tarnished silver bullet: the quest for new antibiotics, *Essays Biochem. 61*, 103-114. DOI:10.1042/EBC20160077
24. (2006) In *Treating Infectious Diseases in a Microbial World: Report of Two Workshops on Novel Antimicrobial Therapeutics*, Washington (DC).
25. Wright, G. D. (2010) Q&A: Antibiotic resistance: where does it come from and what can we do about it?, *BMC Biol. 8*, 123. DOI:10.1186/1741-7007-8-123
26. Dubos, R. J. (1939) Studies on a Bactericidal Agent Extracted from a Soil Bacillus : I. Preparation of the Agent. Its Activity in Vitro, *J. Exp. Med. 70*, 1-10.
27. Van Epps, H. L. (2006) Rene Dubos: unearthing antibiotics, *J. Exp. Med. 203*, 259. DOI:10.1084/jem.2032fta
28. Reddy, K. V., Yedery, R. D., and Aranha, C. (2004) Antimicrobial peptides: premises and promises, *Int. J. Antimicrob. Agents 24*, 536-547. DOI:10.1016/j.ijantimicag.2004.09.005
29. Jenssen, H., Hamill, P., and Hancock, R. E. (2006) Peptide antimicrobial agents, *Clin. Microbiol. Rev. 19*, 491-511. DOI:10.1128/CMR.00056-05
30. Bahar, A. A., and Ren, D. (2013) Antimicrobial peptides, *Pharmaceuticals 6*, 1543-1575. DOI:10.3390/ph6121543
31. Huang, Y., Huang, J., and Chen, Y. (2010) Alpha-helical cationic antimicrobial peptides: relationships of structure and function, *Protein Cell 1*, 143-152. DOI:10.1007/s13238-010-0004-3
32. Giangaspero, A., Sandri, L., and Tossi, A. (2001) Amphipathic alpha helical antimicrobial peptides, *Eur. J. Biochem. 268*, 5589-5600. DOI:10.1046/j.1432-1033.2001.02494.x
33. Tossi, A., Sandri, L., and Giangaspero, A. (2000) Amphipathic, alpha-helical antimicrobial peptides, *Biopolymers 55*, 4-30. DOI:10.1002/1097-0282(2000)55:1<4::AID-BIP30>3.0.CO;2-M
34. Conibear, A. C., and Craik, D. J. (2014) The chemistry and biology of theta defensins, *Angew. Chem., Int. Ed. Engl. 53*, 10612-10623. DOI:10.1002/anie.201402167

35. Fjell, C. D., Hiss, J. A., Hancock, R. E. W., and Schneider, G. (2012) Designing antimicrobial peptides: form follows function, *Nat. Rev. Drug Discovery 11*, 37-51. DOI:10.1038/nrd3591
36. Sai, K. P., Jagannadham, M. V., Vairamani, M., Raju, N. P., Devi, A. S., Nagaraj, R., and Sitaram, N. (2001) Tigerinins: novel antimicrobial peptides from the Indian frog Rana tigerina, *J. Biol. Chem. 276*, 2701-2707. DOI:10.1074/jbc.M006615200
37. Fernandez-Vidal, M., Jayasinghe, S., Ladokhin, A. S., and White, S. H. (2007) Folding amphipathic helices into membranes: amphiphilicity trumps hydrophobicity, *J. Mol. Biol. 370*, 459-470. DOI:10.1016/j.jmb.2007.05.016
38. Romeo, D., Skerlavaj, B., Bolognesi, M., and Gennaro, R. (1988) Structure and bactericidal activity of an antibiotic dodecapeptide purified from bovine neutrophils, *J. Biol. Chem. 263*, 9573-9575.
39. Nakamura, T., Furunaka, H., Miyata, T., Tokunaga, F., Muta, T., Iwanaga, S., Niwa, M., Takao, T., and Shimonishi, Y. (1988) Tachyplesin, a class of antimicrobial peptide from the hemocytes of the horseshoe crab (Tachypleus tridentatus). Isolation and chemical structure, *J. Biol. Chem. 263*, 16709-16713.
40. Miyata, T., Tokunaga, F., Yoneya, T., Yoshikawa, K., Iwanaga, S., Niwa, M., Takao, T., and Shimonishi, Y. (1989) Antimicrobial peptides, isolated from horseshoe crab hemocytes, tachyplesin II, and polyphemusins I and II: chemical structures and biological activity, *J. Biochem. 106*, 663-668.
41. Aumelas, A., Mangoni, M., Roumestand, C., Chiche, L., Despaux, E., Grassy, G., Calas, B., and Chavanieu, A. (1996) Synthesis and solution structure of the antimicrobial peptide protegrin-1, *Eur. J. Biochem. 237*, 575-583. DOI:10.1111/j.1432-1033.1996.0575p.x
42. Mandard, N., Bulet, P., Caille, A., Daffre, S., and Vovelle, F. (2002) The solution structure of gomesin, an antimicrobial cysteine-rich peptide from the spider, *Eur. J. Biochem. 269*, 1190-1198. DOI:10.1046/j.0014-2956.2002.02760.x
43. Conibear, A. C., Rosengren, K. J., Harvey, P. J., and Craik, D. J. (2012) Structural characterization of the cyclic cystine ladder motif of theta-defensins, *Biochemistry 51*, 9718-9726. DOI:10.1021/bi301363a
44. Lee, J. U., Kang, D. I., Zhu, W. L., Shin, S. Y., Hahm, K. S., and Kim, Y. (2007) Solution structures and biological functions of the antimicrobial peptide, arenicin-1, and its linear derivative, *Biopolymers 88*, 208-216. DOI:10.1002/bip.20700
45. Fehlbaum, P., Bulet, P., Chernysh, S., Briand, J. P., Roussel, J. P., Letellier, L., Hetru, C., and Hoffmann, J. A. (1996) Structure-activity analysis of thanatin, a 21-residue inducible insect defense peptide with sequence homology to frog skin antimicrobial peptides, *Proc. Natl. Acad. Sci. U. S. A. 93*, 1221-1225.
46. Tasiemski, A., Jung, S., Boidin-Wichlacz, C., Jollivet, D., Cuvillier-Hot, V., Pradillon, F., Vetriani, C., Hecht, O., Sonnichsen, F. D., Gelhaus, C., Hung, C. W., Tholey, A., Leippe, M., Grotzinger, J., and Gaill, F. (2014) Characterization and function of the first antibiotic isolated from a vent organism: the extremophile metazoan Alvinella pompejana, *PLoS One 9*, e95737. DOI:10.1371/journal.pone.0095737
47. Ehret-Sabatier, L., Loew, D., Goyffon, M., Fehlbaum, P., Hoffmann, J. A., van Dorsselaer, A., and Bulet, P. (1996) Characterization of novel cysteine-rich antimicrobial peptides from scorpion blood, *J. Biol. Chem. 271*, 29537-29544. DOI:10.1074/jbc.271.47.29537
48. Hwang, P. M., Zhou, N., Shan, X., Arrowsmith, C. H., and Vogel, H. J. (1998) Three-dimensional solution structure of lactoferricin B, an antimicrobial peptide derived from bovine lactoferrin, *Biochemistry 37*, 4288-4298. DOI:10.1021/bi972323m
49. Jordan, J. B., Poppe, L., Haniu, M., Arvedson, T., Syed, R., Li, V., Kohno, H., Kim, H., Schnier, P. D., Harvey, T. S., Miranda, L. P., Cheetham, J., and Sasu, B. J. (2009) Hepcidin revisited, disulfide connectivity, dynamics, and structure, *J. Biol. Chem. 284*, 24155-24167. DOI:10.1074/jbc.M109.017764
50. Gorter, E., and Grendel, F. (1925) On Bimolecular Layers of Lipoids on the Chromocytes of the Blood, *J. Exp. Med. 41*, 439-443.

51. Singer, S. J., and Nicolson, G. L. (1972) The fluid mosaic model of the structure of cell membranes, *Science 175*, 720-731. DOI:10.1126/science.175.4023.720
52. Harder, T., Scheiffele, P., Verkade, P., and Simons, K. (1998) Lipid domain structure of the plasma membrane revealed by patching of membrane components, *J. Cell Biol. 141*, 929-942. DOI:10.1083/jcb.141.4.929
53. Cooper, G. (2000) *The Cell: A Molecular Approach*, 2nd ed., Sinauer Associates.
54. Lasic, D. D. (1988) The mechanism of vesicle formation, *Biochem. J. 256*, 1-11.
55. Inagaki, S., Ghirlando, R., and Grisshammer, R. (2013) Biophysical characterization of membrane proteins in nanodiscs, *Methods 59*, 287-300. DOI:10.1016/j.ymeth.2012.11.006
56. Carlson, J. W., Jonas, A., and Sligar, S. G. (1997) Imaging and manipulation of high-density lipoproteins, *Biophys. J. 73*, 1184-1189. DOI:10.1016/S0006-3495(97)78150-5
57. Bayburt, T. H., Grinkova, Y. V., and Sligar, S. G. (2002) Self-assembly of discoidal phospholipid bilayer nanoparticles with membrane scaffold proteins, *Nano Lett. 2*, 853-856. DOI:10.1021/nl025623k
58. Nasr, M. L., Baptista, D., Strauss, M., Sun, Z. J., Grigoriu, S., Huser, S., Pluckthun, A., Hagn, F., Walz, T., Hogle, J. M., and Wagner, G. (2017) Covalently circularized nanodiscs for studying membrane proteins and viral entry, *Nat. Methods 14*, 49-52. DOI:10.1038/nmeth.4079
59. Ritchie, T. K., Grinkova, Y. V., Bayburt, T. H., Denisov, I. G., Zolnerciks, J. K., Atkins, W. M., and Sligar, S. G. (2009) Chapter 11 - Reconstitution of membrane proteins in phospholipid bilayer nanodiscs, *Methods Enzymol. 464*, 211-231. DOI:10.1016/S0076-6879(09)64011-8
60. Yang, L., Harroun, T. A., Weiss, T. M., Ding, L., and Huang, H. W. (2001) Barrel-stave model or toroidal model? A case study on melittin pores, *Biophys. J. 81*, 1475-1485. DOI:10.1016/S0006-3495(01)75802-X
61. Shai, Y. (1995) Molecular recognition between membrane-spanning polypeptides, *Trends Biochem. Sci. 20*, 460-464. DOI:10.1016/S0968-0004(00)89101-X
62. Epand, R. F., Maloy, L., Ramamoorthy, A., and Epand, R. M. (2010) Amphipathic helical cationic antimicrobial peptides promote rapid formation of crystalline states in the presence of phosphatidylglycerol: lipid clustering in anionic membranes, *Biophys. J. 98*, 2564-2573. DOI:10.1016/j.bpj.2010.03.002
63. Nicolas, P. (2009) Multifunctional host defense peptides: intracellular-targeting antimicrobial peptides, *FEBS J. 276*, 6483-6496. DOI:10.1111/j.1742-4658.2009.07359.x
64. Maisetta, G., Vitali, A., Scorciapino, M. A., Rinaldi, A. C., Petruzzelli, R., Brancatisano, F. L., Esin, S., Stringaro, A., Colone, M., Luzi, C., Bozzi, A., Campa, M., and Batoni, G. (2013) pH-dependent disruption of Escherichia coli ATCC 25922 and model membranes by the human antimicrobial peptides hepcidin 20 and 25, *FEBS J. 280*, 2842-2854. DOI:10.1111/febs.12288
65. Lopez-Oyama, A. B., Taboada, P., Burboa, M. G., Rodriguez, E., Mosquera, V., and Valdez, M. A. (2011) Interaction of the cationic peptide bactenecin with mixed phospholipid monolayers at the air-water interface, *J. Colloid Interface Sci. 359*, 279-288. DOI:10.1016/j.jcis.2011.03.081
66. Tang, M., and Hong, M. (2009) Structure and mechanism of beta-hairpin antimicrobial peptides in lipid bilayers from solid-state NMR spectroscopy, *Mol. BioSyst. 5*, 317-322. DOI:10.1039/b820398a
67. Drin, G., and Temsamani, J. (2002) Translocation of protegrin I through phospholipid membranes: role of peptide folding, *Biochim. Biophys. Acta 1559*, 160-170. DOI:10.1016/S0005-2736(01)00447-3
68. Silva, P. I., Jr., Daffre, S., and Bulet, P. (2000) Isolation and characterization of gomesin, an 18-residue cysteine-rich defense peptide from the spider Acanthoscurria gomesiana hemocytes with sequence similarities to horseshoe crab antimicrobial peptides of the tachyplesin family, *J. Biol. Chem. 275*, 33464-33470. DOI:10.1074/jbc.M001491200

69. Moraes, L. G., Fazio, M. A., Vieira, R. F., Nakaie, C. R., Miranda, M. T., Schreier, S., Daffre, S., and Miranda, A. (2007) Conformational and functional studies of gomesin analogues by CD, EPR and fluorescence spectroscopies, *Biochim. Biophys. Acta 1768*, 52-58. DOI:10.1016/j.bbamem.2006.08.016
70. Ovchinnikova, T. V., Shenkarev, Z. O., Balandin, S. V., Nadezhdin, K. D., Paramonov, A. S., Kokryakov, V. N., and Arseniev, A. S. (2008) Molecular insight into mechanism of antimicrobial action of the beta-hairpin peptide arenicin: specific oligomerization in detergent micelles, *Biopolymers 89*, 455-464. DOI:10.1002/bip.20865
71. Shenkarev, Z. O., Balandin, S. V., Trunov, K. I., Paramonov, A. S., Sukhanov, S. V., Barsukov, L. I., Arseniev, A. S., and Ovchinnikova, T. V. (2011) Molecular mechanism of action of beta-hairpin antimicrobial peptide arenicin: oligomeric structure in dodecylphosphocholine micelles and pore formation in planar lipid bilayers, *Biochemistry 50*, 6255-6265. DOI:10.1021/bi200746t
72. Imura, Y., Nishida, M., Ogawa, Y., Takakura, Y., and Matsuzaki, K. (2007) Action mechanism of tachyplesin I and effects of PEGylation, *Biochim. Biophys. Acta 1768*, 1160-1169. DOI:10.1016/j.bbamem.2007.01.005
73. Ohta, M., Ito, H., Masuda, K., Tanaka, S., Arakawa, Y., Wacharotayankun, R., and Kato, N. (1992) Mechanisms of antibacterial action of tachyplesins and polyphemusins, a group of antimicrobial peptides isolated from horseshoe crab hemocytes, *Antimicrob. Agents Chemother. 36*, 1460-1465.
74. Zhang, L., Scott, M. G., Yan, H., Mayer, L. D., and Hancock, R. E. (2000) Interaction of polyphemusin I and structural analogs with bacterial membranes, lipopolysaccharide, and lipid monolayers, *Biochemistry 39*, 14504-14514. DOI:10.1021/bi0011173
75. Imamura, T., Yamamoto, N., Tamura, A., Murabayashi, S., Hashimoto, S., Shimada, H., and Taguchi, S. (2008) NMR based structure-activity relationship analysis of an antimicrobial peptide, thanatin, engineered by site-specific chemical modification: Activity improvement and spectrum alteration, *Biochem. Biophys. Res. Commun. 369*, 609-615. DOI:10.1016/j.bbrc.2008.02.057
76. Hoek, K. S., Milne, J. M., Grieve, P. A., Dionysius, D. A., and Smith, R. (1997) Antibacterial activity in bovine lactoferrin-derived peptides, *Antimicrob. Agents Chemother. 41*, 54-59.
77. Gifford, J. L., Hunter, H. N., and Vogel, H. J. (2005) Lactoferricin: a lactoferrin-derived peptide with antimicrobial, antiviral, antitumor and immunological properties, *Cell. Mol. Life Sci. 62*, 2588-2598. DOI:10.1007/s00018-005-5373-z
78. Umeyama, M., Kira, A., Nishimura, K., and Naito, A. (2006) Interactions of bovine lactoferricin with acidic phospholipid bilayers and its antimicrobial activity as studied by solid-state NMR, *Biochim. Biophys. Acta 1758*, 1523-1528. DOI:10.1016/j.bbamem.2006.06.014
79. Tang, M., Waring, A. J., Lehrer, R. I., and Hong, M. (2006) Orientation of a beta-hairpin antimicrobial peptide in lipid bilayers from two-dimensional dipolar chemical-shift correlation NMR, *Biophys. J. 90*, 3616-3624. DOI:10.1529/biophysj.105.062075
80. Hetru, C., Letellier, L., Oren, Z., Hoffmann, J. A., and Shai, Y. (2000) Androctonin, a hydrophilic disulphide-bridged non-haemolytic anti-microbial peptide: a plausible mode of action, *Biochem. J. 345 Pt 3*, 653-664. DOI:10.1042/bj3450653
81. Peschel, A.; Vuong, C.; Otto, M.; Gotz, F. (2000) The D-alanine residues of Staphylococcus aureus teichoic acids alter the susceptibility to vancomycin and the activity of autolytic enzymes. *Antimicrob. Agents Chemother*. 44 (10), 2845-7.
82. Kawasaki, K., Ernst, R. K., & Miller, S. I. (2005). Inhibition of Salmonella enterica Serovar Typhimurium Lipopolysaccharide Deacylation by Aminoarabinose Membrane Modification. *J. Bacteriol.*, 187(7), 2448–2457. DOI:10.1128/JB.187.7.2448-2457.2005

83. Schmidtchen, A., Frick, I., Andersson, E., Tapper, H. and Björck, L. (2002) Proteinases of common pathogenic bacteria degrade and inactivate the antibacterial peptide LL-37. Mol. Microbiol. 46, 157-168. DOI:10.1046/j.1365-2958.2002.03146.x
84. Guina, T., Yi, E. C., Wang, H., Hackett, M., & Miller, S. I. (2000) A PhoP-Regulated Outer Membrane Protease of Salmonella enterica Serovar Typhimurium Promotes Resistance to Alpha-Helical Antimicrobial Peptides. *J. Bacteriol. 182*(14), 4077–4086.
85. Islam, D., Bandholtz, L., Nilsson, J., Wigzell, H., Christensson, B., Agerberth, B., Gudmundsson, G. H.(2001) Downregulation of bactericidal peptides in enteric infections: A novel immune escape mechanism with bacterial DNA as a potential regulator. *Nat. Med. (N. Y., NY, U. S.) 7*, 180. DOI: 10.1038/84627

Chapter 2 - β-hairpin antimicrobial peptides

This chapter includes the manuscript published in ACS Infectious Diseases journal (2016). The manuscript discussed the relationship between physicochemical properties and antimicrobial properties of six β-hairpin AMPs. This study concluded in a complex balance between charge, amphipathicity, structure, and mode of action for a peptide to be therapeutical valuable. See Appendix II, page 7-122 for supporting information.

The research findings have been published in the manuscript Edwards, Ingrid A., et al. "Contribution of amphipathicity and hydrophobicity to the antimicrobial activity and cytotoxicity of β-hairpin peptides." *ACS Infectious Diseases*, 2016, 2 (6), pp 442–450, DOI: 10.1021/acsinfecdis.6b00045. The publication can be obtained, along with supplementary material associated with the article, from http://pubs.acs.org/doi/abs/10.1021/acsinfecdis.6b00045.

For the purpose of this thesis, the published article has been reproduced on pages 2-26 to 2-44 of chapter 2. As first author, the candidate was the primary contributor to the study design, data acquisition, data analysis and writing of the manuscript. The reader is referred to page V for the contributions by each author to the manuscript.

Contributor	Statement of contribution
Edwards, IA (Candidate)	Conception and design (85%) Analysis and interpretation (80%) Drafting and production (70%)
Elliott, AG	Conception and design (5%) Analysis and interpretation (15%) Drafting and production (20%)
Kavanagh, AM	Conception and design (0%) Analysis and interpretation (5%) Drafting and production (0%)
Zuegg, J	Conception and design (2%) Analysis and interpretation (0%) Drafting and production (0%)
Blaskovich, MAT	Conception and design (4%) Analysis and interpretation (0%) Drafting and production (5%)
Cooper, MA	Conception and design (4%) Analysis and interpretation (0%) Drafting and production (5%)

Research Paper

Contribution of amphipathicity and hydrophobicity to the antimicrobial activity and cytotoxicity of β-hairpin peptides

Ingrid A. Edwards, Alysha G. Elliott, Angela M. Kavanagh, Johannes Zuegg, Mark A.T. Blaskovich and Matthew A. Cooper*

Institute for Molecular Bioscience, 306 Carmody Road (Building 80), The University of Queensland, Brisbane, Queensland 4072 Australia

Correspondence to: m.cooper@uq.edu.au

Keywords: antimicrobial peptides, amphipathicity, β-hairpin, toxicity, Gram-negative bacteria.

2.1 Abstract

Bacteria have acquired extensive resistance mechanisms to protect themselves against antibiotic action. Today the bacterial membrane has become one of the 'final frontiers' in the search for new compounds acting on novel targets to address the threat of MDR and XDR bacterial pathogens. β-hairpin antimicrobial peptides are amphipathic, membrane-binding antibiotics that exhibit a broad range of activities against Gram-positive, Gram-negative and fungal pathogens. However, most members of the class also possess adverse cytotoxicity and hemolytic activity that precludes their development as candidate antimicrobials. We examined peptide hydrophobicity, amphipathicity and structure to better dissect and understand the correlation between antimicrobial activity and toxicity, membrane binding and membrane permeability. The hydrophobicity, pI, net charge at physiological pH, and amphipathic moment for the β-hairpin antimicrobial peptides tachyplesin-1, polyphemusin-1, protegrin-1, gomesin, arenicin-3 and thanatin were determined, and correlated with key antimicrobial activity and toxicity data. These included antimicrobial activity against five key bacterial pathogens and two fungi, cytotoxicity against human cell lines and hemolytic activity in human erythrocytes. Observed antimicrobial activity trends correlated with compound amphipathicity, and to a lesser extent with overall hydrophobicity. Antimicrobial activity increased with amphipathicity, but unfortunately so did toxicity. Of note, tachyplesin-1 was found to be 8-fold more amphipathic than gomesin. These analyses identify tachyplesin-1 as promising scaffold for rational design and synthetic optimisation towards an antibiotic candidate.

2.2 Introduction

Antibiotic-resistant bacteria are a serious and growing threat to human health and national healthcare systems.[1] These 'superbugs' kill 100,000s of people each year and are estimated to add >$20bn in healthcare costs in the US alone.[2] Multi-drug resistant Gram-negative (MDR G-ve) strains of *Klebsiella pneumoniae, Escherichia coli, Acinetobacter baumannii* and *Pseudomonas aeruginosa* that possess extended spectrum beta lactamase (ESBL) and metallo-beta-lactamases (MBL) are of grave concern.[3] There are now extensive and widely dispersed pools of resistance elements that cover all of the classical pathways targeted by current antibiotics: cell wall, folic acid, protein, RNA and DNA synthesis.[4] Most antibiotics target specific receptors, enzymes or proteins that are susceptible to single point mutations that can lead to resistance. However, compounds that target the bacterial membrane (such as antimicrobial peptides, AMPs) or its biosynthesis (such as moenomycin and the recently reported teixobactin[5]), are much less likely to select for spontaneous, single step resistant mutants. Today the only membrane-targeting antibiotics suitable for MDR G-ve infections are the closely related lipopeptides colistin (polymyxin E) and polymyxin B. Unfortunately, resistance to these key 'last resort' antibiotics has appeared, with a recent study[6] demonstrating a plasmid mediated *mcr-1* gene conferring colistin resistance found in China and Europe. Colistin and polymyxin B are both highly nephrotoxic with a low therapeutic index, often imparting severe adverse effects in humans at doses required for efficacy. Therefore there is an urgent unmet medical need for safer antibiotics to treat highly drug-resistant G-ve infections, and this can potentially be achieved by developing drugs that target G-ve bacterial membranes with high selectivity over mammalian membranes.

AMPs are ubiquitous in nature. All multicellular organisms, microorganisms, plants and animals have an innate immune defence system that secretes AMPs. Endogenous AMPs are produced when infections occur, and can also be stored in exposed tissues of animals and plants, constituting a first line of defence that is fast and efficient. These peptides have broad spectrum antimicrobial activity and are also able to host repair and adaptive immune responses in a concerted response to multi-drug resistant bacteria.[7] AMPs are generally small (< 10kDa), characterized by their charge and structural rigidity. They are grouped according to their secondary structure, (α-helical, β-sheet or extended peptides)[8,9] which confer distinct physicochemical properties and biological mechanisms of action. About 2,000 AMPs have been reported (http://aps.unmc.edu/AP/main.php) from eukaryota having antibacterial activity. Approximately 90% of them have been determined to adopt α-helical structure. This category has been extensively explored and reviewed elsewhere.[10]

Less known are the antimicrobial peptides which adopt a β-sheet structure; these include β-hairpin and cyclic α-, β- and θ-defensins.[11] This paper focuses on the β-hairpin AMPs, which have undergone

few studies and limited characterisation. A recent compilation of β-hairpin compounds was reported by Panteleev in 2015.[12] Here we focus on the physiochemical properties of this AMP class, and their contribution to the AMP antimicrobial activity and toxicity. β-Hairpin AMPs are usually small (< 30 amino acid residues), cationic and adopt amphipathic structures that confer excellent binding to the lipid bilayer of bacterial membranes. Fernandez-Vidal et al.[13] demonstrated that amphipathicity is more important than hydrophobicity for binding to microbial membranes. Most of the β-sheet AMPs cause membrane disruption due to electrostatic interactions with the cell membrane.[14,15] However, other modes of action have been suggested.[16,17] Unfortunately, most AMPs are not directly suitable as antibiotic leads for clinical development as they often cause hemolysis and/or mammalian cell cytotoxicity. Modification is required to generate therapeutically valuable molecules.[18] For example, a synthetic cyclic peptide derived from the β-hairpin AMP protegrin-1 has been developed by Polyphor Ltd (Basel, Switzerland)[19], demonstrating the potential for this class of compounds. POL7080 (RG7929) completed a Phase 2 trial for non-cystic fibrosis bronchiectasis in Nov 2015 (clinical trial identifier NTC02096315), and is currently undergoing Phase 2 testing in patients with *P. aeruginosa* ventilator-acquired pneumonia (VAP) co-administered with standard of care (NCT02096328). POL7080 is proposed to act against G-ve bacteria by targeting the β-barrel protein LptD (Imp/OstA), which is involved in the outer-membrane biogenesis of lipopolysaccharide (LPS)[19]. Another β-hairpin AMP is being developed by Adenium Biotech (Denmark), which has been working with variants of arenicin-3, leading to one analog (NZ17074) undergoing preclinical studies.[20, 21]

2.3 Results and discussion

Structure analysis. Some β-hairpin AMPs are intrinsically disordered and require contact with their lipophilic membrane target to adopt an ordered conformation. Others adopt a preferred structural organization, but may change conformation between being in solution and in contact with the surface of a cell membrane. AMPs, often cationic at physiological pH, form amphipathic structures that mirrors that of the phospholipids, allowing the AMPs to interact with bacterial lipid membranes.[7] Previous studies on β-hairpin AMPs have been conducted using different strains of bacteria and assay methods, which does not allow for robust comparison of antimicrobial activity and toxicity. We have now examined representatives of the β-hairpin class under a standard set of conditions in order to directly correlate the therapeutic parameters of the peptides in relation to their origin, length, number of disulfide bridges and turn type.

The β-hairpins originate from diverse sources, including both invertebrates and mammals. They adopt the common characteristic of anti-parallel β-sheets linked by a small turn of 3 to 7 amino acids, forming a hairpin shape that is maintained by interstrand disulfide bridges in both aqueous and lipid-mimicking environments.[22-26] Table 2-1 summarizes the six β-hairpin AMPs chosen for our analysis. The peptides vary from 17 to 21 residues in length, with most containing two disulfide bonds that adopt a common linkage pattern, Cys1-Cys4 and Cys2-Cys3. The exception is thanatin, which has only one disulfide bridge. NMR solution structures indicate that the length of the β-sheet differs between β-hairpins, with the arenicin-3 β-sheet pair rigidifying almost the whole structure, but a less dominant β-sheet conformation in polyphemusin-1 resulting in greater flexibility.

Table 2-1 - β-hairpin AMP origin, turn type, PDB ID and cartoon representation.

Compound	Origin	Type of turn	PDB ID	Cartoon representation	Ref.
arenicin-3	coelomocytes of marine polychaeta lugworm *Arenicola marina*	I' β-turn	-		27
tachyplesin-1	hemocyte debris of *Tachypleus tridentatus*	II four-residue β-turn	1WO0		28
polyphemusin-1	hemocyte debris of *Limulus Polyphemus*	I' four-residue β-turn	1RKK	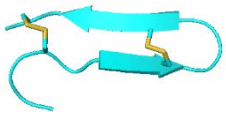	29
gomesin	hemocytes of the spider *Acanthoscurria gomesiana*	noncanonical four-residue β-turn	1KFP		30
protegrin-1	porcine neutrophils	distorted four-residue β-turn	1PG1	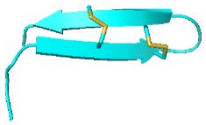	31
thanatin	spined soldier bug, *Podisus maculiventris*	standard β-turn	8TFV		32

The cartoon representation was generated using PyMOL (Schrödinger). Disulfide bridges are shown as sticks.

Table 2-2 - β-hairpin AMPs sequence alignment.

arenicin-3	-	G	F	**C**	W	Y	V	**C**	V	Y	R	N	G	V	R	V	**C**	Y	R	R	**C**	N	-	-	-
tachyplesin-1	-	K	W	**C**	F	R	V	**C**	-	Y	R	G	I	-	-	-	**C**	Y	R	R	**C**	R	*	-	-
polyphemusin-1	R	R	W	**C**	F	R	V	**C**	-	Y	R	G	F	-	-	-	**C**	Y	R	K	**C**	R	*	-	-
gomesin	-	-	Z	**C**	R	R	L	**C**	-	Y	K	Q	R	-	-	-	**C**	V	T	Y	**C**	R	G	R	*
protegrin-1	-	-	R	G	G	R	L	**C**	-	Y	**C**	R	R	-	R	F	**C**	V	-	-	**C**	V	G	R	*
thanatin	G	S	K	K	P	V	P	I	I	Y	**C**	N	R	R	T	G	-	-	-	K	**C**	Q	R	M	*

(*) = C-terminal amidation and Z = N-terminal pyroglutamic acid. The grey sections are the conserved region. The cystines are marked in bold. The cationic residues are marked in red and the hydrophobic in green. The boxes indicate the turn region.

The amino acid sequence alignment, presented in Table 2-2, demonstrates the sequence homology and importance of particular amino acids shared between β-hairpin AMPs. Two areas are defined as conserved: i) tyrosine placed adjacent to a disulfide bond and either included in the turn (tachyplesin-1, polyphemusin-1 and gomesin) or forming part of a β-sheet (arenicin-3, protegrin-1 and thanatin), and ii) the conserved C-terminal cysteine forming the external disulfide bridges of all six compounds. The arrangement of the cationic Arg and Lys residues included in the turn and the distal C- and N-termini regions, flanked by hydrophobic, membrane-insertive Val, Leu, Ile, Tyr or Trp residues, results in an amphipathic structure with one hydrophobic and one basic face, which creates a hydrophobic moment in the structure and allows the molecules to disrupt the bacterial lipid membrane.

The high representation of Tyr and Arg, as displayed by an amino acid frequency graph of all β-hairpin peptide sequences (Appendix II, Figure S7.2-1), consistently confers the elements of hydrophobicity and overall positive charge, respectively to this class of antibiotics.

Physicochemical analysis. Many AMPs, including all of the β-hairpin class, act on the membrane of microorganisms by utilizing physicochemical peptide-lipid interactions to bind to, and disrupt the lipid bilayer of the bacterial membrane. The most important physicochemical property widely reported is amphipathicity, which allows the peptides to attack the membrane by interacting with the hydrophobic-hydrophilic character of the lipids. The physicochemical properties of the β-hairpin AMPs are reported in Table 2-3. The peptide isoelectric point (pI) was calculated using PepCalc.com online tool. Hydrophobicity was calculated based on the normalized consensus scale of Eisenberg.[33]

Table 2-3 - Physicochemical properties of β-hairpin AMPs.

Peptide	pI	Net charge	Hydrophobicity	Amphipathic moment*
arenicin-3	11.17	+4	-0.11	0.44
tachyplesin-1	12.58	+6	-0.43	-0.11
polyphemusin-1	12.41	+7	-0.56	0.48
gomesin	12.58	+6	-0.61	0.83
protegrin-1	13.10	+6	-0.42	0.36
thanatin	12.71	+6	-0.34	-0.69

* see Figure 2-1

The pI is directly correlated with solubility, and proteins are soluble, avoiding aggregation, at greater than one or two pH units on either side of the pI. Since AMPs need to access lipid membranes from an aqueous phase they need to be soluble in both environments. If AMPs aggregate in solution, they will lose their ability to interact with the cell membrane. All of the molecules presented in Table 2-3 have a calculated pI between 11 and 13, which avoids self-association driven by a loss of side chain charges at physiological pH.

Being highly cationic is a key feature of β-hairpin AMPs with net charge varying only slightly, ranging from +4 to +7. It has been demonstrated that the AMP net charge has a direct correlation to their attraction/interaction to negatively charged bacterial membranes, with a lower net charge reducing attraction.[34,35]

The hydrophobicity is relatively similar for all six β-hairpin AMPs with an average value of -0.41. Gomesin has the lowest hydrophobicity at -0.61. Hydrophobic residues facilitate interactions with the fatty acyl chains. The relatively low hydrophobicity prevents binding to the zwitterionic membranes found in mammalian cells, resulting in low toxicity.[36,37] Hydrophobicity is also required for bacterial membrane permeabilisation, but some studies have demonstrated that above an optimum level or threshold (as determined by Glukhov et al.[38]) of hydrophobicity, further increase leads to a loss in antimicrobial activity and increase in toxicity.[39]

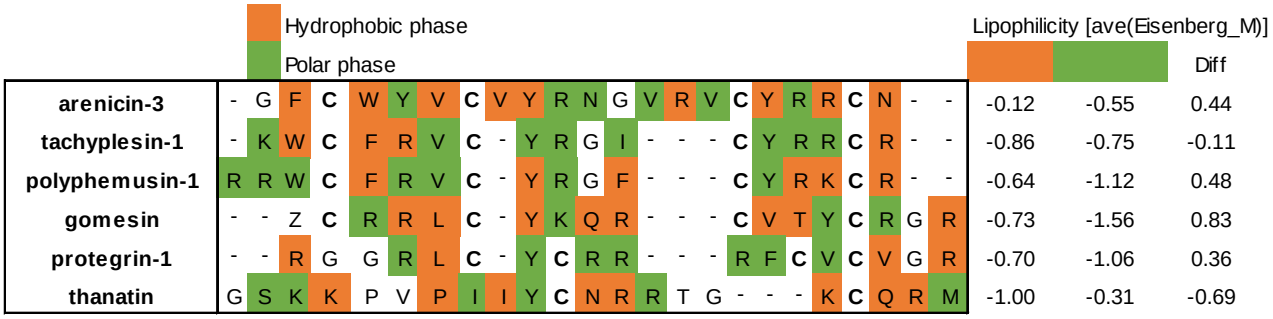

Figure 2-1 - Lipophilicity/amphipathic moment calculation of β-hairpin AMPs. All residues pointing down, toward the membrane, are classified as hydrophobic phase (orange) and those pointing up, away from the membrane, polar phase (green).

Figure 2-1 summarises the lipophilicity, or amphipathic moment, of the β-hairpin AMPs based on analysis of the NMR solution structures, taking the direction of the C_β-atom of each residue (the rest of the side chain being too flexible for accurate calculation). The amphipathic moment (Table 2-3) was calculated using our own model, specific for β-hairpin compounds. Our model considers the most probable orientation of the protein-membrane complex, where the AMPs make contact with the membrane with a perpendicular interaction between the surface of the bacterial or mammalian membrane and the β-sheets, taking into account the twisting of the molecule. This approach agrees with the reported findings of Matsuzaki et al[40], i.e. that the mean axis of the β-sheet of tachyplesin-1 is parallel to the surface of lipid film when binding to the bacteria membrane. For each molecule the amphipathic moment was calculated as the difference between the average value of hydrophobic phase residues and the average value of polar phase residues using the Eisenberg_M scale. The resulting amphipathic moment allowed the classification of the selected hairpin peptides into three groups. The first group constitutes the more amphipathic compounds which have an amphipathic moment <abs|0.4|, including tachyplesin-1 and protegrin-1. The second group consists of those with a medium amphipathic moment between abs|0.4| and abs|0.5| (arenicin-3 and polyphemusin-1), with the third group comprising those which are least amphipathic, including gomesin and thanatin with values > abs|0.5|.

NMR conformational analysis showed that the two-stranded β-sheet in all six β-hairpin AMP structures studied here possess a significant twist. This distortion allows shielding of the hydrophobic side of the β-sheet from contact with the polar solvent. Surface representations that display the electrostatic and molecular hydrophobicity (Figure 2-2) of the six β-hairpin AMPs illustrate the absence or presence of amphipathicity in aqueous solution. Although amphipathic in nature, the charged and hydrophobic residues are scattered throughout the peptide sequences, rather than grouped. Therefore, the structures possess a more distributed amphipathicity compared to the two

clear and distinct faces of opposing properties often seen by other amphipathic molecules, such as the helical AMPs.

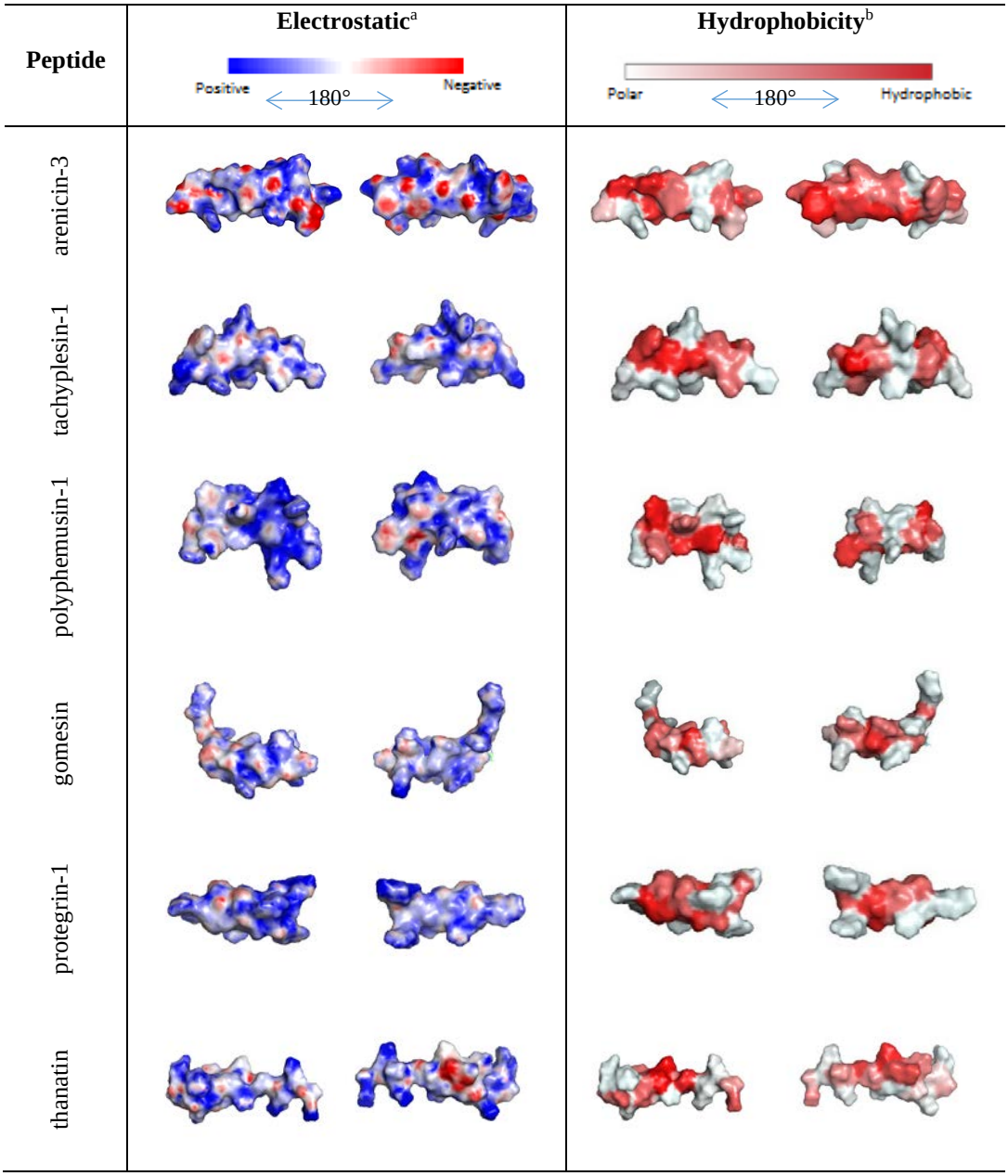

Figure 2-2 - Two-sided view of electrostatic and molecular hydrophobicity. a - The electrostatic views are based on the continuum model of the Poisson-Boltzmann equation. b - The molecular hydrophobicity views are based on the normalized consensus scale value of Eisenberg.[41]

Antimicrobial activity. To determine correlations between the physicochemical properties of the β-hairpin AMPs and their antimicrobial activity and/or toxicity, the selected peptides were tested against a panel of bacteria and fungi, with toxicity determined based on hemolytic activity and cytotoxicity assays against mammalian cells.

Potent and broad-spectrum antimicrobial activity was seen for tachyplesin-1, polyphemusin-1, protegrin-1 and arenicin-3 (Table 2-4). Gomesin showed less potency yet retained broad-spectrum

antimicrobial activity, with the exception of *K. pneumoniae* (ATCC 700603, MDR) and *S. aureus* (ATCC 43300, MRSA) for which the activity was reduced 4-8 fold. Thanatin showed a much narrower spectrum of antimicrobial activity; showing inhibitory preference for Enterobacteriaceae (*E. coli* ATCC 25922 and *K. pneumoniae* ATCC 13883), with activity against other species or resistant strains 8-32 fold less active.

The mechanism of action of β-hairpin AMPs has been suggested to involve disruption of the integrity of the bacterial lipid bilayer.[24,26,42-44] We carried out a fluorescent probe study (SYTOX green dye; data included in the supplementary information) to assess the inner (cytoplasmic) bacteria membrane permeability. The results show that all compounds except thanatin permeabilised the inner bacteria membrane, suggesting that they act via disruption of the membranes of G-ve and G+ve bacteria. The ability of each β-hairpin peptide to permeabilise the *E. coli* cytoplasmic membrane was in agreement with previous studies[31,33,49-51] To further investigate this mechanism, we compared the antimicrobial activity of the peptides against three strains of *E. coli*: (i) a control *E. coli* strain (ATCC 25922) that possessed a 'smooth' lipopolysaccharide (LPS) outer layer, (ii) a membrane mutant, *E. coli* K12 (ATCC 700926), a 'rough' strain deficient in the O-antigen chain of the LPS, and (iii) a membrane mutant, *E. coli* MB 4902, Δ*lpxC* mutant, where LpxC is a key enzyme involved in the biosynthesis of lipid A, a phosphorylated glycolipid that anchors the lipopolysaccharide to the outer membrane of the cell. All peptides were slightly more active (2- to 16-fold) against the 'rough' K12 mutant than the 'smooth' strain, except for thanatin, for which activity remained the same. With the Δ*lpxC* mutant, there was a significant increase in potency for all compounds (4- to 128-fold decrease in MICs), with protegin-1 and polyphemusin-1 showing the greatest potency at 0.015 and 0.03 μg/mL, respectively. Taken together, these data imply the peptides are able to more readily penetrate the lipid bilayer resulting in cell death with decreased lipid A in the outer membrane (OM). The potency of protegin-1 and polyphemusin-1 against the Δ*lpxC E. coli* mutant suggests that their mode of action may differ subtly from the other peptides.

Interestingly, out of the six β-hairpin AMPs tested, one group (arenicin-3, tachyplesin-1 and thanatin) were most active against G-ve bacteria, and in particular *E. coli*, whereas, the second group (polyphemusin-1, protegrin-1 and gomesin) were all more potent (2 to 10 fold) against *B. subtilis* (G+ve bacteria) and *C. neoformans* (fungi) than any other strains of bacteria and fungi. It is likely that this second group of compounds has a different mode of action to the other AMPs studied, an observation supported by the inner bacteria membrane permeabilisation study (data in supplementary information), where all three peptides (polyphemusin-1, protegrin-1 and gomesin) showed permeabilisation at a lower concentration than their MIC for the same *E.coli* ATCC 25922 strain.

Table 2-4 – Antimicrobial activity of β-hairpin AMPs.

Compound name	MIC (μg/mL)											
	Bacteria G-ve								Bacteria G+ve		Fungi Yeast	
	E. coli			*K. pneumoniae*			*A. baumannii*	*P. aeruginosa*	*B. subtilis*	*S. aureus*	*C. albicans*	*C. neoformans*
	ATCC 25922 (control strain)	ATCC 700926 (K12)	MB 4902 (Δ*lpxC*)	ATCC 13883	ATCC 700603 (MDR)	BAA 2146 (NDM-1 pos)	ATCC 19606	ATCC 27853	ATCC 6051	ATCC 43300 (MRSA)	ATCC 90028	ATCC 208821
colistin	0.03	0.03	0.009	0.5	0.125	0.03	0.03	0.25				
vancomycin									0.25	1		
amphotericin B											0.06	0.015
arenicin-3	0.5	0.25	0.125	1	4	4	0.5	1	8	64	64	8
tachyplesin-1	0.06	0.03	0.016	0.125	0.25	0.25	0.125	0.25	0.125	1	4	0.125
polyphemusin-1	0.5	0.06	0.03	0.5	1	2	0.06	2	0.25	2	1	0.06
gomesin	16	8	4	16	64	32	16	16	2	128	16	2
protegrin-1	2	0.25	0.015	0.5	4	4	0.25	4	0.03	4	2	0.06
thanatin	8	8	2	8	64	256	>256	256	128	256	64	64

colistin, vancomycin and amphotericin B were used as positive inhibitor controls for G-ve, G+ve and fungi, respectively. Data: n = 4.

Toxicity. For a peptide to be considered for therapeutic development it not only needs to possess potent antimicrobial activity, it also needs to have low toxicity to human cells. Here we evaluated the hemolytic activity of the profiled peptides, reported in Table 2-5 as a percentage value of hemolysis (compared to 100 % hemolysis induced by 1 % Triton –X100) when tested at 300 μg/mL (Appendix II, Figure S7.2-2). Protegrin-1 showed the highest hemolytic activity with 65 % disruption at the concentration tested. Tachyplesin-1 and polyphemusin-1 both possessed hemolytic activity of approximately 30 %, while arenicin-3 and gomesin were much less hemolytic (4 %). Thanatin was the only compound deemed to be non-hemolytic. Cytotoxicity was assessed using two different human cell lines (kidney and liver) in combination with two serum concentrations, 1 % and 10 %. With reduced serum in the assay, the cells are more susceptible to damage as their growth is not as robust. The compounds were far less toxic when 10 % FBS was present (Table 2-5), but these conditions can potentially lead to false negatives as there is likely to be less unbound active compound available (due to plasma protein binding) to interfere with the cells. Both cell lines were affected to a similar degree and in the same order of magnitude for all compounds except for gomesin, which showed approximately 2-fold more toxicity toward the kidney cells (HEK293) than the liver cells (HepG2). In terms of cytotoxicity, only thanatin remained non-toxic at the highest concentration (300 uM) tested. Plasma Protein Binding (PPB), as measured by ultrafiltration in 100 % human plasma,

ranged from 63 % for polyphemusin-1 to 92 % for thanatin (Table 2-5). The lack of toxicity observed with thanatin may be partly due to its high protein binding, but protegrin-1 (89 %) was similarly highly bound, yet showed the greatest toxicity. The therapeutic potential of β-hairpin AMPs is valued on the basis of their selectivity toward microbial cells as compared to normal mammalian cells. This cell selectivity is expressed as the therapeutic index (TI) of the peptides, which in this study is calculated as the ratio of the average toxicity (the sum of % value of hemolysis plus CC_{50} values of both cytotoxicity using media with minimal serum; 1 % FBS, divided by three) to the median of the MIC determined toward all tested bacteria and fungi strains. A larger therapeutic index value indicates better bacterial / mammalian cell selectivity.

Table 2-5 - Hemolytic activity, cytotoxicity, Therapeutical Index (TI) and Plasma Protein Binding (PPB) of β-hairpin AMPs.

Compound	Hemolysis (%) at 300 µg/mL	Cytotoxicity (CC_{50}) (µg/mL)				TI*	PPB (%)
		HepG2		HEK293			
		1 % FBS	10 % FBS	1 % FBS	10 % FBS		
arenicin-3	4.4 ± 1.1	95.2 ± 4.1	>300	104.6 ± 1.8	>300	17	68
tachyplesin-1	27.8 ± 3.9	65.7 ± 1.5	>300	94.7 ± 1.1	>300	335	76
polyphemusin-1	29.6 ± 2.4	36.5 ± 8.6	254.3 ± 14.2	36.6 ± 1.4	188.5 ± 1.1	46	63
gomesin	4.4 ± 0.1	162.4 ± 1.1	219.7 ± 73.3	102.3 ± 1.1	116.1 ± 25.1	6	87
protegrin-1	64.8 ± 3.5	31.4 ± 2.0	96.1 ± 1.1	19.6 ± 1.2	93.9 ± 1.1	19	89
thanatin	1.3 ± 0.4	>300	>300	>300	>300	3	92

**TI is the therapeutic index calculated as the ratio of the average toxicity (hemolytic and cytotoxic at 1 % FBS) to the median of the MIC determined toward all tested bacteria and fungi strains.*

Based on the activity profiles obtained, the six peptides can be ranked by order of antimicrobial activity and toxicity from the most active/toxic to the least active/toxic, Figure 2-3.

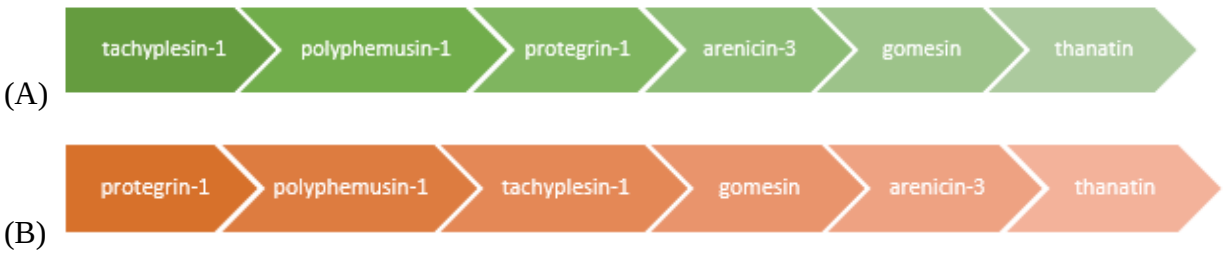

Figure 2-3 - (A) Antimicrobial activity and (B) Toxicity ranking. From left (most) to right (least) comparing the antimicrobial activity across the whole panel of bacterial and fungal strains and the toxicity as a combination of hemolytic activity and cytotoxicity.

From this ranking, two distinct groups form. The first group includes tachyplesin-1, polyphemusin-1 and protegrin-1, constituting the most active but also most toxic (MAMT) compounds. The second group, represented by arenicin-3, gomesin and thanatin, are the least active and least toxic (LALT)

compounds. This correlates with the therapeutic indices calculated for the peptides, where the peptides with best TI values correspond to the MAMT group and the peptides with lower TI values fit into the LALT group.

A comparison of the physicochemical properties (Table 2-3) with antimicrobial activity and toxicity (Figure 2-3) shows that the peptides that are the most amphipathic and the least hydrophobic are those belonging to the MAMT group, like tachyplesin-1, polyphemusin-1 and protegrin-1. Arenicin-3 is moderately amphipathic and quite hydrophobic, which explains it belonging to the LALT group. Gomesin however has poor amphipathicity but the lowest overall hydrophobicity, dis-allowing interaction with either mammalian or bacterial cells, which explain its belonging to the LALT group. The structure-function relationship study from Mattei et al[45] concluded that more hydrophobic analogs of gomesin have higher antimicrobial activity, whereas peptides more hydrophilic abolish antimicrobial activity. It was concluded that the interaction of gomesin with bacterial membranes depends on interplay between surface electrostatic interactions, which drives anchoring to the membrane surface and vesicle aggregation, and insertion of the hydrophobic portion into the membrane core, responsible for causing membrane rupture/permeabilization. Thanatin, unlike gomesin, has good hydrophobicity but is not overly amphipathic, leading to the same behaviour and explains the classification of this compound in the LALT group.

The correlation between antimicrobial activity and toxicity resides in cell selectivity. The cationic property of AMPs contributes to cell selectivity because the surface of bacterial membranes is more negatively charged than that of mammalian cells. However, the hydrophobicity and the amphipathicity, of the peptide are key components of the interaction of AMPs with mammalian cell membranes. Many studies have demonstrated that hemolytic peptides exhibit strong interaction with the zwitterionic phospholipid, phosphatidylcholine, whereas non-hemolytic peptides do not.[46, 47] Our data correlates with these rules, with the most amphipathic compounds being the most hemolytic. For all AMPs, the maintenance of the peptide hydrophobic–hydrophilic balance may be the critical parameter to producing a highly bacterial selective peptide therapeutic.[48]

The key features required for efficient bactericidal or hemolytic activities rise from understanding the secondary and tertiary structures of AMPs. The knowledge of key structure-function relationships may assist in the rational design toward improved analogs for clinical use. As a common supportive structural feature of proteins and peptides, it is highly likely that the disulfide bridges play an important role in β-hairpin AMP antimicrobial activity. The role of disulfide bridges in AMPs has been studied for numerous cases, with their importance appearing to be compound dependent. There are two main categories of compounds; (i) AMPs whose antimicrobial activity is independent of the presence or absence of disulfide bridges, for example human β-defensin-3[22] and bovine β-defensin-2,

(ii) AMPs that display decreased antimicrobial activity in the absence of disulfide bonds, for example human β-defensin-2 and α-defensin HNP-1[22] or bactenecin[22]. The β-hairpin AMPs fall into both categories, but their activity appears dependent on the ability of the peptides to retain their amphipathic structure upon membrane contact.[14,49-52] Therefore, to design new analogs, the secondary structure and amphipathic modifications have to be the key parameters to take into account for developing good structure-activity relationships. Cys could potentially be replaced by aromatic residues like Tyr or Phe which would allow the secondary structure of the peptide to be maintained and increase the hydrophobicity of the peptide which should allow better cell selectivity.[48]

2.4 Materials and methods

Compounds tested. Tachyplesin-1, polyphemusin-1, gomesin, protegrin-1 and thanatin were synthesized by Mimotopes Pty Ltd (Clayton, Australia) using Fmoc-based solid phase peptide synthesis and orthogonal Cys protection (Fmoc Cys(Acm)-OH for C3, C16, and Fmoc Cys(Trt)-OH for C7, C12); the first disulfide bond was formed by air oxidation following cleavage from the resin, with iodine treatment generating the fully cyclized peptide that was purified by RP-HPLC to >95 % purity. Identity and purity were confirmed by LC-MS and HRMS. Arenicin-3 was supplied by Adenium Biotech.

Antimicrobial assay (Minimum Inhibitory Concentration [MIC]). Both antibacterial and antifungal MIC assays were performed by a broth microdilution plate based method as per CLSI guidelines for antimicrobial susceptibility testing.[53, 54] The assay was performed in Mueller Hinton Broth (MHB, Bacto laboratories, 211443) for bacteria and Yeast Extract-Peptone Dextrose (YPD, Sigma-Aldrich, Y1500) for fungi and the MIC was determined as the lowest concentration of compound that prevented microorganism growth after 18-24 h. Full assay details are included in the Appendix II with a full list of strains tested in Table S7.2-1.

Cytotoxicity assay. Cytotoxicity to HEK293 and HepG2 cells was determined using the Alamar Blue (resazurin) assay,[55, 56] with 24h incubation and either 1 % or 10 % serum concentration. Full assay details are included in the supplementary information.

Hemolysis assay. Hemolytic activity was performed as previously descripted in the literature with slight modifications.[57] Full assay details are included in the supplementary information.

Plasma protein binding assay. Plasma protein binding was performed using an Ultrafiltration method.[58]

2.5 Conclusion

Despite the small number of β-hairpin AMPs found in nature, we can start to discern trends to determine key features required for optimal compound design. The AMPs have diverse structural arrangements and physicochemical properties, allowing them to act selectively against bacteria compared to mammalian cell types. However, some key elements are required to remain constant in order to maximize antimicrobial activity and minimize toxicity. The strategy for a good β-hairpin AMP does not involve only one factor but rather requires a good balance between charge, hydrophobicity, amphipathicity, secondary and tertiary structure, and mode of action. β-hairpin AMPs offer a wide spectrum of antimicrobial activity with very limited bacterial resistance observed to date, likely due to the significant change in membrane properties that this would require. β-hairpin AMPs therefore present many advantages over antibiotics already available in the clinic and are worthy of further investigation to develop as replacements for antibiotics that have become ineffective.

2.6 Ancillary information

Supporting Information. *Experimental procedures, amino acid frequency graph, hemolytic activity results, HRMS and LC-MS. This material is available free of charge via the Internet at http://pubs.acs.org.*

Author information. *IAE, MAC, MATB and JZ conceived the study. IAE, AGE and AMK performed the experiments and analysed the data. IAE and AGE wrote the paper with input from all authors. MAC oversaw the research program.*

Acknowledgement. *MAC is a NHMRC principle research fellow (APP1059354). IAE is is supported by an Australian Postgraduate Award (APA) PhD scholarship. AGE, AMK, JZ and MATB are supported in part by Wellcome Trust Strategic grant WT141107. We thank Geraldine Kaeslin for technical contribution in performing the cytotoxicity assays. The mutant E. coli strains MB4902 was generously supplied by Merck Sharp & Dohme Corp. (Kenilworth, NJ), all other strains were sourced from ATCC (American Type Culture Collection). The Arenicin-3 NMR solution structure was provided by Soren Neve, formally of Adenium Biotech as personal communication.*

2.7 References

1. Butler, M. S., Blaskovich, M. A., and Cooper, M. A. (2013) Antibiotics in the clinical pipeline in 2013, *J. Antibiot. 66*, 571-591. DOI:10.1038/ja.2013.86
2. Infectious Diseases Society of, A., Spellberg, B., Blaser, M., Guidos, R. J., Boucher, H. W., Bradley, J. S., Eisenstein, B. I., Gerding, D., Lynfield, R., Reller, L. B., Rex, J., Schwartz, D., Septimus, E., Tenover, F. C., and Gilbert, D. N. (2011) Combating antimicrobial resistance:

policy recommendations to save lives, *Clin. Infect. Dis. 52 Suppl 5*, S397-428. DOI:10.1093/cid/cir153

3. McKenna, M. (2013) Antibiotic resistance: the last resort, *Nature 499*, 394-396. DOI:10.1038/499394a
4. Sahl, H. G., and Shai, Y. (2015) Bacterial resistance to antimicrobial peptides, *Biochim. Biophys. Acta 1848*, 3019-3020. DOI:10.1016/j.bbamem.2015.08.009
5. Ling, L. L., Schneider, T., Peoples, A. J., Spoering, A. L., Engels, I., Conlon, B. P., Mueller, A., Schaberle, T. F., Hughes, D. E., Epstein, S., Jones, M., Lazarides, L., Steadman, V. A., Cohen, D. R., Felix, C. R., Fetterman, K. A., Millett, W. P., Nitti, A. G., Zullo, A. M., Chen, C., and Lewis, K. (2015) A new antibiotic kills pathogens without detectable resistance, *Nature*. DOI:10.1038/nature14098
6. Liu, Y. Y., Wang, Y., Walsh, T. R., Yi, L. X., Zhang, R., Spencer, J., Doi, Y., Tian, G., Dong, B., Huang, X., Yu, L. F., Gu, D., Ren, H., Chen, X., Lv, L., He, D., Zhou, H., Liang, Z., Liu, J. H., and Shen, J. (2016) Emergence of plasmid-mediated colistin resistance mechanism MCR-1 in animals and human beings in China: a microbiological and molecular biological study, *Lancet Infect. Dis. 16*, 161-168. DOI:DOI: 10.1016/S1473-3099(15)00424-7
7. Yeaman, M. R., and Yount, N. Y. (2003) Mechanisms of antimicrobial peptide action and resistance, *Pharmacol Rev 55*, 27-55. DOI:10.1124/pr.55.1.2
8. Reddy, K. V., Yedery, R. D., and Aranha, C. (2004) Antimicrobial peptides: premises and promises, *Int. J. Antimicrob. Agents 24*, 536-547. DOI:10.1016/j.ijantimicag.2004.09.005
9. Nguyen, L. T., Haney, E. F., and Vogel, H. J. (2011) The expanding scope of antimicrobial peptide structures and their modes of action, *Trends Biotechnol. 29*, 464-472. DOI:10.1016/j.tibtech.2011.05.001
10. Huang, Y., Huang, J., and Chen, Y. (2010) Alpha-helical cationic antimicrobial peptides: relationships of structure and function, *Protein Cell 1*, 143-152. DOI:10.1007/s13238-010-0004-3
11. Conibear, A. C., and Craik, D. J. (2014) The chemistry and biology of theta defensins, *Angew. Chem., Int. Ed. Engl. 53*, 10612-10623. DOI:10.1002/anie.201402167
12. Panteleev, P. V., Bolosov, I. A., Balandin, S. V., and Ovchinnikova, T. V. (2015) Structure and Biological Functions of beta-Hairpin Antimicrobial Peptides, *Acta naturae 7*, 37-47.
13. Fernandez-Vidal, M., Jayasinghe, S., Ladokhin, A. S., and White, S. H. (2007) Folding amphipathic helices into membranes: amphiphilicity trumps hydrophobicity, *J. Mol. Biol. 370*, 459-470. DOI:10.1016/j.jmb.2007.05.016
14. Saravanan, R., Mohanram, H., Joshi, M., Domadia, P. N., Torres, J., Ruedl, C., and Bhattacharjya, S. (2012) Structure, activity and interactions of the cysteine deleted analog of tachyplesin-1 with lipopolysaccharide micelle: Mechanistic insights into outer-membrane permeabilization and endotoxin neutralization, *Biochim. Biophys. Acta 1818*, 1613-1624. DOI:10.1016/j.bbamem.2012.03.015
15. Bolintineanu, D., Hazrati, E., Davis, H. T., Lehrer, R. I., and Kaznessis, Y. N. (2010) Antimicrobial mechanism of pore-forming protegrin peptides: 100 pores to kill E. coli, *Peptides 31*, 1-8. DOI:10.1016/j.peptides.2009.11.010
16. Jenssen, H., Hamill, P., and Hancock, R. E. (2006) Peptide antimicrobial agents, *Clin. Microbiol. Rev. 19*, 491-511. DOI:10.1128/CMR.00056-05
17. Cruz, J., Ortiz, C., Guzman, F., Fernandez-Lafuente, R., and Torres, R. (2014) Antimicrobial peptides: promising compounds against pathogenic microorganisms, *Curr. Med. Chem. 21*, 2299-2321. DOI:10.2174/0929867321666140217110155
18. Andres, E. (2012) Cationic antimicrobial peptides in clinical development, with special focus on thanatin and heliomicin, *Eur. J. Clin. Microbiol. Infect. Dis. 31*, 881-888. DOI:10.1007/s10096-011-1430-8
19. Srinivas, N., Jetter, P., Ueberbacher, B. J., Werneburg, M., Zerbe, K., Steinmann, J., Van der Meijden, B., Bernardini, F., Lederer, A., Dias, R. L., Misson, P. E., Henze, H., Zumbrunn, J., Gombert, F. O., Obrecht, D., Hunziker, P., Schauer, S., Ziegler, U., Kach, A., Eberl, L.,

Riedel, K., DeMarco, S. J., and Robinson, J. A. (2010) Peptidomimetic antibiotics target outer-membrane biogenesis in Pseudomonas aeruginosa, *Science 327*, 1010-1013. DOI:10.1126/science.1182749

20. Fox, J. L. (2013) Antimicrobial peptides stage a comeback, *Nat. Biotechnol. 31*, 379-382. DOI:10.1038/nbt.2572
21. Wang, X., Wang, X., Teng, D., Zhang, Y., Mao, R., Xi, D., and Wang, J. (2014) Candidacidal mechanism of the arenicin-3-derived peptide NZ17074 from Arenicola marina, *Appl. Microbiol. Biotechnol. 98*, 7387-7398. DOI:10.1007/s00253-014-5784-6
22. Powers, J. P., Rozek, A., and Hancock, R. E. (2004) Structure-activity relationships for the beta-hairpin cationic antimicrobial peptide polyphemusin I, *Biochim. Biophys. Acta 1698*, 239-250. DOI:10.1016/j.bbapap.2003.12.009
23. Fazio, M. A., Oliveira, V. X., Jr., Bulet, P., Miranda, M. T., Daffre, S., and Miranda, A. (2006) Structure-activity relationship studies of gomesin: importance of the disulfide bridges for conformation, bioactivities, and serum stability, *Biopolymers 84*, 205-218. DOI:10.1002/bip.20396
24. Drin, G., and Temsamani, J. (2002) Translocation of protegrin I through phospholipid membranes: role of peptide folding, *Biochim. Biophys. Acta 1559*, 160-170. DOI:10.1016/S0005-2736(01)00447-3
25. Kushibiki, T., Kamiya, M., Aizawa, T., Kumaki, Y., Kikukawa, T., Mizuguchi, M., Demura, M., Kawabata, S., and Kawano, K. (2014) Interaction between tachyplesin I, an antimicrobial peptide derived from horseshoe crab, and lipopolysaccharide, *Biochim. Biophys. Acta 1844*, 527-534. DOI:10.1016/j.bbapap.2013.12.017
26. Robert, E., Lefevre, T., Fillion, M., Martial, B., Dionne, J., and Auger, M. (2015) Mimicking and Understanding the Agglutination Effect of the Antimicrobial Peptide Thanatin Using Model Phospholipid Vesicles, *Biochemistry 54*, 3932-3941. DOI:10.1021/acs.biochem.5b00442
27. Ravn, B. T., Brinch, K. S., Sandvang, D. H., Hoegenhaug, H. H. K., Segura, D. R., and Neve, S. (2011) Arenicin-3 for use in the treatment of urinary tract infections, WO2011/070032 A1.
28. Nakamura, T., Furunaka, H., Miyata, T., Tokunaga, F., Muta, T., Iwanaga, S., Niwa, M., Takao, T., and Shimonishi, Y. (1988) Tachyplesin, a class of antimicrobial peptide from the hemocytes of the horseshoe crab (Tachypleus tridentatus). Isolation and chemical structure, *J. Biol. Chem. 263*, 16709-16713.
29. Miyata, T., Tokunaga, F., Yoneya, T., Yoshikawa, K., Iwanaga, S., Niwa, M., Takao, T., and Shimonishi, Y. (1989) Antimicrobial peptides, isolated from horseshoe crab hemocytes, tachyplesin II, and polyphemusins I and II: chemical structures and biological activity, *J. Biochem. 106*, 663-668.
30. Mandard, N., Bulet, P., Caille, A., Daffre, S., and Vovelle, F. (2002) The solution structure of gomesin, an antimicrobial cysteine-rich peptide from the spider, *Eur. J. Biochem. 269*, 1190-1198. DOI:10.1046/j.0014-2956.2002.02760.x
31. Aumelas, A., Mangoni, M., Roumestand, C., Chiche, L., Despaux, E., Grassy, G., Calas, B., and Chavanieu, A. (1996) Synthesis and solution structure of the antimicrobial peptide protegrin-1, *Eur. J. Biochem. 237*, 575-583. DOI:10.1111/j.1432-1033.1996.0575p.x
32. Fehlbaum, P., Bulet, P., Chernysh, S., Briand, J. P., Roussel, J. P., Letellier, L., Hetru, C., and Hoffmann, J. A. (1996) Structure-activity analysis of thanatin, a 21-residue inducible insect defense peptide with sequence homology to frog skin antimicrobial peptides, *Proc. Natl. Acad. Sci. U. S. A. 93*, 1221-1225.
33. Sweet, R. M., and Eisenberg, D. (1983) Correlation of sequence hydrophobicities measures similarity in three-dimensional protein structure, *J. Mol. Biol. 171*, 479-488. DOI:10.1016/0022-2836(83)90041-4
34. Giangaspero, A., Sandri, L., and Tossi, A. (2001) Amphipathic alpha helical antimicrobial peptides, *Eur. J. Biochem. 268*, 5589-5600. DOI:10.1046/j.1432-1033.2001.02494.x

35. Tossi, A., Scocchi, M., Skerlavaj, B., and Gennaro, R. (1994) Identification and characterization of a primary antibacterial domain in CAP18, a lipopolysaccharide binding protein from rabbit leukocytes, *FEBS Lett. 339*, 108-112. DOI:10.1016/0014-5793(94)80395-1
36. Mojsoska, B., and Jenssen, H. (2015) Peptides and Peptidomimetics for Antimicrobial Drug Design, *Pharmaceuticals 8*, 366-415. DOI:10.3390/ph8030366
37. Yin, L. M., Edwards, M. A., Li, J., Yip, C. M., and Deber, C. M. (2012) Roles of hydrophobicity and charge distribution of cationic antimicrobial peptides in peptide-membrane interactions, *J. Biol. Chem. 287*, 7738-7745. DOI:10.1074/jbc.M111.303602
38. Glukhov, E., Burrows, L. L., and Deber, C. M. (2008) Membrane interactions of designed cationic antimicrobial peptides: the two thresholds, *Biopolymers 89*, 360-371. DOI:10.1002/bip.20917
39. Chen, Y., Guarnieri, M. T., Vasil, A. I., Vasil, M. L., Mant, C. T., and Hodges, R. S. (2007) Role of peptide hydrophobicity in the mechanism of action of alpha-helical antimicrobial peptides, *Antimicrob. Agents Chemother. 51*, 1398-1406. DOI:10.1128/AAC.00925-06
40. Matsuzaki, K., Nakayama, M., Fukui, M., Otaka, A., Funakoshi, S., Fujii, N., Bessho, K., and Miyajima, K. (1993) Role of disulfide linkages in tachyplesin-lipid interactions, *Biochemistry 32*, 11704-11710.
41. Eisenberg, D., Schwarz, E., Komaromy, M., and Wall, R. (1984) Analysis of membrane and surface protein sequences with the hydrophobic moment plot, *J. Mol. Biol. 179*, 125-142. DOI:10.1016/0022-2836(84)90309-7
42. Hong, J., Guan, W., Jin, G., Zhao, H., Jiang, X., and Dai, J. (2015) Mechanism of tachyplesin I injury to bacterial membranes and intracellular enzymes, determined by laser confocal scanning microscopy and flow cytometry, *Microbiol. Res. 170*, 69-77. DOI:10.1016/j.micres.2014.08.012
43. Powers, J. P., Tan, A., Ramamoorthy, A., and Hancock, R. E. (2005) Solution structure and interaction of the antimicrobial polyphemusins with lipid membranes, *Biochemistry 44*, 15504-15513. DOI:10.1021/bi051302m
44. Domingues, T. M., Perez, K. R., Miranda, A., and Riske, K. A. (2015) Comparative study of the mechanism of action of the antimicrobial peptide gomesin and its linear analogue: The role of the beta-hairpin structure, *Biochim. Biophys. Acta 1848*, 2414-2421. DOI:10.1016/j.bbamem.2015.07.012
45. Mattei, B., Miranda, A., Perez, K. R., and Riske, K. A. (2014) Structure-activity relationship of the antimicrobial peptide gomesin: the role of peptide hydrophobicity in its interaction with model membranes, *Langmuir : the ACS journal of surfaces and colloids 30*, 3513-3521. DOI:10.1021/la500146j
46. Matsuzaki, K. (2009) Control of cell selectivity of antimicrobial peptides, *Biochim. Biophys. Acta 1788*, 1687-1692. DOI:10.1016/j.bbamem.2008.09.013
47. Dathe, M., Schumann, M., Wieprecht, T., Winkler, A., Beyermann, M., Krause, E., Matsuzaki, K., Murase, O., and Bienert, M. (1996) Peptide helicity and membrane surface charge modulate the balance of electrostatic and hydrophobic interactions with lipid bilayers and biological membranes, *Biochemistry 35*, 12612-12622. DOI:10.1021/bi960835f
48. Rao, A. G. (1999) Conformation and antimicrobial activity of linear derivatives of tachyplesin lacking disulfide bonds, *Arch. Biochem. Biophys. 361*, 127-134. DOI:10.1006/abbi.1998.0962
49. Tamamura, H., Ikoma, R., Niwa, M., Funakoshi, S., Murakami, T., and Fujii, N. (1993) Antimicrobial activity and conformation of tachyplesin I and its analogs, *Chem. Pharm. Bull. 41*, 978-980.
50. Harwig, S. S., Waring, A., Yang, H. J., Cho, Y., Tan, L., and Lehrer, R. I. (1996) Intramolecular disulfide bonds enhance the antimicrobial and lytic activities of protegrins at physiological sodium chloride concentrations, *Eur. J. Biochem. 240*, 352-357. DOI:10.1111/j.1432-1033.1996.0352h.x

51. Mohanram, H., and Bhattacharjya, S. (2014) Cysteine deleted protegrin-1 (CDP-1): anti-bacterial activity, outer-membrane disruption and selectivity, *Biochim. Biophys. Acta 1840*, 3006-3016. DOI:10.1016/j.bbagen.2014.06.018
52. Fazio, M. A., Jouvensal, L., Vovelle, F., Bulet, P., Miranda, M. T., Daffre, S., and Miranda, A. (2007) Biological and structural characterization of new linear gomesin analogues with improved therapeutic indices, *Biopolymers 88*, 386-400. DOI:10.1002/bip.20660
53. Cockerill, F. R., Wikler, M. A. (2012) *Methods for dilution Antimicrobial susceptibility tests for bacteria that grow aerobically; Approved standard*, Vol. 32, 9th ed., Clinical and laboratory standards institute, Wayne, PA.
54. Rex, J. H., Alexander, B. D. (2008) *Reference Method for Broth Dilution Antifungal Susceptibility Testing of Yeasts; Approved Standard*, Vol. 22, 3rd ed., Clinical and laboratory standards institute, Wayne , PA.
55. McMillian, M. K., Li, L., Parker, J. B., Patel, L., Zhong, Z., Gunnett, J. W., Powers, W. J., and Johnson, M. D. (2002) An improved resazurin-based cytotoxicity assay for hepatic cells, *Cell Biol. Toxicol. 18*, 157-173.
56. O'Brien, J., Wilson, I., Orton, T., and Pognan, F. (2000) Investigation of the Alamar Blue (resazurin) fluorescent dye for the assessment of mammalian cell cytotoxicity, *Eur. J. Biochem. 267*, 5421-5426. DOI:10.1046/j.1432-1327.2000.01606.x
57. Harder, J., Bartels, J., Christophers, E., and Schroder, J. M. (2001) Isolation and characterization of human beta -defensin-3, a novel human inducible peptide antibiotic, *J. Biol. Chem. 276*, 5707-5713. DOI:10.1074/jbc.M008557200
58. Zhang, F., Xue, J., Shao, J., and Jia, L. (2012) Compilation of 222 drugs' plasma protein binding data and guidance for study designs, *Drug Discov. Today 17*, 475-485. DOI:10.1016/j.drudis.2011.12.018

Chapter 3 - Therapeutical enhancement of tachyplesin-1

The chapter includes the manuscript published in ACS Infectious Diseases journal (2017). The manuscript investigated the structure activity relationship of tachyplesin-1 to design therapeutically valuable peptides. This study concluded in two new tachyplesin-1 analogs with great potential. See Appendix III, page 7-143 for supporting information.

The research findings have been published in the manuscript Edwards, Ingrid A., et al. "Structure–Activity and −Toxicity Relationships of the Antimicrobial Peptide Tachyplesin-1." *ACS Infectious Diseases* 2017, 3 (12), pp 917–926., DOI: 10.1021/acsinfecdis.7b00123. The publication can be obtained, along with supplementary material associated with the article, from http://pubs.acs.org/doi/abs/10.1021/acsinfecdis.7b00123.

For the purpose of this thesis, the published article has been reproduced on pages 3-45 to 3-64 of chapter 3. As first author, the candidate was the primary contributor to the study design, data acquisition, data analysis and writing of the manuscript. The reader is referred to page VI for the contributions by each author to the manuscript.

Contributor	Statement of contribution
Edwards, IA (Candidate)	Conception and design (88%) Analysis and interpretation (90%) Drafting and production (80%)
Elliott, AG	Conception and design (4%) Analysis and interpretation (5%) Drafting and production (10%)
Kavanagh, AM	Conception and design (0%) Analysis and interpretation (5%) Drafting and production (0%)
Blaskovich, MAT	Conception and design (4%) Analysis and interpretation (0%) Drafting and production (5%)
Cooper, MA	Conception and design (4%) Analysis and interpretation (0%) Drafting and production (5%)

Research Paper

Structure-activity and -toxicity relationships of the antimicrobial peptide tachyplesin-1

Ingrid A. Edwards, Alysha G. Elliott, Angela M. Kavanagh, Mark A.T. Blaskovich and Matthew A. Cooper*

306 Carmody Road (Building 80), Institute for Molecular Bioscience, 306 Carmody Road (Building 80), The University of Queensland, Brisbane, Queensland 4072 Australia

Correspondence to: m.cooper@uq.edu.au

Keywords: tachyplesin-1; antimicrobial peptide; β-hairpin; antimicrobial activity/toxicity index; amphiphilicity, membrane, antibiotic, resistance

3.1 Abstract

Tachyplesin-1 (**1**) is a cationic β-hairpin antimicrobial peptide with a membranolytic mechanism of action. Whilst it possesses broad-spectrum, potent antimicrobial activity, **1** is highly hemolytic against mammalian erythrocytes, which precludes it from further development. In this study we report a template-based approach to investigate the structure-function and structure-toxicity relationships of each amino acid of **1**. We modulated charge and hydrophobicity by residue modification and truncation of the peptide. Antimicrobial activity was then assessed against six key bacterial pathogens and two fungi, with toxicity profiled against mammalian cells. The internal disulfide bridge Cys7-Cys12 of **1** was shown to play an important role in broad-spectrum antimicrobial activity against all pathogenic strains tested. Novel peptides based on the progenitor were then designed, including **5** (TP1[F4A]), **12** (TP1[I11A]) and **19** (TP1[C3A,C16A]). These had 26- to 64-fold improved activity/toxicity indices, and show promise for further development. Structural studies of **5** (TP1[F4A]) and **12** (TP1[I11A]) identified a conserved β-hairpin secondary structure motif correlating with their very high stability in mouse and human plasma. Membrane binding affinity determined by surface plasmon resonance confirmed their selectivity toward bacterial membranes, but the degree of membrane binding did not correlate with the degree of hemolysis, suggesting that other factors may drive toxicity.

3.2 Introduction

Increasing rates of bacterial resistance to antibiotics has fueled a dire need for the discovery of new replacement drugs for obsolete antibiotics.[1] Antimicrobial peptides (AMPs) are common in nature, being essential components of the innate immune system in the majority of multicellular organisms. AMPs have been well studied over three decades with more than 2000 AMPs reported from eukaryotes (http://aps.unmc.edu/AP/main.php). AMPs, being short, cationic and amphipathic, are characterized with broad range antimicrobial activity resulting from a membranolytic mechanism of action, which consequently offers a low rate of resistance development. Tachyplesin-1 (TP1) **1** is a member of the closely related tachyplesin and polyphemusin families, both originating from the horseshoe crab.[2,3] **1** is a 17 amino acid AMP (KWCFRVCYRGICYRRCR) extracted from the hemocytes of the horseshoe crab, *Tachypleus tridentatus*. **1**, constrained by two disulfide bridges (Cys3-Cys16, Cys7-Cys12), forms a β-hairpin structure (Figure 3-1), both in aqueous solution and in lipid-mimicking environments.[4,5] **1** exhibits potent activity against Gram-positive (G+ve) and Gram-negative (G-ve) bacteria, as well as fungi. **1** did not induce resistance in short term studies[6], but caused decreased susceptibility under long-term continuous selection conditions[7]. **1** has been shown to compromise the integrity of both the outer and cytoplasmic cell membranes of *Escherichia coli*.[8] In addition to its high antimicrobial activity, **1** unfortunately also displays high toxicity towards mammalian cells, a common detrimental characteristic of many AMPs that renders them unsuitable for therapeutic development. Analogs of **1** have been reported in the past, with amino acid substitutions around the disulfide bridge regions.[9-13] However, no systematic study has been reported to ascertain a clear structure-function relationship for each amino acid in the sequence. In this report, we have conducted an alanine scan of **1** followed by modifications of the overall hydrophobicity by replacement at select positions that the Ala scan indicated were amenable to change. We assessed the effects of amino acid replacements on antimicrobial activity, cytotoxicity, and hemolytic activity. Furthermore, we evaluated the membrane binding affinity of the most interesting peptides by surface plasmon resonance (SPR). We then assessed the stability of the most promising peptides in plasma, and conducted solution phase NMR structrural studies.

3.3 Results and discussion

Peptide design. In this study, we systematically determined the importance of each amino acid in 1 in a search for therapeutically valuable analogs of 1. A schematic representation of 1 (Figure 3-1) illustrates the structural amphipathicity of the peptide. There are two distinct faces; one β-sheet (top)

composed mainly of hydrophobic residues and the other one (bottom) being more hydrophilic and charged. Thus, 1 has been identified as one of the most amphipathic β-hairpin AMPs.[14]

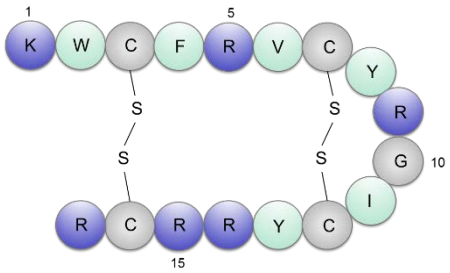

Figure 3-1 - Schematic representation of 1 (TP1). Hydrophobic residues in green and charged residues in blue.

To modulate the properties of a peptide several methodologies are commonly exploited (i) alteration of the hydrophobicity/amphipathicity by replacing hydrophobic residues with less hydrophobic (e.g. Ala, Gly) or more hydrophilic (e.g. Ser) residues, (ii) modification of the charge by replacing basic or acidic residues, (iii) truncation of the peptide, (iv) combination of (i) to (iii).[15,16] Here we have chosen a panel of peptide modifications that encompass all these methods. An alanine scan is commonly employed to ascertain the importance of individual residues within a peptide. Alanine is the most commonly used amino acid to study the amino acid function in a peptide because it eliminates side-chain interactions without altering the main-chain conformation. It has the ability to form α-helices and/or β-sheets, is flexible and has low hydrophobicity.

We studied the physicochemical properties of all **1** analogs (Table 3-1). The peptides ranged from 2009 Da (**29**, 16 residues) to 2293 Da (**23**, 17 residues). The ExPASy ProtParam tool[17] was used to calculate the physicochemical properties of the peptide analogs. The charge of the analogs varied from +4 (**29** and **33**) to +6 (**1**), while their pI varied from 9.25 (**29** and **33**) to 12.71 (**9** and **14**). GRAVY score (grand average of hydropathicity index) is a method used to calculate the hydrophobicity/solubility of a peptide. A negative GRAVY score indicates hydrophilicity and a positive GRAVY score indicates hydrophobicity. All peptides were hydrophilic except for two, **31** with GRAVY = 0.000, and **33** with a positive hydrophobic GRAVY = 0.224.

Table 3-1 - Amino acid sequences and physicochemical properties of tachyplesin-1 and its analogs.

Number	Peptide	H-Sequence-NH2	MW (Da)	Charge	pI	GRAVY
1	TP1	KWCFRVCYRGICYRRCR	2263.7	+6	12.29	-0.518
2	TP1[K1A]	**A**WCFRVCYRGICYRRCR	2206.7	+5	12.28	-0.182
3	TP1[W2A]	K**A**CFRVCYRGICYRRCR	2148.6	+6	12.29	-0.359
4	TP1[C3A,C16S]	KW**A**FRVCYRGICYRR**S**R	2217.6	+6	12.29	-0.753
5	TP1[F4A]	KWC**A**RVCYRGICYRRCR	2187.7	+6	12.29	-0.576
6	TP1[R5A]	KWCF**A**VCYRGICYRRCR	2178.6	+5	12.12	-0.147
7	TP1[V6A]	KWCFR**A**CYRGICYRRCR	2235.7	+6	12.29	-0.659
8	TP1[C7A,C12S]	KWCFRV**A**YRGI**S**YRRCR	2217.7	+6	12.29	-0.753
9	TP1[Y8A]	KWCFRVC**A**RGICYRRCR	2170.0	+6	12.71	-0.335
10	TP1[R9A]	KWCFRVCY**A**GICYRRCR	2178.6	+5	12.12	-0.147
11	TP1[G10A]	KWCFRVCYR**A**ICYRRCR	2277.8	+6	12.29	-0.388
12	TP1[I11A]	KWCFRVCYRG**A**CYRRCR	2221.7	+6	12.29	-0.676
13	TP1[C7S,C12A]	KWCFRV**S**YRGI**A**YRRCR	2217.7	+6	12.29	-0.753
14	TP1[Y13A]	KWCFRVCYRGIC**A**RRCR	2171.7	+6	12.71	-0.335
15	TP1[R14A]	KWCFRVCYRGICY**A**RCR	2178.7	+5	12.12	-0.147
16	TP1[R15A]	KWCFRVCYRGICYR**A**CR	2178.7	+5	12.12	-0.147
17	TP1[C3S,C16A]	KW**S**FRVCYRGICYRR**A**R	2217.7	+6	12.29	-0.753
18	TP1[R17A]	KWCFRVCYRGICYRRC**A**	2178.7	+5	12.12	-0.147
19	TP1[C3A,C16A]	KW**A**FRVCYRGICYRR**A**R	2203.7	+6	12.29	-0.600
20	TP1[C7A,C12A]	KWCFRV**A**YRGI**A**YRRCR	2203.7	+6	12.29	-0.600
21	TP1[C3A,C7A,C12A,C16A]	KW**A**FRV**A**YRGI**A**YRR**A**R	2140.5	+6	11.84	-0.682
22	TP1[V6R,R9A]	KWCFR**R**CY**A**GICYRRCR	2239.8	+6	12.29	-0.659
23	TP1[K1R]	**R**WCFRVCYRGICYRRCR	2292.7	+6	10.16	-0.553
24	TP1[F4G]	KWC**G**RVCYRGICYRRCR	2174.6	+6	9.93	-0.706
25	TP1[F4S]	KWC**S**RVCYRGICYRRCR	2204.6	+6	9.93	-0.729
26	TP1[Y8G]	KWCFRVC**G**RGICYRRCR	2158.6	+6	10.16	-0.465
27	TP1[I11G]	KWCFRVCYRG**G**CYRRCR	2208.6	+6	9.93	-0.806
28	TP1[F4A,Y8A,I11A]	KWC**A**RVC**A**RG**A**CYRRCR	2054.4	+6	10.16	-0.553
29	TP1[-R5,R17G]	KWC - FVCYRGICYRRC**G**	2009.4	+4	9.25	-0.013
30	TP1[K1A,F4A]	**A**WC**A**RVCYRGICYRRCR	2131.5	+5	9.69	-0.241
31	TP1[K1A,Y8A]	**A**WCFRVC**A**RGICYRRCR	2115.5	+5	9.88	0.000
32	TP1[K1A,I11A]	**A**WCFRVCYRG**A**CYRRCR	2165.5	+5	9.69	-0.341
33	TP1[R9A,R17A]	KWCFRVCY**A**GICYRRC**A**	2094.5	+4	9.25	0.224

Antimicrobial activity, toxicity and cell selectivity. 1 was determined previously to possess potent and broad-spectrum antimicrobial activity.[14] Here we assessed the antimicrobial activity of 32 analogs of **1** against a broad range of bacteria, both G-ve and G+ve, as well as fungi. Table 3-2 reports the results of testing against a panel of ATCC reference strains and drug resistant clinical isolates of *Klebsiella pneumoniae*, *Acinetobacter baumannii* and *Pseudomonas aeruginosa* (strain details in Appendix III, Table S7.3-1). The majority of the analogs tested retained potent activity across the range of microbes, even the most resistant ones, as compared to **1**, though no analog displaying increased antimicrobial activity. All peptides, including **1**, showed a marked reduction in activity against *Candida albicans* as compared to other microbes, with at least 8-fold reduction in antifungal activity as compared to *Cryptococcus neoformans*. Similarly, for G+ve bacteria the peptides had lower potency against *Staphylococcus aureus* compared to *Bacillus subtilis*, with antibacterial activity consistently at least 4-fold lower. For *K. pneumoniae,* all peptides demonstrated a reduction in activity between the reference strain, and the multidrug-resistant (MDR) strains of 2- to 8-fold, with no difference between the various MDR strains. Another 4- to 32-fold reduction in activity was noted

when tested against an extensively drug-resistant (XDR) strain across all peptides. This difference in activity was not demonstrated in the case of *A. baumannii* or *P. aeruginosa* with the MIC activity remaining within a tight range (~2-fold, i.e. within accepted assay fluctuation range), between reference strains and resistant strains, including XDR and polymyxin resistant isolates.

The alanine scan showed that single Ala replacements of amino acids at positions 1, 2, 4, 5, 6, 8, 9, 10, 11, 13, 14, 15 or 17 (producing peptides **2**, **3**, **5, 6, 7, 9, 10, 11, 12, 14, 15, 16 or 18**, respectively) gave analogs that retained the broad-spectrum potent antimicrobial activity of **1**; therefore these positions are presumably not key for the antimicrobial activity of the peptide. An NMR and tryptophan fluorescence study performed by Kushibiki *et al*[5] concluded that Trp2 inserted into the hydrophobic acyl chains of LPS and suggested that the residues located at the N- and C-termini of **1** are involved in the binding to LPS, indicating their importance in the mode of action of **1**. Our results do not correlate well with those findings as **3** (TP1[W2A]) showed only 3-fold reduction in antimicrobial activity across all tested strains, with **2** and **18** also showing good activity. Positions 3, 7, 12 and 16 of **1** correspond to Cys residues, forming two disulfide bridges (3-16 and 7-12) that create the disulfide bridge constrained β-hairpin structure as characterized by several earlier studies.[4,5] Removal of the disulfide bridge was achieved via two different approaches: (i) by Ala replacement of one Cys while the partnering Cys residue was replaced by Ser, therefore retaining the same hydrophilic properties of Cys-SH without potential misfolding of the peptide through mismatched disulfide bond formation[18] and (ii) by complete abolition of the disulfide bridge properties by Ala replacement of both Cys residues. The deletion of the internal disulfide bridge (7-12) in **8**, **13** or **20** reduced the antimicrobial activity of **1** by 3- to 12-fold. However, the deletion of the external disulfide bridge (3-16) in **4**, **17** or **19** more significantly reduced the antimicrobial activity of **1**, by 4- to 128-fold. Deletion of both disulfide bridges, **21**, dramatically reduced the overall antimicrobial activity by 64-fold across all tested strains, in accordance with the work performed by Tamamura *et al*.[9] This reduction in antimicrobial activity is presumably due to the subsequent loss of β-sheet stacking, as a direct result of the removal of the disulfide bridges.[7,8,15] In our study, there were several unexpected results. Of the three analogs that removed the external disulfide bond, **19** (TP1[C3A,C16A]) and **17** (TP1[C3S,C16A]) had similar antimicrobial activities across all strains tested, losing only 2 to 16-fold activity as compared to **1**. However, **4** (TP1[C3A,C16S]) showed around 100-fold reduction in antimicrobial activity for most strains tested, except for *B. subtilis* and *C. neoformans* where the reduction was only 10-fold. Cys3 is flanked by hydrophobic residues, Trp2 and Phe4, and Cys16 is flanked by polar residues, Arg15 and Arg17. By inserting the hydrophobic residue Ala into position 3 and hydrophilic residue Ser into position 16, the amphipathicity of the peptide was increased

considerably, potentially creating a repulsive effect between the β-sheets that led to an unfolded structure (1H NMR in Appendix III, Figure S7.3-13).

Several positions were selected for further modifications. The modulation of hydrophobicity/amphipathicity at position 4 was studied by mutating Phe with Ala (F4A) **5**, Gly (F4G) **24** or Ser (F4S) **25**, resulting in reduced antimicrobial activity, around 2-fold at each mutation, as hydrophobicity decreased. A selection of five peptides (**4** (TP1[C3A,C16S]), **19** (TP1[C3A,C7A,C12A,C16A]), **22** (TP1[V6R,R9A]), **28** (TP1[F4A,Y8A,I11A]) and **29** (TP1[-R5,R17G])) showed a considerable loss, at least 100-fold, in antimicrobial activity across the full panel of bacteria and fungi. These five peptides were designed with a range of modifications that comprise physicochemical properties from all regions of the spectrum of MW, charge, pI and hydrophobicity. No trend was identified that correlated physicochemical properties with antimicrobial activity, and it is therefore more likely that the overall peptide structure and sites specific to mode of action are the key elements to increasing and decreasing antimicrobial potential of the **1** peptide scaffold.

Table 3-2 - Antimicrobial activity of tachyplesin-1 and its analogs

Compound name	MIC (μg/mL)												
	Bacteria G-ve									Bacteria G+ve		Fungi Yeast	
	E. coli	*K. pneumoniae*				*A. baumannii*		*P. aeruginosa*		*B. subtilis*	*S. aureus*	*C. albicans*	*C. neoformans*
	ATCC 25922 (control strain)	ATCC 13883	ATCC 700603 (MDR)	BAA 2146 (NDM-1 pos)	clinical isolate 100650661:1 (XDR:PmxR)	ATCC 19606	clinical isolate 100734512:2 (XDR;PmxR)	ATCC 27853	FADDI-FA070 (PmxR)	ATCC 6051	ATCC 43300 (MRSA)	ATCC 90028	ATCC 208821
colistin	0.015	0.125	0.03	0.125	>32	0.06	>32	0.125	>32				
meropenem	≤0.03	0.03	0.06	>32	>64	1	>64	0.5	>32				
vancomycin										0.125	1		
fluconazole												0.5	8
amphotericin B												0.25	0.15
1	0.06	0.06	0.25	0.25	2	0.06	0.125	0.125	0.25	0.06	0.25	2	0.125
2	0.03	0.06	0.125	0.125	2	0.125	0.125	0.25	0.5	0.03	0.5	8	0.25
3	0.25	0.5	1	1	>16	0.5	0.5	0.5	4	0.5	8	8	0.5
4	4	16	16	>16	>16	>16	>16	>16	>16	0.5	>16	>16	4
5	0.125	0.5	0.5	0.5	16	0.5	0.5	0.5	2	0.25	4	8	0.5
6	0.125	0.125	0.5	0.5	8	0.06	0.125	0.25	0.5	0.03	0.5	4	0.25
7	0.25	0.25	1	1	16	0.25	0.5	1	2	0.25	4	8	1
8	0.5	0.5	4	2	16	0.25	0.25	2	4	0.25	2	8	0.5
9	0.06	0.125	0.25	0.5	8	0.125	0.5	1	2	0.25	4	8	0.5
10	0.125	0.03	0.25	0.125	2	0.06	0.125	0.25	1	0.125	1	2	0.25
11	0.06	0.03	0.25	0.25	4	0.06	0.06	0.25	0.5	0.03	0.5	2	0.06
12	0.125	0.25	0.5	0.25	8	0.25	0.25	0.25	1	0.125	2	2	0.5
13	1	4	16	8	16	0.5	1	8	16	0.125	16	2	0.5
14	0.25	0.25	0.5	0.5	8	0.125	0.25	0.5	2	0.06	4	4	0.5
15	0.125	0.06	0.5	0.25	1	0.125	0.125	0.125	0.25	0.125	0.5	8	0.25
16	0.25	0.25	2	1	16	0.25	0.25	4	4	0.03	4	2	0.25
17	0.25	1	2	1	16	0.25	0.25	1	4	0.125	4	4	0.25
18	0.015	0.125	0.25	0.25	4	0.125	0.125	0.25	0.5	0.015	0.5	4	0.25
19	0.25	1	1	1	>16	0.25	0.5	2	8	0.125	8	8	1
20	0.125	0.25	2	1	16	0.25	0.25	1	2	0.125	2	8	1
21	8	16	16	16	>16	4	4	>16	>16	1	16	>16	1
22	0.5	>16	16	>16	>16	16	>16	>16	>16	0.25	>16	>16	4
23	0.125	0.125	0.5	0.25	4	0.125	0.25	0.25	0.5	0.125	1	4	0.25
24	0.25	2	1	2	>16	0.5	2	1	16	0.5	16	8	2
25	0.5	2	4	4	>16	0.5	2	4	>16	0.5	16	>16	4
26	0.5	2	8	8	>16	1	2	8	16	0.5	16	>16	4
27	0.25	0.25	0.5	2	8	0.5	0.5	1	4	0.25	4	8	1
28	8	>16	>16	>16	>16	>16	>16	>16	>16	>16	>16	>16	>16
29	8	>16	>16	>16	>16	16	>16	>16	>16	1	>16	>16	4
30	2	4	4	4	>16	2	16	8	>16	16	>16	>16	>16
31	0.125	0.25	0.5	1	8	0.25	0.5	1	4	0.5	8	>16	2
32	0.125	0.125	0.25	0.5	4	0.25	0.25	0.5	2	0.125	4	>16	1
33	0.03	0.06	0.5	0.5	4	0.25	0.5	0.5	2	0.06	2	8	0.5

colistin, meropenem, vancomycin, fluconazole and amphotericin B were used as positive inhibitor controls for G-ve, G+ve and fungi, respectively. Data: n = 4, XDR (extensively drug resistant), PmxR (polymyxin resistant).

The toxicity of the analogs of **1** was tested against Human Embryonic Kidney cells (HEK293) and human red blood cells (RBC). None of the peptides showed cytotoxicity against HEK293 cells at the highest tested concentration, 100 μg/mL. Hemolytic activity (MHC) is reported in Table 3-3 as the minimum hemolytic concentration that caused 10% hemolysis of fresh RBCs. **1** possessed reasonably

potent hemolytic activity (MHC = 0.25 μg/mL) and most of the peptide analogs did not improve this quality by decreasing hemolytic potency. However, nine of the analogs (**3** (TP1[W2A]), **4** (TP1[C3A,C16S]), **5** (TP1[F4A]), **9** (TP1[Y8A]), **12** (TP1[I11A]), **19** (TP1[C3A,C16A]), **20** (TP1[C7A,C12A]), **22** (TP1[V6R,R9A]) and **30** (TP1[K1A,F4A])) did show promising 32 to 160-fold reductions in MHC. Similarly to antimicrobial activity, this did not correlate with the physicochemical properties of the peptides and no trend or correlation could be discerned. Additionally, for some analogs the reduction in hemolytic activity correlated to the loss of antimicrobial activity, meaning these peptide sequences essentially lost all biological activity. This is the case for **22**, a peptide designed to reduce the hydrophobicity of **1** without change of charge, reducing the overall amphipathicity of **1**. This change was not beneficial, emphasizing again the importance of peptide amphipathicity to its activity.

Commonly, the overall therapeutic potential of a peptide is assessed via a cell selectivity or antimicrobial activity/toxicity index (ATI). The ATI, Table 3-3, can be improved in one of the following ways (i) increase in antimicrobial activity, (ii) decrease in hemolytic activity, or (iii) a combination of both, increasing antimicrobial activity while decreasing hemolytic activity. Here we calculated the ATI from the ratio of the minimum hemolytic concentration (MHC) to the median of the minimum inhibitory concentrations (MIC) determined towards all tested bacteria and fungi (MM). Therefore, a larger ATI value indicates greater desirable cell selectivity. From these ATI calculations, three peptides (**5** (TP1[F4A]), **19** (TP1[C3A,C16A]) and **12** (TP1[I11A])) stood out. These analogs had ATI values that were 26-, 40- and 64-fold improved, respectively, retaining relatively high antimicrobial activity while dramatically decreasing hemolytic activity.

Table 3-3 - Biological activity and activity/toxicity indices of tachyplesin-1 and its analogs

Peptide	MM[a] (μg/mL)	MHC[b] (μg/mL)	ATI[c]
1	0.125	0.25	2.0
2	0.125	2.1	16.8
3	0.4	8	20.0
4	16	8	0.5
5	0.5	40	80.0
6	0.125	2	16.0
7	0.25	1.2	4.8
8	0.5	1	2.0
9	0.25	8	32.0
10	0.125	2	16.0
11	0.125	0.5	4.0
12	0.25	32	128.0
13	1.5	0.6	0.4
14	0.25	1	4.0
15	0.163	0.5	3.1
16	0.25	0.45	1.8
17	0.5	3	6.0
18	0.125	0.45	3.6
19	0.75	40	53.3
20	0.375	8	21.3
21	8	0.24	0.0
22	16	11	0.7
23	0.163	1	6.2
24	1	0.47	0.5
25	2	0.23	0.1
26	3	0.4	0.1
27	0.5	0.2	0.4
28	16	0.9	0.1
29	16	0.3	0.0
30	6.4	32	5.0
31	0.75	0.4	0.5
32	0.5	0.2	0.4
33	0.375	0.2	0.5

[a]The median of the peptide Minimum Inhibitory Concentrations (MICs) against all bacteria and fungi tested (MM).
[b]The MHC was determined as the minimum hemolytic concentration that caused ≤10% hemolysis of fresh red blood cells.
[c]The activity/toxicity index (ATI) is the ratio of the MHC to the MM. Larger values indicate a greater selectivity of the peptides for microbe cells.

The Ala scan peptides that showed an improved ATI, **5** (TP1[F4A]), **9** (TP1[Y8A]) and **12** (TP1[I11A)], were subsequently substituted with Gly instead of Ala, to see if further reduction in side chain hydrophobicity was beneficial. The F4G substitution **24** had similar antimicrobial activity to F4A **5** but almost 100-fold increase in hemolytic activity. Similarly, while Tyr8 and Ile11 substituted by Ala (**9** and **12**) retained **1**'s antimicrobial activity and reduced its hemolytic activity; the analogs with Gly (**26** and **27**) had reduced antimicrobial activity while retaining similar levels of hemolytic activity. In a study by Panteleev *et al*[19], Tyr8 and Ile11 of **1** were substituted by Arg or Ser, in both

cases dramatically reducing the hemolytic activity without detriment to the antimicrobial activity, hence making the compounds very promising for development as antibiotic candidates. In our study, the replacement of the Tyr8 or Ile11 by a less hydrophobic amino acid was also shown to be highly beneficial for the cell selectivity of the peptide. However a fine balance needs to be found, as if the amino acid composition of the peptide becomes too hydrophilic the toxicity increases significantly. This may be influenced by the overall conformation of the peptide as well as the specific conformation of the peptide turn. Residues Tyr8 and Ile11 both form part of the β-turn and the replacement of either residue to a Gly would change the type of structural turn.

The beneficial mutations seen in analogs **5**, **9** and **12** were then combined to see if the effects were additive. Unfortunately, none of **28, 30**, **31**, **32** and **33** showed the desired improvements; while they kept relatively potent antimicrobial activity (except for **28** and **30**), they also concomitantly retained high hemolytic activity (except for **30**).

Another method to increase the activity/toxicity index of **1** was reported by Saravanan *et al*,[12] who deleted the four Cys residues of **1** without replacement (peptide named CDT). In this case, the β-hairpin structure was less rigid but conserved in solution and in the presence of LPS, due to hydrogen bonding and packing interactions across the sheets, allowing the peptide to maintain potent antimicrobial activity while reducing its hemolytic activity. Wood *et al*,[20] studied the SAR of CDT, finding that two analogs [des-Arg^{12,13}] CDT and [Ile^{2,3,6,10}] CDT increased the selectivity index.

Peptide membrane binding followed by Surface Plasmon Resonance. To investigate the cell selectivity, we determined the peptide membrane binding affinity of select peptides by SPR. We selected two model membranes, one mimicking the outer leaflet of the G-ve bacteria *E. coli* (taken as representative of the AMP antimicrobial activity) and the other one mimicking the outer leaflet of the human red blood cell (taken as representative of the AMP hemolytic activity). Bacterial membranes are more negatively charged than mammalian cells due to their lipid composition. Moreover, the cell composition of the outer leaflet of bacterial membranes differs between classes. *E. coli* is predominantly composed of palmitoyloleoyl-phosphatidylethanolamine (POPE), palmitoyloleoyl-phosphatidylglycerol (POPG) and cardiolipin, and was therefore modelled as POPE/POPG/cardiolipin (15:4:1) in our study.[21] In contrast, about half of the mass of the RBC membrane is comprised of protein and the other half is lipids, predominantly phospholipids with the addition of cholesterol.[22] Palmitoyloleoyl-phosphatidylcholine (POPC), a zwitterionic phospholipid forming a fluid bilayer at room temperature, is the major component of eukaryotic cells. However, cholesterol also plays a key role in the membrane composition of RBCs. Therefore, POPC/cholesterol

(4:1) was used here as a simplistic model to reflect the charge and fluidity of the outer leaflet of RBCs. Matsuzaki *et al.*[23] stated that hemolytic peptides exhibited strong interactions with zwitterionic phospholipids, whereas non-hemolytic peptides did not. We thus investigated the relative membrane binding affinities of the three peptides possessing the highest ATI values (**5**, **12** and **19**), as well as less active **1** and **27**, to assess this hypothesis. In our study (Figure 3-1), all five peptides exhibited a stronger interaction to POPE/POPG/cardiolipin, modelling the outer leaflet of *E. coli*, as opposed to POPC/cholesterol, modelling the outer leaflet of RBCs. The cell selectivity was relatively similar amongst the five peptides. These data do not correlate with the findings of Matsuzaki *et al*.[23] and did not correspond with our observed antimicrobial and hemolytic activity and hemolytic activity testing, which showed that all five peptides had similar antimicrobial potency but differed by their hemolytic activity. **1** and **27** exhibited high hemolytic activity compared to the other three peptides. We would therefore have expected to see an increase in binding affinity to RBC with **1** and **27**. This lack of correlation between the model membrane binding affinities and the biological data could be due to several hypotheses (i) our RBC model is too simplistic and does not reflect the full complexity of what occurs *in vitro* with live cells, as the RBC membrane is a very complex ensemble of two asymmetric layers,[24,25] composed mainly of phosphatidylcholine (PC), sphingomyelin (SM) and cholesterol, or (ii) the affinity for the peptide to bind to the membrane is only the first step in the mode of action for activity. It is likely that the peptide not only needs to bind to the membrane but must also act to disrupt the cell to exhibit activity and cause cell death. This is in accordance with the findings of Imura *et al*,[26] suggesting a lipid flip-flop with toroidal pore formation mechanism of action.

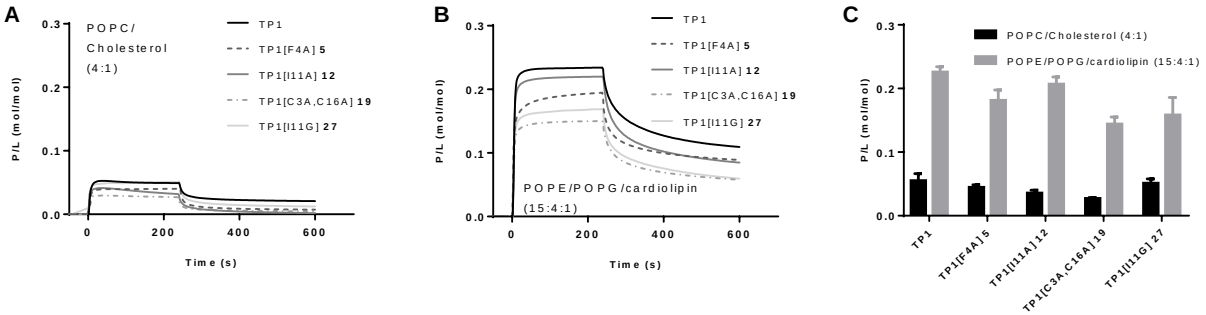

Figure 3-2 - Membrane binding affinity of tachyplesin-1 and its analogs as monitored by surface plasmon resonance. The response to the total amount of lipid deposited on the chip surface was normalized by calculating the peptide-to-lipid ratio (P/L mol/mol) (1RU = 1 pg.mm^{-2}). Sensorgrams obtained upon injection of 64 µg/mL of peptide over (A) POPC/Cholesterol (4:1) [RBC] or (B) POPE/POPG/cardiolipin (15:4:1) [*E. coli*] bilayers. (C) Comparison of the P/L obtained for the five peptides at the reported point at the end of the association phase over both model bilayers. Error bars represent standard error of the mean of three replicates.

Plasma stability. Plasma stability is an important parameter for potential peptidic drug candidates. Compounds with certain functional groups are more susceptible to hydrolysis by plasma enzymes

than others. These include esters, amides, lactones, lactams, carbamides, sulfonamides and peptide mimetics. The plasma stability assay is designed to focus on these classes of compounds. To evaluate the stability of the three peptides possessing the highest ATI values (**5**, **12** and **19**), we performed a plasma stability assay against mouse and human plasma over 2 hours. The percentage of peptide remaining in plasma was followed by LC-MS, as shown in Figure 3-3. Interestingly, **1**, **5** and **12** remained fully stable in both mouse and human plasma, however, **19** was rapidly degraded to leave only 13% or 52% after two hours, in mouse and human plasma, respectively. Loss of the disulfide bridge in **19** TP1[C3A,C16A] improved the activity/toxicity relationship but made **19** TP1[C3A,C16A], more susceptible to hydrolysis in the plasma environment.

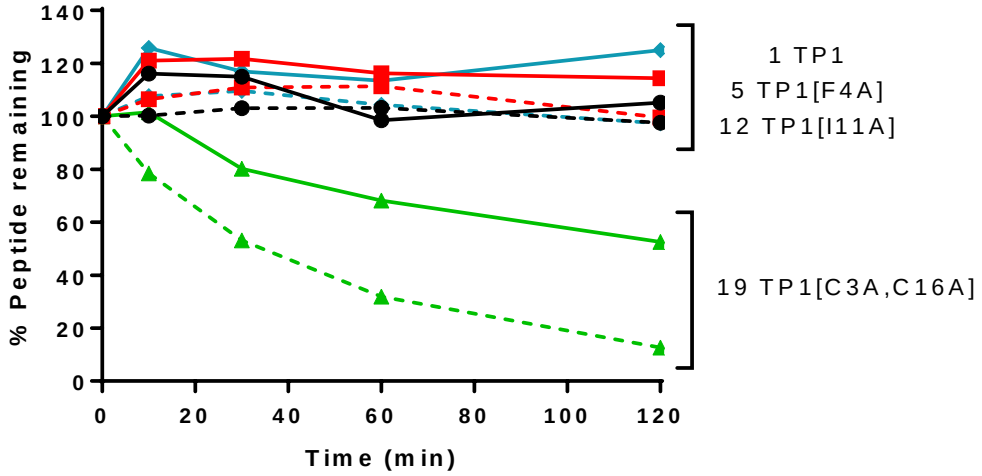

Figure 3-3 – Plasma stability of tachyplesin-1 and its analogs as monitored by LC-MS. Stability of **1** TP1(black), **5** TP1[F4A] (red), **12** TP1[I11A] (blue) and **19** TP1[C3A,C16A] (green) in mouse (dotted line) and human (full line) plasma over 120 min. Points represent the average of two replicates.

Structural characterization. To better understand the observed variation of peptide stability in plasma, the structural characterization of the four peptides was investigated. NMR spectroscopy was used to confirm the folding of the TP1 analogs and to compare their structures. The NMR assignment of **1** was comparable to the chemical shift assignment reported previously, BMRB 5486.[27] A comparison of the Hα chemical shifts of the four TP1 analogs (Figure 3-4A) illustrates that the structures are conserved for **1**, **5** and **12**. However, **19** shows very different Hα chemical shifts as compared to the other three analogs, demonstrating that its secondary structure is not conserved. In Figure 3-4B, secondary chemical shifts were calculated by comparing the experimentally observed Hα chemical shifts (HA) for each residue with the chemical shifts observed for the corresponding residues in random coil (RC) peptides[28], to compare **1** and its analogs in relation to sheet formation.

1, **5** and **12** show a similar pattern, with defined β-hairpin structure as compared to **19,** where the β-hairpin motif is lost due to the reduction of the length of the first β-sheet region, from Trp2-Cys7 to Arg5-Cys7. It is logical to attribute this to the loss of the disulfide bridge Cys3-Cys16, rendering the N- and C-terminal more flexible and reducing the size of the N-terminal β-sheet, changing the overall β-hairpin secondary structure motif.

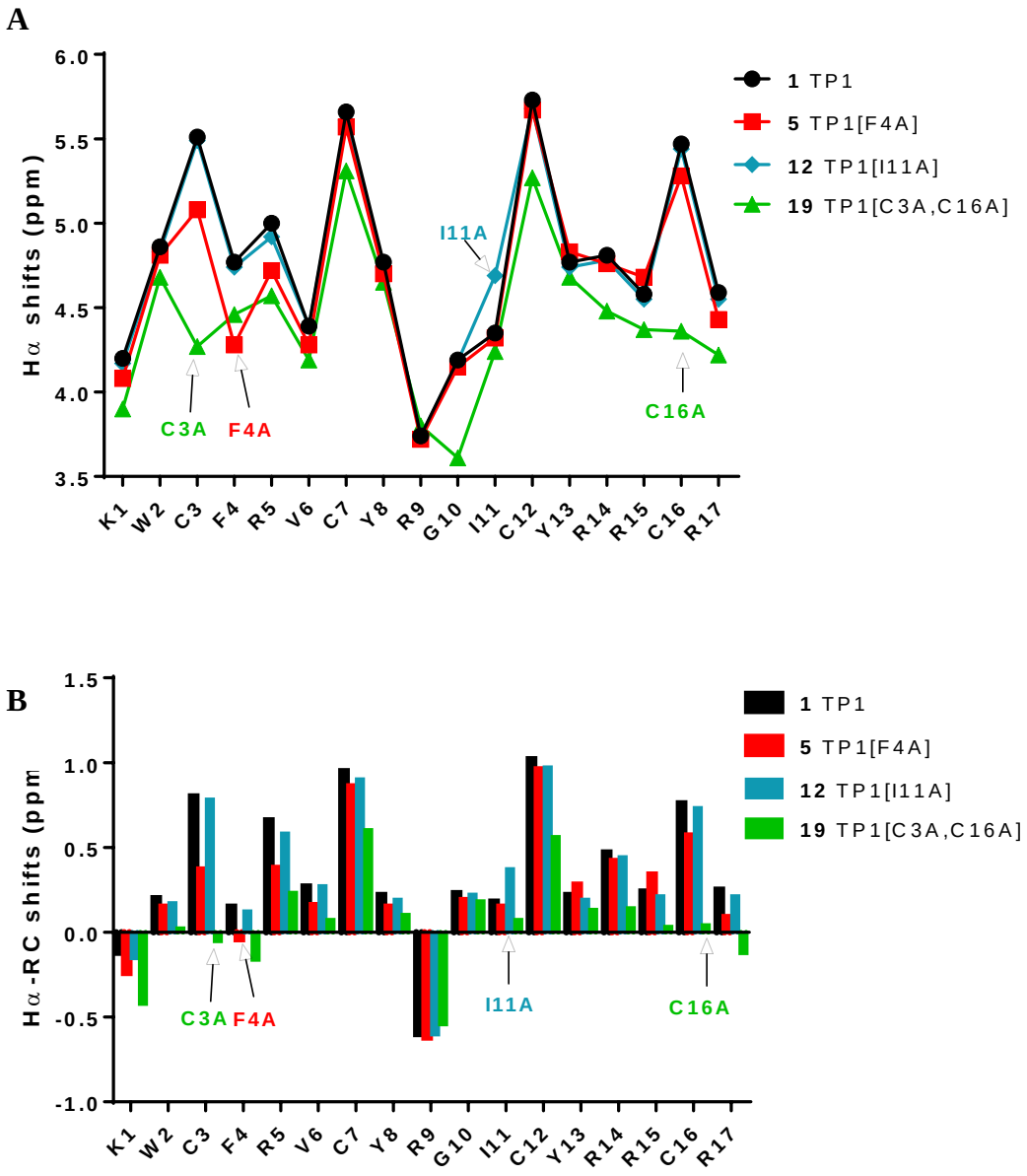

Figure 3-4 – TP1 and analogs chemical shifts. (A) Hα chemical shifts and (B) Hα secondary chemical shifts of TP1 **1** (black) and analogs **5** (red), **12** (blue) and **19** (green). Secondary chemical shifts were calculated by comparing the experimentally observed Hα chemical shifts (HA) for each residue with the chemical shifts observed for the corresponding residues in random coil (RC) peptides.[28] The sequence mutations are annotated.

3.4 Materials and methods

Materials. Tachyplesin-1 and tachyplesin-1 analogs were synthesized by Mimotopes Pty Ltd (Clayton, Australia) and WuXi AppTech (Shanghai, China) using Fmoc-based solid phase peptide synthesis and orthogonal Cys protection (Fmoc Cys(Acm)-OH for Cys3, Cys16, and Fmoc Cys(Trt)-OH for Cys7, Cys12); the first disulfide bridge was formed by air oxidation following cleavage from the resin, with iodine treatment generating the fully cyclized peptide that was purified by RP-HPLC to > 90% purity. Identity and purity were confirmed by LC-MS, HRMS and 1H and 2D TOCSY NMR (Figures S7.3-1 to S7.3-103). Proton chemical shifts of **1** (TP1) were comparable of previously reported tachyplesin-1 (PDB ID 1ma2 and BMRB 5486) and taken as reference for the identity confirmation of **1** analogs.[27] Synthetic lipids palmitoyloleoyl-phosphatidylcholine (POPC), palmitoyloleoyl-phosphatidylglycerol (POPG), palmitoyloleoyl-phosphatidylethanolamine (POPE) and cardiolipin were purchased from Avanti Polar Lipids (Alabaster, AL). All chemicals were used without further purification. The tachyplesin analogs used in this study do not contain any structures with potential PAINS (Pan Assay Interference Compounds) liabilities.

Antimicrobial activity. Both antibacterial and antifungal assays were performed by a broth micro-dilution plate based method as per CLSI guidelines for antimicrobial susceptibility testing.[29, 30] The assay was performed in Mueller Hinton Broth (MHB, Bacto laboratories, 211443) for antibacterial testing and Yeast Extract-Peptone Dextrose (YPD, Sigma-Aldrich, Y1500) for antifungal testing, and the Minimum Inhibitory Concentration (MIC) was determined as the lowest concentration of compound that prevented all visible microorganism growth after 18-24 h. Compounds were prepared at 0.64 mg/mL solution in water:DMSO (4:1).

For antimicrobial assays, the tested strains, Table S7.3-1, were cultured either in Luria broth (LB) (In Vitro Technologies, USB75852), Nutrient Broth (NB) (Becton Dickson, 234000) or MHB at 37 °C overnight. A sample of culture was then diluted 40-fold in fresh MHB and incubated at 37 °C for 1.5-2 h. The compounds were serially diluted two-fold across the wells of 96-well plates (Corning 3641, Non-binding Surface [NBS]), with compound concentrations ranging from 0.015 μg/mL to 64 μg/mL, plated in duplicate. The resultant mid-log phase cultures were diluted to the final concentration of 1×10^6 CFU/mL, then 50 μL was added to each well of the compound-containing plates giving a final compound concentration range of 0.008 μg/mL to 32 μg/mL and a cell density of $5x10^5$ CFU/mL. All plates were then covered and incubated at 37 °C for 18 h. Resazurin was added at 0.001% final concentration to each well and incubated for 2 h before MICs were read by eye. Resazurin was added to assist MIC determination as small spindle tissue or precipitate was present in otherwise clear wells.

For the antifungal assay, fungi strains, Table S7.3-1, were cultured for 3 days on YPD agar at 30 °C. A yeast suspension of $1x10^6$ to $5x10^6$ CFU/mL was prepared from five colonies. These stock suspensions were diluted with Yeast Nitrogen Base (YNB) (Becton Dickinson, 233520) broth to a final concentration of 2.5×10^3 CFU/mL. The compounds were serially diluted two-fold across the wells of 96-well plates (Corning 3641, Non-binding Surface [NBS]), with compound concentrations ranging from 0.015 μg/mL to 64 μg/mL and final volumes of 50 μL, plated in duplicate. Then, 50 μL of the fungi suspension that was previously prepared in YNB broth to the final concentration of 2.5×10^3 CFU/mL, was added to each well of the compound-containing plates, giving a final compound concentration range of 0.008 μg/mL to 32 μg/mL. Plates were covered and incubated at 35 °C for 24 h. *C. albicans* MICs were determined by measuring the absorbance at OD_{530}. For *C. neoformans* resazurin was added at 0.006% final concentration to each well and incubated for a further 3 h before MICs were determined by measuring the absorbance at $OD_{570\text{-}600}$.

Hemolytic assay. The ability of the peptides to hemolyze human red blood cells was determined by a previously reported method.[31] Human red blood cells were separated from serum and washed in phosphate-buffered saline (PBS, pH 7.4) with 4–5 times centrifugation at 4000 rpm. Erythrocytes were then resuspended in phosphate-buffered saline as a 0.25% (v/v) solution. Stock solutions (300 μM) of compounds were prepared. Two-fold serial dilutions were prepared yielding eight solutions in total, which were aliquoted (20 μL) into a 96-well plate (NUNC 96 wells polypropylene plates round bottom, Sigma Aldrich P6866). The erythrocyte solution (100 μL) was dispensed into each well and incubated with diluted peptide solution at 37 °C for 1 h. Triton X-100 solution (1%, v/v, 20 μL) was used as a positive control to represent 100% cell lysis, and PBS solution (20 μL) was used as a negative control (spontaneous lysis after 1 h incubation). The 96-well plate was centrifuged to pellet intact red blood cells, and the supernatant of each well was collected in a fresh plate (NUNC 96 wells polypropylene plates flat bottom, Sigma Aldrich P7366) and measured by visual absorption spectroscopy at 415 nm. The percentage of hemolysis was calculated according to the following equation:

$$Hemolysis\ (\%) = \left[\frac{OD_{415}(sample) - OD_{415}(zero\ lysis)}{OD_{415}(100\%\ lysis) - OD_{415}(zero\ lysis)}\right] x100\%$$

All peptide solutions were assayed in triplicate.

Cytotoxicity. Cytotoxicity to HEK293 cells was determined using the resazurin assay.[32,33] In brief, HEK293 cells were seeded as 4000 cells/well in black-wall, clear-bottom 384-well plates (Corning, Australia) and incubated for 24 h at 37 °C, 5% CO_2. Compounds were then added into each well. After 24 h incubation, 5 μM resazurin was added per well and incubated at 37 °C for 2 h. Fluorescence

intensity was then read using a Polarstar Omega with excitation/emission 560/590. The data were then analyzed using GraphPad Prism 6 software. CC_{50} values were calculated using the following equation: Percentage Viability = ($FI_{TEST} – FI_{Negative}$/$FI_{UNTREATED} – FI_{Negative}$)*100.

Surface Plasmon Resonance. The binding affinity of **1** and its analogs for model membranes composed of POPC/Cholesterol (4:1) and POPE/POPG/cardiolipin (15:4:1) were compared using SPR. Solutions were freshly prepared and filtered (0.22 µM pore size). L1 sensor chip and BIAcore 3000 system (Biacore, GE Healthcare) were used. Small unilamellar vesicles (diameter, 50 nm) were prepared by freeze-thaw fracturing and sized by extrusion. Vesicle suspensions were deposited on an L1 chip over 40 min at a flow rate of 2 µL/min to allow the vesicles to bind, fuse and form a stable lipid bilayer. The association of the peptide sample to the lipid bilayer was evaluated by injection for 240 s at flow rate of 5 µL/min and the dissociation was followed for 600 s at the same flow rate. The L1 chip was regenerated after each injection cycle, by injection of 3-[(3-cholamidopropyl)dimethylammonio]-1-propanesulfonate (CHAPS) (5 µL/min, 60 s), followed by an injection of 10 mM sodium hydroxide in 20 % methanol (w/w) (50 µL/min, 60 s) and to finish an injection of 10 mM sodium hydroxide (50 µL/min, 36 s) buffer. All measurements were conducted at 25 °C. 10 mM HEPES buffer pH7.4 containing 150 mM NaCl (to mimic the physiological conditions) was used as running buffer and to prepare samples and lipid vesicles.[34,35] The peptide samples were prepared at 7 different concentrations, starting from 64 to 1 µg/mL following 2-fold dilution steps. The lipid deposited onto the chip surface is dependent on the lipid mixture, therefore, the response units were converted into peptide to lipid ratio (mol/mol).

Plasma stability. Test compound (final concentration 2 µM) was combined with pre-warmed CD-1 mouse or human plasma at 37 °C (100 µL volume). At each time point (t = 0, 15, 30, 60 and 120 min), 100 µL of 4% H_3PO_4/H_2O was added and the reaction was quenched with 600 µL of cold stop solution (200 ng/mL tolbutamide plus 20 ng/mL buspirone in 50% ACN/MeOH). Upon centrifugation at 4,000 g for 10 min, the clear supernatants (100 µL) were transferred to a 96-well plate and mixed with 100 µL of ultra-pure water. The samples were shaken at 800 rpm for 10 min before being analysed by LC-MS-MS. The percentage of remaining parent compound at each time interval relative to the t = 0 min sample is calculated from peak area ratios in relation to the internal standard. All samples were run in duplicate with propantheline bromide as a positive control and tolbutamide as internal standard.

NMR characterization. 1H and 2D TOCSY NMR were acquired on a Bruker Avance III spectrometer equipped with a cryogenically cooled triple resonance probed operating system at a normal ^1H frequency of 600 MHz at 298 K. Water suppression was performed via excitation sculpting. Secondary chemical shifts were calculated by comparing the experimentally observed Hα

chemical shifts (HA) for each residue with the chemical shifts observed for the corresponding residues in random coil (RC) peptides.[28] The NMR assignment of **1** TP1 was compared to the chemical shifts reported previously, BMRB 5486.[27]

3.5 Conclusion

This work presents a structure-function relationship study of tachyplesin-1 by a systematic amino acid replacement strategy with characterization of the resultant antimicrobial, cytotoxicity and hemolytic activity. We identified three modified peptides: **5** (TP1[F4A]), **12** (TP1[I11A]) and **19** (TP1[C3A,C16A]), that possessed substantially improved therapeutic indexes (26- to 64-fold) over the progenitor. With high potency against broad-spectrum microbes and considerably less hemolytic toxicity, these compounds may be considered as promising hit compounds for further development towards new treatments for infections caused by Gram-negative and Gram-positive bacterial pathogens, as well as potential fungal infections. Structural studies and preliminary ADME testing support further investigations of two of the three promising novel antimicrobial peptides, as **5** and **12** not only conserve the β-hairpin secondary structure motif but are highly stable in mouse and human plasma. Additional studies examining bioavailability, pharmacokinetics, toxicity, mutagenicity and *in vivo* efficacy of **5** and **12** are required to further validate these interesting novel antibiotics.

3.6 Ancillary information

Supporting Information. *Bacterial strain descriptions and QC data of each compound by HRMS, LC–MS and, 1H and 2D NMR. This information is available free of charge via the Internet at http://pubs.acs.org/.*

Abbreviations Used: *TP1, tachyplesin-1; ADME, Adsorption Distribution Metabolism Elimination; AMP, Antimicrobial peptide; GRAVY, grand average of hydropathicity index; MIC, Minimum inhibitory concentration; MM, Median of the peptide MICs against all bacteria and fungi tested; MHC, Minimum hemolytic concentration; ATI, activity/toxicity index; ATCC, American Type Culture Collection; G-ve, Gram-negative; G+ve, Gram-positive; HEK293, human embryonic kidney 293; RBC, Red Blood Cell; RC, Random Coil.*

Corresponding Author Information*: Matthew A Cooper, Institute for Molecular Bioscience, University of Queensland, Brisbane, Australia. E-mail:* m.cooper@uq.edu.au*, Fax +61-7-3346-2090, Phone +61-7-3346-2044*

Author contribution: *IAE, AGE, MAC and MATB conceived the study. IAE, AGE and AMK performed the experiments and analysed the data. IAE wrote the paper with input from all authors. MAC oversaw the research program.*

Acknowledgment: *This project is supported by NHMRC project grant APP1106590. MAC is a NHMRC principle research fellow (APP1059354). IAE is supported by an Australian Postgraduate Award (APA) PhD scholarship. AGE, AMK and MATB are supported in part by Wellcome Trust Strategic Grant WT1104797/Z/14/Z. MAC currently holds a fractional Professorial Research Fellow appointment at the University of Queensland with his remaining time as CEO of Inflazome Ltd. a company headquartered in Dublin, Ireland that is developing drugs to address clinical unmet needs in inflammatory disease by targeting the inflammasome. We thank Geraldine Kaeslin and Janet Reid for technical contribution in performing the cytotoxicity assays. We thank Ilias Karaiskos and Helen Giamarellou (6th Dept. of Internal Medicine, Hygeia General Hospital, Athens, Greece) and Roger L. Nation (Institute of Pharmaceutical Sciences, Monash University, Australia) for providing the Gram-negative clinical isolates for antimicrobial testing.*

3.7 References

1. Butler, M. S., Blaskovich, M. A. T., and Cooper, M. A. (2016) Antibiotics in the clinical pipeline at the end of 2015, *J. Antibiot.* DOI:10.1038/ja.2016.72
2. Nakamura, T., Furunaka, H., Miyata, T., Tokunaga, F., Muta, T., Iwanaga, S., Niwa, M., Takao, T., and Shimonishi, Y. (1988) Tachyplesin, a class of antimicrobial peptide from the hemocytes of the horseshoe crab (Tachypleus tridentatus). Isolation and chemical structure, *J. Biol. Chem. 263*, 16709-16713.
3. Miyata, T., Tokunaga, F., Yoneya, T., Yoshikawa, K., Iwanaga, S., Niwa, M., Takao, T., and Shimonishi, Y. (1989) Antimicrobial peptides, isolated from horseshoe crab hemocytes, tachyplesin II, and polyphemusins I and II: chemical structures and biological activity, *J. Biochem. 106*, 663-668.
4. Kawano, K., Yoneya, T., Miyata, T., Yoshikawa, K., Tokunaga, F., Terada, Y., and Iwanaga, S. (1990) Antimicrobial peptide, tachyplesin I, isolated from hemocytes of the horseshoe crab (Tachypleus tridentatus). NMR determination of the beta-sheet structure, *J. Biol. Chem. 265*, 15365-15367.
5. Kushibiki, T., Kamiya, M., Aizawa, T., Kumaki, Y., Kikukawa, T., Mizuguchi, M., Demura, M., Kawabata, S., and Kawano, K. (2014) Interaction between tachyplesin I, an antimicrobial peptide derived from horseshoe crab, and lipopolysaccharide, *Biochim. Biophys. Acta 1844*, 527-534. DOI:10.1016/j.bbapap.2013.12.017
6. J. Hong, J. G. D., W.T. Guan, G. Jin, Zh.L. Huang, L.J. Zhang, J. Zh. Dang and Y. Zhang. (2012) Tachyplesin I Induce Drug Resistance in Bacteria in vitro., *J. Anim. Vet. Adv. 11*, 939-945. DOI: 10.3923/javaa.2012.939.945
7. Hong, J., Hu, J., and Ke, F. (2016) Experimental Induction of Bacterial Resistance to the Antimicrobial Peptide Tachyplesin I and Investigation of the Resistance Mechanisms, *Antimicrob. Agents Chemother. 60*, 6067-6075. DOI:10.1128/AAC.00640-16

8. Hong, J., Guan, W., Jin, G., Zhao, H., Jiang, X., and Dai, J. (2015) Mechanism of tachyplesin I injury to bacterial membranes and intracellular enzymes, determined by laser confocal scanning microscopy and flow cytometry, *Microbiol. Res. 170*, 69-77. DOI:10.1016/j.micres.2014.08.012
9. Tamamura, H., Ikoma, R., Niwa, M., Funakoshi, S., Murakami, T., and Fujii, N. (1993) Antimicrobial activity and conformation of tachyplesin I and its analogs, *Chem. Pharm. Bull. 41*, 978-980.
10. Rao, A. G. (1999) Conformation and antimicrobial activity of linear derivatives of tachyplesin lacking disulfide bonds, *Arch. Biochem. Biophys. 361*, 127-134. DOI:10.1006/abbi.1998.0962
11. Tam, J. P., Lu, Y. A., and Yang, J. L. (2000) Marked increase in membranolytic selectivity of novel cyclic tachyplesins constrained with an antiparallel two-beta strand cystine knot framework, *Biochem. Biophys. Res. Commun. 267*, 783-790. DOI:10.1006/bbrc.1999.2035
12. Saravanan, R., Mohanram, H., Joshi, M., Domadia, P. N., Torres, J., Ruedl, C., and Bhattacharjya, S. (2012) Structure, activity and interactions of the cysteine deleted analog of tachyplesin-1 with lipopolysaccharide micelle: Mechanistic insights into outer-membrane permeabilization and endotoxin neutralization, *Biochim. Biophys. Acta 1818*, 1613-1624. DOI:10.1016/j.bbamem.2012.03.015
13. Holland-Nell, K., and Meldal, M. (2011) Maintaining biological activity by using triazoles as disulfide bond mimetics, *Angew. Chem. 50*, 5204-5206. DOI:10.1002/anie.201005846
14. Edwards, I. A., Elliott, A. G., Kavanagh, A. M., Zuegg, J., Blaskovich, M. A. T. and Cooper, M. A. (2016) Contribution of Amphipathicity and Hydrophobicity to the Antimicrobial Activity and Cytotoxicity of β-Hairpin Peptides, *ACS Infect. Dis. 2*, 442-450. DOI:10.1021/acsinfecdis.6b00045
15. Brogden, N. K., and Brogden, K. A. (2011) Will new generations of modified antimicrobial peptides improve their potential as pharmaceuticals?, *Int. J. Antimicrob. Agents 38*, 217-225. DOI:10.1016/j.ijantimicag.2011.05.004
16. Chen, Y., Mant, C. T., Farmer, S. W., Hancock, R. E., Vasil, M. L., and Hodges, R. S. (2005) Rational design of alpha-helical antimicrobial peptides with enhanced activities and specificity/therapeutic index, *J. Biol. Chem. 280*, 12316-12329. DOI:10.1074/jbc.M413406200
17. Artimo, P., Jonnalagedda, M., Arnold, K., Baratin, D., Csardi, G., de Castro, E., Duvaud, S., Flegel, V., Fortier, A., Gasteiger, E., Grosdidier, A., Hernandez, C., Ioannidis, V., Kuznetsov, D., Liechti, R., Moretti, S., Mostaguir, K., Redaschi, N., Rossier, G., Xenarios, I., and Stockinger, H. (2012) ExPASy: SIB bioinformatics resource portal, *Nucleic Acids Res. 40*, W597-603. DOI:10.1093/nar/gks400
18. Nagano, N., Ota, M., and Nishikawa, K. (1999) Strong hydrophobic nature of cysteine residues in proteins, *FEBS Lett. 458*, 69-71.
19. Panteleev, P. V., and Ovchinnikova, T. V. (2015) Improved strategy for recombinant production and purification of antimicrobial peptide tachyplesin I and its analogs with high cell selectivity, *Biotechnol. Appl. Biochem.* DOI:DOI: 10.1002/bab.1456
20. Wood, S. J., Park, Y. A., Kanneganti, N. P., Mukkisa, H.R., Crisman, L. L., Davis, S. E., Vandenbosch, J.L., Scaglione, J. B. and Heyl, D. L. (2014) Modified Cysteine-Deleted Tachyplesin (CDT) Analogs as Linear Antimicrobial Peptides: Influence of Chain Length, Positive Charge, and Hydrophobicity on Antimicrobial and Hemolytic Activity, *Int. J. Pept. Res. Ther. 20*, 519-530. DOI:10.1007/s10989-014-9419-7
21. Soblosky, L., Ramamoorthy, A., and Chen, Z. (2015) Membrane interaction of antimicrobial peptides using E-coli lipid extract as model bacterial cell membranes and SFG spectroscopy, *Chem. Phys. Lipids 187*, 20-33. DOI:10.1016/j.chemphyslip.2015.02.003
22. Cooper, G. (2000) *The Cell: A Molecular Approach*, 2nd ed., Sinauer Associates.
23. Matsuzaki, K. (2009) Control of cell selectivity of antimicrobial peptides, *Biochim. Biophys. Acta 1788*, 1687-1692. DOI:10.1016/j.bbamem.2008.09.013

24. Virtanen, J. A., Cheng, K. H., and Somerharju, P. (1998) Phospholipid composition of the mammalian red cell membrane can be rationalized by a superlattice model, *Proc. Natl. Acad. Sci. U. S. A. 95*, 4964-4969.
25. Salvioli, G., Rioli, G., Lugli, R., and Salati, R. (1978) Membrane lipid composition of red blood cells in liver disease: regression of spur cell anaemia after infusion of polyunsaturated phosphatidylcholine, *Gut 19*, 844-850.
26. Imura, Y., Nishida, M., Ogawa, Y., Takakura, Y., and Matsuzaki, K. (2007) Action mechanism of tachyplesin I and effects of PEGylation, *Biochim. Biophys. Acta 1768*, 1160-1169. DOI:10.1016/j.bbamem.2007.01.005
27. Laederach, A., Andreotti, A. H., and Fulton, D. B. (2002) Solution and micelle-bound structures of tachyplesin I and its active aromatic linear derivatives, *Biochemistry 41*, 12359-12368.
28. Wishart, D. S., Bigam, C. G., Holm, A., Hodges, R. S., and Sykes, B. D. (1995) (1)H, (13)C and (15)N random coil NMR chemical shifts of the common amino acids. I. Investigations of nearest-neighbor effects, *J. Biomol. NMR 5*, 332. DOI:10.1007/BF00211764
29. Cockerill, F. R., Wikler, M. A. (2012) *Methods for dilution Antimicrobial susceptibility tests for bacteria that grow aerobically; Approved standard*, Vol. 32, 9th ed., Clinical and laboratory standards institute, Wayne, PA.
30. Rex, J. H., Alexander, B. D. (2008) *Reference Method for Broth Dilution Antifungal Susceptibility Testing of Yeasts; Approved Standard*, Vol. 22, 3rd ed., Clinical and laboratory standards institute, Wayne , PA.
31. Ravipati, A. S., Henriques, S. T., Poth, A. G., Kaas, Q., Wang, C. K., Colgrave, M. L., and Craik, D. J. (2015) Lysine-rich Cyclotides: A New Subclass of Circular Knotted Proteins from Violaceae, *ACS Chem. Biol. 10*, 2491-2500. DOI:10.1021/acschembio.5b00454
32. McMillian, M. K., Li, L., Parker, J. B., Patel, L., Zhong, Z., Gunnett, J. W., Powers, W. J., and Johnson, M. D. (2002) An improved resazurin-based cytotoxicity assay for hepatic cells, *Cell Biol. Toxicol. 18*, 157-173.
33. O'Brien, J., Wilson, I., Orton, T., and Pognan, F. (2000) Investigation of the Alamar Blue (resazurin) fluorescent dye for the assessment of mammalian cell cytotoxicity, *Eur. J. Biochem. 267*, 5421-5426. DOI:10.1046/j.1432-1327.2000.01606.x
34. Henriques, S. T., Huang, Y. H., Rosengren, K. J., Franquelim, H. G., Carvalho, F. A., Johnson, A., Sonza, S., Tachedjian, G., Castanho, M. A., Daly, N. L., and Craik, D. J. (2011) Decoding the membrane activity of the cyclotide kalata B1: the importance of phosphatidylethanolamine phospholipids and lipid organization on hemolytic and anti-HIV activities, *J. Biol. Chem. 286*, 24231-24241. DOI:10.1074/jbc.M111.253393
35. Craik, D. J., Henriques, S. T., Mylne, J. S., and Wang, C. K. (2012) Cyclotide isolation and characterization, *Methods Enzymol. 516*, 37-62. DOI:10.1016/B978-0-12-394291-3.00024-1

Chapter 4 - The antimicrobial activity of AA139 reveals dual mode of action

4.1 Introduction

The overuse and misuse of antibiotics over decades has led to a dramatic increase in the rate of bacterial resistance to current antibiotics. We have, in the last few years, reached a worldwide state of emergency, where simple infections can cause death. The World Health Organization launched a multi-year campaign with the theme “Antibiotics: Handle with care” in November 2015 to tackle the concern of antibiotic resistance. The discovery of new drugs is thus vital for the replacement of obsolete antibiotics.[1]

Antimicrobial peptides (AMPs) are ubiquitous in nature, being part of the innate immune defense system of microorganisms, plants and animals. AMPs are generally small, cationic and amphipathic, ideally adapted for the protection of their host against pathogenic microorganisms. To date over 2,000 AMPs have been reported from eukaryotes (http://aps.unmc.edu/AP/main.php), however their broad range antimicrobial activity is not enough for entry into the clinical pipeline as they often also exhibit mammalian cell toxicity.[2]

Arenicin peptides, originated from a lugworm, *Arenicola marina*, were discovered about a decade ago by Ovchinnikova et al[3]. Arenicin-1 and arenicin-2, both β-hairpin AMPs with one disulfide bond have been the focus of attention of many researches.[4,5] The antimicrobial mode of action of arenicin-1 and -2 is considered to involve binding to and permeabilization of the bacterial membrane.[6] More recently, Adenium Biotech Ltd discovered a third member of the arenicin family, arenicin-3 (GFCWYVCVYRNGVRVCYRRCN), a 21 amino acid β-hairpin AMP constrained by two disulfide bonds.[7] Arenicin-3 was found to be very potent against a broad range of microbial pathogens however the drawback for further clinical study was its toxicity towards mammalian cells.[2] AA139, an arenicin-3 analog (GFCWYVCARRNGARVCYRRCN) retains broad range antimicrobial activity and concomitantly displays reduced mammalian cell toxicity, rendering it the current lead candidate under advanced preclinical development by Adenium Biotech Ltd.

This study focuses on the comparison between arenicin-3 and its synthetic analog, AA139, investigating their mode of action and aiming to understand how simple amino acid mutations reformed arenicin-3 into a suitable candidate for clinical development. To do so, we divided our investigation into three parts. First, we characterized both arenicin peptides, evaluating their physicochemical properties and elucidating their 3D solution structures in solution using NMR. We then focused on their mode of action using lipid bilayer model membranes, investigating their membrane binding affinity, their ability to cause vesicle leakage and aggregation and their secondary structure modification using circular dichroism spectroscopy. We then evaluated the potential of arenicin peptides to permeabilize the cytoplasmic membrane upon interaction with *E. coli* ATCC25922 cells using fluorescence emission assay followed by FACS cytometry.

4.2 Results and discussion

Physicochemical parameters. Arenicin peptides are β-hairpin AMPs, cationic and amphipathic, allowing them to interact with the cell membrane. Their hydrophobic side is formed by the residue predominantly situated toward the N-terminal part of the molecule and the lipophilic side toward the C-terminal end. The AA139 mutations of two valine residues to less hydrophobic alanine, and tyrosine to less hydrophobic arginine lowers the overall hydrophobicity of AA139 as compared to arenicin-3. Moreover, the charge of the entire molecule has been increased by one positive charge from the additional Arginine (Arg^9) in AA139. Thus the combination of the increase in the overall charge and decrease of hydrophobicity leads to an increase in the amphipathic moment of AA139 (Table 4-1).[2]

Table 4-1 – Sequence, molecular weight (MW), number of charges, mean hydrophobicity and amphipathic moment of arenicin-3 and AA139 based on the normalized consensus scale value of Eisenberg_M.

Peptide	Sequence	MW (g/mol)	Charge	Hydrophobicity	Amphipathic moment
arenicin-3	GFCWYVCVYRNGVRVCYRRCN	2611.1	+4	-0.11	+0.44
AA139	GFCWYVCARRNGARVCYRRCN	2548.1	+5	-0.28	-0.10

Mapping of the electrostatic and molecular hydrophobicity surface of arenicin-3 and AA139 produced representations that did not show distinct faces, with charges and hydrophobic residues being evenly distributed along the peptide backbone. Therefore, these results are not shown.

The antimicrobial activity of AA139 has high selectivity for bacterial cells. The arenicin peptides were tested for their antimicrobial activity against G-ve and G+ve bacteria, Table 4-2. Across all pathogenic strains tested, AA139 displayed a 2- to 4-fold increase in antimicrobial activity as compared to arenicin-3. The toxicity of arenicin peptides against HEK293 cells and their hemolytic activity were also tested, Table 4-2. The hemolytic activity, shown as $HC_{20,}$ reflects the concentration to induce 20% hemolysis. AA139 required 15-fold higher concentration to induce 20% hemolysis than arenicin-3. The cytotoxicity was assessed against HEK293 (kidney) cells at 1% serum concentration. Arenicin-3 displayed at least 3-fold more toxicity than AA139. These results highlight the increased therapeutic potential for AA139 as compared to arenicin-3 due to its improved antimicrobial activity and concomitantly reduced mammalian cell interactions.

Table 4-2 - Antimicrobial activity and toxicity of arenicin peptides.

Peptide	**MIC (µg/mL)[a]**						**HC_{20} (µg/mL)**	**CC_{50} (µg/mL)**
	E. coli ATCC 25922	*K. pneumoniae* ATCC 13883	*A. baumannii* ATCC 19606	*P. aeruginosa* ATCC 27853	*B. subtilis* ATCC 6051	*S. aureus* ATCC 43300	RBC	HEK293
arenicin-3	0.5	1	0.5	1	8	>32	1.2 ± 1	104.6 ± 1.8
AA139	0.125	0.25	0.125	0.5	4	16	18.8 ± 1.5	>300

a. Assay performed as n = 4.

NMR. We determined the NMR solution structures of arenicin-3 and AA139, PDB 5V0Y - BMRB 30259 and PDB 5V11 – BMRB 30260, respectively (Figure 4-1 and Table 4-3). Chemical shifts of the protons in both arenicin peptides were measured from 2D $^{1}H–^{1}H$ TOCSY and NOESY NMR spectra. Secondary Hα shifts (Figure 4-2) are reported as the difference between the observed chemical shift of each α-proton and its respective random coil shift, this provides information about the secondary structure of the peptide.[8] Residues with secondary Hα shifts larger than ± 0.1 ppm are generally considered to correspond to structured regions of a peptide, with positive Hα shifts indicating β-sheet secondary structure and negative Hα shifts indicating turns or helices. As shown by the secondary Hα shifts in Figure 4-2, arenicin peptides are composed of two β-strands and a turn forming a β-hairpin structure. A summary of the NMR data obtained for arenicin-3 and AA139 in aqueous solution is shown in Figure S4-5 and Figure S4-6, respectively. The peptide structures are stabilized by two disulfide bridges Cys^{3}-Cys^{20} and Cys^{7}-Cys^{16}. The two β-strands cover residues Cys^{3}-Arg^{10} and Arg^{13}-Cys^{20}. The β-strands are intervened by a type I' β-turn (Asn^{11}/Gly^{12}) forming slightly twisted anti-parallel β-strands in the β-hairpin structure. The distortion created by the right-handed twist of the two-stranded β-sheet offers the possibility for the molecule to create an amphipathic environment where the hydrophobic side of the β-sheet is shielded from contact with the polar solvent.

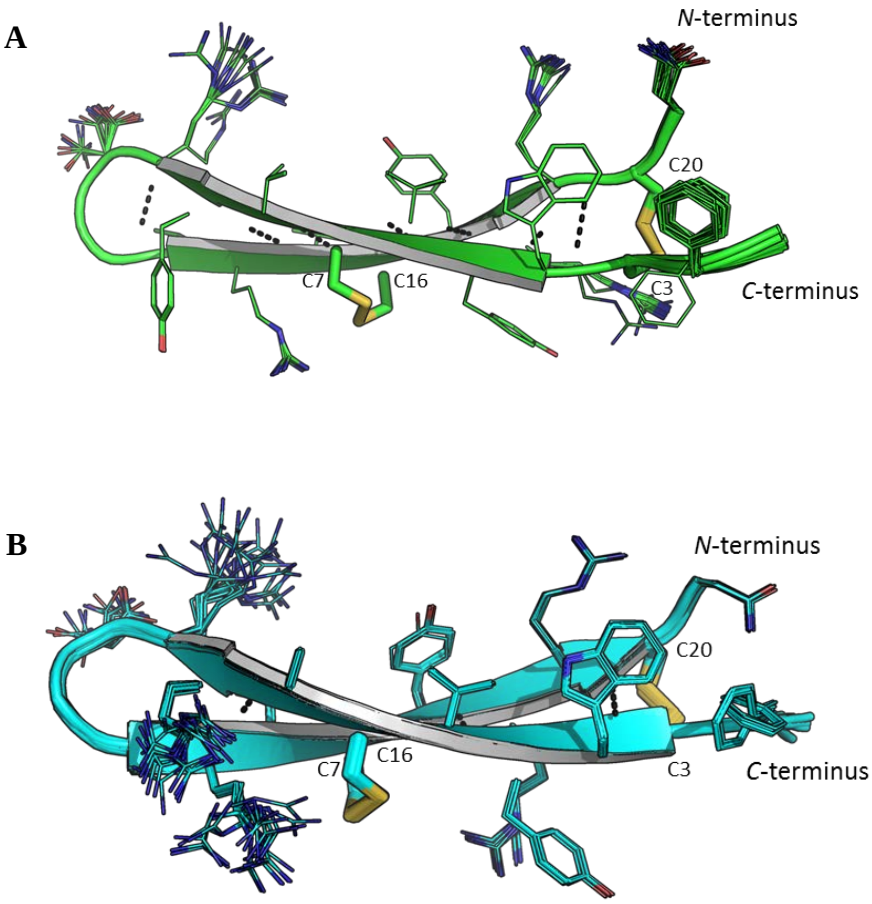

Figure 4-1 – 3-Dimensional NMR solution structures of (A) arenicin-3 (green) and (B) AA139 (cyan). Structures are displayed in cartoon form showing the classic ß-hairpin assembly created by anti-parallel ß-sheets and two stabilizing disulfide bonds (yellow) across the sheets, key residues labelled for orientation and the *N*- and *C*-terminus. Images created using PyMol.

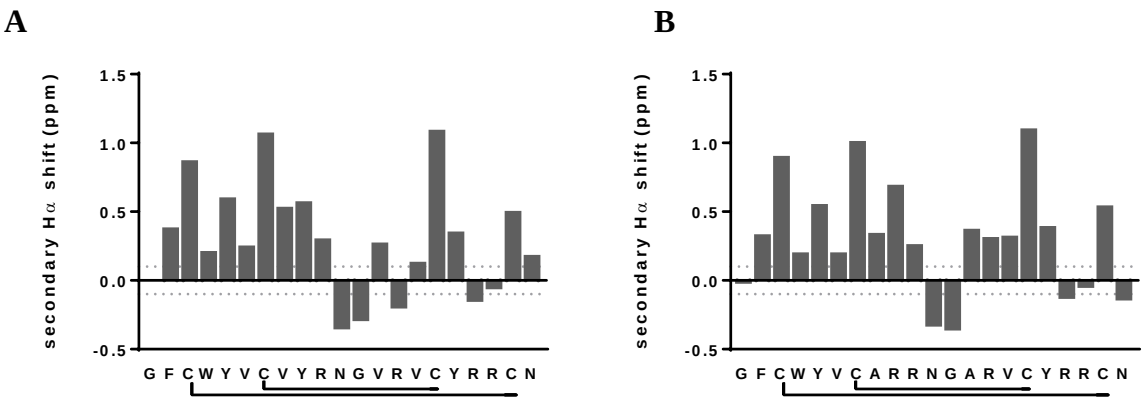

Figure 4-2 - Secondary Hα shifts (variation from random coil) for (A) arenicin-3 and (B) AA139.

Table 4-3 - Statistical analysis of the NMR structures of arenicin-3 and AA139[1]. All statistics are given as mean ± S.D. a. Only structurally relevant restraints, as defined by CYANA, are included. b. Only hydrogen-deuterium exchange were used to define the H-bond restraints. c. As reported by Molprobity (http://molprobity.biochem.duke.edu). d. Defined as number of steric overlaps >0.4 Å per thousand atoms.

	arenicin-3	**AA139**
Experimental restraints[a]		
Interproton distance restraints		
Intraresidue	102	66
Sequential	125	114
Medium range (i–j < 5)	46	45
Long range (i–j > 5[3])	108	108
Dihedral-angle restraints (f, y, c_1)	65	65
Number of H-bond[b]	7	4
Total number of restraints per residue	21.6	19.1
R.m.s. deviation from mean coordinate structure (Å)		
Backbone atoms (residues 1–21)	0.11	0.18
All heavy atoms (residues 1-21)	0.61	0.57
Stereochemical quality[c]		
Residues in most favoured Ramachandran region (%)	100.0 ± 0.0	100.0 ± 0.0
Ramachandran outliers (%)	0 ± 0	0 ± 0
Unfavourable sidechain rotamers (%)	1.3 ± 2.4	16.2 ± 2.6
Clashscore, all atoms[d]	3.06 ± 0.6	0 ± 0
Overall MolProbity score	1.23 ± 0.24 (98^{th} percentile)	1.41 ± 0.06 (96^{th} percentile)

The 3D solution structure supplemented by the H-bond experiments, hydrogen-deuterium exchange (Table S4-2) and amide temperature coefficient (Table S4-3), suggests AA139 to be a more flexible structure than arenicin-3, Figure 4-1.

Despite the higher structural order of arenicin-3 compared to AA139, the activity and toxicity data demonstrate that AA139 is the better candidate for drug development. This data would suggest that the increased flexibility of AA139 may play a role in the improved bacterial toxicity and reduced mammalian cytotoxicity observed. A possible mechanism would be that the flexibility of AA139 allows it to more easily rearrange its structure into an active conformation upon interaction with the bacterial cell membrane.

Arenicin peptides bind to lipid model membranes. The membrane binding affinity of arenicin peptides was followed by SPR using model membranes deposited onto an L1 Chip (Figure 4-3). To mimic the anionic surface of bacterial cell membranes, negatively charged systems (POPC/POPG (1:1 molar ratio) or POPC/POPG (4:1)) were used, and to mimic the neutral surface of mammalian cell membranes, bilayers composed of POPC were used. Membrane-binding studies show that both peptides, have a preference (about 2- to 3-fold) for negatively-charged model membranes

(POPC/POPG), compared to zwitterionic membranes (POPC). This is consistent with the basic nature of these peptides.

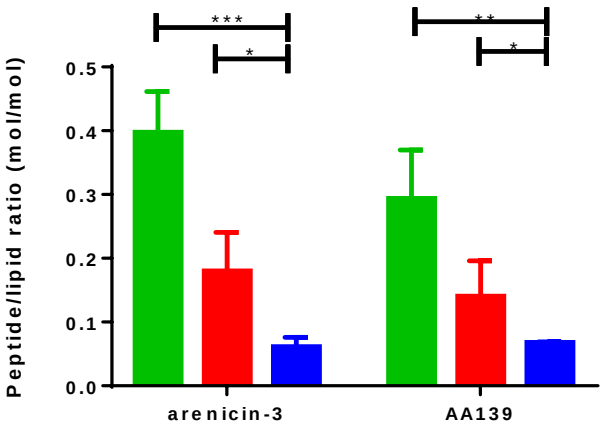

Figure 4-3 - Arenicin-3 and AA139, 25 µM (~64 µg/mL), membrane binding affinity followed by SPR using model membranes composed of POPC/POPG (1:1) (green bar), POPC/POPG (4:1) (red) or POPC (blue). The error bars represent the standard deviation of triplicates. * = $p \leq 0.05$, ** = $p \leq 0.01$, *** = $p \leq 0.0001$.

Both peptides are able to bind to different lipid vesicle compositions, with lower affinity towards the neutral POPC bilayers, compared to the negatively-charged membranes.

Arenicin peptides permeabilize negatively charged lipid model membranes.

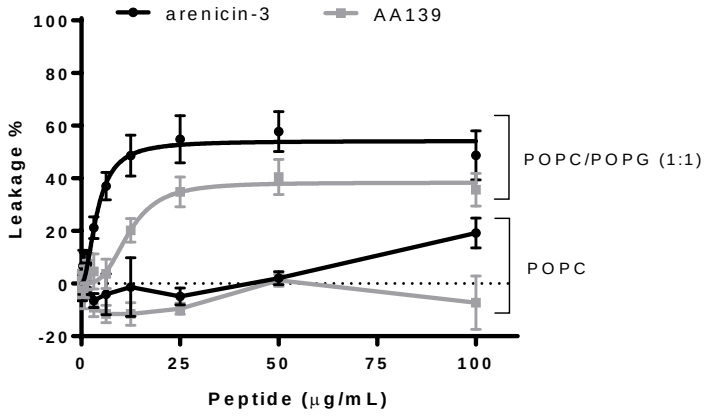

Figure 4-4 - Leakage from POPC and POPC/POPG (1:1) vesicles (lipid concentration at 5 µM) induced by arenicin-3 (black dots) and AA139 (grey squares). 0.1% Triton-X100 was used to establish 100% of leakage and buffer was used as blank to establish 0% leakage.

LUVs (POPC and POPC/POPG (1:1)) (diameter, 100 nm) loaded with carboxyfluorescein (CF) were incubated with a series of 2-fold dilution concentration of arenicin peptides. The vesicle leakage assay[9] evaluated the content leakage from LUVs by CF fluorescence emission quenching induced by arenicin-3 and AA139, Figure 4-4. The results showed that both peptides did not induce leakage of POPC vesicles, over the concentration range tested. However, arenicin peptides induced leakage of POPC/POPG (1:1) vesicles. The maximum leakage was 48% and 35% for arenicin-3 and AA139, respectively, at 100 μg/mL (peptide/lipid ratio 2:1). This suggests that arenicin peptides were able to partly permeabilize the POPC/POPG (1:1) vesicles. The partial leakage induction could be explained by the electrostatic attraction of the cationic peptides to the negatively charged lipid bilayer membranes and therefore suggest that membrane permeabilization is not the only mode of action causing bacterial cell death. This type of weak leakage induced behaviour has previously been shown for Sub3, a cationic AMP, whose mode of action involved permeabilization of the outer membrane and internalisation without permeabilization of the inner cytoplasmic membrane.[10]

Arenicin peptides aggregate negatively charged lipid model membranes.

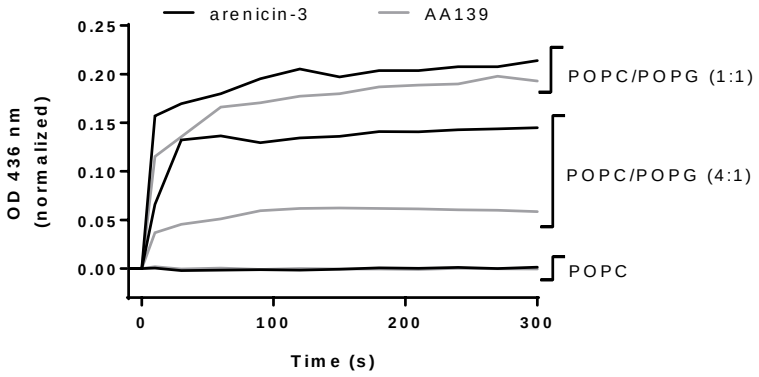

Figure 4-5 - Vesicle aggregation studies. $OD_{436\ nm}$ was monitored after addition of 25 μM (~ 64 μg/mL) of arenicin-3 or AA139 to 500 μM of LUVs prepared in 10 mM HEPES pH 7.4, containing 150 mM NaCl. The OD values were normalized for the baseline.

The ability of arenicin peptides to interact with lipid vesicles was further investigated by following vesicle aggregation. Vesicle integrity is generally kept by inter-vesicle forces such as electrostatics and hydration forces. The addition of a cationic peptide to the negatively charged vesicle environment could cancel repulsive electrostatic forces of negatively charged vesicles and induce dehydration of the lipid polar groups leading to aggregation of the vesicles.[11,12] A solution becoming turbid, reflects aggregation has occurred and leads to an increase in OD_{436} absorbance measurement. In our study,

Figure 4-5, arenicin-3 and AA139 do not induce aggregation of vesicles composed of POPC only. However, they are able to induce aggregation of negatively charged vesicles POPC/POPG (4:1) and (1:1). Arenicin-3 induces more aggregation than AA139 and at a faster rate. These results support our SPR binding and leakage assay findings where arenicin peptides do not bind to or permeabilize the membrane of POPC vesicles but do bind and partially permeabilize the membrane of more negatively charged vesicles POPC/POPG. These results suggest that the antimicrobial mode of action of arenicin peptides might not necessarily be dependent on membrane permeabilization.

Arenicin peptides alter their secondary structure upon interaction with lipid membranes. Circular dichroism spectroscopy is most commonly used to identify the presence of random coil and α-helix secondary structure, and to a lesser extent for determining β-sheet content. We have used this technique to interrogate information about changes in the overall 3D structure of the peptides when bound to lipid bilayers.[13,14] The amide chromophore of the peptide bond dominates the CD spectra of the peptides below 250 nm. Their transitions n->π* and π_0->π* give the signature of an α-helix or β-sheet structure. In the CD study, the lipid mixtures were prepared as LUVs rather than SUVs (as was used previously for SPR studies) due to the curvature effects present in SUVs.[15] Arenicin peptide secondary structures were studied in the absence and presence of LUVs at physiological pH (7.4) as well as in 50% TFE, Figure 4-6. Arenicin-3 and AA139 demonstrate quite atypical CD signatures in solution containing one big positive band at 227 nm and two negative bands at 208 and 195 nm which is not what is expected for β-hairpin structural peptides. This atypical spectrum can be explained by the presence of the two disulfide bridges and the aromatic residues (Try or Trp) as well as the twist in the β-sheet which can affect the CD spectra in the far-UV region (190-250 nm).[16] Both peptides, showed similar secondary structures in solution and in presence of POPC LUVs, further reflecting the weak binding of arenicin peptides with POPC vesicles. Similar secondary structure was observed in 50% TFE, which mimics the hydrophobic environment of microbial membranes. In the presence of POPG, both peptides demonstrated a change in molar ellipticity signature which could be due to two reasons; (i) a change in flexibility of the peptides upon interaction with the lipid model membranes and (ii) the peptides might have precipitated with the vesicles leading to being quenched from the solution which would explain the drop in the overall signal. Although retaining a molar ellipticity signature more typical of an antiparallel β-sheet, AA139 seems to undergo a more significant secondary structure modification. This suggests that the arenicin peptides might undergo a slight twist modification of their β-sheet or align to the lipid bilayer membrane in a particular orientation,[17] but overall keep their β-hairpin structure.

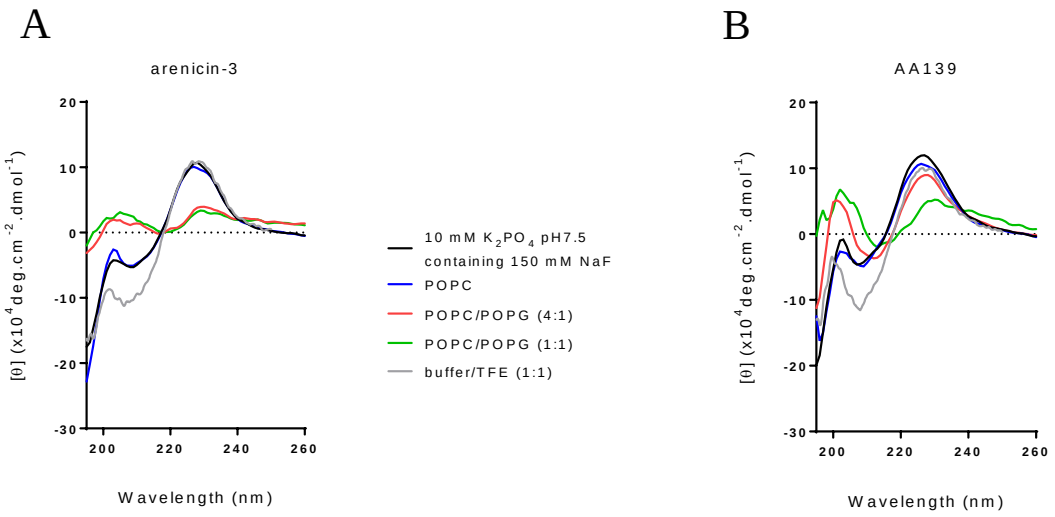

Figure 4-6 - CD spectra of arenicin peptides in the absence or presence of lipid vesicles. CD spectra of 50 μM (~ 128 μg/mL) of arenicin-3 (A) and AA139 (B) prepared in 10 mM PO_4 pH 7.4, containing 150 mM NaF in absence or presence of LUVs at 500 μM (P/L molar ratio of 1/10).

Arenicin peptides insert into lipid membranes. The fluorescence emission spectrum of tryptophan is influenced by the polarity of its local environment.[18] Whilst, in a polar environment, the tryptophan fluorescence emission spectrum shifts toward longer wavelengths, in more hydrophobic environments, the tryptophan fluorescence shifts toward shorter wavelengths (blue shift). Arenicin-3 and AA139 both possess only one Trp in their sequence located at the N-terminal region, in position 4. Tryptophan fluorescence was monitored here to judge the polarity of its environment and thus determine the insertion of the Trp^4 into lipid bilayer vesicles. In the absence of vesicles, the maximum of the fluorescence emission was 347 and 349 nm, for arenicin-3 and AA139, respectively. Upon titration with LUVs POPC/POPG (1:1), the fluorescence emission spectra showed a blue shift for both peptides, Figure 4-7 (A) and (B) and Table 4-4. At the saturation point of the LUVs concentration, the maximum wavelength of tryptophan fluorescence emission was 327 nm for both peptides. These remarkable blue shifts are representative of the tryptophan residue of arenicin peptides inserting into the hydrophobic environment of membranes composed of POPC/POPG (1:1). A comparative study of different LUV compositions was carried out to evaluate whether arenicin peptides have selectivity towards more negatively charged lipid bilayers. No change in the fluorescence emission was observed for both arenicin peptides, upon titration with POPC vesicles. However, when titrating with POPC/POPG (4:1) or POPC/POPG (1:1) vesicles, a typical blue shift in the Trp fluorescence emission spectrum was observed, with a concomitant increase in the fluorescence emission quantum yield, Figure 4-7 (C) and (D). This suggests that Trp^4 of both arenicin

peptides inserts into the lipid bilayer of model membranes containing negatively-charged phospholipids in their composition.

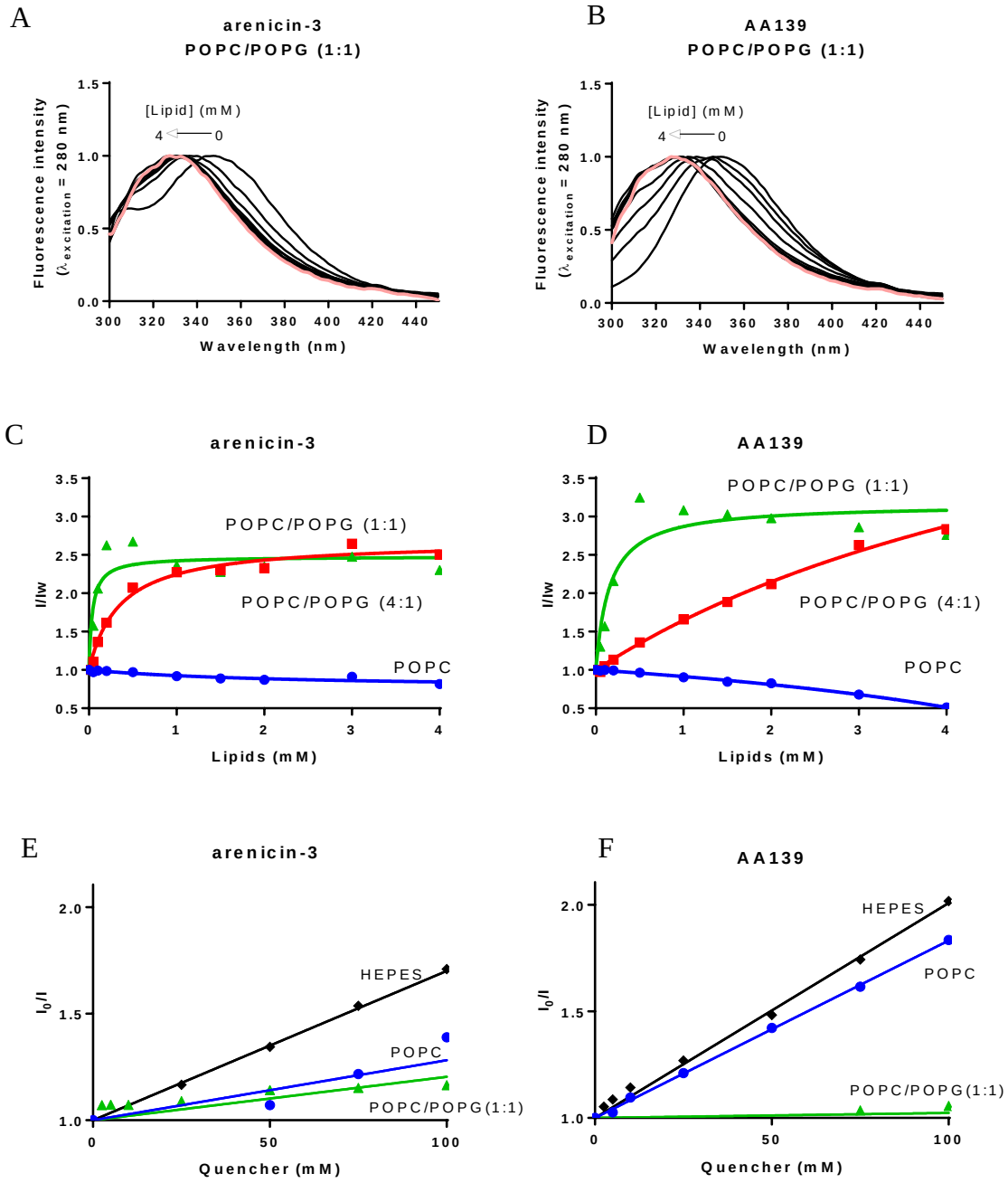

Figure 4-7 – Partitioning of Trp residue of arenicin peptides into model membranes followed with 25 µM (~ 64 µg/mL) of peptide in 10 mM HEPES, pH 7.4, containing 150 mM NaCl. (A) Arenicin-3 and (B) AA139 fluorescence emission spectra ($\lambda_{excitation}$ = 280 nm) upon titration with POPC/POPG (1:1) LUVs with pink trace highlighting the highest concentration of LUVs. (C) and (D) Fluorescence emission of arenicin-3 and AA139, respectively, normalised to [lipid] = 0 (I/Iw) upon titration with POPC (blue dots), POPC/POPG (4:1) (red squares) and POPC/POPG (1:1) (green triangles) LUVs. (E) Arenicin-3 and (F) AA139 emission fluorescence quenching by acrylamide in solution (black diamonds) or in presence of 2 mM LUVs POPC (blue dots) or POPC/POPG (1:1) (green triangles).

The affinity of a peptide for a lipid system can be assessed by the partition coefficient, K_p, ratio of the amount of peptide interacting with the membrane to the amount of peptide in solution. The partition coefficient was calculated as before[19] and results are shown in Table 4-4. Arenicin-3 had the highest partition coefficient when interacting with POPC/POPG (1:1) ($K_P = (3.4 \pm 1.7) \times 10^4$), about 10-fold higher than with POPC/POPG (4:1) and about 4-fold higher than AA139 with POPC/POPG (1:1). None of the peptides had its Trp residue inserting into POPC vesicles under the conditions tested but the Trp partition increased with the increasing amount of POPG in the composition of the vesicles.

Table 4-4 – Partition of arenicin-3 and AA139 into different lipid mixtures as followed by Trp fluorescence emission. The Kp and I_L/I_W parameters were obtained from fitting a non-linear equation. Emission fluorescence quenching of arenicin-3 and AA139 induced by acrylamide.

Peptide	Lipid mixture	K_P (x10^3)	Blue shift (nm)[a]	I_L/I_W	K_{SV}, acrylamide (mM^{-1})
arenicin-3	buffer	-	-	-	7.0 ± 0.3
	POPC	-	0	-	2.8 ± 1.3
	POPC/POPG (4:1)	3.73 ± 0.6	20	2.7 ± 0.8	-
	POPC/POPG (1:1)	33.7 ± 17	20	2.5 ± 2.4	2.0 ± 0.3
AA139	buffer	-	-	-	10.1 ± 0.2
	POPC	-	0	-	8.3 ± 0.1
	POPC/POPG (4:1)	0.19 ± 0.03	12.5	6.1 ± 1.5	-
	POPC/POPG (1:1)	8.3 ± 3.3	22.5	3.2 ± 2.4	0.2 ± 0.5

[a]Fluorescence emission blue shift obtained upon addition of [lipid] = 2 mM.

To assess the degree of solvent exposure of Trp[4] of arenicin peptides, fluorescence quenching studies were carried out for arenicin-3, Figure 4-7 (E), and AA139, Figure 4-7 (F), in the presence and absence of POPC or POPC/POPG (1:1) LUVs using acrylamide, an aqueous fluorescence quencher unable to partition into lipid membranes. The peptides were excited at 290 nm to minimize the relative quencher/fluorophore light absorption ratio. The fluorescence emission intensity data were corrected for the simultaneous light absorption of fluorophore and quencher and analyzed using Stern-Volmer equation as before,[20] Table 4-4. The Trp fluorescence quenching efficiency induced by acrylamide, as quantified with Ksv, calculated from the slope of the Stern-Volmer plots, Table 4-4, was high when both peptides were in buffer, 7.0 ± 0.3 (x10^3) and 10.1 ± 0.2 (x10^3) for arenicin-3 and AA139, respectively. This large quenching of the Trp fluorescence emission confirms exposure of Trp[4] residue to the aqueous solvent. However, in presence of LUVs, the quenching by acrylamide was less efficient. This lower quenching efficiency in the presence of vesicles suggested that the Trp[4] residue in both arenicin peptides inserts into the hydrophobic core of the lipid bilayer and is thus less accessible to acrylamide. The insertion of the Trp[4] residue in vesicles is different for the two arenicin peptides. For arenicin-3, the Trp seems to insert almost similarly in POPC or POPC/POPG (1:1) vesicles with only 1.4-fold reduction from POPC to POPC/POPG (1:1) type of vesicle. However, for AA139, the difference of Ksv between both types of vesicles is quite drastic going from 8.3 ± 0.1

($x10^3$) to 0.2 ± 0.5 ($x10^3$), a 41.5-fold reduction. Overall, in presence of POPC/POPG (1:1) LUVs, the quenching was reduced by 3.5- to 50-fold for arenicin-3 and AA139, respectively, as compared to buffer alone. Taken together, these results show that the Trp^4 residue of both arenicin peptides, and therefore the N-terminus of the peptides, can insert in the hydrophobic region of the phospholipid membrane and more so of the negatively charged ones. The AA139 *N*-terminus seems to insert even deeper than arenicin-3 does with a clear distinction between zwitterionic and negatively charged lipid bilayer vesicles.

Surface charge of model membranes and *E. coli* cells induced by arenicin peptides. The surface charge of lipid vesicles or bacterial cells in aqueous solution can be measured by ζ- potential. Following zeta potential of vesicles or cells upon titration with arenicin peptides allows us to evaluate and determine changes in their surface charge density.[21]

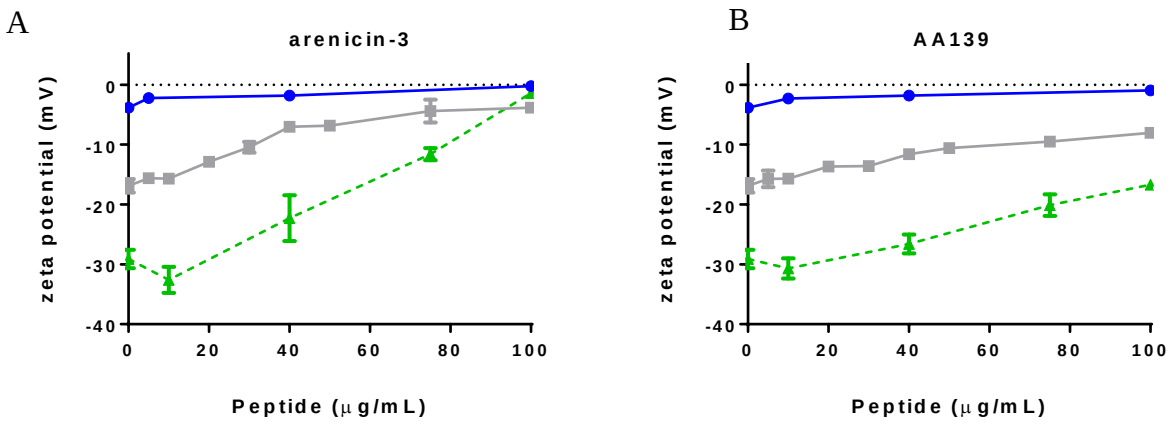

Figure 4-8 – Surface charge of 200 μM POPC (blue dots), POPC/POPG (1:1) (green triangles) vesicles and *E. coli* ATCC 25922 (grey squares) in the presence of (A) arenicin-3 and (B) AA139 as followed by ζ-potential. Average ± SD of three replicates.

Results in Figure 4-8, show that the surface charge of POPC vesicles does not change upon titration with both arenicin peptide (zeta potential values are constant and around neutralization point), suggesting that these two peptides do not interact with POPC vesicles. This correlates well with the low binding affinity or permeabilization shown for zwitterionic lipid bilayers. For POPC/POPG (1:1) LUVs, both arenicin peptides reduce the negative zeta potential of the LUVs. The initial value -29.1 ± 1.56 mV for POPC/POPG (1:1) LUVs steadily climb up to less negative values as the concentration of arenicin peptides increases. Arenicin-3 neutralizes the surface charge of POPC/POPG (1:1) LUVs at 100 μg/mL. AA139 does not neutralize the surface charge of POPC/POPG (1:1) LUVs as efficiently as arenicin-3 does, only reaching -16.7 ± 0.866 mV at 100 μg/mL. This is surprising, considering the overall charge of both peptides, +4 and +5 for arenicin-3 and AA139, respectively.

We would have expected that the more positively charged the peptide is, the faster the neutralization of negatively charged LUVs occur. However, in our case, even though AA139 is more positively charged, it renders the surface charge of the LUVs less negative but does not neutralize the POPC/POPG (1:1) at the highest tested concentration, 100 μg/mL, as arenicin-3 does. For both arenicin peptides, the results suggest that arenicin-3 binds more strongly to the lipids and that the hydrophobicity of arenicin-3 is a stronger determinant of lipid binding than the added charge of AA139.

To get a deeper insight of the mode of action of arenicin peptides and determine whether electrostatic interactions are necessary for their antibacterial activity, the membrane surface potential of *E. coli* was monitored by ζ-potential measurements, Figure 4-8. In the absence of peptides, the *E. coli* cell surface displayed a ζ-potential of -16.9 mV. This negative surface net charge of *E. coli* originates mostly from the lipopolysaccharides and the negatively charged phospholipids covering the outer leaflet of the cells. The titration of *E. coli* cells with arenicin peptides led to a reduction of the negative surface charge, with the values increasing from -16.9 to -3.5 mV or -8.0 mV, when titrating with arenicin-3 or AA139, respectively. The results suggest that both arenicin peptides bind to the *E. coli* cells and affect their surface charge.

Arenicin peptides permeabilize the cytoplasmic bacterial membrane. The cytoplasmic permeabilization activity of arenicin peptides, arenicin-3 and AA139, against the membrane of *E. coli* ATCC 25922 cells were investigated by a fluorescence dye-based assay, using the DNA-binding probe SYTOX® Green. This assay assisted in investigating whether arenicin peptides permeabilize the inner membrane of *E. coli* ATCC 25922 cells. SYTOX® Green is a cell-impermeant nucleic acid stain, allowing the distinction between non-permeabilized from permeabilized cells by the increased fluorescent signal due to DNA-binding of SYTOX® Green. The fluorescence emission followed by flow cytometry was measured as a peptide titration of *E. coli* bacterial cells where SYTOX® Green was added following peptide-cell pre-incubation. For each sample, the fluorescence signals were expressed as a percentage of partial and full cell permeability as compared to intact (untreated) and damaged (treated with isopropanol) cell controls. Polymyxin B was included as a positive control compound, as it has the ability to disrupt the cytoplasmic membrane by pore formation. Meropenem was used as negative control compound, being an antimicrobial compound that enters cells without compromising the bacterial cell membrane.

The results, Figure 4-9, suggest that arenicin peptides permeabilize the cytoplasmic membrane of *E. coli* cells at lethal concentrations (50% of the cells are permeabilized upon treatment with 0.7-1

µg/mL) and induced 100% of cell permeabilization at concentration ≥4 µg/mL for both arenicin peptides. Taking into account the number of cells used in this assay compared to the MIC assays ($9x10^6$ and $5x10^5$ cells/mL respectively, 18-fold difference), arenicin peptides fully permeabilize the inner (cytoplasmic) membrane of *E. coli* cells at the same concentration as their MIC. The permeabilization profile is different for both arenicin peptides, arenicin-3 possess a significantly sharp point of permeabilization whereas AA139 shows a steady increase of permeabilization proportional to the concentration showing probably a different mode of action on the membrane of the cells.

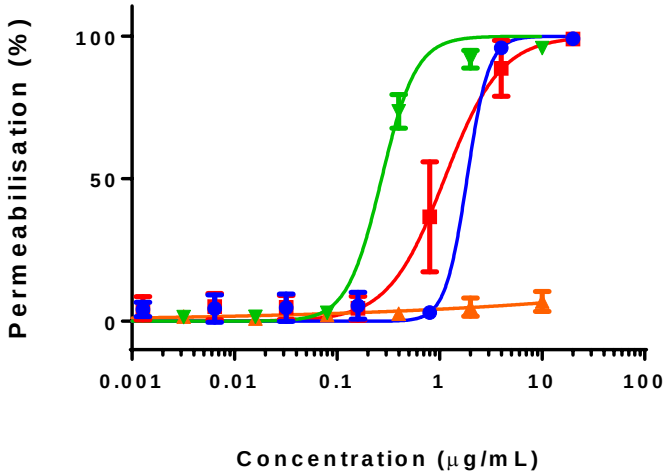

Figure 4-9 – Cytoplasmic membrane permeabilization of *E. coli* ATCC 25922 using arenicin-3 (blue dots), AA139 (red squares), polymyxin B (green down triangles) and meropenem (orange up triangles), evaluated from SYTOX Green fluorescence emission intensity. Average ± SD of three replicates.

4.3 Materials and methods

Materials. Arenicin-3 and AA139 were supplied to us by Adenium Biotech Pty Ltd. Peptides were synthesized using a yeast expression system by GenScript (Denmark) for small scale synthesis (~5 mg), and PolyPeptide Laboratories (Sweden) for larger scale synthesis (>5 mg), on behalf of Adenium Biotech Pty Ltd. Synthetic lipids, palmitoyloleoyl-phosphatidylcholine (POPC) and palmitoyloleoyl-phosphatidylglycerol (POPG) were purchased from Avanti Polar Lipids (Alabaster, AL). All chemicals were used without further purification.

NMR spectroscopy

3D solution structure

Arenicin-3 and AA139 were analyzed at 3.5 and 2.5 mM concentration respectively, in phosphate buffer at pH 3.3 containing 10% D_2O. All NMR experiments were performed on a Bruker Avance III

spectrometer equipped with a cryogenically cooled triple resonance probe operating at a nominal ^{1}H frequency of 700 MHz. The excitation sculpting sequence was used to suppress the solvent (H_2O) resonance. Two-dimensional TOCSY [t_m (MLEV17 spin-lock mixing pulses) = 80 ms], NOESY [t_m (mixing time) = 300 ms], ^{15}N-HSQC and ^{13}C-HSQC were recorded at 25 °C. Chemical shifts were referenced relative to the 2,2-dimethylsilapentane-5-sulfonic acid (DSS) signal at 0 ppm. The assignment of proton resonances was carried out using TOCSY and NOESY data using the CCPNMR software.[22] Torsion angles constraints were obtained using the Talos software.[23] Structure calculations were performed using CYANA 3.0.[24] Additional upper/lower restraints were applied to form disulfide bonds between Cys^{3}- Cys^{20} and Cys^{7}-Cys^{16}.

Hydrogen-deuterium exchange studies

All NMR spectra for the hydrogen-deuterium exchange studies were recorded on the spectrometer described above at 25 °C. Spectra were referenced to DSS at 0 ppm. Lyophilized peptide was initially solubilized in phosphate buffer at pH 3.3. The peptide was then lyophilized. Lyophilized peptide was dissolved in 100% D_2O and immediately placed in the spectrometer for measurement. 1D ^{1}H and TOCSY spectra were recorded at specific time points over a 24 h period. Hydrogen-deuterium exchange rates were measured by integrating each exchangeable amide resonance separately.

Amide temperature coefficient studies

The temperature dependence of amide proton resonances was derived from 1D ^{1}H and TOCSY spectra recorded on a Bruker ARX 500 MHz spectrometer. Spectra were measured between 15 °C to 35 °C, in 5 °C increments, and referenced to DSS at 0 ppm. Assignment of the spectra was performed using the program CCPNMR.[22]

Antimicrobial activity, Minimum Inhibitory Concentration (MIC). Antibacterial assays were performed by a broth micro-dilution plate based method as per CLSI guidelines for antimicrobial susceptibility testing.[25, 26] The assay methodology was previously reported in chapter 3.

Hemolytic assay. The ability of the peptides to hemolyse human red blood cells was determined by a previously reported method in chapter 3.

Cytotoxicity. Cytotoxicity to HEK293 cells was determined using the resazurin assay.[27,28] Cell culturing, cytotoxicity assays and calculation of percentage of cell death were performed as previously described in chapter 3.[29]

Preparation of vesicles. Small unilamellar vesicles (SUVs) (50 nm diameter) for SPR and large unilamellar vesicles (LUVs) (100 nm diameter) for all other assays were used as membrane models and prepared by extrusion method as previously described.[30,31] The synthetic lipids were used to

prepare model membrane composed of POPC, POPC/POPG (4:1 or 1:1molar ratio). All lipid suspensions were prepared in 10 mM HEPES pH 7.4, containing 150 mM NaCl unless otherwise stated.

Surface plasmon resonance. The binding affinity of the peptides for model membranes composed of POPC or POPC/POPG (4:1 or 1:1) were compared using SPR. The methodology was already described in chapter 3.

Vesicles leakage assay. Vesicle leakage was quantified by carboxyfluorescein (CF) dequenching as previously described.[9] LUVs composed of POPC or POPC/POPG (1:1) were prepared containing 50 mM CF and homogenized to a diameter of 100 nm by extrusion. CF-loaded LUVs and non-encapsulated CF were separated by gel filtration on a Sephadex G50 column equilibrated with HEPES buffer. Several concentrations (2-fold dilution starting from 100 µg/mL) of arenicin peptides were incubated during 10 min with LUVs (5 µM final lipid concentration). The fluorescence emission intensity (FI; excitation/emission = 485 nm /520 nm) of the released CF was read using a PHERAstar plate reader (BMG Labtech). Controls with Triton X-100 0.1% (v/v) and with HEPES buffer were included to establish the FI with 100% and 0% of leakage, FI_{Triton} and FI_{buffer}, respectively. The percentage of leakage was calculated using the following equation:

$$\% \text{ Leakage} = (FI_{sample} - FI_{buffer})/(FI_{Triton} - FI_{buffer}) \times 100$$

Vesicle aggregation. Aggregation of POPC or POPC/POPG (4:1 or 1:1) LUVs induced by arenicin peptides was evaluated by optical density at 436 nm (OD_{436}). Arenicin peptides (25 µM) were added to LUVs (500 µM), and optical density was recorded as a function of time.[11]

Circular dichroism (CD) spectroscopy. CD spectra were recorded on a Jasco J-810 Circular Dichroism Spectropolarimeter at ambient temperature using a 1 mm path length cuvette. Wavelengths from 260 to 185 nm were recorded with a 0.1 step and a 50 nm/min speed. Spectra were collected and averaged over 3 scans and corrected for background contributions. LUVs were prepared by extrusion method as mentioned earlier. Samples and lipid vesicles were prepared in 10 mM K_2PO_4 pH 7.4 containing 150 mM NaF. Lipid vesicles were prepared at 0.5 mM and sample peptide at 50 µM giving a peptide to lipid molar ratio (P/L) of 1/10. The lipid vesicles scatter light below 195 nm, therefore no data were recorded below this value. The peptides were also followed upon titration with trifluoroethanol (TFE), up to 50 %, mimicking hydrophobic environment. Signal was recorded in milli-degrees and the following equation was used to normalize the milli-degrees into mean-residue ellipticity, $[\theta]_{MRE} = \theta/(c \times l \times N_t)$, where θ is the data in milli-degrees, c is the peptide concentration in molar, l is the cuvette path length in mm, and N_t is the number of residues.

Partition into lipid vesicles followed by Trp fluorescence emission. Arenicin peptides have intrinsic fluorescence due to a Trp residue in position 4. The involvement of the Trp residue in the interaction of arenicin peptides with POPC or POPC/POPG (4:1 or 1:1) LUVs was examined following the Trp fluorescence properties using a Perkin Elmer LS50 spectrometer with a quartz cuvette (pathlength = 0.5 cm). Tryptophan fluorescence emission spectra were scanned upon titration of a stock solution of LUVs (0-4 mM final lipid concentration) into peptide solution (25 μM). The excitation wavelength was set to 280 nm and emission was monitored from 300 to 450 nm at 25 °C. Partition curves were plotted, and the partition coefficient, Kp, was determined to compare the affinity for the three lipid mixtures.[19]

Fluorescence quenching experiments were performed by stepwise addition of acrylamide from a stock solution (4 M) into peptide solution at room temperature. The results were analyzed by fitting to the Stern-Volmer equation, $I_0/I = 1 + K_{SV}[Q]$ and quenching efficiency quantified with K_{SV} (Stern-Volmer constant).[32] I_0 and I are the fluorescence intensities at appropriate emission wavelength in the absence and presence of quencher (acrylamide), respectively. [Q] is the molar concentration of acrylamide.[20]

ζ potential measurements on model membranes and bacterial cells. Zeta potential measurements were conducted to evaluate changes in the surface charge of lipid bilayer model membranes and in *E. coli* cells in the presence of arenicin peptides at several concentrations. Studies were conducted in a Zetasizer Nano ZS90 (Malvern Instruments) equipped with a 633 nm HeNe laser and disposable DTS1070 ζ cells with gold electrodes. LUVs of POPC and POPC/POPG (1:1) at final concentration of 200 μM were incubated for 15 min at 25 °C with peptide from 0 to 100 μg/mL. Bacterial cells were pelleted, washed three times and resuspended in HEPES buffer at 2 x 10^7 CFU/mL. Peptides were added and samples were incubated for 30 mins at 37 °C. The ζ potential was calculated using the Smoluchowski equation. Ten measurements of 100 runs each were carried out for all the concentrations of peptide with the experiments run in duplicate.[10]

Inner membrane permeability followed by SYTOX Green fluorescence emission. *E. coli* ATCC 25922 cells were grown to exponential phase (OD~0.6), centrifuged at 2500 RCF for 10 min, the pellet washed with PBS buffer three times to remove any trace of nucleic acids and residual growth media, and cells were resuspended in buffer at 1 x 10^7 CFU/mL. Bacterial cell suspensions were incubated with peptides at different concentrations (five-fold dilutions starting from 20 μg/mL) for 1 h at 37 °C, repeated in triplicate. SYTOX™ Green (Life Technologies S7020), a DNA-binding dye that becomes fluorescent when bound to nucleic acids and only enters cells with comprised plasma membranes,[33] was added to the peptide–treated cells at a final concentration of 2 μM, and incubated

for 5 min at room temperature. The fluorescence emission intensity of the bacterial suspensions were then scanned using λ_{ex} = 488 nm and λ_{em} = 530 nm with 30 nm band pass by flow cytometry performed with a BD FACS Canto II (BD biosciences). For each sample 100000 events were recorded and the fluorescence signals were expressed as a percentage of cell permeability as compared to intact (untreated) and damaged (treated with isopropanol) cell controls. Polymyxin B was included as a positive inner membrane permeating compound control and meropenem as negative inner membrane permeating compound control (antimicrobial compound that enters cells without compromising the bacterial cell membrane).

Based on forward and side scattering measurements of the intact versus damaged cell controls, two distinct populations were identified; i) healthy or intact cells, ii) dead/unhealthy or completely/partially permeabilized cells. Healthy cells were deemed as 10^1 to 10^3 range of detection, at 530 nm, and dead or unhealthy cells were deemed as 10^3 to 10^5 range of detection at 530 nm.

4.4 Conclusion

Bacteria are developing resistance to current antibiotics rendering them ineffective even for the treatment of the simplest diseases. The development of new drugs to replace obsolete antibiotics is thus an emergency. AMPs have fascinated scientists for decades due to their large range of antimicrobial activity, however what is suitable for microorganisms, plants and animals is not necessary suitable for human as most AMPs display toxicity towards mammalian cells. To counteract mammalian cell toxicity, the method of choice, is to design analogs of natural AMPs, in order to retain its antimicrobial property and concomitantly reduce its mammalian toxicity. This is what has been achieved, in the case of AA139, a synthetic analog of arenicin-3, offering potent broad-spectrum antimicrobial activity and very low mammalian cell toxicity. In the attempt to develop drug candidates at a faster rate than bacteria develop resistance to antibiotics, the study of the mode of action of those molecules is required.

In this study, we examined the 3D solution structures and mode of action of both arenicin-3 and AA139. The comparison between arenicin-3 and AA139, revealed the significant implications simple amino acid changes, could have on the properties of AMPs. The mutations of two valines for alanine as well as a tyrosine for an arginine, reduced the overall hydrophobicity of the molecule and consequently increased its amphipathicity. We confirmed that these arenicin peptides are β-hairpin right handed twisted peptides, constrained by two disulfides bridges Cys^3-Cys^{20} and Cys^7-Cys^{16}. The mutations of three amino acids between arenicin-3 and AA139 did not affect the peptide backbone, which is almost perfectly superimposable. Although, almost identical, the NMR study revealed that

arenicin-3 has a more rigid and stable structure than AA139 possessing almost 2-fold more H-bonds than AA139. Its more flexible structure offer AA139, the possibility to probably slightly rearrange its structure to maneuver through the lipid bilayer of the cell membranes.

We investigated the mode of action of both peptides against bacterial and mammalian cells. To do so, we evaluated the effect of the peptides on the cell membrane, through assays using lipid bilayer model membranes and bacterial cells. Studies conducted with lipid vesicles using SPR and fluorescence methodologies suggested that arenicin peptides bind, permeabilize and insert into negatively charged lipid vesicles (POPC/POPG). Their β-hairpin secondary structures were not modified, but rather, might slightly twist upon interaction with negatively charged lipid model membrane or might align to the lipid bilayer membrane in a particular orientation. Arenicin-3 induces more aggregation of negatively charged lipid bilayer model membranes than AA139 and at a faster rate. The *N*-terminus of AA139 (Trp^4) inserts deeper into the hydrophobic core of negatively charged phospholipid membranes than zwitterionic ones (41.5-fold difference of Ksv) rendering it more selective for negatively charged phospholipid membranes, as compared to arenicin-3 (1.4-fold difference of Ksv), which seems to have its *N*-terminus inserting quite similarly in both types of membranes. These results correlate well with the difference seen in toxicity of both arenicin peptides, with AA139 displaying a reduced hemolytic activity as compared to arenicin-3. The results obtained with bacterial cells, *E. coli* ATCC 25922, confirmed that arenicin peptides permeabilize the inner bacterial membrane.[34] Our study suggests that arenicin peptides act on the membrane of *E. coli* cells and are most likely attracted to the cell surface due to electrostatic attraction. AA139 permeabilizes the inner (cytoplasmic) membrane of *E. coli* cells with a steady increase proportional to its concentration, thus it is possible to suggest that AA139 antimicrobial mode of action differs from arenicin-3 and AA139 can kill bacteria via an alternative means as opposed to pure membrane disruption.

In summary, the use of lipid bilayer model membranes and bacterial cells, allowed us to propose a model for the mechanism of action of AA139, Figure 4-10, involving three steps: (1) binding the outer membrane through electrostatic interactions, (2) inserting into the hydrophobic core of the outer membrane creating partial permeabilization due to the ability of the peptide to modify its secondary structure allowing it to enter into the lipid bilayer without pore formation, (3) accessing and permeabilizing the cytoplasmic membrane.

AA139 flexibility may be a clue to the difference between both arenicin peptides. Usually, β-hairpin AMPs are extremely rigid and a change in their structure would lead to a loss of antimicrobial activity. However, it was observed, for the case of LytA239–253, a peptide encompassing the β-hairpin core of the third CBR of pneumococcal C-LytA, that this peptide would undergo complete secondary

structure modification when interacting with detergent micelle and SUVs, changing from β-hairpin to α-helical secondary structure.[35] Structural flexibility is also usually observed for most AMPs which adopt random coil secondary structure in solution and become α-helical upon binding to cell membranes. We could imagine that structural modification or rearrangement could lead to a more valuable therapeutic peptide in the case of AA139.

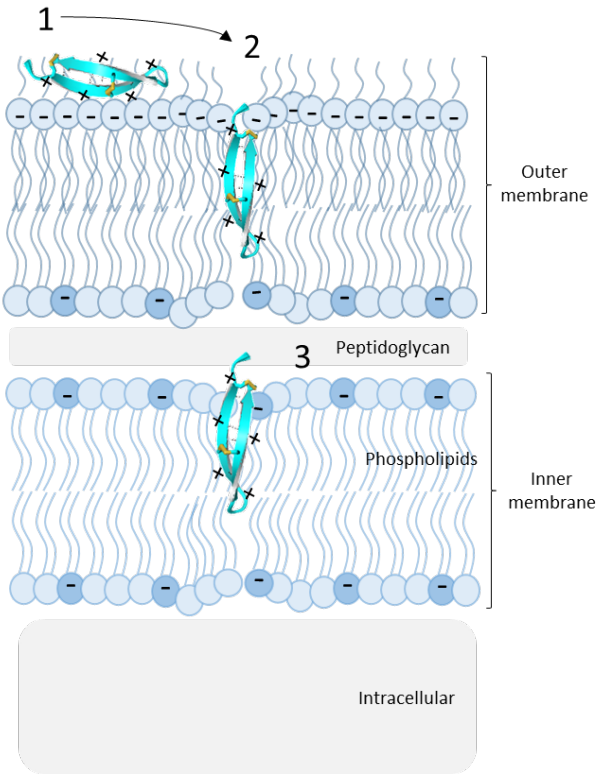

Figure 4-10 - Model of the mechanism of action of AA139 against Gram-negative bacteria cell membrane. 1) AA139 binds to the negatively charged outer membrane of Gram-negative bacteria via electrostatic interactions; 2) AA139 inserts into the hydrophobic core of the outer membrane creating partial permeabilization; 3) AA139 accesses and permeabilizes the cytoplasmic membrane.

We now have a deeper understanding of the mode of action of arenicin peptides and how the mutation of only three amino acids has made a significant increase in the therapeutic value of the peptide. Other β-hairpin AMPs have been reengineered to generate therapeutically valuable molecules. For example, Iseganan, a synthetic analog of protegrin-1 that was redesigned by reducing and redistributing the overall charge and hydrophobicity of the peptide by simple two amino acid deletion/mutations, was shown to be effective for the prevention of oral mucositis. However, this peptide failed phase III clinical trials for the prevention of ventilator-assisted pneumonia due to high toxicity.[36] A 14 amino acid synthetic cyclic peptide derived from protegrin-1, Murepavadin (POL7080), an outer membrane protein targeting antibiotic, was engineered by Polyphor. Polyphor announced on 19th May 2017 the success of a phase II clinical trial and the recruitment of the first patient for a phase III clinical trial in Q1/2018 for the treatment of nosocomial pneumonia (ventilator-associated and hospital-acquired

pneumonia; VAP/HAP) caused by infections of *Pseudomonas aeruginosa*, including its resistant strains. Natural AMPs offer great potential for the fight against resistant bacteria. The redesign of AMPs to produce better therapeutic candidates than the native prototype is now exemplified by AA139, which possesses promising therapeutic qualities for further drug development. AA139 provides an example of successful improvements that should be considered when designing other potential antimicrobial peptides.

4.5 References

1. Butler, M. S., Blaskovich, M. A. T., and Cooper, M. A. (2016) Antibiotics in the clinical pipeline at the end of 2015, *J. Antibiot.* DOI:10.1038/ja.2016.72
2. Edwards, I. A., Elliott, A. G., Kavanagh, A. M., Zuegg, J., Blaskovich, M. A. T. and Cooper, M. A. (2016) Contribution of Amphipathicity and Hydrophobicity to the Antimicrobial Activity and Cytotoxicity of β-Hairpin Peptides, *ACS Infect. Dis. 2*, 442-450. DOI:10.1021/acsinfecdis.6b00045
3. Ovchinnikova, T. V., Aleshina, G. M., Balandin, S. V., Krasnosdembskaya, A. D., Markelov, M. L., Frolova, E. I., Leonova, Y. F., Tagaev, A. A., Krasnodembsky, E. G., and Kokryakov, V. N. (2004) Purification and primary structure of two isoforms of arenicin, a novel antimicrobial peptide from marine polychaeta Arenicola marina, *FEBS Lett. 577*, 209-214. DOI:10.1016/j.febslet.2004.10.012
4. Panteleev, P. V., Bolosov, I. A., Balandin, S. V., and Ovchinnikova, T. V. (2015) Design of antimicrobial peptide arenicin analogs with improved therapeutic indices, *J. Pept. Sci. 21*, 105-113. DOI:10.1002/psc.2732
5. Shenkarev, Z. O., Balandin, S. V., Trunov, K. I., Paramonov, A. S., Sukhanov, S. V., Barsukov, L. I., Arseniev, A. S., and Ovchinnikova, T. V. (2011) Molecular mechanism of action of beta-hairpin antimicrobial peptide arenicin: oligomeric structure in dodecylphosphocholine micelles and pore formation in planar lipid bilayers, *Biochemistry 50*, 6255-6265. DOI:10.1021/bi200746t
6. Andra, J., Jakovkin, I., Grotzinger, J., Hecht, O., Krasnosdembskaya, A. D., Goldmann, T., Gutsmann, T., and Leippe, M. (2008) Structure and mode of action of the antimicrobial peptide arenicin, *Biochem. J. 410*, 113-122. DOI:10.1042/BJ20071051
7. Ravn, B. T., Brinch, K. S., Sandvang, D. H., Hoegenhaug, H. H. K., Segura, D. R., and Neve, S. (2011) Arenicin-3 for use in the treatment of urinary tract infections, WO2011/070032 A1.
8. Wishart, D. S., Bigam, C. G., Holm, A., Hodges, R. S., and Sykes, B. D. (1995) (1)H, (13)C and (15)N random coil NMR chemical shifts of the common amino acids. I. Investigations of nearest-neighbor effects, *J. Biomol. NMR 5*, 332. DOI:10.1007/BF00211764
9. Huang, Y. H., Colgrave, M. L., Daly, N. L., Keleshian, A., Martinac, B., and Craik, D. J. (2009) The biological activity of the prototypic cyclotide kalata b1 is modulated by the formation of multimeric pores, *J. Biol. Chem. 284*, 20699-20707. DOI:10.1074/jbc.M109.003384
10. Torcato, I. M., Huang, Y. H., Franquelim, H. G., Gaspar, D. D., Craik, D. J., Castanho, M. A., and Henriques, S. T. (2013) The antimicrobial activity of Sub3 is dependent on membrane binding and cell-penetrating ability, *ChemBioChem 14*, 2013-2022. DOI:10.1002/cbic.201300274
11. Torcato, I. M., Huang, Y. H., Franquelim, H. G., Gaspar, D., Craik, D. J., Castanho, M. A., and Troeira Henriques, S. (2013) Design and characterization of novel antimicrobial peptides, R-BP100 and RW-BP100, with activity against Gram-negative and Gram-positive bacteria, *Biochim. Biophys. Acta 1828*, 944-955. DOI:10.1016/j.bbamem.2012.12.002

12. Cummings, J. E., and Vanderlick, T. K. (2007) Aggregation and hemi-fusion of anionic vesicles induced by the antimicrobial peptide cryptdin-4, *Biochim. Biophys. Acta 1768*, 1796-1804. DOI:10.1016/j.bbamem.2007.04.016
13. Sreerama, N., Venyaminov, S. Y., and Woody, R. W. (1999) Estimation of the number of alpha-helical and beta-strand segments in proteins using circular dichroism spectroscopy, *Protein Sci. 8*, 370-380. DOI:10.1110/ps.8.2.370
14. Woody, R. W. (1995) Circular dichroism, *Methods Enzymol. 246*, 34-71. DOI:10.1016/0076-6879(95)46006-3
15. Henriques, S. T., Quintas, A., Bagatolli, L. A., Homble, F., and Castanho, M. A. (2007) Energy-independent translocation of cell-penetrating peptides occurs without formation of pores. A biophysical study with pep-1, *Mol. Membr. Biol. 24*, 282-293. DOI:10.1080/09687860601142936
16. Sreerama, N., Manning, M. C., Powers, M. E., Zhang, J. X., Goldenberg, D. P., and Woody, R. W. (1999) Tyrosine, phenylalanine, and disulfide contributions to the circular dichroism of proteins: circular dichroism spectra of wild-type and mutant bovine pancreatic trypsin inhibitor, *Biochemistry 38*, 10814-10822. DOI:10.1021/bi990516z
17. Miles, A. J., and Wallace, B. A. (2016) Circular dichroism spectroscopy of membrane proteins, *Chem. Soc. Rev. 45*, 4859-4872. DOI:10.1039/c5cs00084j
18. Santos, N. C., Prieto, M., and Castanho, M. A. (2003) Quantifying molecular partition into model systems of biomembranes: an emphasis on optical spectroscopic methods, *Biochim. Biophys. Acta 1612*, 123-135. DOI:10.1016/S0005-2736(03)00112-3
19. Henriques, S. T., Pattenden, L. K., Aguilar, M. I., and Castanho, M. A. (2009) The toxicity of prion protein fragment PrP(106-126) is not mediated by membrane permeabilization as shown by a M112W substitution, *Biochemistry 48*, 4198-4208. DOI:10.1021/bi900009d
20. Castanho, M. A., and Prieto, M. J. (1998) Fluorescence quenching data interpretation in biological systems. The use of microscopic models for data analysis and interpretation of complex systems, *Biochim. Biophys. Acta 1373*, 1-16. DOI:10.1016/S0005-2736(98)00081-9
21. Domingues, M. M., Santiago, P. S., Castanho, M. A., and Santos, N. C. (2008) What can light scattering spectroscopy do for membrane-active peptide studies?, *J. Pept. Sci. 14*, 394-400. DOI:10.1002/psc.1007
22. Skinner, S. P., Goult, B. T., Fogh, R. H., Boucher, W., Stevens, T. J., Laue, E. D., and Vuister, G. W. (2015) Structure calculation, refinement and validation using CcpNmr Analysis, *Acta Crystallogr., Sect. D: Biol. Crystallogr. 71*, 154-161. DOI:10.1107/S1399004714026662
23. Shen, Y., Delaglio, F., Cornilescu, G., and Bax, A. (2009) TALOS+: a hybrid method for predicting protein backbone torsion angles from NMR chemical shifts, *J. Biomol. NMR 44*, 213-223. DOI:10.1007/s10858-009-9333-z
24. Guntert, P. (2004) Automated NMR structure calculation with CYANA, *Methods Mol. Biol. 278*, 353-378. DOI:10.1385/1-59259-809-9:353
25. Cockerill, F. R., Wikler, M. A. (2012) *Methods for dilution Antimicrobial susceptibility tests for bacteria that grow aerobically; Approved standard*, Vol. 32, 9th ed., Clinical and laboratory standards institute, Wayne, PA.
26. Rex, J. H., Alexander, B. D. (2008) *Reference Method for Broth Dilution Antifungal Susceptibility Testing of Yeasts; Approved Standard*, Vol. 22, 3rd ed., Clinical and laboratory standards institute, Wayne , PA.
27. McMillian, M. K., Li, L., Parker, J. B., Patel, L., Zhong, Z., Gunnett, J. W., Powers, W. J., and Johnson, M. D. (2002) An improved resazurin-based cytotoxicity assay for hepatic cells, *Cell Biol. Toxicol. 18*, 157-173.
28. O'Brien, J., Wilson, I., Orton, T., and Pognan, F. (2000) Investigation of the Alamar Blue (resazurin) fluorescent dye for the assessment of mammalian cell cytotoxicity, *Eur. J. Biochem. 267*, 5421-5426. DOI:10.1046/j.1432-1327.2000.01606.x

29. Edwards, I. A., Elliott, A. G., Kavanagh, A. M., Blaskovich, M. A. T., and Cooper, M. A. (2017) Structure-Activity and -Toxicity Relationships of the Antimicrobial Peptide Tachyplesin-1, *ACS Infect. Dis.* DOI:10.1021/acsinfecdis.7b00123
30. Craik, D. J., Henriques, S. T., Mylne, J. S., and Wang, C. K. (2012) Cyclotide isolation and characterization, *Methods Enzymol. 516*, 37-62. DOI:10.1016/B978-0-12-394291-3.00024-1
31. Henriques, S. T., Pattenden, L. K., Aguilar, M. I., and Castanho, M. A. (2008) PrP(106-126) does not interact with membranes under physiological conditions, *Biophys. J. 95*, 1877-1889. DOI:10.1529/biophysj.108.131458
32. Henriques, S. T., and Castanho, M. A. (2005) Environmental factors that enhance the action of the cell penetrating peptide pep-1 A spectroscopic study using lipidic vesicles, *Biochim. Biophys. Acta 1669*, 75-86. DOI:10.1016/j.bbamem.2004.11.017
33. Roth, B. L., Poot, M., Yue, S. T., and Millard, P. J. (1997) Bacterial viability and antibiotic susceptibility testing with SYTOX green nucleic acid stain, *Appl. Environ. Microbiol. 63*, 2421-2431.
34. Yang, N., Liu, X., Teng, D., Li, Z., Wang, X., Mao, R., Wang, X., Hao, Y., and Wang, J. (2017) Antibacterial and detoxifying activity of NZ17074 analogues with multi-layers of selective antimicrobial actions against Escherichia coli and Salmonella enteritidis, *Sci. Rep. 7*, 3392. DOI:10.1038/s41598-017-03664-2
35. Héctor, Z. C., Beatriz, M., Erik, S., S., U. A., M., S. J., Ángeles, J. M. (2015) Micelle-Triggered β-Hairpin to α-Helix Transition in a 14-Residue Peptide from a Choline-Binding Repeat of the Pneumococcal Autolysin LytA. *Chemistry – A European Journal*, *21* (22), 8076-8089. DOI: 10.1002/chem.201500447
36. Kollef, M., Pittet, D., Sanchez Garcia, M., Chastre, J., Fagon, J. Y., Bonten, M., Hyzy, R., Fleming, T. R., Fuchs, H., Bellm, L., Mercat, A., Manez, R., Martinez, A., Eggimann, P., Daguerre, M., Luyt, C. E., and Prevention of Pneumonia Study Trial, G. (2006) A randomized double-blind trial of iseganan in prevention of ventilator-associated pneumonia, *Am. J. Respir. Crit. Care Med. 173*, 91-97. DOI:10.1164/rccm.200504-656OC

Chapter 5 - Structural AA139 mode of action study

5.1 Introduction

The label free studies presented in chapter 4 allowed us to gain an insight into the mode of action of arenicin peptides toward bacterial and mammalian cells. To deepen our comprehension, a structural characterization study is beneficial to understand the mechanism on a 3D molecular level. To date, the most established techniques for determination of high-resolution structures are X-ray crystallography and NMR spectroscopy, with both techniques generally yielding highly similar structures. The antimicrobial peptide database reports 2900 AMPs, but only 388 peptides have known 3D structure, of which 87% have been solved by NMR. NMR is the tool most widely employed in this area of research, mostly because peptide–lipid complexes cannot be crystallized. NMR is therefore the most appropriate tool to tackle the structural characterization of the mode of action of AA139. The structural study was performed on AA139 as it is the current lead drug candidate in its class. Bacterial and mammalian cells, as well as phospholipid vesicles, are too large for solution NMR spectroscopy, thus, alternative model systems have been developed to examine the structure of peptides in a membrane mimetic environment.

Historically, aqueous solution of organic solvents such as trifluoroethanol (TFE) were first employed to mimic the cell like lipid environment. However, TFE can induce the formation of α-helical secondary structure, which often does not correlate with biological activity.[1] Then, detergent micelles were introduced, adopting elliptical or rod-like shapes, depending on detergent concentration and chain length. Sodium dodecylsulphate (SDS) is negatively charged and dodecylphosphocholine (DPC) is zwitterionic, therefore mimicking bacterial and mammalian cell membranes, respectively. Discoidal micelles, or bicelles, have also been routinely used. They are formed by long- and short-chain phospholipids like DMPC or DHPC. Micelles/bicelles better mimic the cell membranes than TFE due to the separation of the hydrophobic acyl chains and the hydrophilic head groups. They are small enough for conventional proton NMR techniques without significantly broadening the signals of the peptide. However, micelles/bicelles do not reflect the true complexity of the bacteria and/or mammalian cell membranes due to their monolayer feature, coupled with a really tight curvature radius which can cause peptides to adopt non-native conformations or to aggregate. The mode of action of arenicin-2 was studied using DPC micelles, suggesting dimeric formation of arenicin-2 upon interaction with the micelles and pore formation.[2]

Phospholipid bilayer vesicles are better models of cell membranes. They have been used sporadically in solution NMR due to their relatively big size. The smallest possible vesicles DLPC-d_{64} have been used in some cases, giving a better representation of the peptide conformation and potentially the same conformation as is found in nature.[3] Lipid bilayer vesicles have been extensively used in solid state NMR, where size is not a limiting factor. For instance, the mode of action of protegrin was studied via solid state NMR (ssNMR) using DLPC or POPC bilayers, using static ssNMR and magic angle spinning (MAS) NMR respectively, supporting a toroidal pore mechanism of action.[4]

A more recent innovation, since the beginning of the twenty first century, are lipid bilayer nanodiscs, and their use is rapidly expanding.[5,6] Originally thought to offer advantages for the study of membrane proteins, they are now also employed for the structural and functional studies of membrane active peptides by solution NMR. Shenkarev et al.[7] attempted to study the binding interaction between arenicin-2 and nanodiscs constituted of DLPC/DLPG, however the peptide disintegrated the ND rendering the experiment impossible to accomplish.

In this chapter, three approaches have been explored for the structural characterization of AA139's mode of action against bacterial membranes: (i) a computational modelling study, (ii) a solution NMR study using lipid bilayer nanodiscs and (iii) a solid-state NMR study using lipid bilayer vesicles.

5.2 Results and discussion

Computational modelling. To evaluate the binding and insertion/interaction of arenicin peptides with the cell membranes, computational analysis was performed. We analyzed the aggregation proficiency of arenicin peptide structures by *in silico* means, in solution (*in vitro* aggregation) and in the presence of bacterial membrane (*in vivo* aggregation) by using TANGO (http://tango.crg.es/) and AGGRESCAN 3D (A3D) algorithms respectively. TANGO algorithm predicts β-aggregation proficiency pattern based on; different energy states, hydrophobicity, solvation energetics, electrostatic interactions and hydrogen bonding. The results, as shown in Figure 5-1 – A and B, reveal possible aggregation in solution for both arenicin-3 and AA139 taking part in the *N*-terminal β-sheet at physiological pH. The A3D algorithm assessed the proneness to aggregation of the peptide in *in vivo* conditions. The higher the aggregation score, the more prone is the amino acid for aggregation. This algorithm identified 14 amino acids (Gly1-Tyr9 and Val13-Tyr17) for arenicin-3 and 9 amino acids (Gly1-Cys7 and Cys16-Tyr17) for AA139 which may facilitate interchain bonding and auto-aggregation when in the presence of a lipid environment, Figure 5-1 – C and D. The mutations of Val to Ala and Tyr to Arg when going from arenicin-3 to AA139 lower the aggregation potential of the molecule *in vitro* and *in vivo*.

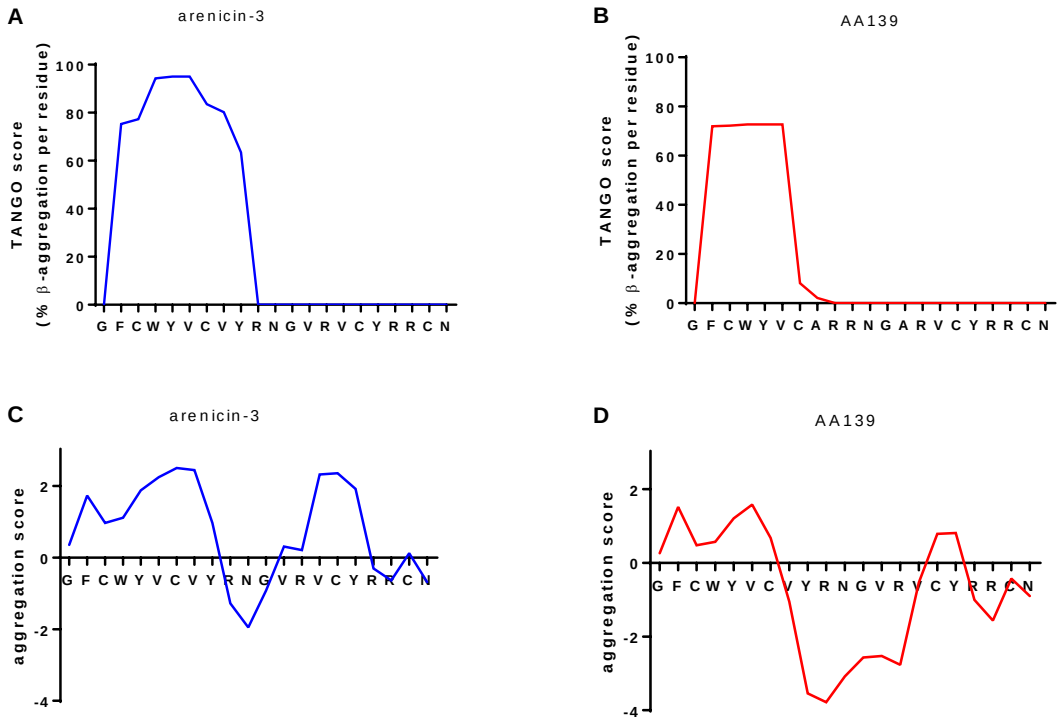

Figure 5-1 - Prediction of aggregation propensity of arenicin peptides by TANGO (A and B) and Aggrescan3D (C and D).

The orientation and potential interaction of arenicin peptides with a lipid membrane were studied by using the Orientation of Proteins in Membrane (OPM) web server[8], where the modeled peptide and dummy atoms of lipid moieties were viewed through FirstGlance in Jmol, V2.51, Figure 5-2. Note that OPM uses a DMPC lipid membrane as a mimic for mammalian cell membranes.

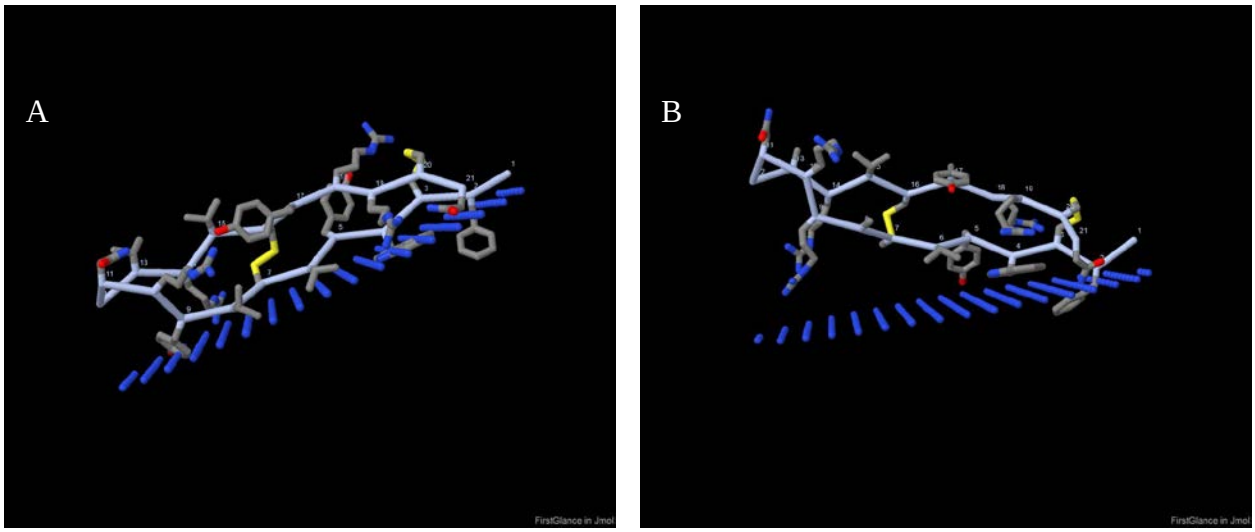

Figure 5-2 – OPM representation of arenicin peptides with DMPC lipid membrane, represented in blue dotted lines, (A) arenicin-3 and (B) AA139.

The results of OPM are summarized in Table 5-1. Both arenicin peptides possess the same number of embedded residues (two), however their orientation toward the membrane differ. Arenicin-3 tends to lay almost parallel (82° tilt angle) to the membrane whilst AA139 is predicted to interact with a much wider angle (67° tilt angle). Arenicin-3 may interact with an increased depth of penetration into the hydrophobic core of the membrane (3.3 ± 1.5 Å) than AA139 (2.1 ± 1.7 Å). The transfer free energy of the molecule from water to the lipid bilayer, or $\Delta G_{transfer,}$ is more important for arenicin-3 (-4.4 kcal/mol) than for AA139 (-3.5 kcal/mol). This trend correlates well with the acrylamide quenching study performed in chapter 4. The acrylamide quenching remains quite large for AA139 as compared to arenicin-3 when exposed to POPC LUVs, still demonstrating exposure of the Trp4 residue to the aqueous solvent for AA139 and less so for arenicin-3, meaning that the arenicin-3 Trp4 residue, would be inserted into the hydrophobic core of the liposome. This could explain the difference in mammalian toxicity between arenicin peptides.

Table 5-1 - OPM results describing the depth/hydrophobic thickness, $\Delta G_{transfer}$ and the tilt angle of arenicin peptides toward DMPC lipid model membrane.

Peptide	Depth/Hydrophobic Thickness (Å)	$\Delta G_{transfer}$ (kcal/mol)	Tilt Angle (°)	Membrane embedded residue
arenicin-3	3.3 ± 1.5	-4.4	82 ± 6	2
AA139	2.1 ± 1.7	-3.5	67 ± 9	2

Nanodisc stability study. Nanodiscs (ND) are the latest lipid bilayer model membranes, sufficiently small (about 10 nm) to be analyzed by solution state NMR. ND are a self-assembled lipid bilayer stabilized by a scaffold protein, mimicking as closely as possible a cell membrane bilayer. By using different compositions of lipids, theoretically any kind of cell membrane could be mimicked. However, because of their liquid phase transition or their charge, some lipids are more or less stable at any chosen temperature in this constrained environment. Therefore, as the use of ND grows,[9] questions are arising about the stability of this kind of membrane mimicking tool. Here, we evaluated the stability of four different ND constructs: (i) two different membrane scaffold proteins were designed, MSP1D1ΔH5 (shortened dH5 for the rest of the chapter) and cNW9 (circularized version of MSP1D1ΔH5)[10] and (ii) two different lipid compositions, POPC (mimicking mammalian cell membranes) and POPC/POPG (4:1) (mimicking G-ve bacterial cell membranes). We evaluated stability over a range of concentrations of ND, pH, buffer type, temperature and length of storage, using size exclusion chromatography (SEC), electron microscopy (EM) and mass spectrometry (MS) for characterization.

The comparison of the size exclusion chromatograms of the different ND compositions revealed promising results. The circularized membrane scaffold protein (cNW9) stabilized the ND of any lipid composition extremely well. This was true for any chosen buffer, temperature, concentration or

storage condition studied. However, the study revealed surprising results for the most commonly used membrane scaffold protein for NMR studies, MSP1D1ΔH5. This scaffold tended to be more homogeneous and stable when the ND was composed only of zwitterionic lipids rather than negatively charged lipids. Moreover, the storage buffer and temperature were found to play an extremely important role on its stability. This scaffold only remained stable over 30 days when stored in 20 mM Tris-HCl pH 7.5, 50 mM NaCl, 1 mM EDTA buffer. For all other conditions, the ND peak broadened and shifted over time, pushed to an extreme in the case of 37 °C storage in as little as two days. The stability study has been summarized in the Table 5-2. All size exclusion traces can be found in the Appendix V, Figures S7.5-1 to S7.5-4.

Table 5-2 – Nanodiscs stability study summary of the number of days the ND remained stable during the length of the stability study experiments. The stability was assessed from the SEC chromatograms (Appendix V, page **7-258 to 7-261**). Any shift and/or broadening of the ND peak would be considered as instability.

Buffer (containing 50 mM NaCl, 1 mM EDTA)	**Temperature (°C)**	**Number of days of ND stability/Number of days of experiment**			
		ND[POPC]		**ND[(POPC/POPG)(4:1)]**	
		dH5	**cNW9**	**dH5**	**cNW9**
20 mM Tris-HCl pH 7.5	4	30/30	30/30	1/30	30/30
20 mM PO4 pH6.5	4	3/30	30/30	1/30	30/30
20 mM Bis-Tris pH6.5	4	3/30	30/30	1/30	30/30
	25	-	-	1/2	2/2
	37	-	-	0/2	2/2
	freeze	-	-	2/2	2/2

A detailed study was conducted for both scaffold protein constructs of ND constituted with POPC/POPG (4:1) to assess degradation in the preferred buffer, 20 mM Bis-Tris pH 6.5, 50 mM NaCl, 1 mM EDTA.

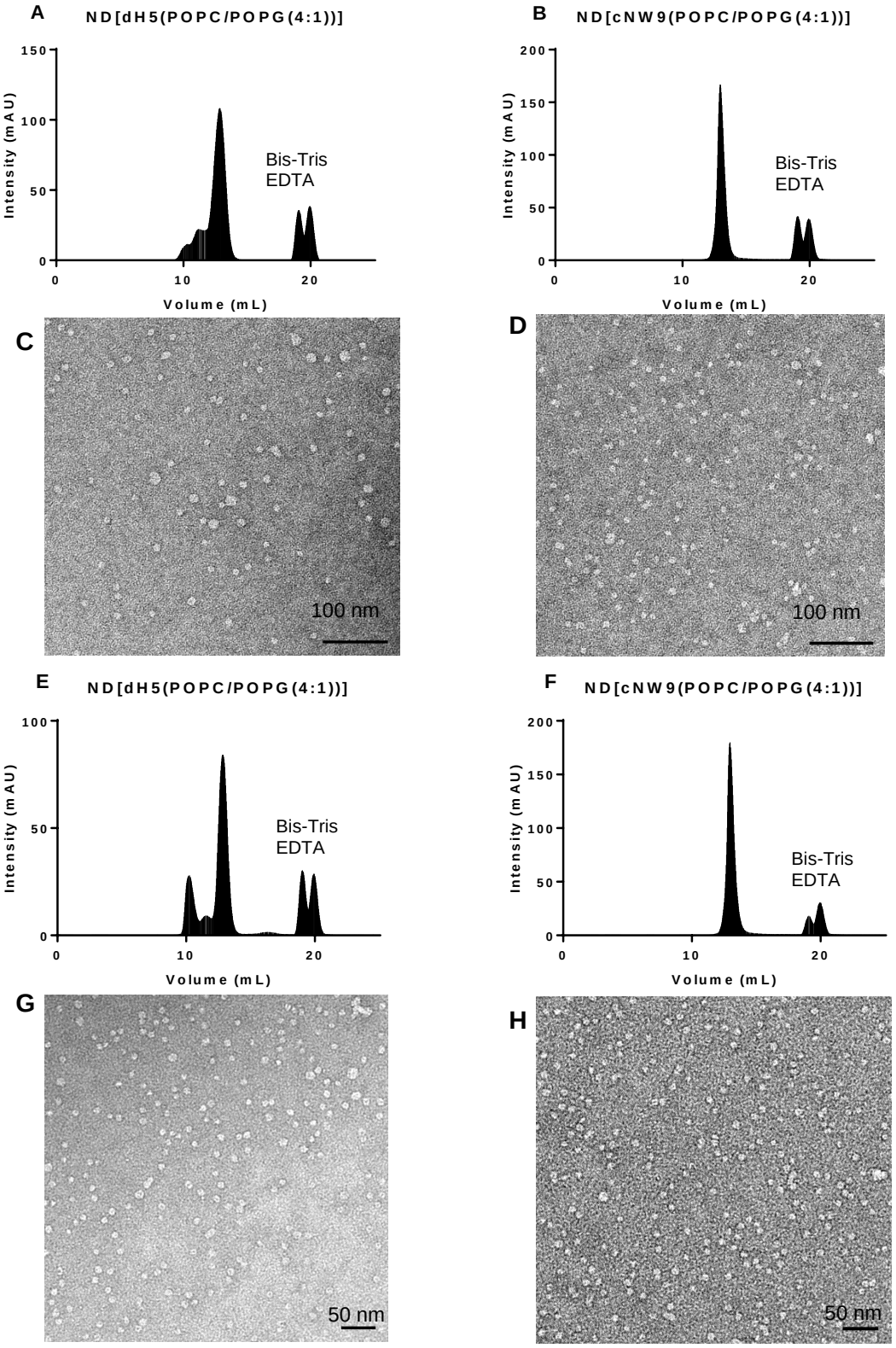

Figure 5-3 – Stability study of ND constituted with POPC/POPG (4:1) using membrane scaffold protein dH5 (A, C, E and G) and cNW9 (B, D, F and H) construct at day 0 (A, B, C and D), time of assembly and day 7 (E, F, G and H) after storage at room temperature. A, B, E and F are size exclusion chromatography traces. While C, D, G and H are negative staining (1% uranyl acetate) EM images.

At time of assembly (day 0), both ND constructs were analyzed by SEC, Figure 5-3 (A and B). Electron microscopy of both constructs was imaged at day 0, Figure 5-3 (C and D), showing discs of around 8-10 nm diameter. The ND were left at room temperature for seven days and reanalyzed via SEC, Figure 5-3 (E and F) and EM, Figure 5-3 (G and H). The SEC were fractionated and each fraction was subjected to LC-MS in positive mode, Figure 5-4 and Figure 5-5. Negative mode MS was performed for select fractions only to confirm the presence of POPG lipids in the ND peaks, Appendix V, Figure S7.5-5. Negative staining, Figure 5-3 (G and H), confirmed the inhomogeneity of ND diameter for dH5 construct while the cNW9 construct remained quite homogenous. Negative staining was also performed for selected fraction of ND[dH5(POPC/POPG(4:1))], confirming the presence of ND of increased diameter after seven days of storage, Appendix V, Figure S7.5-6. The degradation of ND[dH5(POPC/POPG(4:1))] demonstrated aggregation of the ND over time, however for ND[cNW9(POPC/POPG(4:1))] no degradation was observed.

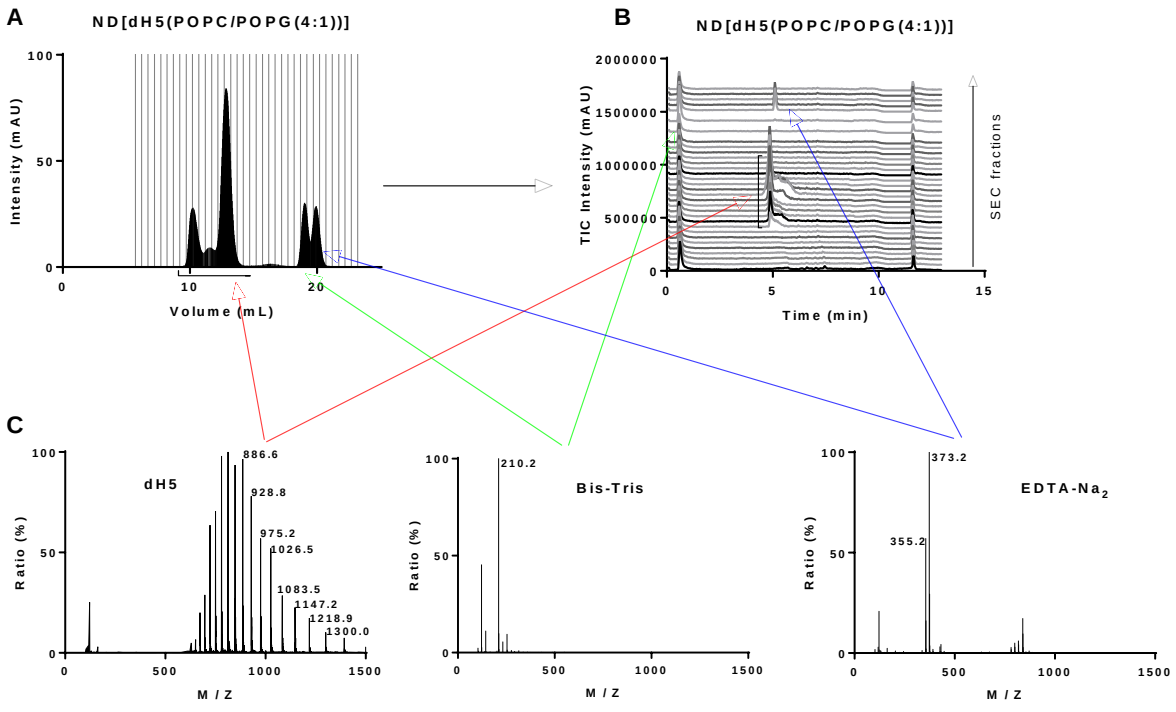

Figure 5-4 – (A) SEC of ND[dH5(POPC/POPG(4:1))] nanodiscs at day 7 stored at room temperature, (B) vertical stacking of LC-MS (ESI in positive mode) of the SEC fractions and (C) M/Z TIC trace of selected peaks. MW(dH5) = 19486 g/mol, MW(Bis-Tris) = 209.2 g/mol and MW(EDTA-Na_2) = 372.2 g/mol.

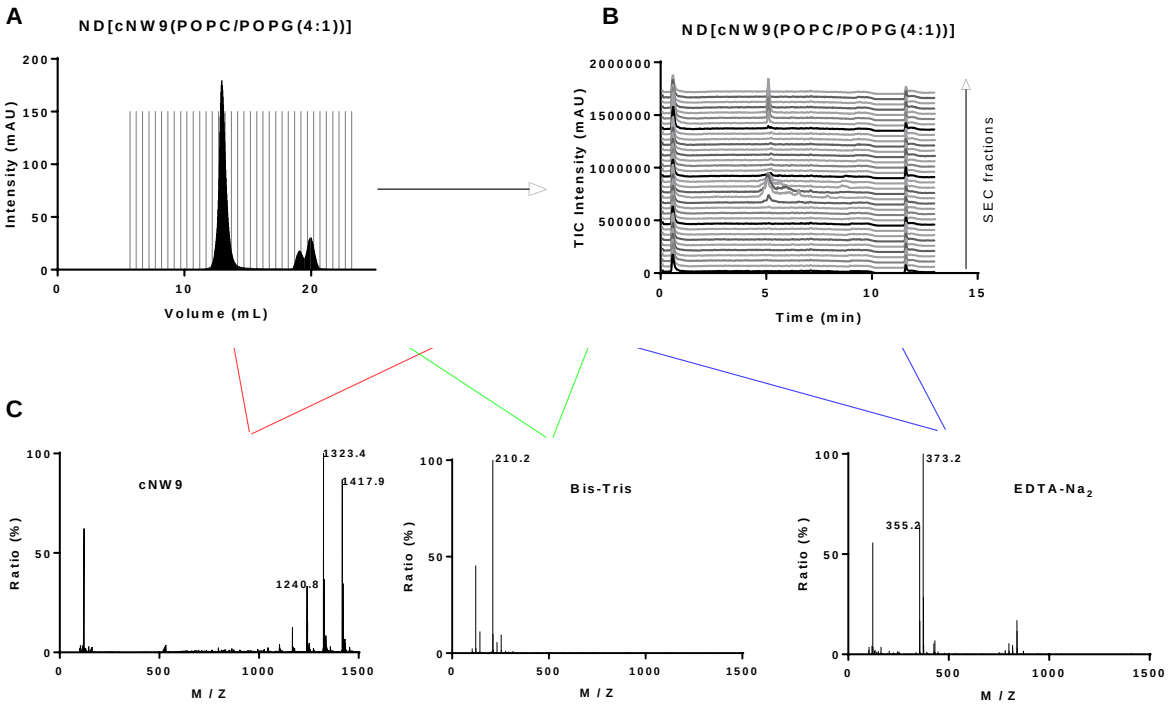

Figure 5-5 - (A) SEC of ND[cNW9(POPC/POPG(4:1))] nanodiscs at day 7 stored at room temperature, (B) vertical stacking of LC-MS (ESI in positive mode) of the SEC fractions and (C) M/Z TIC trace of selected peaks. MW(cNW9) = 19837 g/mol, MW(Bis-Tris) = 209.2 g/mol and MW(EDTA-Na_2) = 372.2 g/mol.

Dynamic Light Scattering (DLS) experiments were performed using MSP1D1ΔH5 membrane scaffold protein either alone or as scaffold for the ND. In this study, the results of the dH5 taken alone demonstrated a mono-disperse particle type with a diameter around 8 nm. This surprising result matched almost perfectly with all other ND studied here, giving mono-dispersed particles with a diameter about 8 nm. This rendered the use of the DLS technique inadequate for our study to evaluate if the ND were correctly assembled. Therefore, it was decided to not pursue the use of the DLS technique for all other ND studies and/or assemblies. The DLS measurements could be found in Appendix V, Figure S7.5-7.

NMR titration experiment. Nanodiscs are detergent free lipid bilayer model membranes and are often an ideal tool to study membrane proteins. However, they can also be used to characterize the interaction of peptides with cell membranes.

A preliminary screen was performed to determine the most suitable buffer for NMR titration experiments of ^{15}N-AA139. To perform the 3D solution NMR structure of AA139, presented in chapter 4, phosphate buffer pH = 3.3 was chosen in order to reduce the solvent exchange and thereby aid the detection of the backbone amides present, leading to 100% of the amide backbone being

visible. However, to evaluate the mode of action of the peptide toward model membranes, a pH closer to physiological conditions would be a more genuine representation. In this case, the ideal buffer would be as close to physiological pH, around 7, as possible and requires at least 80% of the amide backbone to remain visible.

Due to fast exchange of amide protons with the solvent, the higher the pH used, the lower the number of detectable protons. Therefore, a compromise was made in the choice of the buffer, which was 20 mM Bis-Tris pH 6.5, 50 mM NaCl. This buffer allows the detection of 18 out of 21 amide backbone peaks, around 90% of the total amide backbones. Two of the backbone amides are therefore not visible using pH 6.5: Phe2 and Asn11, Figure 5-6 and Appendix V, Figure S7.5-8.

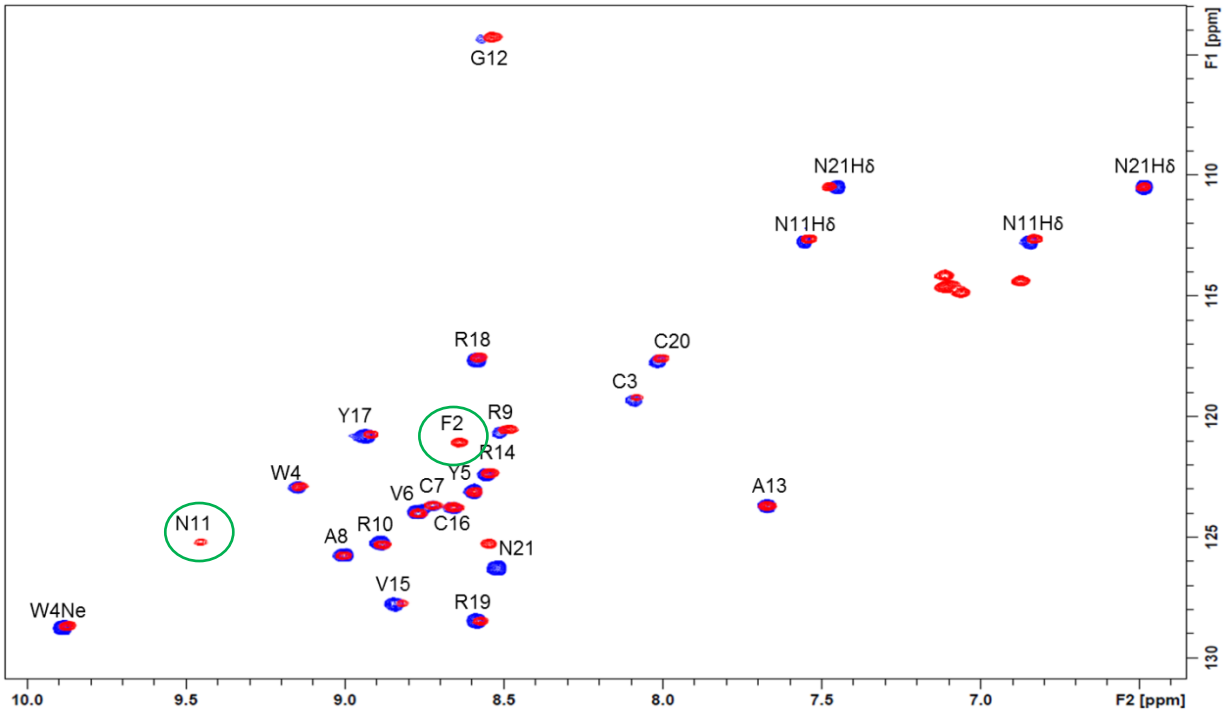

Figure 5-6 - ^{1}H-^{15}N-HSQC of ^{15}N-AA139 in 20 mM PO4 buffer at pH 3.3 in red and 20 mM Bis-Tris pH 6.5 in blue. Peaks have been assigned with both amides backbones only present at pH 3.3 circled in green. Peaks not assigned correspond to side chains.

A titration experiment evaluated the effect of ^{15}N labelled AA139 structure upon titration with ND containing POPC/POPG (4:1) (ND[cNW9(POPC/POPG(4:1))]), mimicking the lipid bilayer membrane of G-ve bacterial cells, such as *E. coli*. This was followed by a series of ^{15}N-HSQC experiments, Figure 5-7, where the concentration of ^{15}N-AA139 was kept constant while the concentration of the ND would increase toward complete saturation, Table 5-3.

Table 5-3 - Experimental design of the solution NMR titration experiment between ^{15}N-AA139 and ND[cNW9((POPC/POPG(4:1))]

Experiment	0	1	2	3	4	5	6
^{15}N-AA139 (µM)	40	40	40	40	40	40	40
ND[cNW9(POPC/POPG(4:1))] (µM)	0	5	7.5	10	12.5	15	20

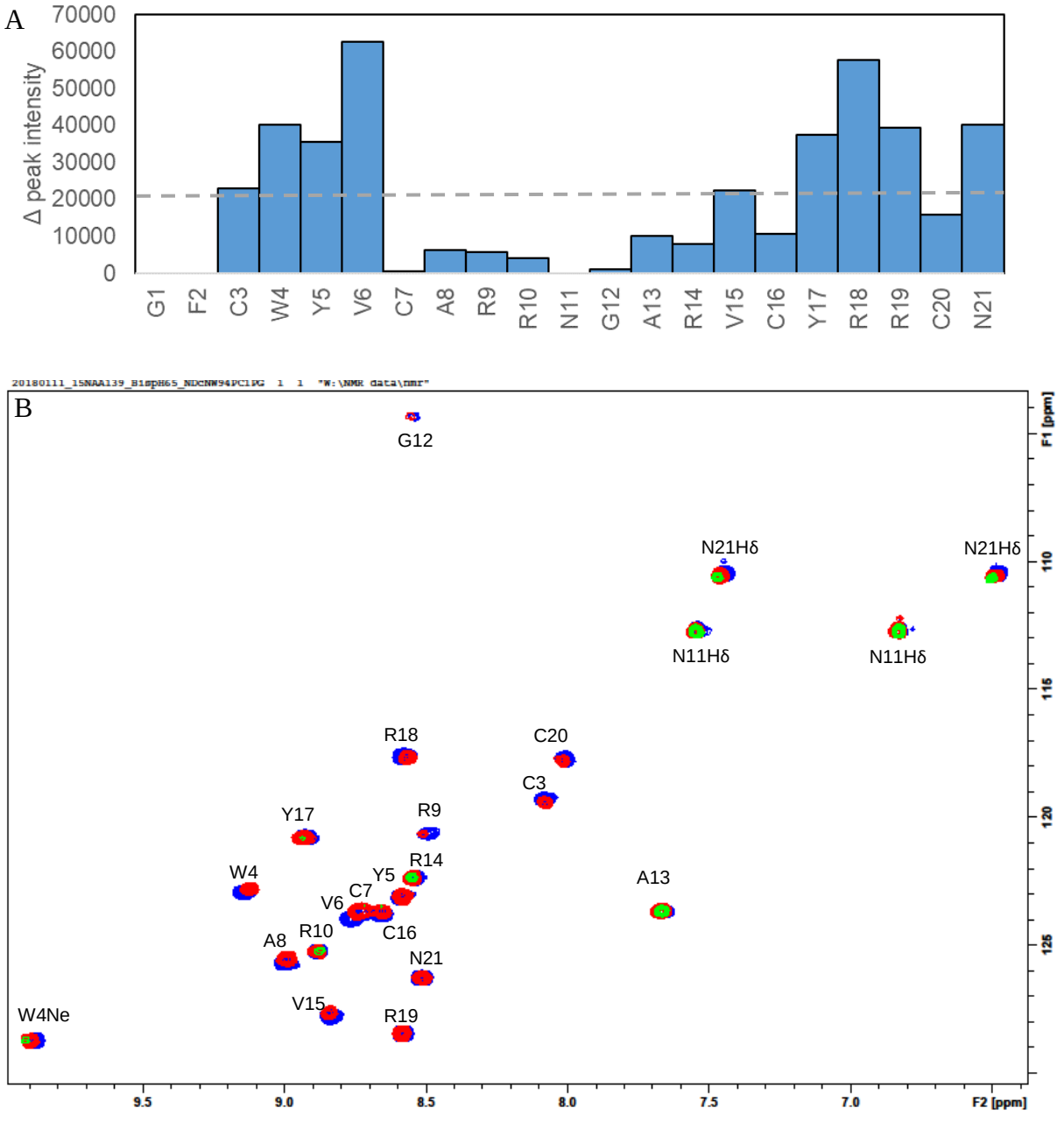

Figure 5-7 – (A) Bar graph of the amide backbone peak intensity change between Peptide/ND ratio (1:0) and (4:1), the grey dash bar represent the average value of all the data points, (B) ^{1}H-^{15}N-HSQC of ^{15}N-AA139 titrated with ND[cNW9(POPC/POPG(4:1))] with varied Peptide/ND molar ratio, (1:0) in blue, (4:1) in red and (2:1) in green.

The addition of ND to the peptide environment could lead to (i) structural modifications upon binding (including self-association and changes in local chemical environment) and/or (ii) change the overall tumbling of the molecule and/or (iii) change the local motion of residues at the binding interface leading to chemical shift movement and/or intensity variation of ^{15}N-AA139 peak signals. Upon binding, the portion of free versus bound peptide changes and the signal of amide (HN) protons of ^{15}N-AA139 residues will be modified depending on the timescale of the binding interaction: (i) fast exchange would mean that the peaks would undergo chemical shift modifications, (ii) intermediate exchange would mean that the peaks would undergo broadening and (iii) slow exchange would mean that two separate set of peaks would be observed. Due to the very large difference in the apparent size of the free and bound state, the bound state will not contribute to the observed signals, except for residues in highly dynamic regions that are not affected by the global tumbling of the molecule (e.g. sidechains of glutamine and asparagine residues and in disordered loops or termini).

The results showed that the amide backbone peaks of ^{15}N-AA139 are not displaying significant changes in chemical shifts along the x (^{1}H) and/or y (^{15}N) axis when titrated with ND, however, intensity change (or broadening) of the peaks was observed. The interaction between ^{15}N-AA139 and ND[cNW9(POPC/POPG(4:1))] is likely to be in the intermediate timescale of interaction (μs-ms).

The data were analysed qualitatively by measuring the difference in peak intensity between Peptide/ND ratio (1:0) and (4:1), as shown in Figure 5-7 (A). The residues with the largest intensity changes (tallest bars), above the average (grey dash bar on the graph), (Cys3, Trp4, Tyr5, Val6, Tyr17, Arg18, Arg19 and Asn21) are most significantly affected by the presence of the NDs. Thus, those residues are most likely to be located at the peptide/ND interface. At a low concentration of ND (peptide/ND ratio of 4:1), ten residues appear unaffected by the presence of the ND (Cys7, Ala8, Arg9, Arg10, Gly12, Ala13, Arg14, Val15, Cys16 and Cys20), showing only minimal peak intensity difference, below the average threshold. Those residues are least likely to be located at the peptide/ND interface.

If the loss in signal can be attributed directly to binding (i.e. the bound state leads to complete loss of signal), it is possible to analyse the data more quantitatively, using the approach proposed by Williamson et al.[11]. Considering the vastly greater size of the bound state, it is reasonable to assume that the observed signals are only from free peptides in solution (i.e. not bound to nanodiscs). Under these circumstances this approach can be applied to determine rough estimates of the K_d of AA139 to NDs. This approach is usually applied for slow or fast exchange regimes, nevertheless as noted above, the model can be applied with some caution under the conditions described here. Thus, the application of this model requires the following assumptions: (i) the ligand is be the ND and the receptor is the peptide, (ii) the peak broadening is only dependant on binding interaction, leading to

observed signals only representing free (unbound) peptides in solution and (iii) an absence of cooperative binding. Moreover, Williamson's equation had to be modified in our case, due to the possibility of a multiple number of equivalent binding sites for the peptide toward the ND, introducing thus another variable, N.

$\Delta\delta_{obs} = \Delta\delta_{max}*((K+P+x*N)-(((K+P+x*N)^2)-4*P*x*N)^{1/2})/(2*P)$, where $\Delta\delta_{obs}$ is the change in the observed intensity from the free state, $\Delta\delta_{max}$ is the maximum intensity change in amplitude, P is the concentration of peptide, x is the concentration of ND, K is the K_d and N is the number of equivalent binding sites. A script was written to perform fitting and plotting of the data to the equation using gnuplot.[12]

The analysis was first run for each residue individually with variable K and N, Table 5-4. The results indicated 7 residues with negative K_d values (Cys7, Ala8, Arg10, Gly12, Ala13, Arg14 and Cys16), indicating that the broadening of these residues does not simply involve binding interaction between AA139 and the ND (i.e. additional exchange processes are occurring that lead to signal loss). Arg9 and Val15 are residues located in the same loop end of the peptide, thus, probably involved in the same type of interaction. For those residues, the broadening of the peaks is potentially due to conformational change. The 9 residues (Cys3, Trp4, Tyr5, Val6, Tyr17, Arg18, Arg19, Cys20 and Asn21), located at the *N*- and *C*-terminal ends of AA139, in contrast show broadening that fits the two-site exchange model used to model the binding interactions. Thus, a second analysis was performed fitting all nine residues as a whole molecule to determine AA139's K_d for NDs. N was first left as a variable then fixed to the closest even integer number, 4. N equal 4 would mean that two AA139 would interact on each side of the ND, Table 5-5. Figure 5-8 shows the graph fitting the intensity of change versus ligand concentration.

Table 5-4 - K_d and N values for each AA139 residues taken individually.

residue	K_d (µM)	N
G1	-	-
F2	-	-
C3	1.26 ± 0.95	5.48 ± 0.63
W4	0.21 ± 0.31	4.68 ± 0.27
Y5	0.56 ± 0.55	3.74 ± 0.29
V6	0.37 ± 0.24	5.05 ± 0.21
C7	-44.15 ± 6.85	4.80 ± 0.87
A8	-0.05 ± 0.29	2.94 ± 0.32
R9	0.08 ± 0.31	2.81 ± 0.20
R10	-1.17 ± 1.67	2.53 ± 0.31
N11	-	-
G12	-0.30 ± 3.38	2.20 ± 0.51
A13	-0.41 ± 1.61	2.58 ± 0.24
R14	-0.39 ± 1.84	2.6 ± 0.27
V15	0.52 ± 0.35	4.09 ± 0.21
C16	-0.43 ± 1.07	2.87 ± 0.23
Y17	0.93 ± 1.10	3.99 ± 0.53
R18	0.70 ± 0.52	4.73 ± 0.34
R19	0.34 ± 0.33	3.51 ± 0.19
C20	0.53 ± 1.02	4.47 ± 0.68
N21	0.62 ± 0.70	3.84 ± 0.37

Table 5-5 - K_d and N value for AA139 taken as a whole.

residue	K_d (µM)	N
overall	0.76 ± 0.31	4.41 ± 0.18
overall	0.34 ± 0.14	4

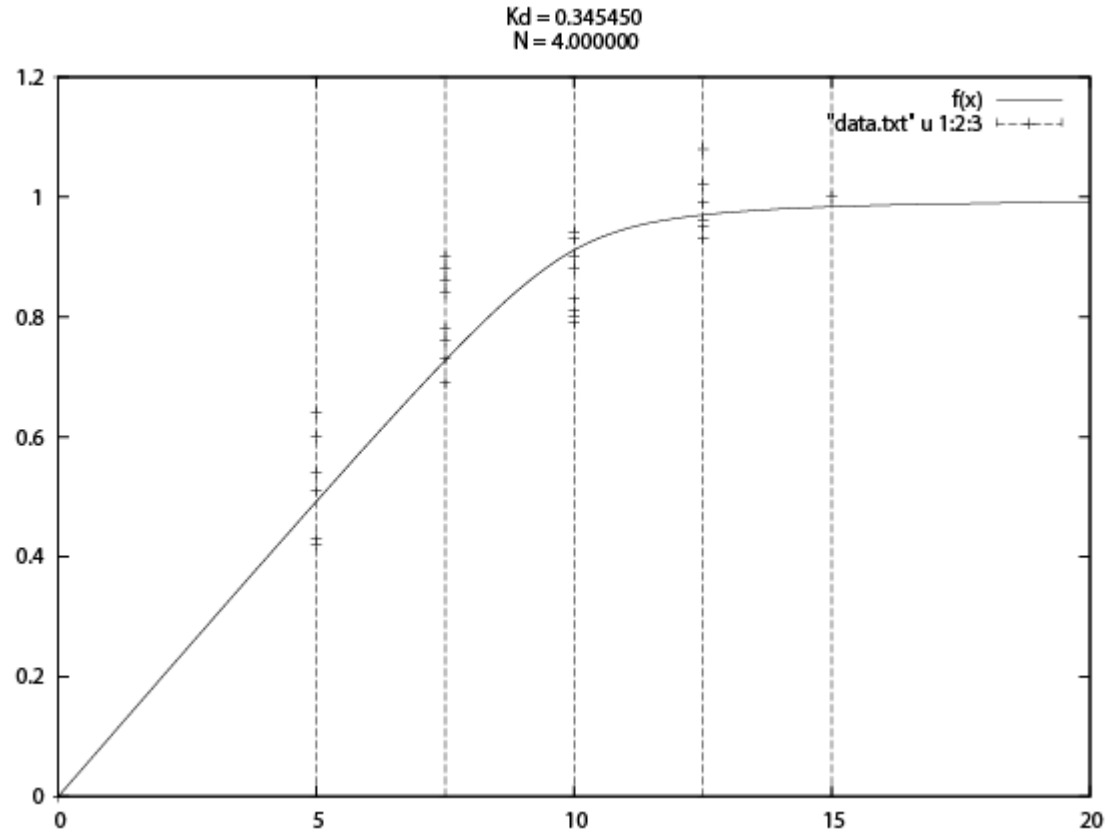

Figure 5-8 - Graph of intensity change versus ligand concentration (μM).

The combination of both data analyses indicated that 8 (qualitatively) and 9 (quantitatively) residues were significantly involved in the binding interaction. Both analysis methods correlated quite well, indicating the same 8 residues (Cys3, Trp4, Tyr5, Val6, Tyr17, Arg18, Arg19 and Asn21) as being involved in the binding interaction. Only one residue, Cys20, does not match between both analysis types. For a more visual representation of the residues most affected by the binding event, a 3D representation was used to illustrate the interaction results, Figure 5-9. This representation shows that the *N*- and *C*-termini of the peptide are dominated by residues involved in the binding interaction, indicating this part of the peptide as potentially the first point of interaction with the lipid bilayer. These results correlate well with the computational modelling examined previously, identifying the *N*-terminus of the peptide as the region to first enter at around 67° tilt angle.

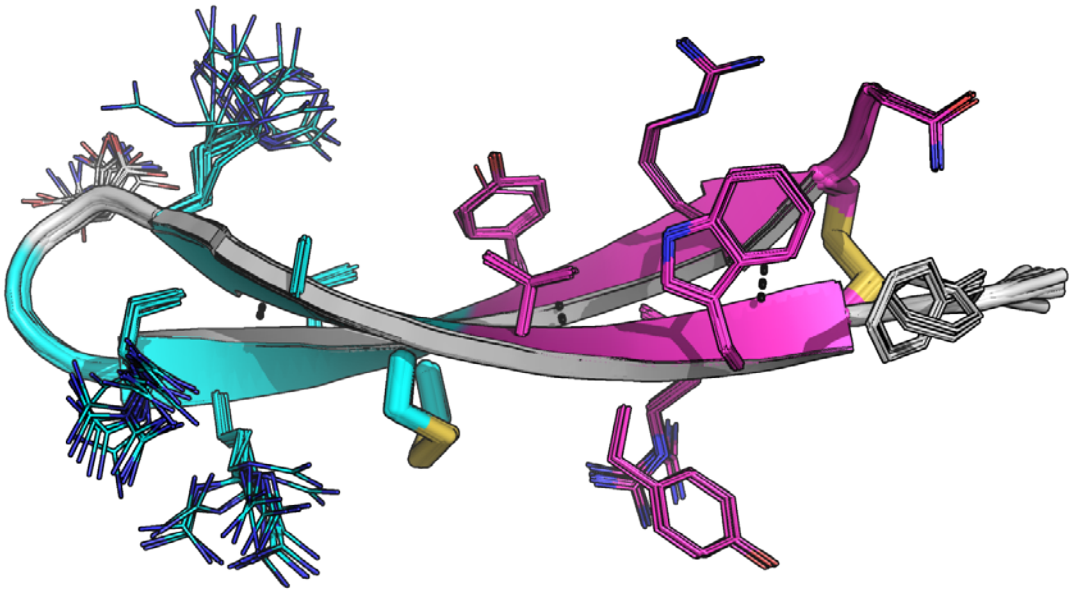

Figure 5-9 - 3D structure of AA139 in cyan with H-bond marked as dashed lines and residues interacting with the lipid bilayer represented in magenta and the undetermined residues in grey.

In this kind of experiment, the type of binding observed needs to be carefully interpreted. To make sure the binding observed corresponds to the interaction between AA139 and the lipid bilayer rather than binding between AA139 and cNW9, a titration experiment control was performed between ND[^{15}N-cNW9(POPC)] and AA139. The ND in this case were made with 100% POPC, as AA139 was previously reported, in chapter 4, of having weaker binding toward POPC than POPC/POPG(4:1) lipid bilayer. Therefore, the control experiment was designed as followed in Table 5-6. Experiment 1 should already reach saturation point due to the ratio of saturation observed in the previous titration experiment between ^{15}N-AA139 and ND[cNW9(POPC/POPG(4:1))], where the saturation was reached at peptide to ND ratio 2:1.

Table 5-6 - Experimental design of the solution NMR titration experiment between AA139 and ND[^{15}N-cNW9(POPC)]

Experiment	0	1	2
AA139 (µM)	0	50	100
ND[^{15}N-cNW9(POPC)] (µM)	100	100	100

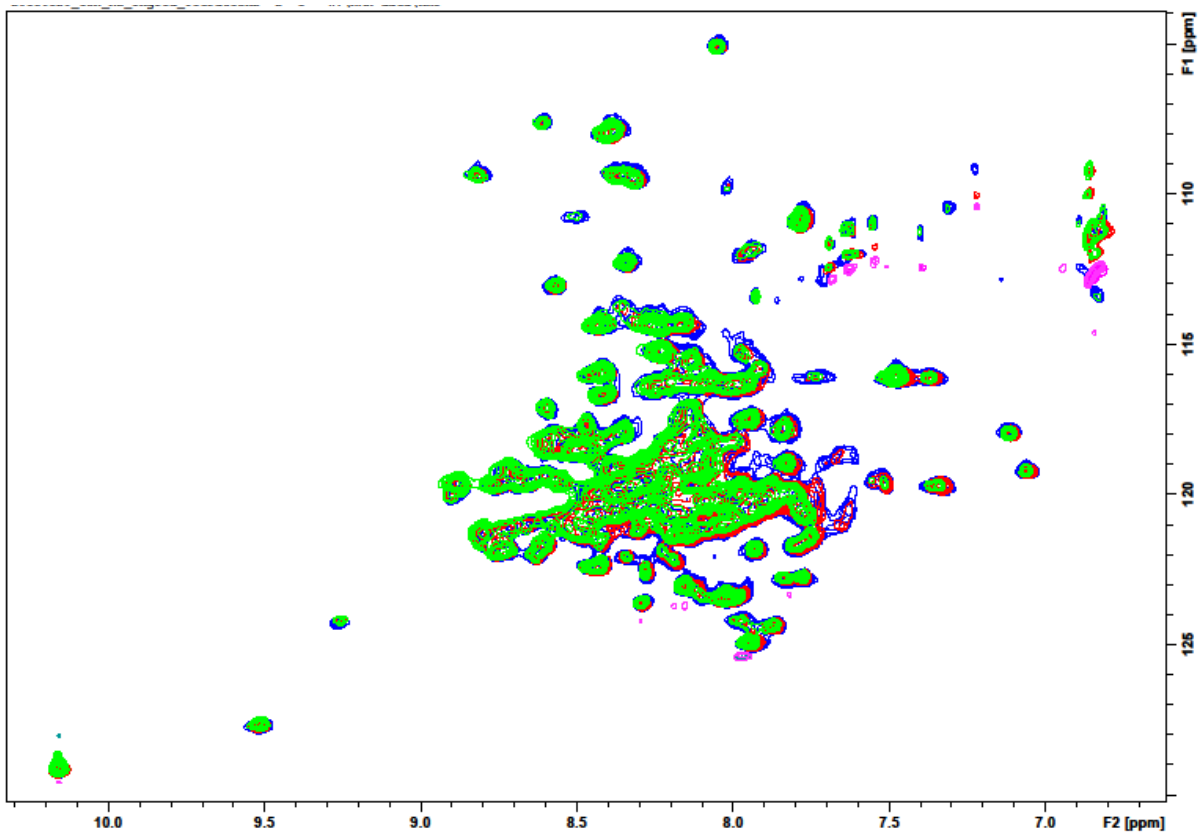

Figure 5-10 – ^{1}H-^{15}N TROSY HSQC recorded at 50 °C of ND[^{15}N-cNW9(POPC)] titrated with AA139 with varied ND/Peptide molar ratio, (1:0) in blue, (2:1) in red and (1:1) in green.

The results, Figure 5-10, showed well distributed spectra for ND[^{15}N-cNW9(POPC)] at 50 °C. The titration was also recorded at 25 °C but the resolution was very poor (data in Appendix V, Figure S7.5-9). Interactions between AA139 and cNW9 could occur from two distinct regions of the helices belt, the external and the internal region. The internal region of the ND belt would only be accessible after previous binding to the lipid bilayer as a secondary interaction. This kind of interaction cannot be avoided and controlled. However, the interaction at the external region needs to be monitored. The titration with non-labelled AA139 did not modify the distribution of the peaks, however slight intensity decrease was observed, when AA139 was titrated. Thirty well defined peaks were picked and the heights were recorded. The percentage of intensity decrease between experiment 1 and/or 2 and experiment 0 was calculated. The percentage of height decrease ranged from 4.6% to 51.4% with an average around 36%. It was noted that the peak intensities were relatively similar between experiment 1 and experiment 2, which correlates with the previous titration experiment, where the saturation point was already reached at a ratio of peptide:ND of 2:1. The intensity decrease in the titration experiment between ND[^{15}N-cNW9(POPC)] and AA139 is negligible as compared to the intensity decrease during the opposite titration experiment, where the average was around 92%, i.e. near complete signal loss. In other words, the interaction between AA139 and cNW9 is significantly

weaker when compared to its interaction with the lipid bilayer and therefore does not affect the derived AA139 K_d value for the interaction with the lipid bilayer POPC/POPG(4:1).

Solid-state NMR study using lipid bilayer vesicles. The results generated from the titration solution state NMR with ND, indicated that AA139 had strong interactions with negatively charged lipid model membranes. However, which conformational state does AA139 adopt when integrated in the lipid bilayer membrane? To answer this question, the characterization of the AA139 structure needs to be monitored while integrated in the lipid bilayer. Solid-state NMR offers adequate tools for this study.

Solid-state NMR spectroscopy (ssNMR) is used for hard to solubilize proteins, membrane proteins and amyloids/fibrils, or micro-crystalline powder of soluble proteins: samples with very slow or inexistent reorientation. ssNMR offers a great advantage over solution NMR, in that it is not limited by the size of the molecule. This is the reason why we have chosen to evaluate the structure of AA139 in lipid vesicles (LUVs) using ssNMR. The absence of molecular tumbling in ssNMR causes extreme line-broadening to render spectra impossible to interpret. However, extremely fast spinning at the magic angle ($\theta = 54.7^{\circ}$ relative to the magnetic field B_0), i.e. MAS, offers the possibility to simulate motional averaging. In MAS, the normally broad lines become narrower due to removal of the anisotropic interaction terms. This increases the resolution of the spectra and renders them interpretable. Unlike solution NMR where most nuclei can be detected, in ssNMR generally only low-γ nuclear spins nuclei, i.e. ^{13}C and ^{15}N can be observed, since the spinning rate has to be larger than the interaction strength.[13]

This work was done collaboratively with the Leibniz-Forschungsinstitut für Molekulare Pharmakologie in Berlin with the group of Professor Hartmut Oschkinart, who is an expert in this field.

In solution NMR, a titration with lipid ND was possible because only the freely tumbling, unbound, peptides were studied. However, the sample for ssNMR needs to be prepared as such that the peptide possesses as few orientations as possible to avoid line broadening. Thus, the sample was prepared as concentrated as possible to render the detection of the peptide possible whilst maintaining an appropriate peptide to lipids ratio, for the peptide to be fully integrated with the LUVs without precipitation. The ideal molar peptide to lipids ratio was found to be 1:80. Figure 5-11 validated the choice of the 1:80 ratio by showing the peptide proton signal disappearance, due to the change of molecular tumbling, when in presence of LUVs. In order to perform a comparison of the solution

NMR to the ssNMR as fairly as possible, the same buffer was chosen, 20 mM Bis-Tris pH 6.5, 50 mM NaCl.

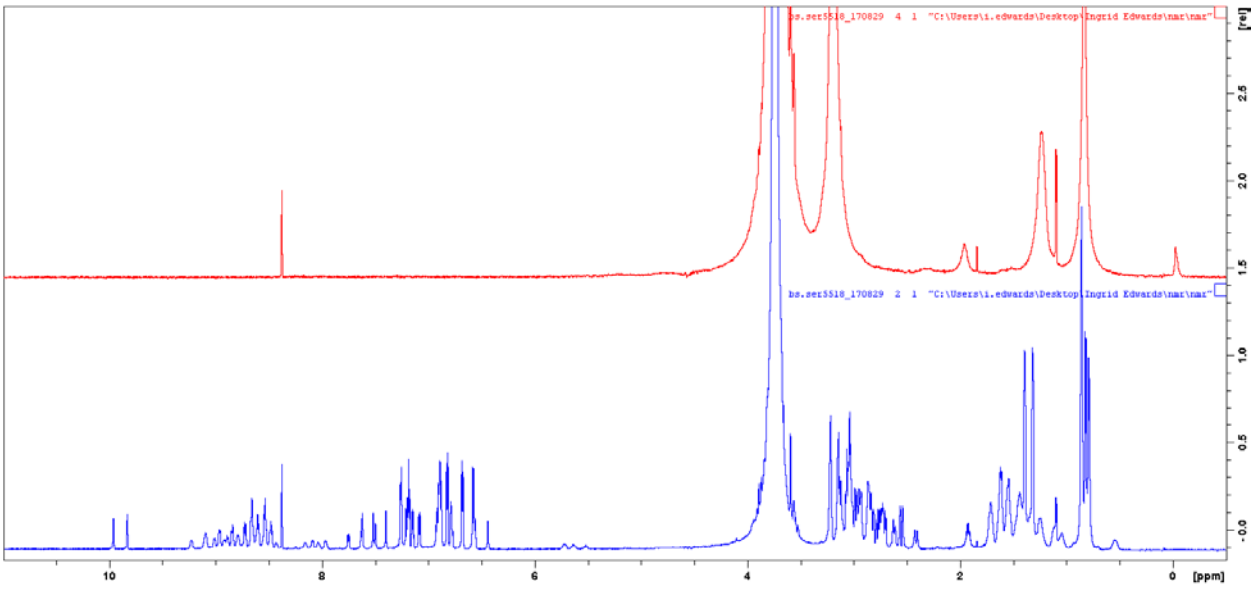

Figure 5-11 – ^{1}H solution NMR of ^{15}N-AA139 at 93 µM free in solution (blue) and in presence of LUVs at 7.5 mM (molar ratio peptide:lipids 1:80) (red) in 20 mM Bis-Tris pH6.5, 50 mM NaCl.

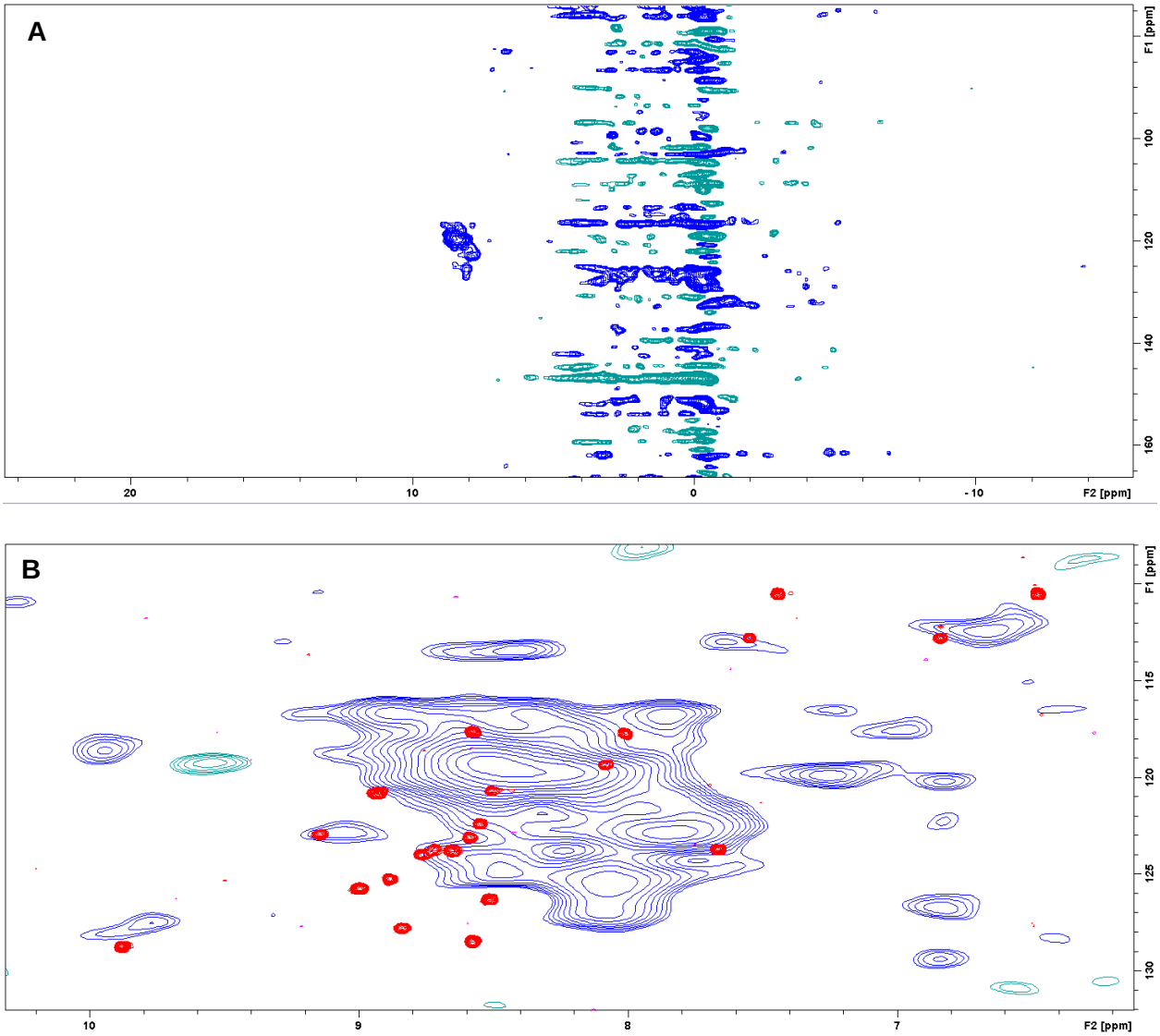

Figure 5-12 – (A) ^{1}H-^{15}N CP with water suppression ssNMR experiment of ^{15}N-AA139 in presence of LUVs at molar ratio 1:80 in 20 mM Bis-Tris pH6.5, 50 mM NaCl. (B) Zoomed ^{1}H-^{15}N superimposed spectra (A) in blue and ^{15}N-AA139 in free solution (red) in 20 mM Bis-Tris pH6.5, 50 mM NaCl.

Figure 5-12 (A) shows the ^{1}H-^{15}N CP with water suppression ssNMR experiment of ^{15}N-AA139 in presence of LUVs at molar ratio 1:80 in 20 mM Bis-Tris pH 6.5, 50 mM NaCl. Peaks in the right region for a peptide were observed, however the signal to noise ratio was poor and therefore limited the spectral interpretation. Figure 5-12 (B) shows ^{1}H-^{15}N superimposed spectra of ^{15}N-AA139 in free solution (red) and in presence of LUVs at molar ratio 1:80 (blue) in 20 mM Bis-Tris pH 6.5, 50 mM NaCl. Even with the poor signal to noise ratio of the ssNMR spectra, we can clearly see that both set of peaks are not superimposing and therefore reflect a different secondary structure of AA139 when free in solution compared to in presence of LUVs that are representative of a bacterial membrane. The ssNMR spectra displayed peaks in the region of random coil secondary structure, as opposed to

the solution NMR free state, which demonstrated a fully structured β-hairpin AA139. These results could mean that the peptide loses its well defined 3D structure when inserting in the liposomes.

DLS was performed to evaluate the size of the LUVs in absence and presence of AA139. The results are detailed in Table 5-7 and the volume distribution versus the size of the particle can be found in Appendix V, Figure S7.5-10. In both samples, the distribution is very mono-disperse, with one single peak observed. The Z-average diameter distribution increased from 118.5 ± 0.8 nm to 135.6 ± 1.2 nm when LUVs are put in presence of AA139 at a ratio 80:1. The results support that AA139 interacts with the LUVs but does not promote aggregation at a peptide/lipid ratio of 1:80, however they seem to increase the size of the LUVs most likely by sitting on the surface or inserting in the particle and slightly expanding their diameter.

Table 5-7 - DLS results showing the Z. average and volume mean of LUVs in absence and presence of AA139 (ratio 80:1)

Sample	Z. Ave (nm)	Volume mean (nm)
LUVs [POPC/POPG (4:1)]	118.5 ± 0.8	111.2 ± 1.0
LUVs [POPC/POPG (4:1)] + AA139 (ratio 80:1)	135.6 ± 1.2	132.8 ± 8.1

5.3 Materials and methods

Material. Synthetic lipids palmitoyloleoyl-phosphatidylcholine (POPC) and palmitoyloleoyl-phosphatidylglycerol (POPG) were purchased from Avanti Polar Lipids (Alabaster, AL). All chemicals were used without further purification.

Recombinant expression of ^{15}N, ^{13}C labelled arenicin-3 and AA139.

Arenicin peptide expression in Escherichia coli

Recombinant isotopically single and double labelled (^{15}N and $^{15}N/^{13}C$) arenicin-3 or AA139, were expressed from a His_6-tagged SUMO fusion protein in *Escherichia coli* shuffle strain cells. The plasmid construct for arenicin-3 and AA139 expression was designed by myself and Zhenling Cui, respectively. The gene fragment containing optimized codons for His_6-SUMO-peptide as well as 5'- and 3'- overlap to pOPINE plasmid was synthesized by IDT. Recombinant plasmid pOPINE-His_6-SUMO-peptide was constructed by ligating the NotI/XhoI double digested pOPINE plasmid with the synthesized gene fragment. The plasmid contains the T7 promoter, the ribosome-binding site while the gene insert encodes the fusion protein with His_6-tag at N-term, plasmid vector represented in Figure 5-13.

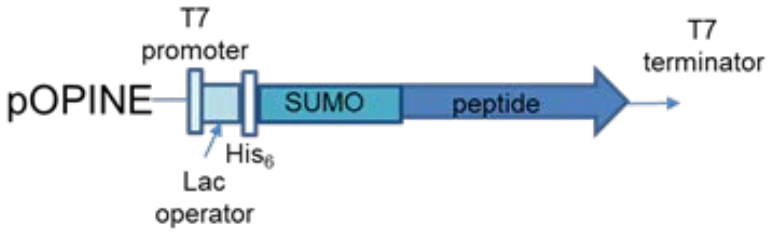

Figure 5-13 - Schematic representation of the expression vector. Schematic representation of the pOPINE-SUMO expression vector used for cytoplasmic expression of disulfide-rich peptides in an *E. coli* shuffle strain. The coding region includes a His6 tag for affinity purification, a SUMO fusion tag to aid solubility and a codon-optimized gene encoding the target peptide. The location of key elements of the vector are shown, including the T7 promoter and lac operator.

Plasmid purification (QIAGEN Plasmid Purification Kit) and transformation were performed according to the standard commercial protocol. After transformation, the clones containing the correct gene insert were screened for and confirmed by sequencing. The *E. coli* shuffle cells (NEB) transformed with pOPINE-His_6-SUMO-AA139 were grown in 10 mL of LB media with 100 µg/mL of ampicillin at 37 °C with shaking at 220 rpm until OD_{600} reached late exponential phase (OD_{600} = 0.8). The culture was then transferred to 50 mL of Minimum Media (MM) with 100 µg/mL of ampicillin supplemented with $^{15}NH_4Cl$ and/or ^{13}C-D-glucose and grown at 37 °C with shaking at 250 rpm overnight. The culture was then transferred in 2 L of MM with 100 µg/mL of ampicillin and grown at 37 °C with shaking at 250 rpm until OD_{600} = 0.8. The culture was then cooled down at 20 °C, followed by induction by adding 0.5 mM isopropyl β-D-1-thiogalactopyranoside (IPTG) at 20 °C

with shaking at 250 rpm overnight. The expression level of His_6-SUMO-peptide was monitored using sodium dodecyl sulfate polyacrylamide gel electrophoresis (SDS-PAGE).

Comments:

- Prior to the design of the pOPINE-His_6-SUMO-AA139 construct, a different construct was designed, taking example of the design presented by Klint *et al.*,[14] for disulfide rich peptides. With the presence of a MalE signal sequence in the coding region, the fusion protein is transported to the periplasm via the Sec translocase system. MalE is removed during this process releasing the fusion protein into the periplasm where the Dsb machinery (DsbA, DsbB, DsbC and DsbD) can assist with disulfide bridge formation. Synthetic genes encoding the arenicin peptides with codon optimization for expression in *E. coli* were cloned into variant of the pLic-MalE-His_6-MBP-peptide expression vector by Lifescience Technology, Geneart AG (Regenburg, Germany). The production of arenicin peptides was attempted using various *E. coli* strains (BL21(DE3), BL21(DE3) gold, BL21(DE3) C43, BL21(DE3) C41[15], BL21(DE3) RP, BL21(DE3) RIL, BL21(DE3) Star, Rosetta-gami(DE3), Rosetta-gami B(DE3), Rosetta 2(DE3), Rosetta blue (DE3) and NEB NiCO21 (Wk6) without success. In all attempted experiments, the fusion protein was retained in the insoluble part of the cell, trapped in the inclusion bodies. This had previously been observed for the recombinant production of arenicin-1 and arenicin-2 by Ovchinnikova et al.[16] Thus various attempts were trialed to retrieve the protein from the inclusion bodies using detergent, without success.[17]
- With pOPINE-His_6-SUMO-AA139 made first, it was thought that pOPINE-His_6-SUMO-arenicin3 could be constructed using Direct Mutagenesis with the Q5 kit from NEB using deletion/insertion PCR methodology. However, after several repeats, the mutagenesis was never fully complete and the construct could not be made. Therefore, pOPINE-His_6-SUMO-arenicin-3 was eventually constructed using the same ligation method previously used for the construction of pOPINE-His_6-SUMO-AA139.
- The Minimum Media composition was optimized for better yield, see final composition below, Table 5-8 and Table 5-9. Due to the high percentage of D-glucose, the shaking speed was increased to 250 rpm to ensure enough available oxygen for optimal cell growth.

Table 5-8 - M9 media recipe

M9 media (5X)	Mass (g) to make 1 L solution
KH_2PO_4	15
Na_2HPO_4	64
NaCl	5
Make up to 1L with H2O and adjust the pH to 7 before autoclave	

Table 5-9 - Minimum media recipe

Minimum media	Volume (mL) to make 1 L solution
M9 (1X)	1000
MEM Vitamin Solution (100×)	10
Thiamine (40 mg/mL)	2
$MgSO_4$ (1 M)	1.6
$CaCl_2$ (1 M)	0.08
(^{15}N)NH4Cl (0.25 mg/mL)	4
(^{13}C)D-glucose (0.2 g/mL)	50
Ampicillin (100 mg/mL)	1

Fusion protein purification and cleavage

The cells were harvested by centrifugation at 7000 rpm for 30 min at 4 °C and resuspended in buffer containing 150 mM sodium phosphate buffer (pH 8), 300 mM NaCl, 20 mM imidazole, EDTA-free protease inhibitor cocktail. The cells were then disrupted using a cell disruptor at 27 KPsi for 1 cycle and subjected to centrifugation at 20000 rpm for 30 min at 4 °C. The supernatant was applied to two attached 5 mL Histrap FF prepacked columns on a FPLC (AKTA instrument). The recombinant protein was eluted with 0.5 M imidazole and the fractions corresponding to the fusion protein were collected and concentrated using Amicon 3 kDa. Buffer exchange was performed by dialysis using 6-8 kDa MW cut off membrane for 6 h against 2 L of the cleavage buffer of 50 mM Tris-HCl (pH 8), 150 mM NaCl. SUMO protease was then used for the cleavage of the fusion protein with a (w/w) ratio of 1:50, shaking overnight at 4 °C.

Comments:

- Throughout the purification and cleavage process, glassware should be used to handle fusion protein and protein alone as arenicin peptides are highly adsorbent on plastic. Thus, the use of plastic containers would highly reduce production yield.

AA139 purification by HPLC

The solution was loaded onto a Gilson HPLC system using C18 column (Zorbax® C18, 9.4 x 100 mm, 5 um) equilibrated with solution A (0.1% trifluoroacetic acid). The chromatography was performed at a flow rate of 3 mL/min with a linear gradient of solution B (100% acetonitrile, 0.1% trifluoroacetic acid): 5% for 6 min, 5–50% for 16 min, 50–100% for 4 min, 100% for 2 min and 5% for 3 min. The peaks monitored at 210 nm were collected and lyophilized. The lyophilized product was then analyzed by LC-MS using Agilent Technologies 1200 Series Instrument with a G1316A variable wavelength detector set at λ= 210 nm, 1200 Series ELSD, 6110 quadrupole ESI-MS, using an Agilent Zorbax Eclipse XDB-Phenyl (3 × 100mm, 3.5 μm particle size, flow rate 1 mL/min, the mobile phases 0.05% formic acid in water and 0.05% formic acid in acetonitrile). ^{1}H and ^{1}H-^{15}N-HSQC NMR spectra were assessed for comparison to the synthetic material.

Comments:

- After the cleavage step, it is of common practice to remove the affinity tags before performing the HPLC step. This can be achieved by applying the cleaved mixture solution to a Ni-NTA column (5 mL Histrap FF prepacked). However, the arenicin peptides were highly retained by the Ni-NTA beads and only a tiny percentage of the peptide would be released leading to very poor yield. Another method was attempted; the addition of 1% TFA to the cleavage mixture solution, however this resulted in co-precipitation of the peptide with the tags and therefore the purification could not be pursued. By avoiding that step completely, the yield of 0.125 mg/L of culture using the reverse purification method by Ni-NTA, increased dramatically to 0.75 mg/L of culture, leading to a total of 6-fold increase in the yield.[14]

Nanodiscs preparation. MSP1D1Δh5 was cloned by PCR mutagenesis to incorporate the DNA encoding for the *C*-terminal LPGT motif to create the cNW9 construct. MSP1D1Δh5 and cNW9 were recombinantly expressed in *E. coli* BL21(DE3) cells from a pET29 vector as a 6-histidine fusion protein and purified on a metal affinity column (Ni-NTA). cNW9 was circularized using sortase A inhibition approach.[10] cNW9 labelled and non-labelled protein were expressed, purified and circularized by Alan Zhang.

To assemble nanodiscs with different lipid compositions, MSP1D1Δh5 or cNW9 protein and lipids were co-dissolved in reconstitution buffer (20 mM Tris.HCl pH 7.4, 100 mM NaCl, 0.5 mM EDTA and 100 mM Cholate) and mixed for 1 h at 4 °C. Molar ratio of 1:50 (membrane scaffold protein (MSP) / lipids) was taken according to the surface area of such type of lipids used, using the equation: $N_L \bullet S = (0.423 \bullet M\text{-}9.75)^2$ with the number of lipids per Nanodisc, N_L, the number of amino acids in the scaffold protein, M and S, the mean surface area per lipid used to form the Nanodisc, measured in $Å^2$.[18] POPC and POPG have been estimated with similar mean surface area at around 70 $Å^2$.[19] 0.6 mg/(mL of reaction) of Bio-Beads SM-2 (Bio-Rad #152-3920) were added to absorb the cholate detergent. The mixture was gently shaken for 4 h at 4 °C. The solution was filtered through a 0.45 µm filter to remove the Bio-Beads and then concentrated to 5 mg/mL (unless otherwise stated) using an Amicon 10 kDa at 4 °C and 3000 g. Size exclusion chromatography was performed to ensure the homogeneity of the sample using a Superdex S200 5/150 gel filtration column pre-equilibrated in 20 mM Tris-HCl pH 7.5, 150 mM NaCl.

Nanodiscs stability study. ND were assembled in 20 mM Tris.HCl pH 7.4, 100 mM NaCl, 0.5 mM EDTA and 100 mM cholate buffer and detergent was removed using Biobeads SM2. The ND solutions were filtered and subjected to buffer exchange on a PD10 column in three different buffer conditions. The buffers were chosen following the literature[7,20] and NMR titration requirements; (i) 20 mM Tris-HCl pH 7.5, 50 mM NaCl, 1 mM EDTA reducing the salt composition of the original

assembly buffer for ease in NMR experiments, (ii) 20 mM Bis-Tris pH 6.5, 50 mM NaCl, 1 mM EDTA reducing the pH of the original buffer in case of exchangeable amide protons in the studied protein and (iii) 20 mM PO4 pH 6.5, 50 mM NaCl, 1 mM EDTA reducing the pH the same way as the buffer (ii) without having any interfering proton signal due to the presence of the Bis-Tris. SEC was then performed to follow the homogeneity of the sample using a Superdex S200 5/150 gel filtration column pre-equilibrated in 20 mM Tris-HCl pH 7.5, 150 mM NaCl, over several days. The detailed study was performed using Superdex S200 10/300 column pre-equilibrated in 20 mM Tris-HCl pH 7.5, 150 mM NaCl.

Solution NMR measurement. Solution NMR titration experiments between ^{15}N-AA139 and ND[cNW9(POPC/POPG(4:1))] were performed on a Bruker Avance III spectrometer equipped with a cryogenically cooled triple resonance probed operating at a nominal ^{1}H frequency of 700 MHz. ^{15}N-HSQC were recorded at 25 °C. Solution NMR titration experiments between AA139 and ND[^{15}N-cNW9(POPC/POPG(4:1))] were performed on a Bruker Avance III spectrometer equipped with a cryogenically cooled triple resonance probed operating at a nominal ^{1}H frequency of 900 MHz. TROSY were recorded at 50 °C.

Dynamic light scattering (DLS). Dynamic light scattering experiments were carried out at 20 °C with DNYAPRO-99 (Wyatt). Size distribution was calculated with the Wyatt software.

Electron microscopy (EM). Nanodiscs were diluted to a final concentration of 200 nM in 20 mM Tris–HCl, pH 7.5, 50 mM NaCl and adsorbed to glow-discharged, carbon-coated EM grids. Samples were prepared by conventional negative staining with 1 % (w/v) uranyl acetate. EM images were collected with a Tecnai 12 electron microscope operated at an acceleration voltage of 120 kV.

Liquid Chromatography – Mass Spectrometry (LC-MS). LC-MS analysis were conducted using Agilent Technologies 1200 Series Instrument with a G1316A variable wavelength detector set at λ= 210 nm, 1200 Series ELSD, 6110 quadrupole ESI-MS, using an Agilent Zorbax Eclipse XDB-Phenyl (3 × 100mm, 3.5 μm particle size, flow rate 1 mL/min, the mobile phases 0.05% formic acid in water and 0.05% formic acid in acetonitrile).

Solid-state NMR.

Lipid bilayer vesicles preparation

LUVs (100 nm diameter) were used as a membrane model and prepared by extrusion method as previously described.[21] The synthetic lipids were used to prepare model membranes composed of POPC, POPC/POPG (4:1 molar ratio).

Solid-state NMR measurement

All solid-state NMR experiments were performed on a Bruker spectrometer operating at a nominal ^{1}H frequency of 800MHz. The probe used was a wide bore probe for very fast MAS of 60 KHz and a 1.3 mm rotor. Temperature of the sample was 18 °C.

5.4 Conclusion

The aim of this study was to evaluate the mode of action of AA139 toward G-ve bacterial cell membranes. A computational modelling study provided an experimental speculation of the orientation of the peptide at the interface with the cell membrane, proposing a slight angle of contact. Then, in order to perform solution NMR characterization, recombinant expression was used to produce labelled AA139, which was then purified via a novel method to produce correctly-folded arenicin peptide in *E. coli*. At the same time, the stability of two ND types were evaluated, concluding that cNW9 ND was the most stable construct over MSP1D1ΔH5, the most commonly construct currently used. cNW9 ND remained highly stable under all conditions tested; including different buffer conditions, pH, temperature and even over relatively long lengths of time (up to 30 days). This cNW9 ND construct was then used to perform a solution NMR titration experiment with ^{15}N-AA139. The results identified the *N*- and *C*-terminal ends of AA139 as the likely first points of contact with the lipid bilayer bacterial model membrane, with a K_d value of around 0.3 μM. The preliminary work performed using ssNMR suggested that AA139 loses its well-defined 3D structure upon insertion in the hydrophobic core of the membrane. This is consistent with the solution state titration studies that also reveal that several residues in the hairpin region undergo broadening due to exchange other than binding interactions. The consensus outcome suggests that the peptide termini bind to the bilayer and that this causes a change in the conformation of the hairpin region which destabilizes the overall 3D structure of the peptide in the membrane.

The structural mode of action study of AA139 allowed us to refine the model of mechanism of action proposed in chapter 4. The refined model, Figure 5-14, includes now the orientation of the peptide toward the lipid bilayer upon interacting (determined by solution NMR) and upon insertion (preliminary data generated by ssNMR). In summary, 1) AA139 binds to the negatively charged outer membrane of G-ve bacteria via electrostatic interactions with a slight angle from its *N*- and *C*-terminal ends; 2) AA139 inserts into the hydrophobic core of the outer membrane creating partial permeabilization most likely losing its well defined 3D structure and 3) AA139 accesses and permeabilizes the cytoplasmic membrane.

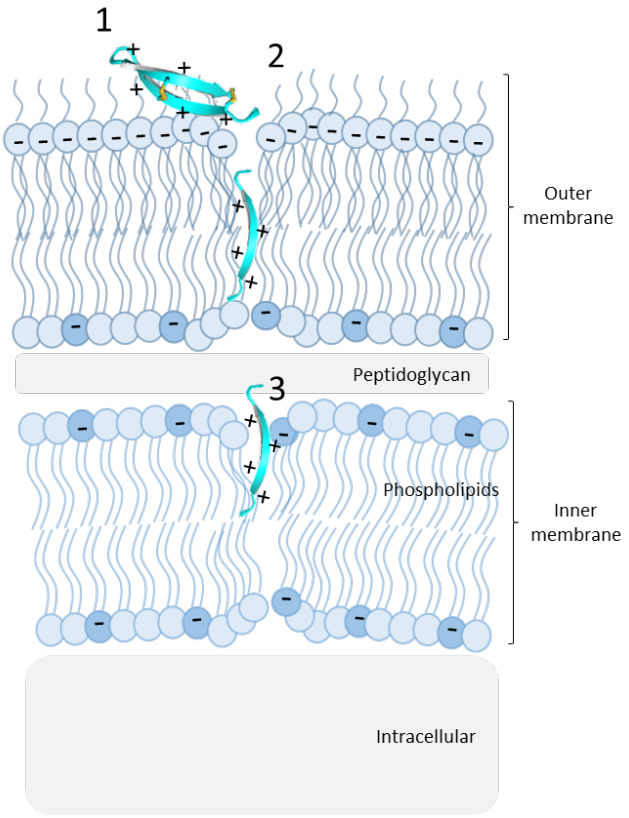

Figure 5-14- Refined proposed model of mechanism of action for AA139 against Gram-negative bacteria cell membranes. 1) AA139 binds to the negatively charged outer membrane of G-ve bacteria via electrostatic interactions with a slight angle from its *N*- and *C*-terminal ends; 2) AA139 inserts into the hydrophobic core of the outer membrane creating partial permeabilization, while most likely losing its well defined 3D structure and 3) AA139 accesses and permeabilizes the cytoplasmic membrane.

This work confirms the great potential of nanodiscs to study the mode of action and the structural characterization of membrane active peptides. The first K_d value was determined using a solution NMR titration experiment to evaluate the binding interaction between the antimicrobial peptide and the lipid bilayer nanodisc. The K_d value could be evaluated using other techniques such as ITC, but the structural information would be lost. More experiments need to be performed to determine the 3D structure of AA139 whilst interacting with the lipid bilayer model membrane. As mentioned by Ramamoorthy[22], the study of membrane-active peptides in lipid bilayers can be very challenging for NMR measurements. While physiological conditions would seem to be more relevant for this type of study to provide meaningful insights into the biological function of these membrane active peptides, those conditions may not be suitable for NMR measurements. This has often led to the use of modified sample conditions or the use of lipid model membranes that poorly mimic the cell complexity. Gramicidin-A was the first antimicrobial peptide whose 3D structure, integrated in oriented phospholipid bilayers, was determined by solid state NMR and reported in the protein databank.[23] Since then, the structure of other antimicrobial peptides have been studied with various tools and lipid

environment. The most recent high-resolution structure of β-hairpin AMPs was performed for thanatin in lipopolysaccharide micelles using solution NMR.[24] However, no one to date has achieved the structural characterization of AMPs in lipid bilayers by solution NMR. Seeing the tremendous potential that nanodiscs offer, the 3D solution NMR structure of AMPs in a lipid bilayer environment would be the next step forward. This would allow us to visualize the true structure of AMPs while integrated in the cell membrane and allow for the design of therapeutically valuable peptides.

5.5 References

1. Rao, A. G. (1999) Conformation and antimicrobial activity of linear derivatives of tachyplesin lacking disulfide bonds, *Arch. Biochem. Biophys. 361*, 127-134. DOI:10.1006/abbi.1998.0962
2. Shenkarev, Z. O., Balandin, S. V., Trunov, K. I., Paramonov, A. S., Sukhanov, S. V., Barsukov, L. I., Arseniev, A. S., and Ovchinnikova, T. V. (2011) Molecular mechanism of action of beta-hairpin antimicrobial peptide arenicin: oligomeric structure in dodecylphosphocholine micelles and pore formation in planar lipid bilayers, *Biochemistry 50*, 6255-6265. DOI:10.1021/bi200746t
3. Wakamatsu, K., Takeda, A., Tachi, T., and Matsuzaki, K. (2002) Dimer structure of magainin 2 bound to phospholipid vesicles, *Biopolymers 64*, 314-327. DOI:10.1002/bip.10198
4. Buffy, J. J., Waring, A. J., Lehrer, R. I., and Hong, M. (2003) Immobilization and aggregation of the antimicrobial peptide protegrin-1 in lipid bilayers investigated by solid-state NMR, *Biochemistry 42*, 13725-13734. DOI:10.1021/bi035187w
5. Bayburt, T. H., Grinkova, Y. V., and Sligar, S. G. (2002) Self-assembly of discoidal phospholipid bilayer nanoparticles with membrane scaffold proteins, *Nano Lett. 2*, 853-856. DOI:10.1021/nl025623k
6. Shaw, A. W., McLean, M. A., and Sligar, S. G. (2004) Phospholipid phase transitions in homogeneous nanometer scale bilayer discs, *FEBS Lett. 556*, 260-264.
7. Shenkarev, Z. O., Lyukmanova, E. N., Paramonov, A. S., Panteleev, P. V., Balandin, S. V., Shulepko, M. A., Mineev, K. S., Ovchinnikova, T. V., Kirpichnikov, M. P., and Arseniev, A. S. (2014) Lipid-protein nanodiscs offer new perspectives for structural and functional studies of water-soluble membrane-active peptides, *Acta Naturae 6*, 84-94.
8. Lomize, M. A., Pogozheva, I. D., Joo, H., Mosberg, H. I., and Lomize, A. L. (2012) OPM database and PPM web server: resources for positioning of proteins in membranes, *Nucleic Acids Res. 40*, D370-376. DOI:10.1093/nar/gkr703
9. Denisov, I. G., and Sligar, S. G. (2017) Nanodiscs in Membrane Biochemistry and Biophysics, *Chem. Rev. (Washington, DC, U. S.)*. DOI:10.1021/acs.chemrev.6b00690
10. Nasr, M. L., Baptista, D., Strauss, M., Sun, Z. J., Grigoriu, S., Huser, S., Pluckthun, A., Hagn, F., Walz, T., Hogle, J. M., and Wagner, G. (2017) Covalently circularized nanodiscs for studying membrane proteins and viral entry, *Nat. Methods 14*, 49-52. DOI:10.1038/nmeth.4079
11. Williamson, M. P. (2013) Using chemical shift perturbation to characterise ligand binding, *Prog. Nucl. Magn. Reson. Spectrosc. 73*, 1-16. DOI:10.1016/j.pnmrs.2013.02.001
12. Phillips, L. (2018) *Gnuplot 5*, Alogus Publishing.
13. Laws, D. D., Bitter, H. M., and Jerschow, A. (2002) Solid-state NMR spectroscopic methods in chemistry, *Angew. Chem., Int. Ed. Engl. 41*, 3096-3129. DOI:10.1002/1521-3773(20020902)41:17<3096::AID-ANIE3096>3.0.CO;2-X
14. Klint, J. K., Senff, S., Saez, N. J., Seshadri, R., Lau, H. Y., Bende, N. S., Undheim, E. A., Rash, L. D., Mobli, M., and King, G. F. (2013) Production of recombinant disulfide-rich

venom peptides for structural and functional analysis via expression in the periplasm of E. coli, *PLoS One 8*, e63865. DOI:10.1371/journal.pone.0063865

15. Dumon-Seignovert, L., Cariot, G., and Vuillard, L. (2004) The toxicity of recombinant proteins in Escherichia coli: a comparison of overexpression in BL21(DE3), C41(DE3), and C43(DE3), *Protein Expression Purif. 37*, 203-206. DOI:10.1016/j.pep.2004.04.025
16. Ovchinnikova, T. V., Shenkarev, Z. O., Nadezhdin, K. D., Balandin, S. V., Zhmak, M. N., Kudelina, I. A., Finkina, E. I., Kokryakov, V. N., and Arseniev, A. S. (2007) Recombinant expression, synthesis, purification, and solution structure of arenicin, *Biochem. Biophys. Res. Commun. 360*, 156-162. DOI:10.1016/j.bbrc.2007.06.029
17. Tao, H., Liu, W., Simmons, B. N., Harris, H. K., Cox, T. C., and Massiah, M. A. (2010) Purifying natively folded proteins from inclusion bodies using sarkosyl, Triton X-100, and CHAPS, *BioTechniques 48*, 61-64. DOI:10.2144/000113304
18. Ritchie, T. K., Grinkova, Y. V., Bayburt, T. H., Denisov, I. G., Zolnerciks, J. K., Atkins, W. M., and Sligar, S. G. (2009) Chapter 11 - Reconstitution of membrane proteins in phospholipid bilayer nanodiscs, *Methods Enzymol. 464*, 211-231. DOI:10.1016/S0076-6879(09)64011-8
19. Janosi, L., and Gorfe, A. A. (2010) Simulating POPC and POPC/POPG Bilayers: Conserved Packing and Altered Surface Reactivity, *J. Chem. Theory Comput. 6*, 3267-3273. DOI:10.1021/ct100381g
20. Susac, L., Horst, R., and Wuthrich, K. (2014) Solution-NMR characterization of outer-membrane protein A from E. coli in lipid bilayer nanodiscs and detergent micelles, *ChemBioChem 15*, 995-1000. DOI:10.1002/cbic.201300729
21. Craik, D. J., Henriques, S. T., Mylne, J. S., and Wang, C. K. (2012) Cyclotide isolation and characterization, *Methods Enzymol. 516*, 37-62. DOI:10.1016/B978-0-12-394291-3.00024-1
22. Ramamoorthy, A. (2009) Beyond NMR spectra of antimicrobial peptides: dynamical images at atomic resolution and functional insights, *Solid State Nucl. Magn. Reson. 35*, 201-207. DOI:10.1016/j.ssnmr.2009.03.003
23. Ketchem, R., Roux, B., and Cross, T. (1997) High-resolution polypeptide structure in a lamellar phase lipid environment from solid state NMR derived orientational constraints, *Structure 5*, 1655-1669.
24. Sinha, S., Zheng, L., Mu, Y., Ng, W. J., and Bhattacharjya, S. (2017) Structure and Interactions of A Host Defense Antimicrobial Peptide Thanatin in Lipopolysaccharide Micelles Reveal Mechanism of Bacterial Cell Agglutination, *Sci. Rep. 7*, 17795. DOI:10.1038/s41598-017-18102-6

Chapter 6 – Conclusions and future directions

6.1 Conclusions

Antimicrobial resistance is a worldwide concern affecting not only the human population but animal, food and the environment. Solutions for new therapies need to be devised and engineered as quickly as possible. AMPs have great potential due to their broad spectrum of antimicrobial activity and their very limited propensity to induce bacterial resistance observed to date. Although discovered more than 80 years ago, very few have reached the market so far (Gramicidin for instance is one of the rare one)[1], due to their high cost of production and their poor stability in human plasma as well as during storage. This thesis offers extensive research on the β-hairpin AMPs as replacement therapies for obsolete antibiotics against Gram-negative bacterial pathogens.

This study started its investigation by evaluating the relationship between physicochemical and antimicrobial properties of β-hairpin AMPs. The panel of six β-hairpin AMPs (arenicin-3, tachyplesin-1, polyphemusin-1, gomesin, protegrin-1 and thanatin) was selected as a representation of the β-hairpin AMP family, due to their sequence length, number of disulfide bridges and their general antimicrobial properties. The findings of this investigation revealed a very complex equilibrium between all properties of their primary, secondary and tertiary structures and their mode of action. Of note, the amphipathic character of the peptides seemed to play an important role on their antimicrobial activity; the more amphipathic, the more active the peptide becomes.

This first study allowed us to gain a general knowledge and background on the β-hairpin AMPs. However, the underlying goal of the thesis is to understand the function and mode of action of β-hairpin AMPs in order to design new and improved therapeutic peptide antimicrobials. To do so, two approaches were investigated: (i) the classical mutagenesis approach evaluated with the study of tachyplesin-1 and (ii) the comprehensive mode of action characterization of the lead drug candidate, AA139.

Our initial comparative study identified tachyplesin-1 as the most promising lead drug candidate for further development due to its 8-fold higher therapeutic index than the other peptides studied. This finding led the study of tachyplesin's structure-function and structure-toxicity relationships with the aim of designing novel therapeutically valuable peptides. An alanine scan of tachyplesin-1 was

performed along with selective positional modifications to assess the significance of each amino acid. The evaluation of the therapeutic properties of each tachyplesin-1 analog in combination with early ADME studies and structural characterization revealed two newly designed peptides, TP1[F4A] and TP1[I11A] with 40- and 64-fold improved antimicrobial activity / toxicity indexes over tachyplesin-1, respectively. Their high microbial potency and relatively low mammalian toxicity, render TP1[F4A] and TP1[I11A] very attractive as potential drug candidates for the treatment of infections caused by bacterial and/or fungal pathogens. Further bioavailability, pharmacokinetics and *in vivo* assays will be required to validate their full potential as novel antibiotics.

The mode of action study focused on arenicin-3 and its synthetic analog, AA139, which is a lead drug candidate developed by Adenium Biotech Ltd, currently in preclinical development for MDR urinary tract infection and pneumonia. This study aimed to understand how simple amino acid mutations can drive one peptide to be toxic but lead to a closely related analog to be developed as a lead drug candidate. Their 3D structures were characterized by solution NMR, identifying two β-hairpin peptides with a right-handed twist that were almost completely superimposable. However, the number of stabilizing interactions along the β-sheets, identified AA139 as a more flexible structure as compared to arenicin-3. Their mode of action was first investigated via label free assays using vesicles as a lipid bilayer model. Assays such as binding affinity, aggregation, permeabilization, insertion and surface charge potential of vesicles were evaluated. The results demonstrated that both arenicin peptides bind, permeabilize and insert into negatively charged lipid vesicles (POPC/POPG). AA139 promoted less vesicle aggregation than arenicin-3. It inserts its *N*-terminus or tryptophan deeper into the hydrophobic core of the negatively charged lipid bilayer model membrane than zwitterionic ones as compared to arenicin-3. These results correlate well with the difference observed for the toxicity of arenicin peptides against mammalian cells, with AA139 displaying reduced hemolytic activity as compared to arenicin-3. Surface charge potential and permeabilization assays were performed using *E. coli* cells. The results suggested that arenicin peptides act on the membrane of *E. coli* cells by neutralizing the outer membrane and permeabilizing the cytoplasm. However, the AA139 rate of permeabilization differed from arenicin-3, suggesting a different mode of action.

Nonetheless, the question remained, which part of the peptide is specifically involved in the membrane interaction and what happens next? This was investigated with assays employing isotopically labelled peptides. A novel method was developed for recombinantly expressing and purifying ^{15}N labelled arenicin peptides, allowing their use for solution and solid-state NMR. The solution NMR titration experiment, using novel nanodisc constructs, evaluated which AA139 amino acid was involved in the interaction with this lipid bilayer model. The results identified that the *N*- and *C*- terminal ends of the peptide were likely the first point of contact with the lipid bilayer, and

suggested that the β-hairpin loop of the peptide undergoes a conformational change upon binding. Furthermore, preliminary work performed using solid-state NMR and vesicles suggested that AA139 loses its well-defined 3D structure upon insertion in the hydrophobic core of the membrane.

The mode of action study of AA139 allowed us to propose a model of mode of action, Figure 5-14. In summary, 1) AA139 binds to the negatively charged outer membrane of Gram-negative bacteria via electrostatic interactions with a slight angle from its *N*- and *C*-terminal ends; 2) AA139 inserts into the hydrophobic core of the outer membrane, creating partial permeabilization while most likely losing its well defined 3D structure; and 3) AA139 accesses and permeabilizes the cytoplasmic membrane.

This suggested mode of action against Gram-negative bacteria may be enough for AA139 to disrupt its membrane target and to promote inactivation of the bacterial cells. However, as seen for numerous other antimicrobial peptides, its mode of action may not only be due to membrane disruption, but linked with a dual mode of action, as suggested by the slope of the *E. coli* cytoplasm permeabilization assays.

Natural AMPs offer great potential for the fight against resistant bacteria. So far, most attempts to produce antimicrobial candidate from AMPs have been focused on α-helical AMPs, however, these have not yet led to any major clinical success. The redesign of natural β-hairpin AMPs, tachyplesin-1 and arenicin-3, produced two examples of analog peptides, possessing improved therapeutic qualities suitable for further drug development. AA139 has progressed into late stage pre-clinical development for urinary tract infection and pneumonia diseases. We could postulate that β-hairpin AMPs might provide better selectivity than with α-helical AMPs due to their mode of action, allowing for better differentiation from cytotoxic effects. Similar strategies for peptide reengineering, as conducted here for tachyplesin-1 and arenicin-3, should be investigated for other potential antimicrobial peptides.

6.2 Future directions

To further understand the mechanism of action of AA139 and its behavioral difference between mammalian and bacterial cell membrane, it would be interesting to extend the solid-state NMR experiments attempted with the use of nanodiscs for instance and characterize its 3D structure when embedded in the membrane. Reverse solid-state NMR experiments, like ^{31}P and ^{2}H would be also valuable to evaluate the effect of the peptide on the lipid membrane.[2] Other more futurist experiments

could also be considered, like in-cell NMR experiments using live bacteria and mammalian cells, which has already been reported for few proteins.[3]

The mode of action studies of peptides and proteins against cell membrane targets requires lipid bilayer model membranes. However, lipid bilayer model membranes do not have the same size and membrane curvature as the target organisms. Indeed, lipid model bilayer membranes, usually range from 100 nm (LUVs) to 8 nm (nanodiscs) diameter, and bacteria cells are about 3 µm (*E. coli*) and 8 µm (red blood cells) in size. This 10-fold difference in size may affect the AMPs behavior and could biased their mode of action results. The membrane curvature is significantly different between cells and LUVs/SUVs, purely due to their size and their spherical constraints. However, thanks to the non-spherical property of the nanodiscs, the latter are better reflecting the curvature of the cell membranes and more closely mimic the natural radius of the different cells.

This thesis explored the great potential that newly developed nanodiscs could have on these type of studies. However, not all nanodisc constructs can be used under any condition. The stability studies of nanodiscs performed in this thesis demonstrated the risk involved in the length of storage, temperature and buffer conditions, on retaining the structure of these intricate lipid bilayer model membranes. This study also highlighted the commensurate improvement made with the use of a circularized nanodisc construct, using cNW9 membrane scaffold protein. This construct remained stable under all tested conditions, including length of time and buffer storage conditions, pH and temperature. The circularized nanodisc construct was tested here using two different compositions of phospholipids, POPC and POPC/POPG (4:1), mimicking mammalian and bacterial cell membranes, respectively. Nanodiscs are one of the most advanced model membrane systems used today, mimicking as closely as possible the cell membranes. However, this mimic replacement provides only a very simplistic model of the true membrane composition complexity. Thus, one could imagine building a nanodisc composed not only of the cNW9 MSP, offering tremendous stability, but also with directly extracted cell membrane, constituting the lipid bilayer. Preliminary work has explored the possibility of such nanodisc constructs. Material and methods can be found in Appendix V, page 7-265.

Results. The lipid membranes of both *E. coli* ATCC 25922 and red blood cells were extracted and characterized to evaluate the lipid type as well as the amount of proteins extracted. The mass spectrometry, Figure 6-1, Figure 6-2 and Figure 6-3, demonstrated the success of the lipid extraction for both cell types. In *E. coli,* the presence of POPG, POPE and cardiolipins were identified. In red blood cells, POPC and sphingomyelin were identified. Cholesterol could not be observed under these conditions due to the ionization mode used, cholesterol only ionizes in positive mode.

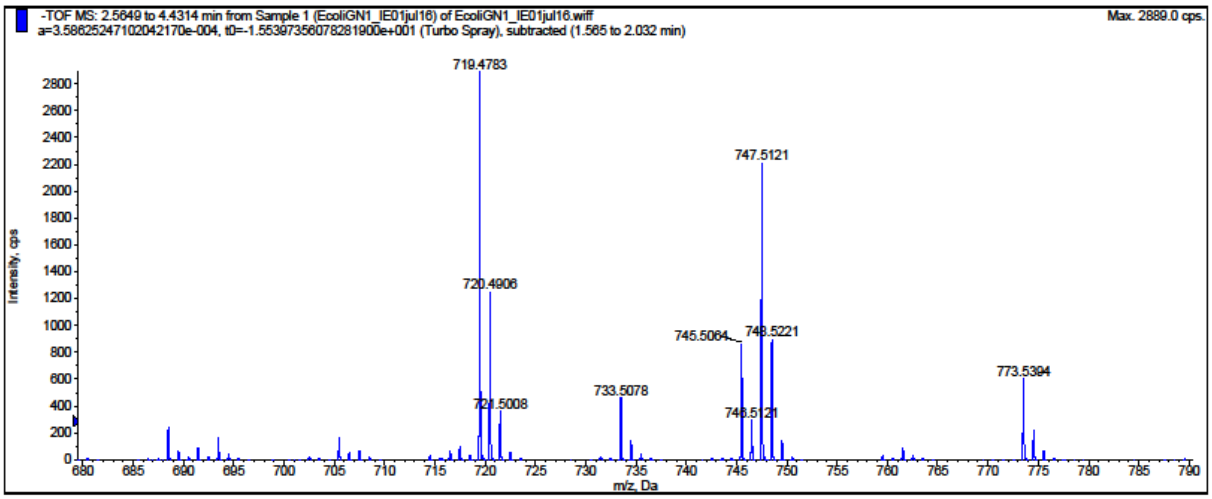

Figure 6-1 - *E. coli* lipid extract of phospholipids characterized by MS-TOF in negative mode ionization. MW(POPG 32:1) = 720.5 Da, MW(POPG) = 734.5 Da, MW(POPG 34:1) = 748.5 Da and MW(POPG 36:2) = 774.5.

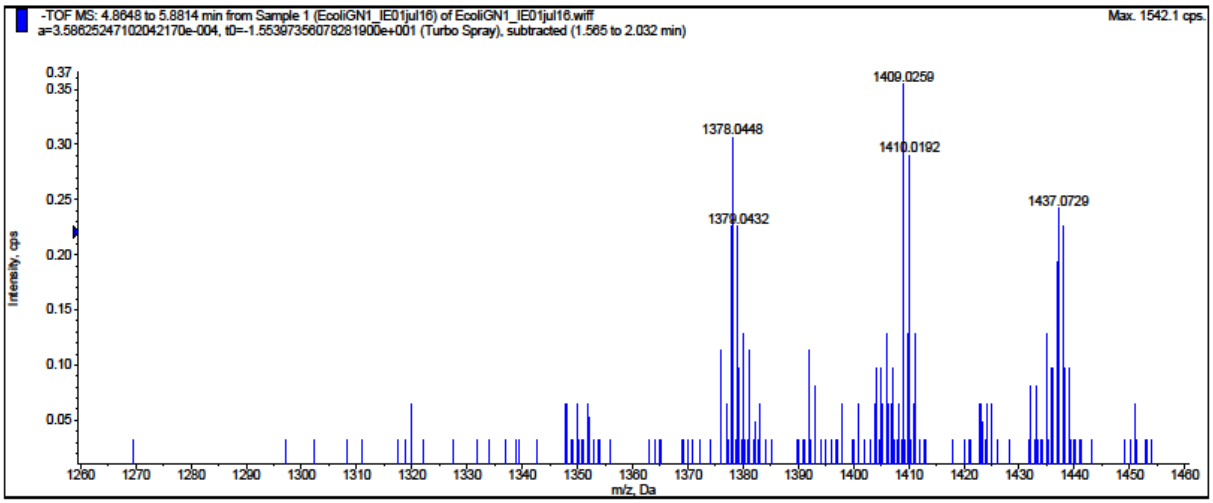

Figure 6-2 - *E. coli* lipid extract of cardiolipins characterized by MS-TOF in negative mode ionization.

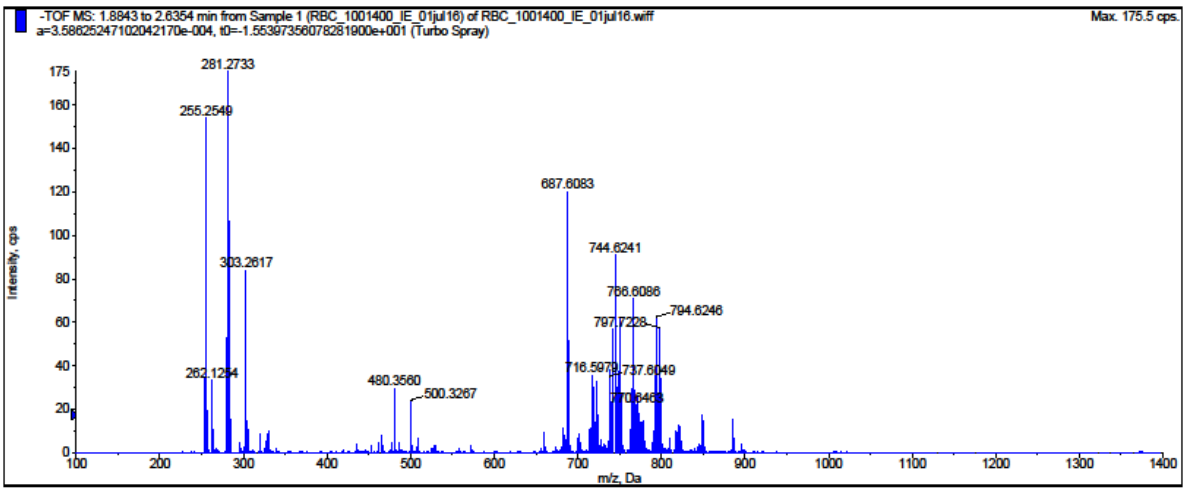

Figure 6-3 – Red blood cells lipid extract of phospholipids characterized by MS-TOF in negative mode ionization. MW(sphingomyelin) = 688.5 Da and MW(POPC) = from 716 to 796 Da.

To quantitate the protein concentration extracted alongside the lipids in both *E.coli* and RBC solutions, a bicinchoninic acid (BCA) assay was performed, Figure 6-4. The substantial amount of proteins extracted alongside the lipids confirm the extraction of a full complex lipid bilayer of both cell membranes.

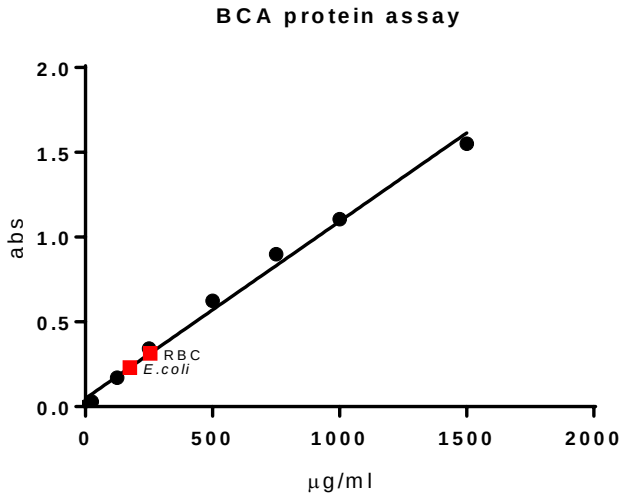

Figure 6-4 - BCA protein assay. For *E. coli* and RBC the concentration of proteins in their respective solutions were 175 and 254 µg/mL, respectively.

The membrane extraction produced solution mixtures of lipids, which were hard to quantitate, and proteins, which were hard to qualitatively identify. The bottleneck of such membrane extractions reside in the fact that the extract cannot be well quantified. Thus, nanodisc production with membrane extracts will be difficult to achieve due to the crucial ratio lipid to MSP required for the auto-formation of the nanodisc. However, one could imagine that the lipid to MSP ratio was only essential

when the MSP was linear. Now using the circularized MSP (cNW9 for example), the circle is already formed and only the lipid bilayer needs to get integrated. The use of the circular MSP reduces the auto-formation steps of the nanodisc. Using an excess amount of lipids, or membrane extract, will probably not affect the formation of the nanodisc but only the propensity of the nanodisc to aggregate. Further experiments and quality control tests would validate or revoke the idea of novel nanodiscs formed by membrane extracts. The latter could revolutionize the mode of action study of peptides, as direct membrane would be used instead of a model mimicking only partially the original.

6.3 References

1. Mishra, B., Reiling, S., Zarena, D., and Wang, G. (2017) Host defense antimicrobial peptides as antibiotics: design and application strategies, *Curr. Opin. Chem. Biol. 38*, 87-96. DOI:10.1016/j.cbpa.2017.03.014
2. Marc-Antoine, S., Frances, S. (2018) Antimicrobial Peptide Structures: From Model Membranes to Live Cells. *Chemistry – A European Journal, 24* (2), 286-291, DOI: 10.1002/chem.201704362
3. Luchinat, E., Banci, L. (2017). In-cell NMR: a topical review. *IUCrJ, 4(Pt 2)*, 108–118, DOI:10.1107/S2052252516020625

Chapter 7 - Appendix

7.1 Appendix I – Ethics approval

THE UNIVERSITY OF QUEENSLAND

Institutional Human Research Ethics Approval

Project Title:	Withdrawing And Using Blood From The Cubital Vein And Use Of Blood Products Obtained From The Red Cross Blood Bank - 17/03/2015 - AMENDMENT
Chief Investigator:	Dr Trent Woodruff
Supervisor:	None
Co-Investigator(s):	Prof Matthew Cooper
School(s):	IMB; SBS
Approval Number:	2014000031
Granting Agency/Degree:	NHMRC, ARC
Duration:	31st December 2019

Comments/Conditions:

Subproject Titles:

"Investigation of Inflammatory Responses in Human Immune Cells"

"Analysis of Haemolysis of Red Blood Cells for Compounds with Antimicrobial Activity"

Note: If this approval is for amendments to an already approved protocol for which a UQ Clinical Trials Protection/Insurance Form was originally submitted, then the researchers must directly notify the UQ Insurance Office of any changes to that Form and Participant Information Sheets & Consent Forms as a result of the amendments, before action.

Name of responsible Committee:
Medical Research Ethics Committee
This project complies with the provisions contained in the *National Statement on Ethical Conduct in Human Research* and complies with the regulations governing experimentation on humans.

Name of Ethics Committee representative:
Professor Bill Vicenzino
Chairperson
Medical Research Ethics Committee

Signature _____ Date 26/3/2015

7.2 Appendix II - Supplementary information Chapter 2

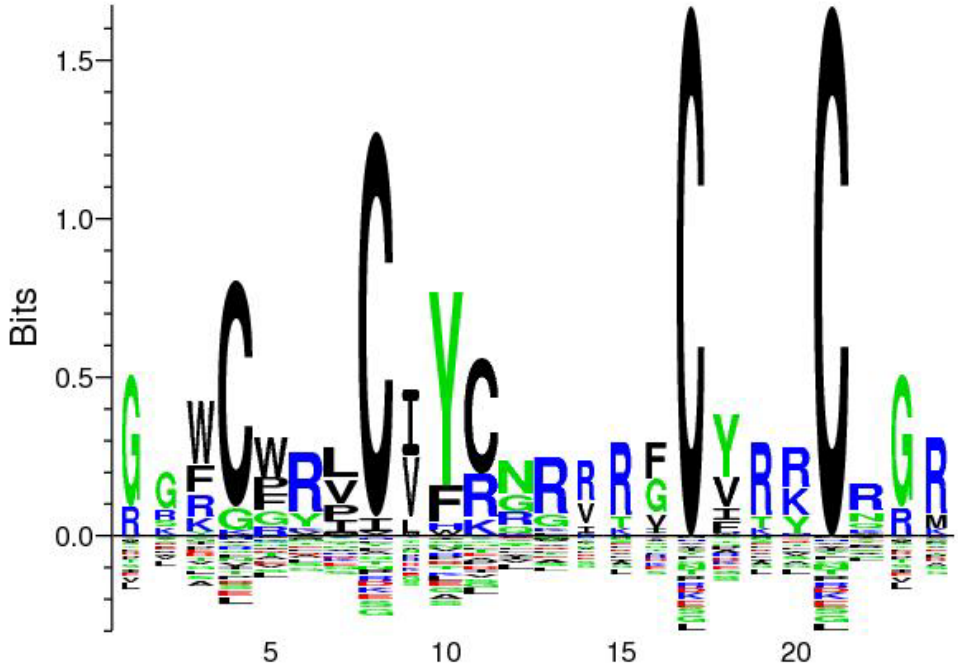

Figure S7.2-1 - Amino acid frequency of β-hairpin AMPs. The amino acid frequency graph has been done using Seq2logo 2.0 server, using P-Weighted Kullback-Leibler logo type and Hobohm 1 clustering method with 0.63 threshold and pseudo counts of 200.

Amino acid frequency graph was performed using Seq2logo 2.0 server online tool. It is a graphical representation of the sequence conservation of amino acids, showing how well residues are conserved at each position within the β-hairpin AMP family. The relative size of the letters indicates their frequency in the compared sequences. As already observed in the standard alignment, the most prominent amino acid represented in the frequency graph is the last cysteine of the peptide sequences, which is the most conversed residue in all β-hairpin AMPs studied here.

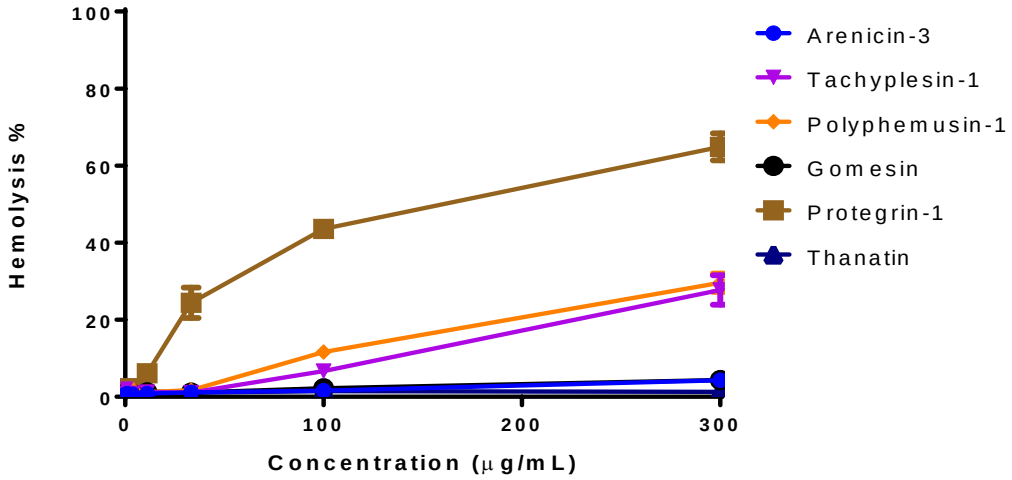

Figure S7.2-2 - Hemolysis activity (%) of β-hairpin compounds tested from 0.1 to 300 μg/mL.

Detailed Methodologies

Antibacterial assay (Minimum Inhibitory Concentration [MIC]). MIC assay was performed by a broth microdilution plate based method as per CLSI guidelines for antimicrobial susceptibility testing of aerobic bacteria.[1] Compounds were prepared at 1.28 mg/mL solution in water. The tested strains, Table S1, were cultured in Luria broth (LB) (In Vitro Technologies, USB75852), at 37 °C overnight. A sample of culture was then diluted 40-fold in fresh Muller Hinton broth (MHB) (Bacto laboratories, 211443) and incubated at 37 °C for 1.5-2 h. The compounds were serially diluted two-fold across the wells, with compound concentrations ranging from 0.015 μg/mL to 512 μg/mL, plated in duplicate. The resultant mid-log phase cultures were diluted to the final concentration of 1×10^6 CFU/mL, then 50 μL was added to each well of the compound-containing 96-well plates (Corning 3641, Non-binding Surface [NBS]), giving a final compound concentration range of 0.008 μg/mL to 256 μg/mL and $5x10^5$ CFU/mL. All the plates were covered and incubated at 37 °C for 18 h. MICs were determined visually, being defined as the lowest concentration showing no visible growth. Resazurin was added at 0.001% final concentration to each well and incubated for 2 h before MICs were re-read for confirmation using the colour change from blue to pink to indicate wells containing viable cells. The resazurin assay was added in some wells where some form of precipitate was present in otherwise clear wells, making it difficult to ascertain which wells had visible growth.

Antifungal assay (Minimum Inhibitory Concentration [MIC]). MIC assay was performed by a broth microdilution plate based method as per CLSI guidelines for antimicrobial susceptibility testing.[2] Fungi strains, Table S1, were cultured for 3 days on Yeast Extract-Peptone Dextrose (YPD) (Sigma-Aldrich, Y1500) agar at 30 °C. A yeast suspension of $1x10^6$ to $5x10^6$ CFU/mL was prepared from five colonies. These stock suspensions were diluted with Yeast Nitrogen Base (YNB) (Becton Dickinson, 233520) broth to a final concentration of 2.5×10^3 CFU/mL. All samples, compounds and standards were plated in 96-well plates (Corning 3641, Non-binding Surface [NBS]), by adding 10 μL of 1.28 mg/mL stock solution to each well and 90 μL of media. Then, the samples were serial diluted (1:2) in 12 concentrations across the plate. The standard antifungal ranged from 256 μg/mL to 0.12 μg/mL and compounds from 128 μg/mL to 0.06 μg/mL with final volumes of 50 μL per well, plated in duplicate. Then, 50 μL of the fungi suspension that

was previously prepared in YNB broth to the final concentration of 2.5×10^3 CFU/mL, was added to each well of the compound-containing plates, giving a final standard compound concentration range of 128 μg/mL to 0.06 μg/mL and tested compound from 64 μg/mL to 0.03 μg/mL. Plates were covered and incubated at 35 °C for 24 h. *Candida albicans* MICs were determined by measuring the absorbance at OD_{530}. For *Cryptococcus neoformans* 10 μL of 0.06 % resazurin were added to the 24 h incubated plates. Then, these plates were incubated for another 3 h. *Cryptococcus neoformans* MICs were determined by measuring the absorbance at $OD_{570\text{-}600}$.

Table S7.2-1 – Microbial strains and cell line used for the antimicrobial assay.

Organism	Strains	Comment
Escherichia coli	ATCC 25922	FDA control, CLSI QC Strain
Escherichia coli	MB 4902	ΔlpxC mutant
Escherichia coli	ATCC 700926	MG 1655; K12 substr
Klebsiella pneumoniae	ATCC 700603	Multi-drug Resistant (MDR)
Klebsiella pneumoniae	ATCC 13883	Type strain
Klebsiella pneumoniae	ATCC BAA-2146	New Delhi Metallo-beta-lactamase-1 (NDM-1) positive
Acinetobacter baumannii	ATCC 19606	Type strain
Pseudomonas aeruginosa	ATCC 27053	Quality Control strain
Bacillus subtilis	ATCC 6051	Type strain
Staphylococcus aureus	ATCC 43300	Methicillin Resistant *Staphylococcus aureus* (MRSA)
Candida albicans	ATCC 90028	CLSI reference strain
Cryptococcus neoformans var grubii	ATCC 208821	H99, Type strain
HepG2	ATCC HB-8065	Hepatocellular carcinoma liver cells
HEK293	ATCC CRL-1573	Embryonic kidney cells

Cytotoxicity. Cytotoxicity to HEK293 and HepG2 cells was determined using the Alamar Blue (resazurin) assay,[3, 4] For the assays supplemented with 1 % FBS as final concentration the cells were seeded one day prior to the assay (3,000 per 20 µL for HEK293 and 4,000 per 20 µL for HepG2) with DMEM + 2 % FBS. The compounds were prepared as described below, using DMEM with no FBS instead to give the final FBS concentration of 1 %.

The highest concentration the compounds were tested was 300 µg/mL. A dilution series of 1:3 fold steps in DMEM (GIBCO-Invitrogen, cat. no. 11995-073) + 10 % FBS was created (concentration range of 600 µg/mL – 0.28 µg/mL), and 20 µL of these 2x concentrated compound dilutions were added in duplicates to wells of a black wall, clear bottom 384-wells cell culture plate. For the assays with 1 % FBS the compounds in 0 % FBS were added to the existing cell plates in 2 % FBS. 200 µM Tamoxifen (Sigma T5648) served as negative control and in addition a serial dilution of tamoxifen, starting at 200 µM (74 µg/mL), was included as a dose response control (1 in 2 dilution series for tamoxifen). For the assay with 10 % FBS, HepG2 cells were seeded at 5000 cells per well, in a volume of 20 µL in DMEM medium + 10 % of FBS and added to the 20 µL of compound solution (total volume of 40 µL), resulting in a final compound concentration range of 300 µg/mL to 0.14 µg/mL. Cells were incubated together with the compounds for 20 h at 37 ^{o}C, 5 % CO_2.

After the incubation, 5 µL of 100 µM (25 µg/mL) resazurin dissolved in PBS (final concentration was approximately 11 µM) was added to each well. The plates were then incubated for 3 h at 37 ^{o}C, 5 % CO_2. The fluorescence intensity was read using the TECAN Infinite M1000 PRO with excitation/emission 560/590. The data was analysed by Graph Pad Prism software. The data were plotted as the average percentage of control ± SD for each set of duplicate wells using the following equation: Cell survival % = (FI_{SAMPLE} – $FI_{Negative}$/$FI_{UNTREATED}$ –$FI_{Negative}$)*100. (100 µg/mL tamoxifen was set as 0 % survival, media control as 100 %). From those graphs, the CC_{50}, the Cytotoxic Concentration of the peptide to cause death to 50% of viable cells in the host, were calculated and reported.

Hemolysis assay. Hemolytic activity was performed as previously descripted in the literature with slight modifications.[5] In brief, human erythrocytes were isolated from anonymous fresh human blood and adjusted to $1x10^9$ blood cells/mL in PBS buffer. Control compounds and peptides were prepared to 3 mg/mL solutions in PBS. Then up to 300 µg/mL of peptide were added and incubated for 3 h at 37 °C. Following incubation, samples were centrifuged at 3,000 rpm for 20 min, and the supernatants, 100 µL, were carefully collected for measurement. The degree of hemolysis in the samples was determined by measurement of the absorption of the supernatants at 540 nm using the Polarstar-Omega plate reader. 1 % Triton-X100 was used as positive control for inducing 100 % hemolysis. Full graph results available in Figure S2.

Inner membrane permeability measured by SYTOX green fluorescence emission. *E. coli* ATCC 25922 cells were grown to exponential phase (OD~0.6), centrifuged at 2,500 RCF for 10 min, the pellet washed with PBS buffer (x3) to remove any trace of nucleic acids and residual growth media, and then a cell suspension prepared at $1x10^7$ cells/mL. Bacterial cell suspensions were then incubated with compounds at different concentrations (five-fold dilutions starting from 20 μg/mL) for 1 h at 37 °C, repeated in triplicate. SYTOX green (Life Technologies S7020), a DNA-binding dye that becomes fluorescent when bound to nucleic acids and only enters cells with comprised plasma membranes,[6] was added to the peptide–treated cells at a final concentration of 2 μM, and incubated for 5 min at room temperature. The fluorescence emission intensity of the bacterial suspensions were scanned using λ_{ex} = 488 nm and λ_{em} = 530 nm with 30 nm bandpass by flow cytometry performed with a BD FACSCanto II (BD biosciences).[7] For each sample 100,000 events were recorded and the fluorescence signals were expressed as a percentage of cell permeability as compared to in-tact (un-treated) and damaged (treated with isopropanol) cell controls. Polymyxin B was included as a positive inner membrane permeating compound control and meropenem as negative inner membrane permeating compound control (antimicrobial compound that enters cells without compromising the bacterial cell membrane).

Based on forward and side scattering measurements of the in-tact versus damaged cell controls two distinct populations were identified; i) healthy or in-tact cells, ii) dead/unhealthy or completely/partially permeabilised cells. Healthy cells were deemed as 10^1 to 10^3 range of detection, at 530 nm, and dead or unhealthy cells were deemed as 10^3 to 10^5 range of detection at 530 nm.

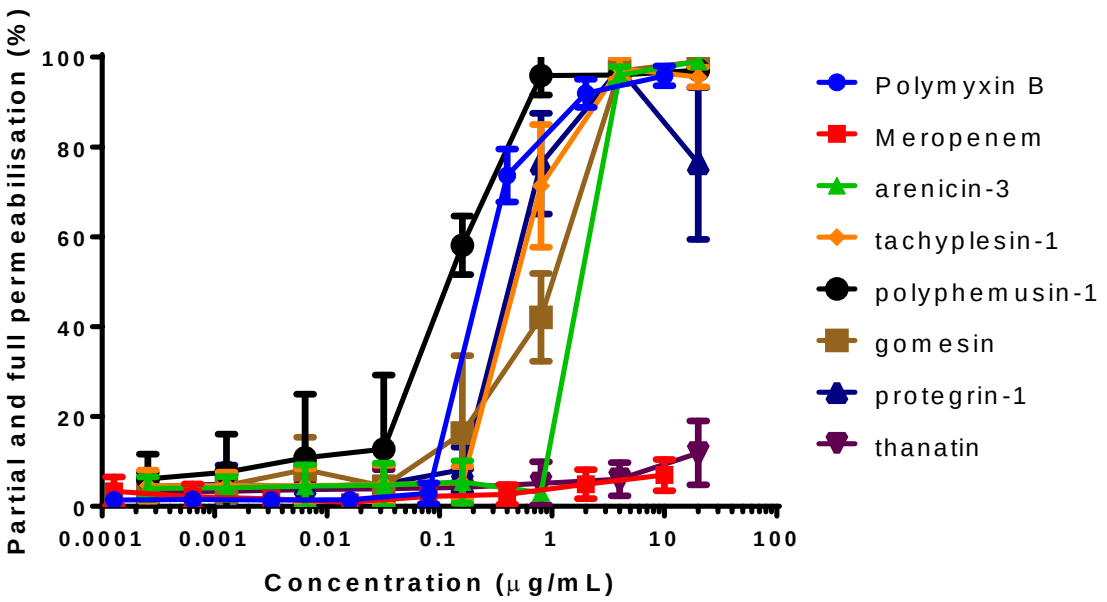

Figure S7.2-3 – Inner bacterial membrane permeability in *E. coli* ATCC 25922 evaluated from SYTOX green fluorescence emission intensity. Average ± SD of three replicates.

The SYTOX green data suggests that arenicin-3, tachyplesin-1, polyphemusin-1, gomesin and protegrin-1 permeabilise the cytoplasmic membrane of *E. coli* cells at lethal concentrations (50% cell damage 0.1-1 μg/mL). However, thanatin does not permeabilise *E. coli* cells at lethal concentrations. The ability of each β-hairpin peptide to permeabilise or not permeabilise the *E. coli* cytoplasmic bacterial membrane is in agreement with previous studies in the literature. For example, Hong *et al.*,[8] demonstrate that tachyplesin-1 compromises the integrity of the *E. coli* cell membrane via flow cytometric analysis of cells following single- or double-staining with carboxyfluorescein diacetate or propidium iodide; Powers *et al.*,[9] found the mechanism of action of polyphemusin-1 to be a lipid flip-flop mechanism; Domingues *et al.*,[10] display lipid leakage induced by gomesin in the presence of a lipid mimicking environment; Drin *et al.*,[11] showed that protegrin-1 translocates into the membrane via tryptophan fluorescence assay data; Robert *et al.*,[12] suggests that the cytoplasmic membrane is not the target for thanatin but instead the peptide agglutinates the cells in order to cause cell death.

Plasma protein binding assay. Plasma protein binding was performed using an Ultrafiltration method.[13] Fresh frozen human plasma was pooled from O Negative (Product number 1274512) blood from the R & D division of the Australian Red Cross Blood Services (Brisbane). Stock solutions (20 mg/mL) of the test compounds were prepared in H_2O. Test compounds (40 µg/mL) were incubated in 100 % human plasma at 37 °C for 30 min (1 mL volume). For unfiltered samples, an aliquot (50 µL) was removed, diluted with PBS (50 µL) and quenched with ice-cold precipitating solution comprising 0.5 µM carbutamide MS internal standard in acetonitrile : methanol : formic acid (1: 1 : 0.001). Samples were incubated at 4 °C for 30 min then centrifuged at 14000 × g for 8 min, with the clear supernatant transferred to a vial for LC-MS-MS analysis. For filtered samples, the plasma sample (250 µL) was filtered using Amicon Ultra-0.5 Centrifugal Filter Devices 30K NMWL at 14000 × g for 7 min and then an aliquot (50 µL) was processed as described for unfiltered samples. The fraction of unbound compound was calculated by determining the concentration of the filtered sample and the concentration of unfiltered sample. All samples were performed in triplicate with sulfamethoxazole as a control.

Peptide Characterisation

Final purity of more than 95 % for all compounds was confirmed by LC-MS analysis using both ELSD and UV (210 nm) detection. LC-MS analysis were conducted using Agilent Technologies 1200 Series Instrument with a G1316A variable wavelength detector set at λ= 210 nm, 1200 Series ELSD, 6110 quadrupole ESI-MS, using an Agilent Zorbax Eclipse XDB-Phenyl (3 × 100mm, 3.5 µm particle size, flow rate 1 mL/min, the mobile phases 0.05% formic acid in water and 0.05% formic acid in acetonitrile). Identities of final products were confirmed by high resolution mass spectrometry (HRMS), performed on a Bruker Micro TOF mass spectrometer using (+)-ESI calibrated to sodium formate.

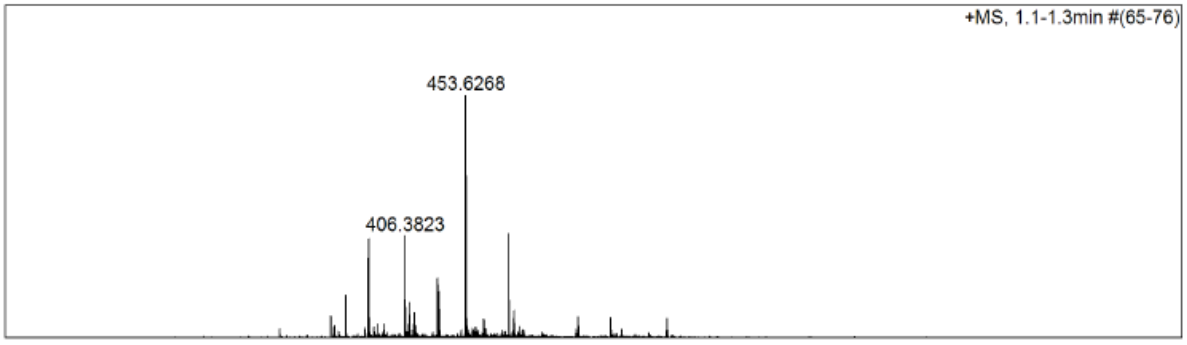

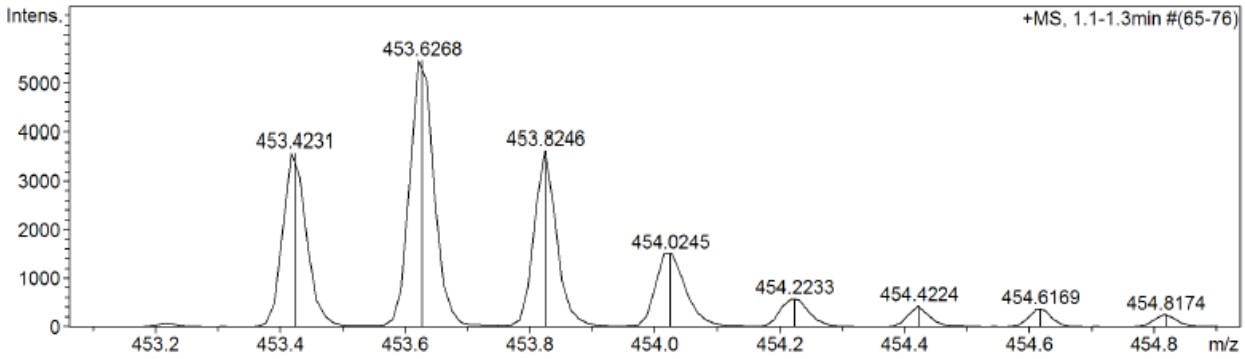

Sum Formula	Sigma	m/z	Err [ppm]	Mean Err [ppm]	Err [mDa]	rdb	N Rule	e⁻
C 99 H 156 N 35 O 19 S 4	0.109	453.4234	0.80	-0.70	0.36	39.50	ok	even

Figure S7.2-4 – HRMS of tachyplesin-1
HRMS-ESI (*m/z*): $[M + 5H]^{5+}$ calculated for $(C_{99}H_{151}N_{35}O_{19}S_4 + 5H)/5$, 453.4162; found 453.4234.

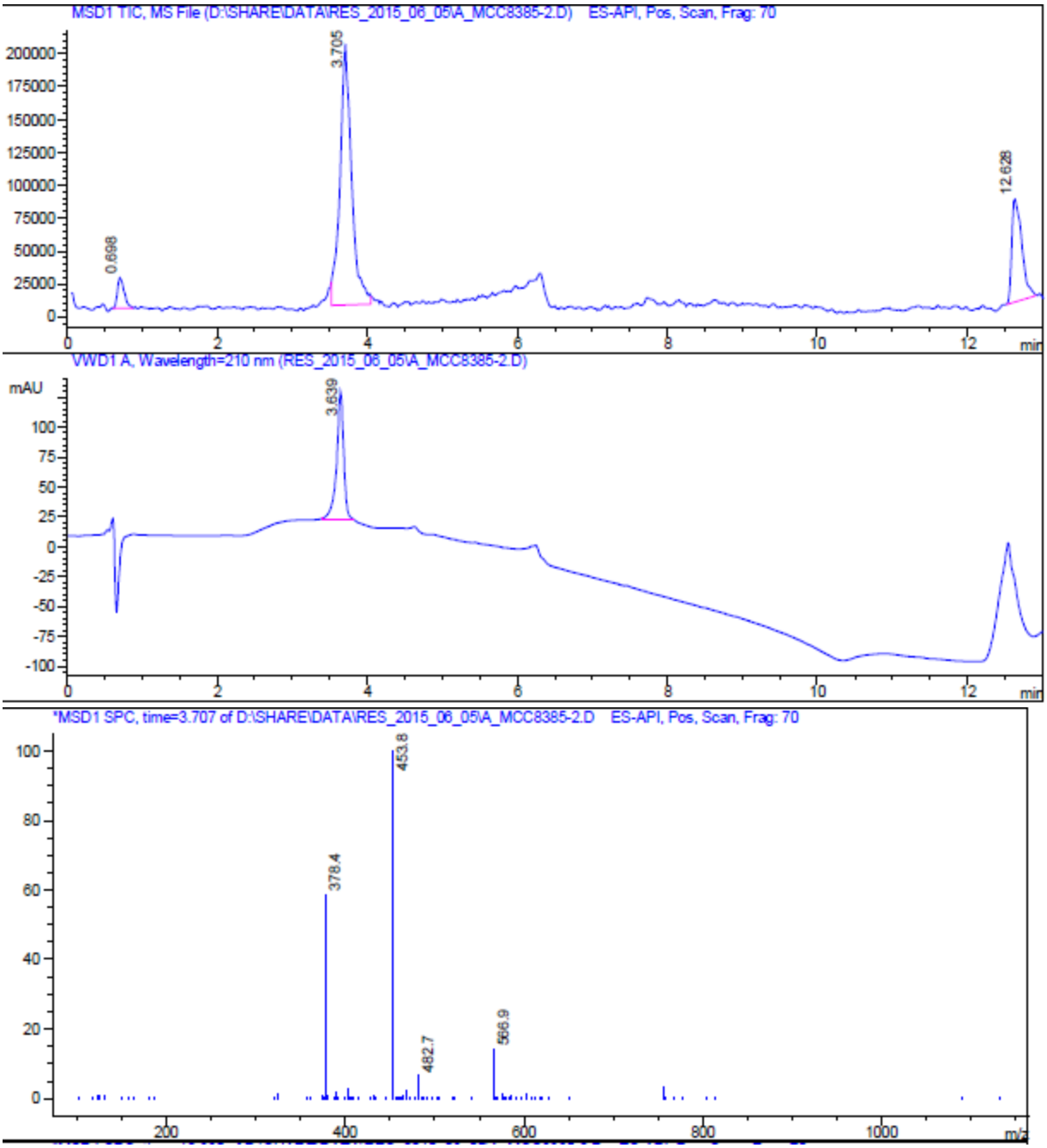

Figure S7.2-5 – LC-MS of tachyplesin-1

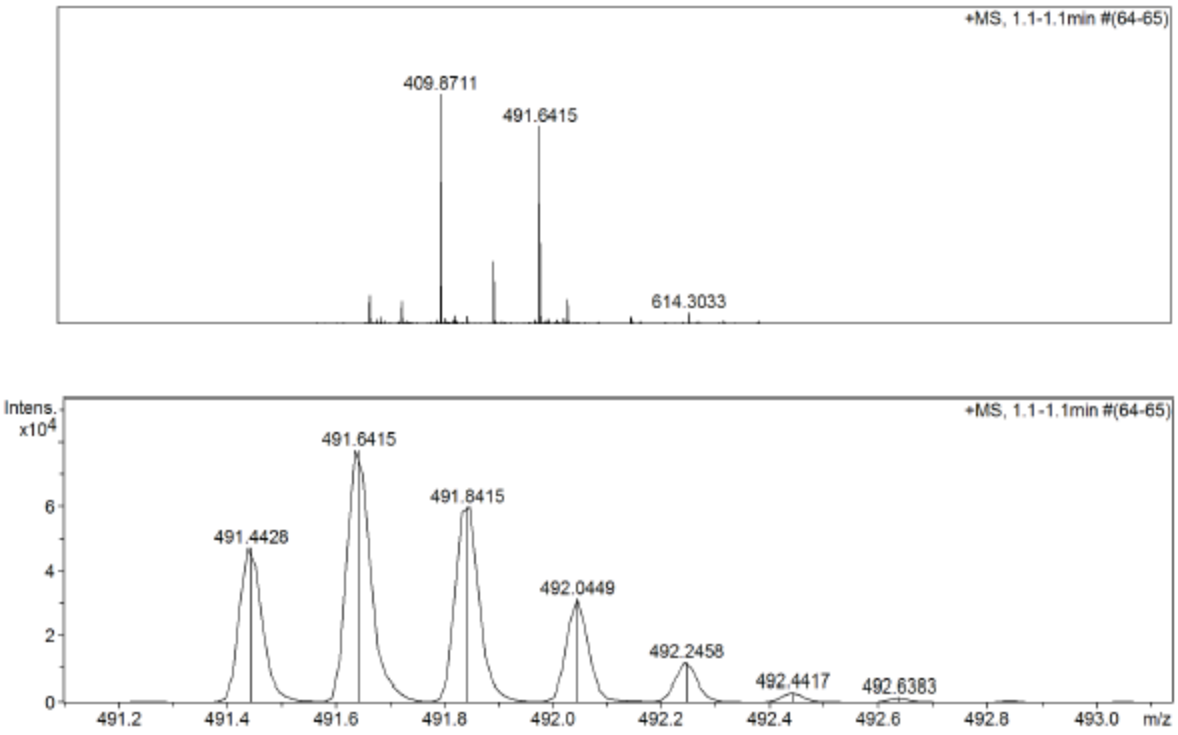

Sum Formula	Sigma	m/z	Err [ppm]	Mean Err [ppm]	Err [mDa]	rdb	N Rule	e⁻
C 108 H 166 N 39 O 20 S 4	0.082	491.4405	-4.58	-2.52	-2.25	45.50	ok	even

Figure S7.2-6 – HRMS of polyphemusin-1
HRMS-ESI (*m/z*): $[M + 5H]^{5+}$ calculated for ($C_{108}H_{161}N_{39}O_{20}S_4$ + 5H)/5, 491.4333; found 491.4405.

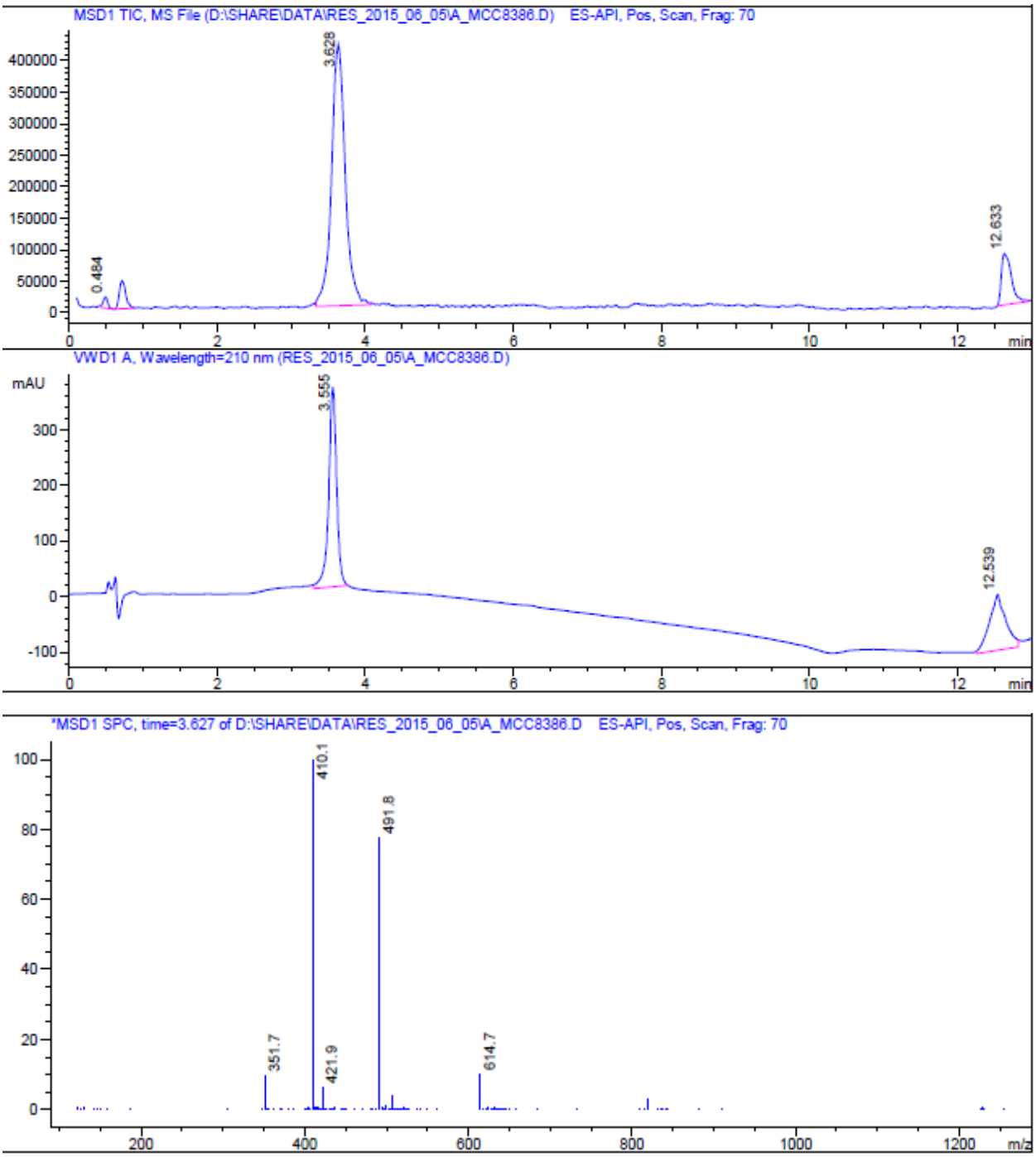

Figure S7.2-7 – LC-MS of polyphemusin-1

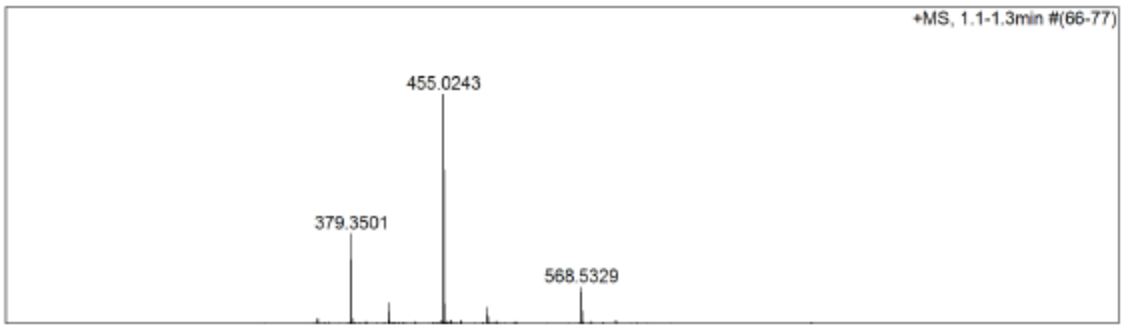

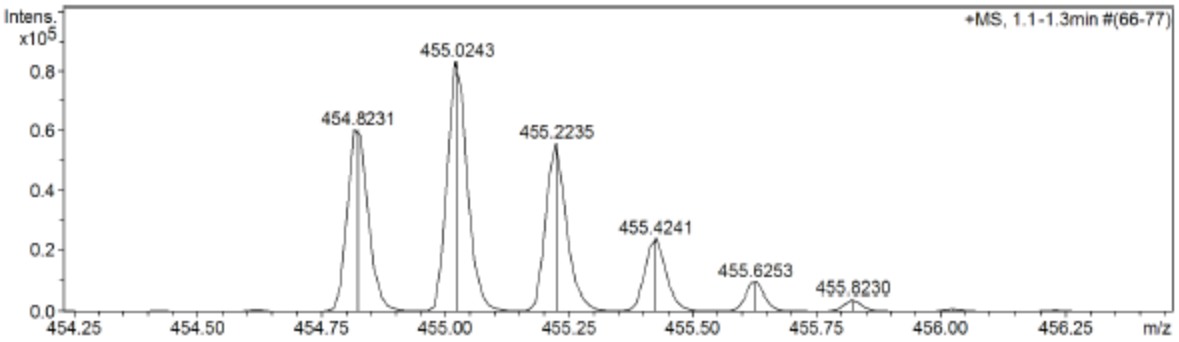

Sum Formula	Sigma	m/z	Err [ppm]	Mean Err [ppm]	Err [mDa]	rdb	N Rule	e⁻
C 93 H 157 N 36 O 23 S 4	0.094	454.8216	-3.32	-3.75	-1.51	33.50	ok	even

Figure S7.2-8 – HRMS of gomesin
HRMS-ESI (*m/z*): $[M + 5H]^{5+}$ calculated for ($C_{93}H_{152}N_{36}O_{23}S_4$ + 5H)/5, 454.8143; found 454.8216.

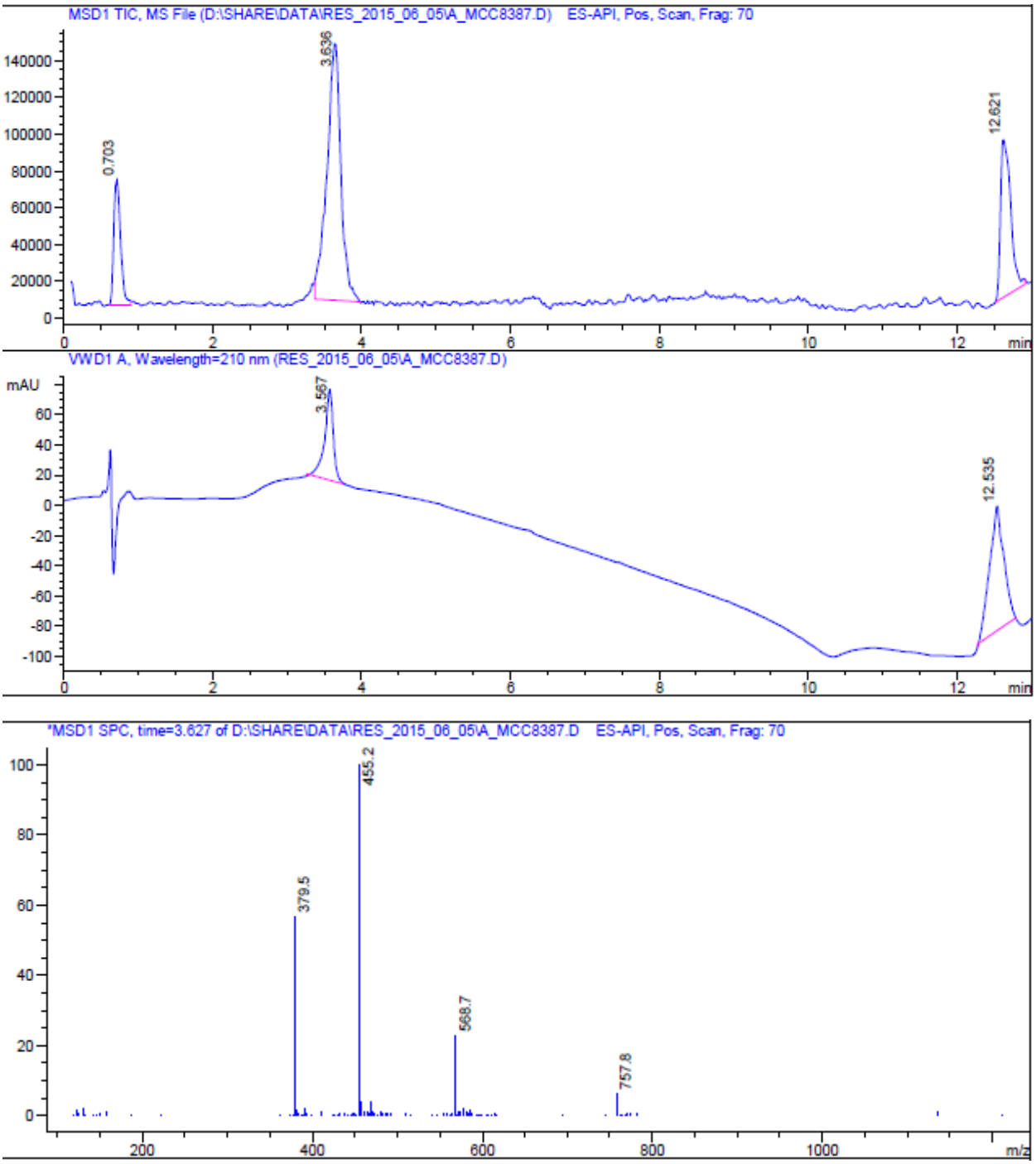

Figure S7.2-9 – LC-MS of gomesin

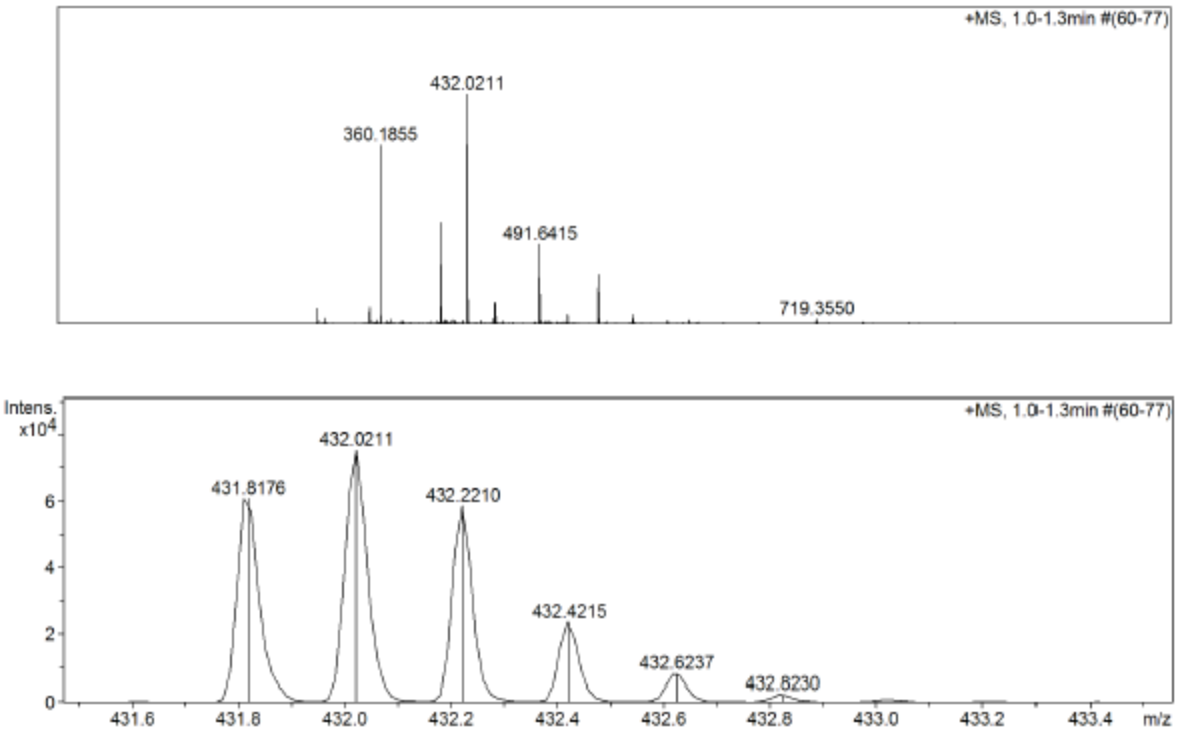

Sum Formula	Sigma	m/z	Err [ppm]	Mean Err [ppm]	Err [mDa]	rdb	N Rule	e⁻
C 88 H 152 N 37 O 19 S 4	0.063	431.8184	1.85	-3.44	0.80	31.50	ok	even

Figure S7.2-10 – HRMS of protegrin-1
HRMS-ESI (*m/z*): $[M + 5H]^{5+}$ calculated for ($C_{88}H_{147}N_{37}O_{19}S_4$ + 5H)/5, 431.8111; found 431.8184.

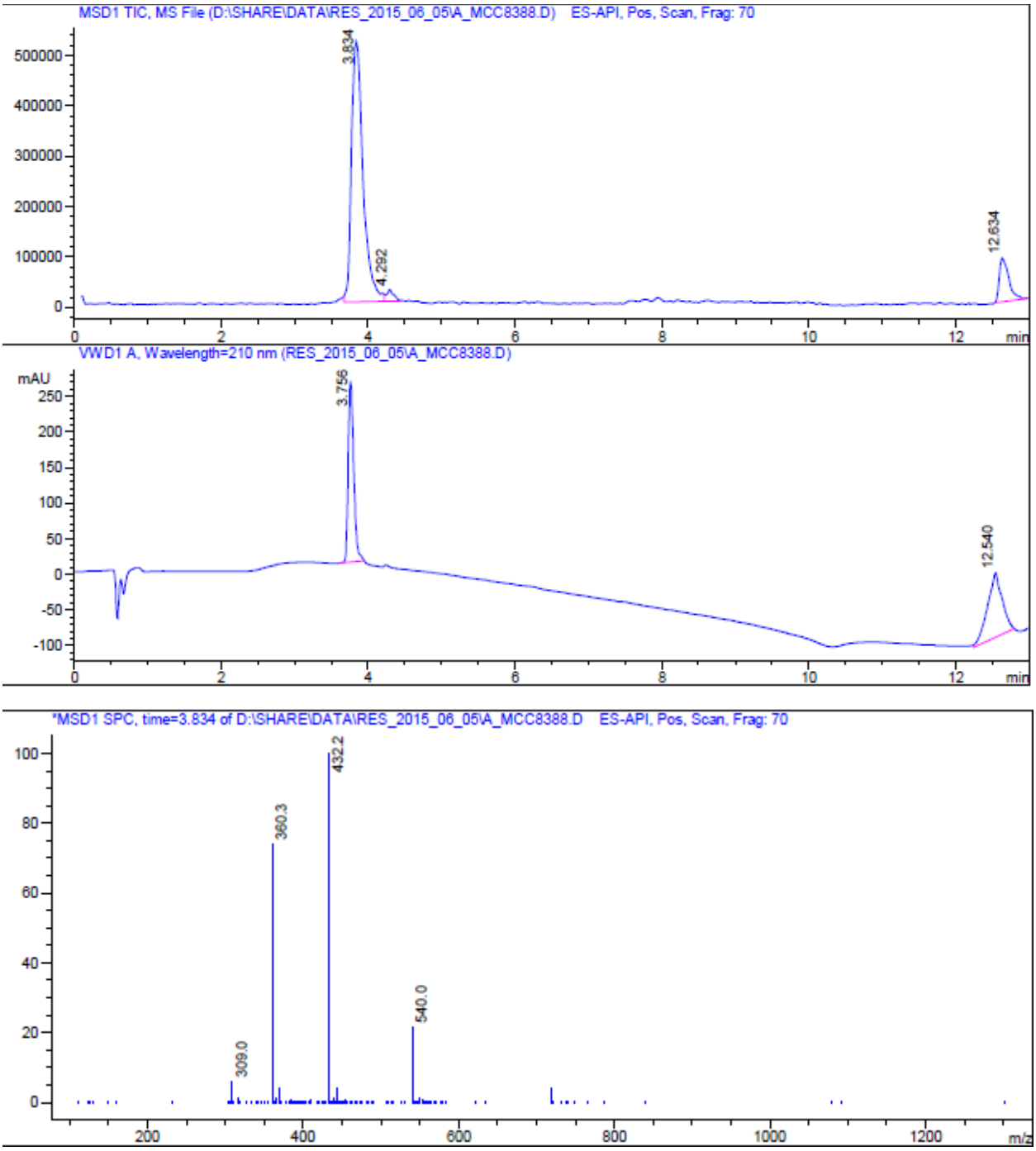

Figure S7.2-11 – LC-MS of protegrin-1

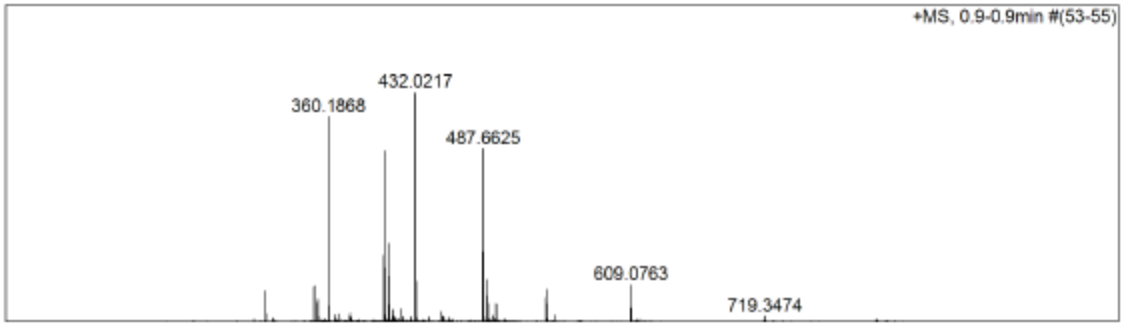

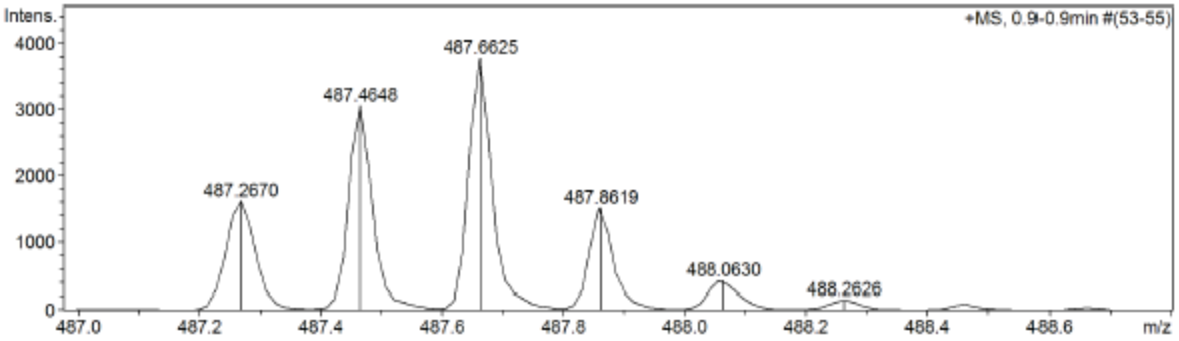

Sum Formula	Sigma	m/z	Err [ppm]	Mean Err [ppm]	Err [mDa]	rdb	N Rule	e⁻
C 103 H 183 N 36 O 26 S 3	0.163	487.2648	-4.60	3.27	-2.24	30.50	ok	even

Figure S7.2-12 – HRMS of thanatin
HRMS-ESI (*m/z*): $[M + 5H]^{5+}$ calculated for ($C_{103}H_{178}N_{36}O_{26}S_3$ + 5H)/5, 487.2575; found 487.2648.

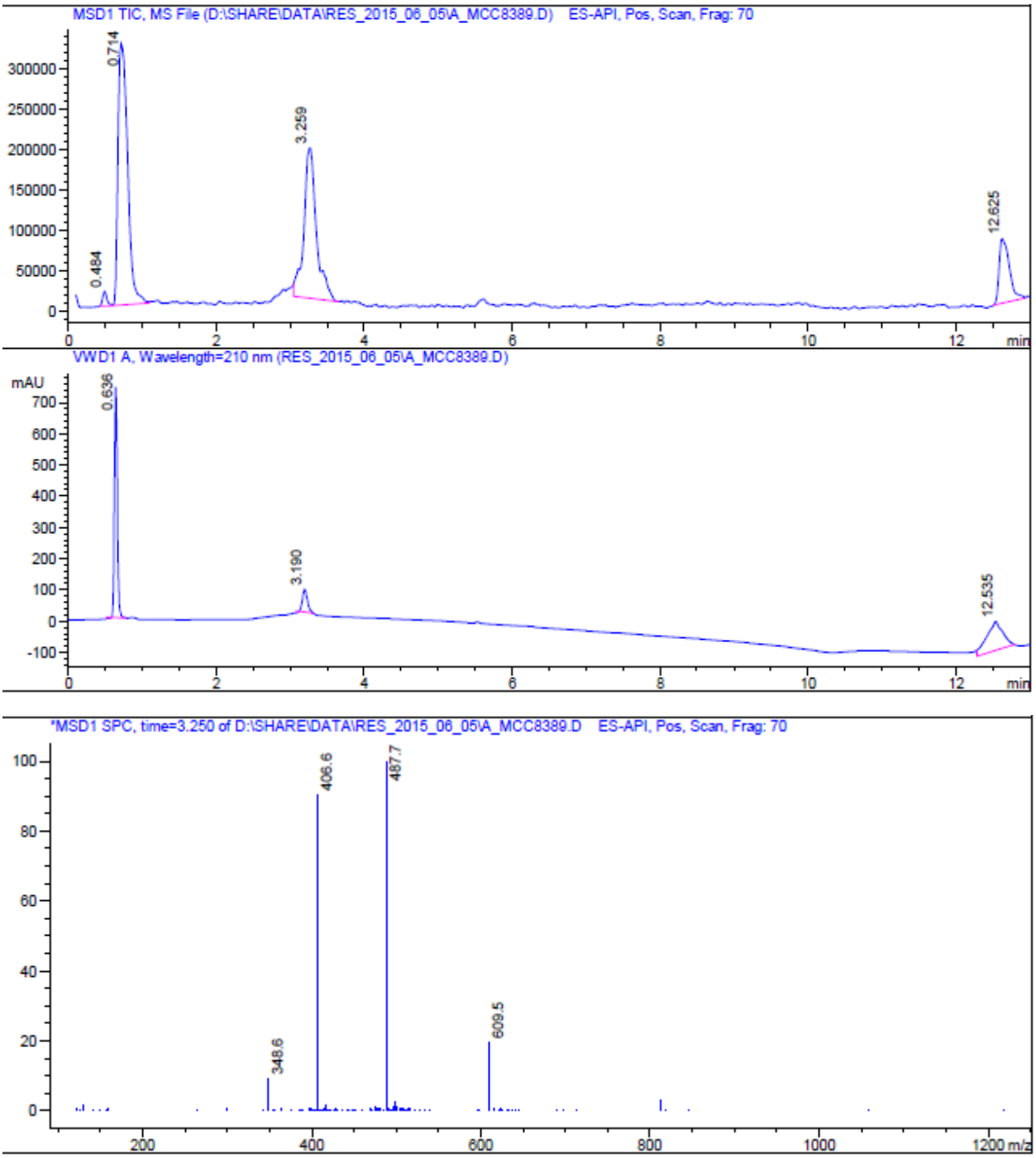

Figure S7.2-13 – LC-MS of thanatin

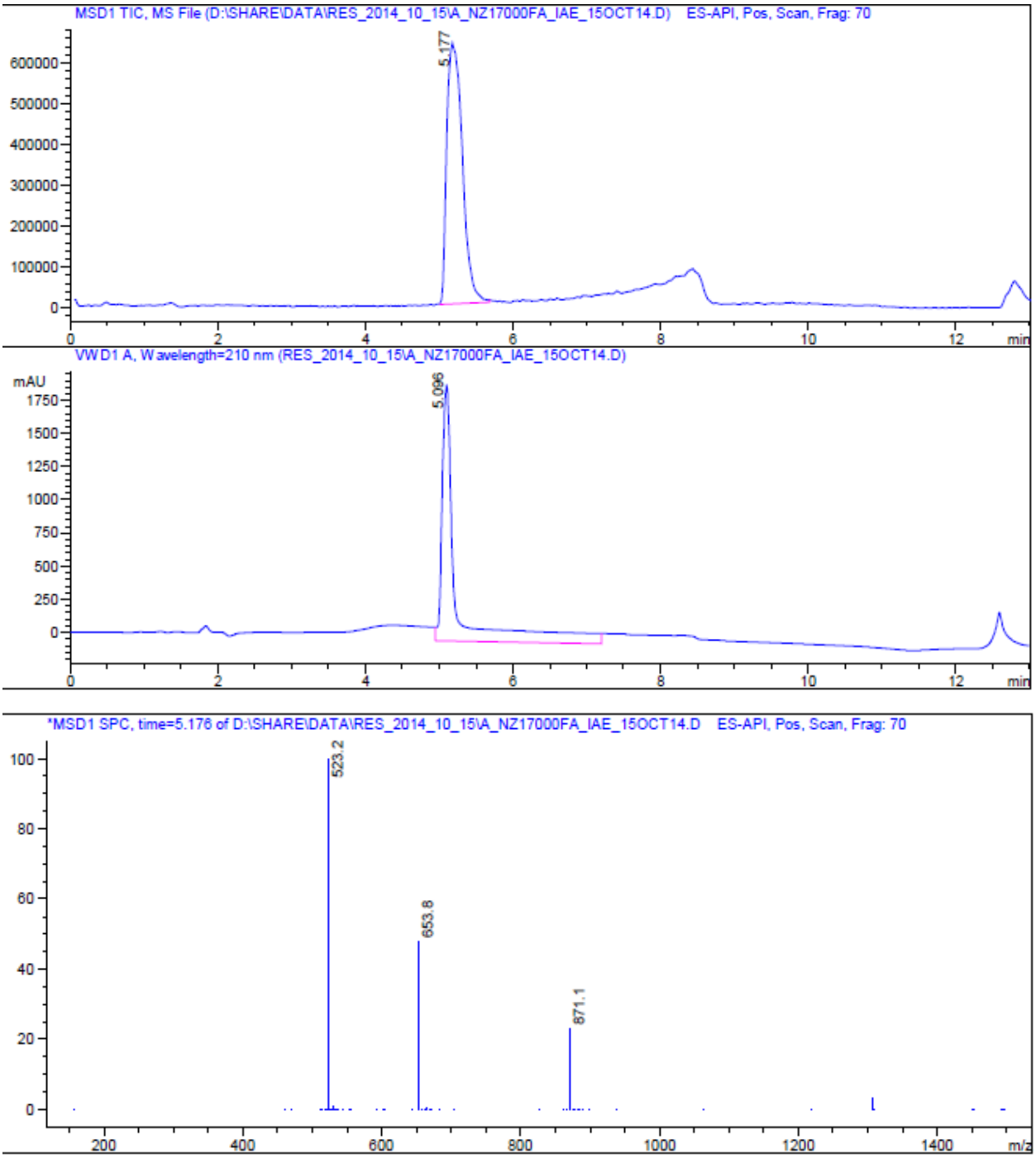

Figure S7.2-14 – LC-MS of arenicin-3

References:

1. Wayne, P. (2012) *CLSI. Methods for dilution Antimicrobial susceptibility tests for bacteria that grow aerobically*, Vol. 32, Ninth Edition ed., Clinical and laboratory standards institute.
2. Wayne (2002) *Reference Method for Broth Dilution Antifungal Susceptibility Testing of Yeasts; Approved Standard*, Vol. 22, 2nd ed., Clinical and laboratory standards institute.
3. McMillian, M. K., Li, L., Parker, J. B., Patel, L., Zhong, Z., Gunnett, J. W., Powers, W. J., and Johnson, M. D. (2002) An improved resazurin-based cytotoxicity assay for hepatic cells, *Cell biology and toxicology 18*, 157-173.
4. O'Brien, J., Wilson, I., Orton, T., and Pognan, F. (2000) Investigation of the Alamar Blue (resazurin) fluorescent dye for the assessment of mammalian cell cytotoxicity, *Eur. J. Biochem. 267*, 5421-5426.
5. Harder, J., Bartels, J., Christophers, E., and Schroder, J. M. (2001) Isolation and characterization of human beta -defensin-3, a novel human inducible peptide antibiotic, *The Journal of biological chemistry 276*, 5707-5713.
6. Roth, B. L., Poot, M., Yue, S. T., and Millard, P. J. (1997) Bacterial viability and antibiotic susceptibility testing with SYTOX green nucleic acid stain, *Appl. Environ. Microbiol. 63*, 2421-2431.
7. Torcato, I. M., Huang, Y. H., Franquelim, H. G., Gaspar, D. D., Craik, D. J., Castanho, M. A., and Henriques, S. T. (2013) The antimicrobial activity of Sub3 is dependent on membrane binding and cell-penetrating ability, *ChemBioChem 14*, 2013-2022.
8. Hong, J., Guan, W., Jin, G., Zhao, H., Jiang, X., and Dai, J. (2015) Mechanism of tachyplesin I injury to bacterial membranes and intracellular enzymes, determined by laser confocal scanning microscopy and flow cytometry, *Microbiological research 170*, 69-77.
9. Powers, J. P., Tan, A., Ramamoorthy, A., and Hancock, R. E. (2005) Solution structure and interaction of the antimicrobial polyphemusins with lipid membranes, *Biochemistry 44*, 15504-15513.
10. Domingues, T. M., Perez, K. R., Miranda, A., and Riske, K. A. (2015) Comparative study of the mechanism of action of the antimicrobial peptide gomesin and its linear analogue: The role of the beta-hairpin structure, *Biochimica et biophysica acta 1848*, 2414-2421.
11. Drin, G., and Temsamani, J. (2002) Translocation of protegrin I through phospholipid membranes: role of peptide folding, *Biochimica et biophysica acta 1559*, 160-170.
12. Robert, E., Lefevre, T., Fillion, M., Martial, B., Dionne, J., and Auger, M. (2015) Mimicking and Understanding the Agglutination Effect of the Antimicrobial Peptide Thanatin Using Model Phospholipid Vesicles, *Biochemistry 54*, 3932-3941.
13. Zhang, F., Xue, J., Shao, J., and Jia, L. (2012) Compilation of 222 drugs' plasma protein binding data and guidance for study designs, *Drug discovery today 17*, 475-485.

7.3 Appendix III - Supplementary information Chapter 3

Table S7.3-1 – Microbial strains and cell line used for the antimicrobial assay and cytotoxicity assays

Organism	Strains	Description
Escherichia coli	ATCC 25922	FDA control strain
Klebsiella quasipneumoniae subsp. similipneumoniae	ATCC 700603	Multi-drug Resistant (MDR)
Klebsiella pneumoniae	ATCC 13883	Type strain (polymyxin hetero-resistant)
Klebsiella pneumoniae	ATCC BAA-2146	New Delhi Metallo-beta-lactamase-1 (NDM-1) positive
Klebsiella pneumoniae	CI 100650661:1	Extensively-drug Resistant (XDR)
Acinetobacter baumannii	ATCC 19606	Type strain
Acinetobacter baumannii	CI 100734512:2	Extensively-drug Resistant (XDR)
Pseudomonas aeruginosa	ATCC27053	Quality control strain
Pseudomonas aeruginosa	FADDI-PA070	Polymyxin resistant
Bacillus subtilis	ATCC 6051	Type strain
Staphylococcus aureus	ATCC 43300	Methicillin Resistant *Staphylococcus aureus* (MRSA)
Candida albicans	ATCC 90028	CLSI reference strain
Cryptococcus neoformans var grubii	ATCC 208821	H99, Type strain
HEK293	ATCC CRL-1573	Human Embryonic kidney cells

Peptide Characterisation

Final purity of more than 90 % for all compounds was confirmed by HPLC analysis using UV (214 nm) detection. HPLC analysis were conducted using Agilent Technologies 1200 Series Instrument with a G1316A variable wavelength detector set at λ= 214 nm, using an Agilent Zorbax Eclipse XDB-Phenyl (3 × 100mm, 3.5 μm particle size, flow rate 1 mL/min). Two different solvent systems were used, 0.1% trifluoroacetic acid in water / 0.1% trifluoroacetic acid in acetonitrile and 0.1% trifluoroacetic acid in water / 0.1% trifluoroacetic acid in methanol). Identities of final products were confirmed by high resolution mass spectrometry (HRMS), performed on a Bruker Micro TOF mass spectrometer using (+)-ESI calibrated to sodium formate. 1H and 2D TOCSY NMR were acquired on Bruker Avance III spectrometer equipped with a cryogenically cooled triple resonance probed operating at a normal ^{1}H frequency of 600 MHz at 298 K. Water suppression was done via excitation sculpting unless otherwise stated.

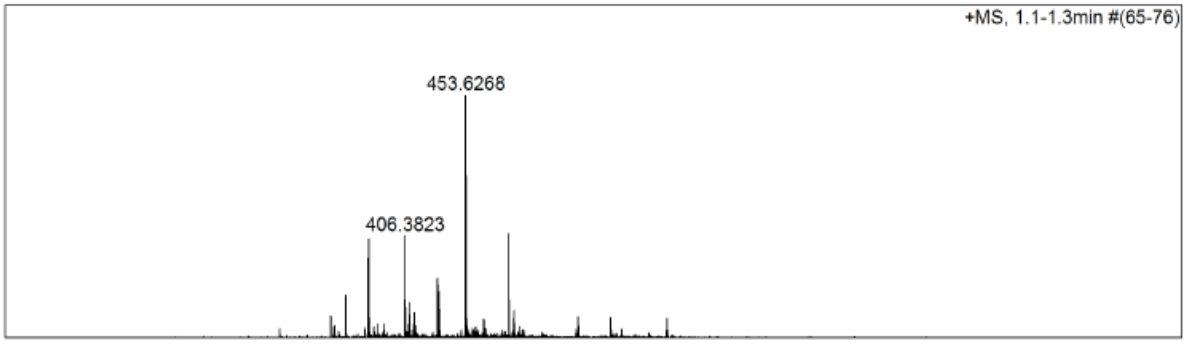

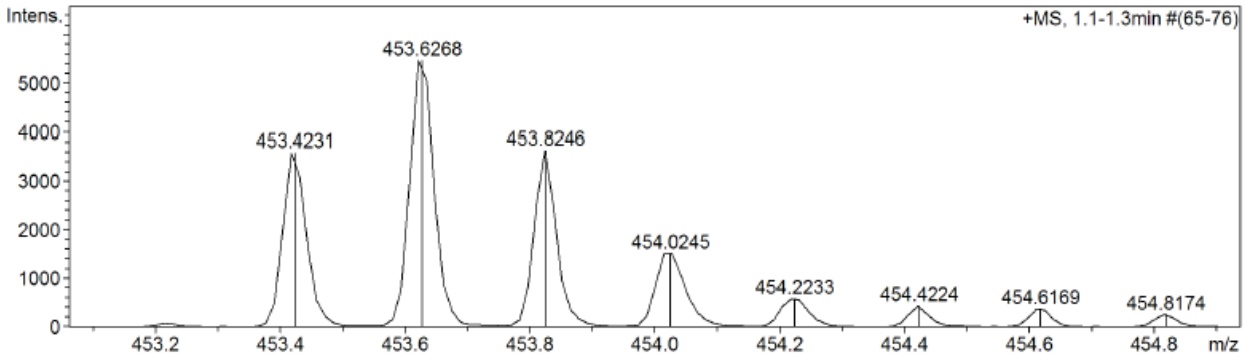

Sum Formula	Sigma	m/z	Err [ppm]	Mean Err [ppm]	Err [mDa]	rdb	N Rule	e⁻
C 99 H 156 N 35 O 19 S 4	0.109	453.4234	0.80	-0.70	0.36	39.50	ok	even

Figure S7.3-1 – HRMS of 1 (TP1)
HRMS-ESI (*m/z*): $[M + 5H]^{5+}$ calculated for $(C_{99}H_{151}N_{35}O_{19}S_4 + 5H)/5$, 453.4234; found 453.4231.

A

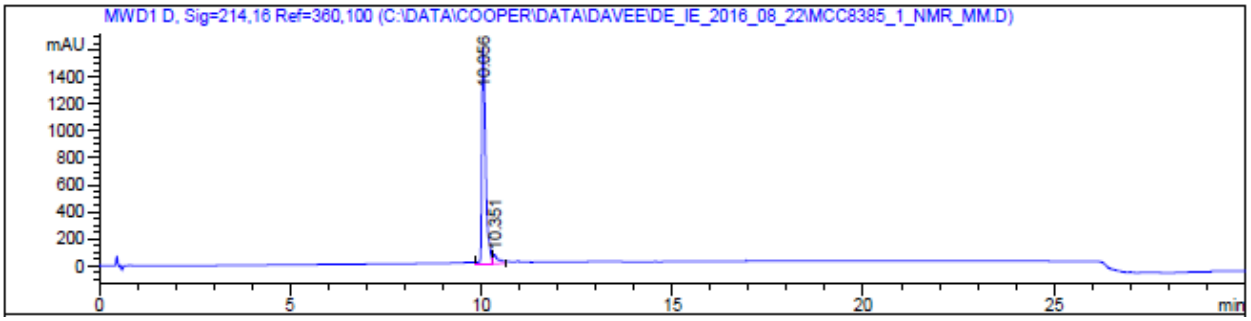

Peak #	RetTime [min]	Type	Width [min]	Area [mAU*s]	Height [mAU]	Area %
1	10.056	VV	0.0985	1.05828e4	1613.07642	93.7489
2	10.351	VV	0.1495	705.64661	63.56611	6.2511

B

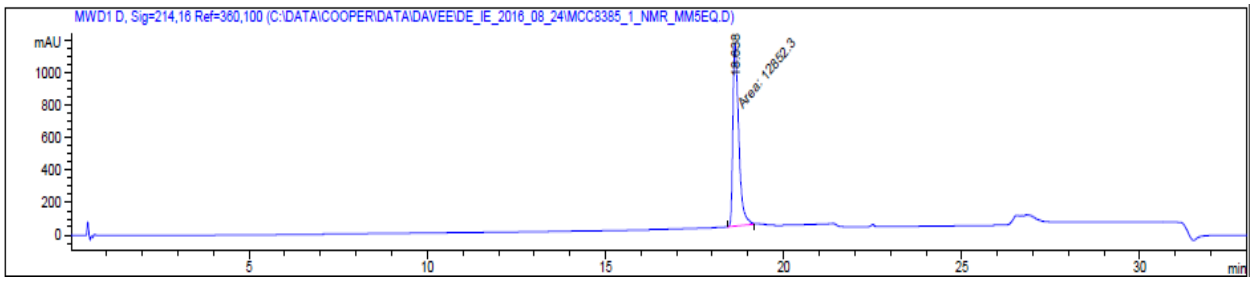

Peak #	RetTime [min]	Type	Width [min]	Area [mAU*s]	Height [mAU]	Area %
1	18.638	MM	0.1904	1.28523e4	1125.19165	100.0000

Figure S7.3-2 – HPLC of 1 (TP1). A – In Acetonitrile solvent system. B – In Methanol solvent system.

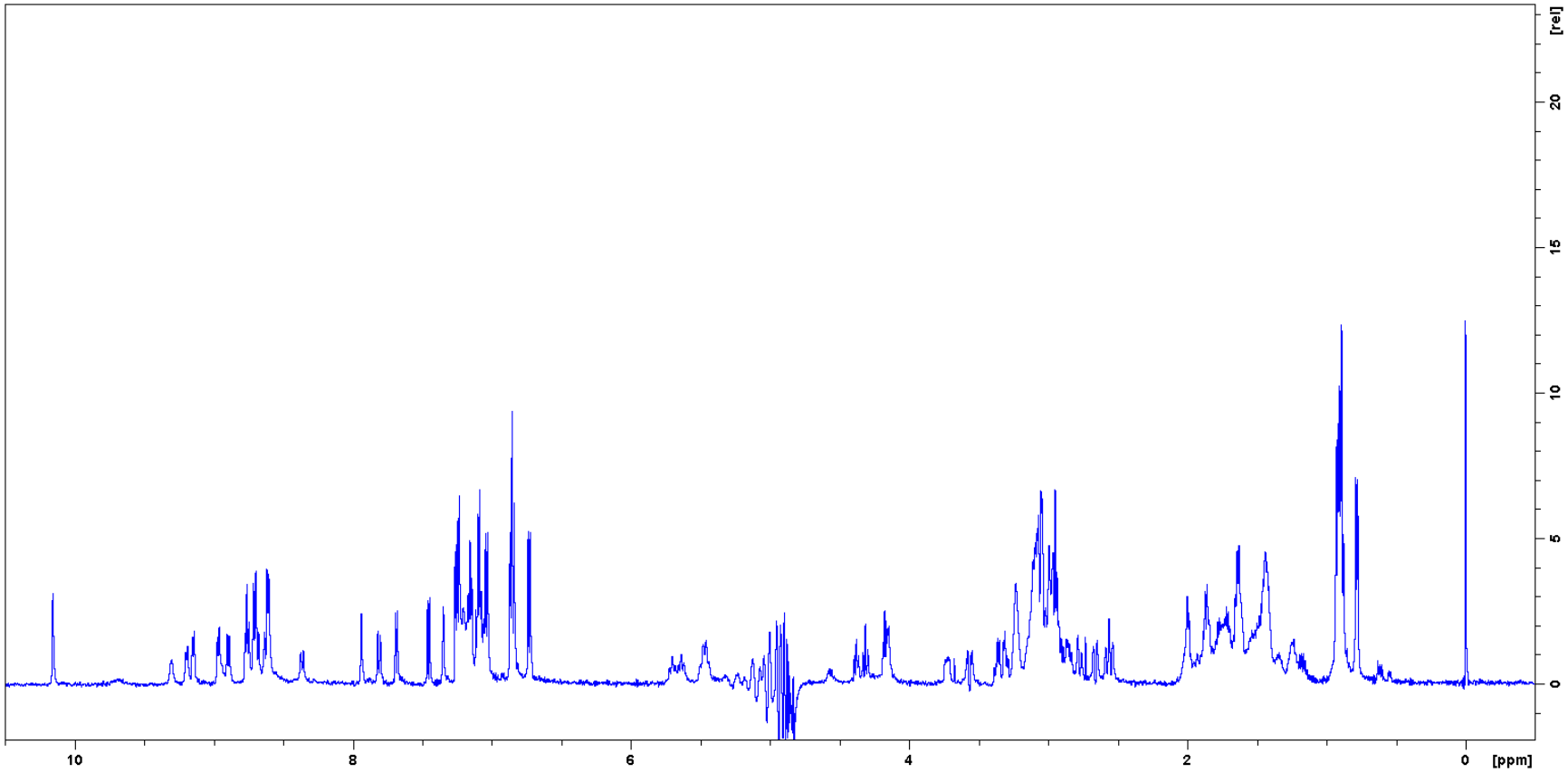

Figure S7.3-3 – ^{1}H NMR of 1 (TP1)

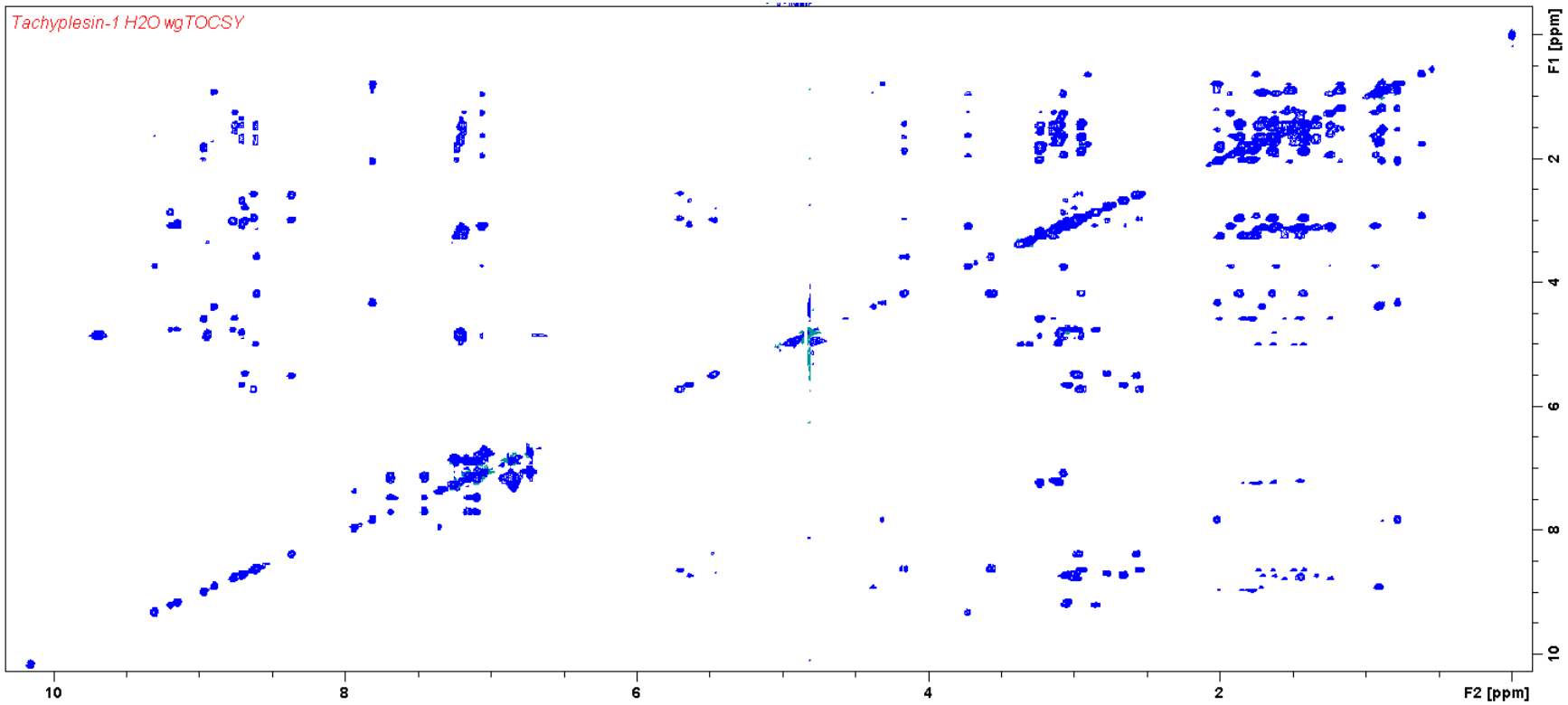

Figure S7.3-4 – 2D TOCSY NMR of 1 (TP1), MLEV17 spin-lock mixing pulses = 80 ms, water suppression was performed using Watergate sequence.

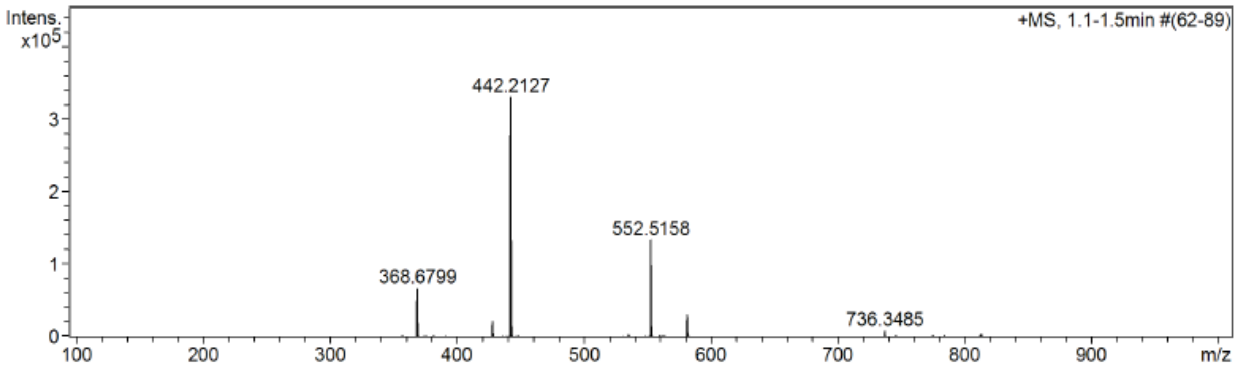

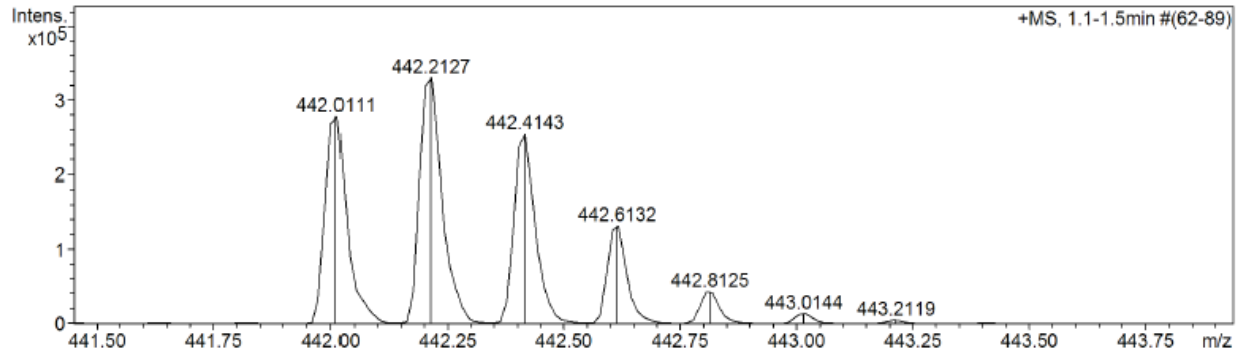

Sum Formula	Sigma	m/z	Err [ppm]	Mean Err [ppm]	Err [mDa]	rdb	N Rule	e⁻
C 96 H 149 N 34 O 19 S 4	0.044	442.0119	1.78	-0.70	0.79	39.50	ok	even

Figure S7.3-5 – HRMS of 2 (TP1[K1A])
HRMS-ESI (*m/z*): $[M + 5H]^{5+}$ calculated for ($C_{96}H_{144}N_{34}O_{19}S_4$ + 5H)/5, 442.0119; found 442.0111.

A

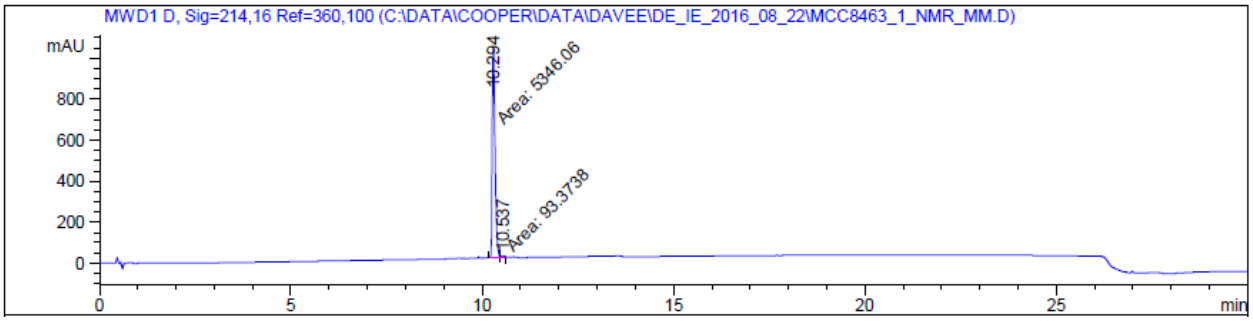

Peak #	RetTime [min]	Type	Width [min]	Area [mAU*s]	Height [mAU]	Area %
1	10.294	MF	0.0863	5346.05664	1032.87158	98.2834
2	10.537	FM	0.1310	93.37376	11.87540	1.7166

B

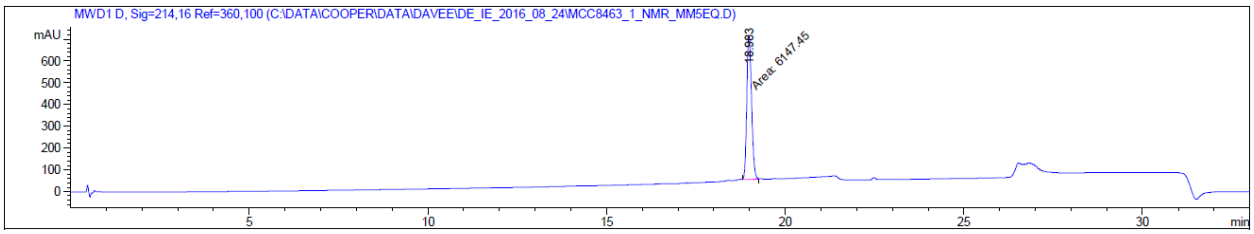

Peak #	RetTime [min]	Type	Width [min]	Area [mAU*s]	Height [mAU]	Area %
1	18.983	MM	0.1550	6147.45459	661.16681	100.0000

Figure S7.3-6 – HPLC of 2 (TP1[K1A]). A – In Acetonitrile solvent system. B – In Methanol solvent system.

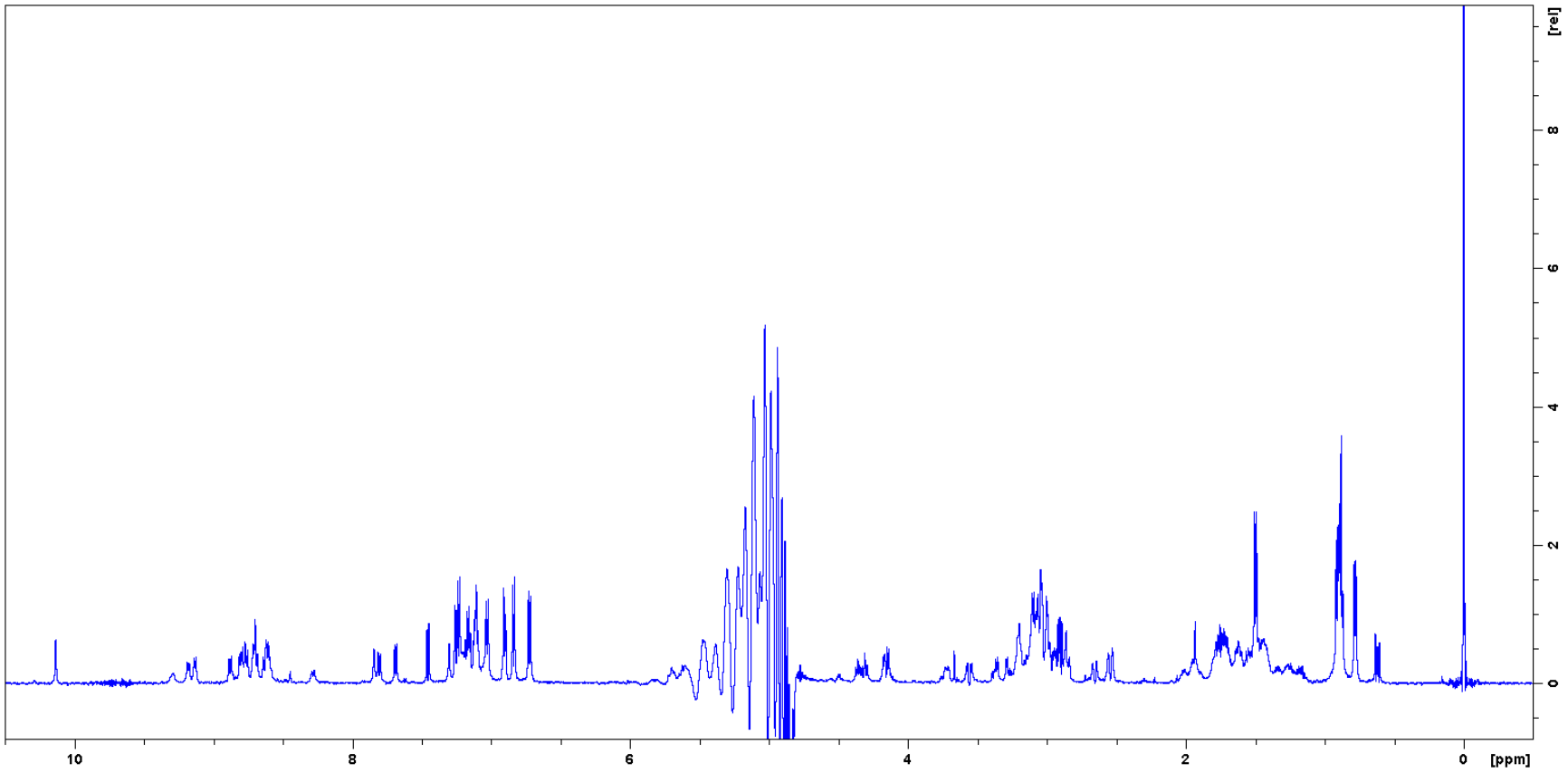

Figure S7.3-7 – ^{1}H NMR of 2 (TP1[K1A])

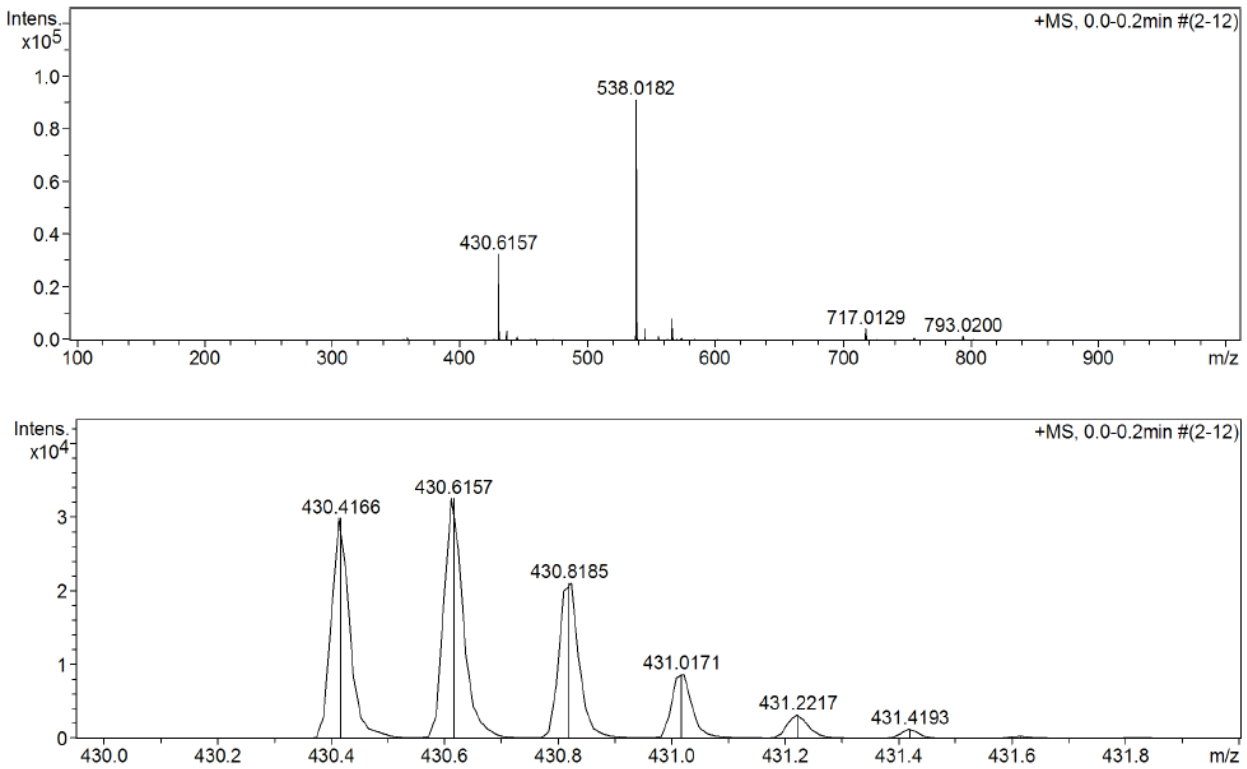

Sum Formula	Sigma	m/z	Err [ppm]	Mean Err [ppm]	Err [mDa]	rdb	N Rule	e⁻
C 91 H 151 N 34 O 19 S 4	0.087	430.4150	-3.82	-3.62	-1.64	33.50	ok	even

Figure S7.3-8 – HRMS of 3 (TP1[W2A])
HRMS-ESI (*m/z*): $[M + 5H]^{5+}$ calculated for ($C_{91}H_{146}N_{34}O_{19}S_4$ + 5H)/5, 430.4150; found 430.4166.

A

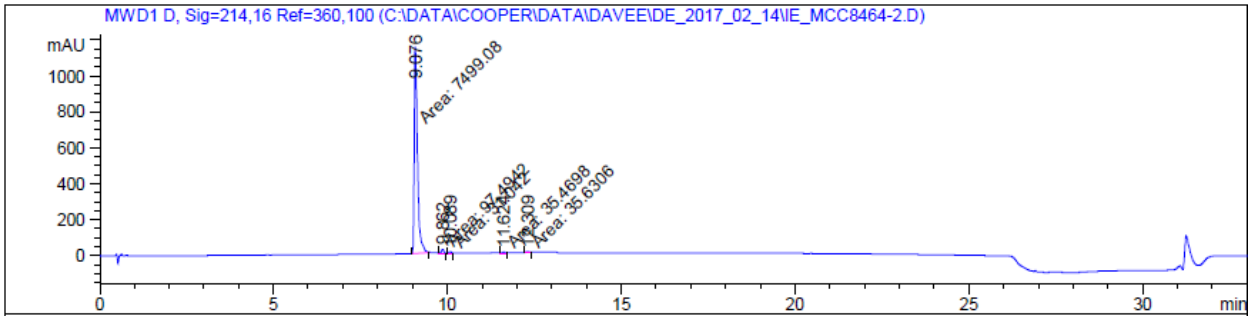

Peak #	RetTime [min]	Type	Width [min]	Area [mAU*s]	Height [mAU]	Area %
1	9.076	MM	0.1084	7499.08447	1153.26575	97.4069
2	9.862	MM	0.0801	97.49422	20.29183	1.2664
3	10.089	MM	0.0668	31.04198	7.75037	0.4032
4	11.624	MM	0.1342	35.46975	4.40386	0.4607
5	12.309	MM	0.1227	35.63057	4.83964	0.4628

B

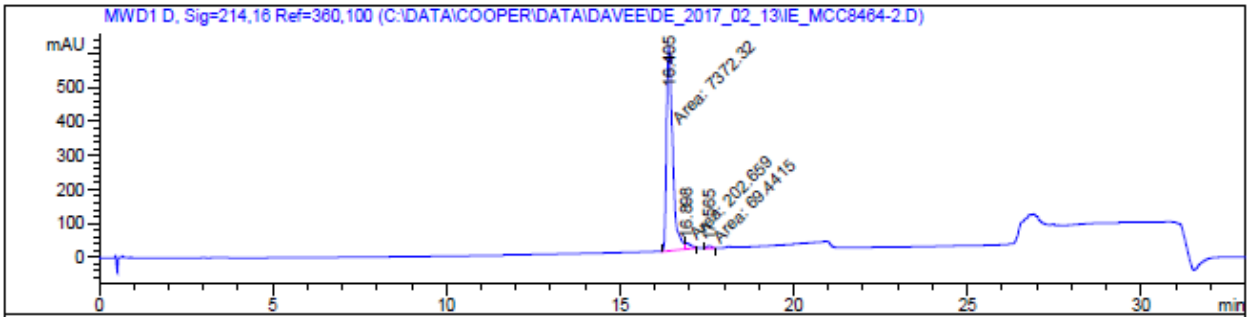

Peak #	RetTime [min]	Type	Width [min]	Area [mAU*s]	Height [mAU]	Area %
1	16.405	MF	0.2037	7372.31543	603.11798	96.4405
2	16.898	FM	0.1911	202.65860	17.67676	2.6511
3	17.565	MM	0.1617	69.44147	7.15540	0.9084

Figure S7.3-9 – HPLC of 3 (TP1[W2A]) – A – In Acetonitrile solvent system. B – In Methanol solvent system.

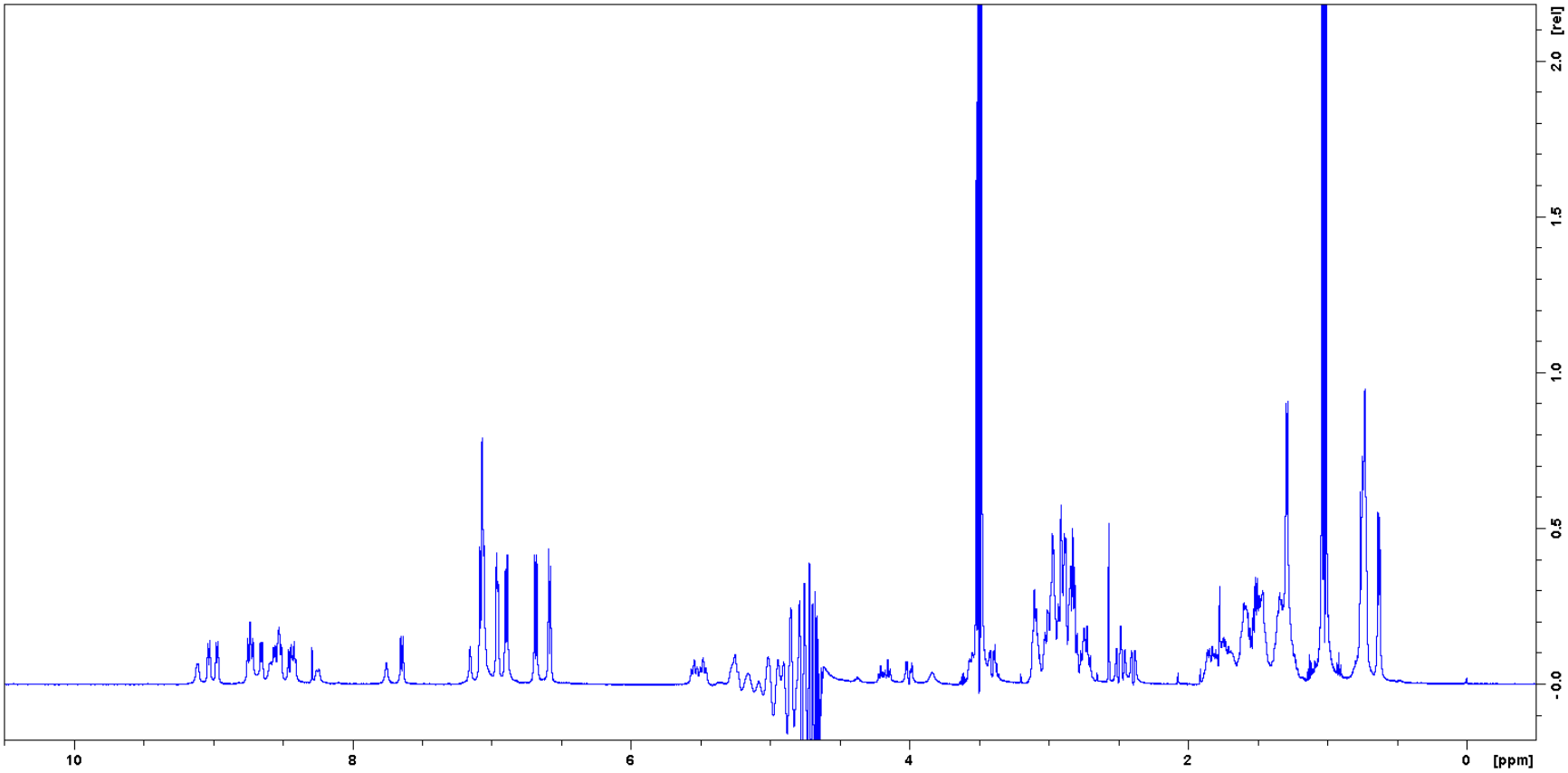

Figure S7.3-10 – ^{1}H NMR of 3 (TP1[W2A]). The quadruplet at 3.65 and the triplet at 1.17 ppm are residual ethanol.

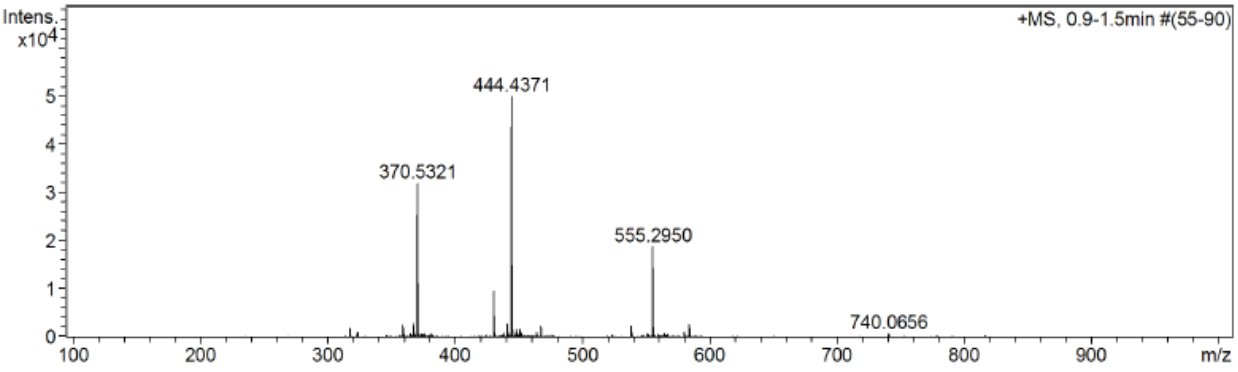

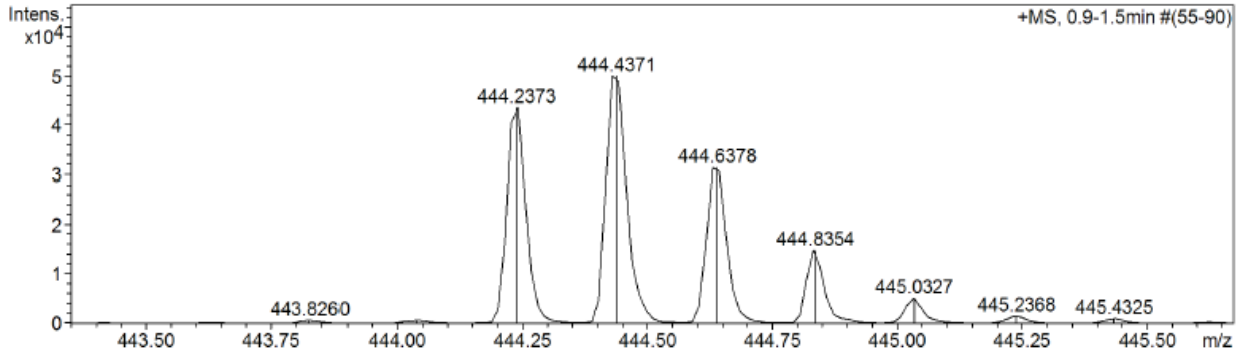

Sum Formula	Sigma	m/z	Err [ppm]	Mean Err [ppm]	Err [mDa]	rdb	N Rule	e⁻
C 99 H 158 N 35 O 20 S 2	0.060	444.2367	-1.38	1.14	-0.61	38.50	ok	even

Figure S7.3-11 – HRMS of 4 (TP1[C3A,C16S])
HRMS-ESI (*m/z*): $[M + 5H]^{5+}$ calculated for ($C_{99}H_{153}N_{35}O_{20}S_2$ + 5H)/5, 444.2367; found 444.2373.

A

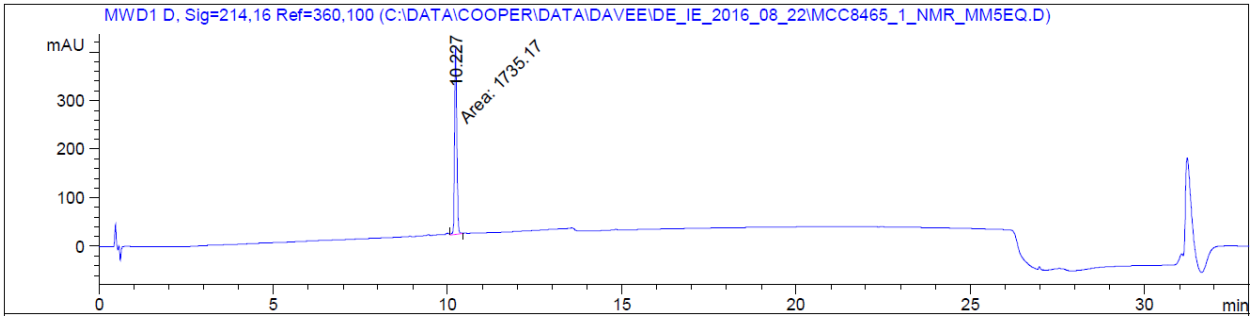

Peak #	RetTime [min]	Type	Width [min]	Area [mAU*s]	Height [mAU]	Area %
1	10.227	MM	0.0743	1735.17078	389.39505	100.0000

B

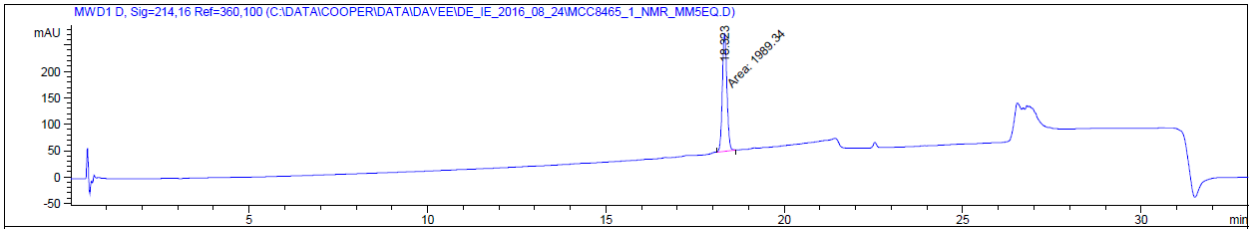

Peak #	RetTime [min]	Type	Width [min]	Area [mAU*s]	Height [mAU]	Area %
1	18.323	MM	0.1483	1989.34351	223.50307	100.0000

Figure S7.3-12 – HPLC of 4 (TP1[C3A,C16S]). A – In Acetonitrile solvent system. B – In Methanol solvent system.

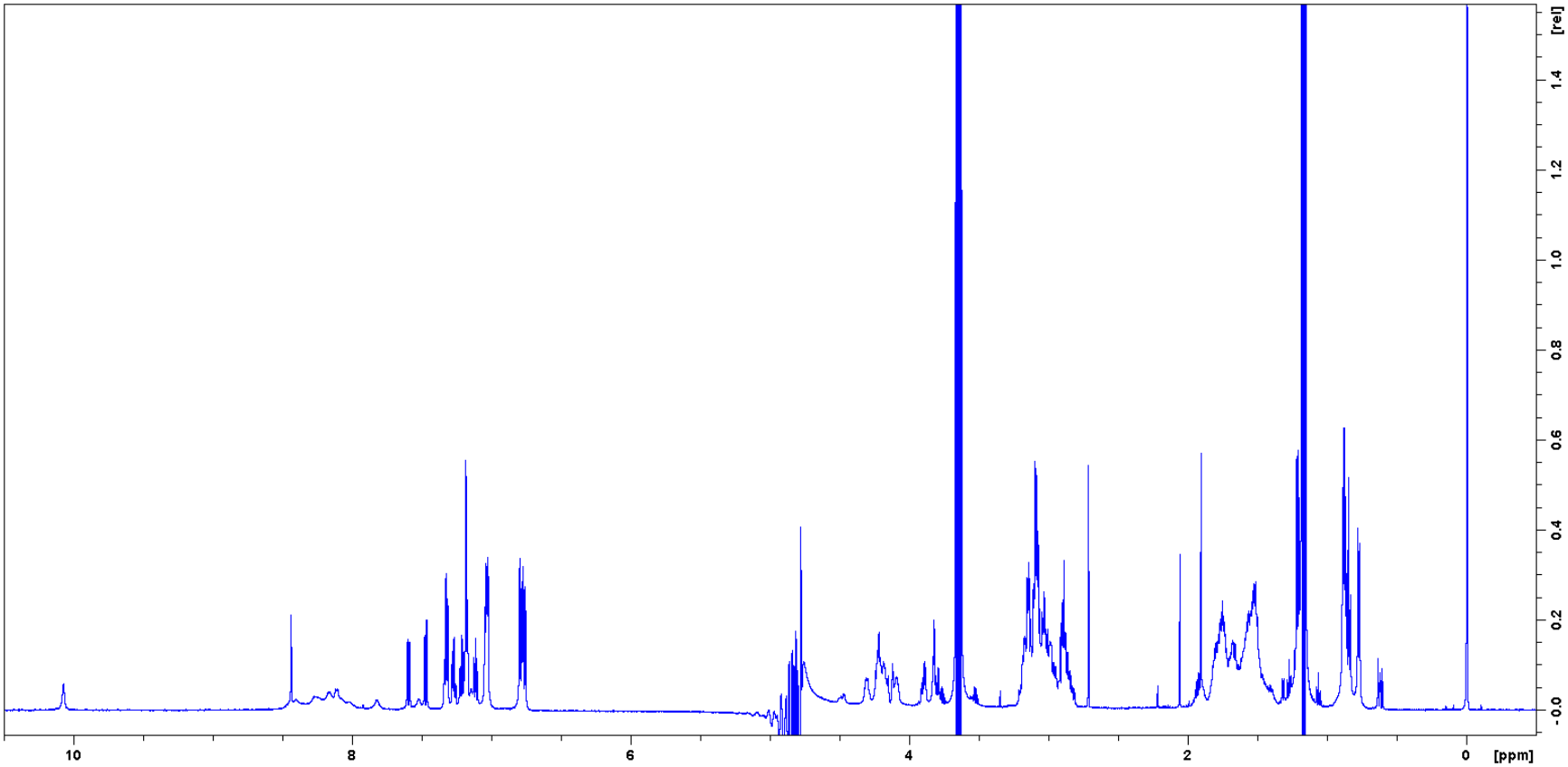

Figure S7.3-13 – ^{1}H NMR of 4 (TP1[C3A,C16S]). The quadruplet at 3.65 and the triplet at 1.17 ppm are residual ethanol.

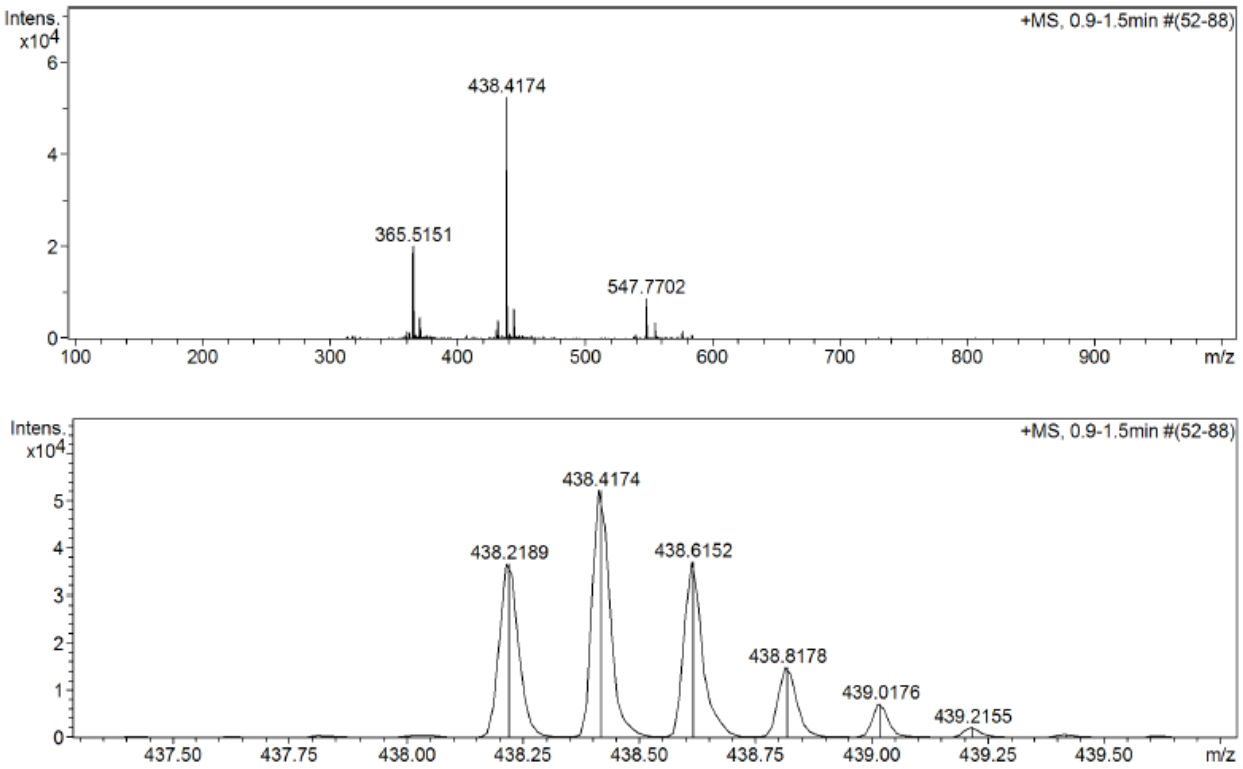

Sum Formula	Sigma	m/z	Err [ppm]	Mean Err [ppm]	Err [mDa]	rdb	N Rule	e⁻
C 93 H 152 N 35 O 19 S 4	0.087	438.2172	-3.95	1.06	-1.73	35.50	ok	even

Figure S7.3-14 – HRMS of 5 (TP1[F4A])
HRMS-ESI (*m/z*): $[M + 5H]^{5+}$ calculated for ($C_{93}H_{147}N_{35}O_{19}S_4$ + 5H)/5, 438.2172; found 438.2189.

A

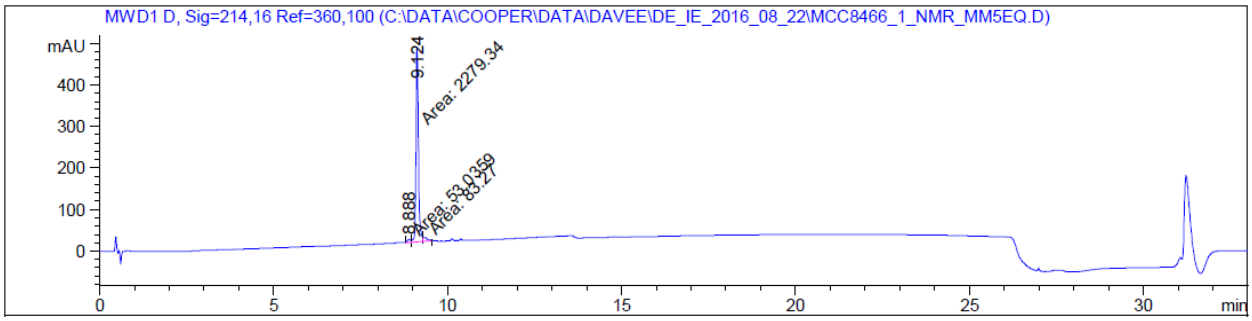

Peak #	RetTime [min]	Type	Width [min]	Area [mAU*s]	Height [mAU]	Area %
1	8.888	MF	0.1071	53.03590	8.25302	2.1955
2	9.124	MF	0.0808	2279.33862	470.36792	94.3574
3	9.353	FM	0.1451	83.27000	9.56678	3.4471

B

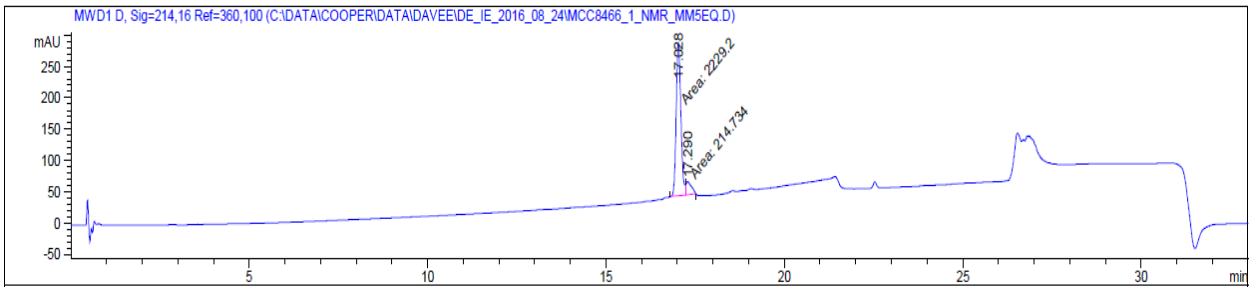

Peak #	RetTime [min]	Type	Width [min]	Area [mAU*s]	Height [mAU]	Area %
1	17.028	MF	0.1523	2229.20190	243.96825	91.2136
2	17.290	FM	0.1738	214.73389	20.59522	8.7864

Figure S7.3-15 – HPLC of 5 (TP1[F4A]). A – In Acetonitrile solvent system. B – In Methanol solvent system.

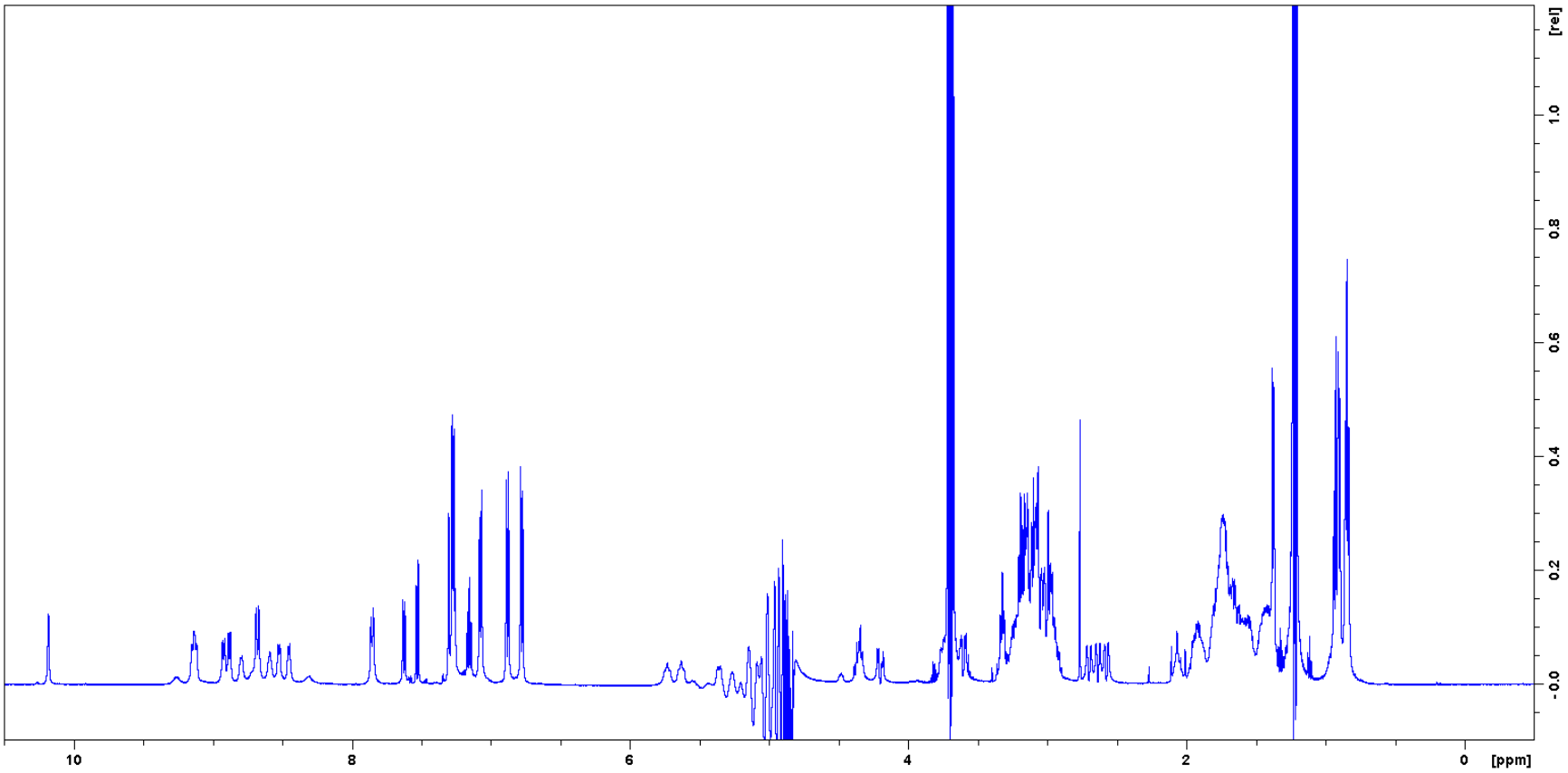

Figure S7.3-16 – ^{1}H NMR of 5 (TP1[F4A]). The quadruplet at 3.65 and the triplet at 1.17 ppm are residual ethanol.

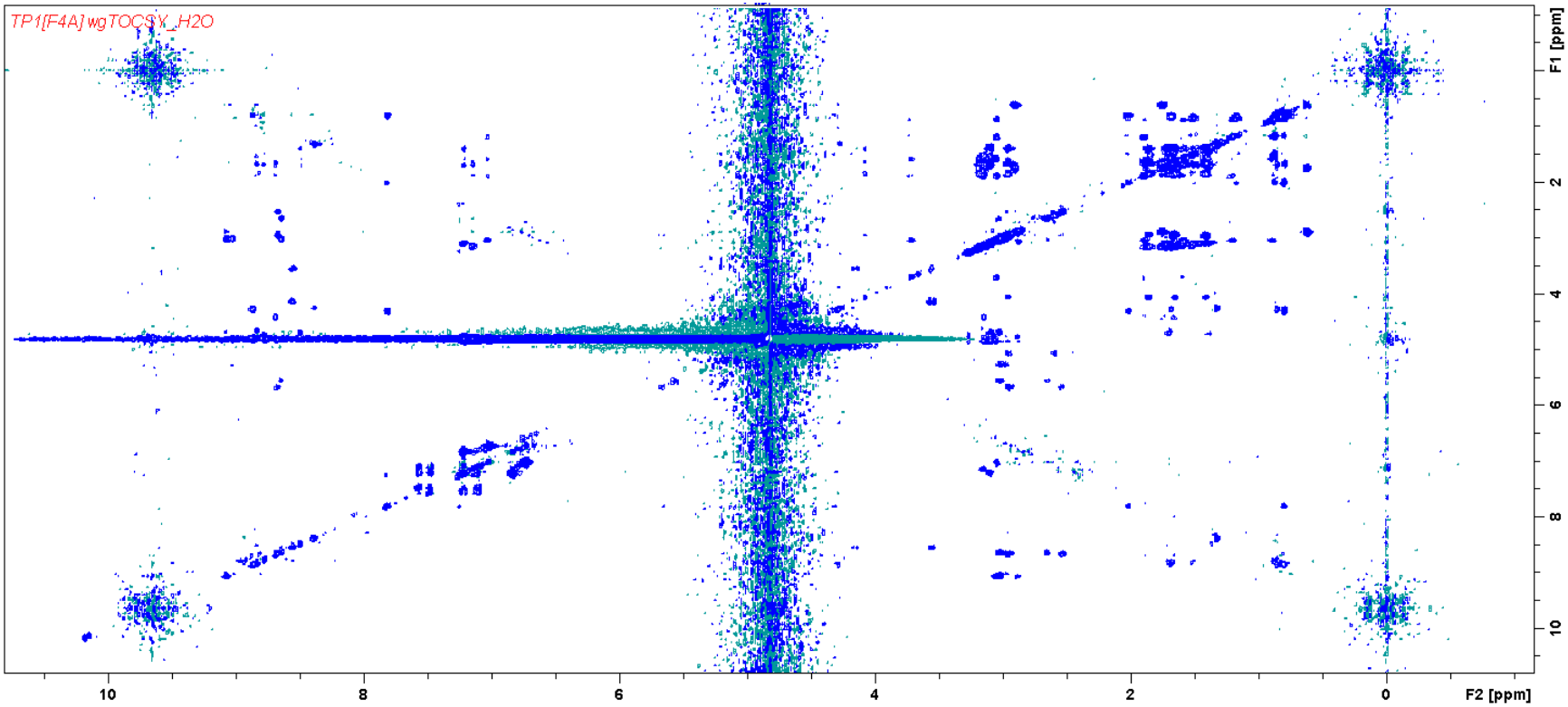

Figure S7.3-17 – 2D TOCSY NMR of 5 (TP1[F4A]), MLEV17 spin-lock mixing pulses = 80 ms, water suppression was performed using Watergate sequence.

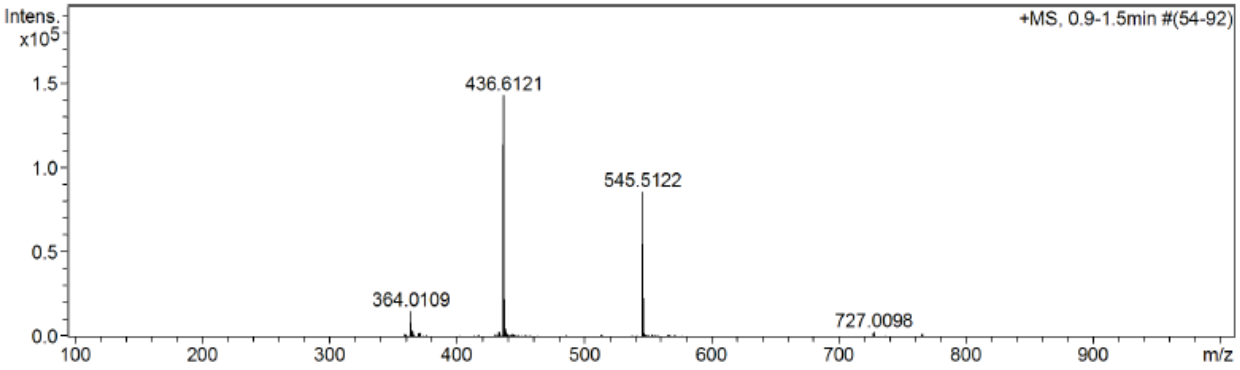

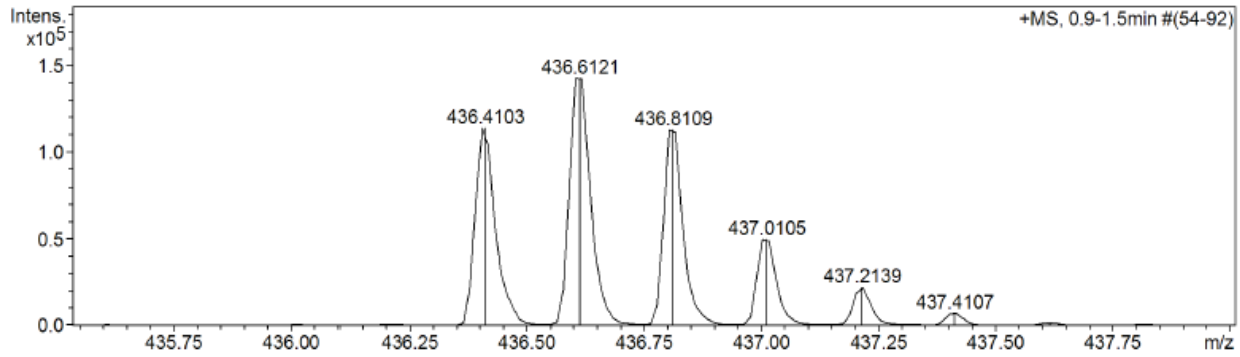

Sum Formula	Sigma	m/z	Err [ppm]	Mean Err [ppm]	Err [mDa]	rdb	N Rule	e⁻
C 96 H 149 N 32 O 19 S 4	0.049	436.4106	0.83	-0.25	0.36	38.50	ok	even

Figure S7.3-18 – HRMS of 6 (TP1[R5A])
HRMS-ESI (*m/z*): $[M + 5H]^{5+}$ calculated for ($C_{96}H_{144}N_{32}O_{19}S_4$ + 5H)/5, 436.4106; found 436.4103.

A

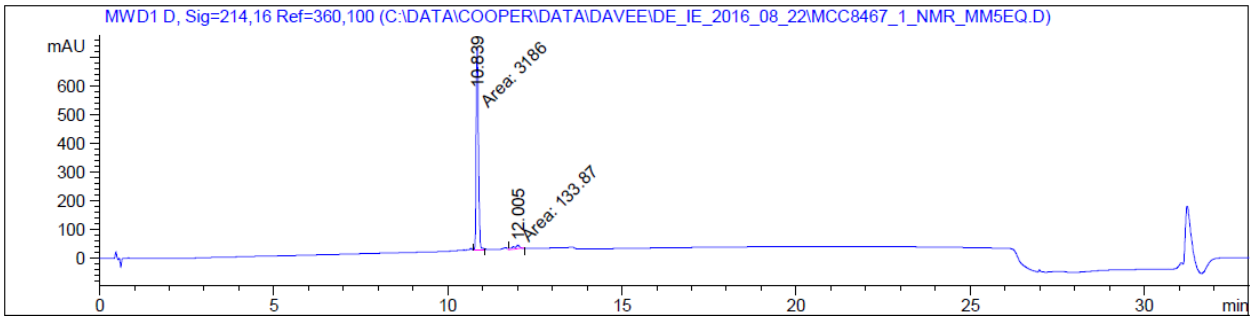

Peak #	RetTime [min]	Type	Width [min]	Area [mAU*s]	Height [mAU]	Area %
1	10.839	MM	0.0748	3185.99536	710.05774	95.9676
2	12.005	MM	0.1812	133.87025	12.31468	4.0324

B

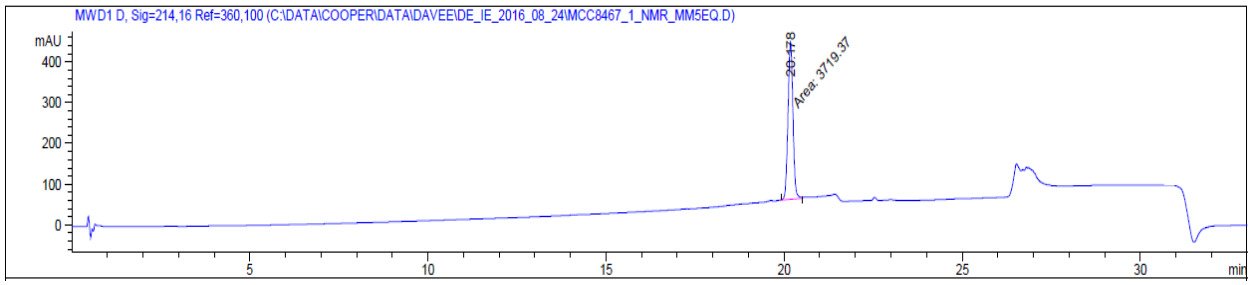

Peak #	RetTime [min]	Type	Width [min]	Area [mAU*s]	Height [mAU]	Area %
1	20.178	MM	0.1604	3719.37231	386.57819	100.0000

Figure S7.3-19 – HPLC of 6 (TP1[R5A]). A – In Acetonitrile solvent system. B – In Methanol solvent system.

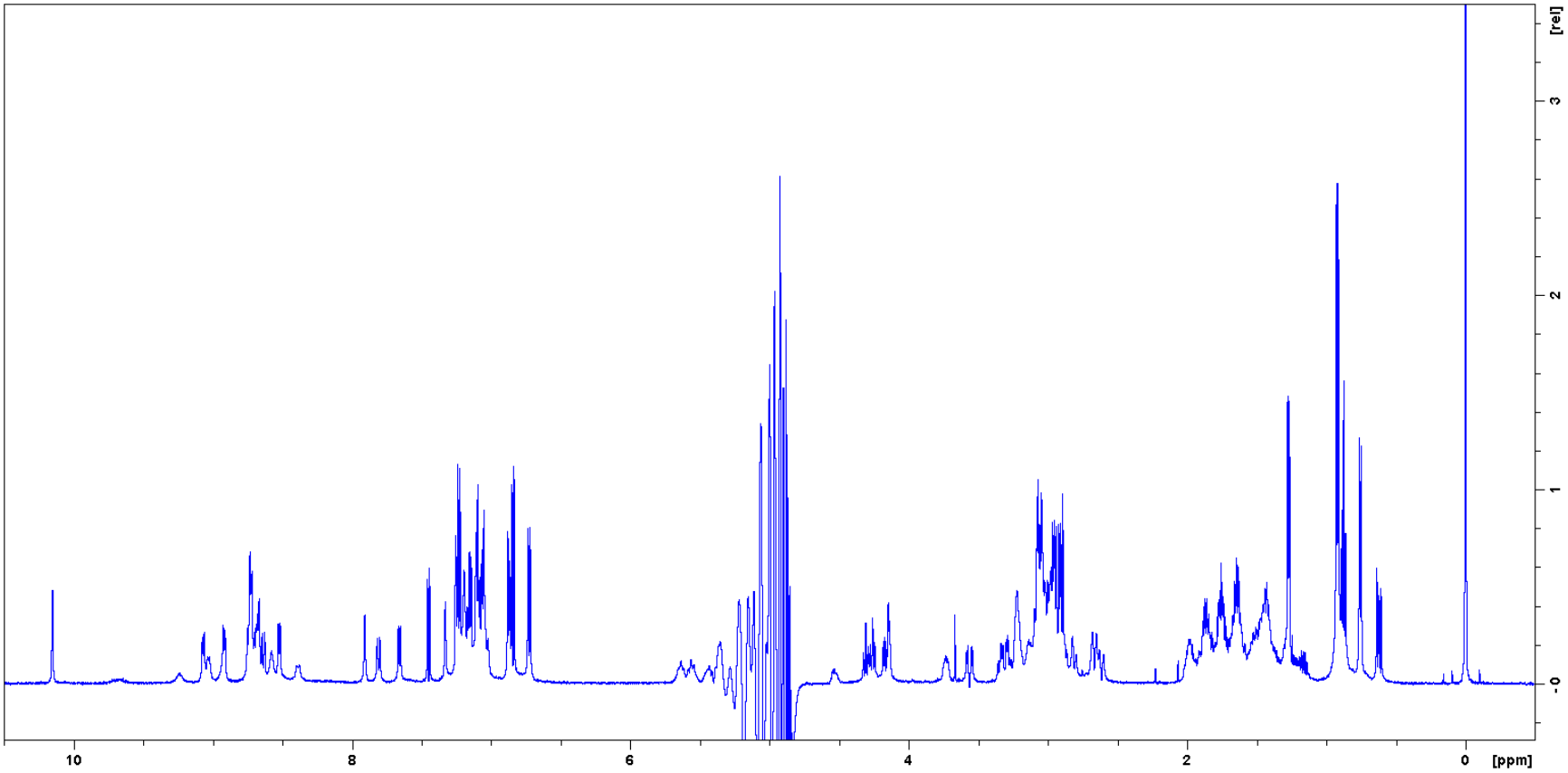

Figure S7.3-20 – ^{1}H NMR of 6 (TP1[R5A])

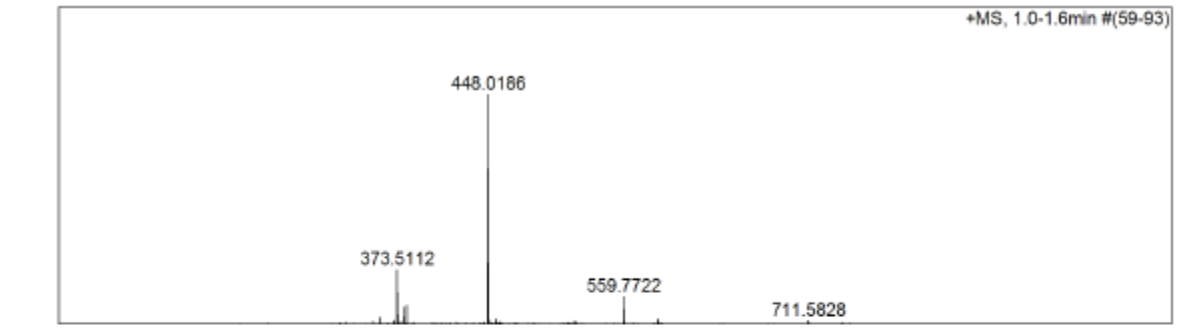

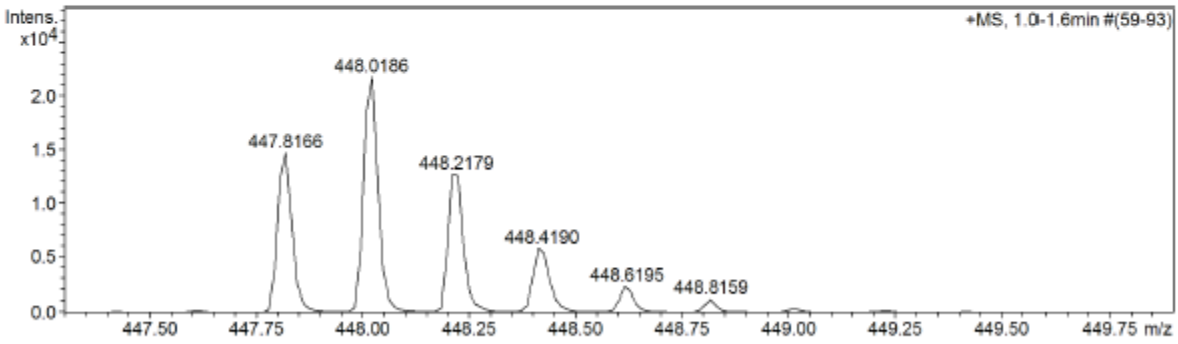

Sum Formula	Sigma	m/z	Err [ppm]	Mean Err [ppm]	Err [mDa]	rdb	N Rule	e⁻
C 97 H 152 N 35 O 19 S 4	0.122	447.8172	1.27	-0.64	0.57	39.50	ok	even

Figure S7.3-21 – HRMS of 7 (TP1[V6A])
HRMS-ESI (*m/z*): $[M + 5H]^{5+}$ calculated for ($C_{97}H_{147}N_{35}O_{19}S_4$ + 5H)/5, 447.8172; found 447.8166.

A

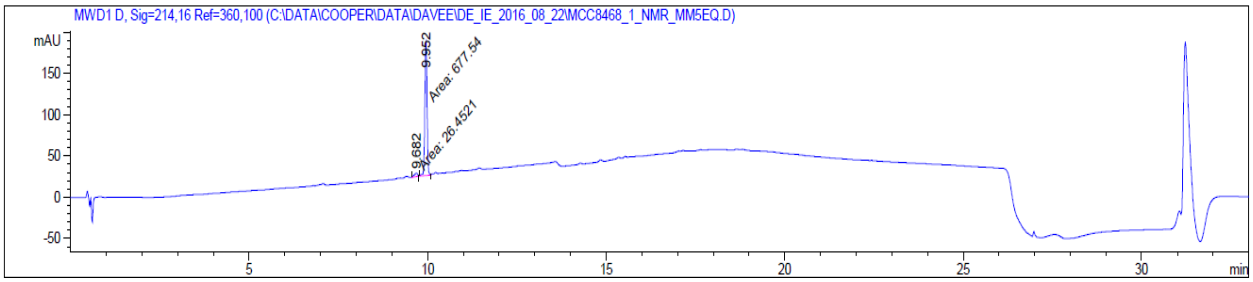

Peak #	RetTime [min]	Type	Width [min]	Area [mAU*s]	Height [mAU]	Area %
1	9.682	MM	0.1113	26.45213	3.96237	3.7574
2	9.952	MM	0.0691	677.53961	163.37051	96.2426

B

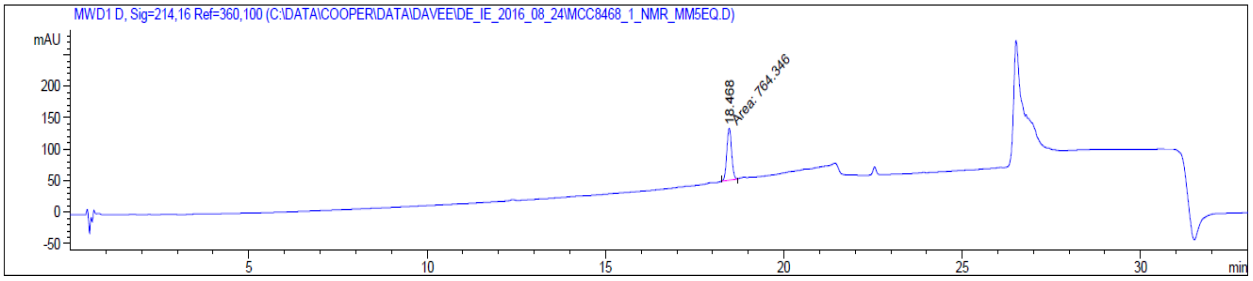

Peak #	RetTime [min]	Type	Width [min]	Area [mAU*s]	Height [mAU]	Area %
1	18.468	MM	0.1549	764.34570	82.26044	100.0000

Figure S7.3-22 – HPLC of 7 (TP1[V6A]). A – In Acetonitrile solvent system. B – In Methanol solvent system.

NMR could not be carried out for TP1 V6A as this analog was not soluble in 100% H_2O.

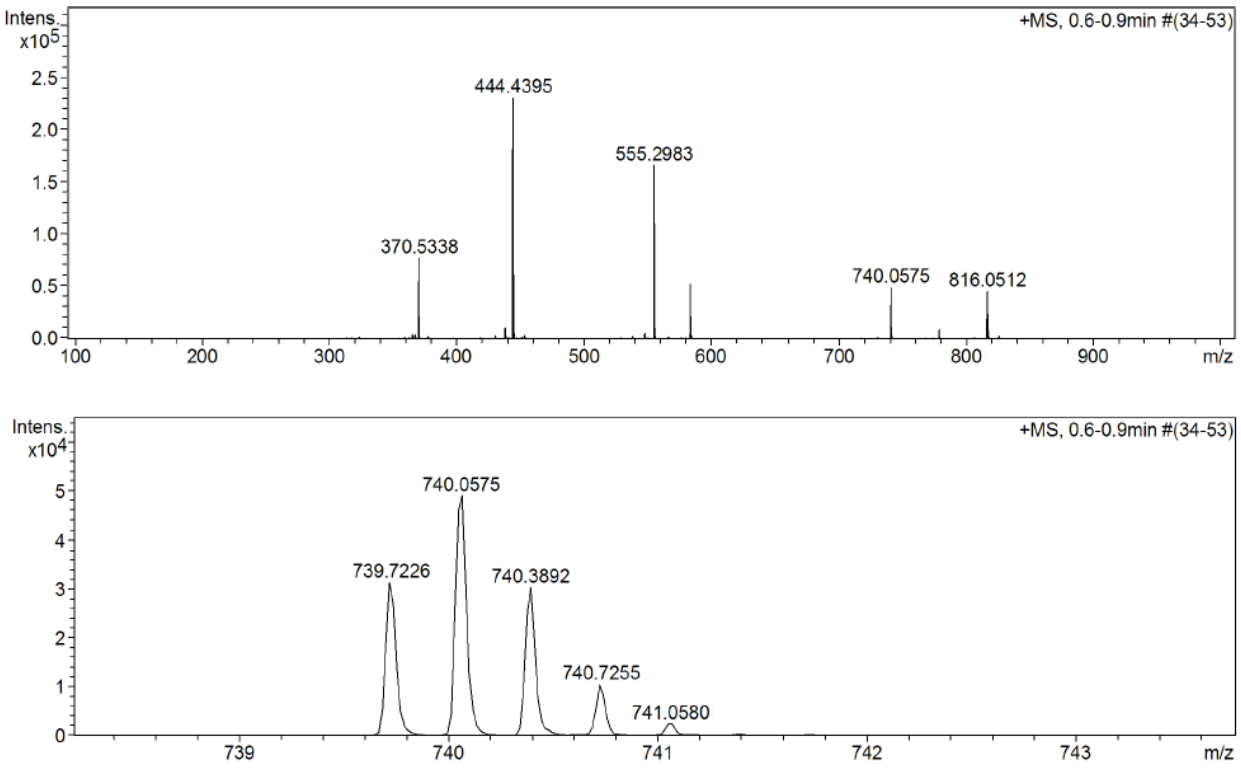

Sum Formula	Sigma	m/z	Err [ppm]	Mean Err [ppm]	Err [mDa]	rdb	N Rule	e⁻
C 99 H 156 N 35 O 20 S 2	0.108	739.7230	0.54	0.76	0.40	39.50	ok	even

Figure S7.3-23 – HRMS of 8 (TP1[C7A,C12S])
HRMS-ESI (*m/z*): $[M + 3H]^{3+}$ calculated for ($C_{99}H_{153}N_{35}O_{20}S_2$ + 3H)/3, 739.7230; found 739.7226.

A

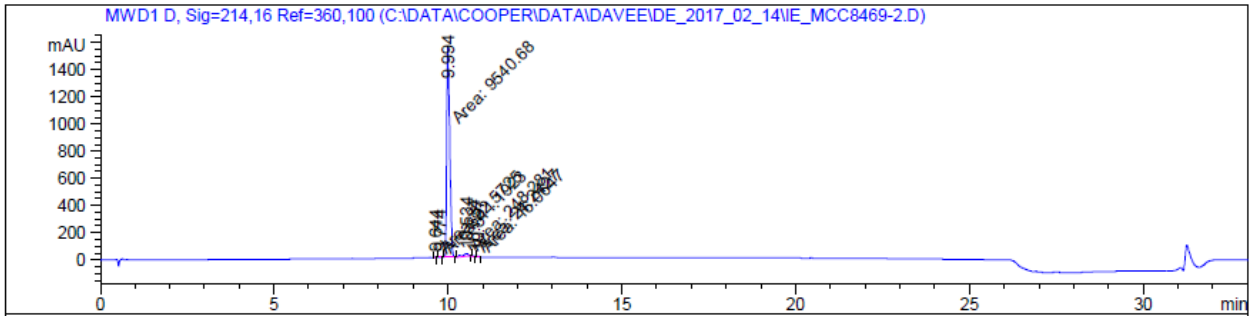

Peak #	RetTime [min]	Type	Width [min]	Area [mAU*s]	Height [mAU]	Area %
1	9.644	MM	0.0734	22.57248	5.12507	0.2289
2	9.774	MM	0.0631	11.19231	2.95857	0.1135
3	9.994	MM	0.1024	9540.67578	1553.22595	96.7317
4	10.534	MM	0.1943	248.28114	21.30013	2.5173
5	10.734	MM	0.0727	24.24271	5.55457	0.2458
6	10.867	MM	0.0575	16.06471	4.66041	0.1629

B

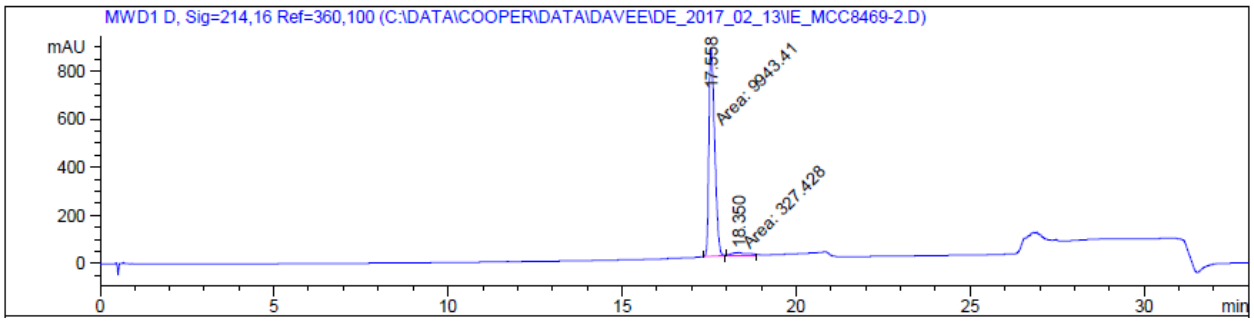

Peak #	RetTime [min]	Type	Width [min]	Area [mAU*s]	Height [mAU]	Area %
1	17.558	MM	0.1910	9943.41016	867.72925	96.8121
2	18.350	MM	0.5320	327.42804	10.25710	3.1879

Figure S7.3-24 – HPLC of 8 (TP1[C7A,C12S]). A – In Acetonitrile solvent system. B – In Methanol solvent system.

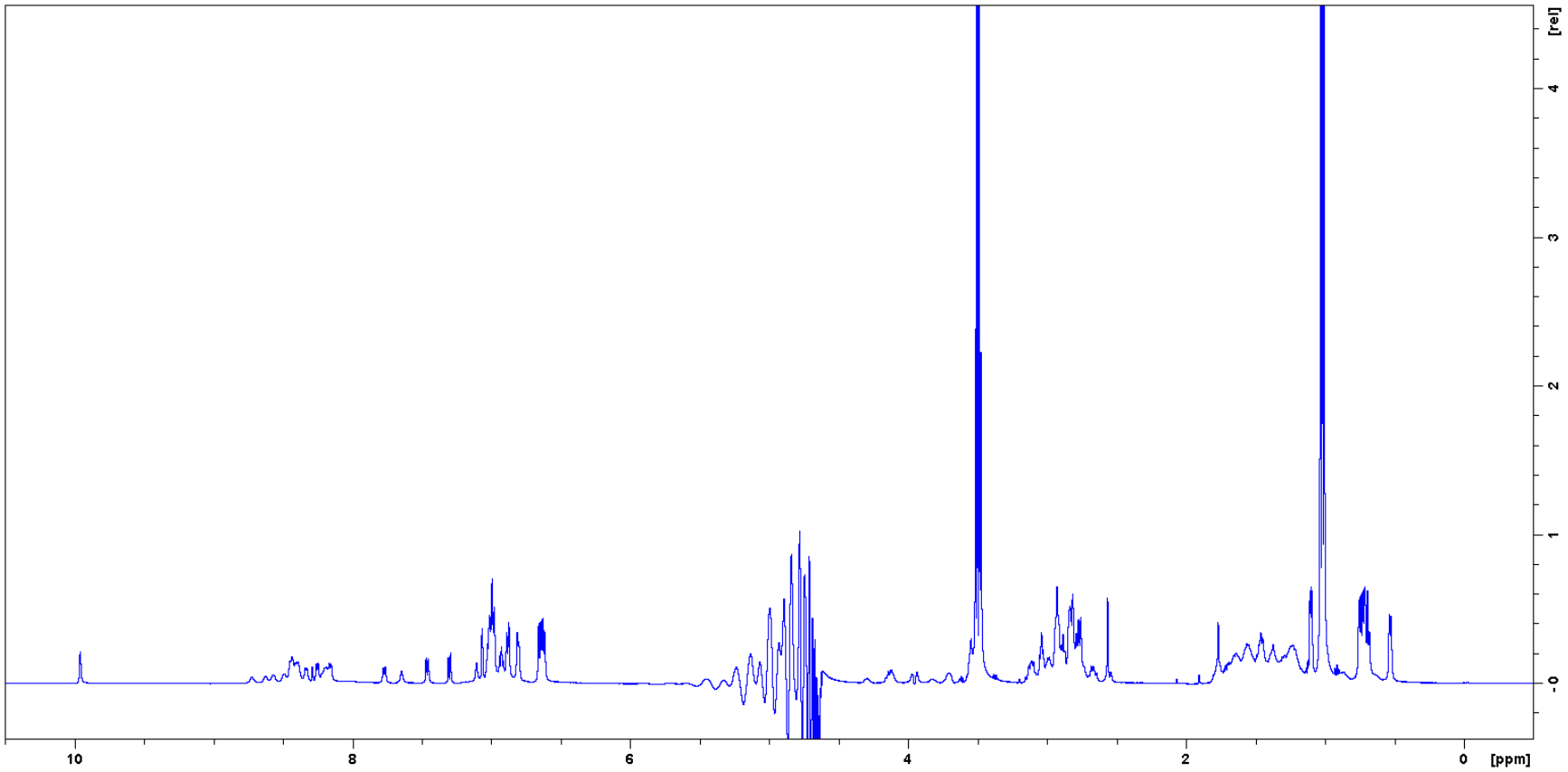

Figure S7.3-25 – ^{1}H NMR of 8 (TP1[C7A,C12S]). The quadruplet at 3.65 and the triplet at 1.17 ppm are residual ethanol.

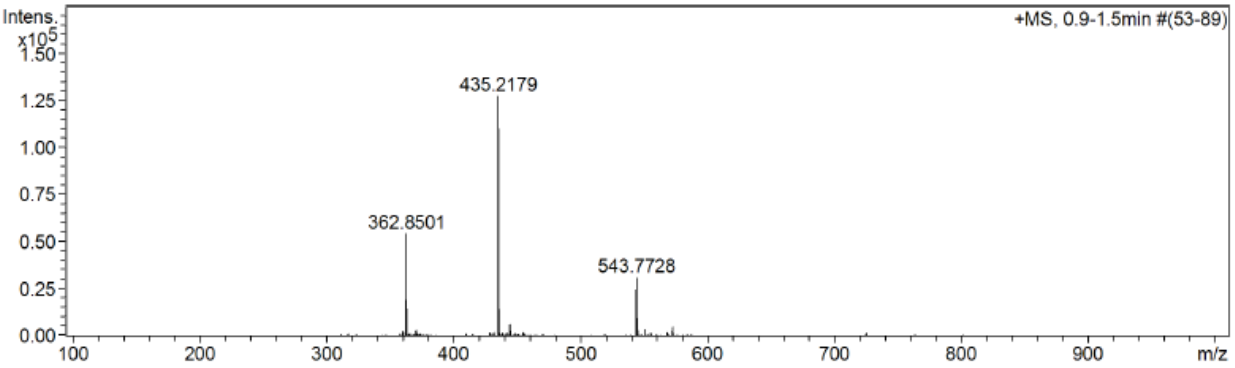

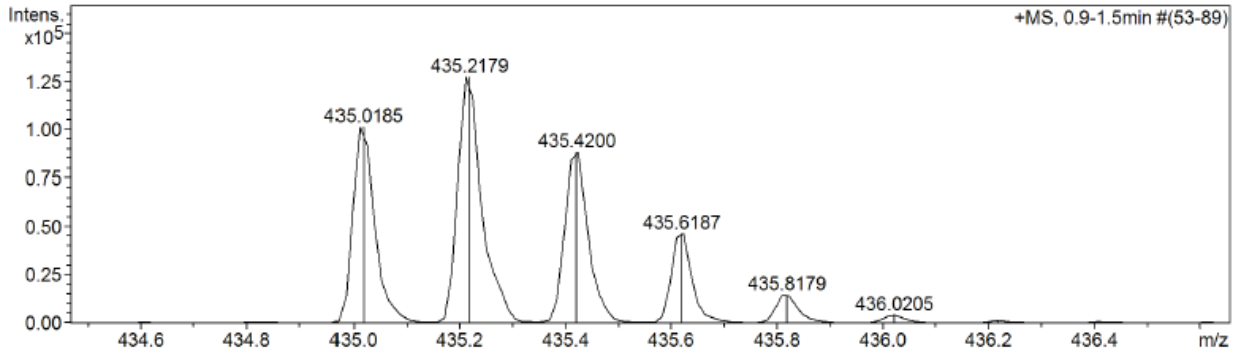

Sum Formula	Sigma	m/z	Err [ppm]	Mean Err [ppm]	Err [mDa]	rdb	N Rule	e⁻
C 93 H 152 N 35 O 18 S 4	0.061	435.0182	-0.62	0.06	-0.27	35.50	ok	even

Figure S7.3-26 – HRMS of 9 (TP1[Y8A])
HRMS-ESI (*m/z*): $[M + 5H]^{5+}$ calculated for ($C_{93}H_{147}N_{35}O_{18}S_4$ + 5H)/5, 435.0182; found 435.0185.

A

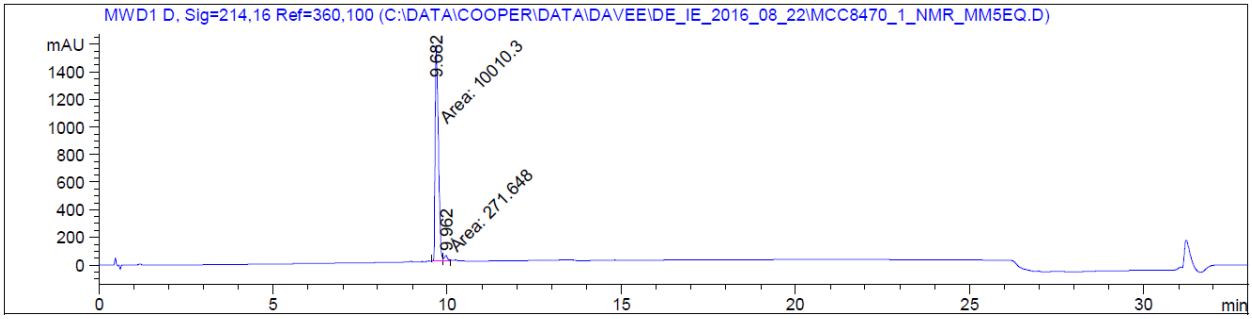

Peak #	RetTime [min]	Type	Width [min]	Area [mAU*s]	Height [mAU]	Area %
1	9.682	MF	0.1066	1.00103e4	1564.92139	97.3580
2	9.962	FM	0.1134	271.64825	39.92057	2.6420

B

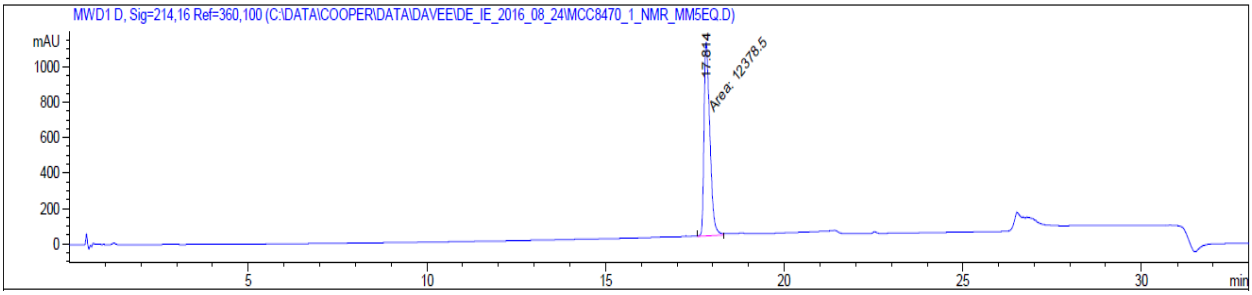

Peak #	RetTime [min]	Type	Width [min]	Area [mAU*s]	Height [mAU]	Area %
1	17.814	MM	0.1882	1.23785e4	1096.01990	100.0000

Figure S7.3-27 – HPLC of 9 (TP1[Y8A]). A – In Acetonitrile solvent system. B – In Methanol solvent system.

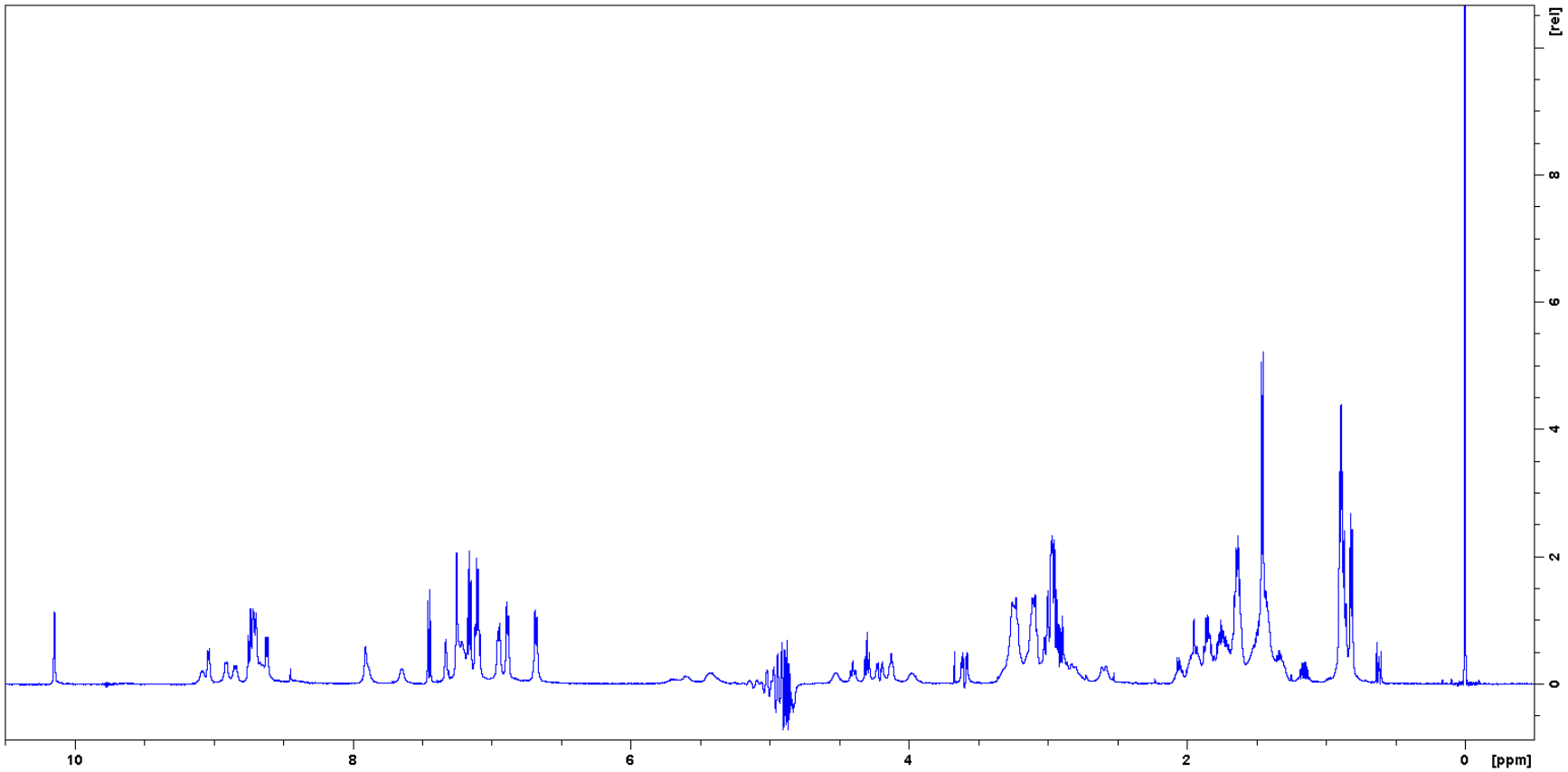

Figure S7.3-28 – ^{1}H NMR of 9 (TP1[Y8A])

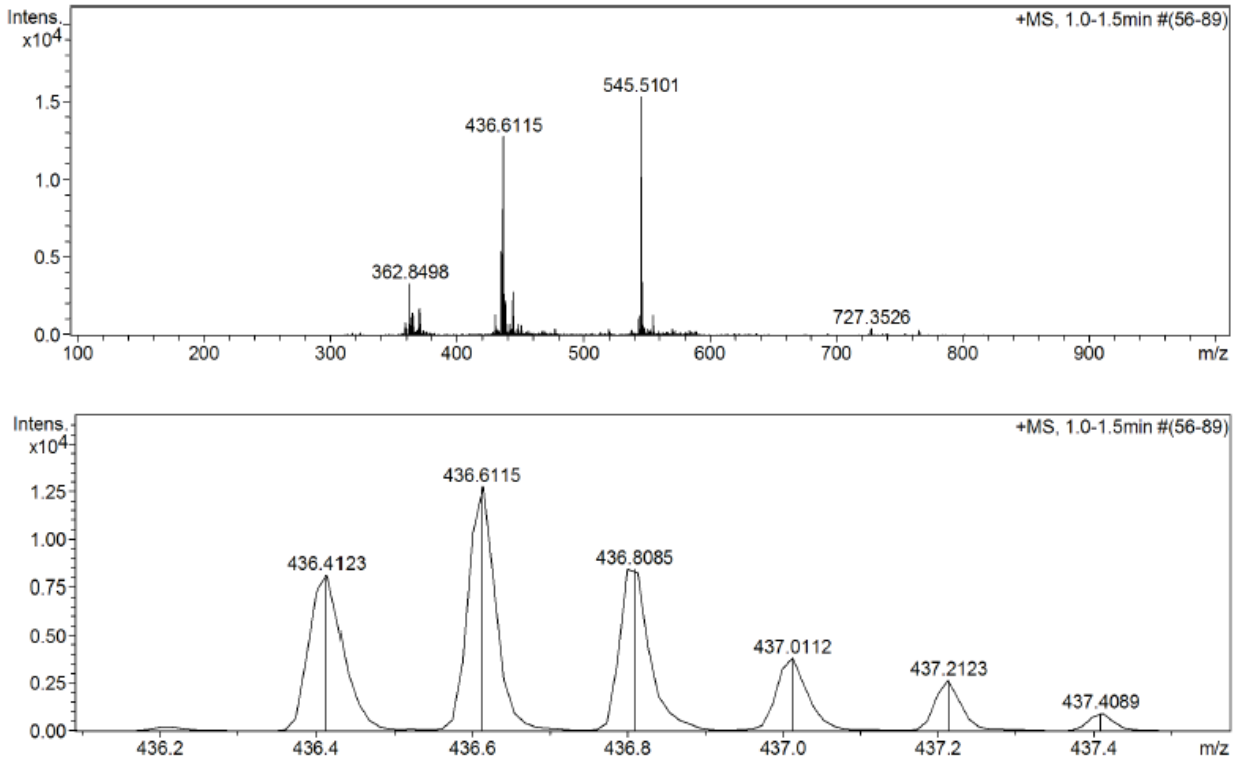

Sum Formula	Sigma	m/z	Err [ppm]	Mean Err [ppm]	Err [mDa]	rdb	N Rule	e⁻
C 96 H 149 N 32 O 19 S 4	0.099	436.4106	-3.85	0.51	-1.68	38.50	ok	even

Figure S7.3-29 – HRMS of 10 (TP1[R9A])
HRMS-ESI (*m/z*): $[M + 5H]^{5+}$ calculated for ($C_{96}H_{144}N_{32}O_{19}S_4$ + 5H)/5, 436.4106; found 436.4123.

A

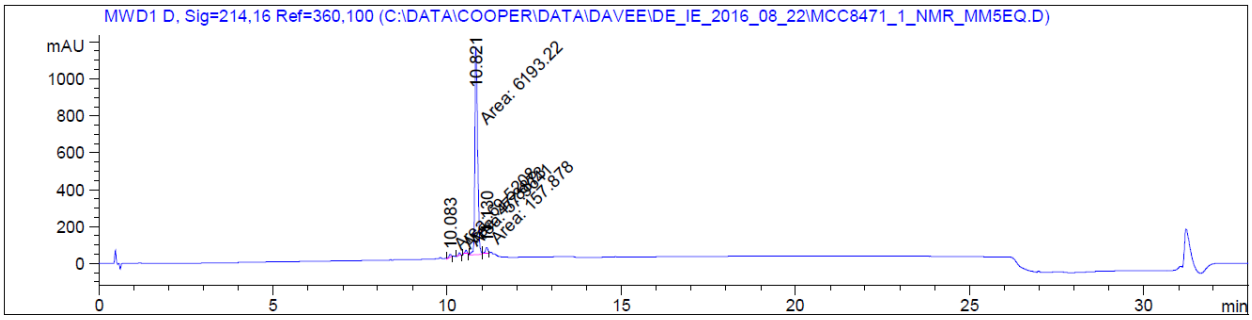

Peak #	RetTime [min]	Type	Width [min]	Area [mAU*s]	Height [mAU]	Area %
1	10.083	MM	0.0704	69.52084	16.46930	1.0652
2	10.347	MM	0.0520	47.88727	15.34116	0.7337
3	10.540	MM	0.0619	57.96414	15.60855	0.8881
4	10.821	MM	0.0912	6193.21582	1131.25891	94.8939
5	11.130	MM	0.0834	157.87781	31.54144	2.4190

B

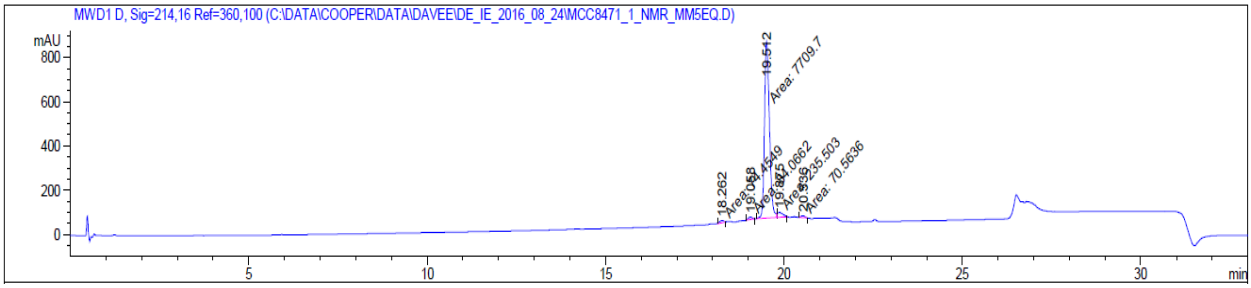

Peak #	RetTime [min]	Type	Width [min]	Area [mAU*s]	Height [mAU]	Area %
1	18.262	MM	0.1240	74.45493	10.00465	0.9108
2	19.058	MM	0.1277	84.06622	10.97340	1.0284
3	19.512	MF	0.1604	7709.69824	801.06329	94.3165
4	19.875	FM	0.1825	235.50288	21.51109	2.8810

Figure S7.3-30 – HPLC of 10 (TP1[R9A]). A – In Acetonitrile solvent system. B – In Methanol solvent system.

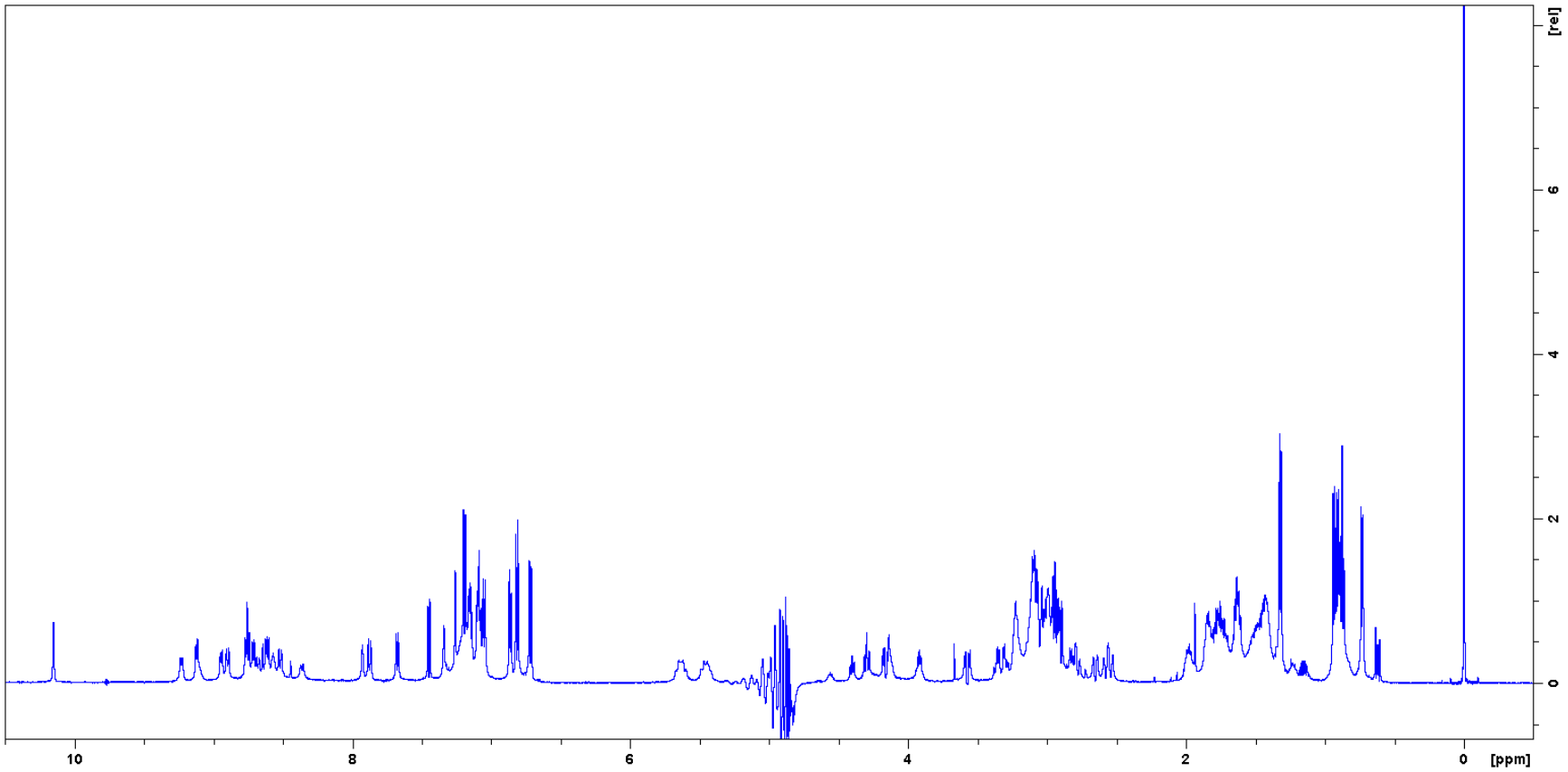

Figure S7.3-31 – ^{1}H NMR of 10 (TP1[R9A])

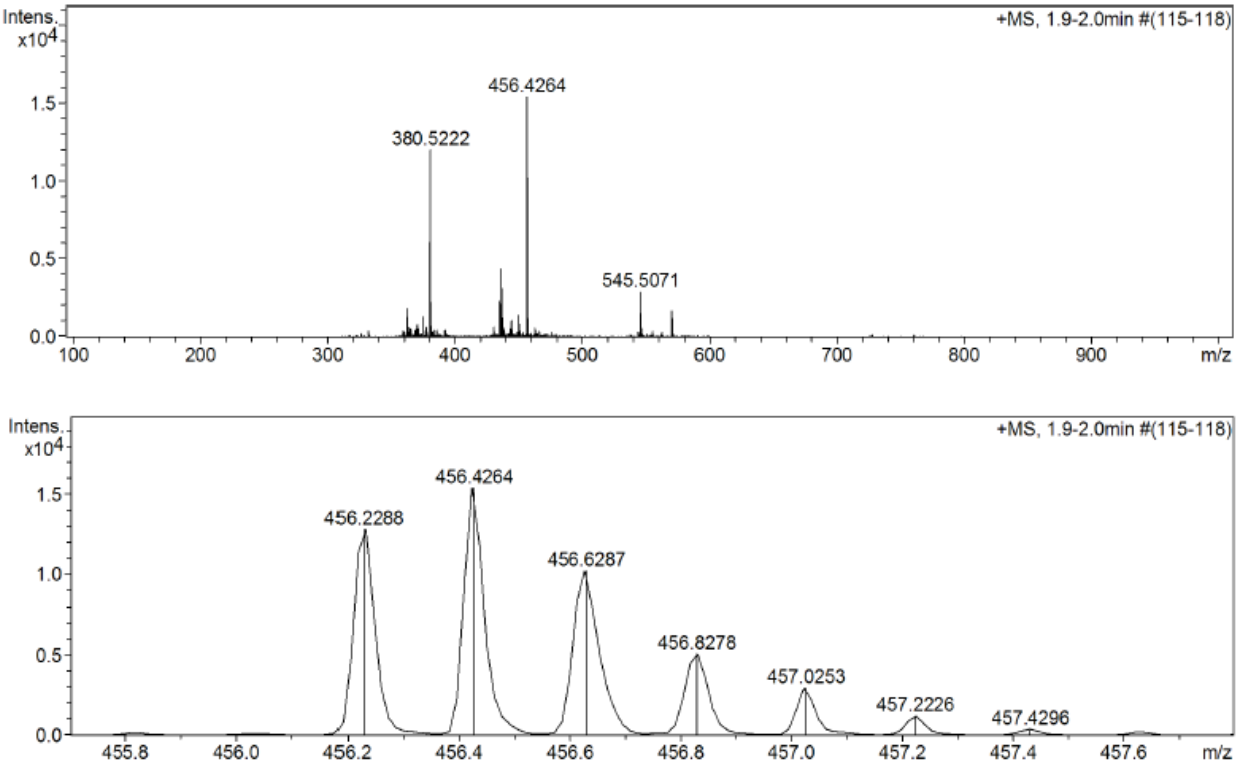

Sum Formula	Sigma	m/z	Err [ppm]	Mean Err [ppm]	Err [mDa]	rdb	N Rule	e⁻
C 100 H 158 N 35 O 19 S 4	0.077	456.2266	-4.87	-0.86	-2.22	39.50	ok	even

Figure S7.3-32 – HRMS of 11 (TP1[G10A])
HRMS-ESI (*m/z*): $[M + 5H]^{5+}$ calculated for ($C_{100}H_{153}N_{35}O_{19}S_4$ + 5H)/5, 456.2266; found 456.2288.

A

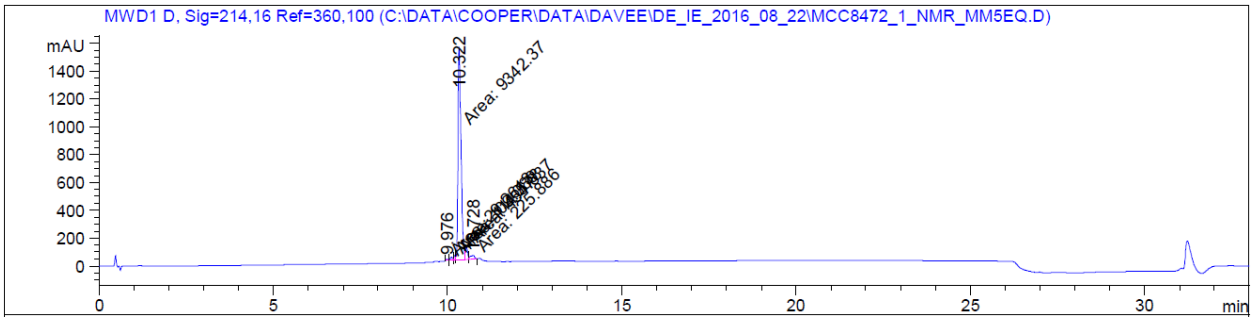

Peak #	RetTime [min]	Type	Width [min]	Area [mAU*s]	Height [mAU]	Area %
1	9.976	MF	0.0581	29.26125	8.40014	0.2848
2	10.106	MF	0.0873	109.08946	20.81790	1.0619
3	10.201	FM	0.0581	111.57804	31.98828	1.0861
4	10.322	MF	0.1011	9342.36719	1540.37402	90.9426
5	10.532	MF	0.0793	454.63693	95.56071	4.4256
6	10.728	FM	0.1412	225.88580	26.65364	2.1989

B

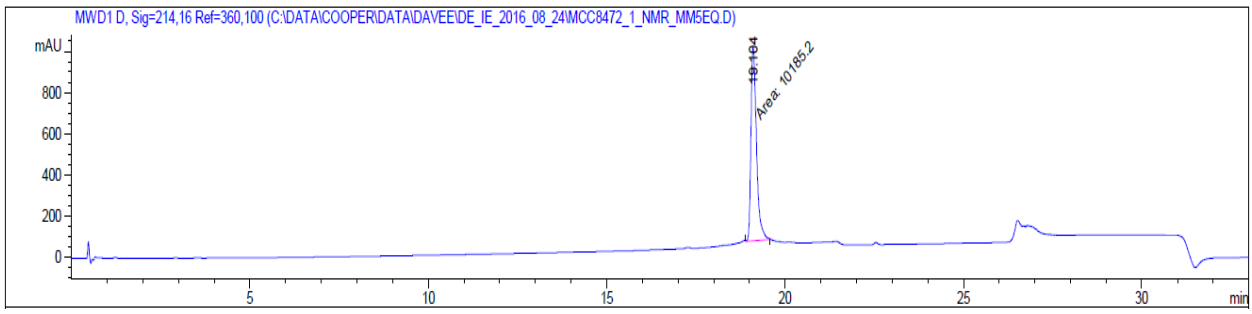

Peak #	RetTime [min]	Type	Width [min]	Area [mAU*s]	Height [mAU]	Area %
1	19.104	MM	0.1793	1.01852e4	946.74231	100.0000

Figure S7.3-33 – HPLC of 11 (TP1[G10A]). A – In Acetonitrile solvent system. B – In Methanol solvent system.

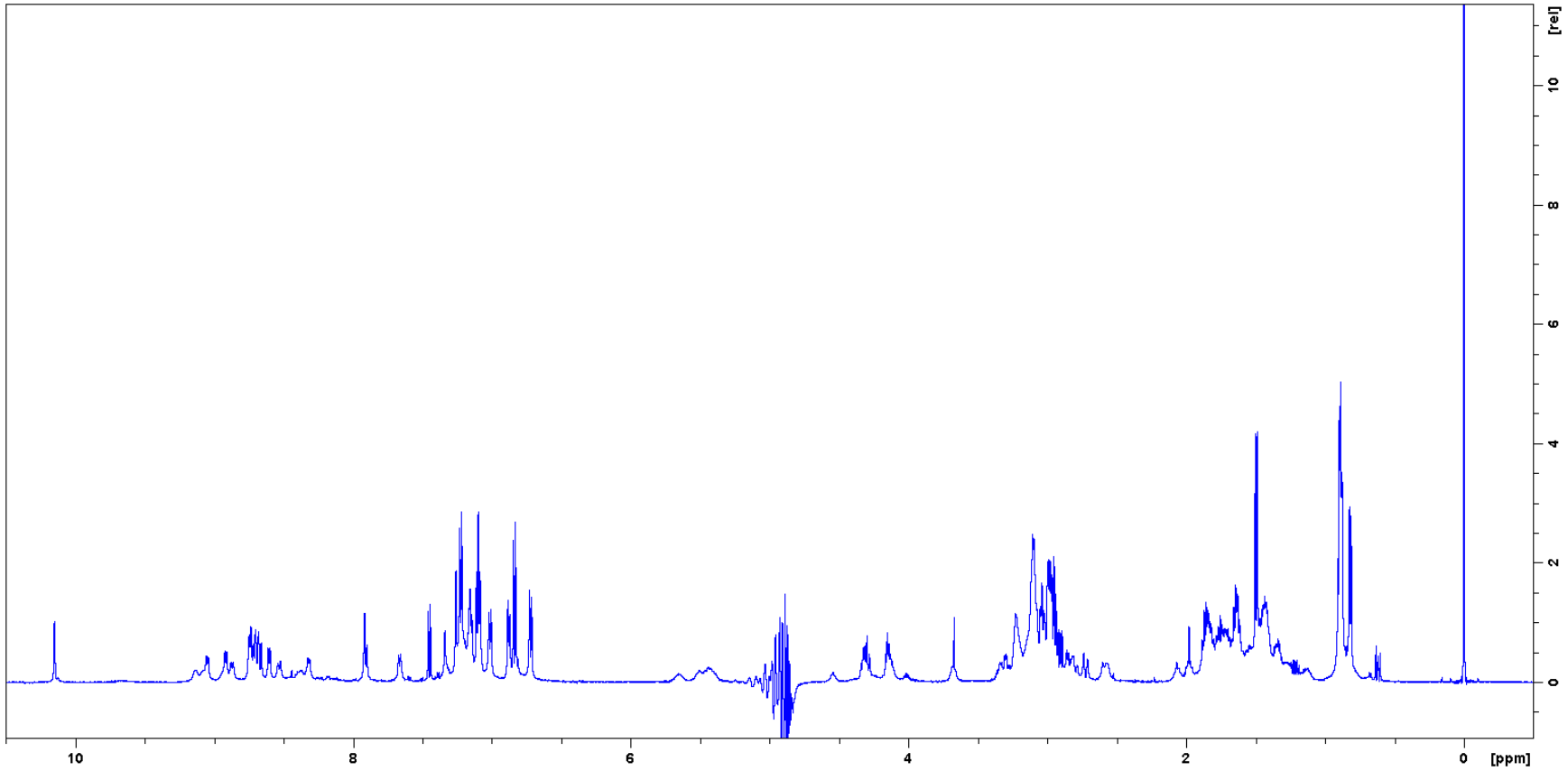

Figure S7.3-34 – ^{1}H NMR of 11 (TP1[G10A])

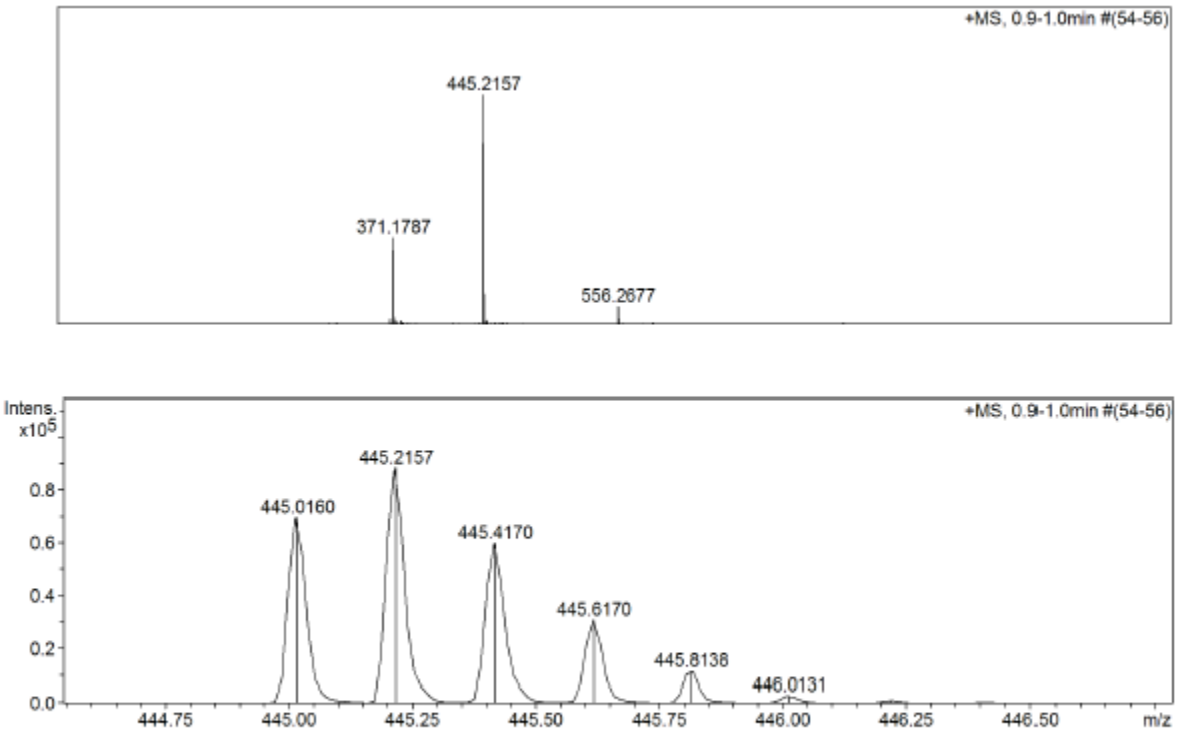

Sum Formula	Sigma	m/z	Err [ppm]	Mean Err [ppm]	Err [mDa]	rdb	N Rule	e⁻
C 96 H 150 N 35 O 19 S 4	0.070	445.0141	-4.31	-3.31	-1.92	39.50	ok	even

Figure S7.3-35 – HRMS of 12 (TP1[I11A])
HRMS-ESI (*m/z*): $[M + 5H]^{5+}$ calculated for $(C_{96}H_{145}N_{35}O_{19}S_4 + 5H)/5$, 445.0141; found 445.0160.

A

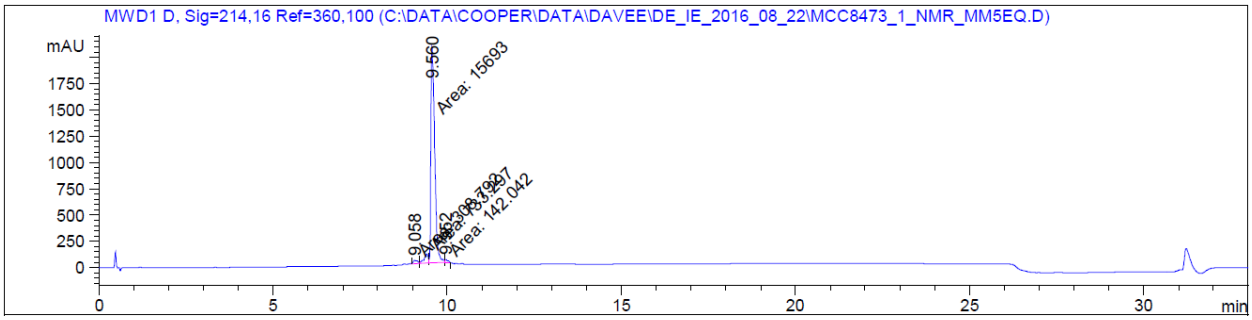

Peak #	RetTime [min]	Type	Width [min]	Area [mAU*s]	Height [mAU]	Area %
1	9.058	MF	0.1469	308.79227	35.03418	1.8296
2	9.411	FM	0.1393	733.29688	87.76018	4.3449
3	9.560	MF	0.1272	1.56930e4	2056.78003	92.9838
4	9.952	FM	0.0858	142.04214	27.58723	0.8416

B

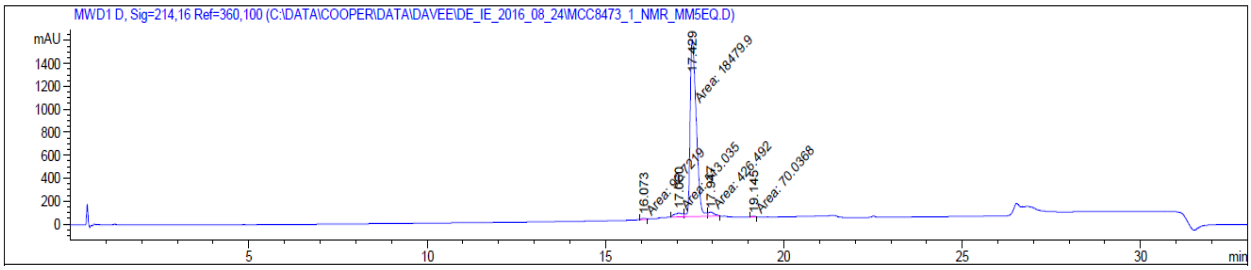

Peak #	RetTime [min]	Type	Width [min]	Area [mAU*s]	Height [mAU]	Area %
1	16.073	MM	0.1344	92.72194	11.50004	0.4735
2	17.060	MF	0.2589	513.03503	33.02238	2.6199
3	17.429	FM	0.1995	1.84799e4	1543.78174	94.3710
4	17.947	FM	0.2006	426.49222	35.42899	2.1780

Figure S7.3-36 – HPLC of 12 (TP1[I11A]). A – In Acetonitrile solvent system. B – In Methanol solvent system.

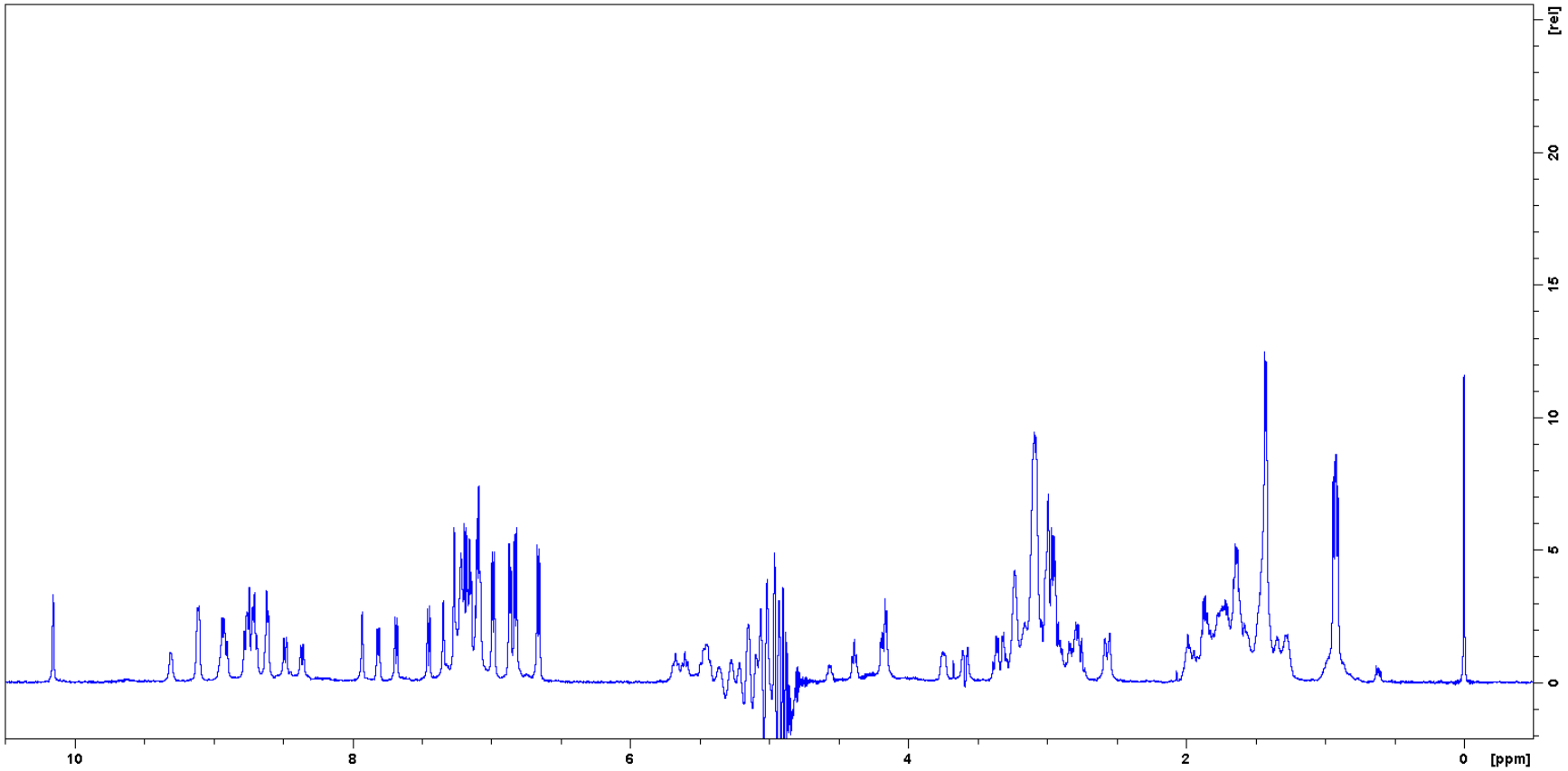

Figure S7.3-37 – ^{1}H NMR of 12 (TP1[I11A])

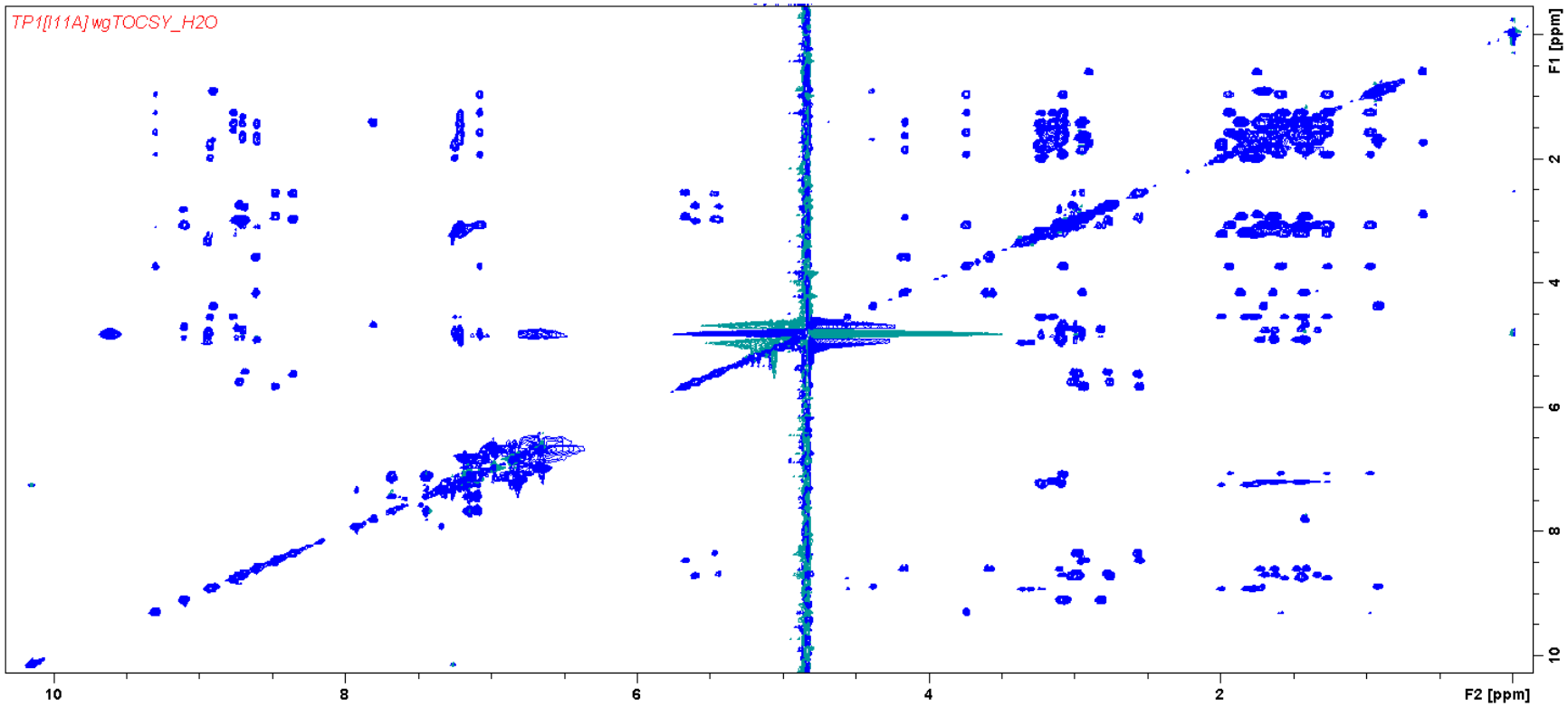

Figure S7.3-38 – 2D TOCSY NMR of 12 (TP1[I11A]), MLEV17 spin-lock mixing pulses = 80 ms, water suppression was performed using Watergate sequence.

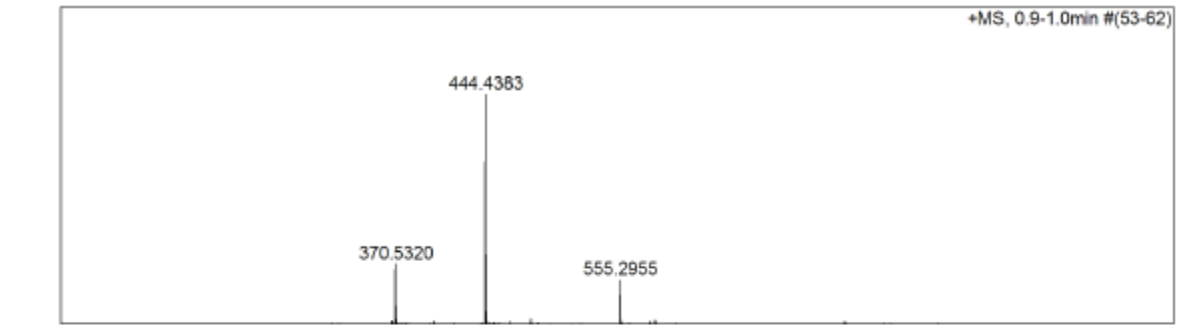

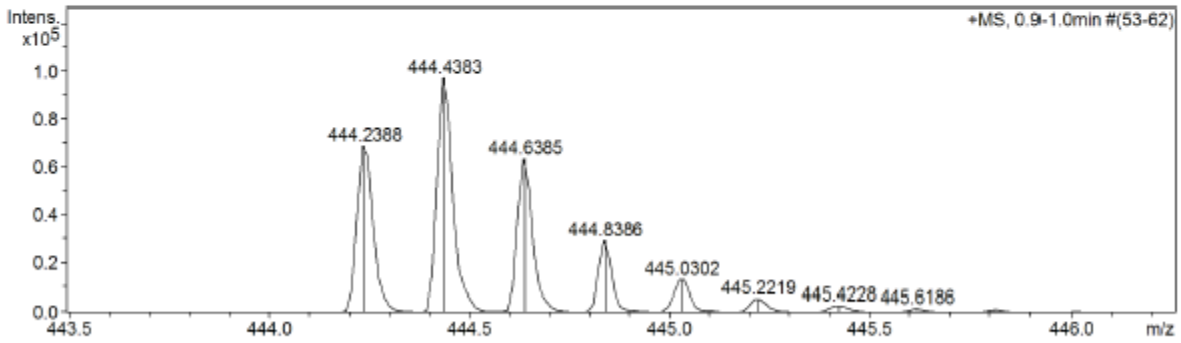

Sum Formula	Sigma	m/z	Err [ppm]	Mean Err [ppm]	Err [mDa]	rdb	N Rule	e⁻
C 99 H 158 N 35 O 20 S 2	0.057	444.2367	-4.66	-0.08	-2.07	38.50	ok	even

Figure S7.3-39 – HRMS of 13 (TP1[C7S,C12A])
HRMS-ESI (*m/z*): $[M + 5H]^{5+}$ calculated for ($C_{99}H_{153}N_{35}O_{20}S_2$ + 5H)/5, 444.2367; found 444.2388.

A

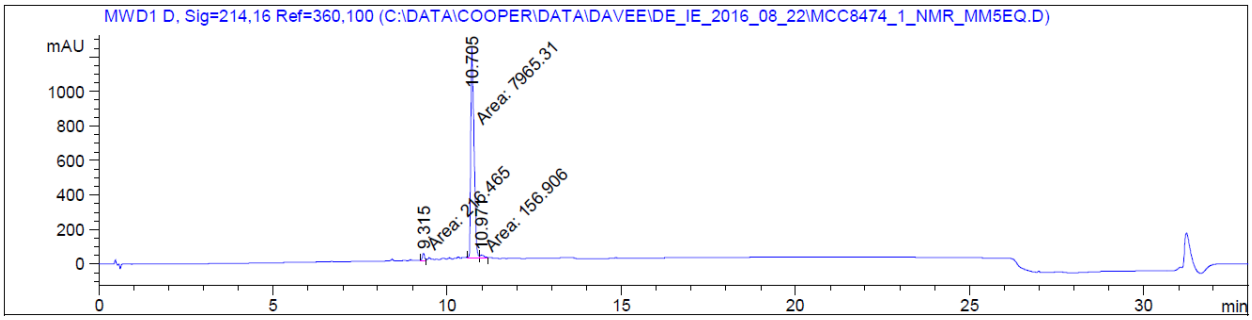

Peak #	RetTime [min]	Type	Width [min]	Area [mAU*s]	Height [mAU]	Area %
1	9.315	MM	0.0813	216.46452	44.38278	2.5959
2	10.705	MF	0.1081	7965.31445	1228.36230	95.5224
3	10.971	FM	0.1582	156.90649	16.53472	1.8817

B

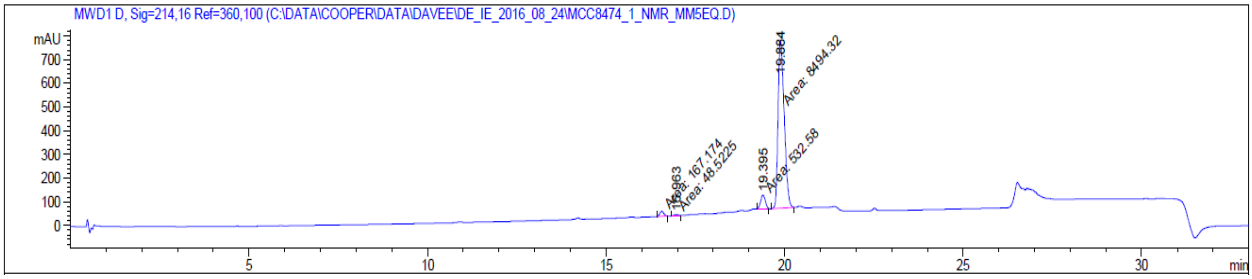

Peak #	RetTime [min]	Type	Width [min]	Area [mAU*s]	Height [mAU]	Area %
1	16.559	MM	0.1330	167.17435	20.95232	1.8087
2	16.963	MM	0.1428	48.52246	5.66488	0.5250
3	19.395	MM	0.1532	532.58002	57.92709	5.7622
4	19.884	MM	0.1989	8494.32324	711.89496	91.9040

Figure S7.3-40 – HPLC of 13 (TP1[C7S,C12A]). A – In Acetonitrile solvent system. B – In Methanol solvent system.

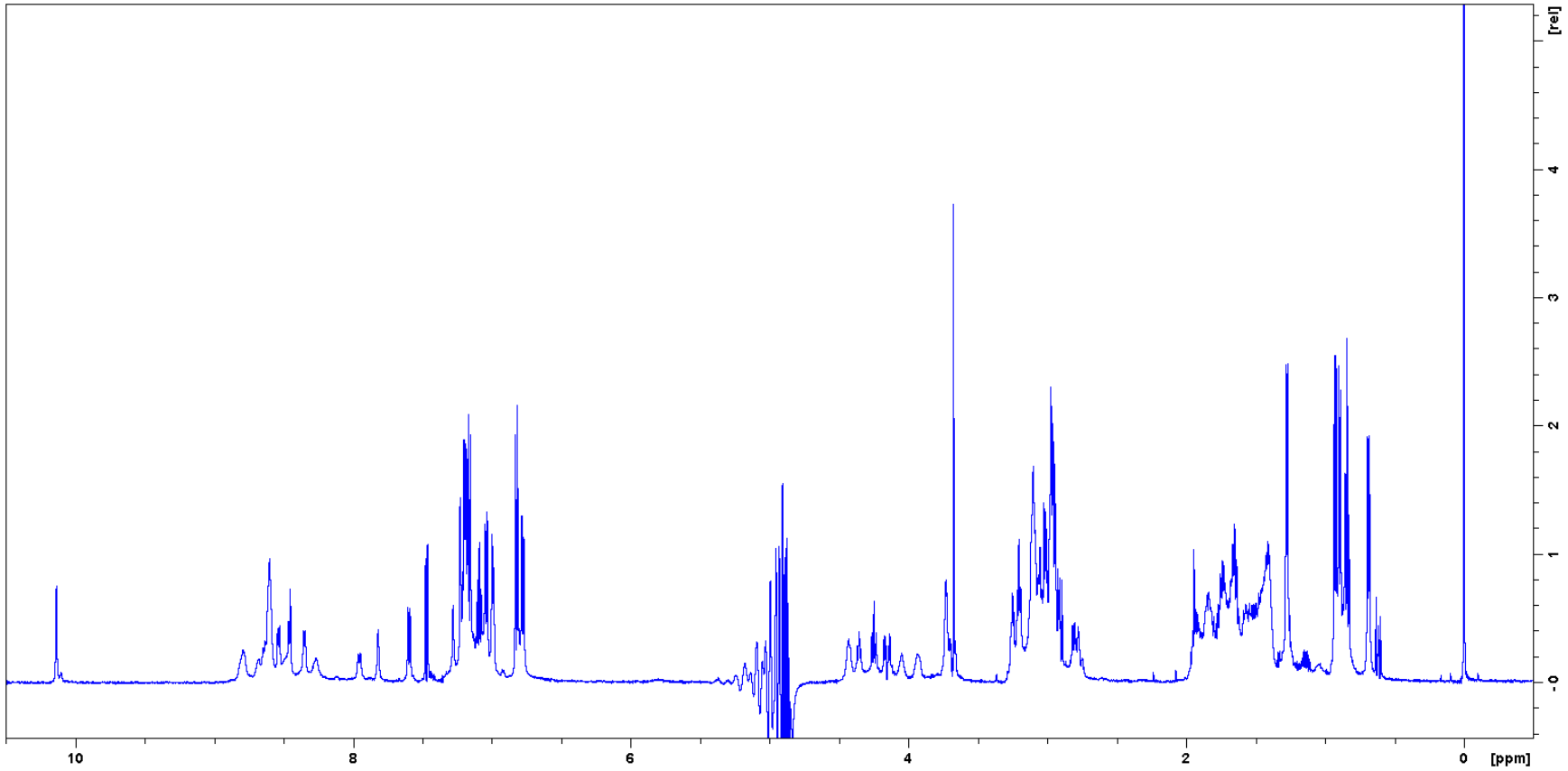

Figure S7.3-41 – ^{1}H NMR of 13 (TP1[C7S,C12A])

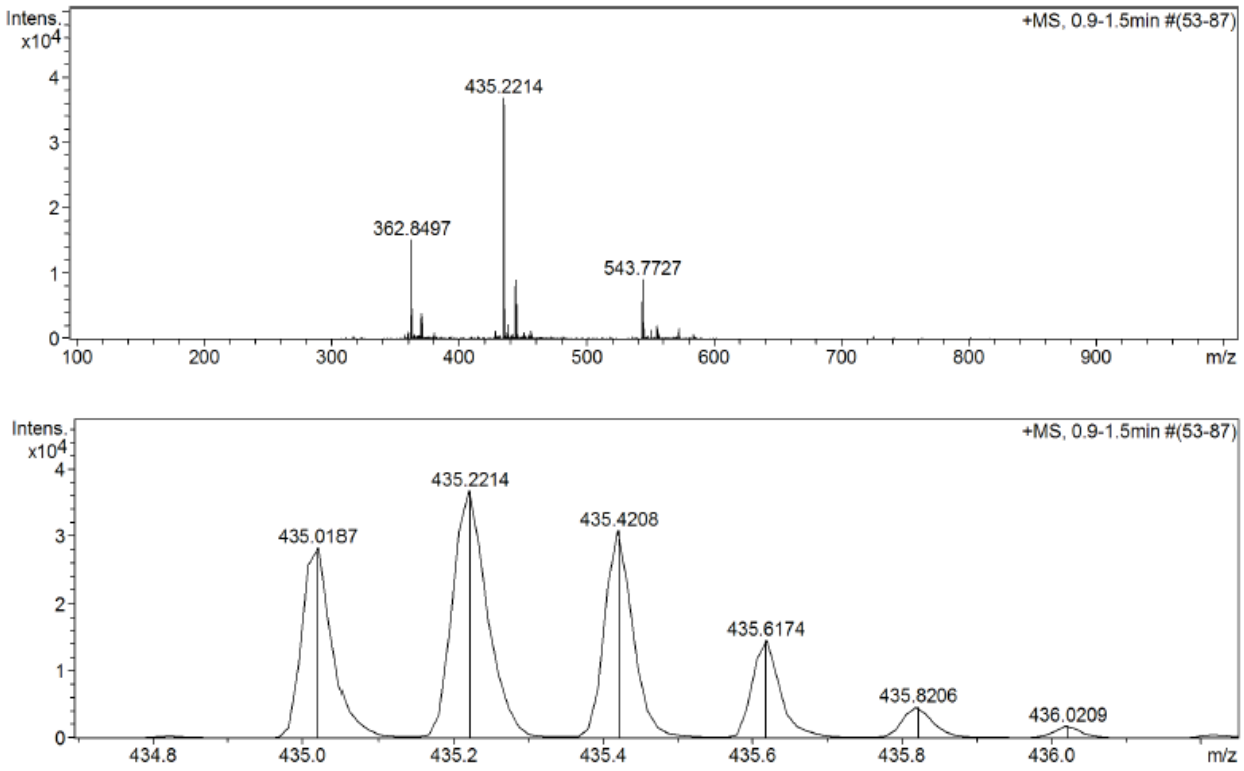

Sum Formula	Sigma	m/z	Err [ppm]	Mean Err [ppm]	Err [mDa]	rdb	N Rule	e⁻
C 93 H 152 N 35 O 18 S 4	0.052	435.0182	-1.05	-3.04	-0.46	35.50	ok	even

Figure S7.3-42 – HRMS of 14 (TP1[Y13A])
HRMS-ESI (*m/z*): $[M + 5H]^{5+}$ calculated for ($C_{93}H_{147}N_{35}O_{18}S_4$ + 5H)/5, 435.0182; found 435.0187.

A

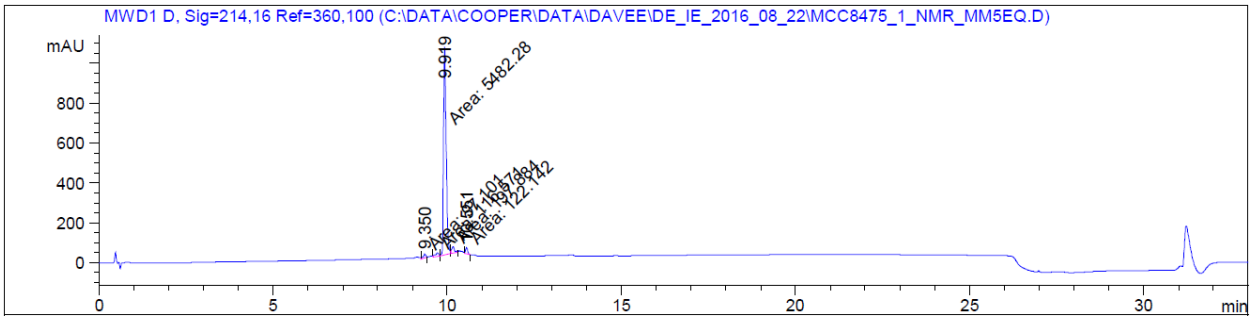

Peak #	RetTime [min]	Type	Width [min]	Area [mAU*s]	Height [mAU]	Area %
1	9.350	MM	0.0865	97.10098	18.71880	1.6141
2	9.714	MF	0.1164	116.57051	16.69056	1.9377
3	9.919	MF	0.0874	5482.27930	1045.82373	91.1287
4	10.163	FM	0.0982	197.88428	33.57885	3.2893
5	10.551	MM	0.0697	122.14211	29.20605	2.0303

B

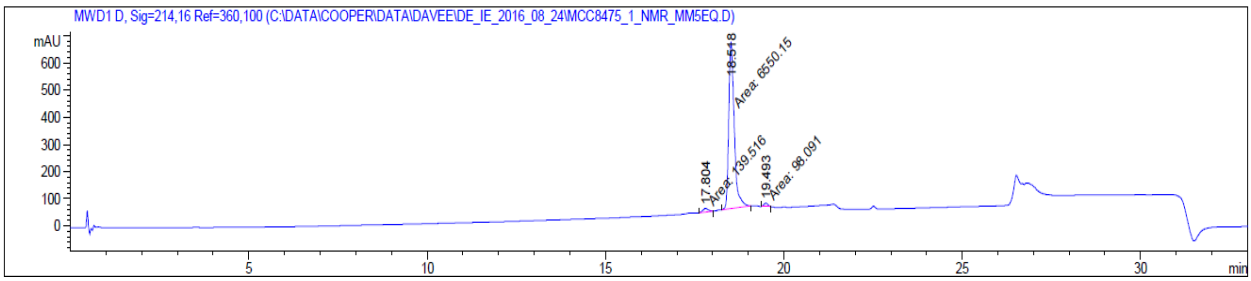

Peak #	RetTime [min]	Type	Width [min]	Area [mAU*s]	Height [mAU]	Area %
1	17.804	MM	0.1806	139.51576	12.87500	2.0554
2	18.518	MM	0.1784	6550.14600	611.91870	96.4995
3	19.493	MM	0.1308	98.09105	12.49893	1.4451

Figure S7.3-43 – HPLC of 14 (TP1[Y13A]). A – In Acetonitrile solvent system. B – In Methanol solvent system.

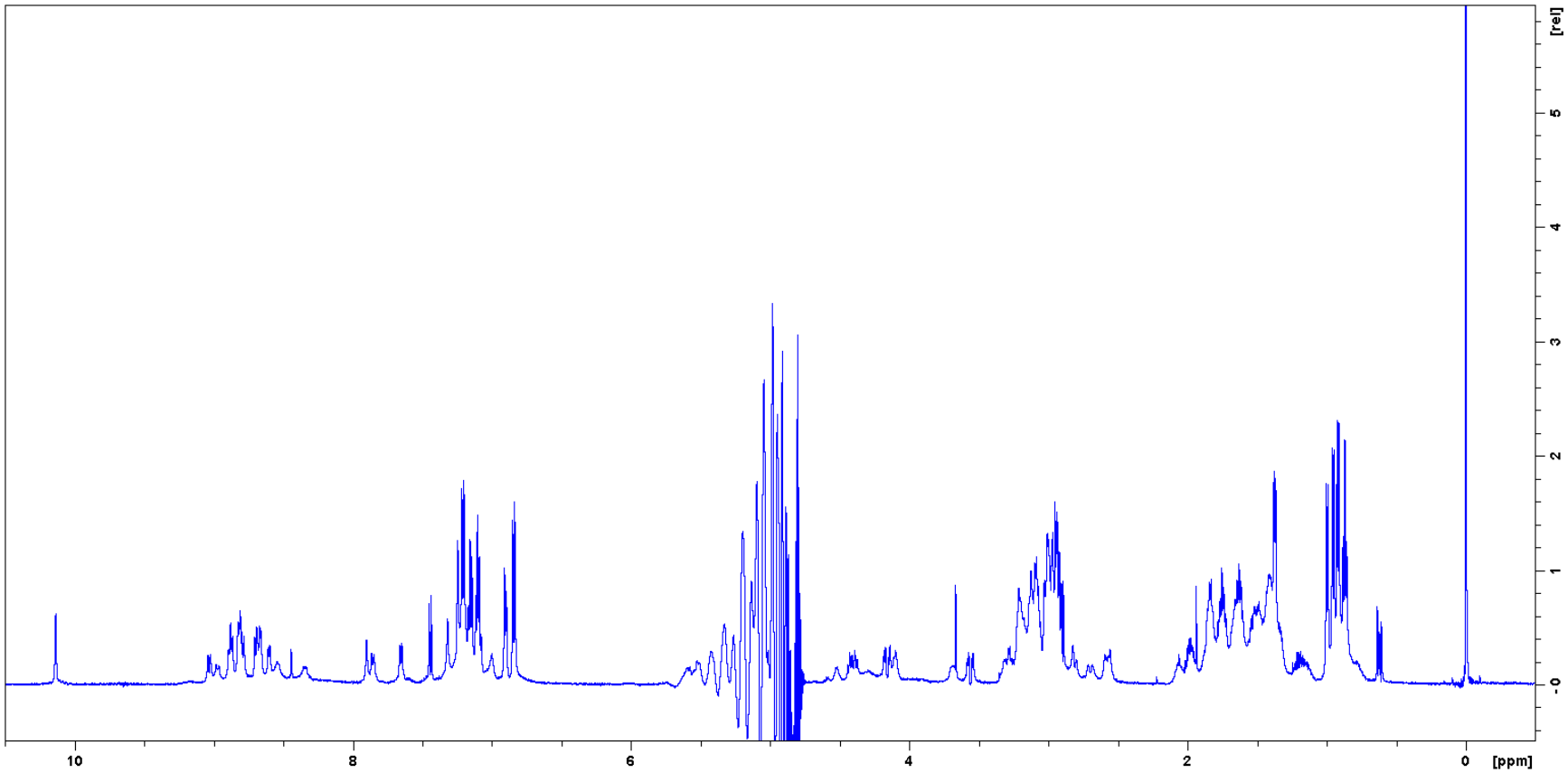

Figure S7.3-44 – ^{1}H NMR of 14 (TP1[Y13A])

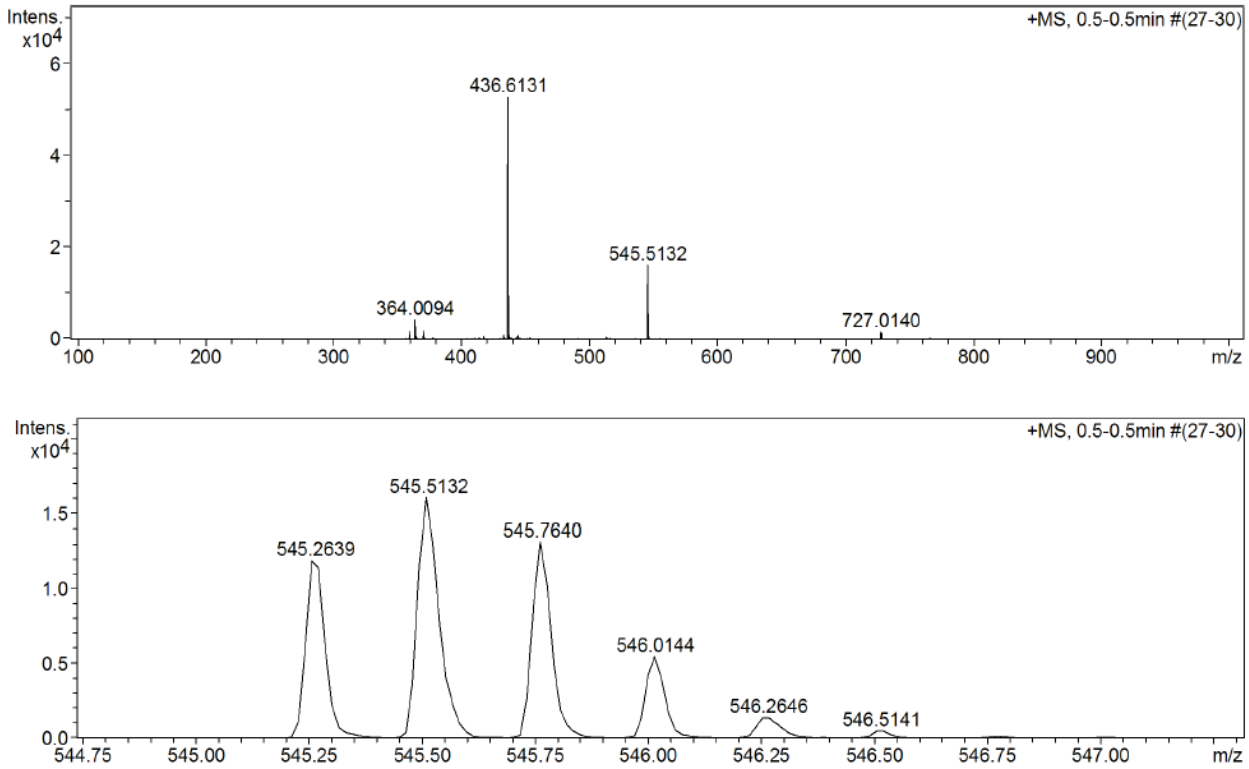

Sum Formula	Sigma	m/z	Err [ppm]	Mean Err [ppm]	Err [mDa]	rdb	N Rule	e⁻
C 96 H 148 N 32 O 19 S 4	0.074	545.2615	-4.35	-3.23	-2.37	39.00	ok	even

Figure S7.3-45 – HRMS of 15 (TP1[R14A])
HRMS-ESI (*m/z*): $[M + 5H]^{5+}$ calculated for $(C_{96}H_{144}N_{32}O_{19}S_4 + 4H)/4$, 545.2615; found 545.2639.

A

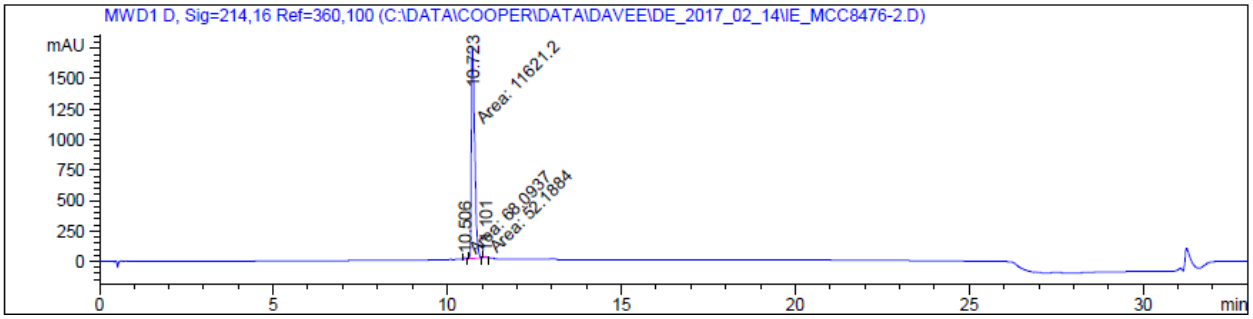

Peak #	RetTime [min]	Type	Width [min]	Area [mAU*s]	Height [mAU]	Area %
1	10.506	MM	0.0915	68.09374	12.40871	0.5799
2	10.723	MM	0.1112	1.16212e4	1741.15417	98.9756
3	11.101	MM	0.0815	52.18843	10.67304	0.4445

B

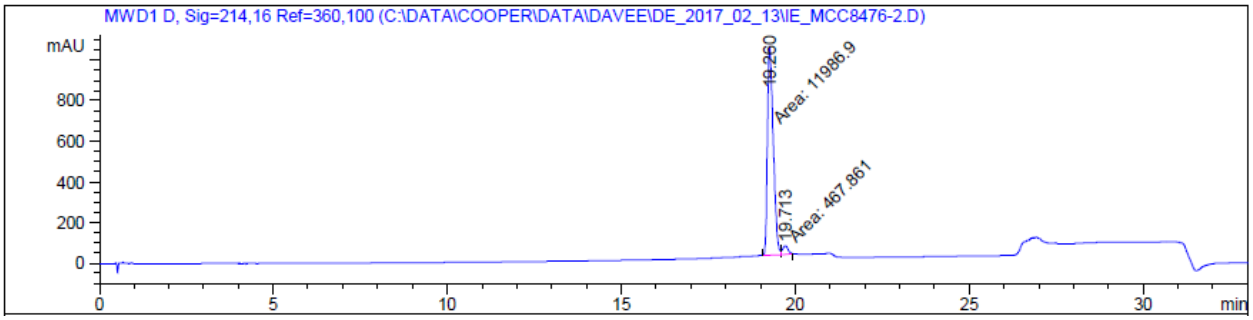

Peak #	RetTime [min]	Type	Width [min]	Area [mAU*s]	Height [mAU]	Area %
1	19.260	MF	0.1948	1.19869e4	1025.37378	96.2435
2	19.713	FM	0.1867	467.86084	41.76830	3.7565

Figure S7.3-46 – HPLC of 15 (TP1[R14A]). A – In Acetonitrile solvent system. B – In Methanol solvent system.

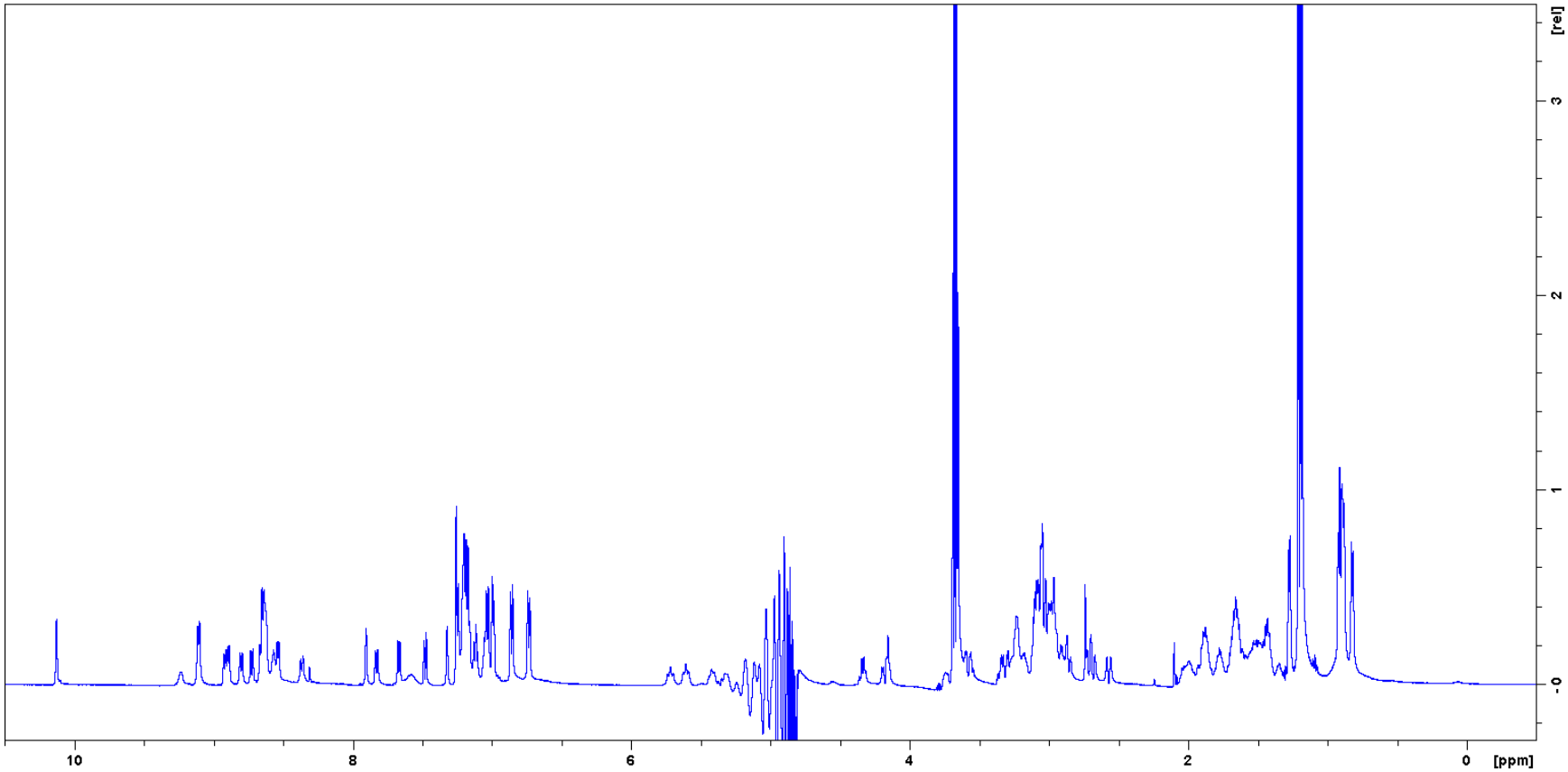

Figure S7.3-47 – ^{1}H NMR of 15 (TP1[R14A]). The quadruplet at 3.65 and the triplet at 1.17 ppm are residual ethanol.

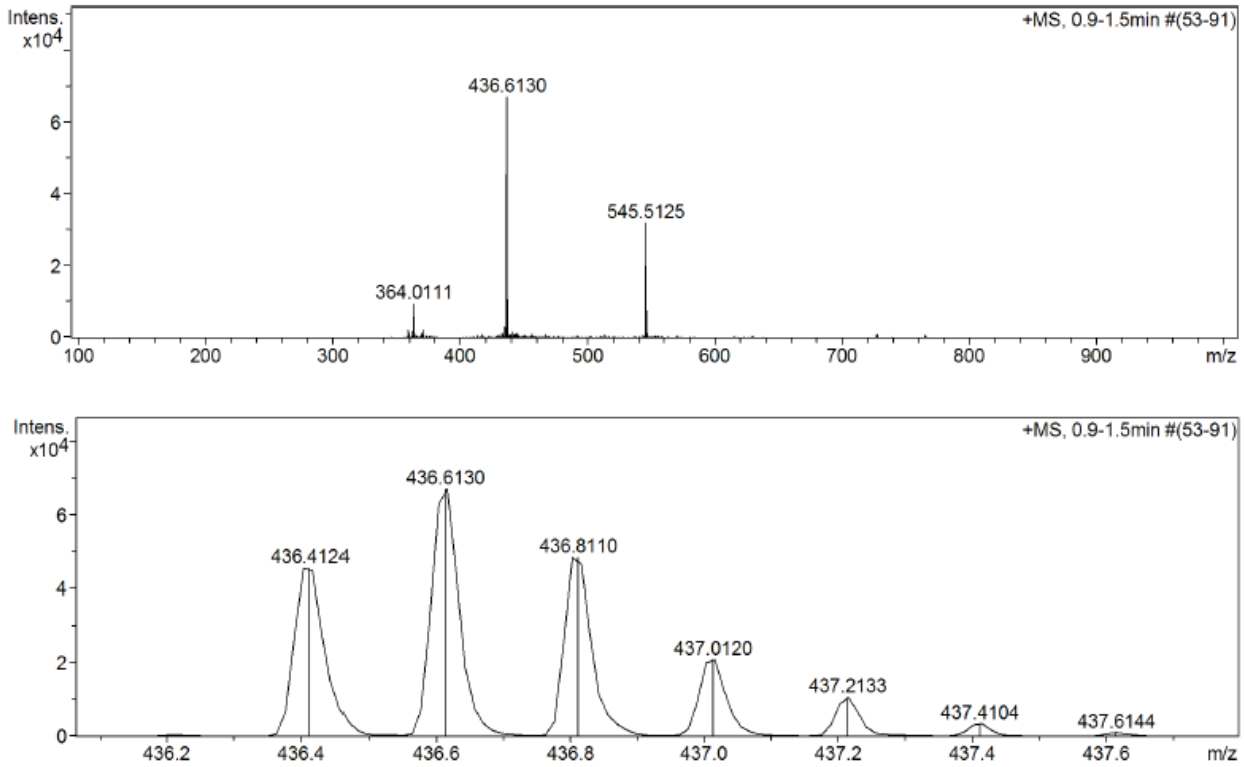

Sum Formula	Sigma	m/z	Err [ppm]	Mean Err [ppm]	Err [mDa]	rdb	N Rule	e⁻
C 96 H 149 N 32 O 19 S 4	0.080	436.4106	-4.14	-2.45	-1.81	38.50	ok	even

Figure S7.3-48 – HRMS of 16 (TP1[R15A])
HRMS-ESI (*m/z*): $[M + 5H]^{5+}$ calculated for ($C_{96}H_{144}N_{32}O_{19}S_4$ + 5H)/5, 436.4106; found 436.4124.

A

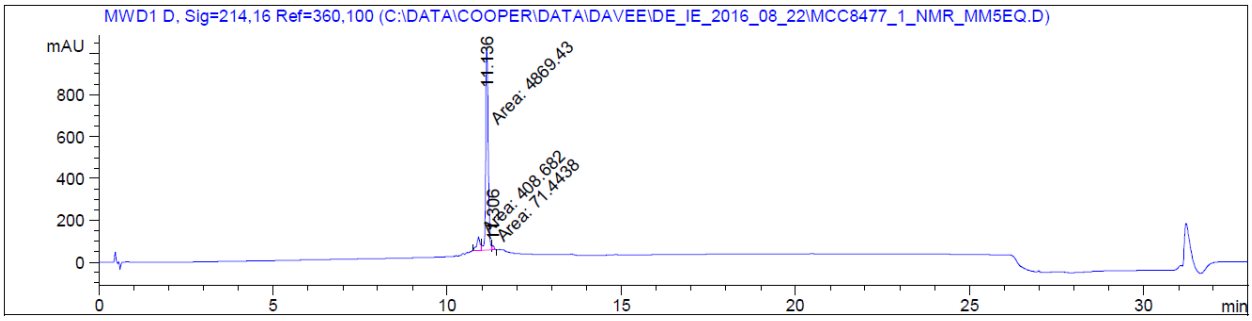

Peak #	RetTime [min]	Type	Width [min]	Area [mAU*s]	Height [mAU]	Area %
1	10.896	MF	0.1113	408.68198	61.17282	7.6395
2	11.136	MF	0.0834	4869.43457	972.69623	91.0249
3	11.306	FM	0.0599	71.44379	19.87618	1.3355

B

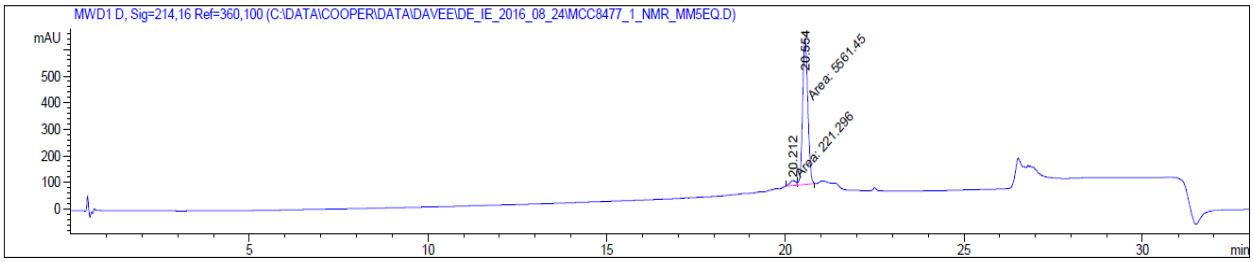

Peak #	RetTime [min]	Type	Width [min]	Area [mAU*s]	Height [mAU]	Area %
1	20.212	MF	0.1981	221.29593	18.61413	3.8268
2	20.554	FM	0.1689	5561.45020	548.89484	96.1732

Figure S7.3-49 – HPLC of 16 (TP1[R15A]). A – In Acetonitrile solvent system. B – In Methanol solvent system.

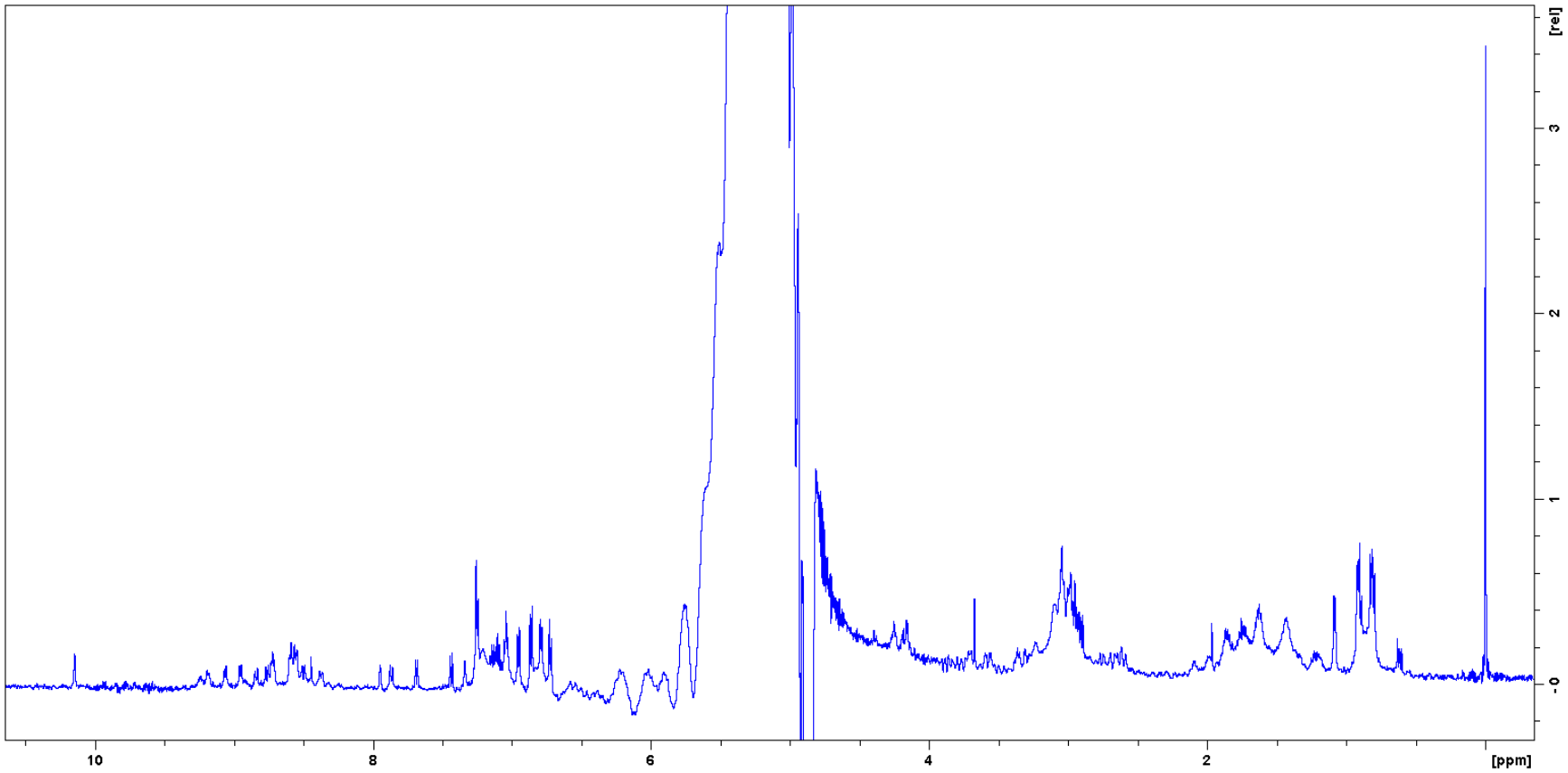

Figure S7.3-50 – ^{1}H NMR of 16 (TP1[R15A])

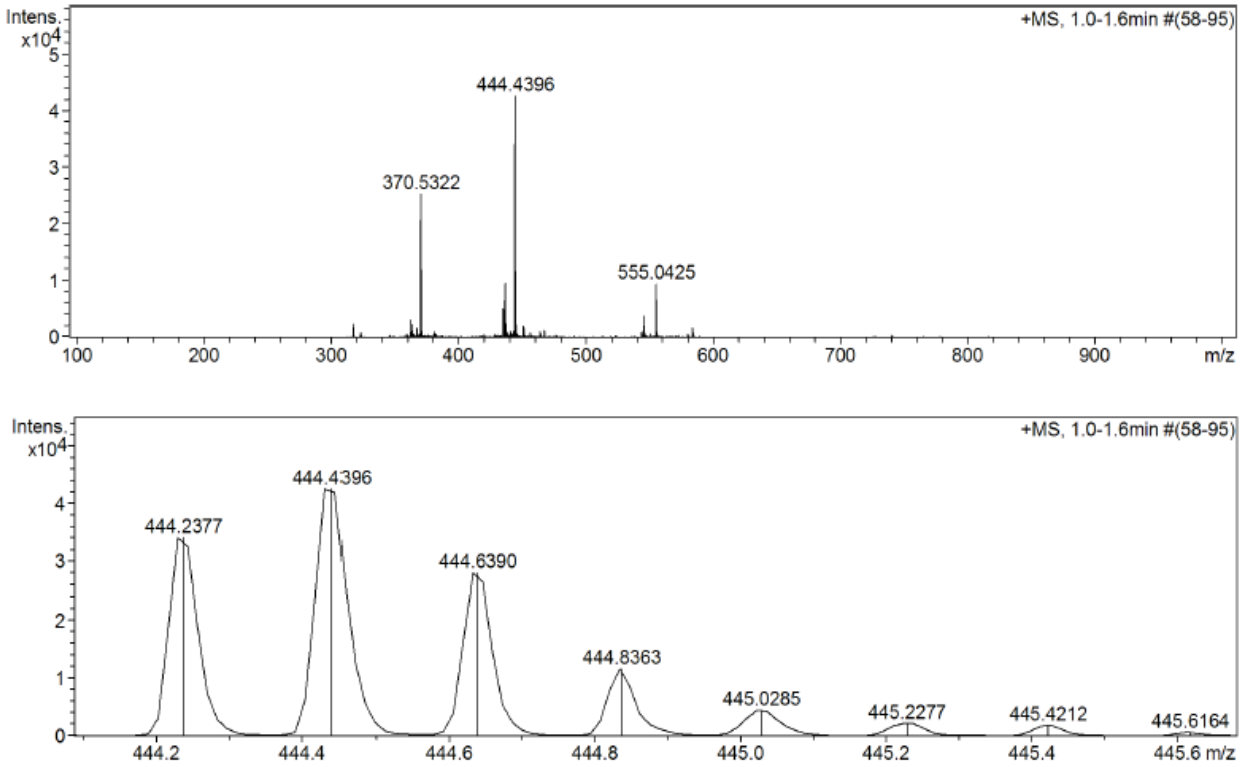

Sum Formula	Sigma	m/z	Err [ppm]	Mean Err [ppm]	Err [mDa]	rdb	N Rule	e⁻
C 99 H 158 N 35 O 20 S 2	0.054	444.2367	-2.25	-0.06	-1.00	38.50	ok	even

Figure S7.3-51 – HRMS of 17 (TP1[C3S,C16A])
HRMS-ESI (*m/z*): $[M + 5H]^{5+}$ calculated for ($C_{99}H_{153}N_{35}O_{20}S_2$ + 5H)/5, 444.2367; found 444.2377.

A

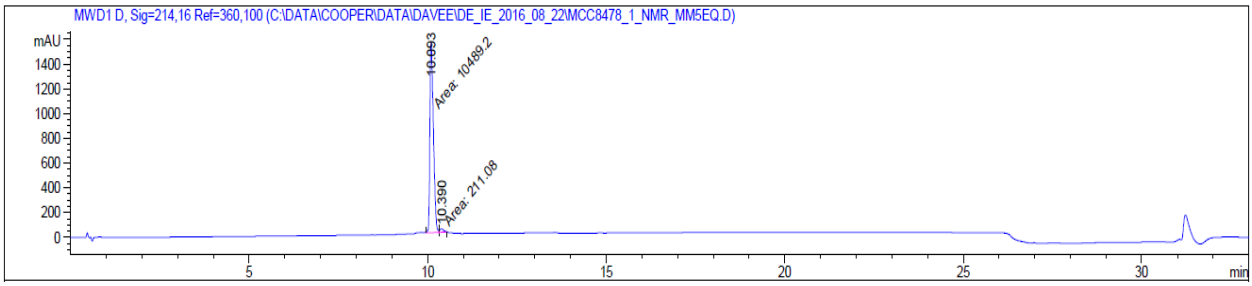

Peak #	RetTime [min]	Type	Width [min]	Area [mAU*s]	Height [mAU]	Area %
1	10.093	MF	0.1132	1.04892e4	1544.39185	98.0273
2	10.390	FM	0.1258	211.08011	27.95553	1.9727

B

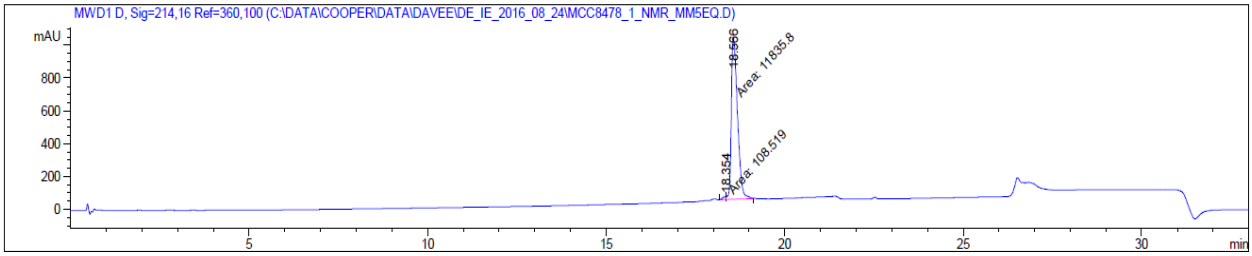

Peak #	RetTime [min]	Type	Width [min]	Area [mAU*s]	Height [mAU]	Area %
1	18.354	MF	0.1111	108.51890	16.27588	0.9085
2	18.566	FM	0.1990	1.18358e4	991.04279	99.0915

Figure S7.3-52 – HPLC of 17 (TP1[C3S,C16A]). A – In Acetonitrile solvent system. B – In Methanol solvent system.

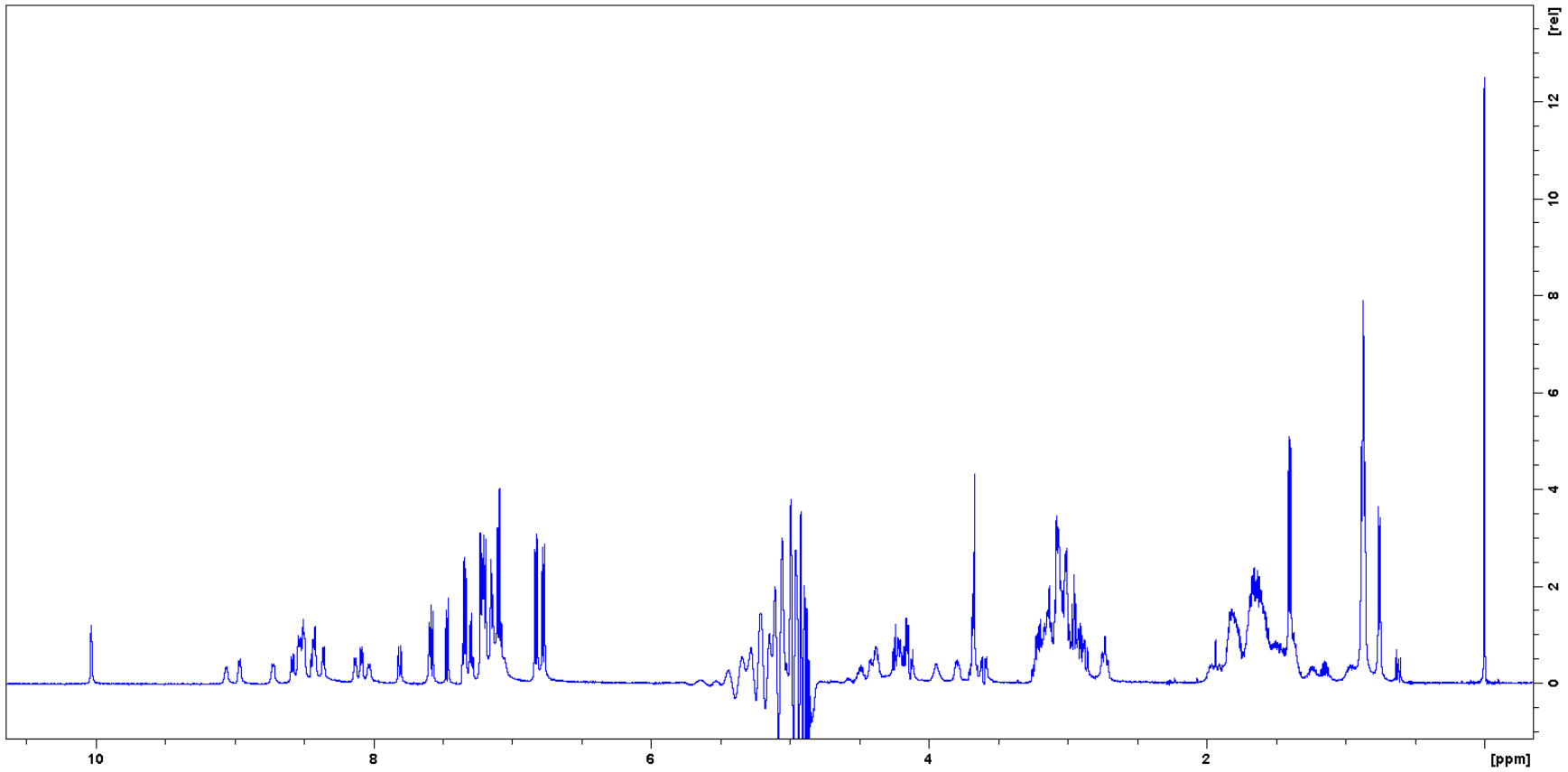

Figure S7.3-53 – ^{1}H NMR of 17 (TP1[C3S,C16A])

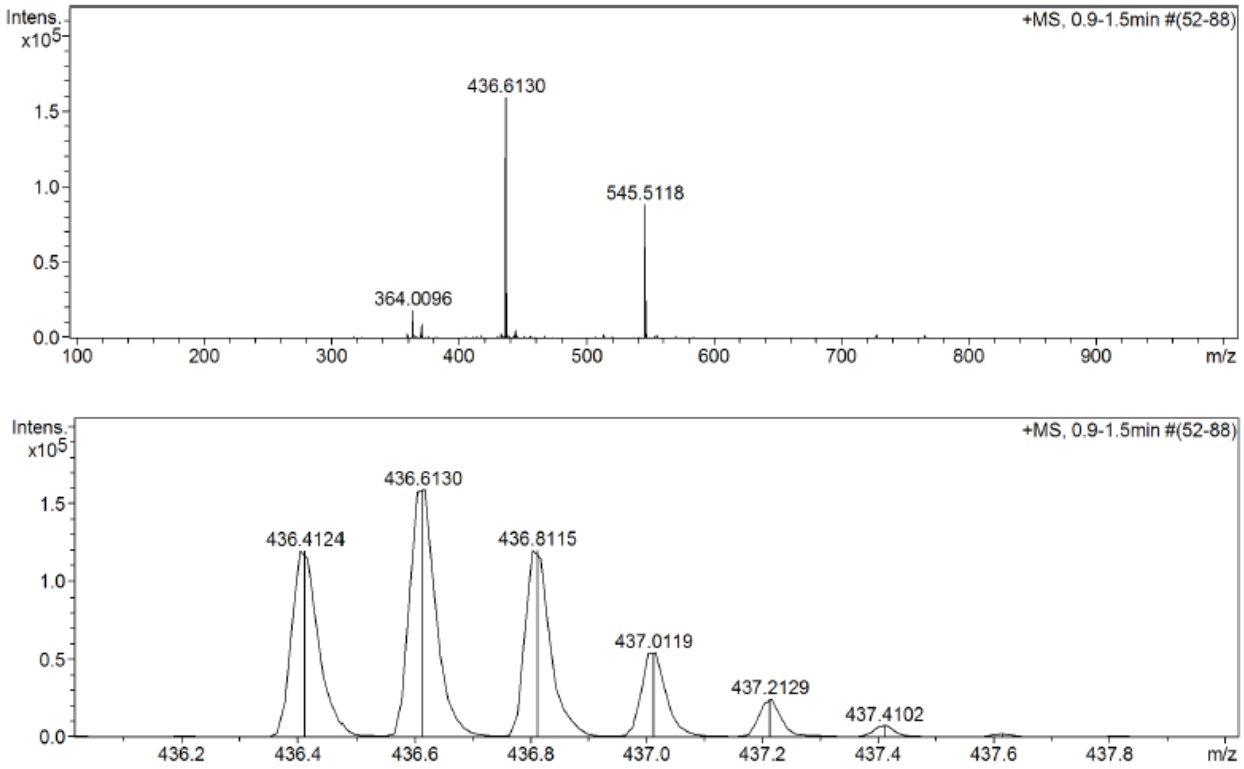

Sum Formula	Sigma	m/z	Err [ppm]	Mean Err [ppm]	Err [mDa]	rdb	N Rule	e⁻
C 96 H 149 N 32 O 19 S 4	0.058	436.4106	-4.12	-2.59	-1.80	38.50	ok	even

Figure S7.3-54 – HRMS of 18 (TP1[R17A])
HRMS-ESI (*m/z*): $[M + 5H]^{5+}$ calculated for ($C_{96}H_{144}N_{32}O_{19}S_4$ + 5H)/5, 436.4106; found 436.4124.

A

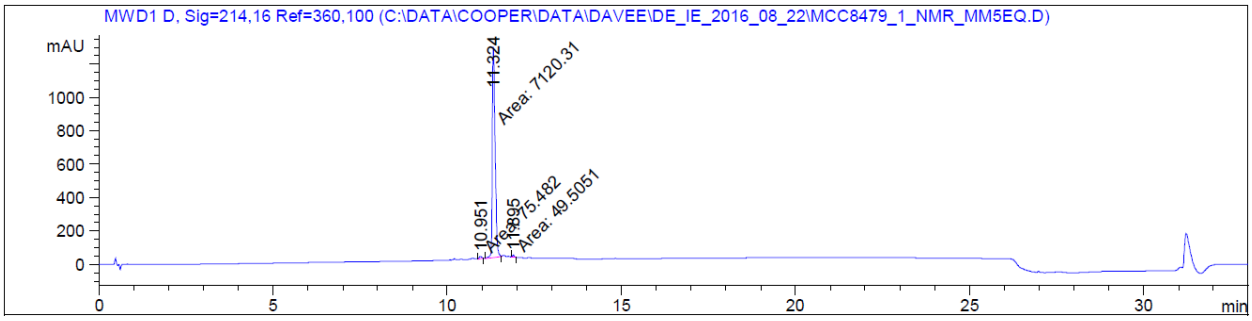

Peak #	RetTime [min]	Type	Width [min]	Area [mAU*s]	Height [mAU]	Area %
1	10.951	MM	0.0861	75.48200	14.61552	1.0418
2	11.324	MM	0.0939	7120.30615	1263.75635	98.2749
3	11.895	MM	0.0650	49.50505	12.69810	0.6833

B

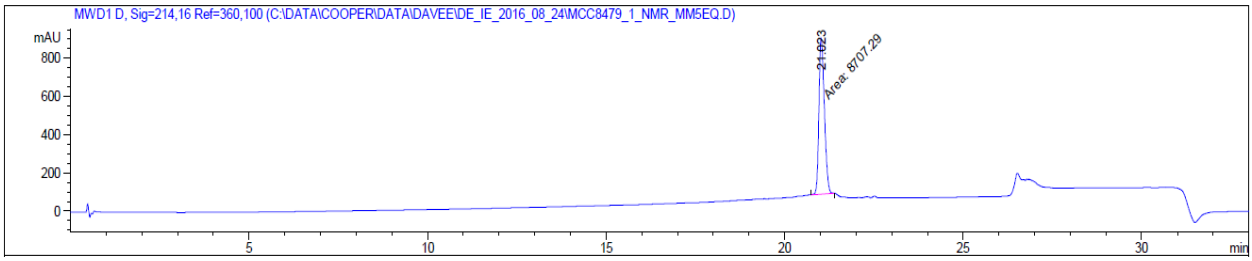

Peak #	RetTime [min]	Type	Width [min]	Area [mAU*s]	Height [mAU]	Area %
1	21.023	MM	0.1778	8707.29199	816.24091	100.0000

Figure S7.3-55 – HPLC of 18 (TP1[R17A]). A – In Acetonitrile solvent system. B – In Methanol solvent system.

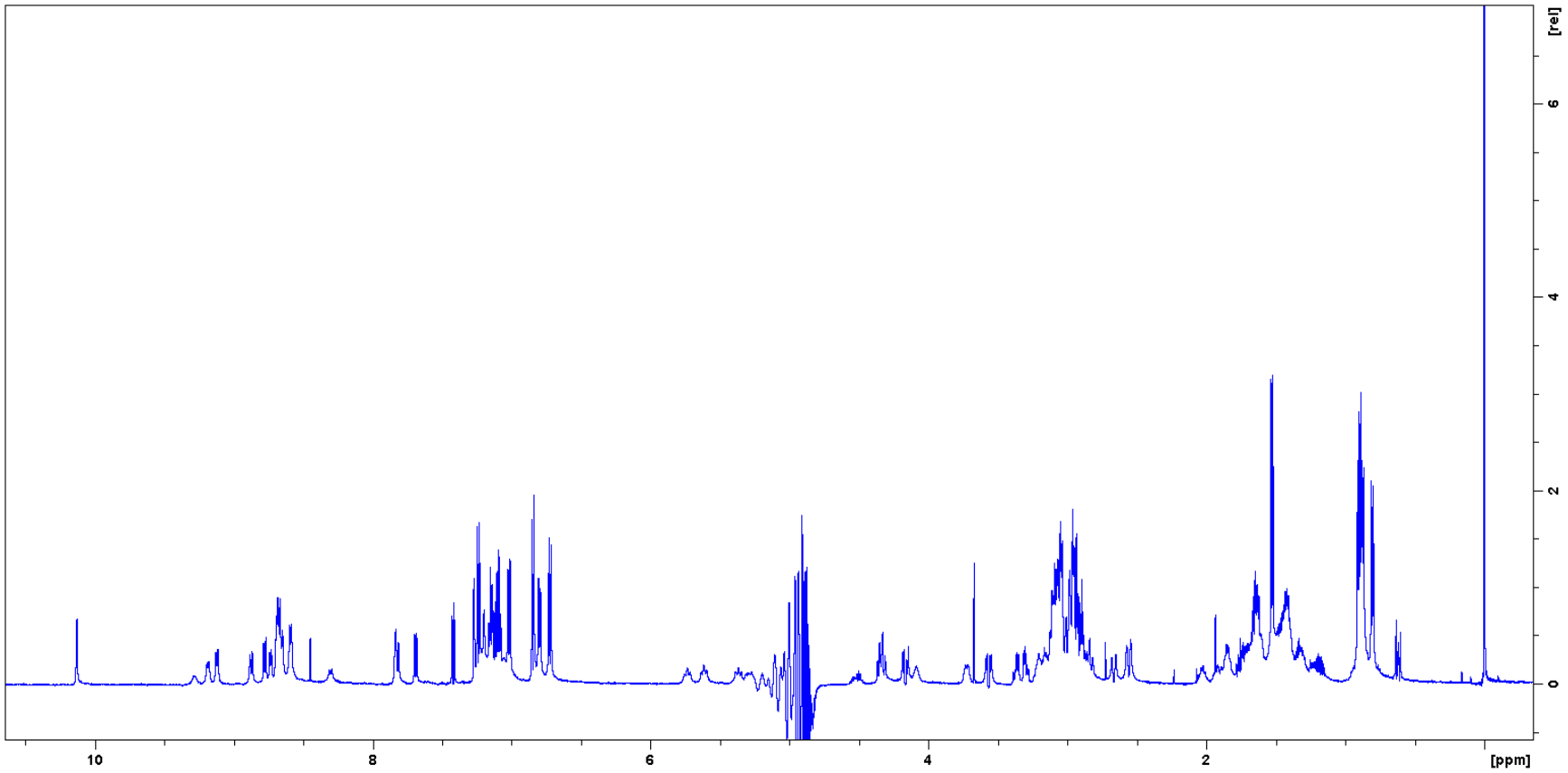

Figure S7.3-56 – ^{1}H NMR of 18 (TP1[R17A])

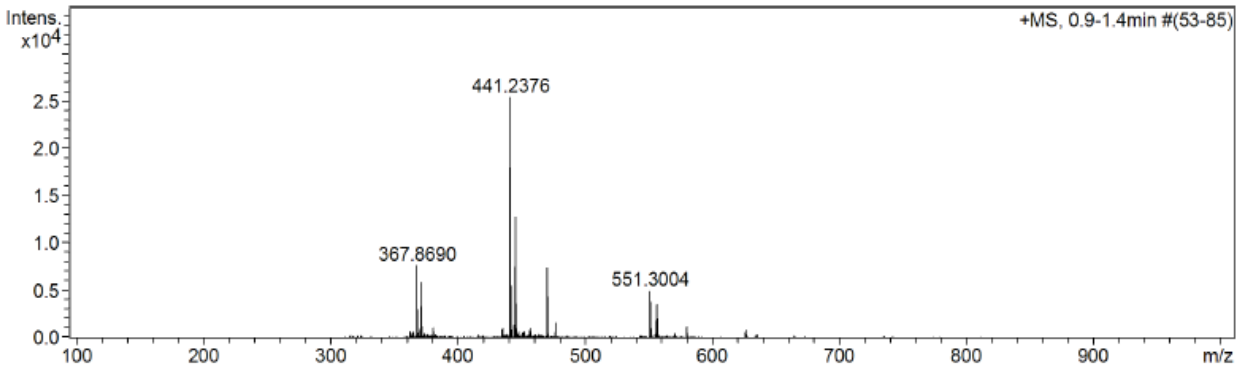

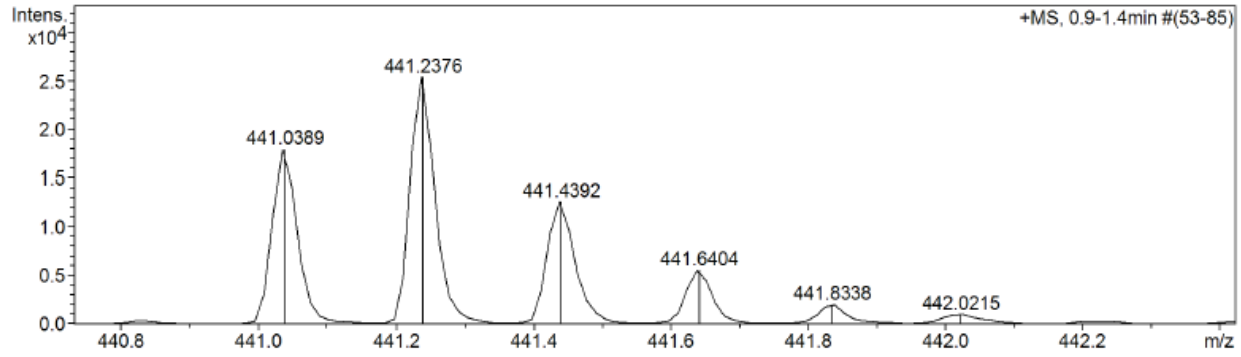

Sum Formula	Sigma	m/z	Err [ppm]	Mean Err [ppm]	Err [mDa]	rdb	N Rule	e⁻
C 99 H 158 N 35 O 19 S 2	0.116	441.0377	-2.53	1.45	-1.12	38.50	ok	even

Figure S7.3-57 – HRMS of 19 (TP1[C3A,C16A])
HRMS-ESI (*m/z*): $[M + 5H]^{5+}$ calculated for $(C_{99}H_{153}N_{35}O_{19}S_2 + 5H)/5$, 441.0377; found 441.0389.

A

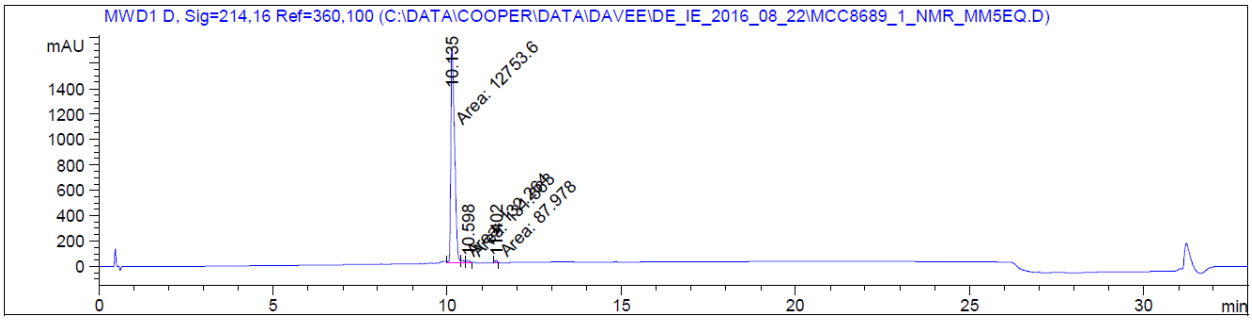

Peak #	RetTime [min]	Type	Width [min]	Area [mAU*s]	Height [mAU]	Area %
1	10.135	MF	0.1249	1.27536e4	1702.42053	97.3156
2	10.439	MF	0.1013	132.26416	21.76858	1.0092
3	10.598	FM	0.1029	131.56314	21.30974	1.0039
4	11.402	MM	0.0689	87.97800	21.28057	0.6713

B

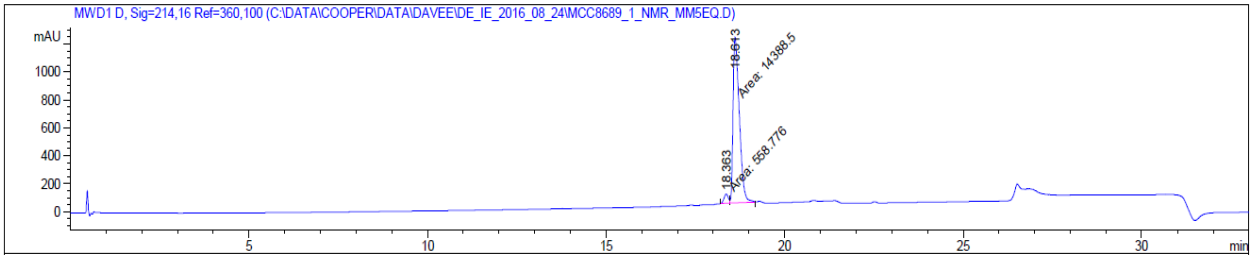

Peak #	RetTime [min]	Type	Width [min]	Area [mAU*s]	Height [mAU]	Area %
1	18.363	MF	0.1392	558.77643	66.92471	3.7383
2	18.613	FM	0.2026	1.43885e4	1183.55908	96.2617

Figure S7.3-58 – HPLC of 19 (TP1[C3A,C16A]). A – In Acetonitrile solvent system. B – In Methanol solvent system.

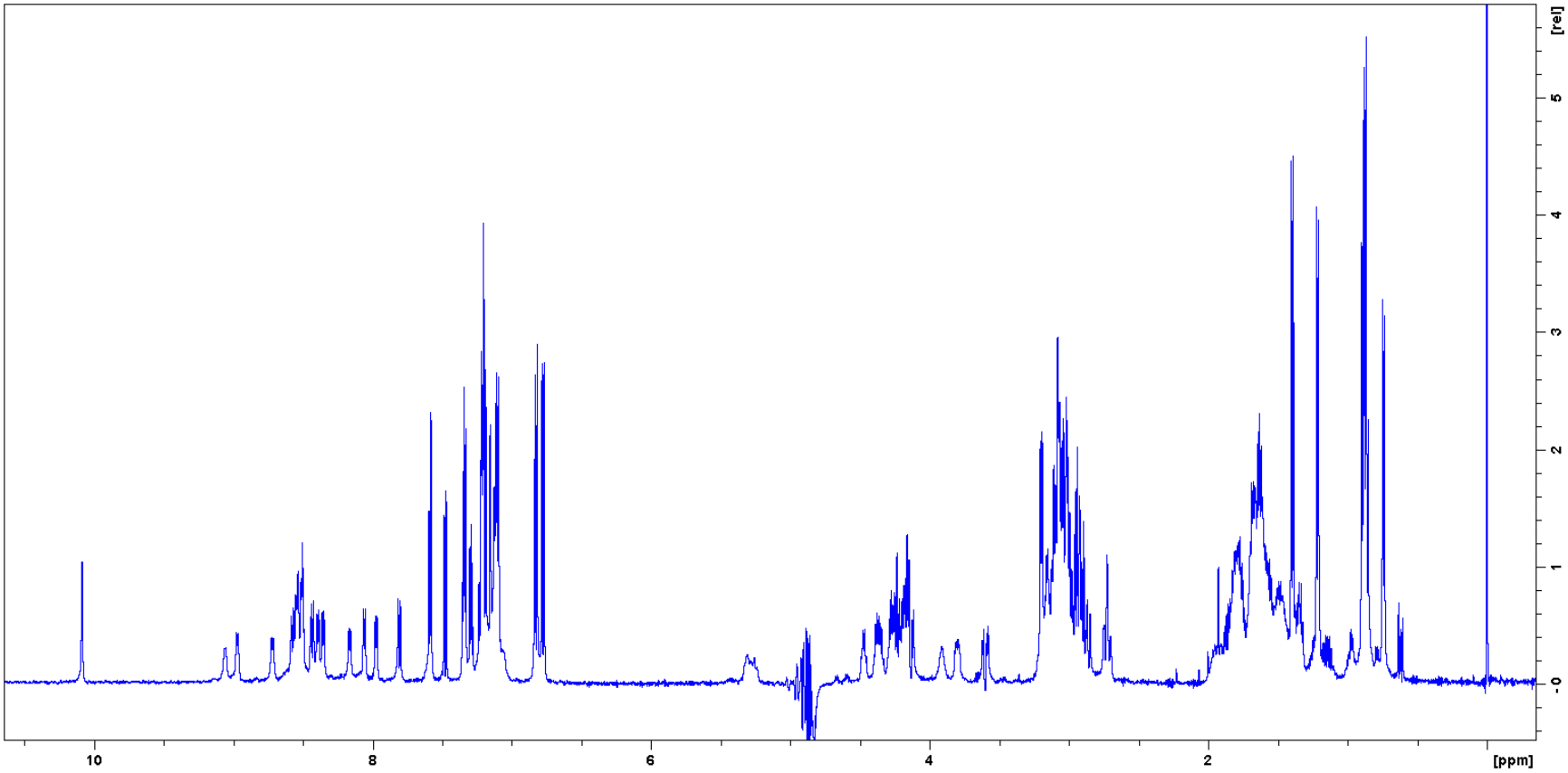

Figure S7.3-59 – ^{1}H NMR of 19 (TP1[C3A,C16A])

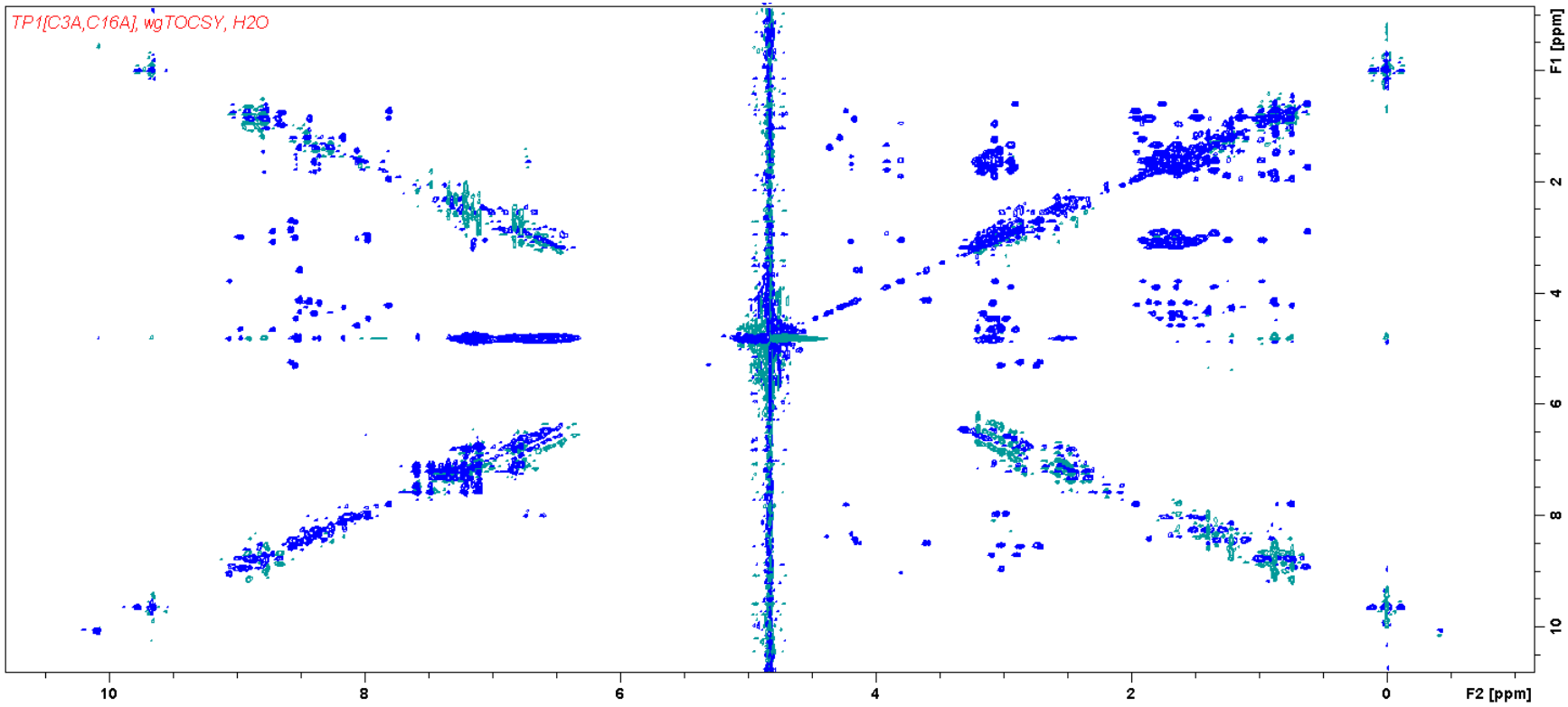

Figure S7.3-60 – 2D TOCSY NMR of 19 (TP1[C3A,C16A]), MLEV17 spin-lock mixing pulses = 80 ms, water suppression was performed using Watergate sequence.

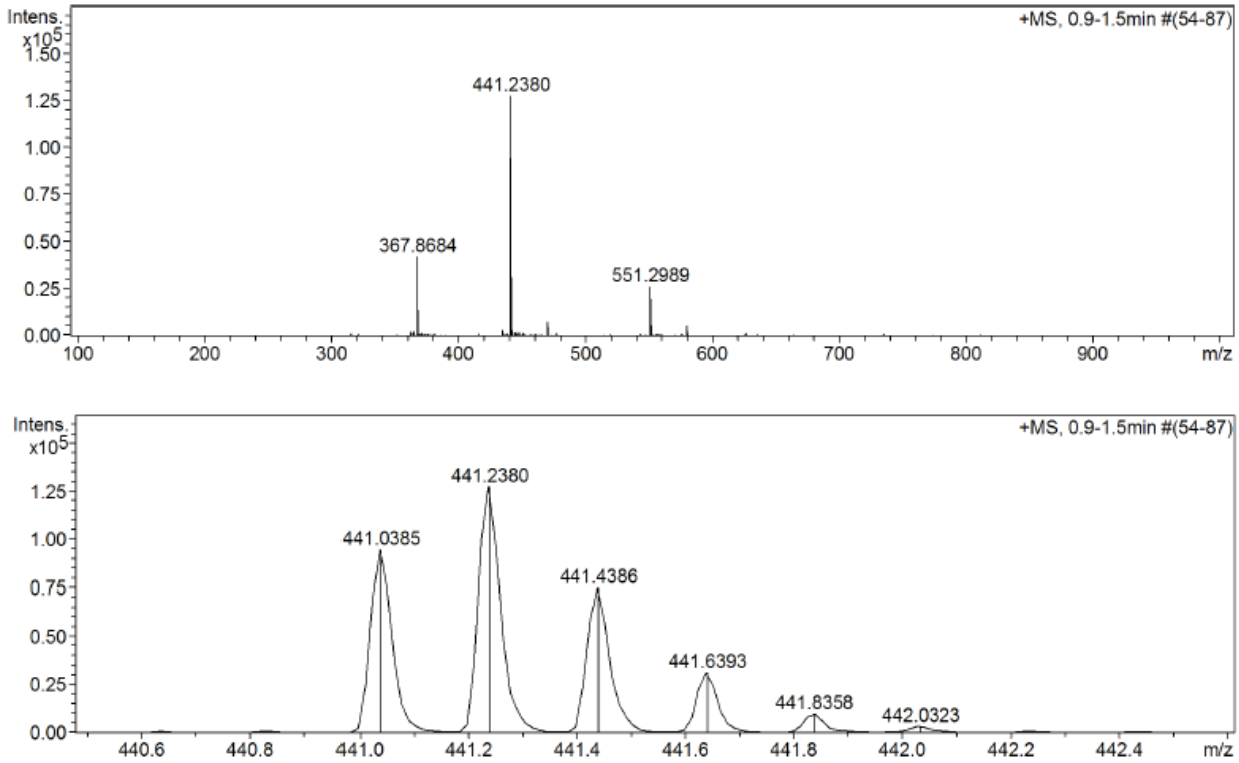

Sum Formula	Sigma	m/z	Err [ppm]	Mean Err [ppm]	Err [mDa]	rdb	N Rule	e⁻
C 99 H 158 N 35 O 19 S 2	0.083	441.0377	-1.64	0.73	-0.73	38.50	ok	even

Figure S7.3-61 – HRMS of 20 (TP1[C7A,C12A])
HRMS-ESI (*m/z*): $[M + 5H]^{5+}$ calculated for ($C_{99}H_{153}N_{35}O_{19}S_2$ + 5H)/5, 441.0377; found 441.0385.

A

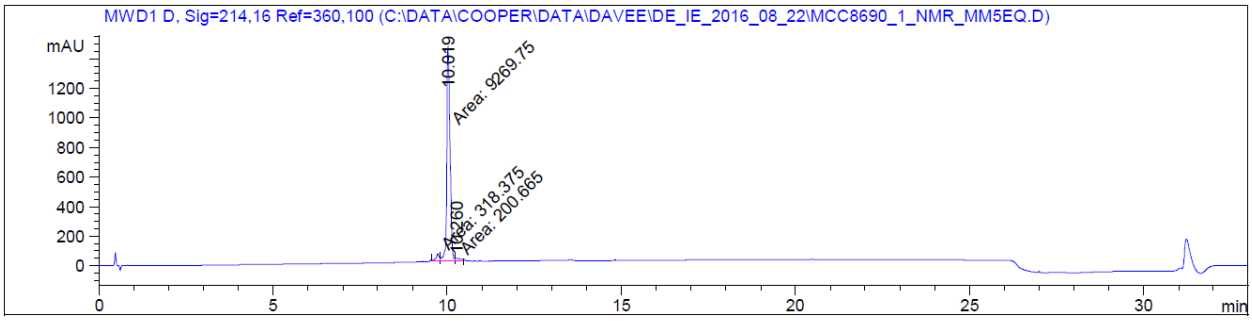

Peak #	RetTime [min]	Type	Width [min]	Area [mAU*s]	Height [mAU]	Area %
1	9.723	MF	0.1077	318.37512	49.27920	3.2524
2	10.019	MF	0.1061	9269.74902	1455.65747	94.6976
3	10.260	FM	0.1841	200.66455	18.16937	2.0499

B

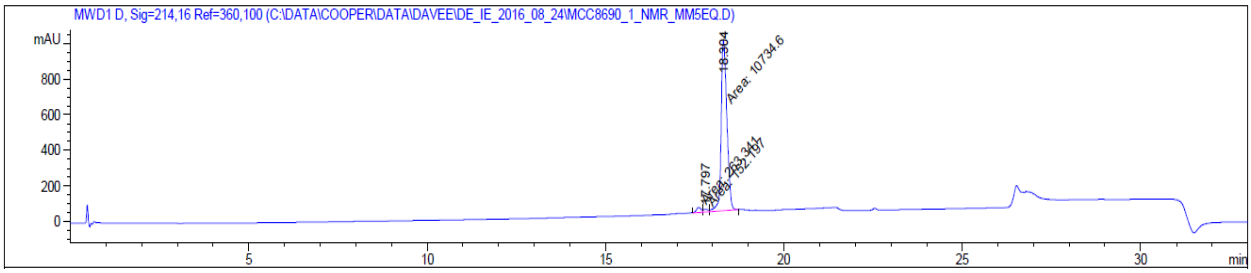

Peak #	RetTime [min]	Type	Width [min]	Area [mAU*s]	Height [mAU]	Area %
1	17.610	MF	0.1492	263.34085	29.41039	2.3618
2	17.797	FM	0.1705	152.19653	14.87825	1.3650
3	18.304	FM	0.1865	1.07346e4	959.54895	96.2733

Figure S7.3-62 – HPLC of 20 (TP1[C7A,C12A]). A – In Acetonitrile solvent system. B – In Methanol solvent system.

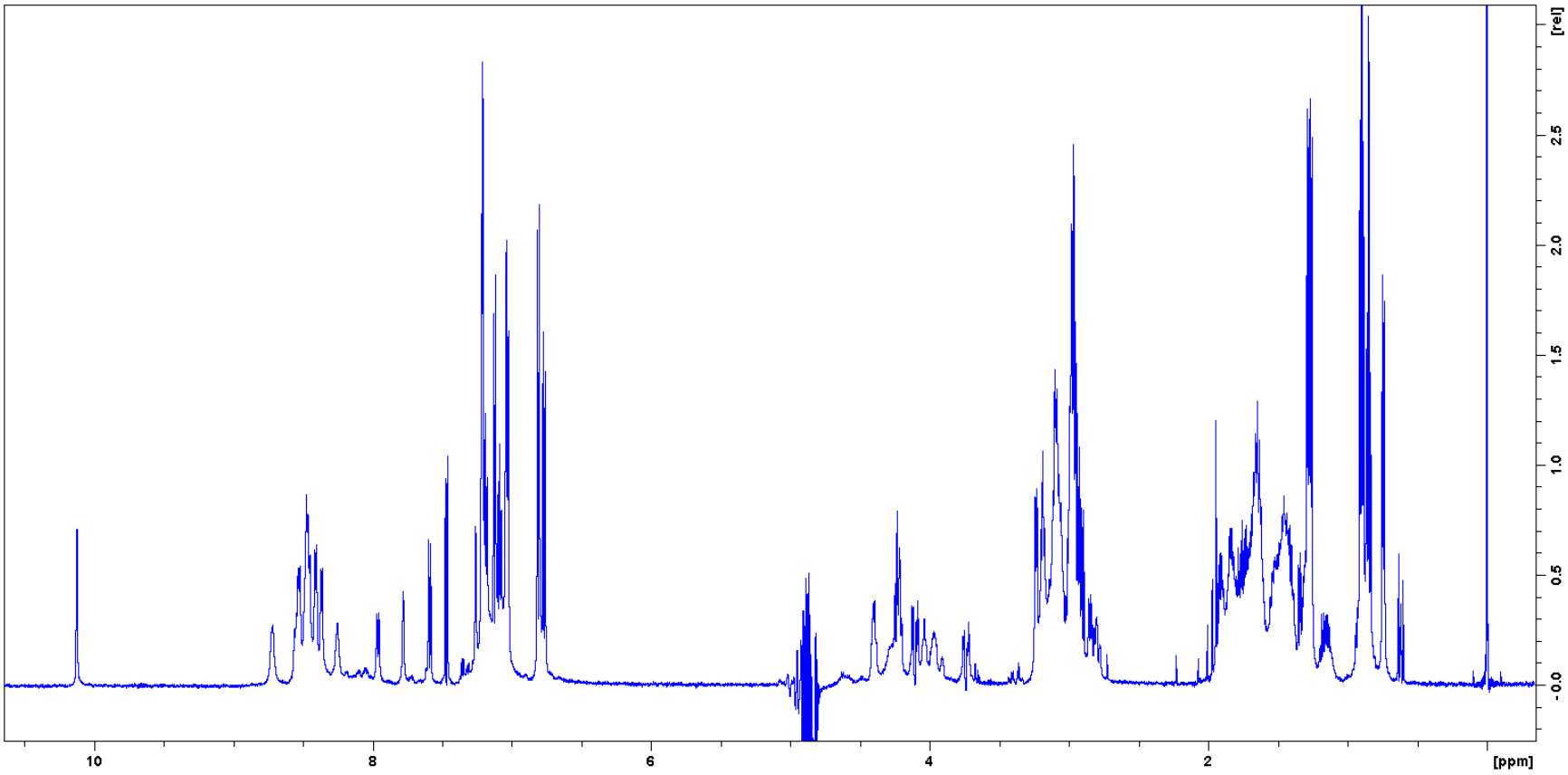

Figure S7.3-63 – ^{1}H NMR of 20 (TP1[C7A,C12A])

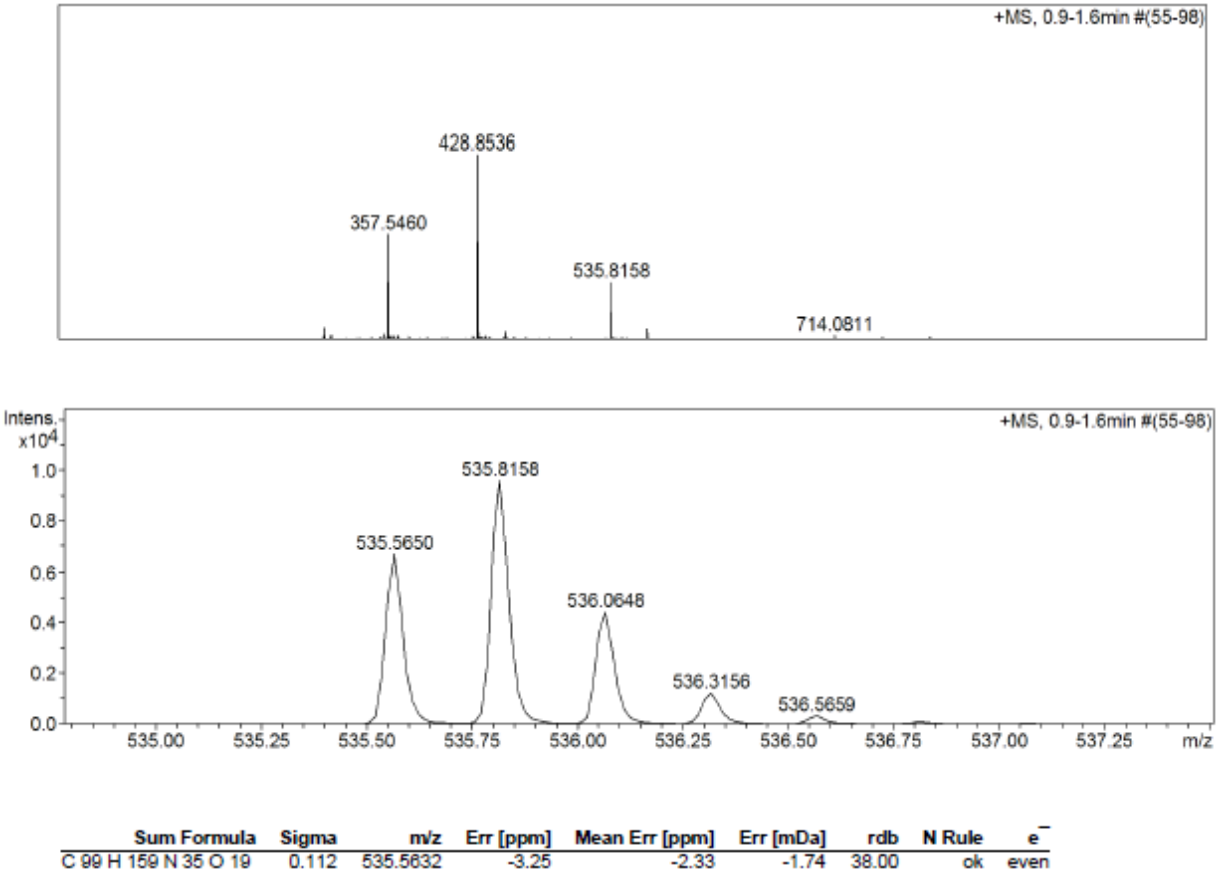

Sum Formula	Sigma	m/z	Err [ppm]	Mean Err [ppm]	Err [mDa]	rdb	N Rule	e⁻
C 99 H 159 N 35 O 19	0.112	535.5632	-3.25	-2.33	-1.74	38.00	ok	even

Figure S7.3-64 – HRMS of 21 (TP1[C3A,C7A,C12A,C16A])
HRMS-ESI (*m/z*): $[M + 4H]^{4+}$ calculated for ($C_{99}H_{155}N_{35}O_{19}$ + 4H)/4, 535.5632; found 535.5650.

A

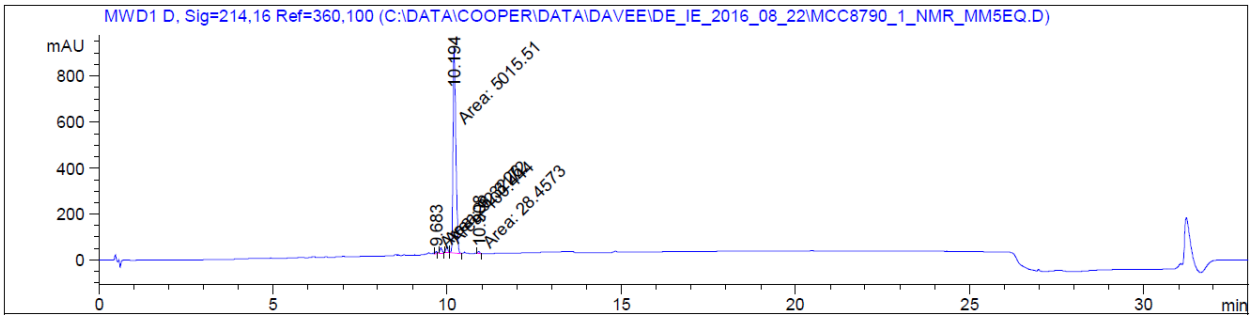

Peak #	RetTime [min]	Type	Width [min]	Area [mAU*s]	Height [mAU]	Area %
1	9.683	MM	0.0575	26.32258	7.62627	0.5001
2	9.818	MM	0.0720	92.31723	21.38323	1.7541
3	9.990	MM	0.0702	100.44353	23.86150	1.9085
4	10.194	MM	0.0930	5015.51465	898.81195	95.2966
5	10.908	MM	0.0658	28.45732	7.20558	0.5407

B

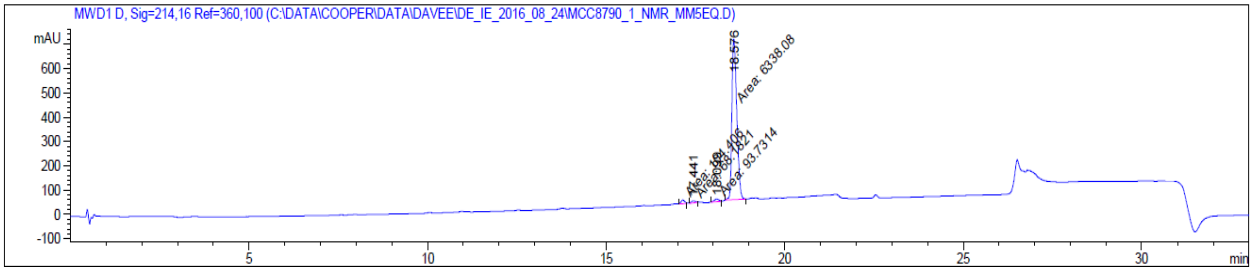

Peak #	RetTime [min]	Type	Width [min]	Area [mAU*s]	Height [mAU]	Area %
1	17.148	MM	0.1178	104.40572	14.77721	1.5809
2	17.441	MM	0.1310	68.18211	8.67207	1.0324
3	18.099	MM	0.1532	93.73144	10.19717	1.4192
4	18.576	MM	0.1594	6338.07520	662.77356	95.9675

Figure S7.3-65 – HPLC of 21 (TP1[C3A,C7A,C12A,C16A]). A – In Acetonitrile solvent system. B – In Methanol solvent system.

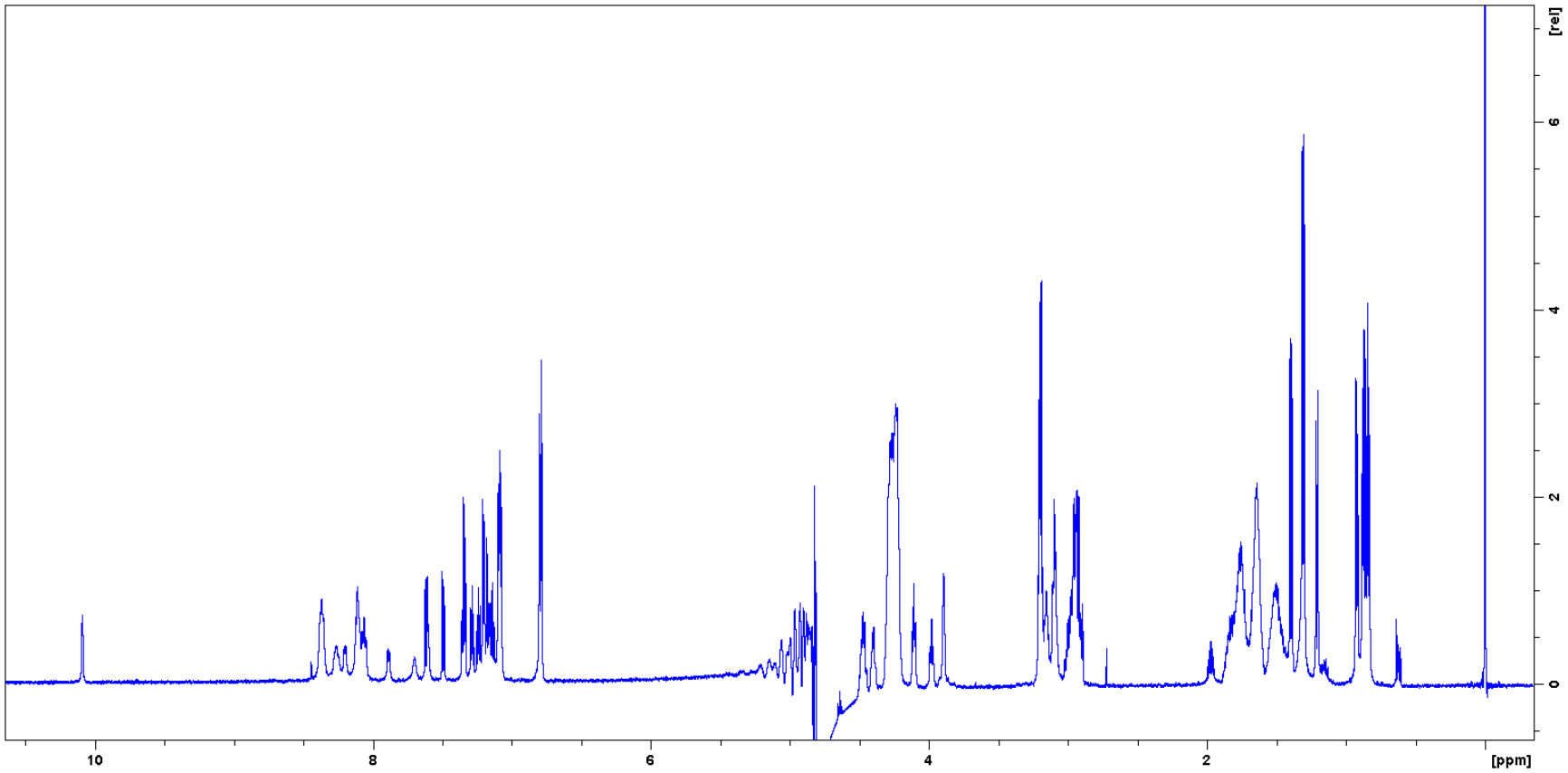

Figure S7.3-66 – ^{1}H NMR of 21 (TP1[C3A,C7A,C12A,C16A])

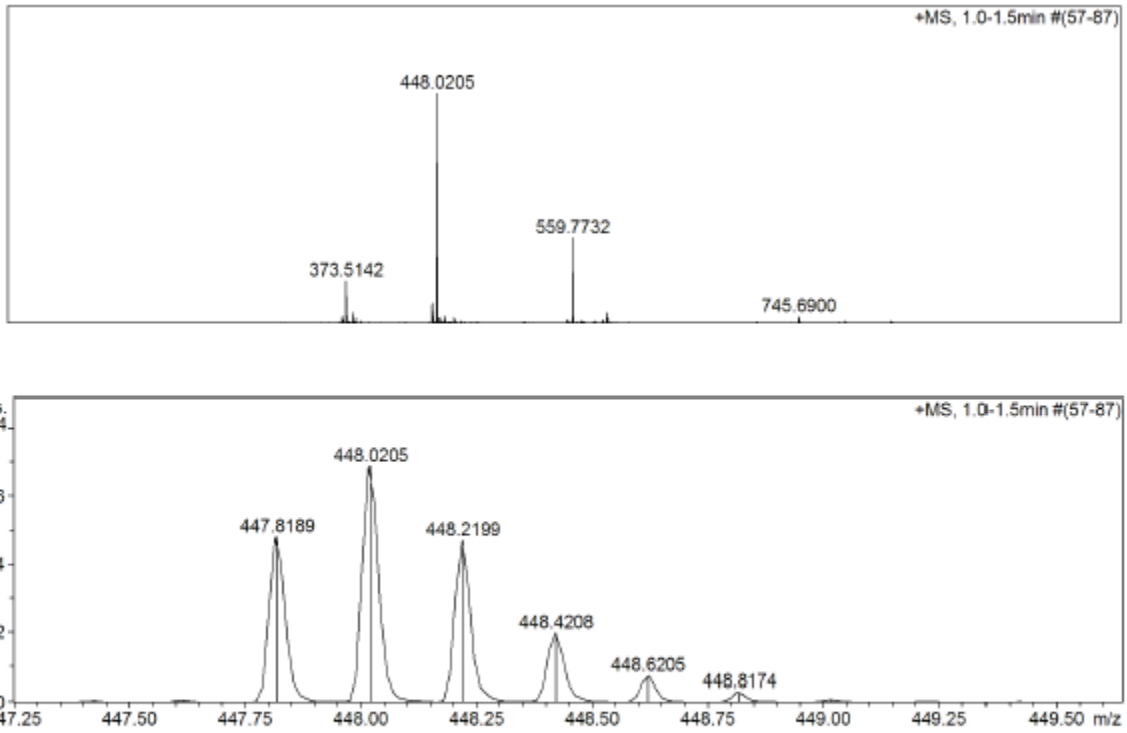

Sum Formula	Sigma	m/z	Err [ppm]	Mean Err [ppm]	Err [mDa]	rdb	N Rule	e⁻
C 97 H 152 N 35 O 19 S 4	0.097	447.8172	-3.93	-4.63	-1.76	39.50	ok	even

Figure S7.3-67 – HRMS of 22 (TP1[V6R,R9A])
HRMS-ESI (*m/z*): $[M + 5H]^{5+}$ calculated for ($C_{97}H_{147}N_{35}O_{19}S_4$ + 5H)/5, 447.8172; found 447.8189.

A

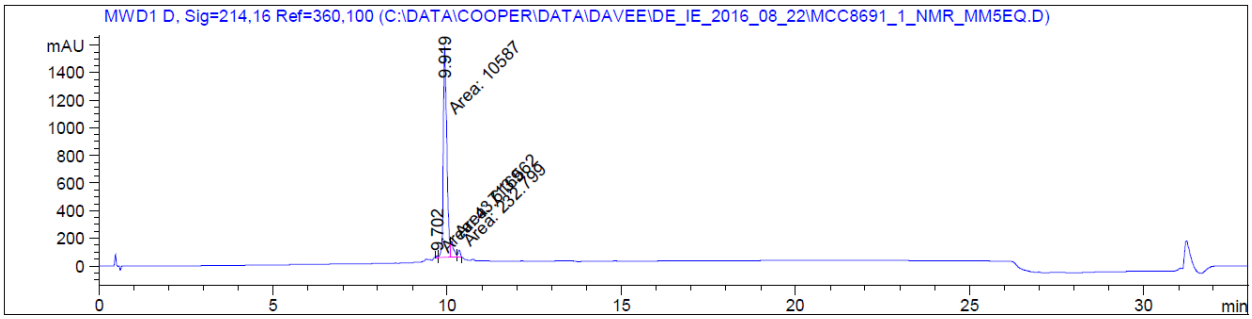

Peak #	RetTime [min]	Type	Width [min]	Area [mAU*s]	Height [mAU]	Area %
1	9.702	MF	0.0581	43.61690	12.51987	0.3768
2	9.919	MF	0.1155	1.05870e4	1528.03296	91.4487
3	10.122	MF	0.1013	713.56183	117.36015	6.1636
4	10.341	FM	0.0764	232.79851	50.81728	2.0109

B

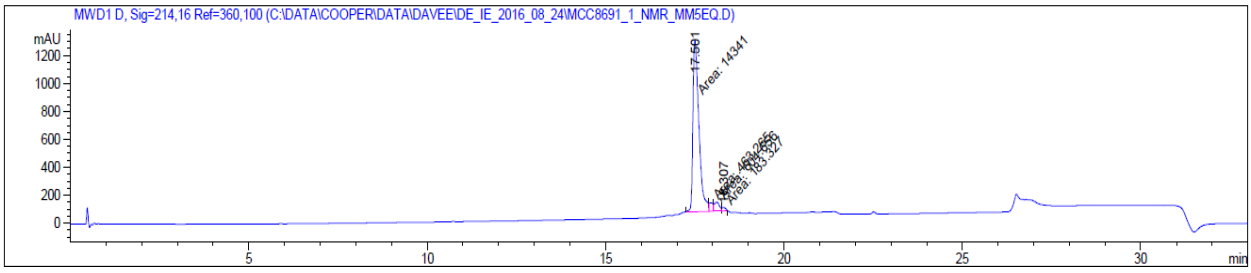

Peak #	RetTime [min]	Type	Width [min]	Area [mAU*s]	Height [mAU]	Area %
1	17.501	MF	0.1938	1.43410e4	1233.31299	91.9752
2	17.946	MF	0.1281	463.26532	60.27827	2.9711
3	18.116	FM	0.1560	604.65582	64.61996	3.8779
4	18.307	FM	0.1327	183.32738	23.02361	1.1758

Figure S7.3-68 – HPLC of 22 (TP1[V6R,R9A]). A – In Acetonitrile solvent system. B – In Methanol solvent system.

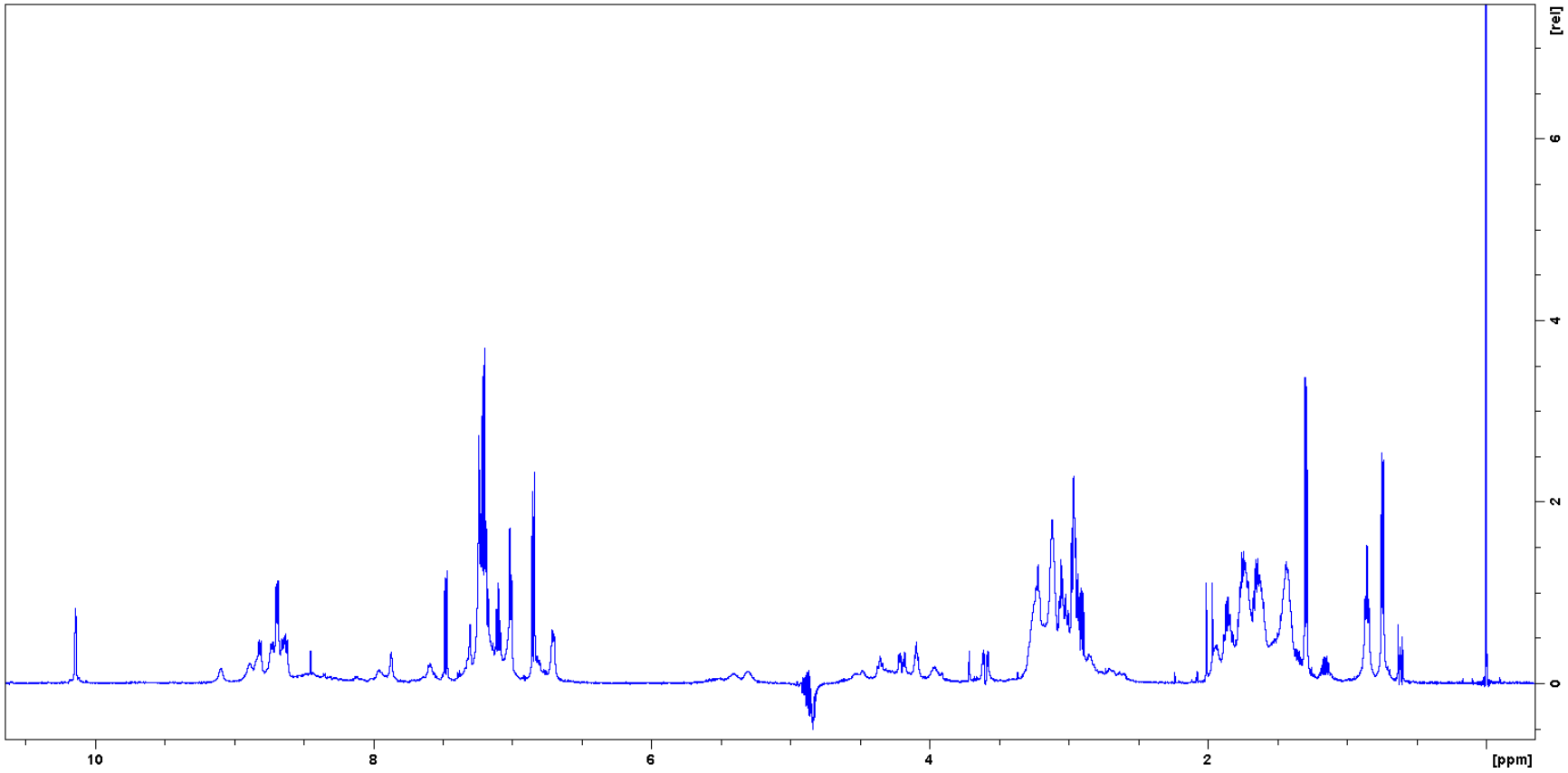

Figure S7.3-69 – ^{1}H NMR of 22 (TP1[V6R,R9A])

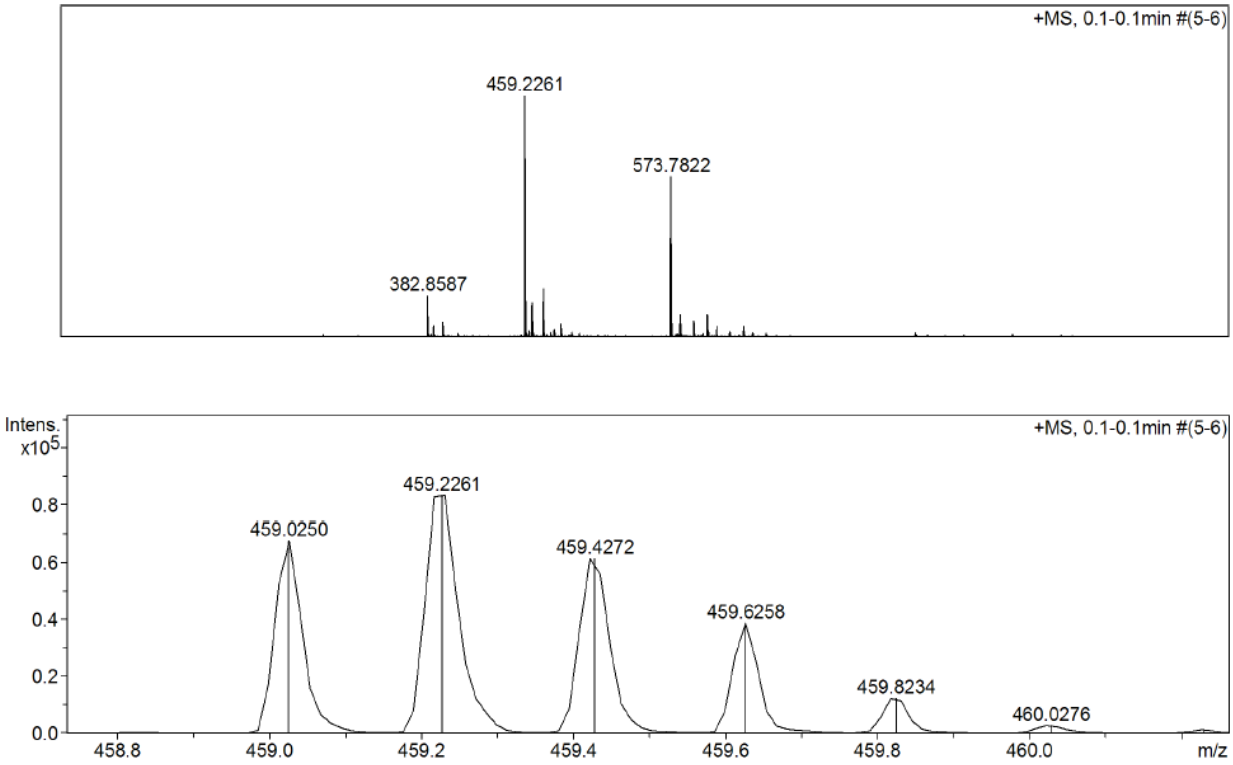

Sum Formula	Sigma	m/z	Err [ppm]	Mean Err [ppm]	Err [mDa]	rdb	N Rule	e⁻
C 99 H 156 N 37 O 19 S 4	0.047	459.0247	-0.66	-1.63	-0.30	40.50	ok	even

Figure S7.3-70 – HRMS of 23 (TP1[K1R])
HRMS-ESI (*m/z*): $[M + 5H]^{5+}$ calculated for ($C_{99}H_{151}N_{37}O_{19}S_4$ + 5H)/5, 459.0247; found 459.0250.

A

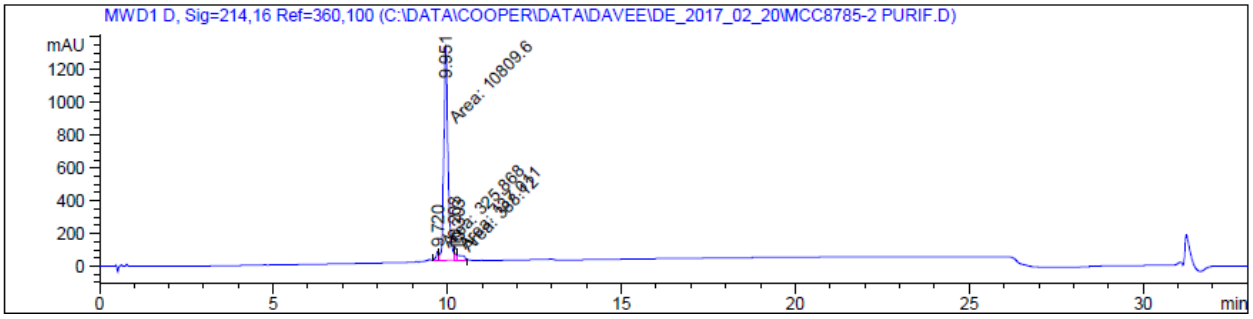

Peak #	RetTime [min]	Type	Width [min]	Area [mAU*s]	Height [mAU]	Area %
1	9.720	MF	0.1010	325.86838	53.76357	2.7946
2	9.951	MF	0.1379	1.08096e4	1305.98303	92.7019
3	10.203	FM	0.0525	137.01128	43.53272	1.1750
4	10.303	FM	0.2148	388.11993	30.12170	3.3285

B

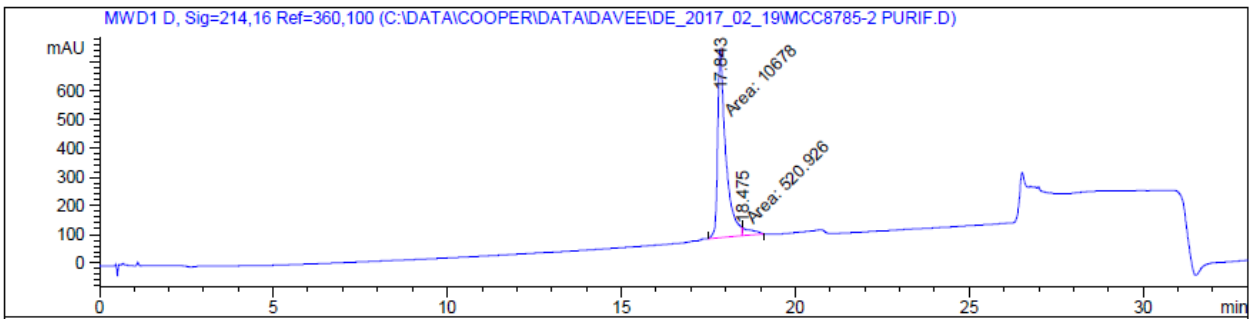

Peak #	RetTime [min]	Type	Width [min]	Area [mAU*s]	Height [mAU]	Area %
1	17.843	MF	0.2706	1.06780e4	657.62469	95.3484
2	18.475	FM	0.2948	520.92639	29.44866	4.6516

Figure S7.3-71 – HPLC of 23 (TP1[K1R]). A – In Acetonitrile solvent system. B – In Methanol solvent system.

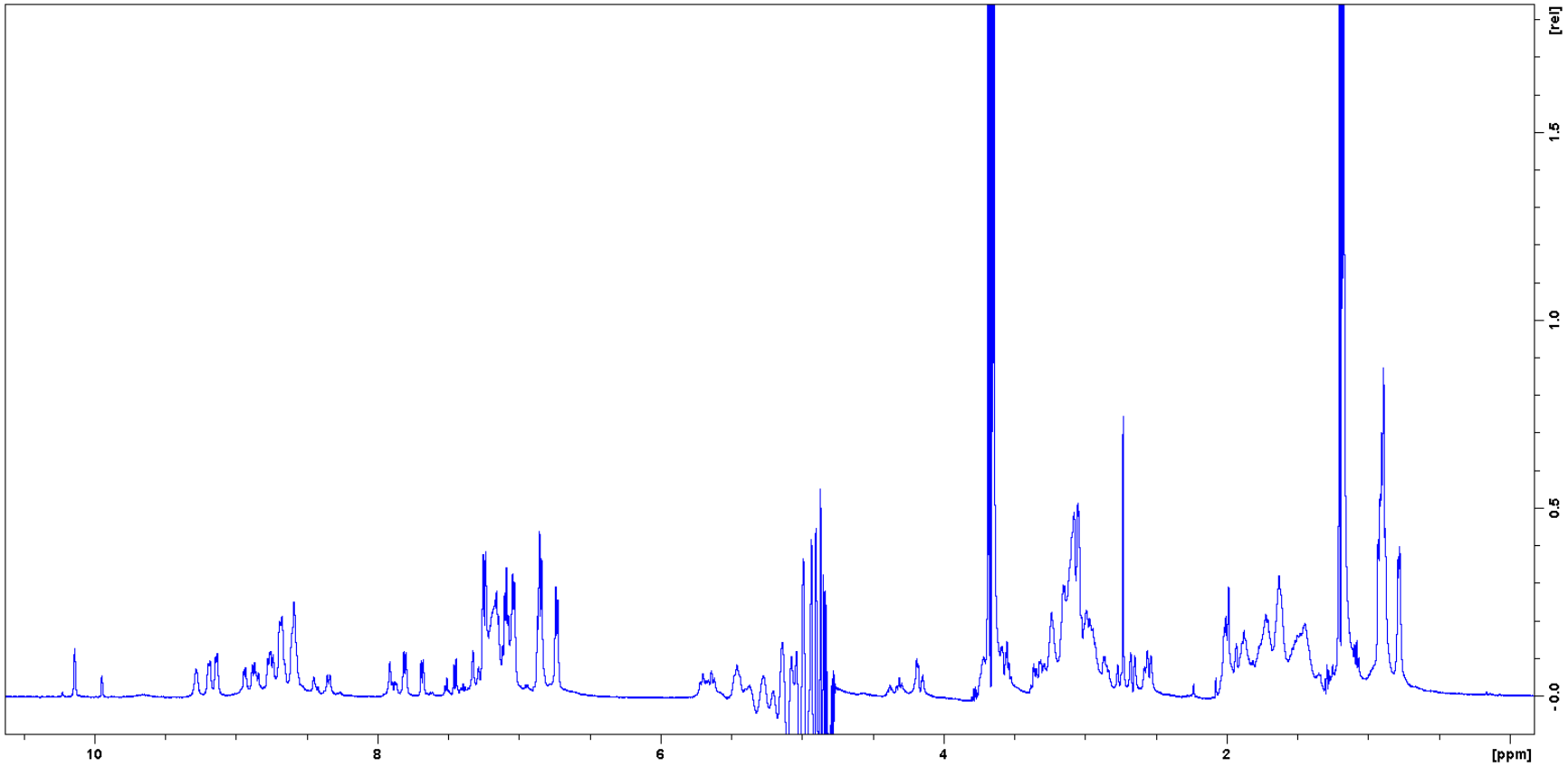

Figure S7.3-72 – ^{1}H NMR of 23 (TP1[K1R]). The quadruplet at 3.65 and the triplet at 1.17 ppm are residual ethanol.

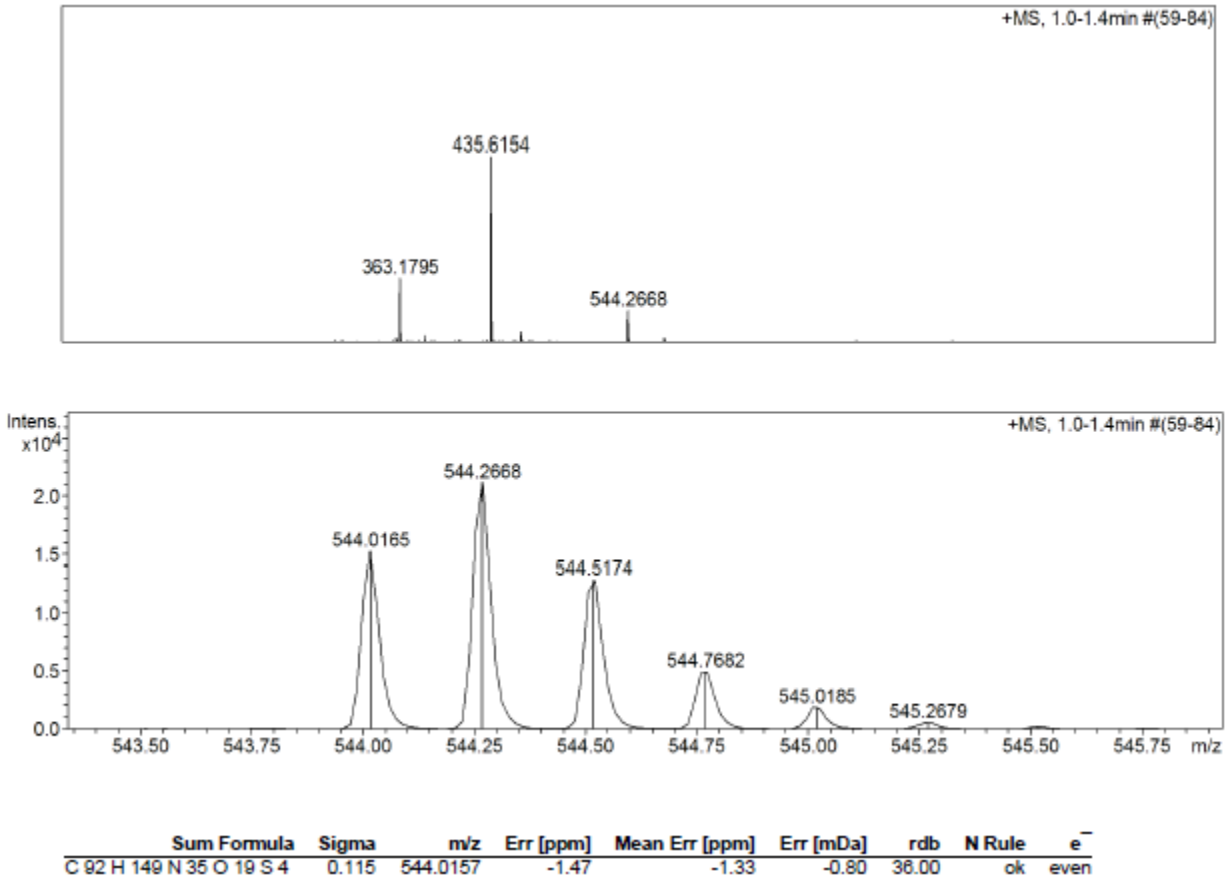

Sum Formula	Sigma	m/z	Err [ppm]	Mean Err [ppm]	Err [mDa]	rdb	N Rule	e⁻
C 92 H 149 N 35 O 19 S 4	0.115	544.0157	-1.47	-1.33	-0.80	36.00	ok	even

Figure S7.3-73 – HRMS of 24 (TP1[F4G])
HRMS-ESI (*m/z*): $[M + 4H]^{4+}$ calculated for $(C_{92}H_{145}N_{35}O_{19}S_4 + 4H)/4$, 544.0157; found 544.0165.

A

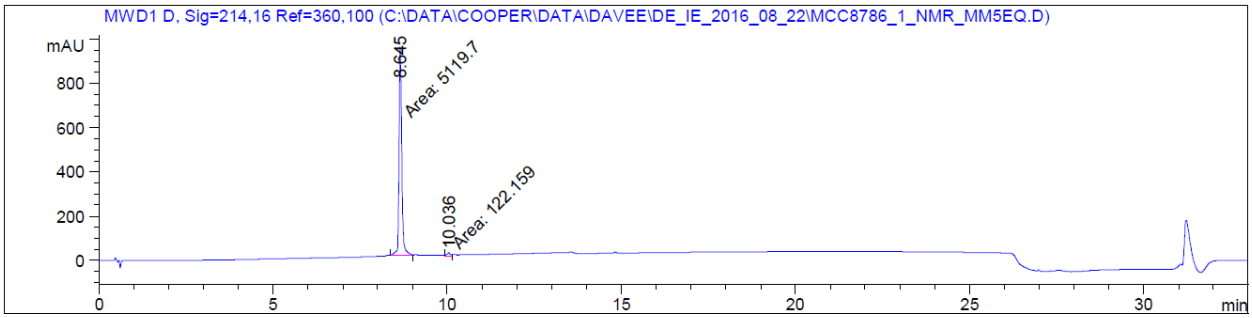

Peak #	RetTime [min]	Type	Width [min]	Area [mAU*s]	Height [mAU]	Area %
1	8.645	MM	0.0904	5119.69873	943.92566	97.6695
2	10.036	MM	0.1273	122.15916	15.99638	2.3305

B

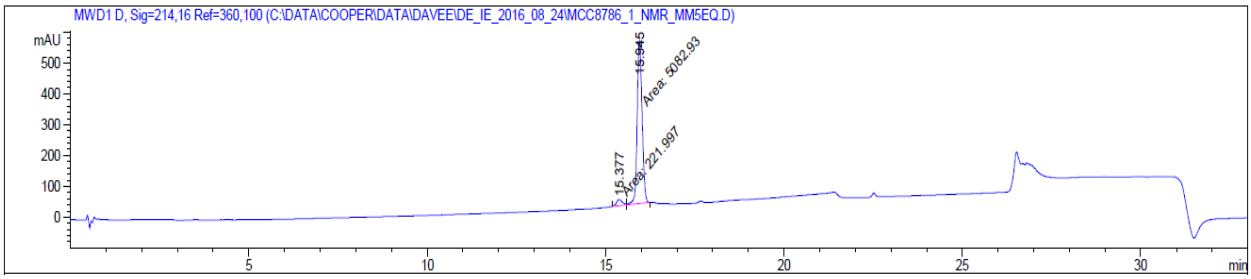

Peak #	RetTime [min]	Type	Width [min]	Area [mAU*s]	Height [mAU]	Area %
1	15.377	MF	0.1845	221.99724	20.05425	4.1847
2	15.945	FM	0.1604	5082.93066	528.22681	95.8153

Figure S7.3-74 – HPLC of 24 (TP1[F4G]). A – In Acetonitrile solvent system. B – In Methanol solvent system.

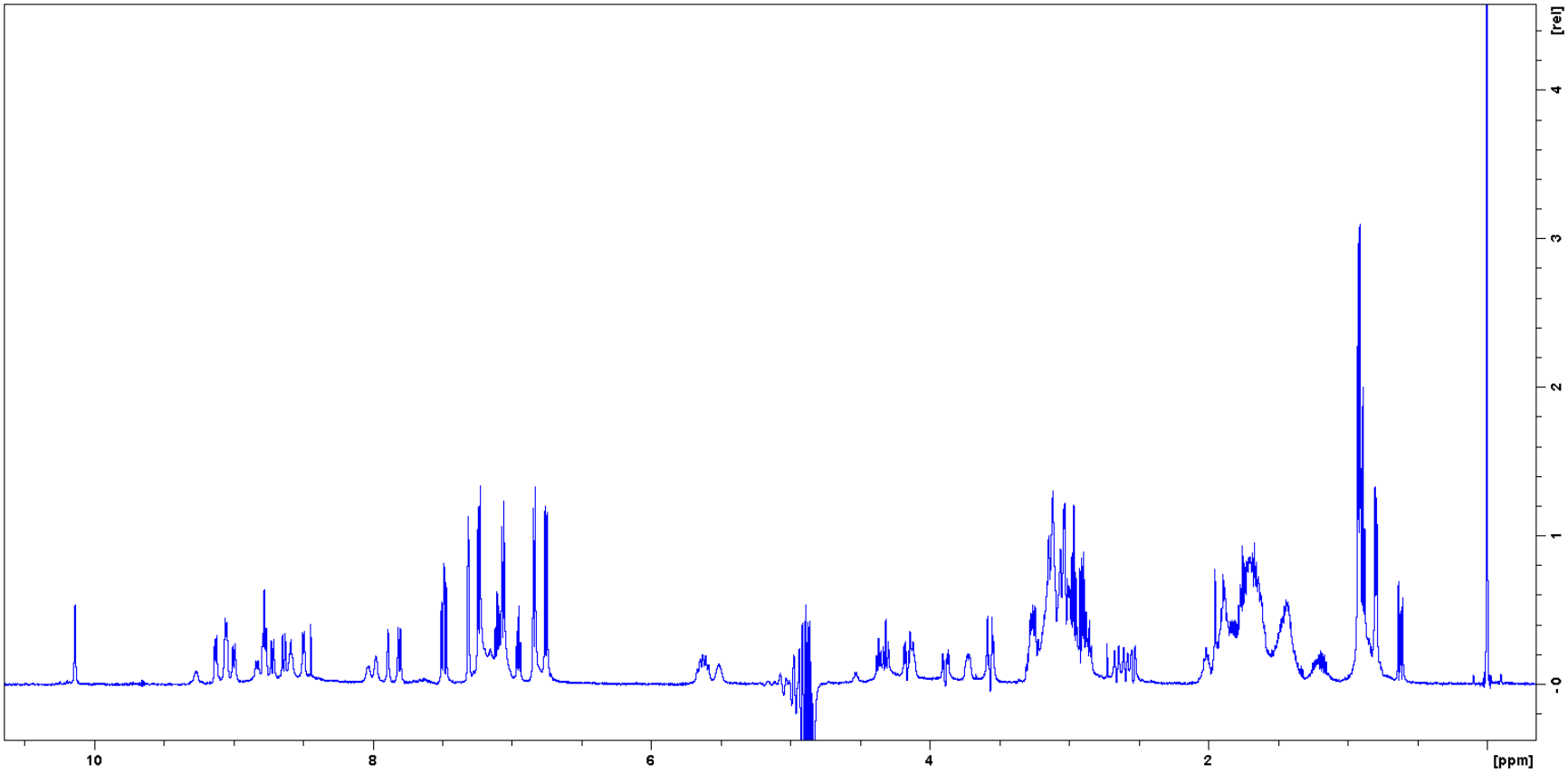

Figure S7.3-75 – ^{1}H NMR of 24 (TP1[F4G])

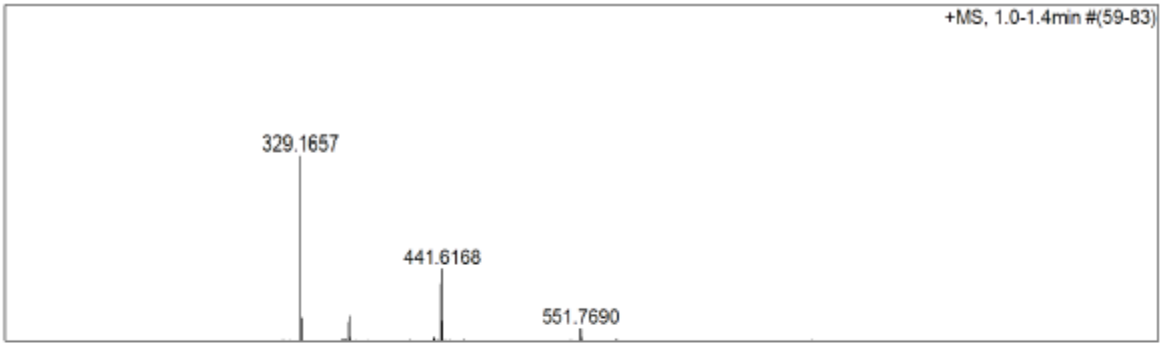

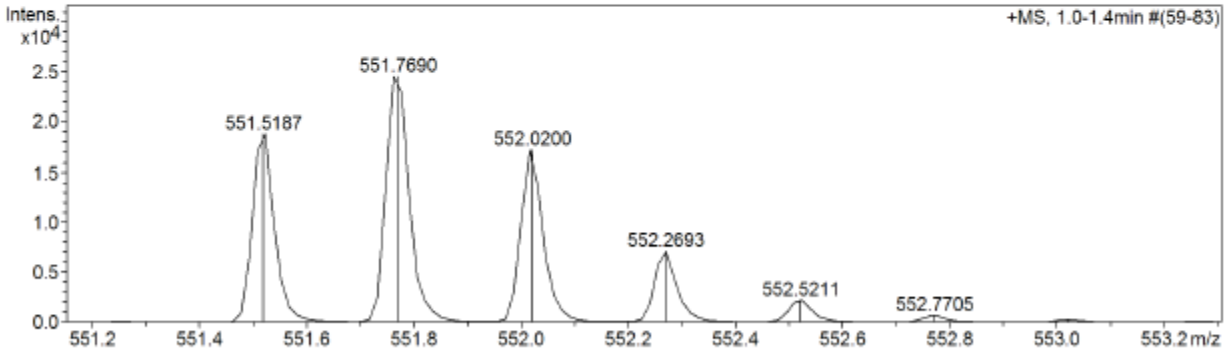

Sum Formula	Sigma	m/z	Err [ppm]	Mean Err [ppm]	Err [mDa]	rdb	N Rule	e⁻
C 93 H 151 N 35 O 20 S 4	0.085	551.5184	-0.55	-0.63	-0.30	36.00	ok	even

Figure S7.3-76 – HRMS of 25 (TP1[F4S])
HRMS-ESI (*m/z*): $[M + 4H]^{4+}$ calculated for $(C_{93}H_{147}N_{35}O_{20}S_4 + 4H)/5$, 551.5184; found 551.5187.

A

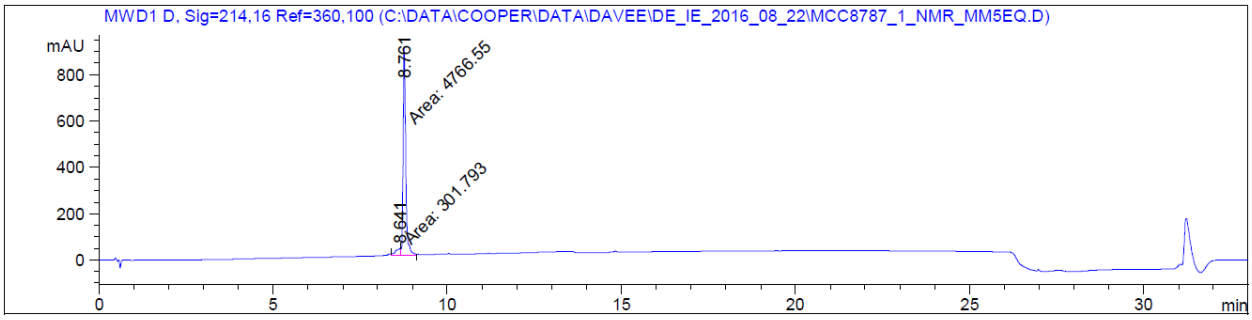

Peak #	RetTime [min]	Type	Width [min]	Area [mAU*s]	Height [mAU]	Area %
1	8.641	MF	0.1720	301.79297	29.24299	5.9545
2	8.761	FM	0.0880	4766.54688	903.08929	94.0455

B

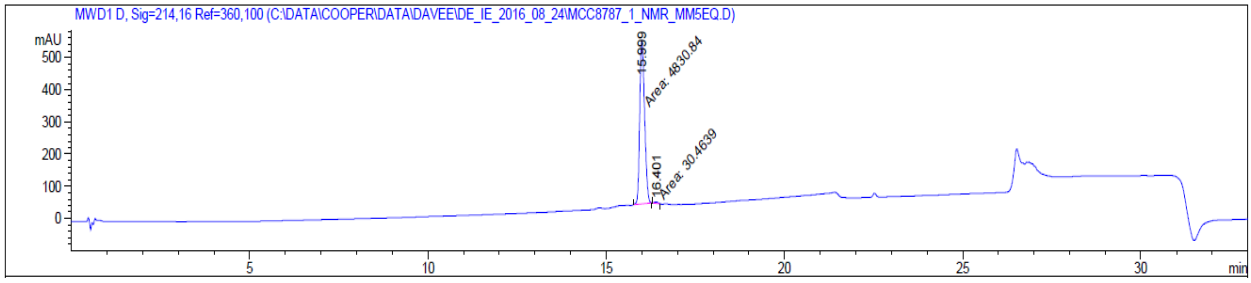

Peak #	RetTime [min]	Type	Width [min]	Area [mAU*s]	Height [mAU]	Area %
1	15.999	MM	0.1586	4830.84424	507.76233	99.3733
2	16.401	MM	0.1146	30.46392	4.42855	0.6267

Figure S7.3-77 – HPLC of 25 (TP1[F4S]). A – In Acetonitrile solvent system. B – In Methanol solvent system.

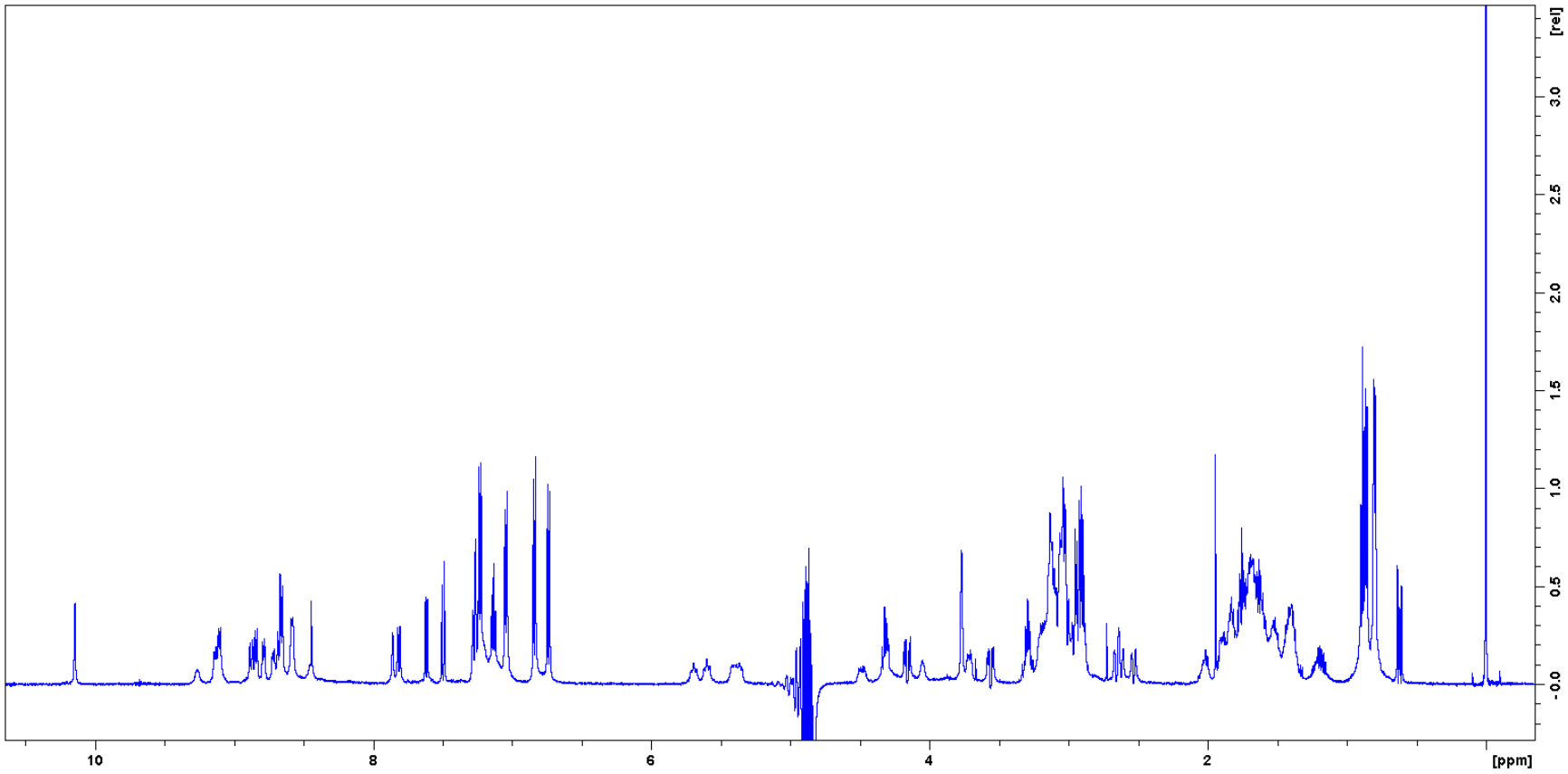

Figure S7.3-78 – ^{1}H NMR of 25 (TP1[F4S])

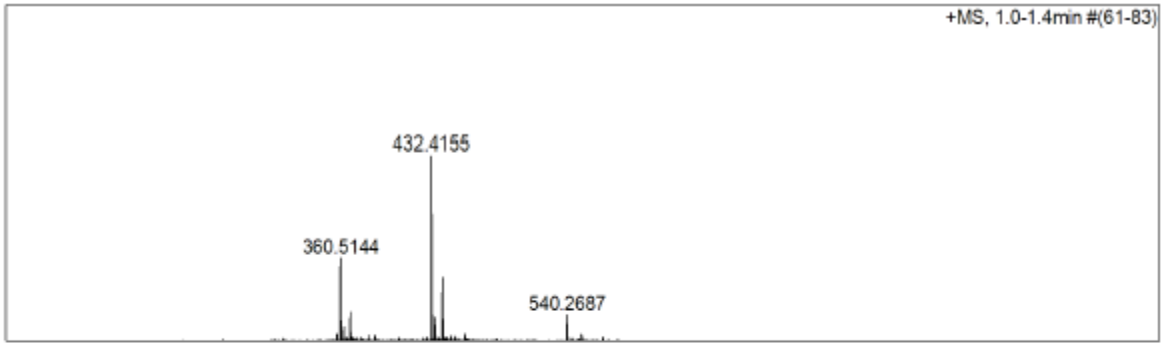

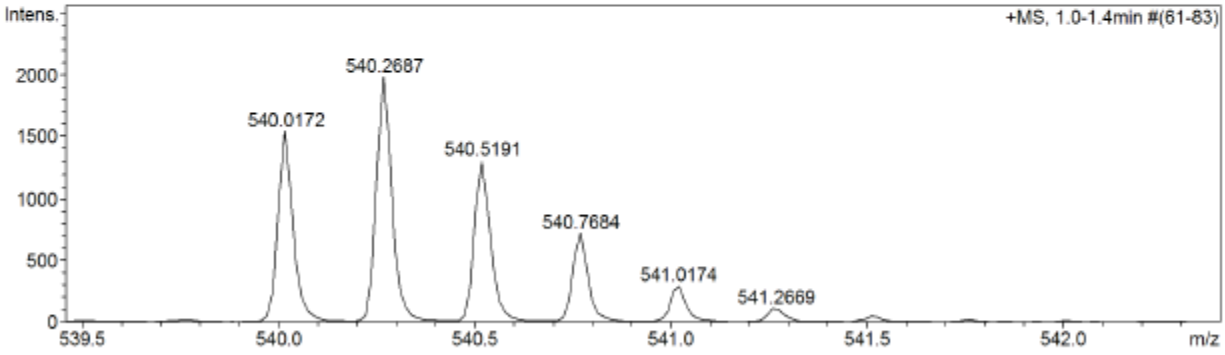

Sum Formula	Sigma	m/z	Err [ppm]	Mean Err [ppm]	Err [mDa]	rdb	N Rule	e⁻
C 92 H 149 N 35 O 18 S 4	0.061	540.0170	-0.29	-1.15	-0.16	36.00	ok	even

Figure S7.3-79 – HRMS of 26 (TP1[Y8G])
HRMS-ESI (*m/z*): $[M + 4H]^{4+}$ calculated for ($C_{92}H_{145}N_{35}O_{18}S_4$ + 4H)/4, 540.0170; found 540.0172.

A

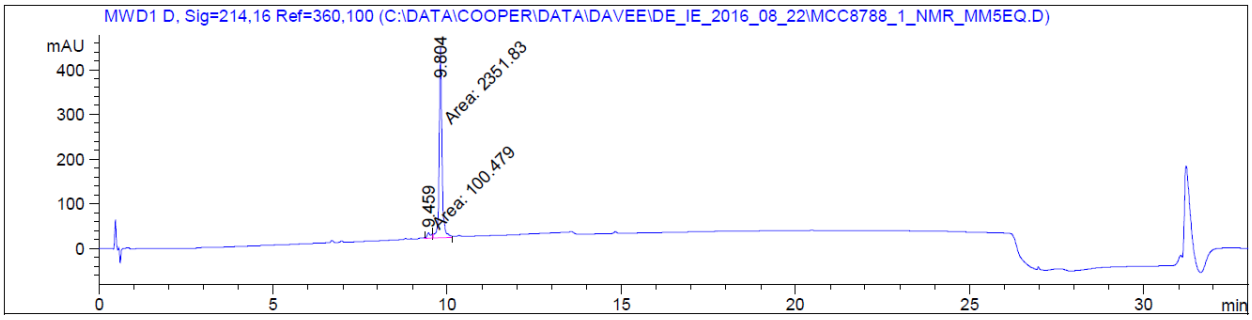

Peak #	RetTime [min]	Type	Width [min]	Area [mAU*s]	Height [mAU]	Area %
1	9.459	MF	0.1361	100.47942	12.30400	4.0973
2	9.804	FM	0.0913	2351.83252	429.37296	95.9027

B

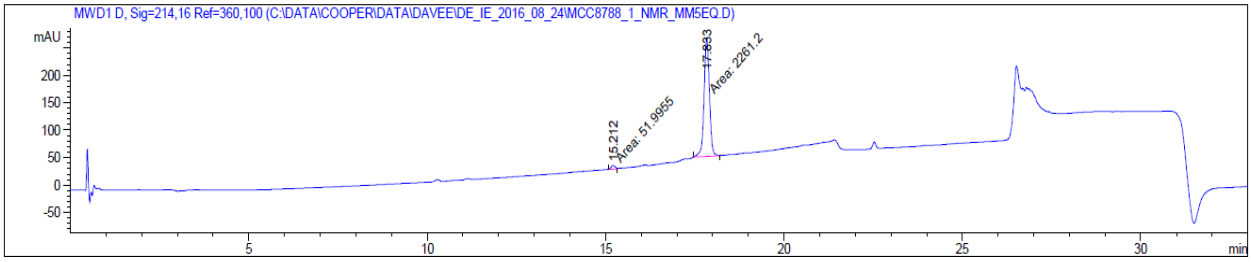

Peak #	RetTime [min]	Type	Width [min]	Area [mAU*s]	Height [mAU]	Area %
1	15.212	MM	0.1276	51.99551	6.78900	2.2478
2	17.833	MM	0.1734	2261.19824	217.30592	97.7522

Figure S7.3-80 – HPLC of 26 (TP1[Y8G]). A – In Acetonitrile solvent system. B – In Methanol solvent system.

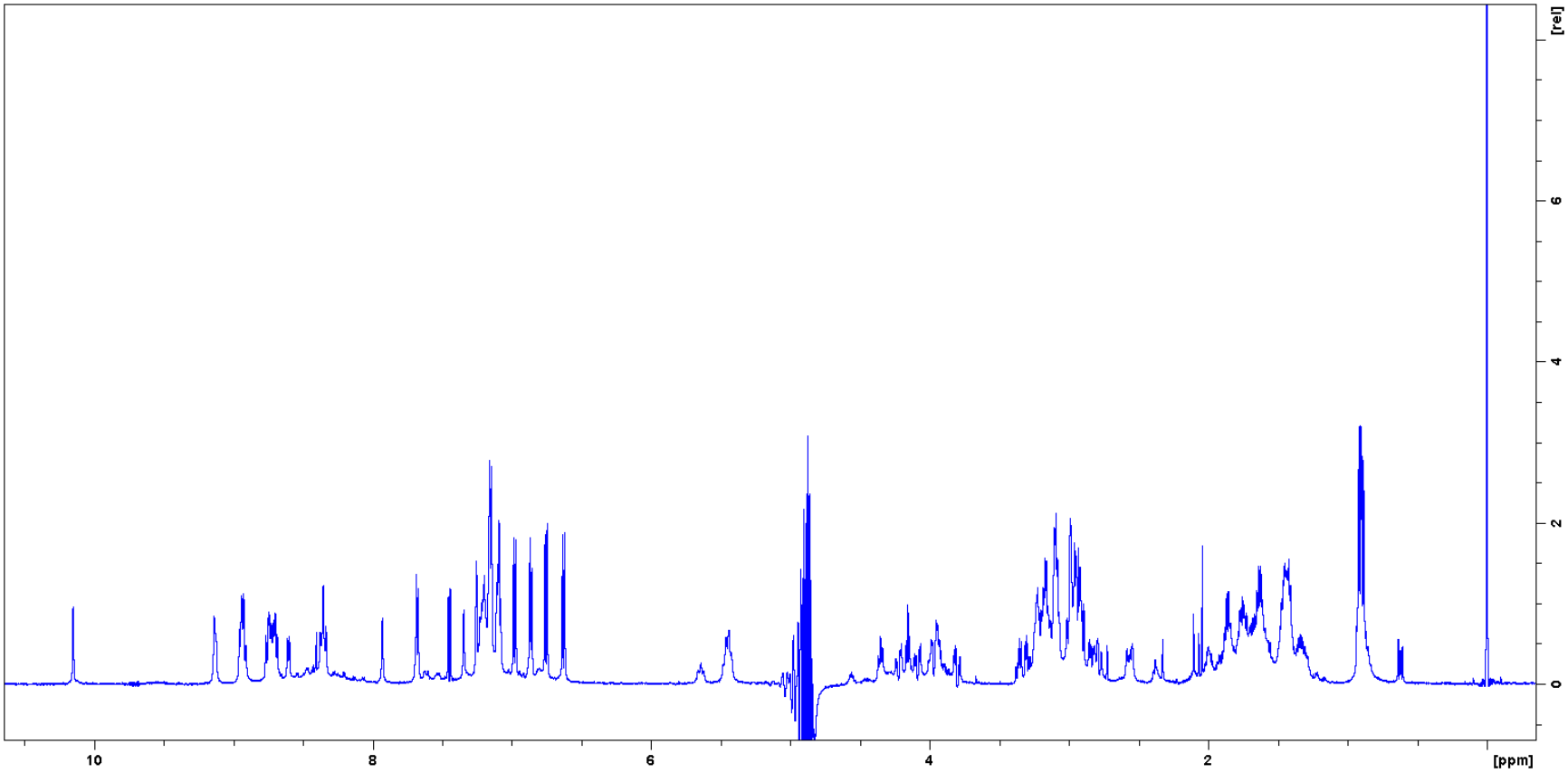

Figure S7.3-81 – ^{1}H NMR of 26 (TP1[Y8G])

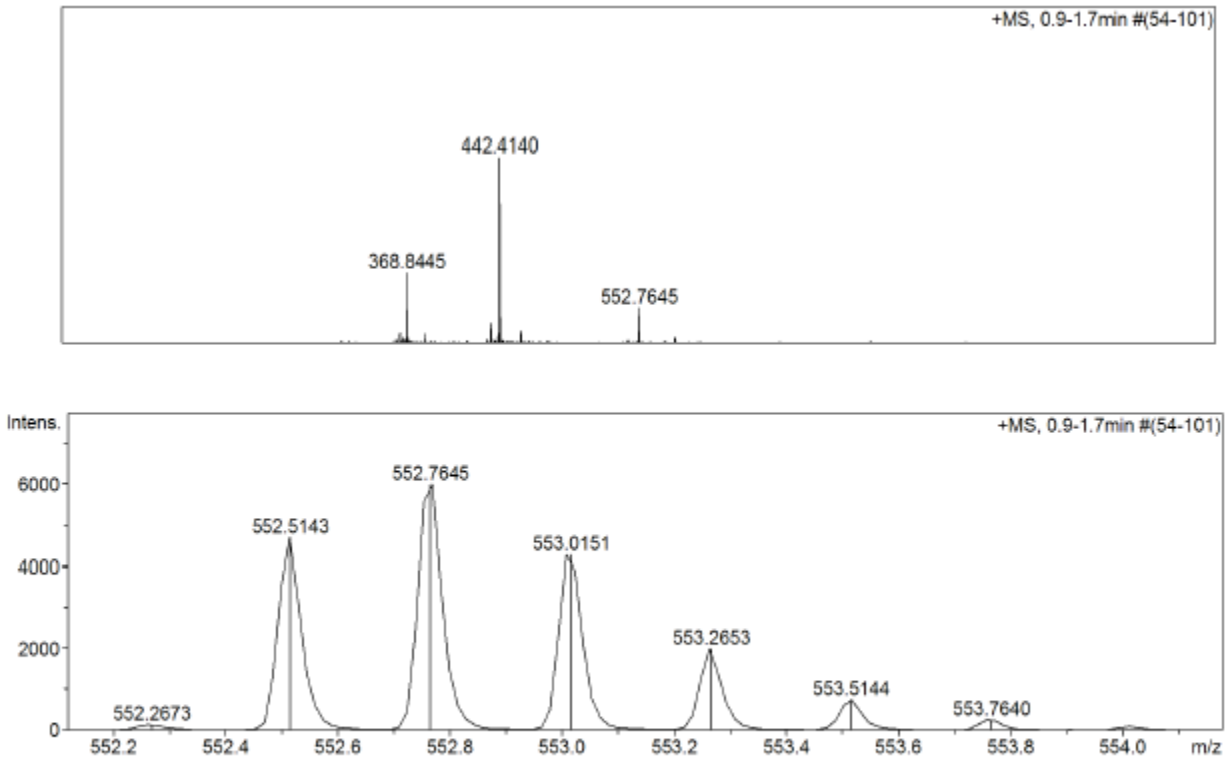

Sum Formula	Sigma	m/z	Err [ppm]	Mean Err [ppm]	Err [mDa]	rdb	N Rule	e⁻
C 95 H 147 N 35 O 19 S 4	0.067	552.5118	-4.37	-3.87	-2.42	40.00	ok	even

Figure S7.3-82 – HRMS of 27 (TP1[I11G])
HRMS-ESI (*m/z*): $[M + 4H]^{4+}$ calculated for ($C_{95}H_{143}N_{35}O_{19}S_4$ + 4H)/4, 552.5118; found 552.5143.

A

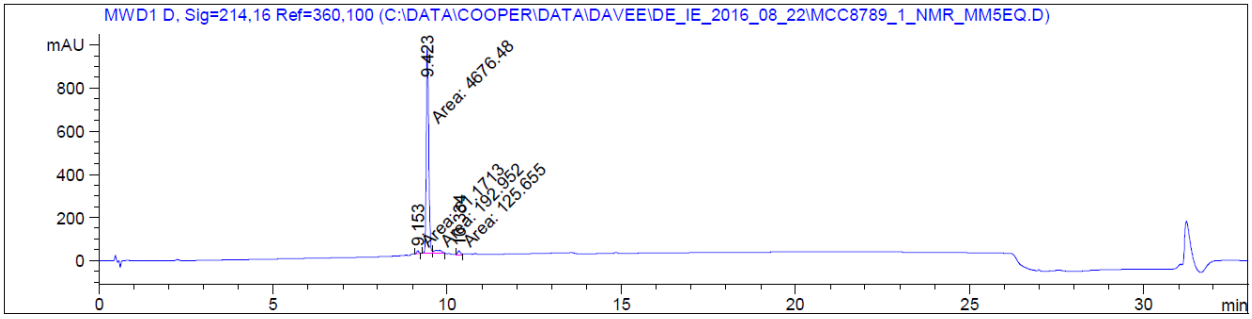

Peak #	RetTime [min]	Type	Width [min]	Area [mAU*s]	Height [mAU]	Area %
1	9.153	MM	0.0743	61.17129	13.72766	1.2098
2	9.423	MF	0.0805	4676.48389	967.70148	92.4890
3	9.686	FM	0.2349	192.95206	13.68803	3.8161
4	10.334	MM	0.1011	125.65485	20.70683	2.4851

B

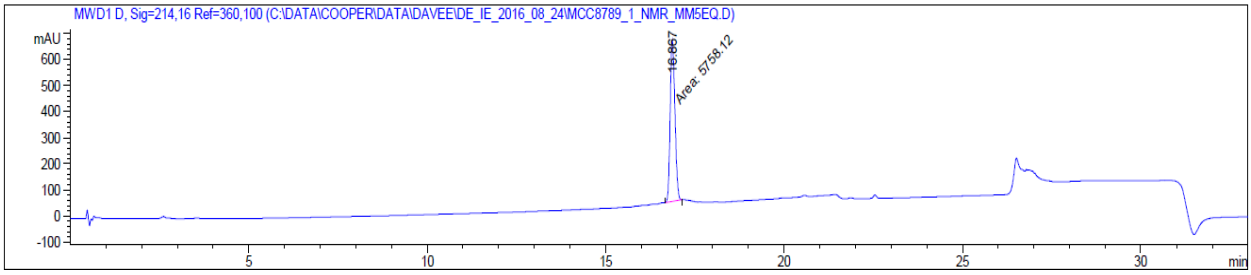

Peak #	RetTime [min]	Type	Width [min]	Area [mAU*s]	Height [mAU]	Area %
1	16.867	MM	0.1544	5758.11670	621.60376	100.0000

Figure S7.3-83 – HPLC of 27 (TP1[I11G]). A – In Acetonitrile solvent system. B – In Methanol solvent system.

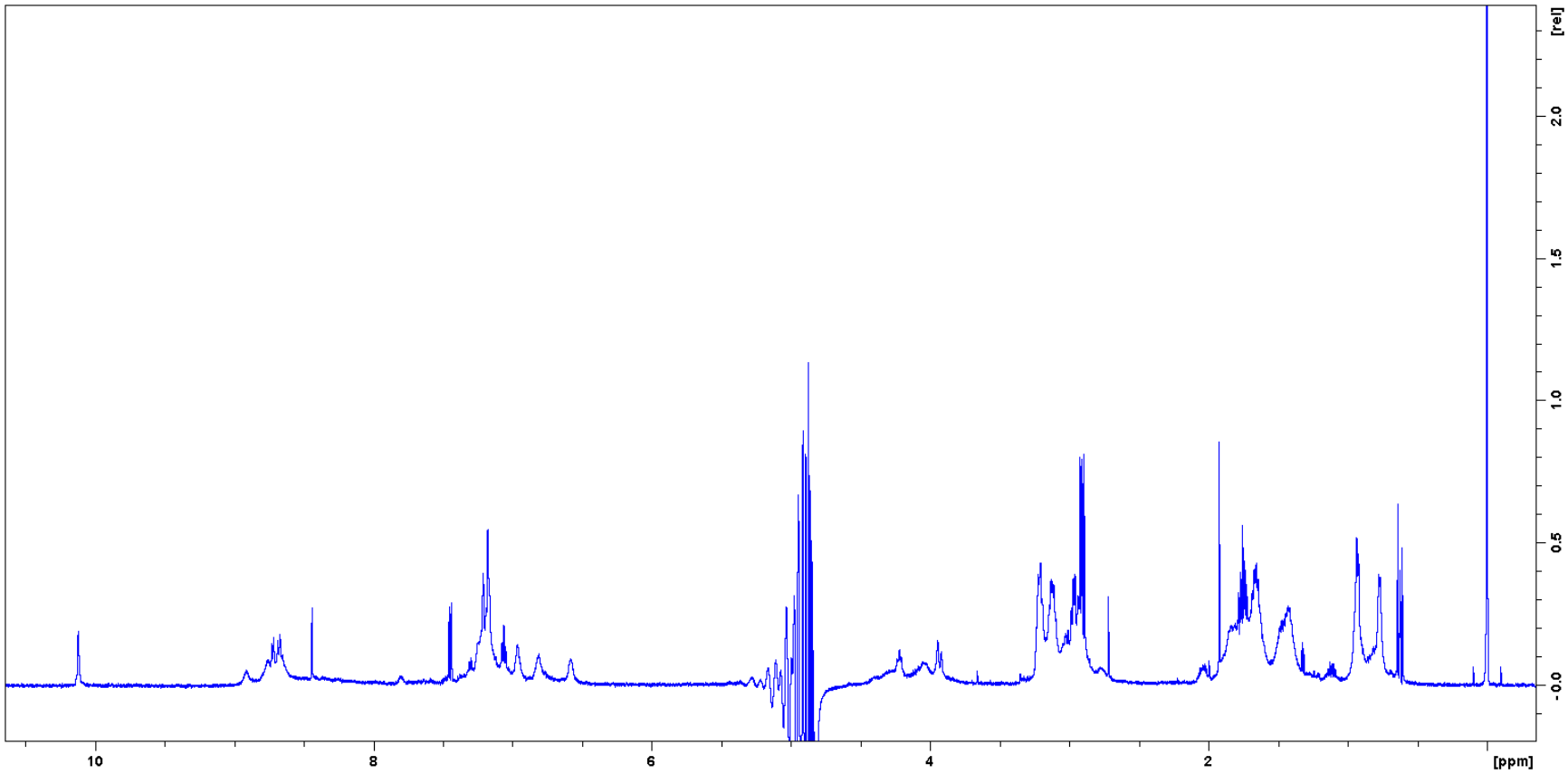

Figure S7.3-84 – ^{1}H NMR of 27 (TP1[I11G])

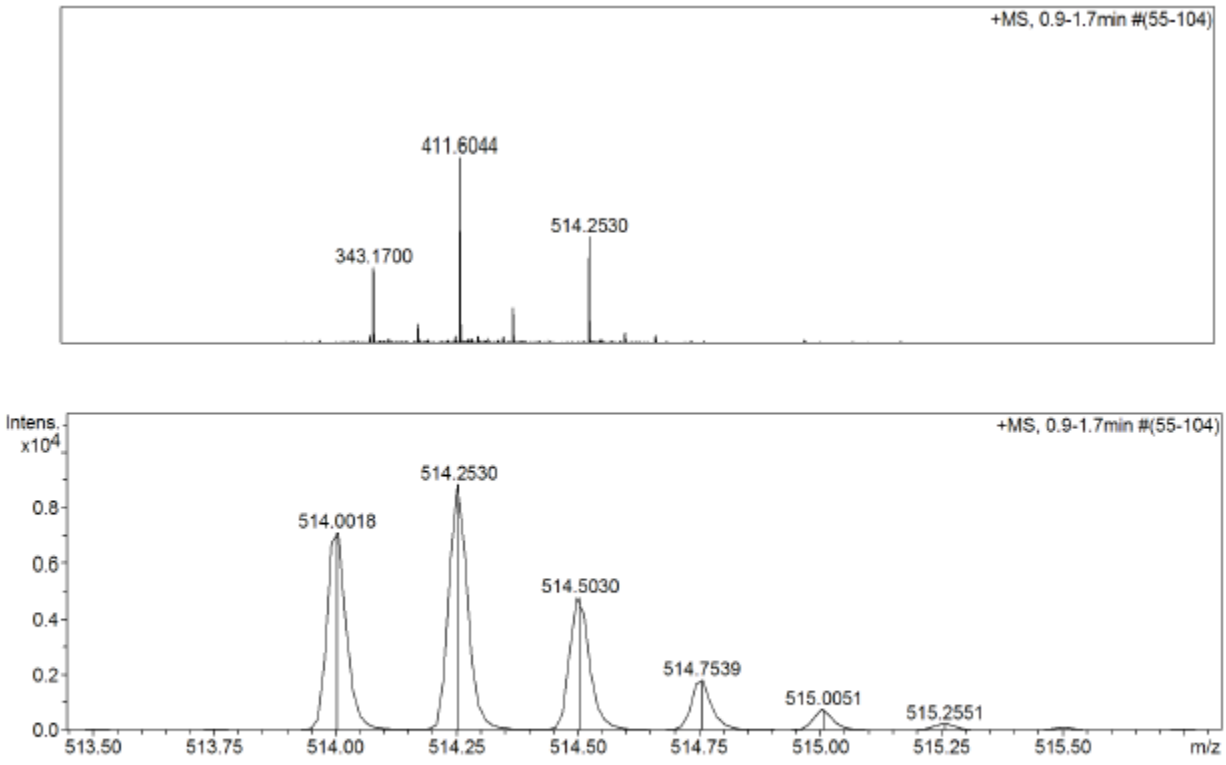

Sum Formula	Sigma	m/z	Err [ppm]	Mean Err [ppm]	Err [mDa]	rdb	N Rule	e⁻
C 84 H 141 N 35 O 18 S 4	0.124	514.0014	-0.84	-1.96	-0.43	32.00	ok	even

Figure S7.3-85 – HRMS of 28 (TP1[F4A,Y8A,I11A])
HRMS-ESI (*m/z*): $[M + 4H]^{4+}$ calculated for ($C_{84}H_{137}N_{35}O_{18}S_4$ + 4H)/4, 514.0022; found 514.0014.

A

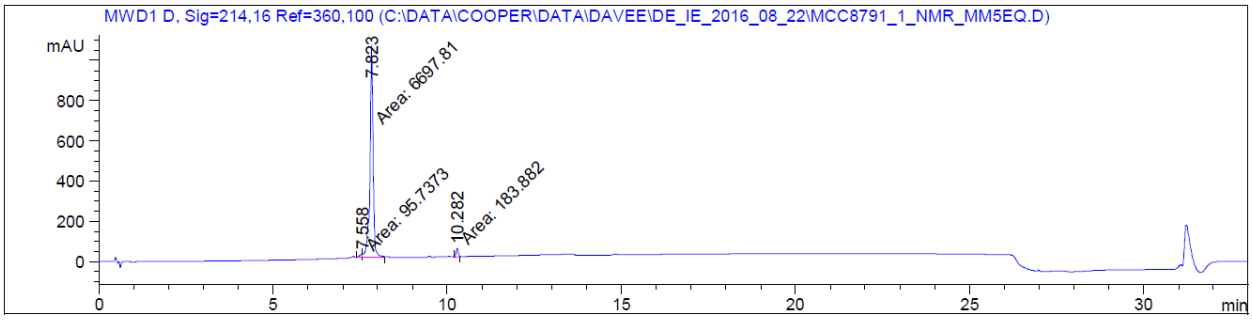

Peak #	RetTime [min]	Type	Width [min]	Area [mAU*s]	Height [mAU]	Area %
1	7.558	MF	0.1016	95.73730	15.70359	1.3721
2	7.823	FM	0.1063	6697.81445	1050.10937	95.9925
3	10.282	MM	0.0707	183.88239	43.33925	2.6354

B

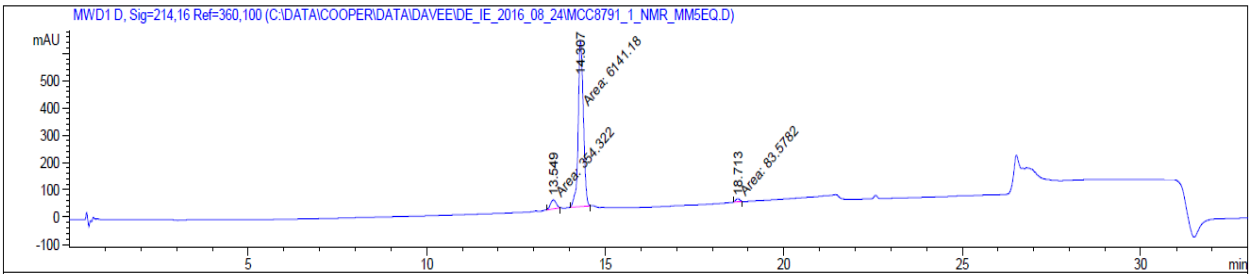

Peak #	RetTime [min]	Type	Width [min]	Area [mAU*s]	Height [mAU]	Area %
1	13.549	MM	0.1815	354.32153	32.52795	5.3856
2	14.307	MM	0.1684	6141.18311	607.96539	93.3441
3	18.713	MM	0.1245	83.57817	11.19143	1.2704

Figure S7.3-86 – HPLC of 28 (TP1[F4A,Y8A,I11A]). A – In Acetonitrile solvent system. B – In Methanol solvent system.

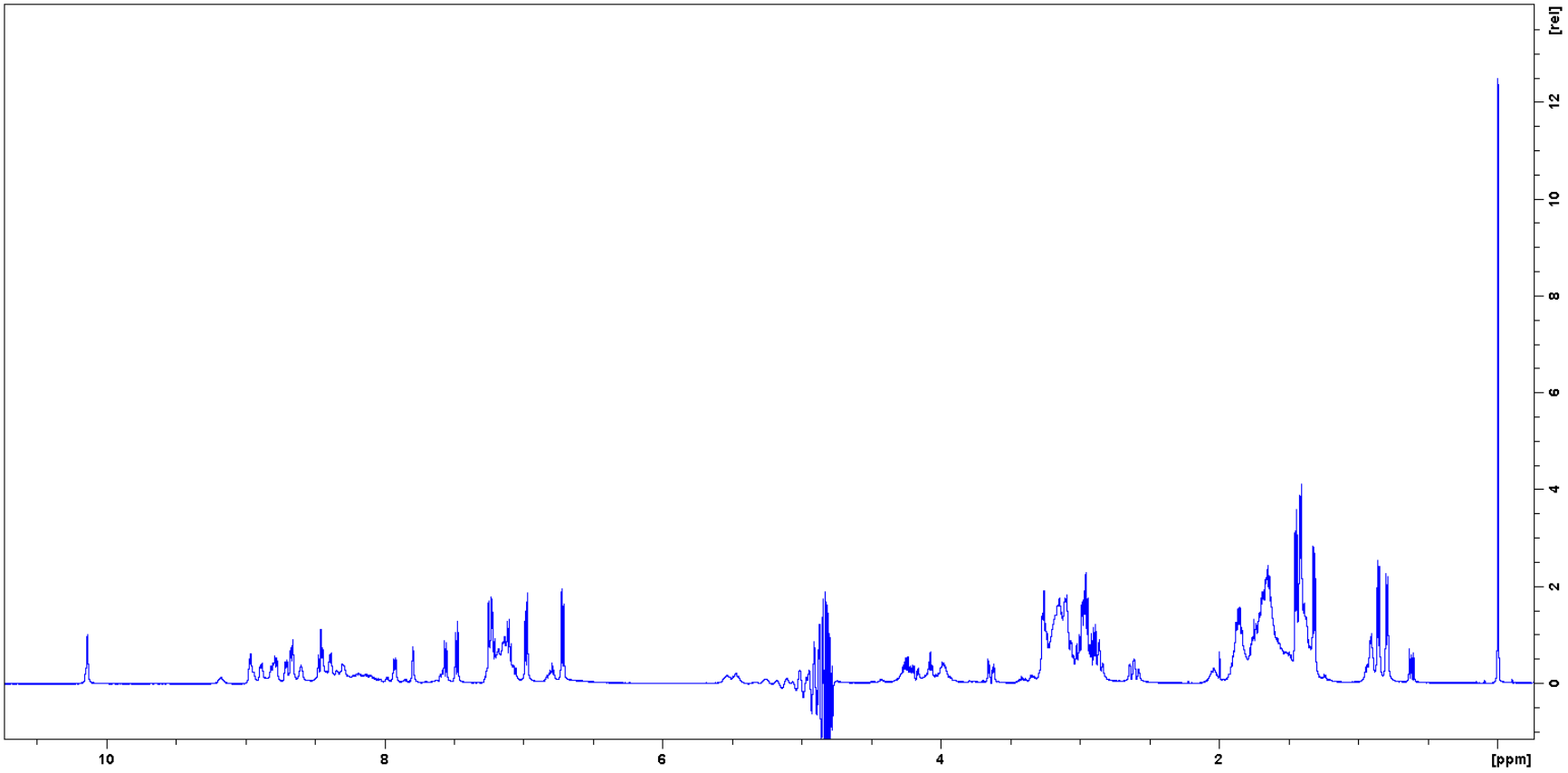

Figure S7.3-87 – ^{1}H NMR of 28 (TP1[F4A,Y8A,I11A])

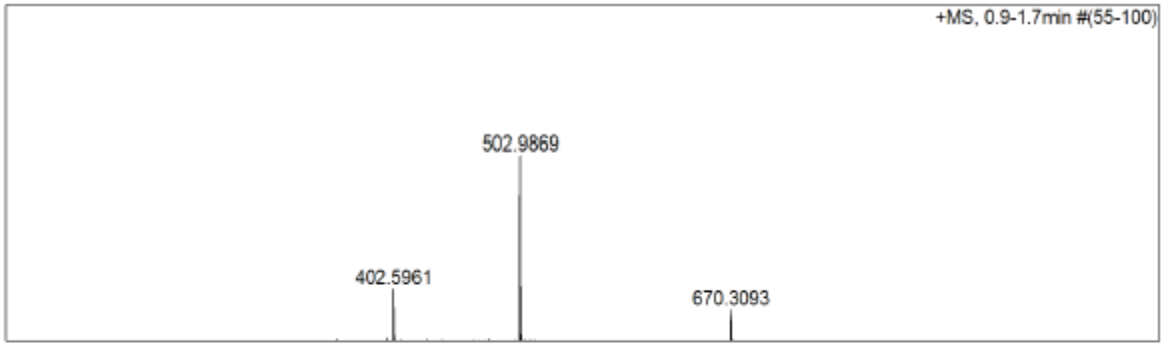

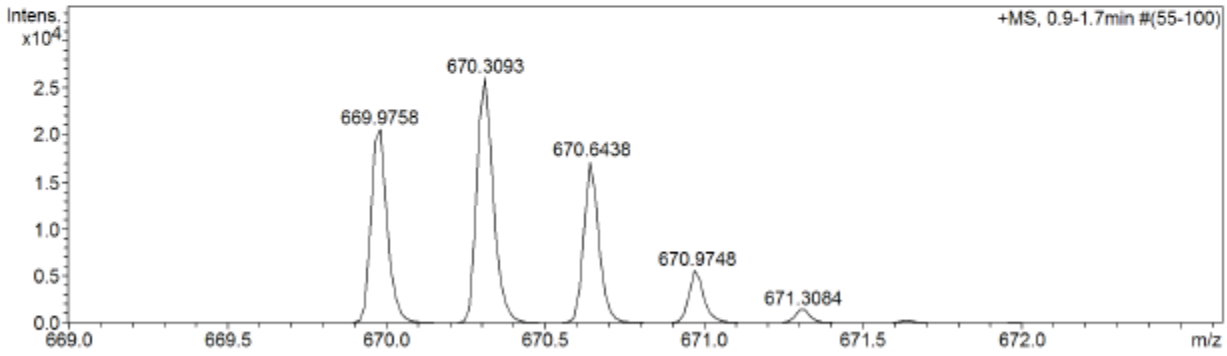

Sum Formula	Sigma	m/z	Err [ppm]	Mean Err [ppm]	Err [mDa]	rdb	N Rule	e⁻
C 89 H 133 N 28 O 18 S 4	0.111	669.9740	-2.78	-2.08	-1.86	37.50	ok	even

Figure S7.3-88 – HRMS of 29 (TP1[–R5,R17G])
HRMS-ESI (*m/z*): $[M + 3H]^{3+}$ calculated for ($C_{89}H_{130}N_{28}O_{18}S_4$ + 3H)/3, 669.9740; found 669.9758.

A

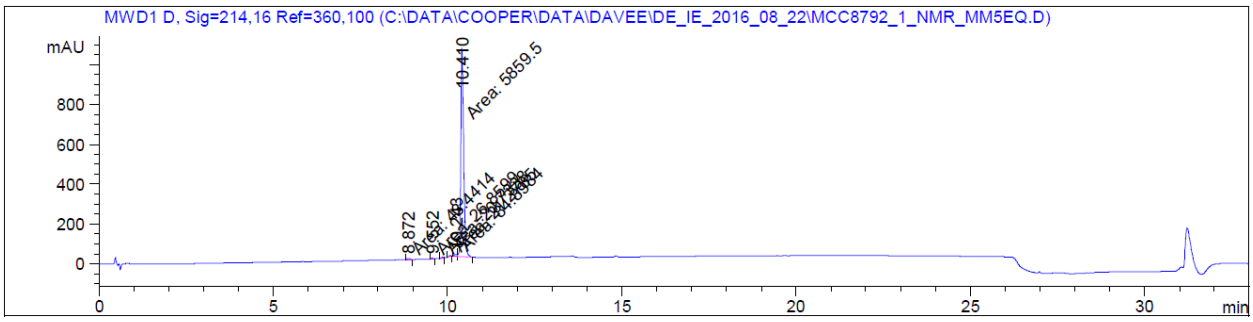

Peak #	RetTime [min]	Type	Width [min]	Area [mAU*s]	Height [mAU]	Area %
1	8.872	MM	0.1115	43.44145	6.49556	0.7172
2	9.552	MM	0.0931	26.85991	4.80887	0.4435
3	9.849	MM	0.0779	20.73376	4.43836	0.3423
4	10.070	MM	0.0662	21.27855	5.35526	0.3513
5	10.243	MF	0.1153	84.89840	12.26987	1.4017
6	10.410	FM	0.0928	5859.50146	1052.74414	96.7439

B

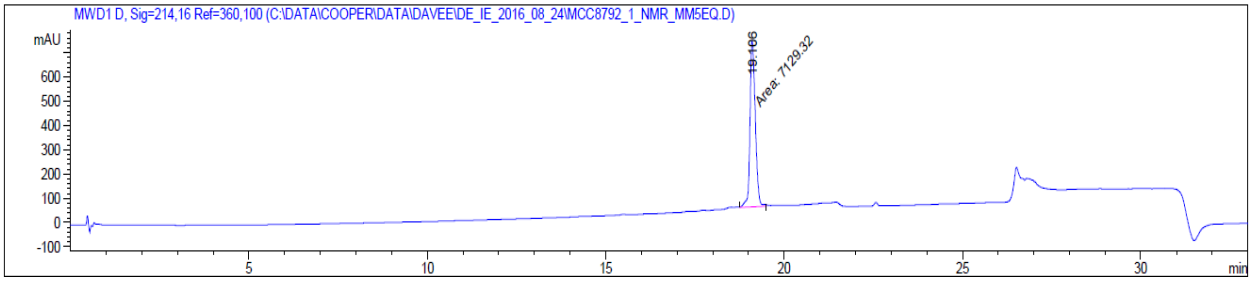

Peak #	RetTime [min]	Type	Width [min]	Area [mAU*s]	Height [mAU]	Area %
1	19.106	MM	0.1730	7129.32031	686.99573	100.0000

Figure S7.3-89 – HPLC of 29 (TP1[–R5,R17G]). A – In Acetonitrile solvent system. B – In Methanol solvent system.

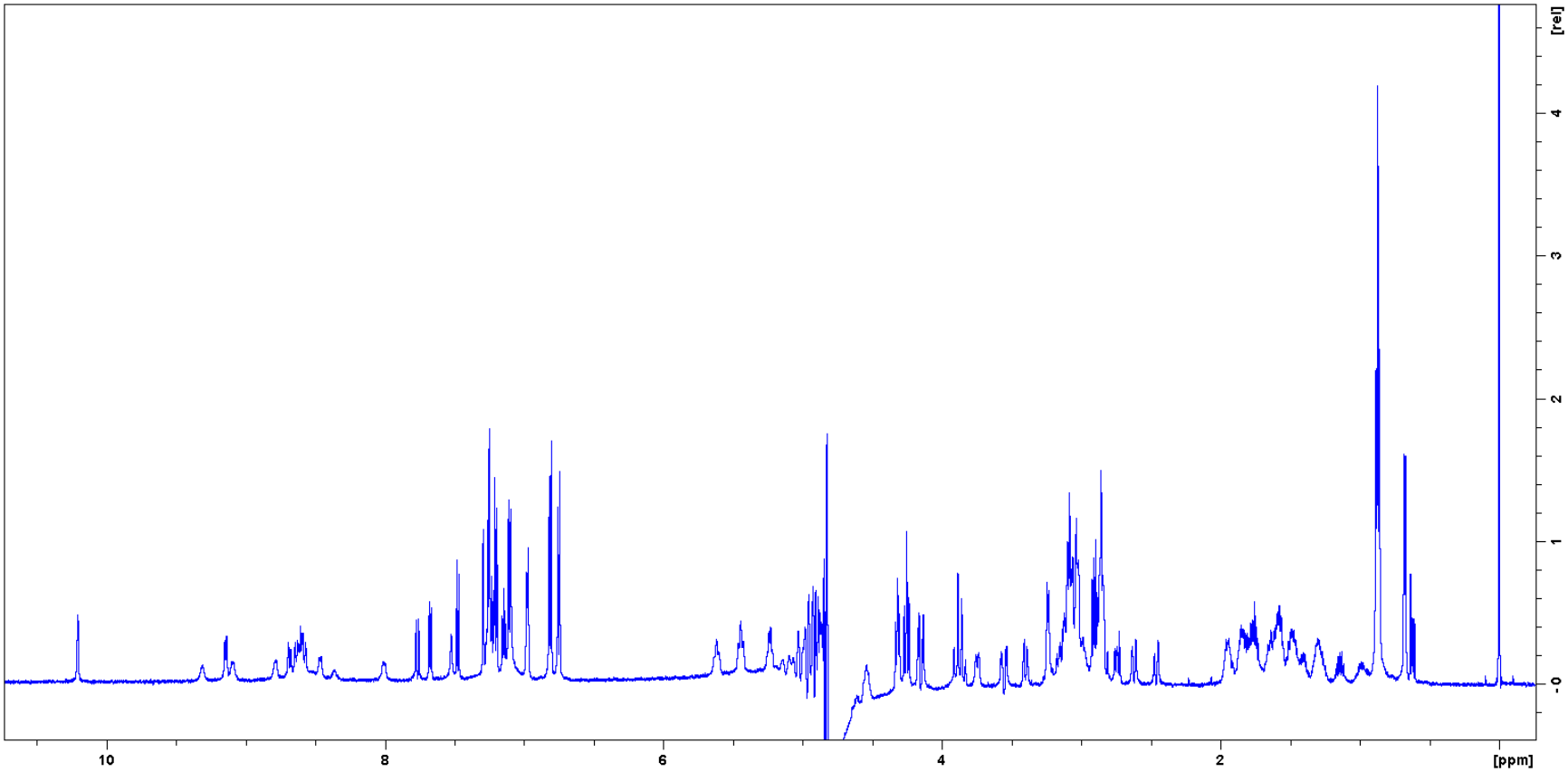

Figure S7.3-90 – ^{1}H NMR of 29 (TP1[–R5,R17G])

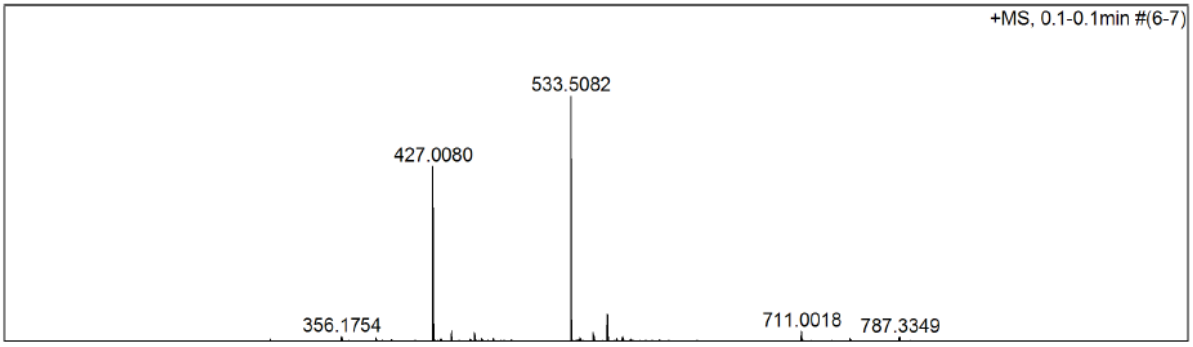

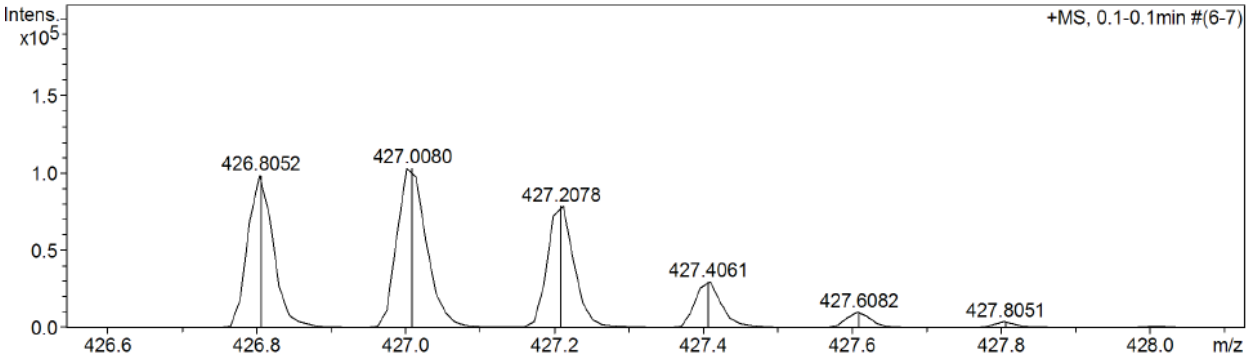

Sum Formula	Sigma	m/z	Err [ppm]	Mean Err [ppm]	Err [mDa]	rdb	N Rule	e⁻
C 90 H 145 N 34 O 19 S 4	0.074	426.8056	0.91	-1.82	0.39	35.50	ok	even

Figure S7.3-91 – HRMS of 30 (TP1[K1A,F4A])
HRMS-ESI (*m/z*): $[M + 5H]^{5+}$ calculated for ($C_{90}H_{140}N_{34}O_{19}S_4$ + 5H)/5, 426.8056; found 426.8052.

A

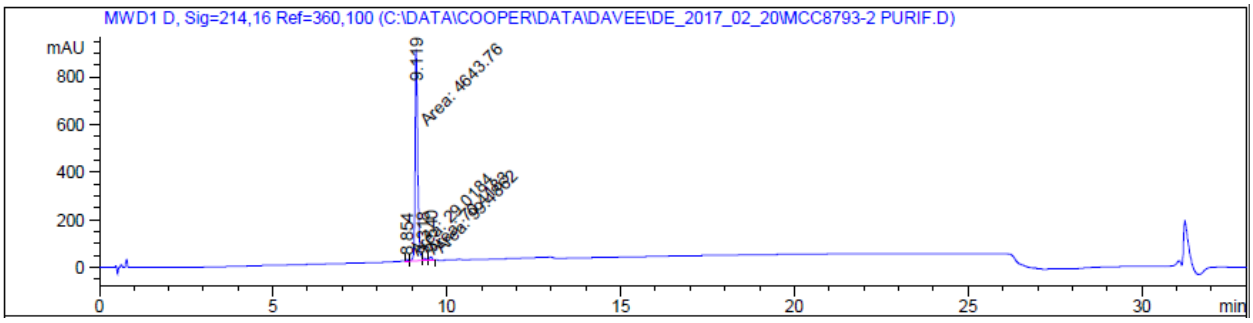

Peak #	RetTime [min]	Type	Width [min]	Area [mAU*s]	Height [mAU]	Area %
1	8.854	MM	0.0751	29.01841	6.44127	0.5992
2	9.119	MF	0.0869	4643.75732	890.50659	95.8923
3	9.318	MF	0.0907	70.41832	9.93906	1.4541
4	9.540	FM	0.0995	99.48624	16.65638	2.0544

B

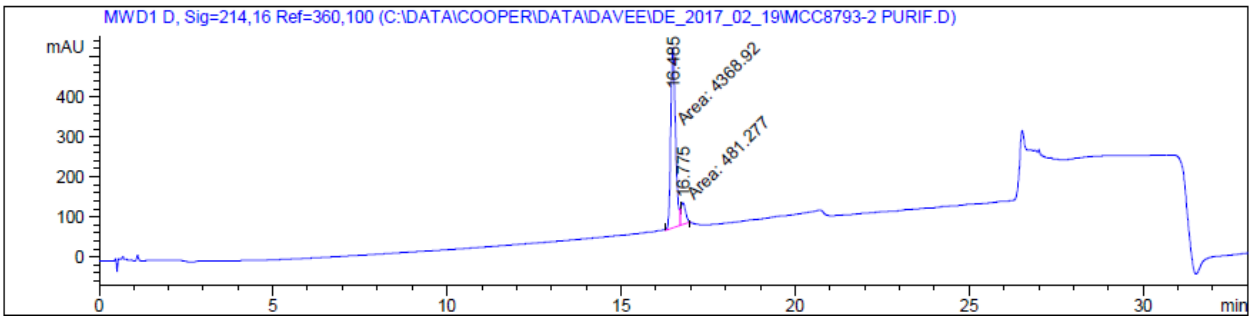

Peak #	RetTime [min]	Type	Width [min]	Area [mAU*s]	Height [mAU]	Area %
1	16.485	MF	0.1620	4368.91650	449.44083	90.0772
2	16.775	FM	0.1488	481.27704	53.91403	9.9228

Figure S7.3-92 – HPLC of 30 (TP1[K1A,F4A]). A – In Acetonitrile solvent system. B – In Methanol solvent system.

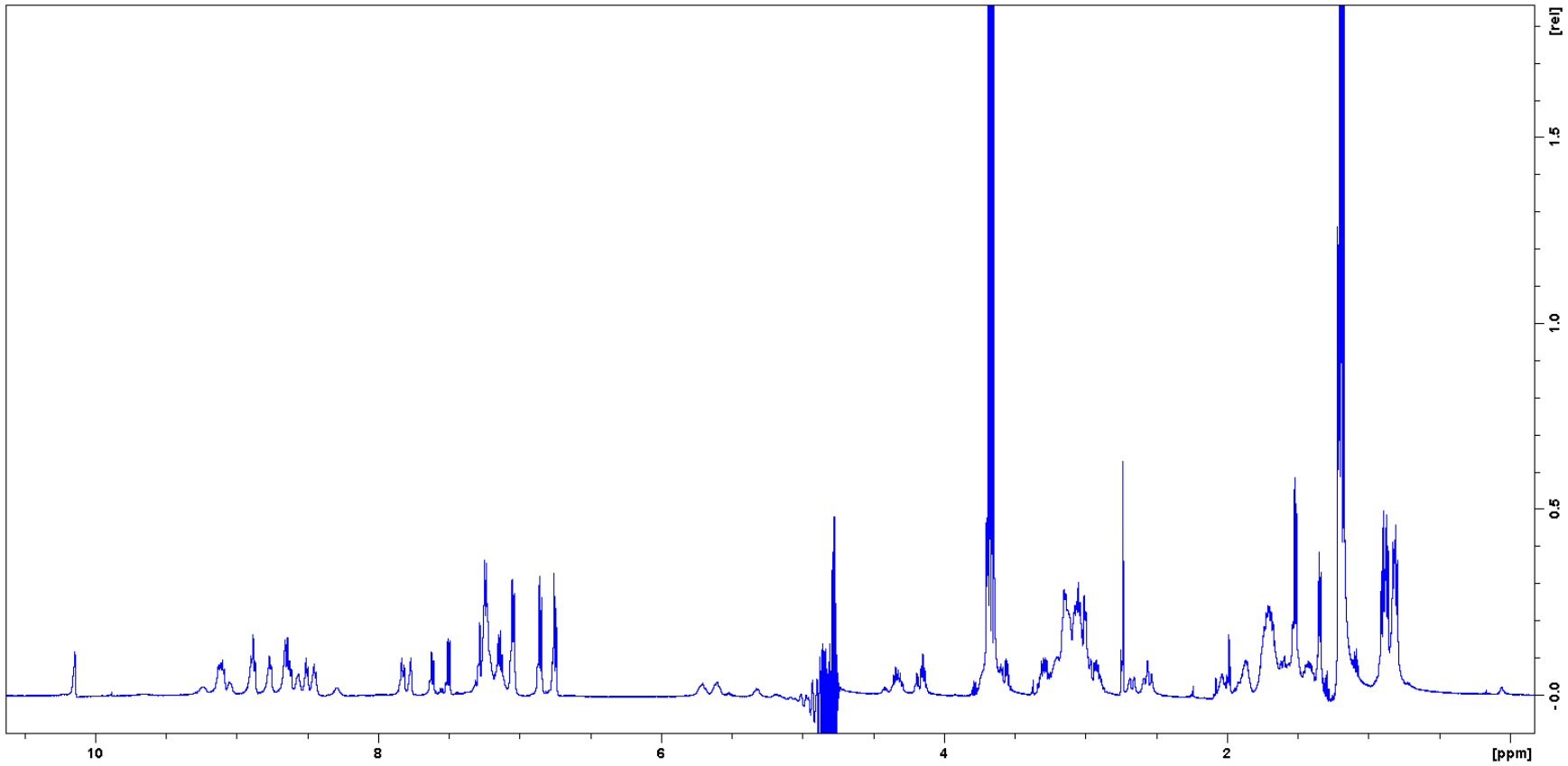

Figure S7.3-93 -^{1}H NMR of 30 (TP1[K1A,F4A]). The quadruplet at 3.65 and the triplet at 1.17 ppm are residual ethanol.

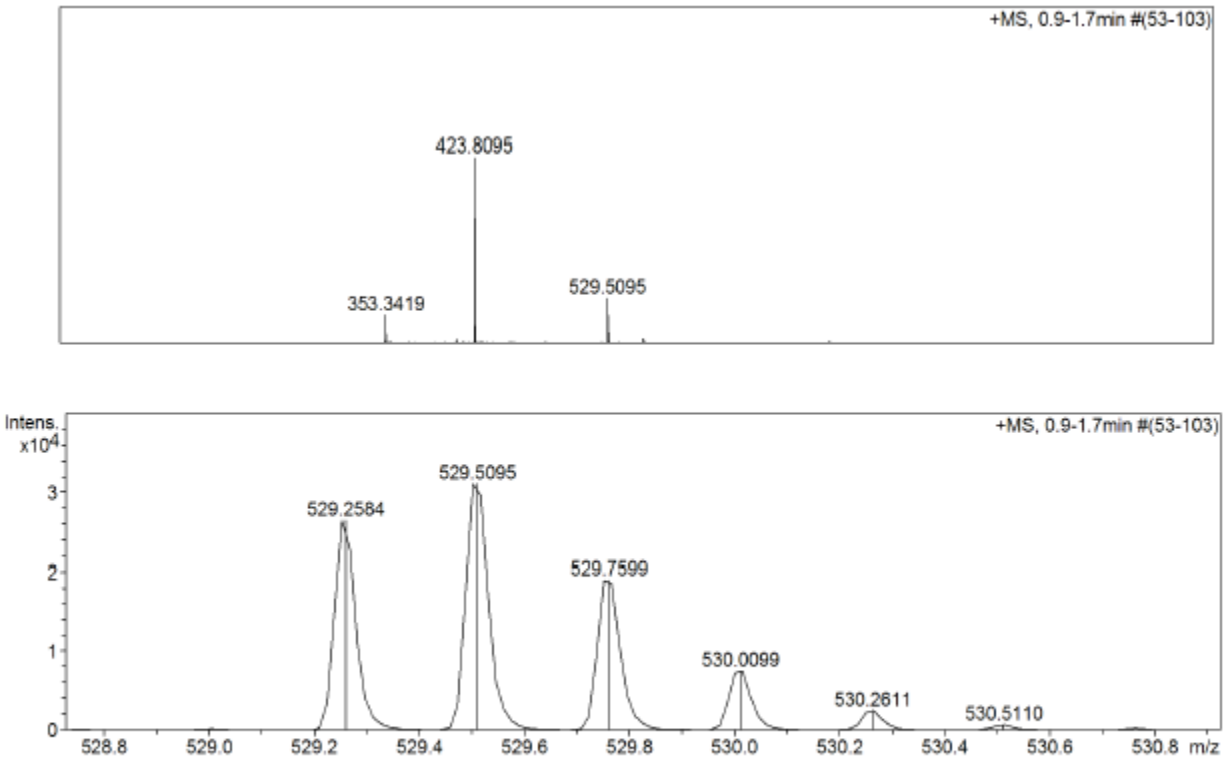

Sum Formula	Sigma	m/z	Err [ppm]	Mean Err [ppm]	Err [mDa]	rdb	N Rule	e⁻
C 90 H 144 N 34 O 18 S 4	0.099	529.2565	-3.74	-4.40	-1.98	36.00	ok	even

Figure S7.3-94 – HRMS of 31 (TP1[K1A,Y8A])
HRMS-ESI (*m/z*): $[M + 4H]^{4+}$ calculated for ($C_{90}H_{140}N_{34}O_{18}S_4$ + 4H)/4, 529.2565; found 529.2584.

A

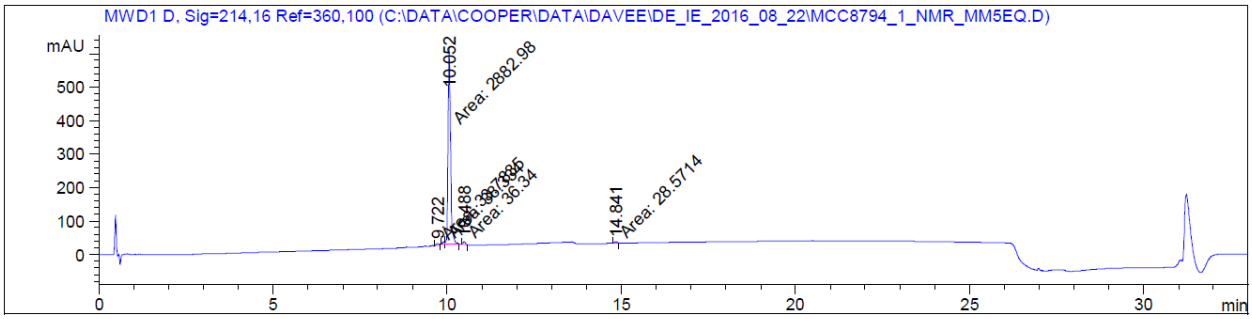

Peak #	RetTime [min]	Type	Width [min]	Area [mAU*s]	Height [mAU]	Area %
1	9.722	MM	0.0961	33.78354	5.85687	1.1187
2	9.900	MF	0.0829	38.33397	7.70273	1.2693
3	10.052	FM	0.0810	2882.97559	592.88971	95.4626
4	10.488	MM	0.0719	36.33997	8.42234	1.2033
5	14.841	MM	0.0886	28.57145	5.37686	0.9461

B

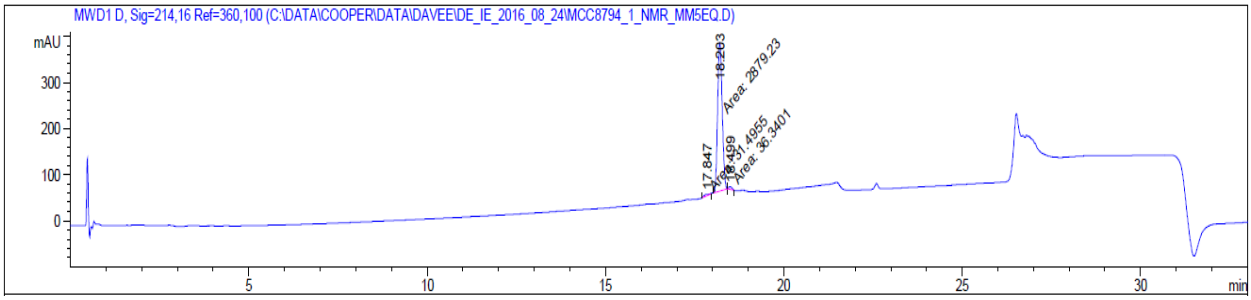

Peak #	RetTime [min]	Type	Width [min]	Area [mAU*s]	Height [mAU]	Area %
1	17.847	MM	0.1870	31.49552	2.80703	1.0687
2	18.203	MM	0.1494	2879.23462	321.27274	97.6982
3	18.499	MM	0.1048	36.34012	5.77761	1.2331

Figure S7.3-95 – HPLC of 31 (TP1[K1A,Y8A]). A – In Acetonitrile solvent system. B – In Methanol solvent system.

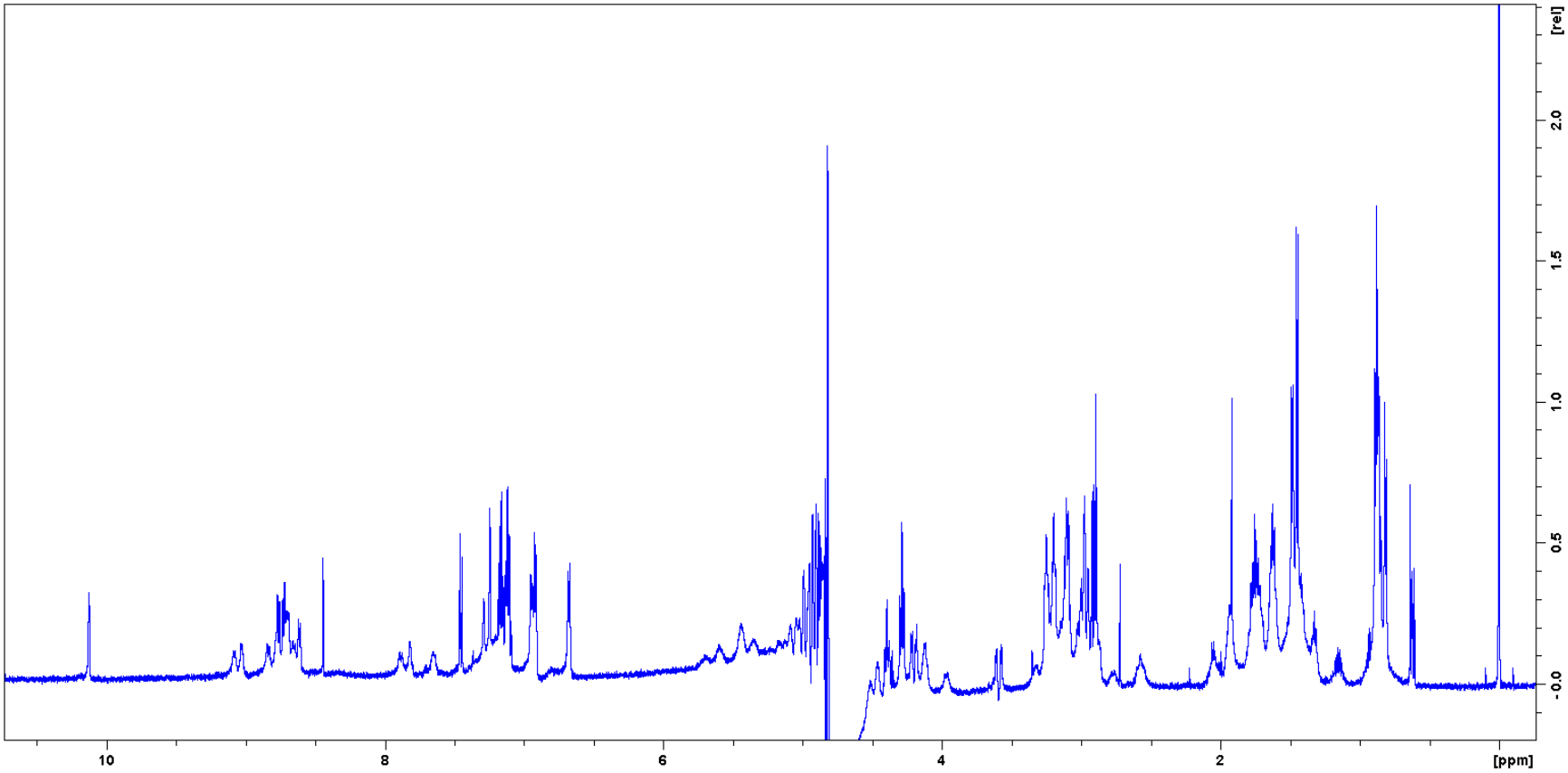

Figure S7.3-96 – ^{1}H NMR of 31 (TP1[K1A,Y8A])

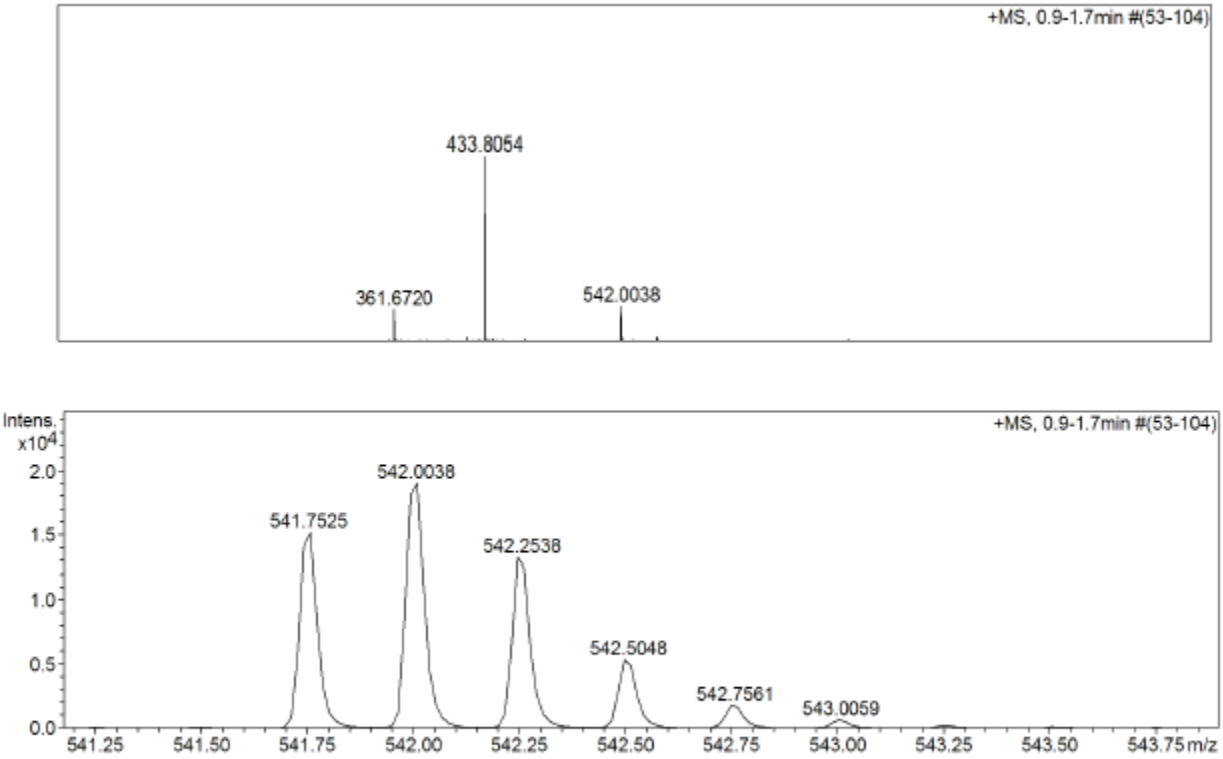

Sum Formula	Sigma	m/z	Err [ppm]	Mean Err [ppm]	Err [mDa]	rdb	N Rule	e⁻
C 93 H 142 N 34 O 19 S 4	0.082	541.7513	-2.29	-3.45	-1.24	40.00	ok	even

Figure S7.3-97 – HRMS of 32 (TP1[K1A,I11A])
HRMS-ESI (*m/z*): $[M + 4H]^{4+}$ calculated for ($C_{93}H_{138}N_{34}O_{19}S_4$ + 4H)/4, 541.7513; found 541.7525.

A

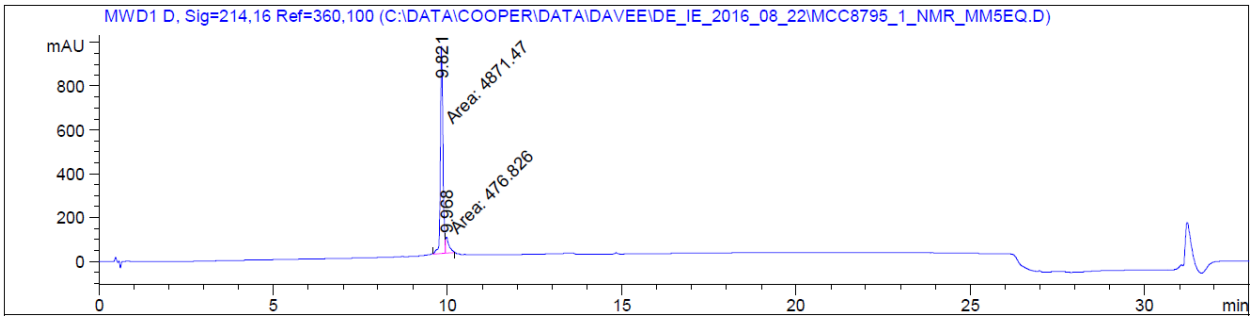

Peak #	RetTime [min]	Type	Width [min]	Area [mAU*s]	Height [mAU]	Area %
1	9.821	MF	0.0853	4871.46875	951.43951	91.0845
2	9.968	FM	0.1102	476.82648	72.12893	8.9155

B

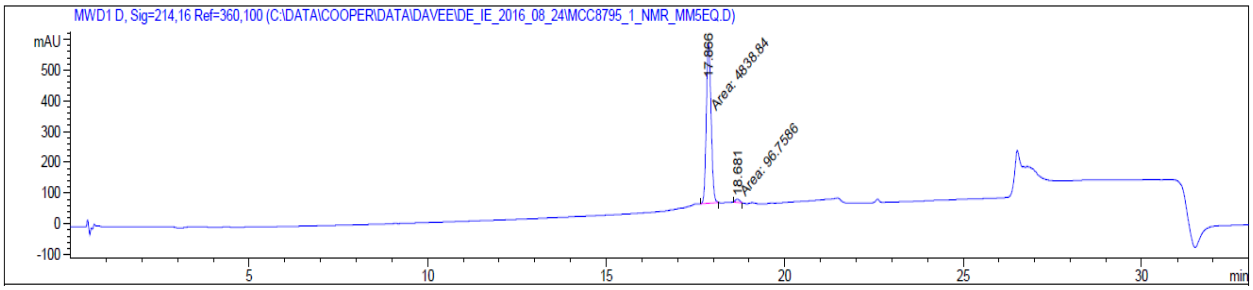

Peak #	RetTime [min]	Type	Width [min]	Area [mAU*s]	Height [mAU]	Area %
1	17.866	MM	0.1541	4838.83691	523.31207	98.0396
2	18.681	MM	0.1416	96.75859	11.39091	1.9604

Figure S7.3-98 – HPLC of 32 (TP1[K1A,I11A]). A – In Acetonitrile solvent system. B – In Methanol solvent system.

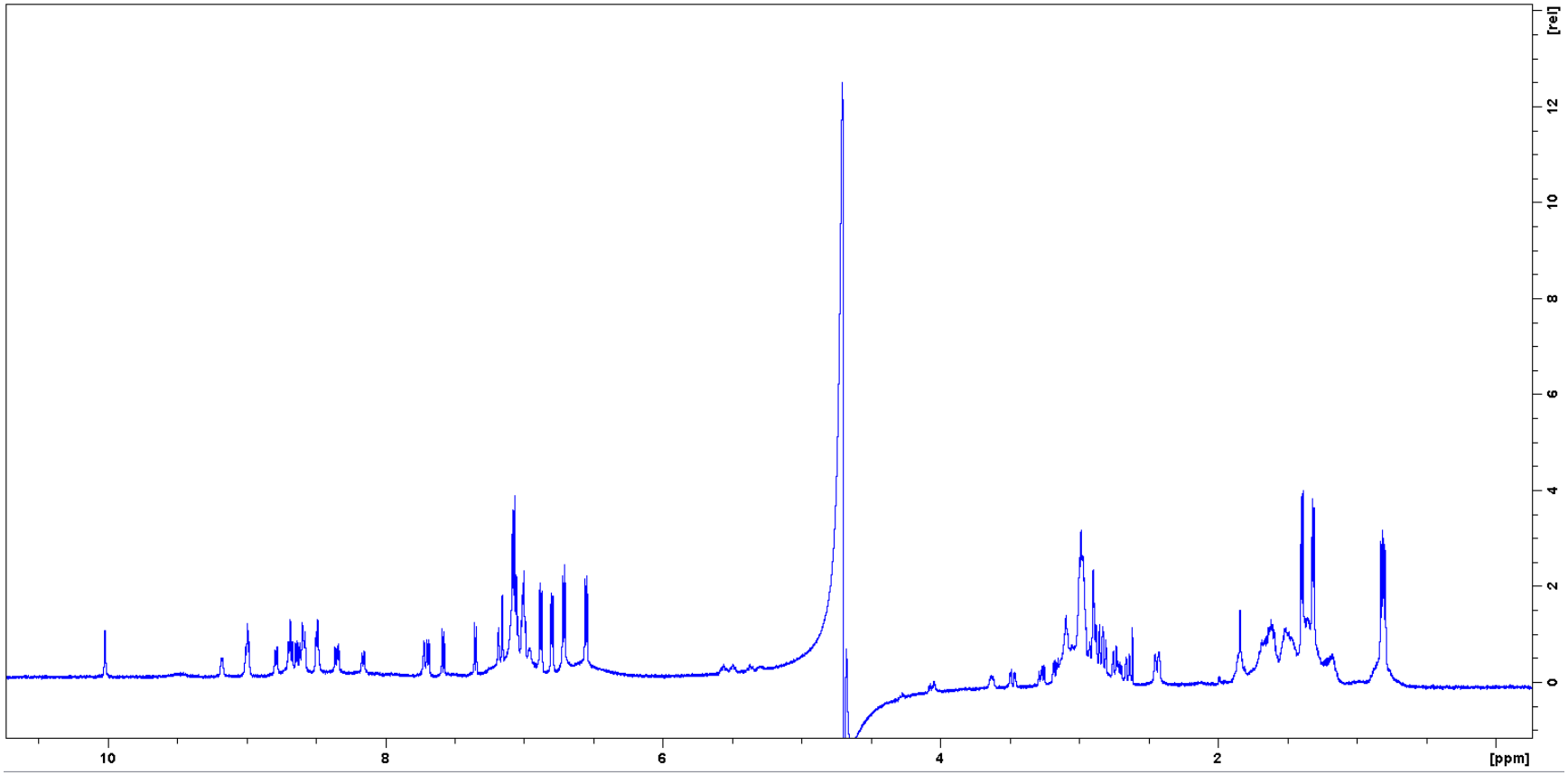

Figure S7.3-99 – ^{1}H NMR of 32 (TP1[K1A,I11A])

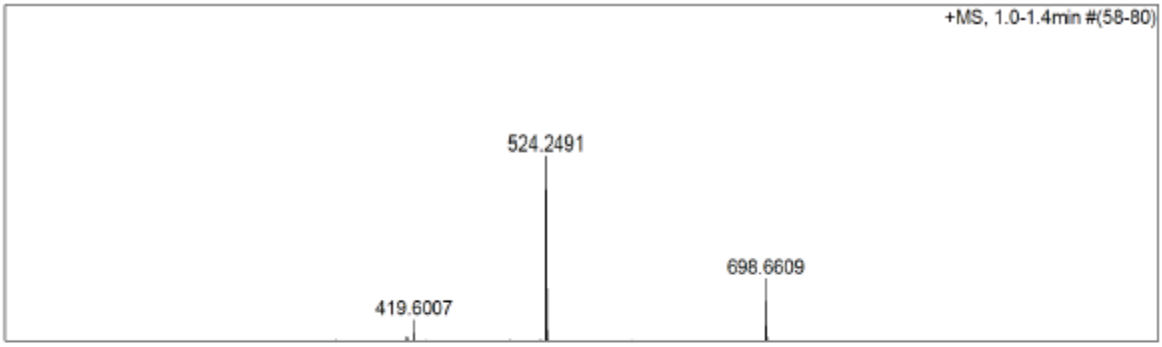

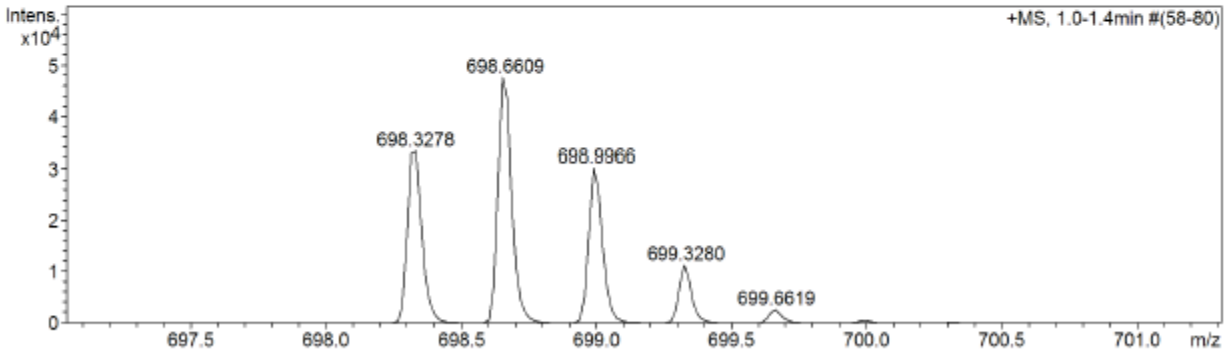

Sum Formula	Sigma	m/z	Err [ppm]	Mean Err [ppm]	Err [mDa]	rdb	N Rule	e⁻
C 93 H 140 N 29 O 19 S 4	0.120	698.3249	-4.14	-3.34	-2.89	38.50	ok	even

Figure S7.3-100 – HRMS of 33 (TP1[R9A,R17A])
HRMS-ESI (*m/z*): $[M + 3H]^{3+}$ calculated for ($C_{93}H_{137}N_{29}O_{19}S_4$ + 3H)/3, 698.3249; found 698.3278.

A

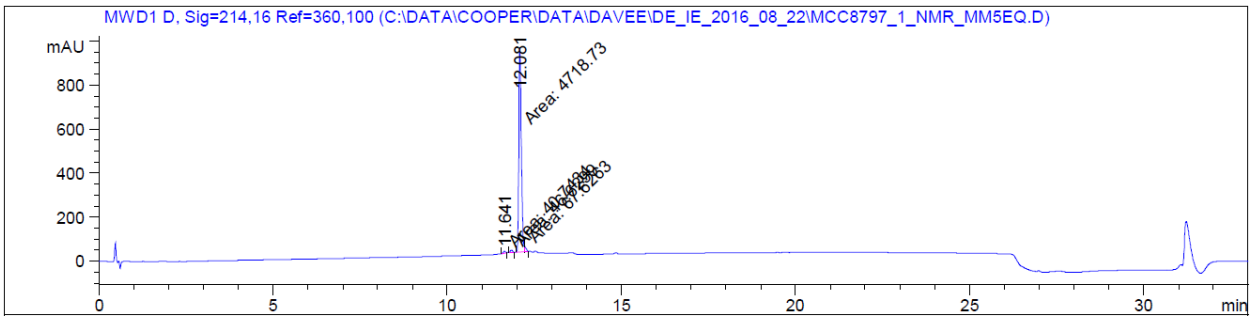

Peak #	RetTime [min]	Type	Width [min]	Area [mAU*s]	Height [mAU]	Area %
1	11.641	MM	0.0807	40.74339	8.41289	0.8360
2	11.842	MM	0.0784	46.62994	9.91646	0.9568
3	12.081	MF	0.0845	4718.73438	930.66034	96.8197
4	12.224	FM	0.0467	67.62631	24.13194	1.3876

B

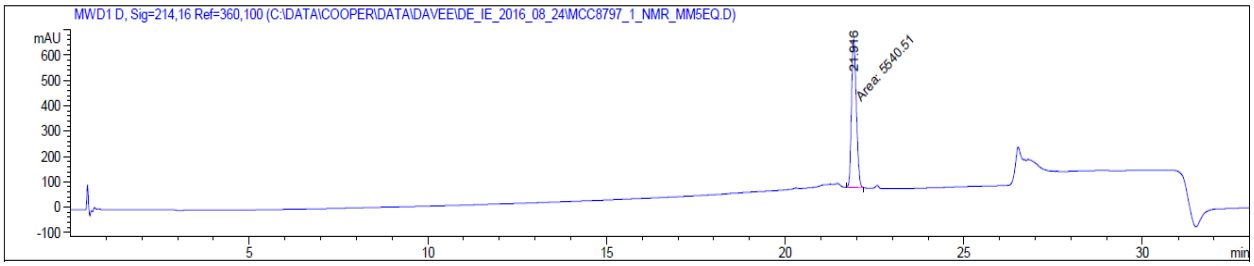

Peak #	RetTime [min]	Type	Width [min]	Area [mAU*s]	Height [mAU]	Area %
1	21.916	MM	0.1574	5540.50586	586.57788	100.0000

Figure S7.3-101 – HPLC of 33 (TP1[R9A,R17A]). A – In Acetonitrile solvent system. B – In Methanol solvent system.

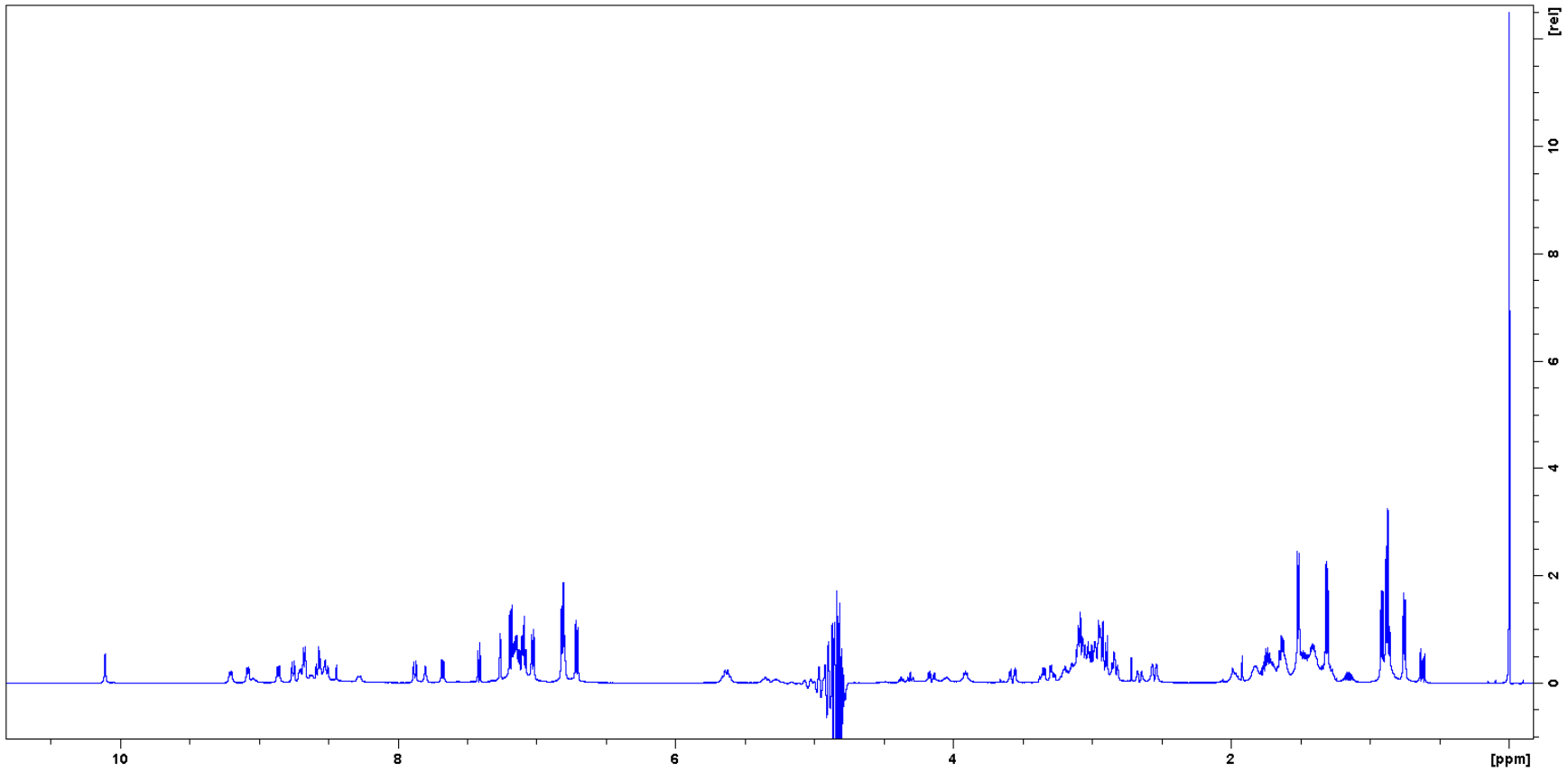

Figure S7.3-102 – ^{1}H NMR of 33 (TP1[R9A,R17A])

A

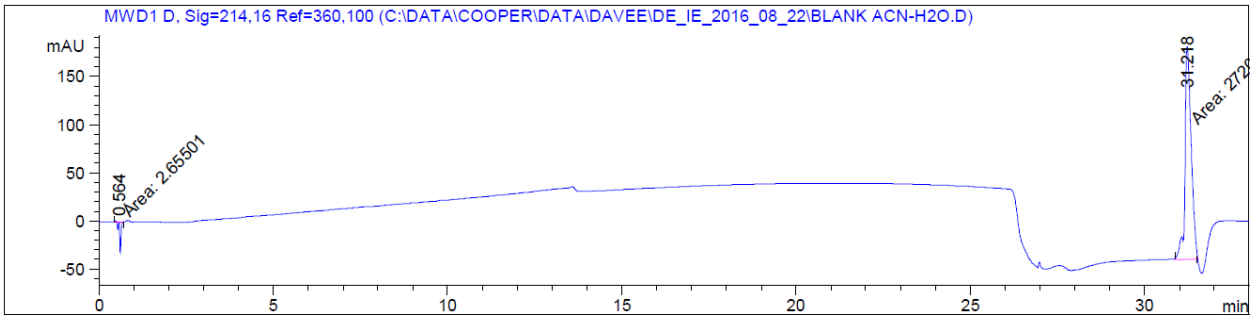

B

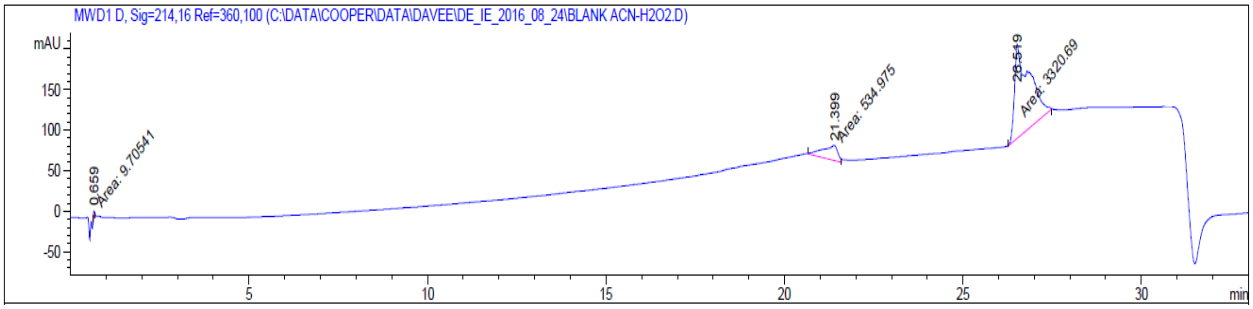

Figure S7.3-103 – HPLC of blank solution. A – In Acetonitrile solvent system. B – In Methanol solvent system.

Table S7.3-104 – Analytical data of TP1 and analogs.

Peptide	HPLC	
	k'[a]	k'[b]
1	15.0	27.3
2	15.4	27.8
3	13.5	23.9
4	15.3	26.8
5	13.5	24.8
6	16.3	29.6
7	14.8	27.0
8	14.9	25.6
9	14.4	26.0
10	16.2	28.6
11	15.4	28.0
12	14.2	25.4
13	16.0	29.2
14	14.8	27.1
15	16.1	28.2
16	16.7	30.2
17	15.1	27.2
18	17.0	30.9
19	15.1	27.2
20	15.0	26.8
21	15.2	27.2
22	14.8	25.6
23	14.8	26.1
24	12.8	23.2
25	13.0	23.3
26	14.6	26.1
27	14.0	24.6
28	11.5	20.7
29	15.6	28.0
30	13.5	24.0
31	15.0	26.6
32	14.6	26.1
33	18.2	32.3

k’ = [(peptide retention time – solvent retention time)/solvent retention time].
in 0.1% TFA in H2O / 0.1% TFA in AcN at 214 nm
in 0.1% TFA in H2O / 0.1% TFA in MeOH at 214 nm

7.4 Appendix IV - Supplementary information Chapter 4

Table S7.4-1 – Microbial strains and cell line used for the antimicrobial assay.

Organism	Strains	Comment
Escherichia coli	ATCC 25922	FDA control
Escherichia coli	CGSC 7139	DC2
Escherichia coli	MB 4902	lpxC mutant
Escherichia coli	MB 5747	tolC mutant
Escherichia coli	MB 5746	lpxC and tolC mutant
Escherichia coli	ATCC 700926	MG 1655; K12 substr
Escherichia coli	CGSC 5167	D31; Ampicillin resistant
Klebsiella pneumoniae	ATCC 700603	Multi-drug Resistant (MDR)
Klebsiella pneumoniae	ATCC 13883	Type strain
Klebsiella pneumoniae	ATCC BAA-2146	New Delhi Metallo-beta-lactamase-1 (NDM-1) positive
Acinetobacter baumannii	ATCC 19606	Type strain
Pseudomonas aeruginosa	ATCC27053	Type strain
Bacillus subtilis	ATCC 6051	Type strain
Staphylococcus aureus	ATCC 43300	Methicillin Resistant *Staphylococcus aureus* (MRSA)
Candida albicans	ATCC 90028	CLSI reference strain
Cryptococcus neoformans var grubii	ATCC 208821	H99, Type strain
HepG2	ATCC HB-8065	Hepatocellular carcinoma liver cells
HEK293	ATCC CRL-1573	Embryonic kidney cells

Peptide Characterisation

Final purity of more than 95 % for all compounds was confirmed by LC-MS analysis using both ELSD and UV (210 nm) detection. LC-MS analysis were conducted using Agilent Technologies 1200 Series Instrument with a G1316A variable wavelength detector set at λ= 210 nm, 1200 Series ELSD, 6110 quadrupole ESI-MS, using an Agilent Zorbax Eclipse XDB-Phenyl (3 × 100mm, 3.5 μm particle size, flow rate 1 mL/min, the mobile phases 0.05% formic acid in water and 0.05% formic acid in acetonitrile). Identities of final products were confirmed by high resolution mass spectrometry (HRMS), performed on a Bruker Micro TOF mass spectrometer using (+)-ESI calibrated to sodium formate.

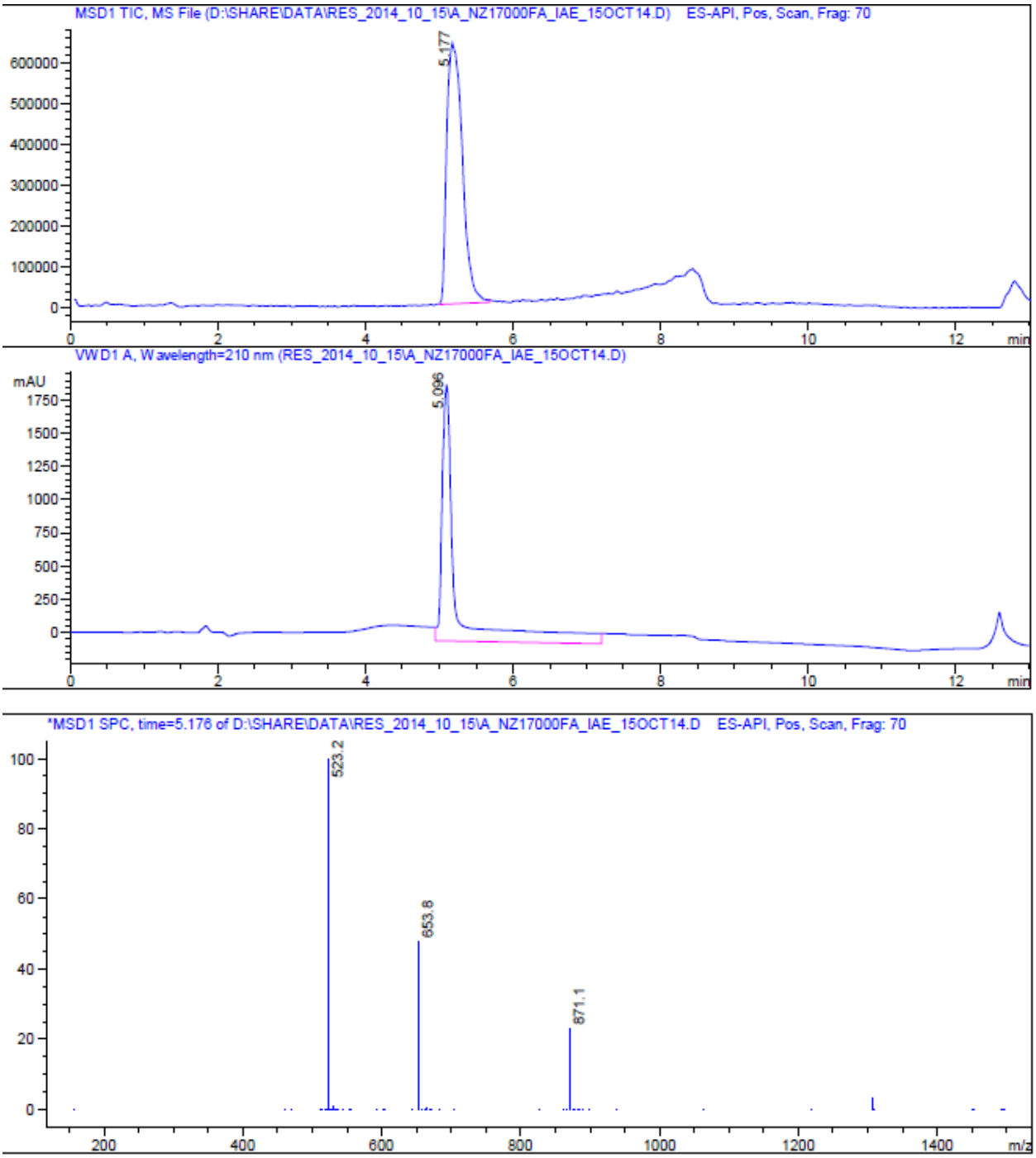

Figure S7.4-1 – LC-MS of arenicin-3. MW(arenicin-3) = 2611.1 Da

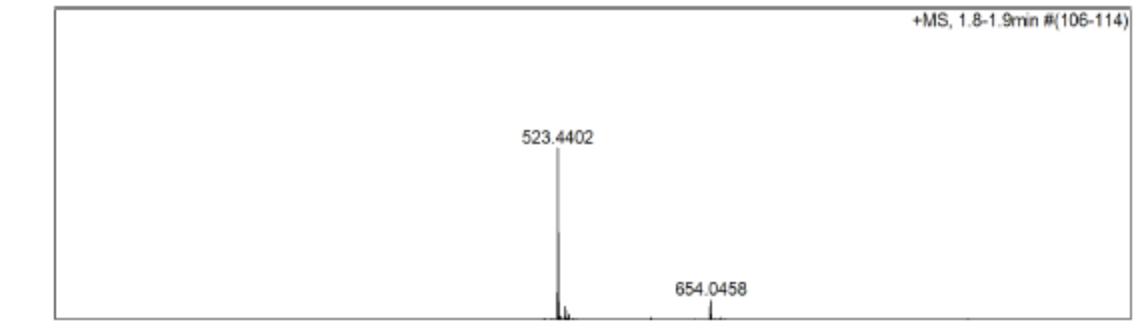

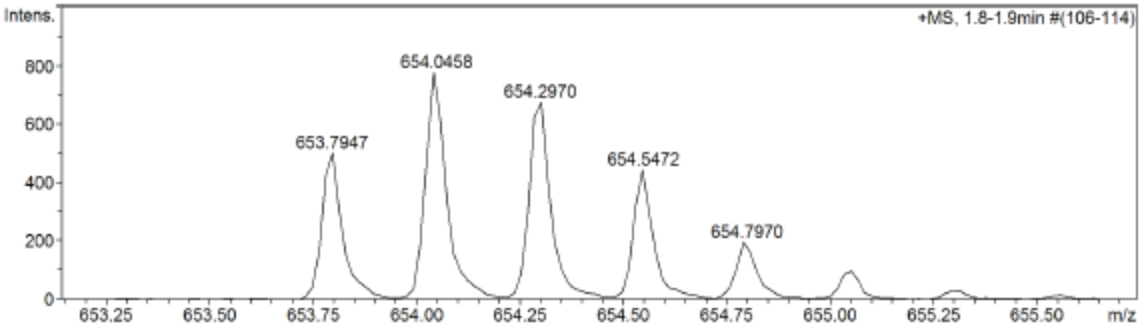

Sum Formula	Sigma	m/z	Err [ppm]	Mean Err [ppm]	Err [mDa]	rdb	N Rule	e⁻
C 115 H 170 N 36 O 27 S 4	0.059	653.7974	4.23	3.03	2.77	49.00	ok	even

Figure S7.4-2 – HRMS of arenicin-3

HRMS-ESI (*m/z*): $[M + 4H]^{4+}$ calculated for $(C_{115}H_{166}N_{36}O_{27}S_4 + 4H)/4$, 653.7974; found 653.7947.

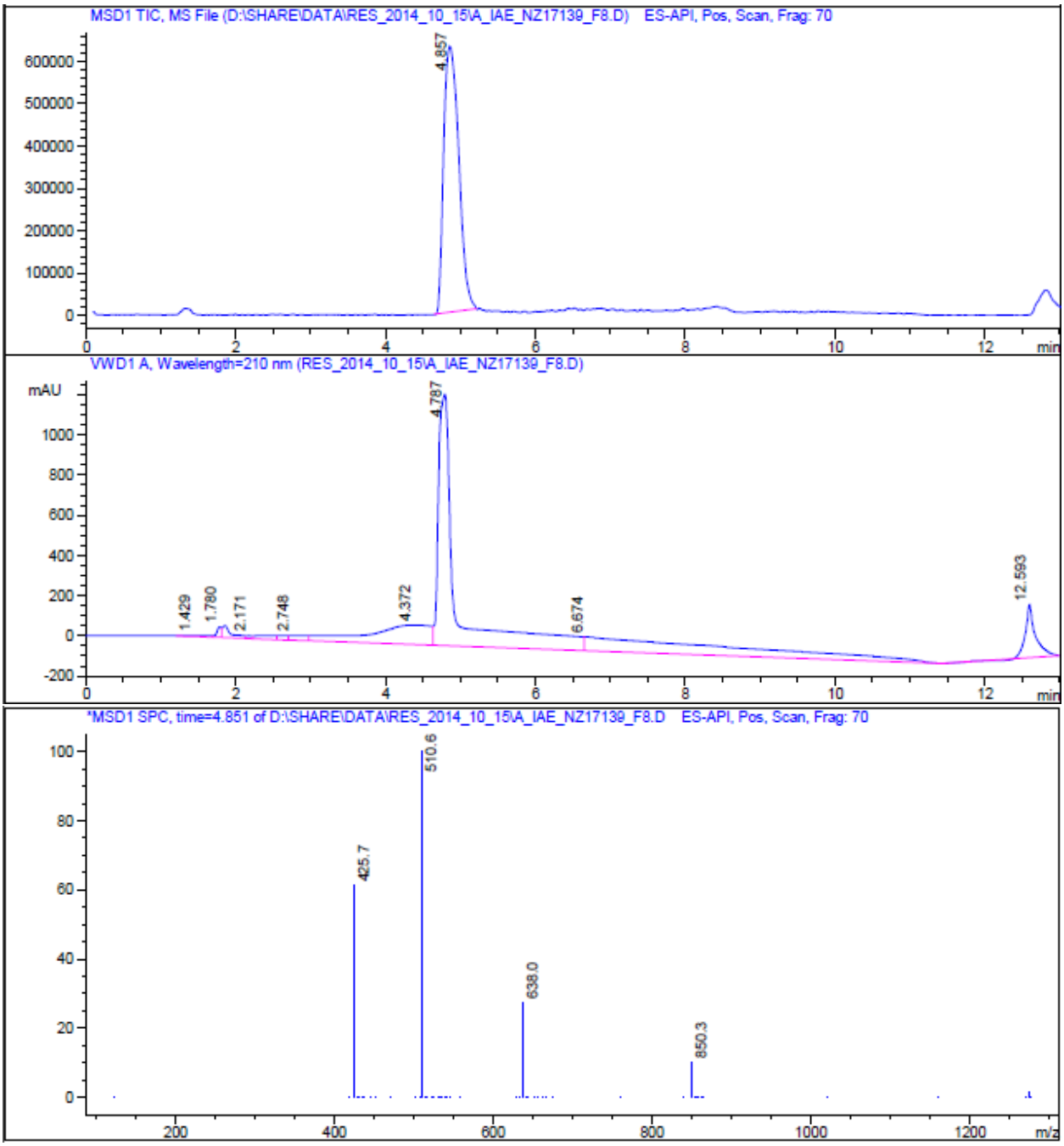

Figure S7.4-3 – LC-MS of AA139. MW(AA139) = 2548.1 Da

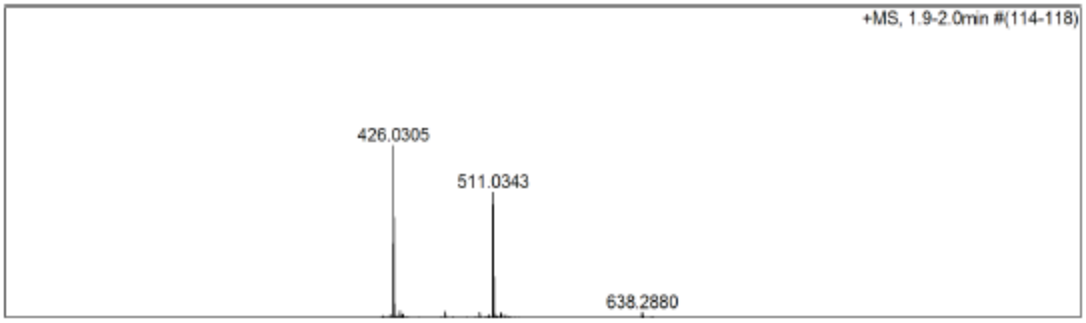

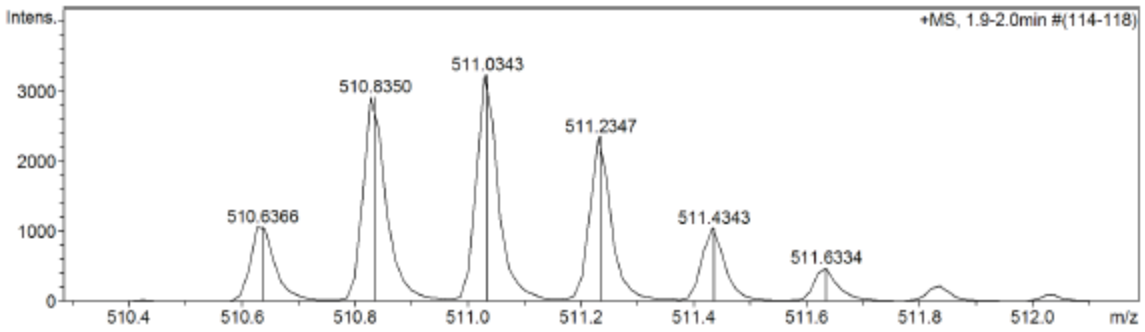

Sum Formula	Sigma	m/z	Err [ppm]	Mean Err [ppm]	Err [mDa]	rdb	N Rule	e⁻
C 108 H 166 N 39 O 26 S 4	0.170	510.6344	-4.22	0.74	-2.15	45.50	ok	even

Figure S7.4-4 – HRMS of AA139

HRMS-ESI (*m/z*): $[M + 5H]^{5+}$ calculated for $(C_{108}H_{161}N_{39}O_{26}S_4 + 5H)/5$, 510.6344; found 510.6366.

	Chemical Shift (ppm)[a]														
Residue	N	NH	Cα	Hα	Cβ	Hβ	Cγ	Cδ	Hγ	Hδ	Hε	Hζ	Hη	Nε	Nδ2
Gly[1]			43.43	3.96		3.96									
Phe[2]	120.59	8.60	57.27	4.99	40.98	3.25,				7.36	7.24	7.21			
Cys[3]	119.00	8.19	55.81	5.57	48.27	2.50, 2.85									
Trp[4]	122.85	9.24		4.86	31.80	3.33,				6.96	9.98, 7.11	7.29, 6.82	6.98	128.69	
Tyr[5]		8.70	57.69	5.14		2.71, 2.84				6.88	6.76				
Val[6]	123.94	8.92	60.90	4.36	33.82	1.66	20.99		0.94						
Cys[7]	123.60	8.77	55.14	5.77	47.53	2.44, 3.00									
Val[8]	119.47	9.17	59.38	4.64	35.80	2.27	21.42		0.93, 1.01						
Tyr[9]		8.69	57.56	5.11		2.72, 2.84				6.90	6.78				
Arg[10]	124.48	9.09	54.85	4.63	32.29	1.65, 1.78	26.93	43.49	1.54, 1.65	3.21	7.22			124.81	
Asn[11]	125.63	9.64	54.31	4.40	37.55	2.80, 3.10				7.64, 6.95					112.77
Gly[12]	102.63	8.58	45.33	3.68, 4.25											
Val[13]	120.36	7.72	61.09	4.38	34.55	2.11	18.88		0.95						
Arg[14]	123.26	8.63	55.30	4.15	30.68	1.31, 1.69	27.82	43.57	0.92, 1.22	3.03	7.09			124.48	
Val[15]	129.72	9.16	61.49	4.24	34.32	1.91	20.77		0.81, 0.92						
Cys[16]	122.93	8.59	54.88	5.79	48.49	2.60, 2.98									
Tyr[17]	121.35	9.16		4.89		2.91, 3.00				6.97	6.65				
Arg[18]	123.26	8.71	55.30	4.20	31.76	1.36, 1.63	27.79	43.55	0.88, 1.13	2.95	6.97				
Arg[19]	128.63	8.67	54.08	4.29	32.60	0.55, 0.94	26.71	43.21	1.21, 1.34	3.12	7.14			124.94	
Cys[20]	116.84	8.09	55.07	5.20	48.78	2.82, 2.97									
Asn[21]	121.55	8.75	51.86	4.91	39.30	3.28, 2.97				6.66, 7.71					110.79

[a]Chemical shift are relative to DSS (0 ppm)

Figure S7.4-5 – NMR data of arenicin-3 in PO4 buffer pH3.3.

	Chemical Shift (ppm)[a]																	
Residue	N	NH	Cα	Hα	Cβ	Hβ	Cγ	Cδ	Cε	Cζ	Cη	Hγ	Hδ	Hε	Hζ	Hη	Nε	Nδ2
Gly[1]			43.54	3.95														
Phe[2]	121.25	8.80	55.97	4.94	40.89	3.23		132.25	131.55	129.80			7.33	7.26	7.22			
Cys[3]	119.28	8.19	55.82	5.60	48.18	2.49, 2.86												
Trp[4]	122.88	9.26		4.85	31.88	3.31		127.34	122.81	113.91, 121.83	123.86		6.98	9.98, 7.16	7.28, 6.89	7.00	128.71	
Tyr[5]	123.12	8.69	57.57	5.09	43.56	2.94		132.66	118.01				6.90	6.76				
Val[6]	123.97	8.87	61.30	4.31		1.55	21					0.88						
Cys[7]	123.68	8.84	55.23	5.71	48.21	2.63, 3.05												
Ala[8]	125.82	9.11	50.97	4.65	22.35	1.47												
Arg[9]	120.58	8.62	55.17	5.02	27.44	1.39, 1.69	27.36					1.52	3.12	6.78				
Arg[10]	125.30	9.00	55.23	4.59	32.47	1.71, 1.79	33.48	43.4				1.54	3.21	7.22				
Asn[11]	125.26	9.58	54.23	4.42	37.51	2.80, 3.09							7.65, 6.96					112.68
Gly[12]	104.30	8.66	45.56	3.61, 4.21														
Ala[13]	123.74	7.78	50.66	4.68	21.30	1.40												
Arg[14]	122.34	8.66	56.28	4.64	30.90	1.80	28.1	43.42				1.46, 1.62	3.14					
Val[15]	127.77	8.94	61.22	4.43	34.46	2.00	20.85					0.94						
Cys[16]	123.81	8.77	55.14	5.80	48.82	2.63, 3.04												
Tyr[17]	120.80	9.04	57.38	4.93	40.45	2.93, 3.01		133.67	117.71				6.96	6.66				
Arg[18]	117.68	8.69	55.24	4.22	27.77	0.86, 1.12	31.93	40.7				1.33, 1.63	2.70, 2.83					
Arg[19]	128.47	8.69	54.23	4.30	32.62	0.62, 0.92	26.85	43.23				1.19, 1.52	3.11					
Cys[20]	117.74	8.12	55.20	5.24	48.46	2.81, 3.06												
Asn[21]	126.34	8.64	54.08	4.61		3.04, 2.92							6.59, 7.55					110.31

[a]Chemical shift are relative to DSS (0 ppm)

Figure S7.4-6 - NMR data of AA139 in PO4 buffer pH3.3.

Table S7.4-2 – Hydrogen-deuterium exchange of arenicin peptides

Peptides	residues with slowly exchanging amides			Hydrogen bonds
	1 h (weak)	3-4 h (medium)	>24 h (strong)	
arenicin-3	C3, C7, N11, G12, C16, C20, N21	F2, Y5, R14, R18	W4, V6, V8, V13, V15, Y17, R19	W4-R19 (HN=O)
				V6-Y17 (HN=O)
				V8-V15 (HN=O)
				V13-R10 (HN-O)
AA139	C3, C7, R9, R10, N11, G12, R14, C16, C20, N21	A8, A13, R18	W4, V6, V15, Y17	W4-R19 (HN-O)
				V6-Y17 (HN=O)
				V15-V8 (HN-O)

Table S7.4-3 – Amide temperature coefficient of arenicin peptides

arenicin-3	slope (ppb/K)	AA139	slope (ppb/K)
Phe^{2}	-3.4	Phe^{2}	-3.6
Cys^{3}	-6.4	Cys^{3}	-6
Trp^{4}	-3.2	Trp^{4}	-4
Tyr^{5}	-6.8	Tyr^{5}	-6.2
Val^{6}	-4	Val^{6}	-7.6
Cys^{7}	-8.2	Cys^{7}	-9.2
Val^{8}	-2.4	Ala^{8}	-2.4
Tyr^{9}	-6.8	Arg^{9}	-7.6
Arg^{10}	-4.2	Arg^{10}	-6.4
Asn^{11}	-9.8	Asn^{11}	-10
Gly^{12}	-10	Gly^{12}	-7.6
Val^{13}	-3	Ala^{13}	-1.4
Arg^{14}	-7.8	Arg^{14}	-6
Val^{15}	-4.4	Val^{15}	-6
Cys^{16}	-8	Cys^{16}	-9
Tyr^{17}	-2.4	Tyr^{17}	-2.2
Arg^{18}	-6	Arg^{18}	-5
Arg^{19}	-6.2	Arg^{19}	-5
Cys^{20}	-2.2	Cys^{20}	-3
Asn^{21}	-4	Asn^{21}	-5

7.5 Supplementary information Chapter 5

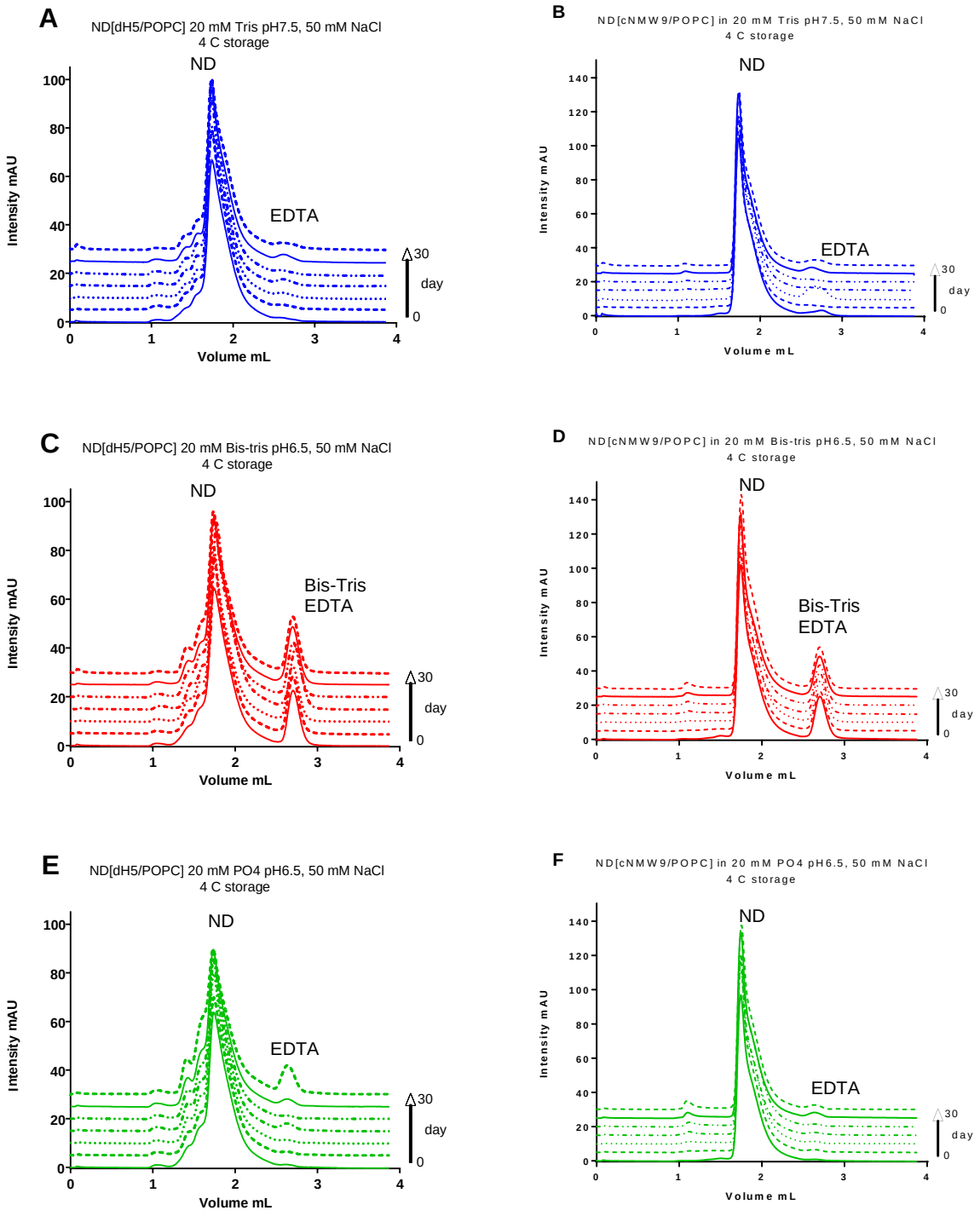

Figure S7.5-1 – Nanodiscs, composed of POPC, stability over 30 days at 4 °C storage. (A), (C) and (E) use dH5 construct while (B), (D) and (F) use cNW9 construct. From top to bottom; (A) and (B) Tris buffer pH7.5 (blue), (C) and (D) Bis-Tris buffer pH 6.5 (red), (E) and (F) PO4 buffer pH 6.5 (green).

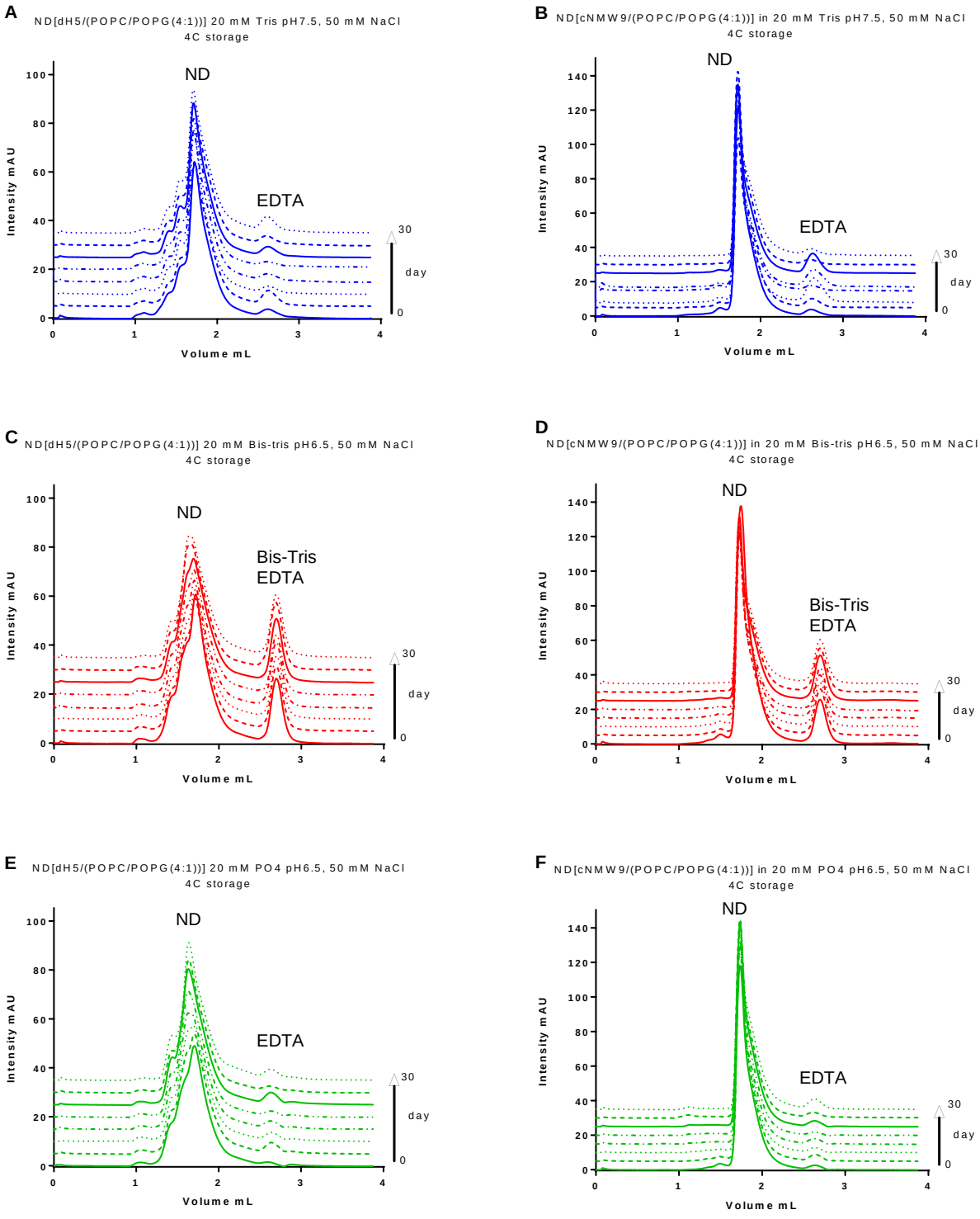

Figure S7.5-2 – Nanodiscs, composed of POPC/POPG (4:1), stability over 30 days at 4 °C storage. (A), (C) and (E) use dH5 construct while (B), (D) and (F) use cNW9 construct. From top to bottom; (A) and (B) Tris buffer pH7.5 (blue), (C) and (D) Bis-Tris buffer pH 6.5 (red), (E) and (F) PO4 buffer pH 6.5 (green).

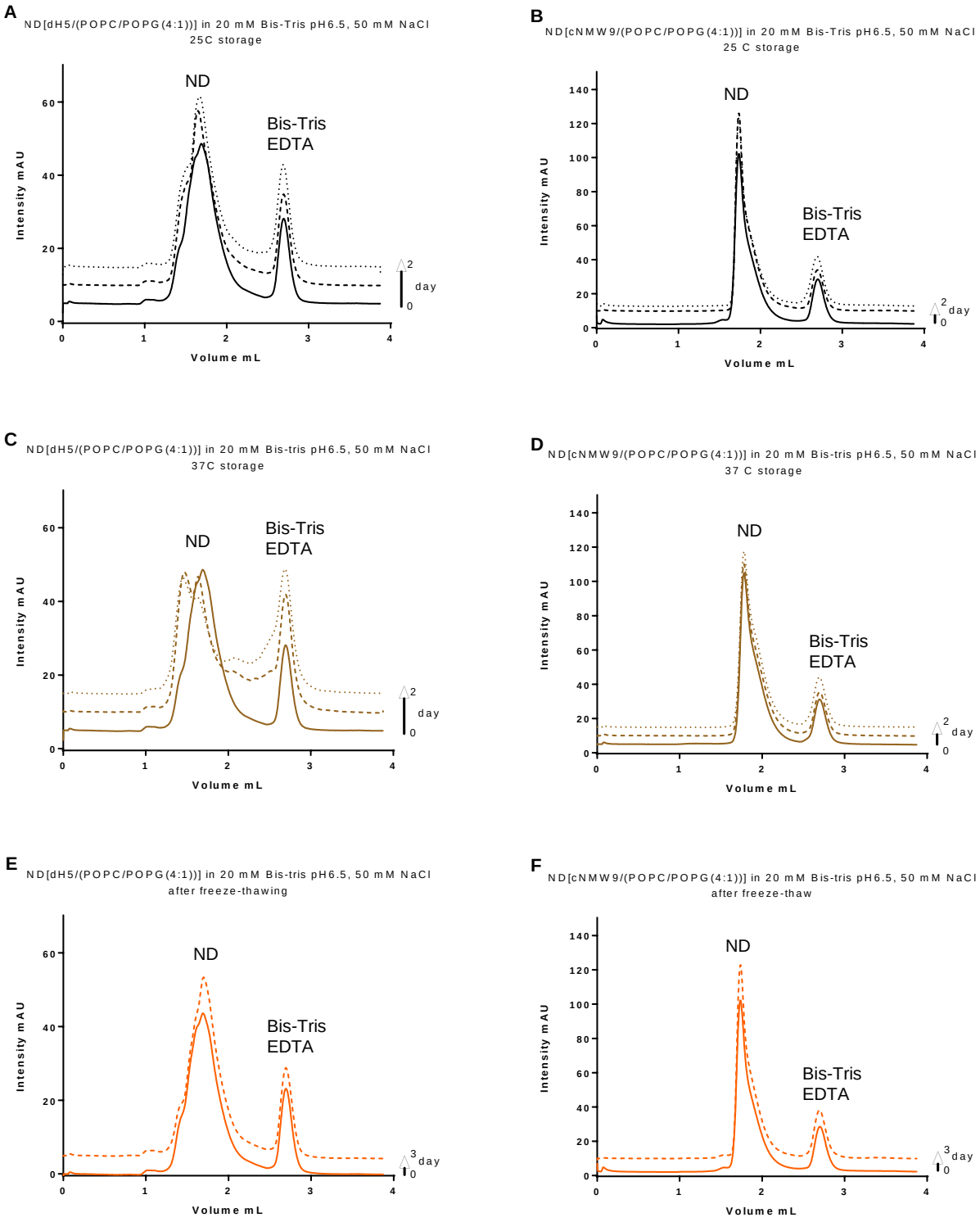

Figure S7.5-3 - Nanodiscs, composed of POPC/POPG (4:1) in Bis-Tris buffer pH 6.5, stability over 2-3 days. (A) and (B) 25 °C, (C) and (D) 37 °C, (E) and (F) after freeze-thawing. (A), (C) and (E) use dH5 construct while (B), (D) and (F) use cNW9 construct.

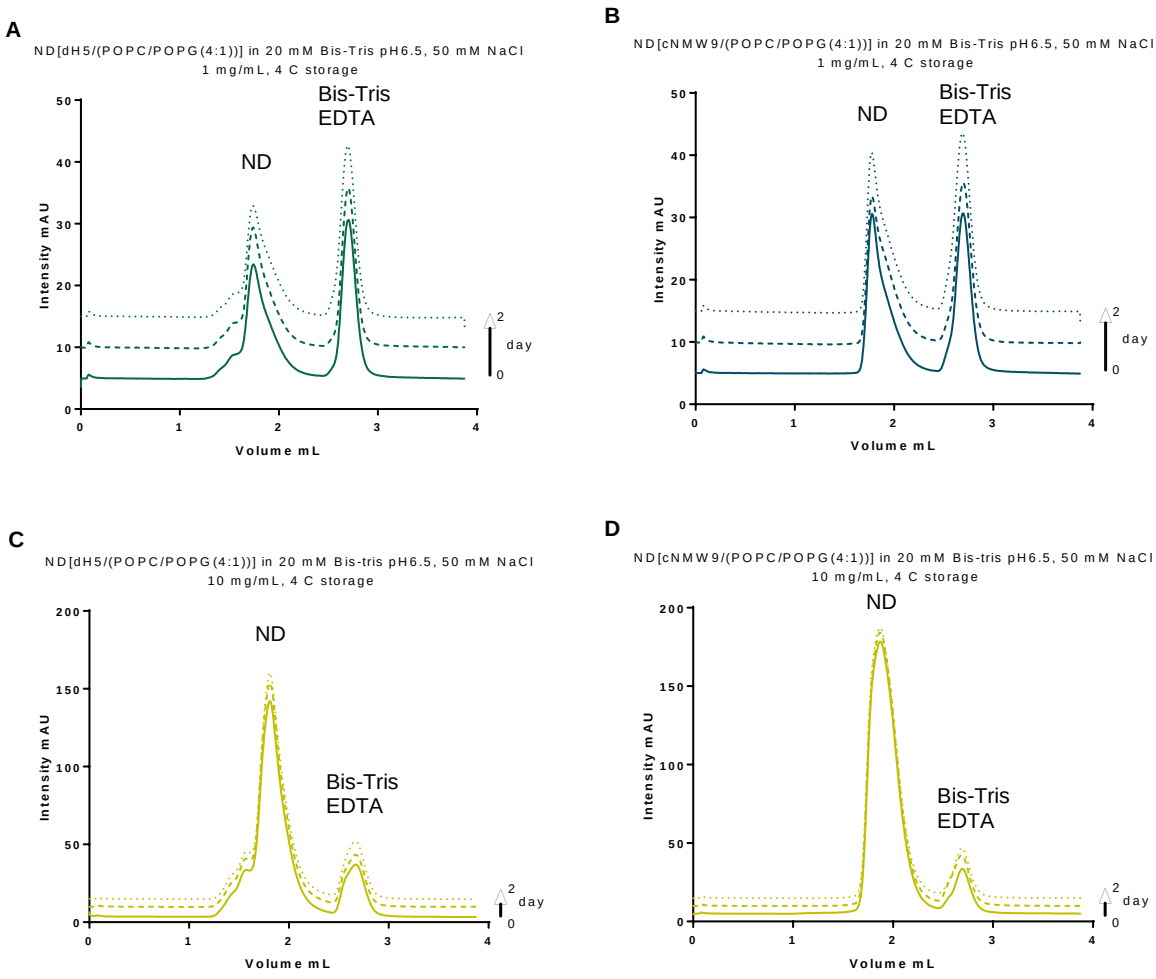

Figure S7.5-4 - Nanodiscs, composed of POPC/POPG (4:1) in Bis-Tris buffer pH 6.5, stability over 2 days. (A) and (B) stored at 1 mg/mL, (C) and (D) stored at 10 mg/mL. (A) and (C) use dH5 construct while (B) and (D) use cNW9 construct.

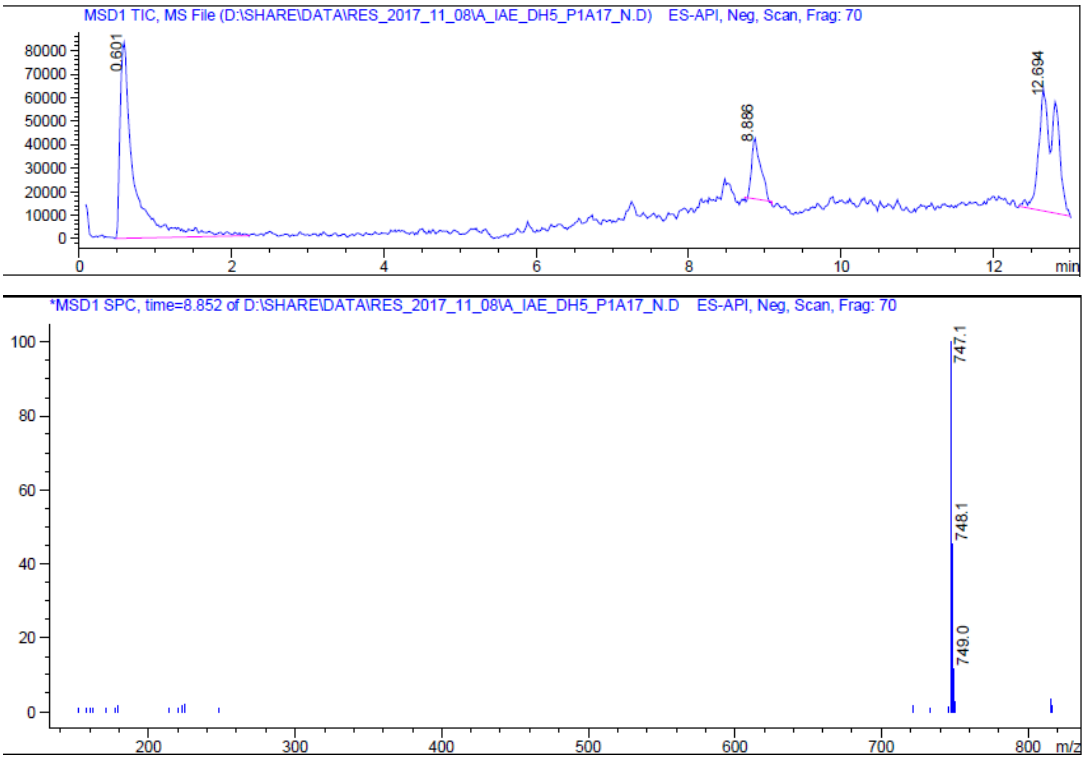

Figure S7.5-5 - LC-MS in negative mode of the SEC of ND[dH5(POPC/POPG(4:1))], shown Figure 5-10 (A), of fractions 10 to 19, fraction corresponding to the ND region, red arrow in Figure 5-10. MW(POPG) = 749.2 g/mol

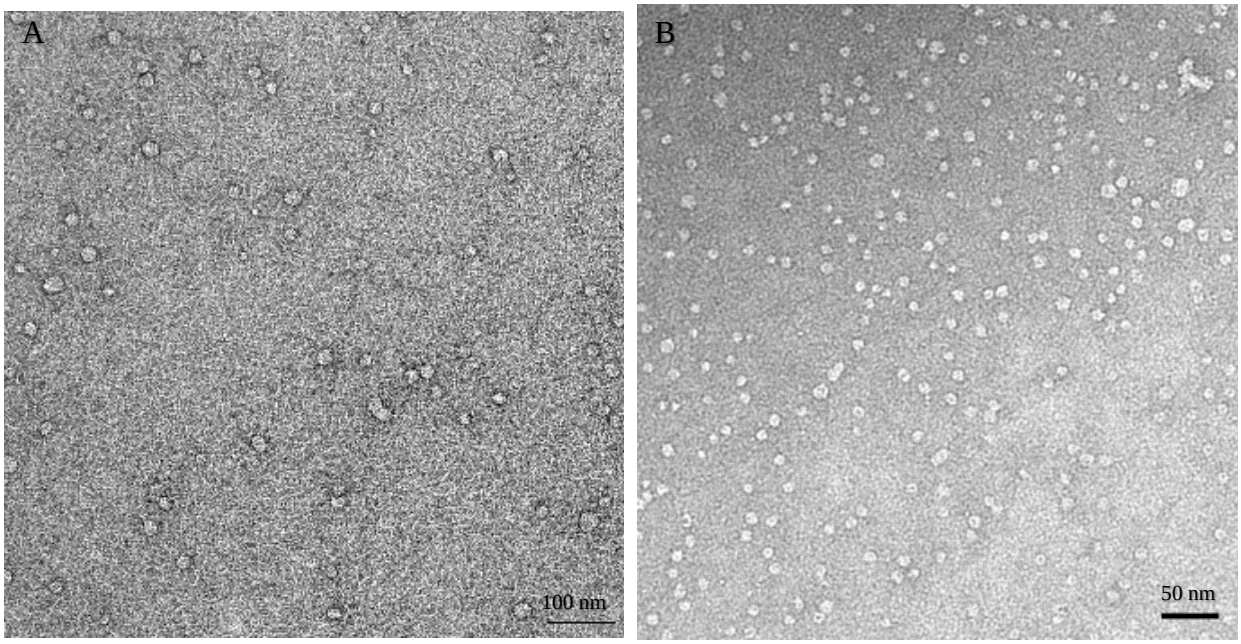

Figure S7.5-6 - Negative staining electron microscopy of (A) fraction 10 showing ND aggregates and **(B)** fraction 16 showing homogeneous ND, of ND[dH5(POPC/POPG(4:1))] at day 7 after storage at room temperature, Figure 5-10(A).

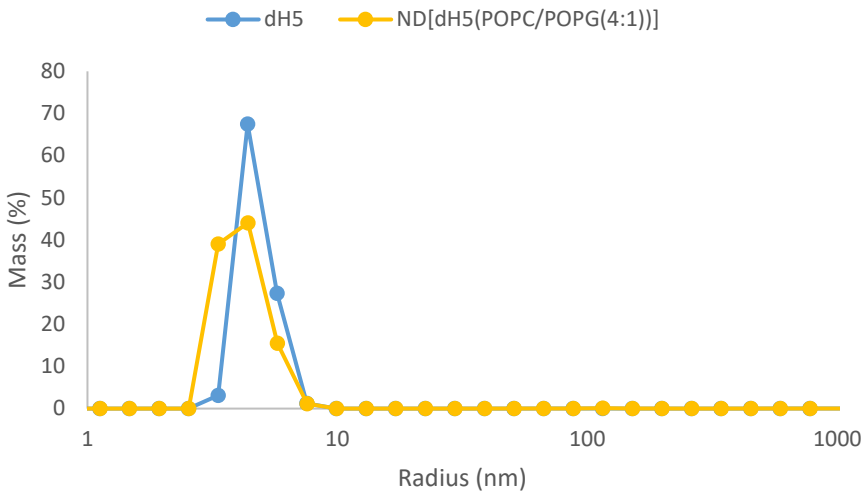

Figure S7.5-7 - DLS experiments of dH5 either alone or as a scaffold for the ND formation showing the mass distribution of the particles.

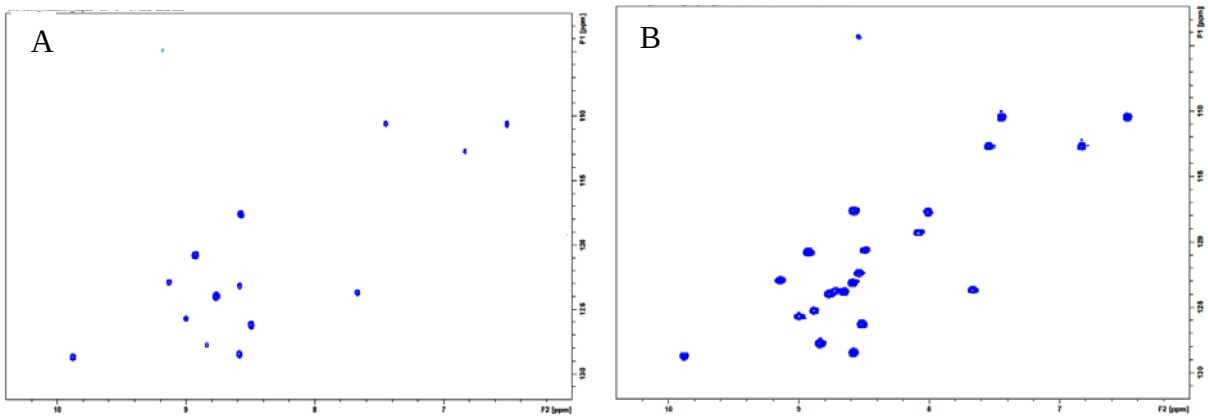

Figure S7.5-8 - ^{1}H-^{15}N-HSQC of ^{15}N-AA139 in (A) 20 mM HEPES buffer pH 7.5 containing 50 mM NaCl and (B) 20 mM Bis-Tris buffer pH6.5 containing 50 mM NaCl.

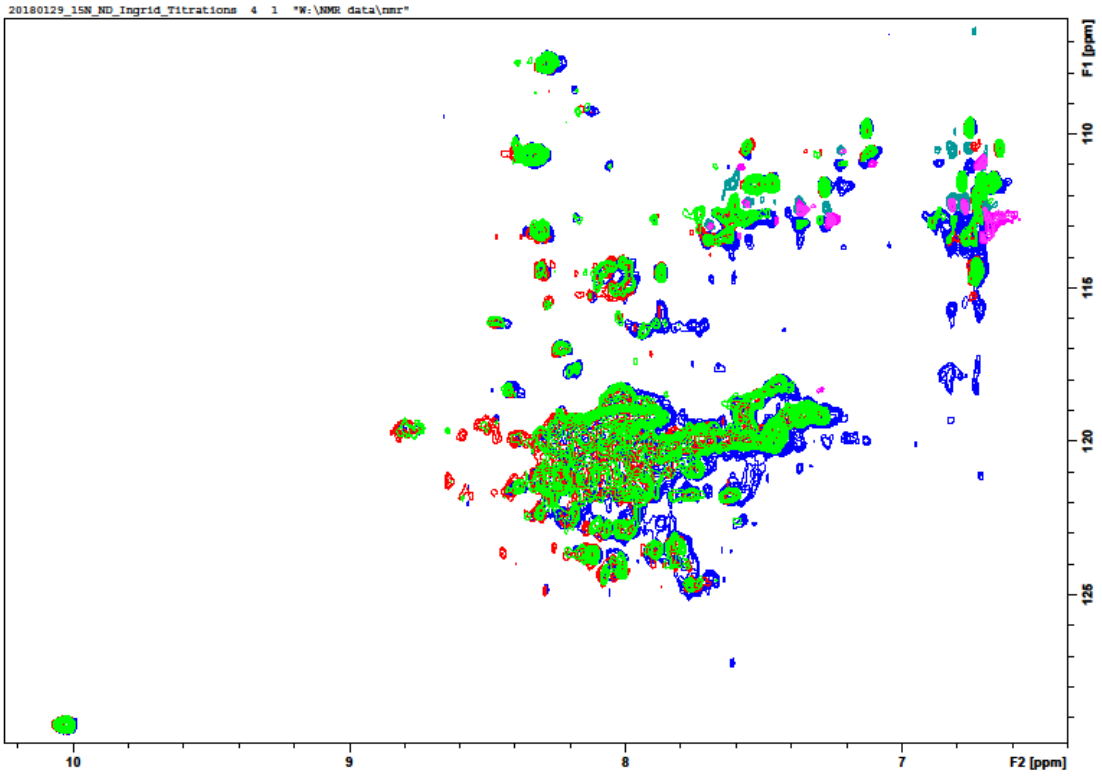

Figure S7.5-9 - Solution NMR titration experiment of AA139 with ND[^{15}N-cNW9(POPC)]. Ratio ND/peptide were 1:0 in blue, 2:1 in red and 1:1 in green.

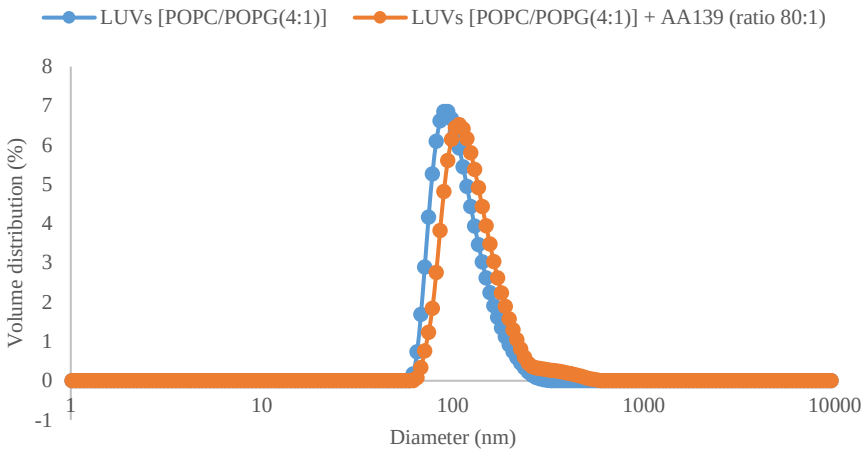

Figure S7.5-10 - DLS of LUVs [POPC/POPG(4:1)] in absence (blue) and presence (orange) of AA139 (ratio 80:1).

7.6 Supplementary information Chapter 6

Materials and methods.

Membrane extraction was perform from E. coli ATCC 25922 and from red blood cells. For *E. coli* cells, the cells were grown in 500 mL of LB media at 37 °C with shaking at 220 rpm until OD_{600} reached late exponential phase (OD_{600} = 0.8). The cells were pelleted by centrifugation at 10000 rpm, for 15 mins at 4 °C. The pellets were washed once with PBS. The pellets were transferred to Teflon tubes and dissolved and incubated for one hour in solvent mixture chloroform/MeOH/H2O (1:2:0.8) with occasional shaking. The cells were washed three times with this solvent mixture, collecting each time the solvent as it is where the lipids are located. Lipid membranes were finally extracted using solvent ratio chloroform/MeOH/H2O (2:2:1.8). The solution was placed in a separatory funnel for decantation. The chloroform phase was removed, evaporated and left under nitrogen flow overnight for complete drying. The lipid extract was then weighted out and characterized.

For red blood cells (RBC), 200 mL of blood taken from the Red Cross were centrifuged at 4000 rpm for 20 min to separate the plasma from the red blood cells. The plasma was removed and the pelleted RBC were washed three times with PBS or until the supernatant becomes clear. Deionized water was added to the RBC to lyse the cells. Cells were pelleted by centrifugation at 4000 rpm for 20 mins and the hemoglobin was removed. The “ghost” membrane of the RBC transferred to Teflon tubes and solubilized in solvent mixture chloroform/MeOH/H2O (1:2:0.8) and incubated for one hour with occasional shaking. The cells were washed three times with this solvent mixture, collecting each time the solvent as it is where the lipids are located. Lipid membranes were finally extracted using solvent ratio chloroform/MeOH/H2O (2:2:1.8). The solution was placed in a separatory funnel for decantation. The chloroform phase was removed, evaporated and left under nitrogen flow overnight for complete drying. The lipid extract was then weighted out and characterized.

Both *E. coli* and RBC lipid membrane extracts were dissolved in 500 µL MeOH. Samples we injected into a QSTAR Elite (Applied Biosystems) hybrid quadrupole Time-of-Flight (TOF) mass spectrometer. Direct infusion on negative mode was performed.

BCA assay. 25 µL of the MeOH solution used for MS was dried up under nitrogen flow and reconstituted in 80 and 160 µL of PBS for *E. coli* and RBC, respectively. The BCA assay was

performed as per provider instruction and the 96 wells plates cooled to room temperature before absorption at 562 nm were measured using Tecan M1000 Pro plate reader.